FHWA - TS - 82 - 216

PB83-185595

HUD-0002712

STRUCTURAL PLASTICS DESIGN MANUAL

Phases 2 and 3; Chapters 5 - 10

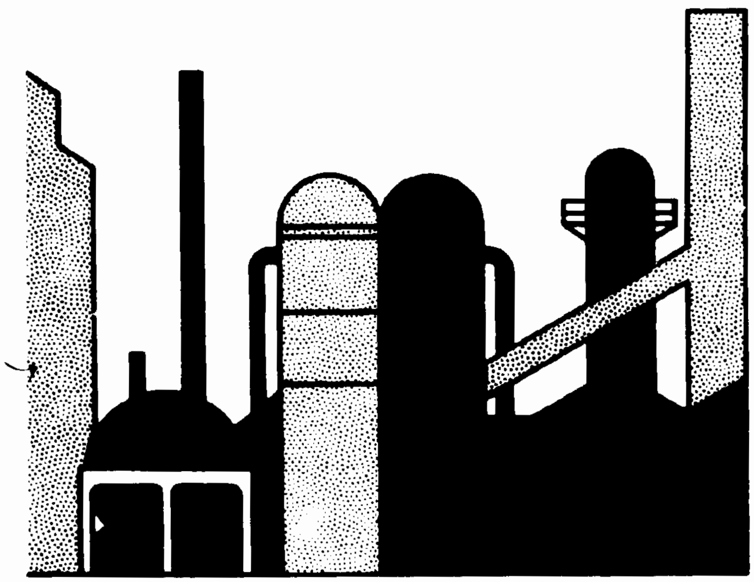

SPONSORED BY

U.S. Department of Transportation
Federal Highway Administration
Urban Mass Transportation Administration

U.S. Department of Housing and Urban Development
and
Participating Industrial Corporations

AUGUST 1982

BIBLIOGRAPHIC INFORMATION

PB83-185595

Structural Plastics Design Manual, Volume 2. Phases 2 and 3, Chapters 5 to 10,

Aug 82

Frank J. Heger, Richard E. Chambers, and Albert G. Dietz.
PERFORMER: Simpson Gumpertz and Heger, Inc., Cambridge, MA.

SPONSOR: Federal Highway Administration, Washington, DC.
HUD-0002712 FHWA/TS-82/216

Sponsored in part by Urban Mass Transportation Administration, Washington, DC., Department of Housing and Urban Development, Washington, DC. American Society of Civil Engineers, New York, Dow Chemical Co., Midland, MI. Monsanto Co., St. Louis, MO. Owens-Corning Fiberglass Corp., Toledo, OH. DuPont de Nemours (E.I.) and Co., Inc., Wilmington, DE. and Rohm and Haas Co., Philadelphia, PA.

This manual provides guidelines to structural engineers designing plastics and reinforced plastics structural components. It discusses applications commonly used in building construction, transportation structures and vehicles, process industries, sanitary facilities, and marine vessels and structures. The volume devotes space to the fundamentals of elastic response of structures and provides quantitative methods for analysis and design of plates, beams and axial stressed members, flat sandwich structures, and thin rings and shells fabricated from plastic materials. It also reviews the tests and standards used for evaluating structural plastics' fire resistance. Tables, diagrams and chapter notes and references are supplied.
KEYWORDS: *Structural members.

Available from the National Technical Information Service, Springfield, Va. 22161

PRICE CODE: PC A99/MF A01

STRUCTURAL PLASTICS DESIGN MANUAL - VOL. 2

Phases 2 and 3 – Chapters 5 to 10

Simpson Gumpertz & Heger Inc.

Frank J. Heger, Principal
Richard E. Chambers, Senior Associate
Albert G. H. Dietz, Consultant

This publication was prepared under a contract from the American Society of Civil Engineers with financial support provided by the sponsoring organizations listed on the reverse side.

SPONSORING ORGANIZATIONS

Ciba-Geigy Corp.

Dow Chemical U.S.A.

E. I. duPont de Nemours & Co. Inc.

Federal Highway Administration

Manufacturing Chemists' Association, Inc.

Monsanto Company

Morrison Molded Fiberglass Corp.

Owens-Corning Fiberglas Corp.

Pittsburgh Plate Glass — Fiberglass Division

Reichhold Chemical, Inc.

Rohm and Haas Company

Shell Chemical Company

U. S. Department of Housing and Urban Development

Urban Mass Transportation Administration

NOTICE

This document is disseminated under the sponsorship of the Department of Housing and Urban Development, the Department of Transportation, the sponsoring industrial organizations for this project, and ASCE in the interests of information exchange. The United States Government, ASCE, the industrial sponsors, and the contracting organization assume no liability for its contents or use thereof.

The contents of this report reflect the views of the contracting organization, and do not necessarily reflect the official views or policy of the sponsors. The purpose of the project is to summarize and interpret state-of-the-art information and concepts from various sources. Example designs and typical properties and behavior are provided only to illustrate engineering concepts. Neither the sponsors nor the contracting organization are responsible for their use in specific applications. This report does not constitute a standard, specification, or regulation. It creates no rights and imposes no duties on any person or organization.

The United States Government does not endorse products, services, or manufacturers. Trade or manufacturer's names appear herein only because they are considered essential to the object of this document.

FORWORD – BY ASCE TASK COMMITTEE ON DESIGN MANUAL

In order that this Manual be truly representative of up-to-date design practices and current technical information, the Task Committee on Design Manual invites responses from the readers and users of this portion of the Manual. The responses may take the form of comments, discussion, questions, etc. and should be sent to:

Harry N. Tuvel, Manager
Technical Services
American Society of Civil Engineers
345 East 47th Street
New York, New York 10017

Your responses will assist in any pertinent editing which will be implemented prior to issuance of the formal Design Manual.

Eugene Gray, Jr., Chairman, ASCE
Task Committee on Design Manual

TASK COMMITTEE ON DESIGN
STRUCTURAL PLASTICS RESEARCH COUNCIL
AMERICAN SOCIETY OF CIVIL ENGINEERS
SEPTEMBER 1981

Membership of Task Committee on Design:

Eugene Gray, Jr., Chairman	Owens-Corning Fiberglas Corp. Granville, Ohio
H. C. Browne	Monsanto Company St. Louis, Missouri
T. J. Fowler	Monsanto Company St. Louis, Missouri
A. M. Lizzio	Department of Transportation Washington, D.C.
J. F. McDermott IV	U. S. Steel Monroeville, Pennsylvania
D. E. White	Dept. of Housing and Urban Development Washington, D.C.
G. O. Widera	University of Illinois Chicago, Illinois
S. J. Gozzo (I. Litant, alternate)	Transportation System Center Cambridge, Massachusetts
A. Green	Composite Technology Inc. Fort Worth, Texas

PREFACE

This Manual was written to provide practical assistance and guidelines to structural engineers engaged in the design of plastics and reinforced plastics structural components. In the first phase of the work, the structural behavior of plastics-based materials is characterized in general; the significant types of structural plastics in current use are listed and described; and practical design criteria are synthesized and proposed for use in the design of structural plastics. Design approaches that lead to the most efficient use of plastics for structural applications are described and illustrated by design examples. These are presented in Volume I of the Manual, published in 1979 by the United States Government Printing Office, and available for distribution through ASCE.

This volume presents the results of Phases 2 and 3 in the development of the Manual, consisting of Chapters 5 through 10. Chapter 5 presents a brief review of fundamental concepts of structural behavior. Chapters 6 through 9 provide quantitative methods for analysis and design of plates, beams and axial stressed members, sandwich components and thin rings and shells that are fabricated from plastic materials with either isotropic or orthotropic elastic properties. Chapter 10 presents general information about the fire resistance of structural plastics and the tests and standards used for evaluating this aspect of their behavior. These chapters complete the Structural Plastics Design Manual.

The Manual is intended as a basic text for engineers interested in a wide variety of structural applications for plastics; in particular, the applications discussed include those commonly used in building construction, transportation structures and vehicles, process industries, sanitary facilities, and marine structures and vessels. It is assumed that engineers and structural designers using the Manual have a basic knowledge of strength of materials, but do not necessarily have a background in plastics and reinforced plastics.

The Manual has been prepared by Simpson Gumpertz & Heger Inc., of Cambridge, Massachusetts, under a research and development contract from the ASCE, with the Society's Structural Plastics Research Council monitoring the effort. The undersigned, a Senior Principal in the consulting engineering firm of Simpson Gumpertz & Heger Inc., developed the conceptual outline for the content of the Manual, and is principal author

of Chapters 4, 5, 6, 7 and 9. Richard E. Chambers, Senior Associate, Simpson Gumpertz & Heger, Inc., is principal author of Chapters 2, 3 and 8. Albert G. H. Dietz, Professor Emeritus, Department of Architecture and Planning, Massachusetts Institute of Technology, was retained as a consultant to assist with certain portions of the Manual and is principal author of Chapters 1 and 10. The text was typed by Cynthia B. Topping and other word processing staff at Simpson Gumpertz & Heger Inc. The illustrations were prepared by the drafting department at Simpson Gumpertz & Heger Inc.

The financial support and technical review of the ASCE Structural Plastics Research Council and its task committee, which has made possible the development of the Manual, is gratefully acknowledged. Howard Browne, chairman of the Council, was an early initiator of the project to develop a Structural Plastics Design Manual and has been, over the years, the prime mover in the effort to obtain financial support. Dr. Timothy Fowler, original chairman of the Council's task committee for the project, and Eugene Gray, current chairman have made valuable suggestions on the scope, organization, and content of the Manual — as have other members of the committee.

Financial support for the project has been provided to the ASCE from the U.S. Department of Housing and Urban Development, the U.S. Department of Transportation, Monsanto Co., Owens-Corning Fiberglas Corporation, Manufacturing Chemists' Association, Inc., Dow Chemical U.S.A., Rohm and Haas Company, and E.I. duPont de Nemours & Co. Inc.

The development of a practical plastics design manual specifically designed to meet the needs of structural engineers is the first project to result from the efforts of the ASCE Structural Plastics Research Council. The Manual was initiated to accomplish one of the Council's primary objectives — to further the rational use of plastics in structural applications. It is hoped that the Manual will serve as a guide that indicates the type of structural design data needed by structural engineers for rational design with structural plastics, as well as a catalyst to foster increased cooperation between industry, government, and the engineering profession in behalf of the future work of the Council.

Frank J. Heger, ScD, P.E., F.ASCE
Simpson Gumpertz & Heger Inc.
Cambridge, Massachusetts

September 1981

TABLE OF CONTENTS - VOL. 2

10. FIRE SAFETY CONSIDERATIONS

ASCE Structural Plastics Design Manual

CHAPTER 5 – FUNDAMENTALS OF ELASTIC RESPONSE OF STRUCTURES

By Frank J. Heger

TABLE OF CONTENTS

NOTATION - Chapter 5

a	diameter of hole; distance from concentrated load to support; long radius of ellipse; crack length; dimensions
a_f	crack length at failure
A	section area
A_n	section area of part n
A_p	area enclosed by the centerline of a closed thin-wall section
A_w	section area of web (I, ⊏, or box beams)
b, b_f, b_w, b_n	width; width of flange; width of web, width of part n
b	spacing between holes; distance to concentrated load from support; short radius of ellipse; dimension
b_t	transformed width used in transformed section
C	constant coefficient
c	dimension; damping coefficient
c_L, c_m	effective load (or force) coefficient, effective mass coefficient
c_r	critical damping coefficient
c_s	shape factor for maximum shear stress
d	dimension; reduced width between notches (Fig. 5-9)
D	overall width without notches (Fig. 5-9)
DLF	dynamic load factor

e_x, e_y	strain in x and y directions
e	strain; eccentricity
E	elastic modulus
E_v	viscoelastic modulus (Chapters 2 and 3)
E_x	elastic modulus in x direction
E_{11}, E_{22}	elastic modulus in materials direction 1, or 2, for normal stress in direction 1, or 2
f	natural frequency of vibration, correction factor for stress intensity
F, F_e	dynamically applied force, effective dynamically applied force
F_t	force at time t
F_1	force at time 1
G	shear modulus
G_{12}	shear modulus for shear in plane of materials axes 1 and 2
$\bar{G}$	energy release rate when cracks extend
h	height of rectangle; height of notch
H	horizontal reaction on loading diagram
I	moment of inertia of section
I_x, I_y	moment of inertia about x and y axes, respectively
I_o, I_{xon}	moment of inertia about centroidal axis, and about centroidal axis parallel to x axis of part n

I_u, I_v — moment of inertia about u and v axes, respectively

I_{up} — moment of inertia about principal axis, u_{px}

I_1, I_2 — moment of inertia about axes 1 and 2, respectively, in member cross section

I_{xy}, $I_{x_o y_o}$ — product of inertia about axes x and y, and product of inertia about centroidal axes parallel to axes x and y

I_z — polar moment of inertia

J — torsion constant for cross section

k — part generalized designation; stiffness (spring constant)

K — stiffness, or spring constant

K, K_I, K_{II}, K_{III} — stress intensity factors

K_m, K_v, K_a — coefficients for bending, shear and axial deflections, respectively

K_t, K_{tx}, K_{tg} — stress concentration factor; stress concentration factor for stress in direction of x-axis; stress concentration factor for nominal stress on gross section

K_c, K_{Ic}, K_{IIc}, K_{IIIc} — critical stress intensity factors for statically applied load

K_{Id} — critical stress intensity factor for dynamically applied load

L — member length

L_p — length of periphery of closed tubular section

m — dimension to centroid from reference axis

M	bending moment
M_p	bending moment due to load, P
M_s	bending moment in spring
M_{x_1}, M_{x_2}	bending moment at a point along reference axis x about centroidal axes 1-1 and 2-2, respectively, in member section
$\bar{M}, \bar{M}_e$	mass; effective mass
n	modular ratio, E_n/E_v; dimension; general part designation
N	axial force per unit width
N_x	axial force in x direction
P	concentrated load
P_{cr}	critical buckling load
q_m	shear flow at centroidal axis 1-1 (usually maximum for section)
$\bar{Q}_{sy}$	first moment of the area of section above (or below) a distance y from the centroidal axis about the centroidal axis
$\bar{Q}_{s1}$	first moment of the entire area above (or below) centroidal axis 1-1 about axis 1-1
r	radius of notch or fillet
r_o	polar radius of gyration
r_x, r_y	radius of gyration about x and y axes
r, R	radial distance from centroid of section to point stressed in shear due to twisting; and maximum radial distance

R	outer radius of circular section; reaction on loading diagram
S	section modulus
S_{xt}, S_{xb}	section modulus for top and bottom of section with respect to x_o axis
S_1, S_2	section modulus with respect to centroidal axes 1 and 2, respectively
t, t_f, t_w, t_n	thickness; thickness of flange; thickness of web; thickness of part n
t	time
T	torsional reaction in loading diagram; natural period of vibration
T_x	torque at point along x axis
V	transverse shear force
V_{x_1}, V_{x_2}	transverse shear force at point along x axis for bending about centroidal axis 1-1, 2-2
w	uniformly distributed load per unit length
W	total uniformly distributed load
x	distance in direction of x axis, from a reference point
$\bar{x}$, $\bar{y}$	distance in direction of x axis from reference y axis to centroid; same in direction of y axis
x_o, y_o	distance form y axis parallel to x axis to centroid of area, and distance from x axis parallel to y axis to centroid of area

y, z	distance in y, and x axes directions, respectively, from section centroid to another point in a member cross section
y_i	initial displacement in y direction
y_{max}, z_{max}	distance in y and z axes directions, respectively, from section centroid to the extreme point on member cross section
α	coefficient in equation for twisting shear; angle of principal normal stress with beam axis
γ	shear strain
γ_e	elastic surface energy of material when crack extends
δ, δ_o	deflection, initial deflection
$\delta_m, \delta_v, \delta_a$	bending, shear and axial deflections, respectively
δ_s	static deflection
δ_x, δ_y	deflection in direction of x, and y axes, respectively
Δ	lateral deflection of frame
ν	Poisson's Ratio
ν_{12}	Poisson's Ratio for stress in materials direction 1 and strain in direction 2
η	percent of critical damping
ω	circular natural frequency of harmonic vibration
Ω	circular forcing frequency of harmonic vibration
ϕ	total angle of twist due to torque

ϕ_1	coefficient for estimating natural frequency
ϕ_{x_1}	curvature (change in slope)
ρ	radius of curvature
ρ_{x1}	radius of curvature associated with ϕ_{x_1}
σ	normal stress
$\sigma_{max}, \sigma_{nom}$	maximum normal stress; nominal normal stress
σ_x	stress in direction x
σ_{xc}	critical buckling stress in direction x
σ_{xf}	nominal tensile failure stress in direction x
σ_{xu}	ultimate strength of material in direction x
τ	shear stress
τ_x, τ_{xm}	shear stress at point along x axis, and maximum shear stress at this point
τ_{xr}	shear stress at distance r from centroid due to torque at a point along x axis
θ	angle of axis, U, from reference axis, x; slope; angle of twist per unit length due to torque; angle of rotation per unit length
θ_p	angle of principal axis, U_p, from reference axis x
θ_o	initial rotation
θ_x	slope of elastic beam axis at point x, angle of twist per unit length at point x

CHAPTER 5 - FUNDAMENTALS OF ELASTIC RESPONSE OF STRUCTURES

F.J. Heger

5.1 INTRODUCTION

The Chapter summarizes certain basic concepts and important geometric properties of members that define elastic structural behavior. These should be familiar to the practicing structural engineer, but for readers less familiar with conventional structural practice, they should serve as a review and summary of basics needed to understand structural analysis and design methods presented in subsequent chapters. First, the stress resultants that represent the effects of applied loads on members in a structural system are defined. Determination of stress resultants is illustrated by a table covering certain common beam cases, as well as by solving an example problem. Next, important geometric properties of a member cross section are described, and equations are given for determining these sectional properties. Finally, conventional elastic "beam theory" is described and used to show how stresses and deflections are determined from stress resultants, member section properties and member support conditions. In later chapters, these concepts are employed to determine stresses and deflections in common types of structural members such as plates, columns, tension members, beams and shells.

The Chapter also presents a summary of the effects of notches, holes and other changes in geometry on structural behavior of plastics which is another topic of critical importance for design. These produce sharply increased local stresses, called stress concentrations, with an increased potential for brittle fracture in plastics materials. Next, the concepts of non-linear response and buckling are introduced. These are needed to determine effects of large deformations and instability on the behavior and design of practical members. The problem of brittle fracture is further examined in an introductory discussion of fracture toughness and the effects of flaws in the presence of tension. Finally, a brief discussion of structural vibration is presented to familiarize the reader with the effects of rapidly applied loads.

5.2 STRESS RESULTANTS

When a system of loads is applied to an assembly of beams and columns, as shown idealized in Fig. 5-1, the members resist these loads and transfer them to the structural supports by bending and extension. Such bending and extension produces internal stresses whose overall effects at any cross section are termed the stress resultants at that section. Stress resultants that are considered in this Chapter are bending moments, M_{x1} and M_{x2}, thrust, N_x, shears V_{x1} and V_{x2}, and twisting moment, T_x, as shown in Fig. 5-1. The planes in which these stress resultants act are also shown in Fig. 5-1. The concepts that are explained here with respect to linear members may also be applied to more complex systems of stress resultants that occur in two and three dimensional components like plates and shells. These are discussed in Chapters 6 and 9.

Statically Determinate and Indeterminate Systems

Stress resultants are determined from the laws of statics and compatibility of deformation at joints and supports. Two dimensional assemblies of linear members (bars) and supports are statically determinate when all of the support reactions to a system of applied loads can be determined by the three equations of static equilibrium:

- Sum of load and reaction components in both the x and y directions are zero. (two equations)
- Sum of moments of loads and reactions about any point in the plane of forces is zero. (one equation)

For three-dimensional assemblies, six equations of equilibrium are available:

- Sum of load and reaction components in each of x, y and z directions are zero. (three equations)
- Sum of moments of load and reaction components in each of the x-y, x-z, and y-z planes about any point in the respective planes are zero. (three equations)

Example 5-1 illustrates the determination of stress resultants for the statically determinate assembly of members and applied loadings shown in Fig. 5-1.

Whenever the number of unknown reaction components, or the internal restraints at joints in a structure exceeds the number of unknowns needed to satisfy the static laws, the structure and its supports, or the structural assembly, is statically indeterminate. In such assemblies, stress resultants must be determined so that deformations at joints between connected structural members and/or between members and their supports are compatible. This requires a more complex analysis that is usually based on elastic bending theory. Methods of elastic analysis for indeterminate structures are well established and they are presented in many textbooks on structural theory. The most widely used methods for manual calculations are the "Method of Superposition" (5.1) and the "Method of Moment Distribution" (5.1, 5.2). The most widely used method for computer analysis is the "stiffness method" (5.1, 5.3). Analysis methods for indeterminate structures will not be treated in detail here.

Determination of Stress Resultants

Stress resultants in the form of shear and bending moment diagrams, or coefficients for maximum shear, thrust and bending moment for many different loading cases and assemblies of beams, columns, and frames are found in various handbooks (5.2, 5.4, 5.5, 5.6, 5.7). A few of the most common cases for individual beams are given in Table 5-1 to illustrate the type of information that is available and for use in the examples presented later. See (5.5) for more information about these cases and for other common cases.

Stress resultants for more complex loading cases frequently can be determined by resolving the total load to combinations of simpler cases, for which solutions for stress resultants are available. The stress resultants for each loading case may be superimposed to obtain stress resultants for the combined case. The law of superposition for elastic deformations is an important theorem that may also be used to determine the stress resultants that produce compatible deformations at joints and supports in indeterminate structures (Method of Superposition (5.1)).

Example 5-1: Determine the reactions and the maximum bending moment, twisting moment, shear force and thrust force in the beam member 1-4 shown in Fig. 5-1, if w = 1 kip/ft. (1 kip = 1000 lbs). P_{3z} = 5k, P_{3x} = 4k, L = 20 ft., a = 8 ft., b = 12 ft., c = 2 ft.*

1. Determine reactions using equations of equilibrium, since the structure is "statically determinate".

$\Sigma F_z = 0$ $\qquad R_1 + R_4 = wL + P_{3z} = 1.0 \times 20 + 5 = 25k$

$\Sigma M_y = \Sigma M_4 = 0;$ $\qquad 20R_1 = wL^2/2 + P_{3z}b = 1.0 \times 20^2/2 + 5 \times 12 = 260'k$

$\qquad R_1 = 13k; R_4 = 25 - 13 = 12k$

$\Sigma F_x = 0$ $\qquad N_4 = P_{3x} = 4.0k$

$\Sigma F_y = 0$ $\qquad H_1 - H_4 = 0; H_1 = H_4$

$\Sigma M_z = \Sigma M_4 = 0$ $\qquad 20H_1 = 2P_{3x} = 2 \times 4; H_1 = 0.4k; H_4 = 0.4k$

$\Sigma M_x = 0$ $\qquad T_1 = 2P_{3z} = 2 \times 5 = 10'k$

2. Stress resultants at distance x from origin, point 1;

$V_{x1} = R_1 - wx;$	$0 \le x \le 8$	$V_{x1} = R_1 - wx - P_{3z}$	$8 \le x \le 20$
$M_{x1} = R_1x - wx^2/2$	$0 \le x \le 8$	$M_{x1} = R_1x - wx^2/2 - P_{3z}(x-8)$	$8 \le x \le 20$
$V_{x2} = H_1$	$0 \le x \le 20$		
$M_{x2} = H_1x - P_{3x}c$	$8 \le x \le 20$	$M_{x2} = H_1x$	$0 \le x \le 8$
$T_{xx} = T_1 - P_{3z}c = 0$	$8 \le x \le 20$	$T_{xx} = T_1$	$0 \le x \le 8$
$N_{xx} = N_1 - P_{3x} = -P_{3x}$	$8 \le x \le 20$	$N_{xx} = N_1 = 0$	$0 \le x \le 8$

See Fig. 5-1 for plots of above equations giving variation of stress resultants with x.

3. Maximum stress resultants

V_{x1max} is at dVx/dx = 0. This occurs at x = 0, or at x = 20; $V_{x1\,max} = R_1$ or R_4

$V_{x1max} = R_1 = 13k$

$M_{x1\,max}$ is at $dM_{x1}/dx = 0;\ R_1 - wx - P_{3z} = 0$

Thus $M_{x1\,max}$ is at point of zero shear; x = 8'

$M_{x1\,max} = 13 \times 8 - 1 \times 8^2/2 = 72'k$

$V_{x2\,max} = H_1 = 0.4k$

$M_{x2\,max}$ at $dM_{x2}/dx = 0$, but there is no singular solution. At x = 8':

$M_{x2\,max} = 8H_1 = 8 \times 0.4 = 3.2'k$, or

$M_{x2\,max} = 8H_1 - 2P_{3x} = 3.2 - 2 \times 4 = -4.8'k$

$T_{xx\,max} = T_1 = 10'k$

$N_{xx\,max} = -P_{3x} = -4k$, from x = 8' to x = 20'

Note: 1 ft = 0.3048m; 1 kip-force = 4.448kN; 1 ft-kip = 1.356 kN-m; 1 kip/ft = 14.593 kN/m

* Design loads, design criteria (such as safety factors, load factors and capacity reduction factors, etc.) and materials properties used in design examples are for illustrative purposes only. The user of this Manual is cautioned to develop his own loads, criteria and materials properties based on the requirements and conditions of his specific design project.

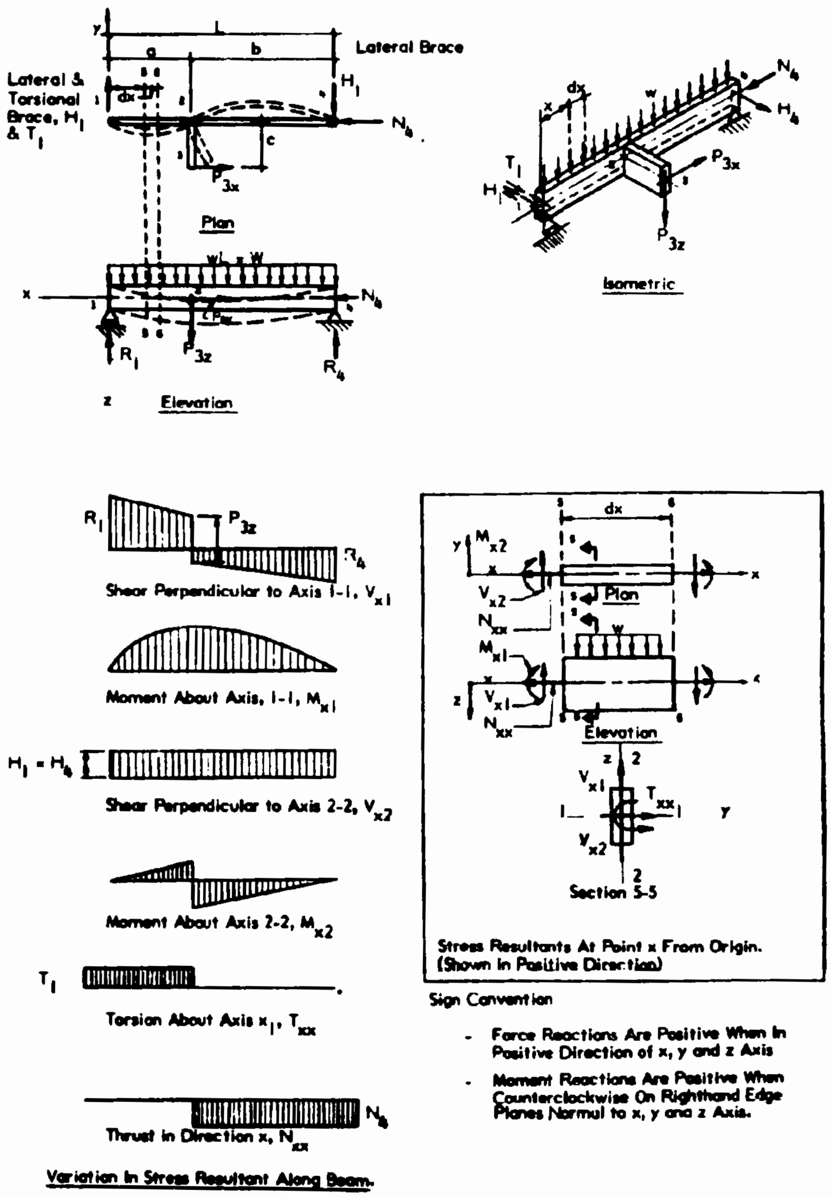

Fig. 5-1 LOADS, REACTIONS AND STRESS RESULTANTS

Table 5-1

Stress Resultants in Beams and Columns for Common Loading and Support Cases

Member and load arrangement*	Maximum stress resultants and location						Maximum bending, shear, and axial deflection coefficients**		
							Bending, K_m	Shear, K_v	Axial, K_a
	M	@ x =	V	@ x =	N		at x = L/2	at x = L/2	at x = L
1. Beam - uniformly distributed load									
(a) 	$\frac{WL}{8}$	$\frac{L}{2}$	$\frac{W}{2}$	0, L	–		$\frac{5}{384}$	$\frac{1}{8}$	–
(b) 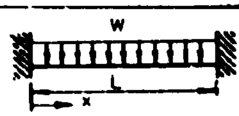	$+\frac{WL}{24}$	$\frac{L}{2}$	$\frac{W}{2}$	0, L	–		$\frac{1}{384}$	$\frac{1}{8}$	–
	$-\frac{WL}{12}$	0, L							
2. Beam - concentrated load							when a = b = L/2:		
(a) 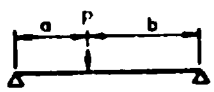	$+\frac{Pab}{L}$	a	$\frac{Pb}{L}$	0	–		$\frac{1}{48}$	$\frac{1}{4}$	–
			$\frac{Pa}{L}$	L					
b) 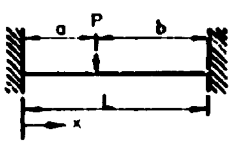	$+\frac{2Pa^2b^2}{L^3}$	a	$\frac{Pb^2}{L^3}(3a+b)$	0	–		when a = b = L/2:		
	$-\frac{Pab^2}{L^2}$	0					$\frac{1}{192}$	$\frac{1}{4}$	–
	$-\frac{Pa^2b}{L^2}$	L	$\frac{Pa^2}{L^3}(a+3b)$	L	–				
3. Column with axial load									
	0	–	0	–	P		–	–	1.0
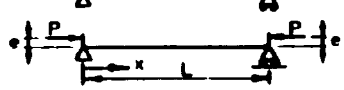	Pe	constant	0	–	P		$\frac{e}{8L}$	–	1.0

Notes

- * See (5.5) for bending moment and shear diagrams, equations of moment, shear, and deflection for 42 common support and load conditions.

** Deflection equations:

Bending deflection, $\delta_m = K_m \frac{WL^3}{EI}$ or $K_m \frac{PL^3}{EI}$

Shear deflection, $\delta_v = K_v \frac{WL}{GA_w}$ or $K_m \frac{PL}{GA_w}$

Axial deflection, $\delta_a = K_a \frac{PL}{EA}$

Once the stress resultants that act at various points along structural members are determined, the designer can determine the expected member stresses and deflections when member sections and structural properties are known, or he can proportion member sections to safely resist the applied stress resultants. How this is accomplished conceptually is presented in the next two sections of this chapter. However, detailed explanations of design procedures for various types of members in actual components are deferred to later chapters.

Methods for determining the properties of cross sections that are either simple solid shapes, or assemblies of thin plates, are presented in the next section. These section properties, together with the stress resultants caused by applied loads, or environmental conditions, are needed in the analysis for stresses and deflections for the many structural configurations considered in subsequent chapters.

5.3 SECTION PROPERTIES

Section properties are structural characteristics of members that are defined by geometric properties of their cross sections. The principal section properties needed for design of most columns, tension members, beams, and ribbed panels are summarized in Table 5-2. Member cross sections used for such components usually have at least one axis of symmetry and this results in simpler behavior in flexure, compression and buckling than occurs with unsymmetrical cross sections. Common sections used for plastics components are illustrated in Fig. 5-2.

Symmetrical Sections

The generalized cross section shown in Table 5-2 has one axis of symmetry. Various reference axes and dimensional parameters that relate to the calculation of the section properties are shown. The x - y axes are arbitrary rectangular reference axes. They are often chosen to take advantage of symmetry, and/or to pass through the centroid of local parts of a composite section. This reduces the calculations required to locate the centroid of complex, or composite sections. The x_o - y_o axes are the axes parallel to the x - y axes that pass through the centroid (center of gravity) of the area.

Table 5-2
Section Properties Needed in Structural Design for Shapes with One or More Axes of Symmetry

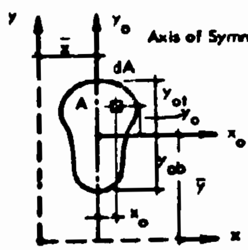

General Section

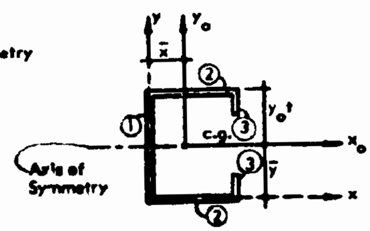

Section Composed of Regular Parts

Property	Equation General	For section with regular parts	Equation Number
1. Area:	$A = \int dA$	$\sum_{n=1}^{n=k} A_n$	5.1
2. Centroid (center of gravity)	$\bar{y} = \dfrac{\int y dA}{\int dA}$	$\dfrac{\Sigma y_n A_n}{\Sigma A_n}$	5.2
	$\bar{x} = \dfrac{\int y dA}{\int dA}$	$\dfrac{\Sigma x_n A_n}{\Sigma A_n}$	5.3
3. Moment of inertia	$I_x = \int y^2 dA;$		5.4
	$I_{xo} = \int y_o^2 dA$	$\sum_{n=1}^{n=k} I_{xon} + A_n \bar{y}_n^2$	5.4a
	$I_y = \int x^2 dA;$		5.5
	$I_{yo} = \int x_o^2 dA$	$\sum_{n=1}^{n=k} I_{yon} + A_n \bar{x}_n^2$	5.5a
4. Radius of gyration	$r_x = \sqrt{\dfrac{I_x}{A}}$		5.6
	$r_y = \sqrt{\dfrac{I_y}{A}}$		5.7
5. Polar moment of inertia	$I_z = \int r^2 dA$		
	$= I_x + I_y$		5.8
6. Section moduli 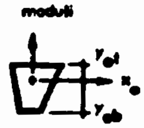	$S_{xt} = \dfrac{I_{xo}}{y_{ot}}$		5.9a
	$S_{xb} = \dfrac{I_{xo}}{y_{ob}}$		5.9b

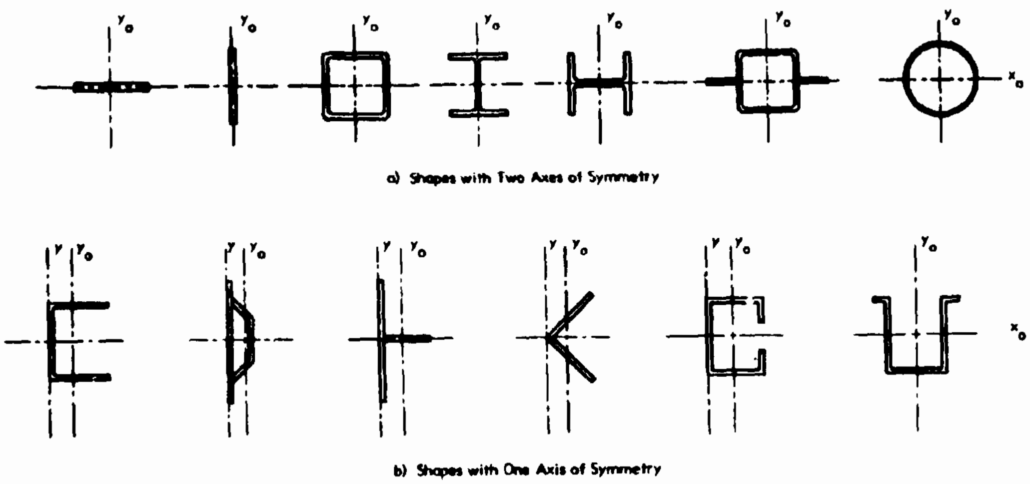

Fig. 5-2 TYPICAL CROSS-SECTION SHAPES

When a section has an axis of symmetry, several theorems can be applied to simplify calculations for section properties:

1. An axis of symmetry is always a centroidal axis.

2. If one axis of a pair of rectangular axes is an axis of symmetry, these axes are principal axes. Princpal axes of an area, with respect to a point in the plane of the area, are mutually perpendicular axes, lying in the plane with origin at the point, that give the largest moment of inertia for one of the axes and the smallest for the other. Determination of principal axes is discussed later with respect to properties of non-symmetrical sections.

A cross section composed of regular elements is also shown in Table 5-2. The calculation of the moment of inertia of such sections can be simplified by using the transfer theorem, as given by Eqs. 5.4a and 5.5a in the Table. The transfer theorem relates moment of inertia about any axis, I, to moment of inertia about a parallel centroidal axis, o, as follows:

$$I_1 = I_o + A\bar{y}^2 \qquad \text{Eq. 5.10}$$

where I_o is the moment of inertia of area A about a centroidal axis o, $\bar{y}$ is the perpendicular distance between centroidal axis o and a parallel axis 1, and I_1, is the moment of inertia of area A about axis I. Thus, in Eqs. 5.4a in the Table, I_{xon} is the moment of inertia about the centroid of part n, and I_{xn} is the contribution of the area of part n to the total moment of inertia about the centroid of the composite section, I_{xo}.

The area, location of centroid and moment of inertia about centroidal axes of regular shapes are found in handbooks (5.4) (5.5). Some common cases are given in Table 5-3 as a design aid to the reader. Since plastic parts frequently contain fillets, properties of quarter circles, ellipses and parabolas are included to facilitate calculations of section properties when these elements are present. The Table also contains equations for section modulus with respect to the edges, of the element (Eq. 5.9). Section properties for various standard I, [and tubular shapes are often given in handbooks prepared by manufacturers or trade associations. Where plastic members are manufactured to match common steel shapes, section properties of such shapes are found in (5.5).

Example 5-2 illustrates the calculation of section properties for a section composed of rectangular elements. Note the selection of reference axes and organization of calculation steps that are used to obtain the needed properties with a minimum of numerical operations. The transfer theorem is used to determine moment of inertias about the centroidal axes of the composite section.

Transformed Section Concept for Elements with Different Stiffnesses

When a cross section is comprised of materials having different elastic modulii, it is convenient to work with a psuedo cross section that is termed the "transformed section". A reference elastic modulus for the transformed section is established, and this is usually taken as the elastic modulus of one of the materials in the cross-section. Furthermore, the actual width of each element is established parallel to the axis about which the moment of inertia is to be determined. The transformed width of each element is obtained by multiplying the actual width by a ratio of the element modulus to the reference modulus, $n = E_n/E_{ref}$. The ratio n is termed the "modular ratio".

Example 5-2: Locate the centroid and determine the moment of inertia and section modulus about both the x_o and the y_o centroidal axes for the thin wall hat section shown.*

Refer to Table 5-2 for nomenclature and equations.

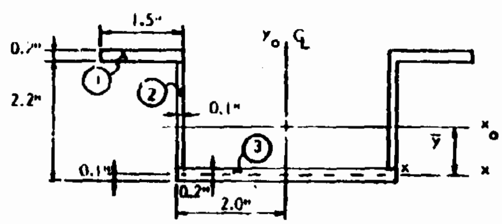

1. Properties about x_o: Set up tabular solution to determine $\bar{y}$ and I_{xo}. Use half the symmetrical section.

	Centroid				Moment of Inertia	
n	Area, A_n	y_n	$A_n y_n$	$\bar{y}_n$	$A_n \bar{y}_n^{\,2}$	$I_{xon} = \frac{bh^3}{12}$
1	1.5 x 0.2 = 0.3	2.2	0.66	1.22	0.447	1.5 x $2^3/12$ = .001
2	2.0 x 0.1 = 0.2	1.1	0.22	0.12	0.003	0.1 x $2^3/12$ = .067
3	2.0 x 0.2 = 0.4	0	0	-0.98	0.383	2.0 x $2^3/12$ = .001
Σ	0.9		0.88		0.833	.069

$$\bar{y} = \frac{\Sigma A_n y_n}{\Sigma A_n} = \frac{0.88}{0.9} = 0.978 \text{ in.}; \quad \bar{y}_n = y_n - \bar{y}$$

$$I_{xo} = 2\,(\Sigma I_{xon} + \Sigma A_n \bar{y}_n^{\,2}) = 2 \times 0.902 = 1.804 \text{ in.}^4$$

$$S_{xt} = \frac{I_{xo}}{y_{ot}} = \frac{1.804}{1.322} = 1.365 \text{ in.}^3; \quad S_{xb} = \frac{I_{xo}}{y_{ob}} = \frac{1.804}{1.078} = 1.673 \text{ in.}^3$$

2. Properties about y_o: Set up tabular solution to determine I_{xo}. Use half the symmetrical section.

n	A_n	I_{yon}	=	$\frac{bh^3}{12}$	$A_n \bar{x}_n^{\,2}$	=	
1	0.3	0.2 x $1.5^3/12$	=	0.0563	0.3 x 2.65^2	=	2.1068
2	0.2	2.0 x $0.1^3/12$	=	0.0002	0.2 x 1.95^2	=	.7605
3	0.4	0.2 x $2^3/12$	=	0.1333	0.4 x 1^2	=	0.4000
Σ				0.190			3.267

$$I_{yo} = 2(\Sigma I_{yon} + \Sigma A_n x_n^2) = 2.0 \times 3.457 = 6.914 \text{ in.}^4; \quad S_{y\,edge} = \frac{6.914}{3.4} = 2.034 \text{ in.}^3$$

Note: 1 in. = 2.54 mm.

* See note on Example 5-1, page 5-4.

Table 5-3
Section Properties for Common Shapes

Shape	Area	Distance from centroid to edge m	n	I_{xo}, Moment of Inertia about centroidal axis, x_o	Section Modulus about S_x axis
1. Rectangle 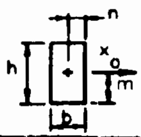	bh	$\frac{h}{2}$	$\frac{b}{2}$	$\frac{bh^3}{12}$	$\frac{bh^2}{6}$
2. Triangle 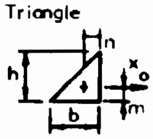	$\frac{bh}{2}$	$\frac{h}{3}$	–	$\frac{bh^3}{36}$	$\frac{bh^2}{12}$ bottom $\frac{bh^2}{24}$ top
3. Solid Circle or Ellipse 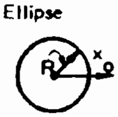	πR^2	R		$\frac{\pi R^4}{4}$	$\frac{\pi R^3}{4}$
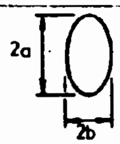	πab	a	b	$\frac{\pi ba^3}{4}$	$\frac{\pi ba^2}{4}$
4. Quarter Circle* or Ellipse 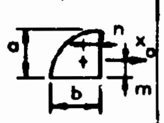 Note: for circle a = b	$\frac{\pi ab}{4}$	$\frac{4a}{3\pi}$	$\frac{4b}{3\pi}$	$a^3b\left(\frac{\pi}{16} - \frac{4}{9\pi}\right)$	
5. Complement of quarter circle* or ellipse 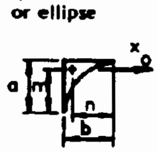 Note: for circle a = b, n = m	$ab\left(1 - \frac{\pi}{4}\right)$	$\frac{a}{6\left(1 - \frac{\pi}{4}\right)}$	$\frac{b}{6\left(1 - \frac{\pi}{4}\right)}$	$a^3b\left(\frac{1}{3} - \frac{\pi}{16} - \frac{1}{36\left(1 - \frac{\pi}{4}\right)}\right)$	

Table 5-3 (cont'd)

Shape	Area	Distance from centroid to edge m	n	I_{xo}, Moment of Inertia about centroidal axis, x_o	Section Modulus about S_x axis
6. Half parabola 	$\frac{2}{3}ab$	$\frac{2}{5}a$	$\frac{3}{8}b$	$\frac{8}{175}a^3b$ $(I_{yo} = \frac{19}{480}ab^3)$	
7. Complement of half parabola 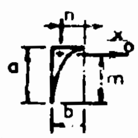	$\frac{1}{3}ab$	$\frac{7}{10}a$	$\frac{3}{4}b$	$\frac{37}{2100}a^3b$ $(I_{yo} = \frac{1}{80}ab^3)$	
8. Parabolic fillet 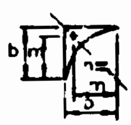	$\frac{b^2}{6}$	$\frac{4}{5}b$	$\frac{4}{5}b$	$\frac{11}{2100}b^4$	
9. Very thin rectangular tube 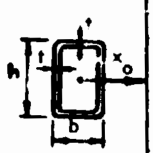	$2t(h+b)$	$\frac{h}{2}$	$\frac{b}{2}$	$\frac{th^2}{6}(h+3b)$	$\frac{th}{3}(h+3b)$
10. Very thin annulus 	$2\pi Rt$	R		$\pi R^3 t$	$\pi R^2 t$
11. Sector of thin annulus 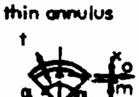 (α in radians)	$2\alpha Rt$	$R\left(\frac{\sin\alpha}{\alpha} - \cos\alpha\right)$		$R^3 t\left(\alpha + \sin\alpha\cos\alpha - \frac{2\sin^2\alpha}{\alpha}\right)$	

Thus, the transformed width, for use in calculating the section properties of the transformed section, is:

$$b_t \quad = \quad n\,b = \frac{E_n}{E_{ref}} \quad b \qquad \text{Eq. 5.11}$$

Since this concept is very useful in the analysis of sandwich sections, it is described in more detail in Section 8.4 of Chapter 8. Its use is illustrated in Examples 8-1 to 8-4. The effect of time-dependent variations in material stiffness properties is illustrated in Example 8-3.

Unsymmetrical Section

For those cases where section properties are required referenced to axes that are not principal axes in symmetrical shapes, or that are either principal or arbitrary axes in non-symmetrical shapes, additional section properties are needed, along with the properties given in Table 5-2. Reference axes, dimensions, and section properties for a generalized unsymmetrical cross section are given in Table 5-4. As in the symmetrical case given in Table 5-2, the x - y axes are arbitrary rectangular reference axes, and the x_o - y_o axes are parallel reference axes with their origin at the centroid of the area. The rectangular axes, u - v, have the same origin as the x - y axes, but are rotated an angle θ, and the rectangular axes, u_p - v_p, at an angle θ_p, are the principal axes through point a. The rectangular axes u_{po} - v_{po}, are the principal central axes through point b, the centroid of the area.

Again, there is a transfer theorem for product of inertia, I_{xy}, that is similar to the transfer theorem for moment of inertia:

$$I_{x_1y_1} = I_{x_oy_o} + A x_o y_o \qquad \text{Eq. 5.18}$$

This theorem is used to calculate the product of inertia of each regular element of a cross section composed of an assembly of regular elements about the centroid of the composite section. Note that for regular elements with an axis of symmetry, such as rectangles, $I_{x_oy_o} = 0$.

Table 5-4

Additional Section Properties Needed with Unsymmetrical or Complex Shapes

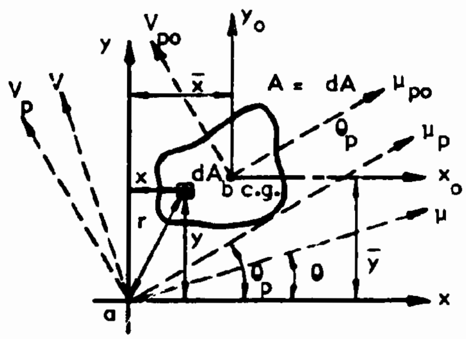

General Section

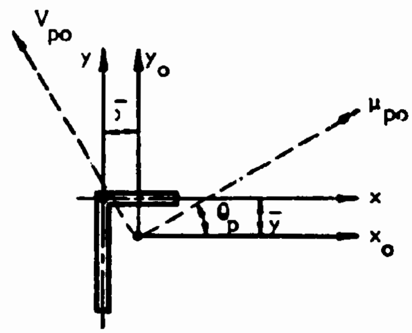

Section Composed of Regular Parts

	Property	Equation General	For cross section with regular parts	Equation Number
1.	Product of inertia	$I_{xy} = \int xy\, dA$		5.12
		$I_{x_o y_o} = \int x_o y_o\, dA$	$\sum_{n=1}^{n=k} I_{xon\ yon} + A\bar{x}_n\bar{y}_n$	5.12a
Note:	If either the y axis or the x axis is an axis of symmetry:	$I_{xy} = 0$		
2.	Moment of inertia about axes u-v at angle, θ, with reference axes x-y	$I_u = I_x \cos^2\theta + I_y \sin^2\theta - I_{xy} \sin 2\theta$		5.13
		$I_v = I_x \sin^2\theta + I_y \cos^2\theta + I_{xy} \sin 2\theta$		5.13a
3.	Polar moment of inertia	$I_z = I_x + I_y = I_u + I_v$		5.14
4.	Polar radius of gyration	$r_o = \sqrt{\frac{I_z}{A}}$		5.15
5.	Angle of principal axes, θ_p, from reference axes x-y.	$\tan 2\theta_p = \frac{2 I_{xy}}{I_y - I_x}$		5.16
6.	Moment of inertia about principal axes, u_p-v_p	$I_{up} = \frac{1}{2}(I_x + I_y) \pm \sqrt{\frac{1}{4}(I_y - I_x)^2 + I_{xy}^2}$ + if max. I - if min. I		5.17

Example 5-3 illustrates the use of the equations in Table 5-4 to determine the angle of principal axes and section properties of a Z-section. With a Z-section, the load axis frequently lies in the plane of the web, while the direction of the principal axes is unrelated to the direction of loads.

Shear Center

The shear center, or center of twist, of a cross section is a point through which the transverse shear stress resultant, V, must be applied to avoid twisting a member. This is the point about which the sum of moments produced by the internal shear stress is zero. (See Eq. 5.30 in the next Section for internal shear stress.) Determination of the shear center is presented in more detail in (5.8), where it is shown that the shear center is a property of the cross section. Also, if a section has an axis of symmetry the shear center is always located on this symmetry axis. Thus, for doubly symmetric sections, the shear center always occurs at the intersection of the symmetry axes. This is also the centroid. For other sections, the shear center and the centroid do not coincide. Equations for the shear centers of some common sections with a single axis of symmetry are given in Table 5-5. See (5.4) for a Table that gives the location of the shear centers of additional sections.

5.4 BASIC RELATIONS FOR STRESS AND DEFORMATION

Member design requires an evaluation of basic response to load in terms of stress and deformation. Stresses within a member are a function of the member section properties and the stress resultants caused by the applied loading. Usually, stresses at the locations of maximum stress resultants govern the design, although if section properties vary with length, other stress resultants that are not maximum may produce maximum stresses.

The design of plastic structural components is usually based on the assumption that member response is elastic (5.9), (i.e., stress is proportional to strain at all points along a member length and over the entire member cross section). The same type of simplifying assumption is usually made for reinforced plastics, except that these materials often have elastic properties that vary with direction, requiring the consideration of anisotropic elasticity. See Chapters 2, 3 and 4 for discussions of complexities introduced by variation in elastic properties with time, temperature, environment and directional characteristics.

Example 5-3: Determine the angle of principal axes and the moment of inertia about both the x_o and y_o axes and the principal axes of the Z section shown.*

1. Properties about x_o: The centroid and I_{xo} are the same as determined for the half section in Example 5-2, since in this direction the Z section has the same configuration and dimensions of half the hat section of the previous example.

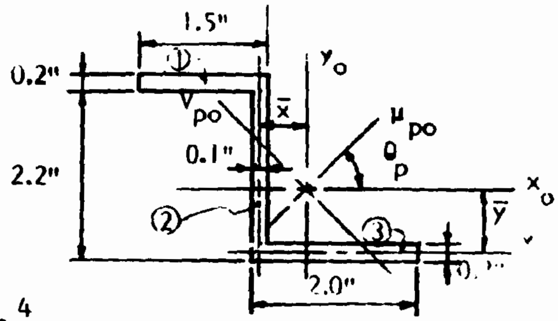

$\bar{y} = 0.978$ in.; $I_{xo} = 1.804/2 = 0.902$ in.^{4}

2. Properties about y_o

	Centroid			Moment of Inertia				Product of Inertia	
n	Area, A_n	x_y	Ax_y	$\bar{x}_n$	$A_n\bar{x}^2_n$	I_{yon}		$\bar{y}_n$	$A_n\bar{x}_n\bar{y}_n$
1	0.3	-0.70	-0.21	-0.889	0.2371	$0.2 \times 1.5^3/12 =$	0.0563	1.22	-0.3254
2	0.2	0	0	-0.189	0.0071	$2.0 \times 0.1^3/12 =$	0.0002	0.12	-0.0045
3	0.4	+0.95	0.38	0.761	0.2316	$0.2 \times 2^3/12 =$	0.1333	-0.98	-0.2983
	0.9		0.17		0.4758		0.190		-0.6282

$\bar{x} = \dfrac{0.17}{0.9} = 0.189$ in.; $I_{yo} = 0.190 + 0.476 = 0.666$ in.^{4}

3. Product of inertia

$$I_{x_oy_o} = \Sigma I_{xon\,yon} + \Sigma A_n\bar{x}_n\bar{y}_n$$

Parts 1, 2 and 3 all are rectangles with axes of symmetry, $I_{xon\,yon} = 0$ for each part; thus:

$$I_{x_oy_o} = \Sigma A_n\bar{x}_n\bar{y}_n = -0.628 \text{ in.}^4$$

4. Direction of two principal axes, with x_o axis

Eq. 5.16; $\tan 2\theta_p = \dfrac{2(-0.628)}{0.666 - 0.902} = 5.322$; $2\theta_{p_o} = 79.36^\circ$; $\theta_p = 39.68^\circ$

5. Moment of inertia about principal axes

Eq. 5.17; $I_{up_o} = \frac{1}{2}(0.902 + 0.666) + \sqrt{\frac{1}{4}(0.666 - 0.902)^2 + (-0.628)^2} = 1.423$ in^4

$I_{vp_o} = \frac{1}{2}(0.902 + 0.666) - \sqrt{\frac{1}{4}(0.666 - 0.902)^2 + (-0.628)^2} = 0.145$ in^4

* See note on Example 5-1, page 5-4.

1 in. = 25.4 mm

Table 5-5

Shear Center for Some Common Thin-Wall Sections with One Axis of Symmetry

Section	Location of Shear Center e
1. Channel 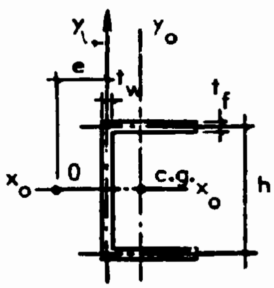	$h \dfrac{I'_{xy}}{I_x}$ I'_{xy} is product of inertia of half section (above x_o) with respect to x_o and y axes.
2. Tee 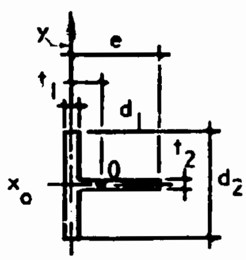	$\frac{1}{2}(t_1 + d_1) \dfrac{1}{1 + \dfrac{d_2^{\,3} t_1}{t_2^{\,3} d_1}}$ Note: for thin tee section, $e \approx 0$
3. I with unequal flanges, thin web 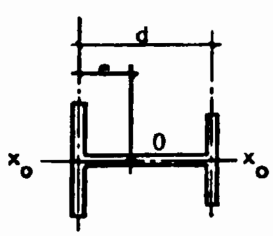	$b \dfrac{I_2}{I_1 + I_2}$ I_1 and I_2 are moments of inertia of flanges 1 and 2 respectively about x-axis.
4. Equal leg angle 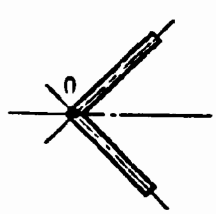	Shear center is at 0 Note: If leg thickness, t, is small relative to leg width, shear center is also at 0 for unequal leg angles

For a linear isotropic elastic member, the basic relation of stress to strain is:

$$\sigma_x = E_x e_x \qquad \text{Eq. 5.19}$$

Deformations of a member are a function of the magnitude and variation of applied stress resultants, the section properties provided along its length, length dimensions, conditions of end restraint and the elastic modulus, E_x (stiffness), of the material in the direction of stress.

The basic equations for determining stress and deformation at a cross section in terms of stress resultants produced by the application of external loading to linear members are presented below, and used in later chapters for the analysis and design of various structural components. The derivations of these expressions are found in textbooks on elementary mechanics of materials and are not included here.

Normal Stress

Normal stress is stress that acts in a direction perpendicular (normal) to a cross section. Normal stress is produced by thrust and bending stress resultants.

Equations for normal stress are derived based on the assumption that "plane sections before bending remain plane after bending." Normal stresses produced by axial force (thrust) are constant over a member cross section as shown in Fig. 5-3, and normal stresses produced by bending moment vary linearly across the depth of a beam in the plane of bending as shown in Fig. 5-4. Bending compresses the cross section above a plane of zero longitudinal displacement, called the neutral axis, and elongates it below the neutral axis. Under pure bending without axial load, the neutral axis passes through the centroid (center of gravity) of the section.

Equations for calculating normal stress at any point a distance y and z from the centroid (Fig. 5-4) of a section which is located at x along the member are (5.8):

Stress Resultant	Normal Stress	Eqs.
Thrust, N_x	$\sigma_x = \frac{N_x}{A}$	5.20
Bending, M_{x_1}	$\sigma_x = \frac{M_{x_1} y}{I_1}$	5.21
Bending, M_{x_2}	$\sigma_x = \frac{M_{x_2} z}{I_2}$	5.22
Combined thrust and bending, N_x and M_x	$\sigma_x = \frac{N_x}{A} + \frac{M_{x_1} y}{I_1} + \frac{M_{x_2} z}{I_2}$	5.23

Since y and z may be plus or minus, thrust may increase or decrease the bending stresses.

The maximum bending stresses occur at the extreme fibers (farthest points from the neutral axis), where y and z attain their maximum values. The section modulus, S, is defined as the cross section property:

$$S_1 = \frac{I_1}{y_{max}} \; ; \; S_2 = \frac{I_2}{z_{max}} \qquad \text{Eqs. 5.24}$$

For symmetrical sections, where S for each edge is the same:

Stress Resultant	Maximum Normal Stress	Eqs.
Bending, M_{x1}	$\sigma_x = \frac{M_{x_1}}{S_1}$	5.25
Bending, M_{x2}	$\sigma_x = \frac{M_{x_2}}{S_2}$	5.26
Combined thrust and bending, N_x and M_x	$\sigma_x = \frac{N_x}{A} + \frac{M_{x_1}}{S_1} + \frac{M_{x_2}}{S_2}$	5.27

See Tables 5-2 and 5-3 for methods and equations for determining I and S.

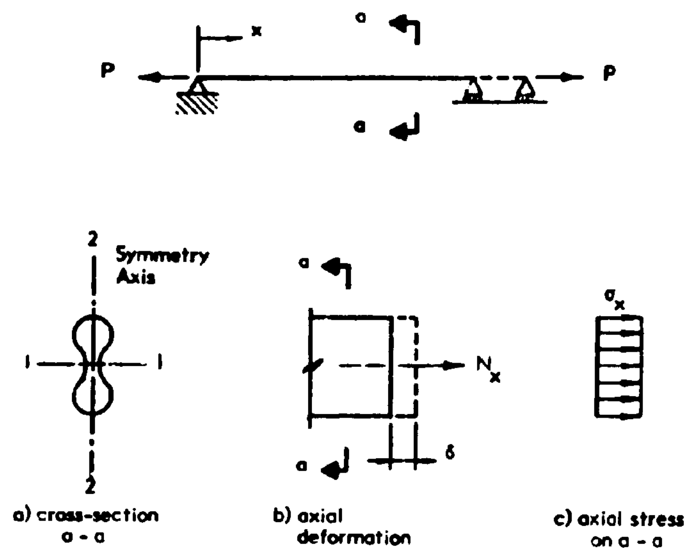

Fig. 5-3 UNIFORM AXIAL NORMAL STRESS

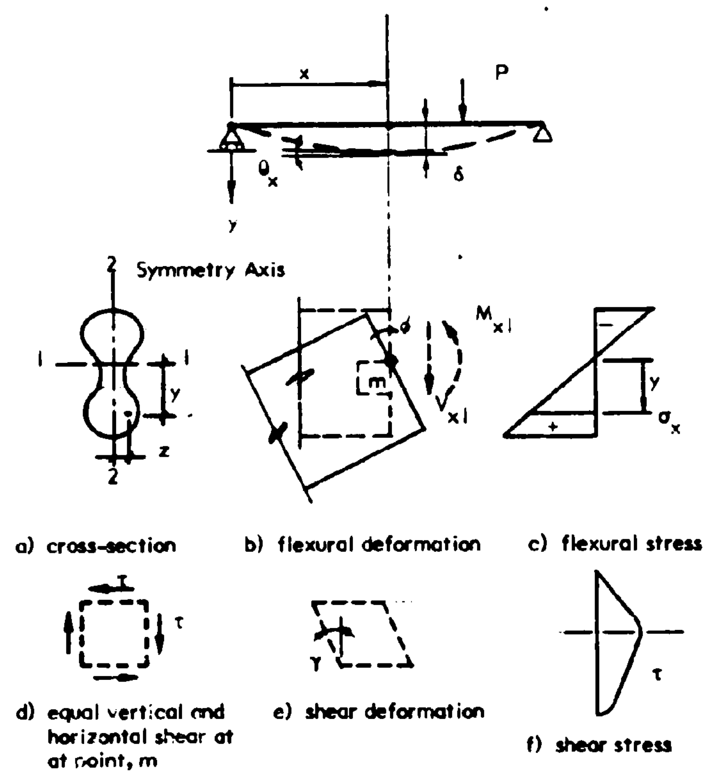

Fig. 5-4 ELASTIC FLEXURAL NORMAL AND SHEAR STRESSES IN BEAMS

Example 5-4 gives calculations for the maximum normal stresses produced in member 1-2 of Fig. 5-1 by the thrust and bending stress resultants determined in Example 5-1. The maximum compressive and tensile normal stresses produced by the combined effects of thrust and moments are also given.

Deformation Due to Normal Stress

Axial force, or thrust, produces the following linear deformation in a member having a length, L, and constant area, A (Fig. 5-3):

$$\delta_x = \frac{N_x L}{A E} \qquad \text{Eq. 5.28}$$

Moment produces curvature, defined as a change in slope over a unit length (Fig. 5-4):

$$\phi_{x_1} = \frac{1}{\rho_{x_1}} = \frac{d\theta}{dx} = \frac{d^2 y}{dx^2} = \frac{M_{x_1}}{E I_1} \qquad \text{Eq. 5.29}$$

ϕ_{x_1} is the curvature, and ρ_{x_1} the radius of curvature, about axis 1 at point x.

Transverse deflection*, y, and slope, θ, at a point x along a beam depend on the length of the member, the variation of moment along the length and the conditions of end restraint. The **conjugate beam analogy** (5.1) (5.8) is useful for determining the slope of the tangent to the elastic curve and the deflection at points on a bent elastic member. In order to use the method, the bending stress resultants (moments) in the member must first be determined. This includes any indeterminate moments at supports that have rotational restraints.

The conjugate beam has the same length and support locations as the actual beam, but with all support points allowed to rotate (regardless of end fixity conditions in the actual beam). Apply a distributed load intensity on the conjugate beam that is equal, at any point to the bending stress resultant along the beam divided by the section bending stiffness (EI) at each point. Thus, the loading diagram for the conjugate beam is the same as the bending moment diagram of the actual beam, divided by EI at each section.

---

* Note: In accordance with common usage, y is also used to denote transverse deflection of the beam, which is not to be confused with the y distance from the section centroid as used in Eqs. 5.21 & 5.23 and in Fig. 5-4 a and c.

Example 5-4: Determine the maximum compressive and tensile normal stresses in member 1-4 of Fig. 5-1. Use the dimensions and loads given in Example 5-1. The thrust and bending stress resultants are calculated in that example. The member is a hollow tubular member as shown below.*

1. Member properties - Refer to Table 5-3, Shape #9: b = 9.5"; h = 19.5"

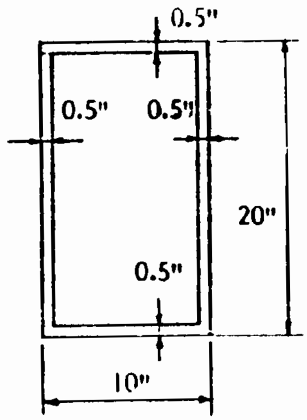

$$A = 2 \times 0.5\,(9.5 + 19.5) = 29 \text{ in.}^2$$

$$I_1 = \frac{0.5 \times 19.5^2}{6}\,(19.5 + 3 \times 9.5) = 1521 \text{ in.}^4$$

$$S_1 = \frac{0.5 \times 19.5}{3}\,(19.5 + 3 \times 9.5) = 156 \text{ in}^3;$$

$$\left(\text{or } S_1 = \frac{1521}{10} = 152.1 \text{ in.}^3\right)$$

$$I_2 = \frac{0.5 \times 9.5^2}{6}\,(9.5 + 3 \times 19.5) = 511$$

$$S_2 = \frac{511}{5} = 102.3 \text{ in.}^3$$

2. Maximum thrust, $N_x = -4.0$k at points 2 to 4

   normal stress: Eq. 5.20 $\quad \sigma_x = \dfrac{-4000}{29} = -138$ psi

3. Maximum bending, $M_{x1} = 72$'k at point 2

   max normal stress: Eq. 5.25: $\sigma_x = \pm \dfrac{72{,}000 \times 12}{152.1} = \pm 5680$ psi

4. Maximum bending, $M_{x2} = +3.2$'k. or -4.8'k at point 2

   max. normal stress: Eq. 5.26: $\sigma_x = \pm \dfrac{4800 \times 12}{102.3} = \pm 563$ psi

5. Maximum combined compressive stress just to right of point 2

   Eq. 5.27: max. $\sigma_x = -138 - 5680 - 563 = -6381$ psi (compression)

6. Maximum combined tensile stress either just to right, or just to left of point 2

   6.1 Just to right of point 2: Same stress resultants as for max. compression

   $\sigma_x = -138 + 5680 + 563 = 6105$ psi

   6.2 Just to left of point 2: $N_x = 0$; $M_{x1} = 72$'k; $M_{x2} = 3.2$'k

   $\sigma_x = 0 + 5680 + \dfrac{3200 \times 12}{102.3} = 6055$ psi

   6.3 Location just to right of point 2 governs.

Note: 1 in. = 25.4 mm; 1 kip-force = 4.448 kN; 1 ft-kip = 1.356 kN-m; 1 psi = 6.895 kPa.

* See note on Example 5-1, page 5-4.

The deformations of the actual beam are determined from certain stress resultants in the conjugate beam as follows:

- The slope (angle of tangent to elastic curve with original axis of beam before bending) at any point on the actual beam is the shear at that point in the conjugate beam.
- The bending deflection at any point on the actual beam is the bending moment at that point in the conjugate beam.

The above is summarized in Fig. 5-5. The areas and centroid locations given in Table 5-3 for parabolas are useful for determining areas and moments of the loads (parabolic moment diagram) on the conjugate beam. Also, calculations are often simplified when moments used as loads on a conjugate beam are broken down to reflect the separate application of each applied load, as well as the separate application of each end moment due to support restraints.

The conjugate beam method for determining deflections and slopes is further illustrated in **Example** 5-5, which gives the deflections and slopes at certain points in beam 1-4 shown in Fig. 5-1.

Deflection of specific types of members and components is discussed in each of the Chapters that follow. Also, see Table 5-1 for the maximum bending and axial deflections for certain common loading and support cases.

Flexural Shear Stress

In addition to bending moment, transverse loads also produce shear stress resultants that act on the plane of the beam cross section. Stresses caused by shear force are termed "flexural shear" stresses or simply "shear" stresses. These may also be determined using the elastic beam theory. Shear stresses act as shown in Fig. 5-4; they are usually maximum at the neutral axis and reducing to zero at the upper and lower extremities of the sections. However, in sections of variable width, maximum shear stress may not always be at the neutral axis. Shear force is related to the change in bending moment along the beam. Also, equilibrium demands that at any point in the beam, the vertical shear stress produced by shear force on the section have an equal horizontal shear stress as shown in sketch (d) of Fig.5-4.

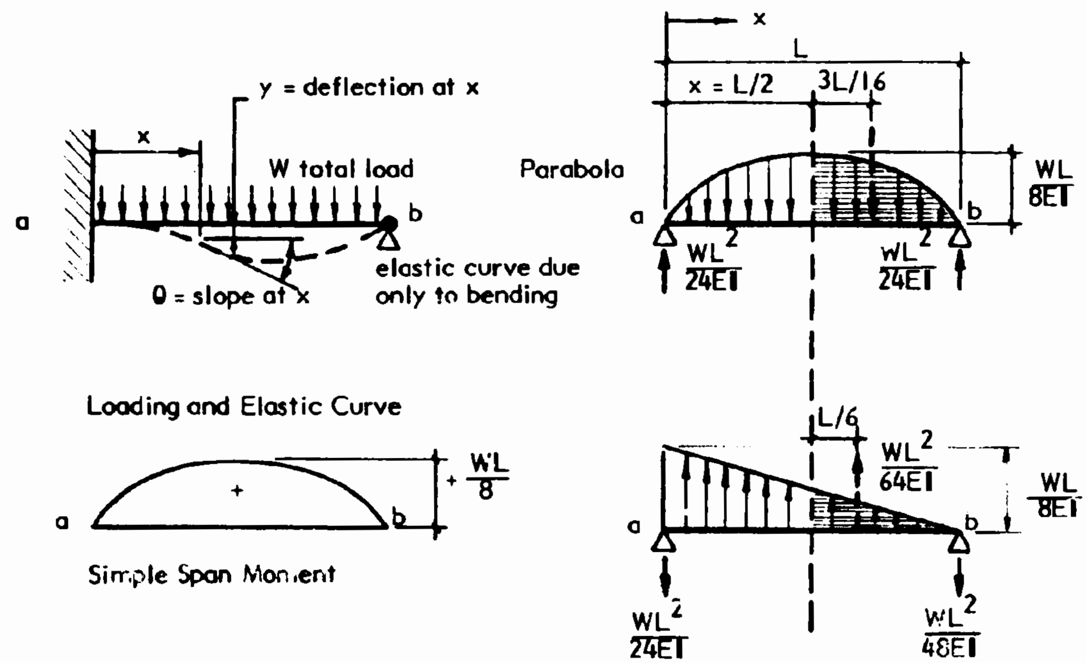

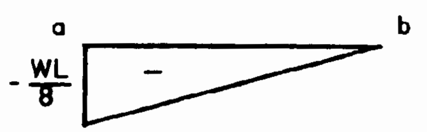

Moment Due to End Restraint

<u>ACTUAL BEAM & BENDING MOMENT DIAGRAM IN 2 PARTS</u>

<u>CONJUGATE BEAM</u>

Slope at a: $\frac{WL^2}{24EI} - \frac{WL^2}{24EI} = 0$

Slope at b: $\frac{WL^2}{24EI} - \frac{WL^2}{48EI} = \frac{WL^2}{48EI}$

Deflection at x = L/2:

$EIy = \frac{WL^3}{48} - \frac{WL^3}{128} - \frac{WL^3}{96} + \frac{WL^3}{384} = \frac{WL^3}{192}$

Fig. 5-5 CONJUGATE BEAM ANALOGY FOR BENDING DEFLECTIONS AND SLOPES

Example 5-5: Determine bending deflections at mid-span of member 1-4, Fig. 5-1, in the z and y directions. Refer to Example 5-1 for loads, dimensions and stress resultants and to Example 5-4 for member section properties. Assume E = 2000 kips per sq. in.*

1. Mid-span deflection in z direction, produced by M_{x1}

1.1 Consider conjugate beam loaded by M_{x1}/EI, diagram due to each load type separately.

(a) Uniformly distributed load

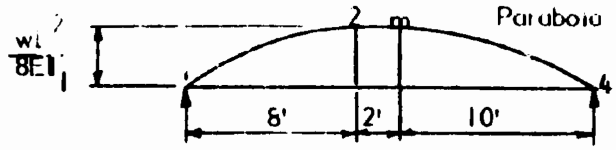

(b) Concentrated load

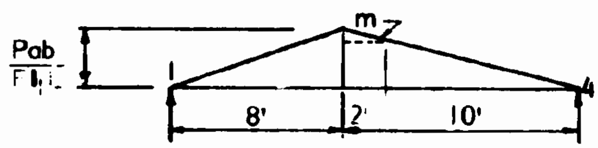

1.2 Moment (M_{x1}) ordinates on conjugate beams

(a) $M_m = 1.0 \times \frac{20^2}{8} = 50'k$

(b) $M_2 = \frac{5.0 \times 8 \times 12}{20} = 24'k$

$M_m = \frac{24 \times 10}{12} = 20'k$

1.3 Reactions on conjugate beams

(a) $EI_1\theta_1 = EI\theta_4 = \frac{2}{3} \times 50 \times 10 = 333.3 \text{ k-ft}^2$

(b) $EI_1\theta_1 = \frac{24 \times 8 \times (8 \times 0.33 + 12)}{2 \times 20} + \frac{24 \times 12}{2} \times \frac{12 \times .67}{20} = 70.4 + 57.6 = 128.0 \text{ k-ft}^2$

$EI_1\theta_4 = 24 \times 20 \times 0.5 - 128.0 = 112.0 \text{ k-ft}^2$

1.4 Deflection at m, δ_{zm} = bending moment in conjugate beam at m

(a) From Table 5-3, Case 6: e.g. for half parabola, $n = \frac{3}{8} \times 10 = 3.75$

$EI_1\ \delta_{zm} = 333.3 \times 10 - 333.3 \times 3.75 = 2083 \text{ k-ft}^3$

(b) $EI_1\ \delta_{zm} = 128. \times 10 - \frac{24 \times 8 \times (2 + 8/3)}{2} - 20 \times 2 \times 1 - \frac{4 \times 2}{2} \times \frac{2 \times 2}{3} = 786.7 \text{ k-ft}^3$

$\delta_{zm} = \frac{(2083 + 786.7) \times 1728}{2 \times 10^3 \times 1521} = 1.63 \text{ in.}$

---

* See note on Example 5-1, page 5-4.

Example 5-5 (continued)

2. Mid-span deflection in y direction produced by M_{x2}

2.1 Consider conjugate beam loaded by M_{x2}/EI_2 diagram

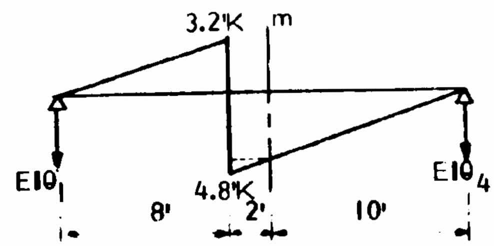

2.2 Moment ordinates

at 2: From Example 5-1 $M_2 = 3.2'k$; $M_2 = -4.8'k$

at m: $M_m = -4.8 \times \frac{10}{12} = -4.0'k$

2.3 Conjugate beam reactions

$$EI\theta_1 = \frac{3.2 \times 8}{2} \times \frac{14.67}{20} - \frac{4.3 \times 12}{2} \times \frac{8}{20} = -2.13 \text{ k-ft}^2$$

$$EI\theta_4 = \frac{3.2 \times 8}{2} \times \frac{5.33}{20} - \frac{4.8 \times 12}{2} \times \frac{12}{20} = -13.86 \text{ k-ft}^2$$

check: $\frac{3.2 \times 8}{2} - \frac{4.8 \times 12}{2} = -16.0$; o.k.

2.4 Deflection at m, δ_{ym} = bending moment in conjugate beam at m

$$EI_2\, \delta_{ym} = -2.13 \times 10 - \frac{3.2 \times 8}{2} \times (\frac{8}{3} + 2) + 4.0 \times 2 \times 1 + \frac{0.8 \times 2 \times 2 \times 2}{2 \times 3} = -72.0 \text{ k-ft}^3$$

$$\delta_{ym} = \frac{-72.0 \times 1728}{2 \times 10^3 \times 511} = -0.12 \text{ in.}$$

Note: 1 in. = 25.4 mm; 1 ft = 0.3048 m ; 1 kip-force = 4.448 kN; 1 ft-kip = 1.356 kN-m.

Shear stress at any distance y from the neutral axis is (5.8):

$$\tau_x = \frac{V_{x_1} \bar{Q}_{sy}}{b\, I_1} \qquad \text{Eq. 5.30}$$

$\bar{Q}_{sy}$ is the first moment of the area above (or below) a distance y from the neutral axis, about the neutral axis. The maximum value of $\bar{Q}_{sy}$ occurs when $y = 0$ and is called $\bar{Q}_{s1}$, the first moment of the area above or below the neutral axis about that axis.

In thin wall sections, "Shear flow" is a term used for the force represented by the shear stress times the width of a cross section at a distance y from the neutral axis, and thus, equals $\tau_x b$. Also, it follows from the above discussion that the maximum value of shear flow occurs at the neutral axis.

$$\text{max shear flow, } q_m = \tau_{xm} b = \frac{V_{x_1} \bar{Q}_{s1}}{I_1} \qquad \text{Eq. 5.31}$$

Shear flow is the force per unit length required to connect elements such as flanges to webs of beams.

When thin wall cross sections, such as **I**, **C** or tubular sections, are used for beams, a simpler relation for determining the approximate maximum shear stress in the web of beam is useful (5.8) (5.10):

$$\tau_{xm} = \frac{V_{x_1}}{A_w} \qquad \text{Eq. 5.32}$$

A_w is the cross section area of the thin web from inside to inside of flanges. With sections having more than one web, include all the webs when calculating A_w.

Eq. 5.32 is only valid for sections that have substantial flanges connected by thin webs. In these sections, most of the bending normal stress is carried in the flanges. Since the shear flow equilibrates the change in total bending force above or below the shear plane for a unit length of member, the shear stress in the web of such a beam is nearly constant between the inside edges of the flanges. Eq. 5.32 may be used for other cross sections if A_w is replaced by

A/c_s where A is the total area of the cross section and c_s is a shape factor that relates the maximum shear stress at the neutral axis to the average shear stress on the entire cross section, A. For solid rectangular sections, $c_s = 1.5$, and for solid circular sections, $c_s = 1.33$.

Shear Deformation

Shear stress deforms a square element into a rhombic shape (Fig. 5-4e). The shear strain is the angle change imposed during this deformation. The basic elastic relation between shear stress and shear strain is:

$$\tau = G\gamma \qquad \text{Eq. 5.33}$$

Shear deformation produces transverse deflection in members that are subject to shear force. For most practical beams, frames, plates, and shells, shear deflection is small relative to bending deflection and is usually neglected when calculating deflections and rotations of typical members. In fact, the usual assumption of beam flexure theory given previously that "plane sections before bending remain plane after bending" is based on neglect of shear deformation. An exception is sandwich panels with "shear flexible" plastic foam cores. Shear deflection can be very significant in such structures, and methods for calculating this deflection are given in Section 8.6 of Chapter 8. Maximum shear deflections for some common loading and support arrangements are given in Table 5-1.

Principal Normal Stress

For any element in stressed body, there is a unique set of perpendicular axes on which only normal stresses act; shear stresses are zero. These axes are the principal stress axes and the corresponding stresses are the principal normal stresses acting on the element.

Element 1 in Fig. 5-6 has principal normal stresses shown on planes at angles, α, and $(90 + \alpha)$ with the planes that are parallel to and normal to the beam axis. The planes of principal stress are not related to the principal axes of the cross section discussed earlier. An important characteristic of principal stresses is that they represent the maximum and minimum normal stresses obtainable on two mutually perpendicular axes within the plane of the element. Another important characteristic is that the maximum shear stress acts on a set of mutually perpendicular axes oriented at an angle of 45^{o} to the principal axes.

The principal stresses, and the angle of the axes of principal stress, can be calculated from the stresses applied to any arbitrary axis. Eq. 6.69 in Chapter 6 give the angle of the planes of principal stresses and the magnitude of these stresses when the stress state on any two mutually perpendicular planes at the point is known. See also (5.8).

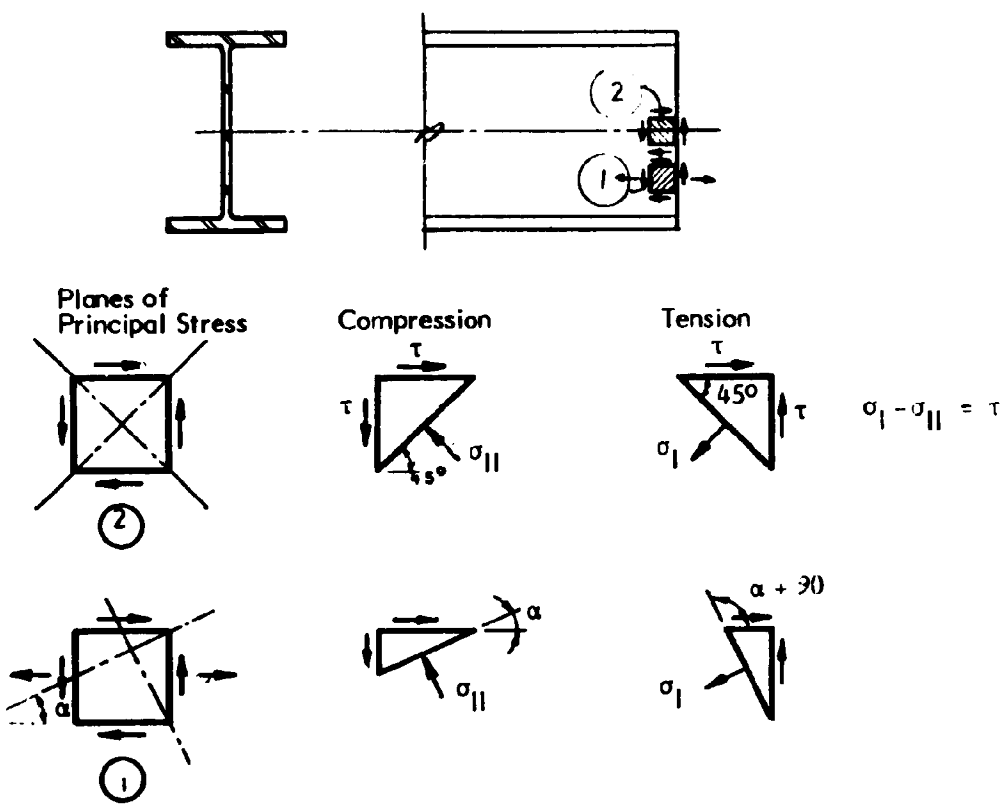

Fig. 5-6 PRINCIPAL NORMAL STRESS

For the majority of bending problems, the maximum normal stress occurs at the extremity of the cross section, and since shear stress is zero at this point, the normal stress there is a principal stress. The principal stresses at other points within the beam are all lower. In a few cases, such as the diaphragms, and deep beams discussed in Chapter 6, principal stresses must be calculated at points away from the extreme fibers. Another case where principal stress governs design is in the evaluation of web buckling in beams with thin webs. Element 2 in Fig. 5-6 illustrates this condition where the principal compressive stress at the neutral axis of a beam acts at 45 degrees to the planes of maximum shear stress. This is discussed further in Section 7.4

Torsion

Torsion also produces shear stress and shear deformation. The simplest model of torsion behavior is the response of a solid or hollow circular shaft under axial torque. The hollow circular tube is also the most efficient section for resisting torsion. Other compact shapes such as solid square, or single-cell and multi-cell closed tubular sections (Fig. 5-7) also provide efficient torsional resistance.

Shear stresses produced by a simple primary torque, T_x, applied to a solid, or tubular circular shaft (Fig. 5-7) are determined by the elastic theory for torsion (5.8):

$$\tau_{xr} = \frac{T_x r}{I_z} \qquad \text{Eq. 5.34}$$

where r is the radial distance to the location of the point stressed in shear, and I_z is the polar moment of inertia of the shaft. The maximum shear occurs at the extreme fibers of the shaft.

The deformation of the twisted circular shaft results in an angle of twist per unit length of (5.8):

$$\theta_x = \frac{T_x}{G I_z} \qquad \text{Eq. 5.35}$$

I_z, the polar moment of inertia of the circular area, is termed the torsion constant and is designated, J, for use with other shapes that exhibit more complex behavior in torsion. Thus, the general relations for maximum shear stress, and angle of twist per unit length are:

$$\tau_{xm} = \frac{T_x R}{J} \qquad \text{Eq. 5.34 a}$$

$$\theta_x = \frac{T_x}{G J} \qquad \text{Eq. 5.35 a}$$

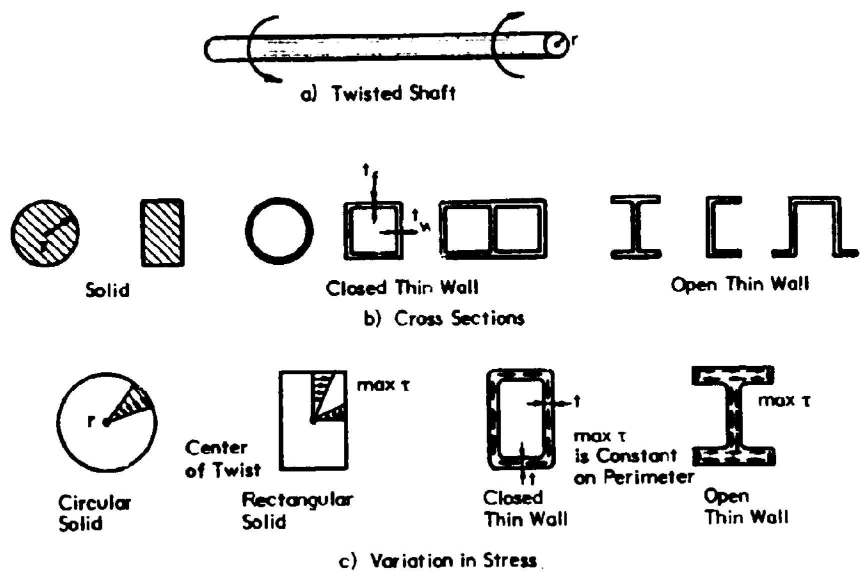

Fig. 5-7 PURE TORSION OF SOLID AND THIN-WALL SHAFTS

If the twisting moment is constant over a shaft length, L, the total twist of the shaft is:

$$\phi = \frac{T L}{G J} \qquad \text{Eq. 5.36}$$

When the shaft cross section is a closed thin walled section of constant thickness t having any closed shape (Fig. 5-7), the torsional shear stress is constant around the perimeter of the shaft and is (5.10):

$$\tau_x = \frac{T_x}{2 A_p t} \qquad \text{Eq. 5.37}$$

where A_p is the area enclosed by the centerline of the closed thin wall section. The torsion constant for any closed thin wall tube of constant wall thickness, t, is:

$$J = \frac{4 A^2 t}{L_p} \qquad \text{Eq. 5.38}$$

where L_p is the length of the periphery of the tube. If the wall thickness of the tube varies, replace L_p/t in Eq. 5.38 with the integral from o to L_p of $d(L_p)/t$.

Example 5-6 illustrates the calculation of combined flexural and torsional shear stresses in the hollow tubular section used for member 1-3 (Fig. 5-1) in previous examples showing calculation of stress resultants (Example 5-1), normal stresses (Example 5-4) and deflections (Example 5-5).

The torsional behavior of non-circular sections that are not thin-walled closed tubular sections is more complex, involving warping of cross sections. The maximum shear stress produced by a simple primary torque applied to a shaft having a rectangular cross section is (5.8):

$$\tau_{xm} = \frac{\alpha T_x}{b\,t^2/3} \qquad \text{Eq. 5.39}$$

where b is the greater dimension and α is a coefficient that may be calculated with the following approximate relation (5.8):

$$\alpha = (1 + 0.6\frac{t}{b}) \qquad \text{Eq. 5.40}$$

α is usually taken as 1.0 for narrow rectangles having $b/t \geq 10$. For such sections, the torsional constant is:

$$J = \frac{b\,t^3}{3} \qquad \text{Eq. 5.41}$$

An open thin-walled cross section comprised of an assembly of narrow rectangular sections is commonly used for various structural members. This type of section includes I, [, angle and hat shapes (Fig. 5-7). The torsional constant for such shapes is (5.11):

Example 5-6: Determine the maximum flexural shear stress, the maximum torsional shear stress and the maximum combined flexural and torsional shear stress in member 1-4 (Fig. 5-1) for the loads, dimensions and stress resultants of Example 5-1. Also, determine the maximum principal normal stress in the flanges of this member. Dimensions and properties of the hollow tubular cross section to be used for member 1-4 are given in Example 5-4 (See sketch).*

1. Max. flexural shear stress caused by V_{x1} occurs at point 1, where max. V_{x1} = 13k.

1.1 Max. shear stress occurs at neutral axis 1-1, where $\overline{Q}_{sy1}$ in Eq. 5.30 is maximum.

$\overline{Q}_{sy1} = 0.5 \times 10 \times \frac{19.5}{2} + 0.5 \times 2 \times \frac{19}{2} \times \frac{19}{4} = 93.9 \text{ in.}^3$; I_1 is given in Example 5-4.

1.2 Eq. 5.30 $\tau_{xm1} = \frac{13,000 \times 93.9}{0.5 \times 2 \times 1521} = 802$ psi

or Eq. 5.32 $\tau_{xm1} = \frac{13,000}{0.5 \times 2 \times 19} = 684$ psi (approximate solution)

2. Max. flexural shear stress caused by V_{x2} occurs anywhere between points 1 and 4, since V_{x2} = 0.4k at all points on the beam.

2.1 Max. $\overline{Q}_{sy2}$ in Eq. 5.30 occurs at neutral axis 2-2:

$\overline{Q}_{sy2} = 0.5 \times 20 \times \frac{9.5}{2} + 0.5 \times 2 \times \frac{9}{2} \times \frac{9}{4} = 57.6 \text{ in}^3$; I_2 is given in Example 5-4

2.2 Eq. 5.30: $\tau_{xm2} = \frac{400 \times 57.6}{0.5 \times 2 \times 511} = 45$ psi

or Eq. 5.32: $\tau_{xm2} = \frac{400}{0.5 \times 2 \times 9} = 44$ psi (approximate solution)

3. Max. torsional shear stress caused by T_{xx} = 10 ft-k occurs between points 1 and 2:

3.1 Eq. 5.37: $\tau_{xm1} = \tau_{xm2} = \frac{10,000 \times 12}{2 \times 19.5 \times 9.5 \times 0.5} = 648$ psi

4. Max. combined shear stress:

4.1 At point 1: $\tau_{xm1} = \tau_{xm1}$ flexure $+ \tau_{xm1}$ torsion $= 802 + 648 = 1450$ psi

4.2 Anywhere between points 1 and 2: $\tau_{xm2} = 45 + 648 = 693$ psi

4.3 At point 1 corner: V_{x1} = 1300 lbs.

$\overline{Q}_{sx} = 0.5 \times 10 \times \frac{19.5}{2} = 48.8 \text{ in}^3$; $\tau_{x1} = \frac{1300 \times 48.4}{0.5 \times 2 \times 1521} = 417$ psi

$\overline{Q}_{sy} = 0.5 \times 19 \times \frac{9.5}{2} = 45.1 \text{ in}^3$; $\tau_{x2} = \frac{400 \times 45.1}{.5 \times 2 \times 522} = 35$ psi

$\tau_x = (\tau_{x1} + \tau_{x2})$ flexure $+ \tau_x$ torsion $= 417 + 35 + 648 = 1100$ psi

5. Max. principal stress in flange occurs at left of point 2 where maximum flexural tension combines with torsional shear stress:

5.1 Max. normal stress at left of point 2 at the corner of the tube (from Example 5-4): $\sigma_x = +6055$ psi

5.2 Shear stress at corner of tube at left of point 2:

$V_{x1} = 5000$ lbs; $\tau_{x1} = \frac{5000 \times 48.8}{0.5 \times 2 \times 1521} = 160$ psi

$V_{x2} = 400$ lbs; $\tau_{x2} = 35$ psi

$\tau_x = (\tau_{x1} + \tau_{x2})$ flexure $+ \tau_x$ torsion $= 160 + 35 + 648 = 843$ psi

5.3 Referring to Eq. 6.69a in Section 6.8 of the next Chapter:

$\tau_m = 0.5\,(6055 + 0) \pm 0.5 \sqrt{(6055 - 0)^2 + 4 \times 843^2} = 6170$ psi

---

Note: 1 in. = 25.4mm; 1 kip-force = 4.448KN; 1 ft-kip = 1.356kN-m; 1 psi = 6.895 kPa

* See note on Example 5-1, page 5-4.

$$J = \Sigma \frac{b_f t_f^3}{3} + \Sigma \frac{b_w t_w^3}{3} = \sum_{n=1}^{n=k} \frac{b_n t_n^3}{3} \qquad \text{Eq. 5.42}$$

The maximum torsional shear stress produced by a simple applied torque on a shaft of open thin-wall section that is free to warp (Fig. 5-7) is (5.10):

$$\text{flange ;} \quad \tau_{xfm} = \frac{T_x t_f}{J} \qquad \text{Eq. 5.43}$$

$$\text{web ;} \quad \tau_{xwm} = \frac{T_x t_w}{J} \qquad \text{Eq. 5.44}$$

Any part, n, with flange, t_n:

$$\tau_{xnm} = \frac{T_x t_n}{J} \qquad \text{Eq. 5.45}$$

The torsional constant, J, will be increased by the presence of fillets in a thin-walled cross section, and the maximum shear stress will also increase somewhat from the value given by Eq. 5.45. If a more exact evaluation is not made, the possibility of increased shear in the fillets can be taken into account in the safety factor.

In general, open sections do not provide efficient resistance to applied torque; hence, they are seldom used as shafts designed to resist torsion. However, shapes with open sections frequently are used as beams or columns. When applied loads produce twist, torsional behavior of the thin-wall open shapes must be evaluated. This requires consideration of lateral bending associated with restraint of warping, as well as consideration of torsional shear.

Torsion with Warping Restraint

When warping of an open thin-walled section is restrained, some parts of the section resist twisting by bending (Fig. 5-8). This reduces the portion of the twisting moment resisted by torsion. The total twisting moment produces a combination of torsional and flexural shear stress and flexural normal stresses on the cross section, as shown in Fig. 5-8. A detailed solution for these stresses is complex and outside the scope of this elementary presentation. Detailed explanations and equations for warping flexural and torsional stresses are found in (5.10 and 5.11).

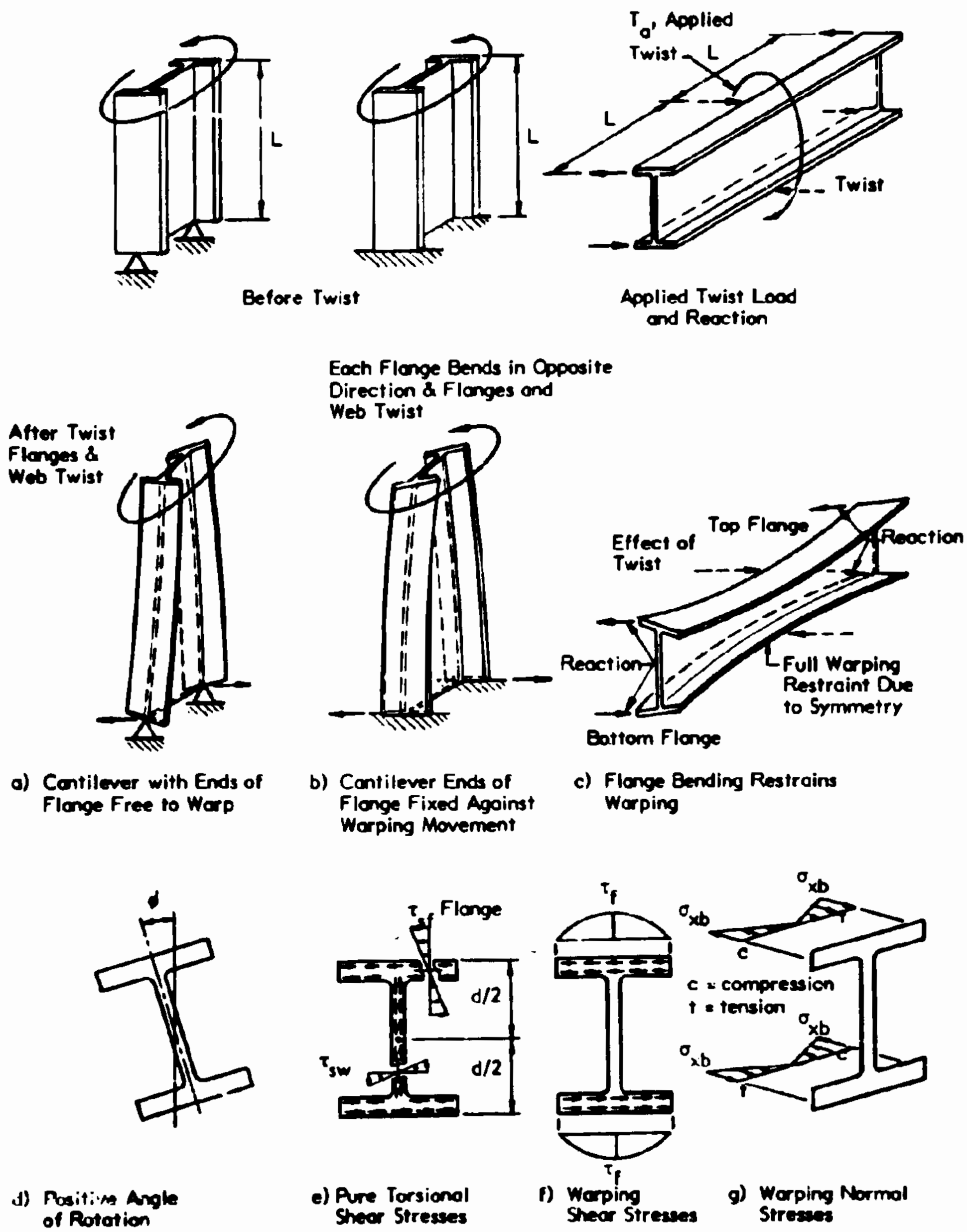

Fig. 5-8 TORSION OF I SHAPED BEAM WITH AND WITHOUT RESTRAINT OF FLANGE WARPING

A useful approximation that accounts for the warping resistance of a doubly symmetric I section is discussed and illustrated with a design example in Section 7.4 of Chapter 7. Equations are provided for calculating the flexural normal and shear stresses that arise when the flanges bend as the beam is twisted, and also for determining the torsional shear stresses, as reduced by the restraint of warping. The reduced twisting deformation resulting because of warping resistance is also given.

The warping resistance of closed sections is much smaller than their torsional resistance, except for very short members. Thus, warping stresses are not usually investigated for closed thin-walled sections such as rectangular tubes and hollow ribs that are subject to twist (5.10).

Shear center

A transversely loaded beam will not be subject to torsion if the applied loads pass through the "shear center" (also sometimes called "center of twist" or "flexural center"). Loads that are applied in a plane of symmetry of the cross section (Fig. 5-2a, axes y_o and x_o, Fig. 5-2b, axis x_o except y_o in sketch on right) always pass through the shear center. When load action lines pass through the shear center, the equations presented previously for flexural normal stress and shear stress may be applied for both symmetrical and non-symmetrical cross sections. When load action lines do not pass through the shear center, loads may be resolved into a direct load applied at that location, and a twisting moment equal to the direct load times the perpendicular distance from its line of action to the shear center.

The location of the shear center is determined from the geometry of the cross section. For sections with two axes of symmetry, the shear center is located at the intersection of the symmetry axes, and therefore it coincides with the centroid. For sections, with one symmetry axis, it is located on this axis, as discussed in Section 5.3. See Table 5-5 in that Section for the location of the shear center for some common cross sections with one axis of symmetry. See (5.8) for the general case of sections without symmetry axes.

5.5 STRESS CONCENTRATIONS

When local discontinuities occur at member cross sections subject to stresses, maximum stresses may be substantially higher than the stress levels calculated for the general stress field. Examples of significant discontinuities include holes, notches, cracks and abrupt changes in thickness, width or depth. Failure to account for such effects has been a major factor in the failure of plastics structural components, but the problem has not been unique to plastics.

An evaluation of the increased stresses at points of stress concentration is particularly important when materials do not exhibit a ductile stress-strain relation prior to rupture. Since some plastics and reinforced plastics behave essentially elastically to rupture, consideration of the effects of stress concentrations are crucial in design. Even those plastics that exhibit large ductility and yielding before failure under short-term load may in effect lose much of this ductility under long-term stress, particularly when exposed to various aggressive environments (including daylight).

Stress concentrations are also significant when plastic materials are subject to cyclic stress or strains well below their short-term yield values. Also, parts subject to only a few cycles of reversing stresses and strains above yield may fail prematurely by low cycle fatigue.

Design details that produce stress concentrations should be avoided whenever possible. The more brittle the material, the more careful the designer should be to eliminate or reduce stress concentrations. These effects are reduced by the use of fillets of adequate size when cross sections change size or shape, by the proper spacing of holes for connections, and by the design of bonded joints for gradual transfer of forces. See Section 4.5 for guidelines that minimize stress concentrations in molded components.

Most plastics cannot be characterized as completely brittle or as completely ductile materials. Many thermoplastics have a yield point in short term tests, but also often have suffered micro cracking and other structural damage at stresses below yield. This may result in dramatic reductions in strength and ductility under long term stress and/or in aggressive environments. Reinforced plastics generally do not exhibit a marked yield in short term tests, but may also develop micro cracks that damage and alter the structural properties of the resin matrix at stress levels well below the ultimate strength of the composite. See Chapters 2 and 3 for a detailed description of the mechanical behavior of thermoplastics and reinforced plastics.

The structural changes that occur prior to ultimate strength complicate the accurate consideration of stress concentrations at structural discontinuities. The emerging science of fracture mechanics provides a means for developing more precise and generally less conservative assessments of the quantitative effects of stress concentrations in plastics. Some elementary concepts of fracture mechanics are presented later in Section 5.8, but detailed analysis of specific plastics and composites is beyond the scope of this Design Manual. The following elementary summary of information about the effects of several common types of stress concentrations in materials that behave elastically up to ultimate is presented to guide the designer toward an understanding of structural behavior under this often simplified assumption. He can then assess the need for a more thorough analysis using refined theoretical or experimental approaches.

The existence of bi-axial or tri-axial stress conditions also complicates assessment of behavior at stress concentrations. Some stress raisers produce bi-axial or tri-axial stresses even when the general stress field is uniaxial. Again, fracture mechanics and/or careful experimental work is needed for an accurate consideration of the impact of the stress raiser on structural behavior with specific materials. This more detailed treatment is not within the scope of this Manual.

Stress concentrations in homogeneous elastic materials may not be accurate for non-homogeneous materials such as layered fiber reinforced composites. For example, limited research on the effect of holes in infinitely wide plates that show much lower stress concentration for small holes than for large holes, while the elastic theory for homogeneous materials indicates that the maximum stress concentration at a hole in an infinitely wide plate is not a function of hole size.

Stress Concentration Factor

The degree of stress concentration is usually expressed by the "stress concentration factor," K_t, (5.12) where:

$$K_t = \frac{\text{peak stress}}{\text{nominal stress on net section}} = \frac{\sigma_{max}}{\sigma_{nom}} \qquad \text{Eq. 5.46}$$

σ_{nom} is obtained from the elementary formulas given in the previous Section using the section properties of the net cross section. (Occasionally stress concentration factors are related to stresses on the gross section, instead of the net section.) The nominal and maximum stresses for axial tension and bending in a notched bar are shown in Fig. 5-9.

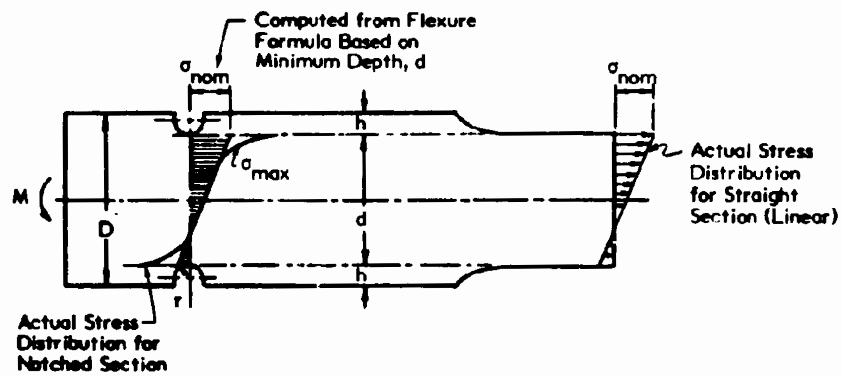

Fig. 5-9 NOMINAL AND MAXIMUM NORMAL STRESS AT NOTCH

The peak stresses caused by stress concentration usually are of most concern in elements subject to axial or flexural tension, and to diagonal tension resulting from shear. Peak stresses at discontinuities could also reduce compressive strength if materials behavior in compression remains linear elastic up to crushing. For most materials, however, yielding, creep or local instability tend to dissipate peak compressive stresses, and thus to reduce the severity of stress concentrations in compression.

Stress concentration factors are obtained from the theory of elasticity and/or from experimental methods such as photoelasticity, precision strain gages, and membrane and electrical analogies for torsion. Much of the available information on stress concentration factors for elastic homogeneous isotropic materials is summarized in (5.12).

Notches

Notches can cause very high peak stresses in structural members. Cracks are a particularly severe type of notch. Deep scratches, gouges and similar damage caused by improper handling can reduce the load-resisting capacity of a member because "notch effects" result from such damage. Threads also are notches and reduce the strength of materials to a greater extent than the loss of cross section because of the stress concentration effect. Threads in shafts also cause torsional stress concentrations.

The information given below for notch effects is not intended for evaluating the effects of cracks in plastics. Fracture mechanics provides a quantitative approach that may be used in conjunction with the proper tests and experiments to assess the behavior of plastics that have been subject to various stages of cracking. See Section 5.8.

Approximate values of K_t for determining peak stresses covering a range of notch proportions are given in Fig. 5-10 for notched flat bar tension and bending in homogeneous isotropic members. Additional charts giving more accurate values of K_t and values of K_t for larger ratios of r/d are given in (5.12). Also, see (5.12) for charts for notches on one side, multiple notches and notches in circular members.

Fillets

When member cross sections change, fillets are usually needed to reduce the peak stress caused by stress concentrations. The effect of changing the fillet radius at changes in the width of a thin flat bar subject to tension or to bending is shown in Fig. 5-11. The reduction in stress concentration that occurs with larger radii is readily apparent from the sharp reduction in K_t with increasing r/d. Fig. 5-11 applies to cases where the section having the larger dimension, D, extends for a considerable distance along the member axis beyond the fillets, and the material is homogeneous and isotropic.

Graphs for K_t with short lengths of shoulder are also given in (5.12), as are graphs for round members, shafts stressed in torsion and other conditions.

Fillets with variable radii, as shown in Fig. 5-12, produce lower stress concentrations than the circular fillets shown in Fig. 5-11. Some of these optimized fillets are discussed in (5.12).

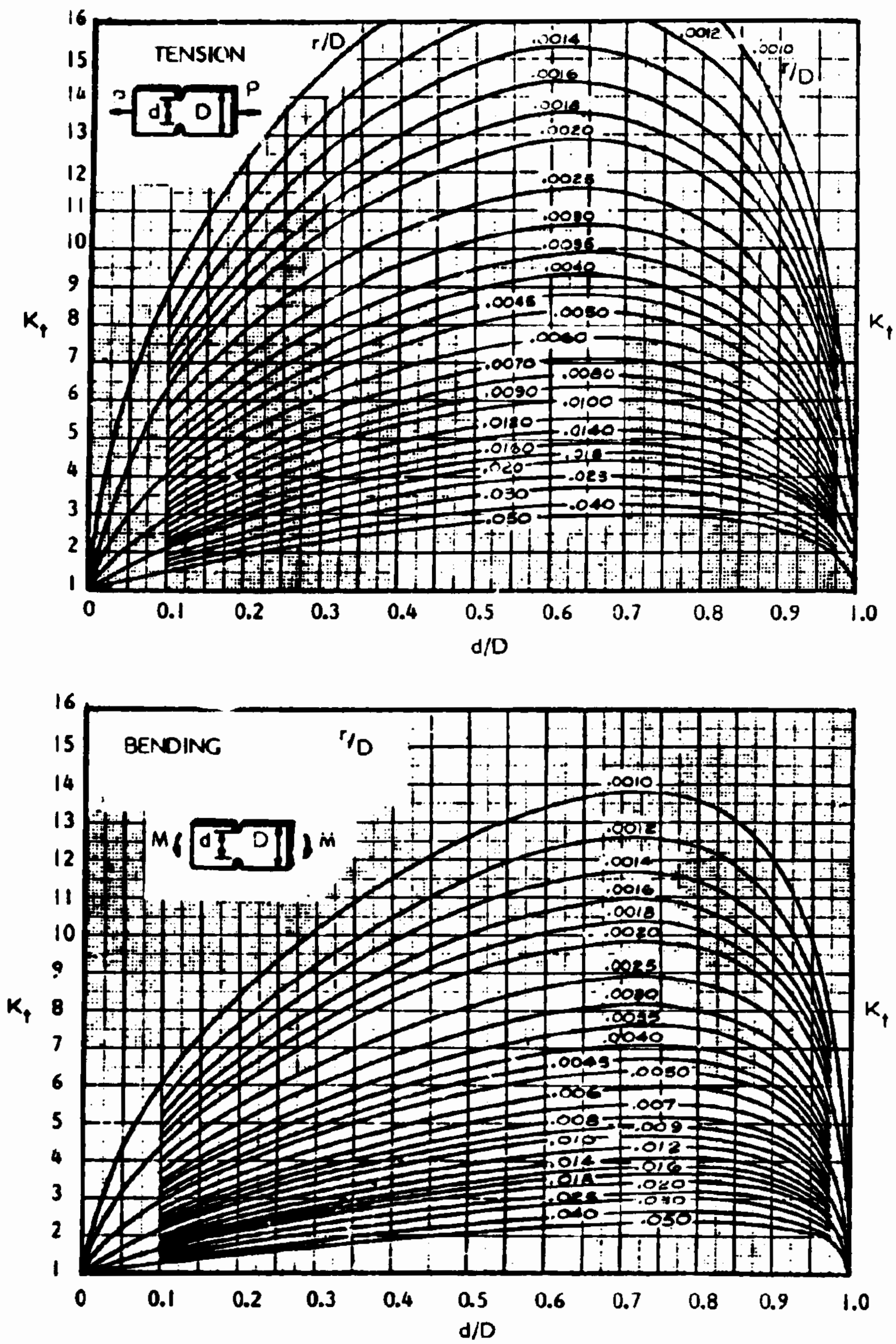

Fig. 5-10 STRESS CONCENTRATION FACTOR, K_t FOR A NOTCHED FLAT BAR SUBJECT TO TENSION AND BENDING (5.12)

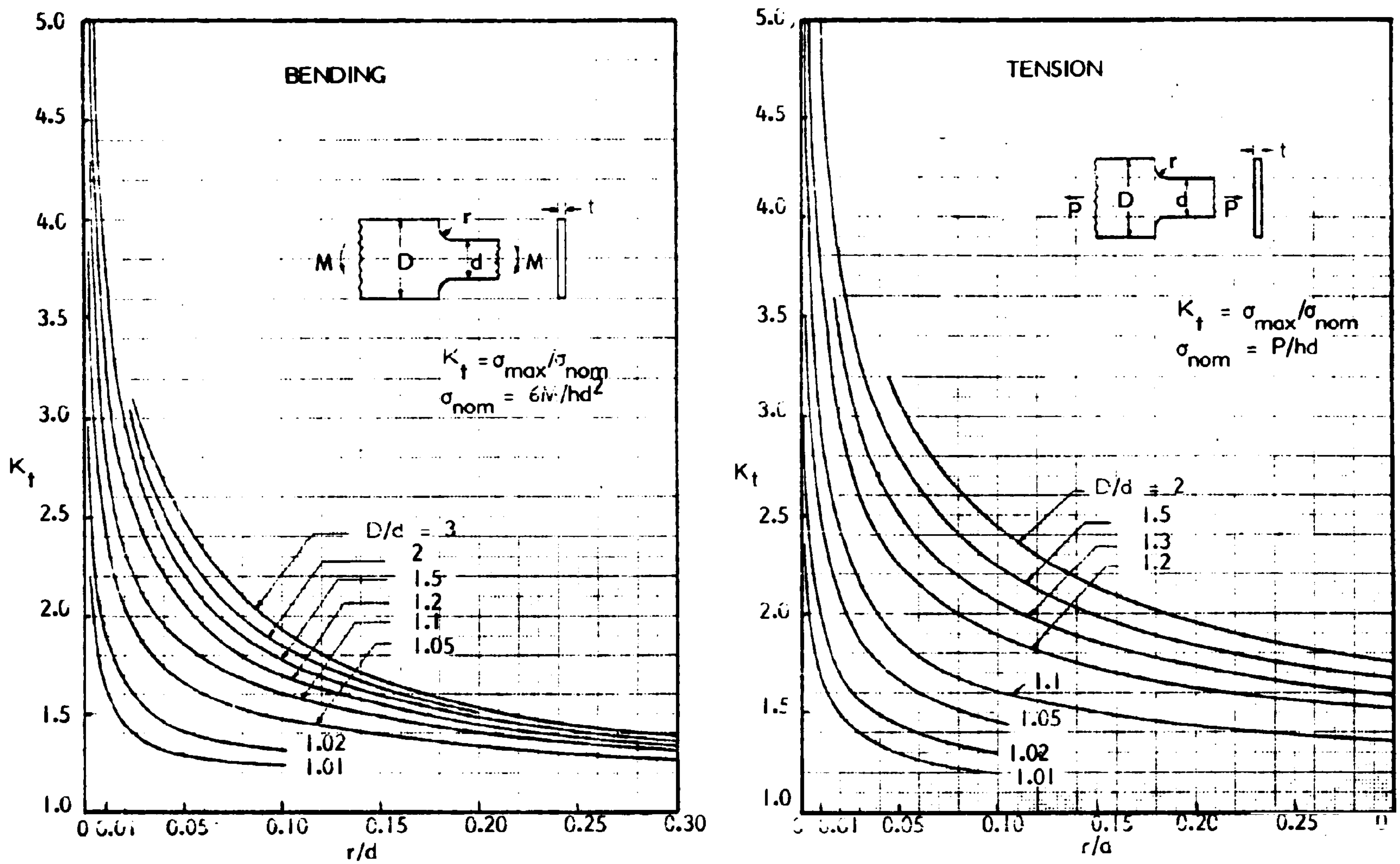

Fig. 5-11 STRESS CONCENTRATION FACTORS FOR STEPPED FLAT BAR WITH FILLETS SUBJECT TO TENSION AND BENDING (5.12)

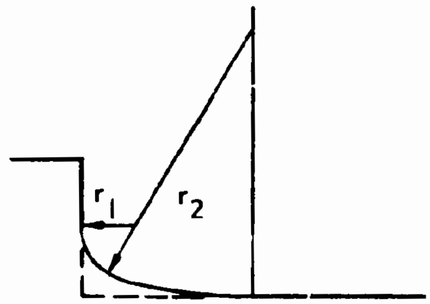

Fig. 5-12 COMPOUND FILLET

Holes

Holes are another common type of discontinuity that causes stress concentrations. A single circular hole in an infinite plate produces $K_t = 3.0$ for uniaxial tension in homogeneous, isotropic materials. For biaxial stresses, σ_x and σ_y, calculate:

$$K_{tx} = 3 - \left(\frac{\sigma_y}{\sigma_x}\right) \qquad \text{Eq. 5.47}$$

to obtain maximum tension stress in the x direction.

For a homogeneous orthotropic plate of infinite width under uniaxial stress in direction 1-1, the stress concentration factor at a hole is (5.23):

$$K_t = 1 + \sqrt{2\left(\frac{E_{11}}{E_{22}} - \nu_{12}\right) + \frac{E_{11}}{G_{12}}} \qquad \text{Eq. 5.48}$$

For a homogeneous isotropic plate of finite width, b, and a single hole of diameter, a, subject to uniaxial tension perpendicular to b, a good approximation for K_t, to be applied to stress on the net section, is:

$$K_t = 2 + \left(1 - \frac{a}{b}\right)^3 \qquad \text{Eq. 5.49}$$

A more useful factor for static design purposes is K_{tg}, to be applied to stress on the gross section, where:

$$K_{tg} = \frac{K_t}{\left(1 - \frac{a}{b}\right)} \qquad \text{Eq. 5.49 a}$$

Graphs giving K_{tg} for eccentrically located circular holes, for various patterns of multiple circular holes, for plates with circular holes subject to shear, and for holes in solid and tubular cylindrical elements are given in (5.12). Fig. 5-13 is a graph that gives K_t for shear stress in an infinite plate of homogeneous, isotropic material with 2 holes, as well as for a plate with infinite number of holes in a single line.

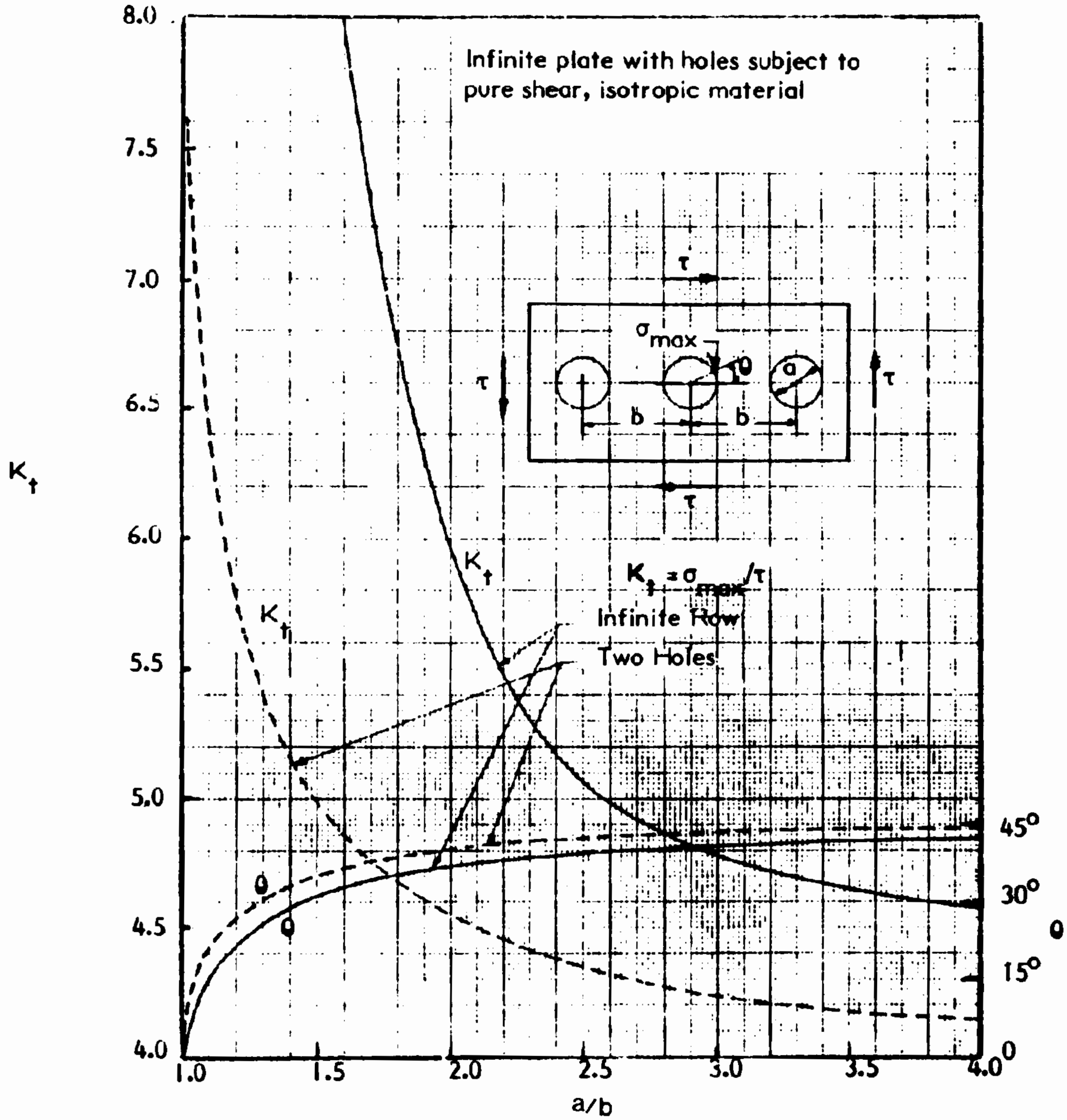

Fig. 5-13 STRESS CONCENTRATION FACTOR, K_t, FOR PRINCIPAL STRESS IN INFINITE PLATE WITH SINGLE ROW OF HOLES SUBJECT TO SHEAR (5.12)

The above stress concentration factors, based on completely elastic behavior, may be too severe for small holes in reinforced plastics. At such discontinuities, a relatively minor degree of micro cracking at the very localized points of peak stress may relieve much of the stress concentration caused by the hole (5.23). Thus, for small holes in fiber reinforced composites, the overall strength reduction can be less than the factor K_{tx} given by Eqs. 5.47 or 5.48 for the peak elastic stress at a hole. For example, in experiments on one example plate comprised of a glass fiber epoxy laminate of uni-directional layers at 0^o and $\pm 45^o$, K_t was found to equal about 2.0 for a 1/8 inch diameter hole, 2.45 for a 1/4 inch diameter hole and 3.07 for a 1/2 inch diameter hole (5.24). In contrast to the above findings, stress concentration factors, presented in (5.25), based on 3-dimensional finite element analyses, are larger for the relatively thick example plates of boron epoxy laminates with holes of varying sizes, than for similar plates of isotropic materials.

See also (5.26) for detailed consideration and equations for stress concentration factors for holes in plates comprised of advanced fiber laminates.

Reference (5.12) gives K_t values for hole shapes other than circular, including elliptical, rectangular with rounded corners, and narrow slits. The graphs provided cover uniaxial tension, biaxial stress and shear stress. Also, see Section 5.8 for an equation for stress concentration with a particular elliptical hole.

Other Types

Stress concentration factors are also given in (5.12) for a number of common structural and mechanical components that have been investigated for stress concentrations. Included are bolts loaded in tension where threads, nuts and heads cause severe stress concentration. K_t values ranging from 2 to 9 are reported for bolts of various types.

Comments on Design Practice

Because high peak stresses caused by stress concentrations can cause premature failure of some plastics materials, design practice for structural use of materials such as acrylic is to avoid completely the use of holes, notches or other such discontinuities in connections or other details of strucural components. With reinforced plastics, strength at holes used for connections is determined by mechanical testing as discussed in Section 4.11. For any materials that behave elastically, at peak stresses the types of structural discontinuities described in this Section can be estimated with the stress concentration factors given herein, or in (5.12), and component design developed to hold these stresses below appropriate materials strength limits.

Stress concentrations can severly reduce the fatigue strength of plastics; thus, it is particularly important to minimize stress concentrations by careful detailing of components subject to fatigue to avoid notches, holes and changes in cross section as much as possible.

See Example 7-1 in Section 7.2 for an illustration of the use of stress concentration factors in the design of a tension member.

Fracture Mechanics

Fracture mechanics provides a rational approach to account for the effects of stress concentrations caused by flaws, cracks, and sharp notches. These cause very localized maximum stresses that usually exceed the theoretical ultimate tensile strength of materials. However, most materials can accomodate such effects by plastic yielding of local material near the crack tip or by other mechanisms inherant to various materials. See Section 5.8 for a summary of Fracture Mechanics concepts that provide a rational approach for determining the fracture strength of members with sharp cracks, flaws or other crack-like discontinuities. The effects of such discontinuities on fatigue strength and on stress-corrosion cracking in hostile environments are also treated in that Section.

5.6 NON-LINEAR RESPONSE

The stresses and deformations described in the preceding sections are determined based on the elastic response of structures whose initial geometry is assumed to remain unchanged after deformation. This assumption facilitates simple structural analyses that give results of acceptable accuracy for the large majority of design applications with structural plastics materials.

There are important structural applications, however, where the above assumption may not produce designs of acceptable accuracy. An example is the behavior of transversely loaded thin plates with edges held against translation. Here, changes in geometry as the plate deflects enable it to develop a significant increase in resistance to transverse loading. The same behavior occurs with flexible tension members such as cables. In Chapter 6, charts are provided which facilitate a simple evaluation of both bending and membrane (in-plane) stresses in plates with edges held against lateral translation. Equations are also given for stresses and deflections of membranes, or flexible plates without bending stiffness. Equations given for long rectangular membranes also apply to cables held at their ends.

Changes in initial geometry can also result in significant reduction in load supporting capability of slender linear members subject to the combined effects of bending and compression. When these members deflect in bending, the bending deflection results in an eccentric application of compressive thrust that amplifies the initial bending effect. This problem is treated later in Section 7.5 which covers the design of beam-columns. It is also treated in Section 6.9 relative to behavior of plates subject to combined direct compression and lateral load.

Non-linear response also occurs when a flexible moment resisting frame deflects under lateral load. Any vertical load on the frame amplifies bending due to lateral loads because of the eccentricities introduced by the lateral deflection of the frame. This is termed the P-Δ effect and is also discussed further in Section 7.5.

Buckling is a special type of non-linear structural response in members subject to compression. This is discussed in the next Section.

Non-linear behavior may also result from non-linear stress-strain behavior of plastics materials. As noted previously, most conventional methods for determining stresses and deflections are based upon the linear relation between stress and strain represented by E, the elastic modulus. However, plastics materials do not always exhibit a linear relation between stress and strain. Two types on non-linearities may occur: (1) E reduces with increasing stress in short-time tests; (2) E reduces with time under load at a constant stress (or strain). The above cases are considered in detail in Chapters 2 and 3.

Exact analysis of materials with a non-linear stress-strain relation, where E reduces with increasing stress, or strain, is complex. When the stress-strain curve can be approximated by two straight lines at different slopes (bi-linear, with two values of E), simplifications are possible such as those developed for steel, a material idealized as having a constant stress for all values of strain above the yield point. Computer solutions have been developed to provide more general solutions for stresses and deformations in members with non-linear materials. Some of these are discussed in Chapter 4. However, they are seldom used in practical design and are not considered here.

When E reduces with time under load, pseudo-elastic analyses are possible if the reduced E is not stress-dependent also. As explained in Chapters 2 and 3, the reduced E is termed the viscoelastic modulus, E_v. In this approach, elastic methods are used to determine stresses and deflections, with E_v (for the appropriate duration of load and expected service conditions of temperature and exposure) used in place of E.

5.7 BUCKLING UNDER COMPRESSIVE STRESS

Except for tension members, all components of structures, as well as structures in their entirety, can be subject to buckling. Therefore, the designer of plastic structures must thoroughly understand of the nature of structural instability. The fundamental concept of buckling or structural instabiity is illustrated by the simple model in Fig. 5-14 (5.10). This elementary structure is comprised of two very stiff struts connected at their midheight by a rotationally flexible spring having a stiffness or spring constant, K, where K is the moment in the spring required to rotate each adjacent strut through an angle $\theta = 1$ radian. Thus, by definition:

$$M_s = 2 K \theta \qquad \text{Eq. 5.49}$$

If the structure is subject to an axial load, P, as shown in the Fig. 5-14a, there appears to be no force that would make the elastic hinge move horizontally (i.e. buckle the column), regardless of the magnitude of P. However, further investigation reveals that this is not true, and that at some load, P_{cr}, the column will buckle laterally at the spring.

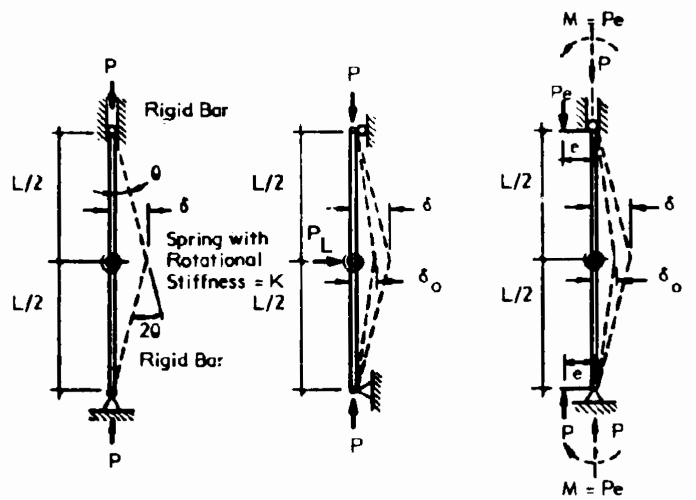

a) Concentric Load b) Lateral Load c) Eccentric Load or End Moments

Fig. 5-14 DEFORMATION OF AXIALLY LOADED BAR WITH STIFFNESS CONCENTRATED AT MID-HEIGHT

The critical load may be determined by investigating equilibrium of the column in a slightly deflected position with the hinge point deflected an amount, δ, causing the hinge to undergo a total rotation of 2θ. In this position, the bending moment applied by the load, P, at the spring is:

$$M_p = P\delta \qquad \text{Eq. 5.50}$$

Also, the spring has rotated an amount:

$$\theta = \frac{\delta}{L/2} \qquad \text{Eq. 5.51}$$

Thus:

$$M_s = 4K\frac{\delta}{L} \qquad \text{Eq. 5.52}$$

The laws of statics require that $M_p = M_s$. Thus:

$$P\delta = \frac{4K\delta}{L} \qquad \text{Eq. 5.53}$$

Eq. 5.53 can be satisfied in two ways: (1), $\delta = 0$, and any value of P; and (2), $\delta \neq 0$ and a unique value of $P = P_{cr}$, where

$$P_{cr} = \frac{4K}{L} \qquad \text{Eq. 5.54}$$

In the second case, Eq. 5.53 is satisfied for any value of δ.

The above analysis shows that up to the critical load, the column stays straight. If it is deflected horizontally a small amount, δ, the spring stiffness, K, is high enough to return the column to a straight position as long as $P < P_{cr}$. When P equals P_{cr}, any arbitrary deflection may be applied and the column will not be returned to a straight position by the spring because the spring stiffness is not high enough to return the structure to its initially straight position. Of course, if initially, the column was perfectly straight and no external force, however slight, occurred to produce horizontal deflection, then the structure would continue to carry the axial force P. In any real structure, however, slight imperfections, such as initial crookedness and load eccentricities, would inevitably lead to buckling at a load at, or just below, P_{cr}.

If the idealized column shown in Fig. 5-14(b) is assumed to have been assembled with an initial deflection δ_o, the equality of external moment at midheight to internal moment in the spring, under a larger deflection, δ, becomes:

$$P\delta = 2(\theta - \theta_o)K = (\delta - \delta_o)\frac{4K}{L} = (\delta - \delta_o)P_{cr}$$

Solving this equation for δ:

$$\delta = \delta_o \frac{1}{(1 - P/P_{cr})} \qquad \text{Eq. 5.55}$$

Eq. 5.55 shows that if the structure starts with an initial deformation δ_o, that deformation will be magnified by any axial load $P < P_{cr}$ on the structure to become δ. The quantity, $1/(1 - P/P_{cr})$, is termed the "magnification," or "amplification" factor. Also, if a member that supports axial compression is also subject to lateral load (Fig. 5-14b), or to end moments (Fig. 5-14c), the deflection and bending stresses caused by the lateral load or end moment will be magnified by the factor $1/(1 - P/P_{cr})$. Eq. 5.55 is plotted in Fig. 5-15. The Figure shows that the amplification of δ_o is fairly small until the axial load approaches 0.6 P_{cr}.

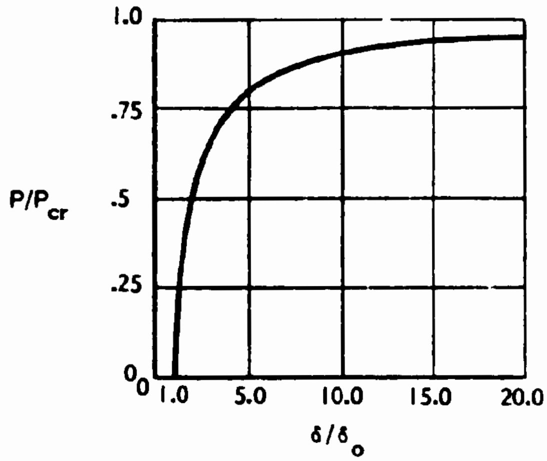

Fig. 5-15 LOAD-DEFLECTION PLOT FOR MEMBER WITH AXIAL LOAD AND INITIAL DEFLECTION

The concept of determining the approximate non-linear deflection or bending moment by applying the amplification factor to the linear deflection or bending moment is extremely useful in a wide variety of problems involving combined bending and axial compression. It also applies to cases of combined bending and axial tension, where the presence of tension reduces the linear bending deflections and stresses.

In practice, the stiffness of structural members is not concentrated at one point, as in the case of the idealized column in Fig. 5-14. For linear members, the stiffness, EI is distributed over the length of the member. Buckling of centrally loaded columns is treated in Section 7.3 of Chapter 7. The magnification of bending effects in beams and frames that also carry axial compression is covered in Section 7.5.

Laterally unbraced beams that are bent about their strong axis may become unstable and deflect laterally at their compression flange while rotating about their tension flange. This is termed lateral-torsional buckling and is treated in Section 7.4.

In-plane compressive stresses develop in plates from constant or variable in-plane compressive stress resultants directed along either or both plate axes, or from in-plane shear stress resultants. Resistance to buckling is a function of flexural stiffness in both directions. Longitudinally compressed long plates, supported along edges parallel to the load, resist buckling by virtue of their transverse flexural stiffness. Buckling of plates is treated in Sections 6.9 and 6.10. The results presented there are used in Chapter 7 for determining the local buckling resistance of thin flanges and webs of column and beam members.

Plates exhibit post-buckling strength. After initial elastic buckling occurs, the compressed plate does not collapse, but additional compressive load capacity develops as the stress continues to increase along the edges of the plate. Even through the interior region of the plate has buckled, compressive forces can continue to be resisted in regions close to transversely supported edges so long as the ultimate strength of the edge region is not exceeded. In the post buckling range, the plate is considered to support in-plane compressive load on a reduced effective width. This is explained in Section 6.9.

Thin faces of sandwich panels may buckle if the core does not provide sufficient elastic support. Buckling resistance of sandwich facings and requirements for core stiffness are given in Section 8.8. Buckling of sandwich columns and plates is also covered in that Section.

The buckling resistances of shells depends upon a combination of axial, or in-plane, stiffness in one direction and flexural stiffness in the other. Because axial stiffness is reduced by local imperfections and eccentricities in stress, shells do not develop the full buckling resistance predicted by the "linear elastic" buckling theory exemplified by the simple model described above. "Large deflection" theory is needed for accurate analyses of shell buckling. Because of the complexity of such analyses, however, the results of linear elastic analyses are often used together with semi-empirical "knockdown" factors that account for the effects of large deflections. These are determined from model tests and/or from a limited number of "large deflection" solutions for simplified basic cases. Equations for buckling resistance of uniform thickness, ribbed and sandwich shells are given in Section 9.10.

5.8 BRITTLE FRACTURE UNDER TENSILE STRESS

All structural members contain crack-like flaws that cause local increases in stress. Quantitative methods for determining the magnitude of these stress concentrations for certain types of discontinuities such as holes, notches with rounded ends and changes in cross section are presented in Section 5.5. In general, the magnitude of the stress concentration increases with the length and sharpness of the flaw or discontinuity. For example, the stress concentration factor for an elliptical hole in an infinite plate subject to a tension stress field, as shown in Fig. 5-16, is (5.14):

$$K_{tg} = 1 + \frac{2a}{b} \qquad \text{Eq. 5.56}$$

The radius of curvature at the end of an ellipse is

$$\rho = \frac{b^2}{a} \qquad \text{Eq. 5.57}$$

Thus, the maximum stress adjacent to an elliptical hole is

$$\sigma_{max} = (1 + 2 \cdot \sqrt{a/\rho}\,) \qquad \text{Eq. 5.58}$$

where σ is the average or nominal stress on the gross area.

If an elliptical hole becomes severly elongated, the radius at the end approaches zero and the ellipse represents a model for the crack-like discontinuity shown in Fig. 5-17. Since for small radii of curvature, $2\sqrt{a/\rho}$ is large compared to 1.0:

$$\sigma_{max} \approx 2\sigma \cdot \sqrt{a/\rho} \propto \sigma\sqrt{a} \qquad \text{Eq. 5.59}$$

As the crack tip radius approaches zero, the peak stress adjacent to the crack approaches infinity.

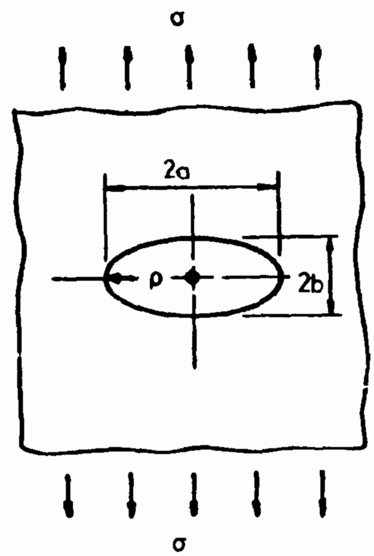

Fig. 5-16 ELLIPTICAL HOLE IN INFINITELY LARGE PLATE UNDER PLANE STRESS

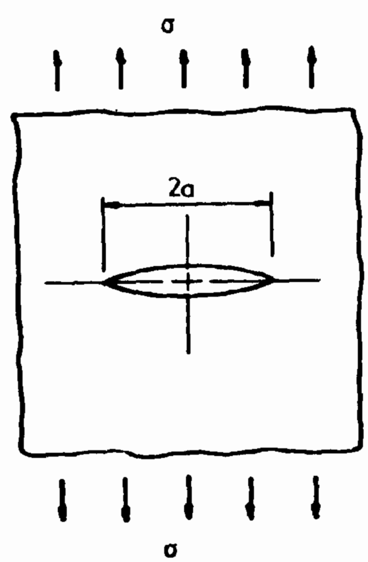

Fig. 5-17 A TYPICAL CRACK-LIKE DISCONTINUITY IN A STRESSED BODY

Because the "Stress Concentration Factor" in Eq. 5.59, $K_{tg} = 2\sqrt{a/\rho}$, approaches infinity for sharp cracks, the elastic analyses used to develop stress concentration factors (Section 5.5) do not provide adequate information to define the behavior of practical materials in the presence of notches. In order to overcome the shortcomings of elastic stress concentration analysis applied to crack-like discontinuities, Griffith (5.13) first examined the behavior of a local zone at the tip of a small crack in a large component in terms of the energy balance required to propagate a crack. His pioneering work provided a foundation for the science of **Fracture Mechanics.** Inglis (5.14) postulated that fracture proceeds in a brittle material when the stress at the crack tip exceeds the theoretical cohesive strength of the material (which can be very high, possibly of the order of E/10), breaking atomic bonds ahead of the crack tip, to create new fracture surfaces. Irwin (5.15) used the above concepts to define a parameter known as the "stress Intensity Factor", K. This factor is a measure of the magnitude, extent, and distribution of stress intensification at sharp notches of various types, and can be used to characterize the materials susceptibility to brittle fracture. It can be used with brittle materials, as well as with materials where fracture is preceded by some yielding and redistribution of stress at the crack tip.

While Griffith's approach was widely used in the early development of Fracture Mechanics, it has largely been replaced by Irwin's concept of "Stress Intensity Factor". The Stress Intensity Factor approach will be described first in this section and then later compared with the Griffith theory of brittle fracture. However, the approaches of Inglis, Irwin and Griffith's all lead to the same general conclusions about the fracture behavior of brittle and pseudo-brittle materials.

Fracture mechanics provides concepts for assessing the safety and reliability of tension members or tension parts of members against failure by brittle fracture. The "Stress Intensity Factor" provides a measure of the overall magnitude of the applied stress field around a crack (as related to a stress and crack length). In applying "fracture mechanics", a limiting or "Critical Stress Intensity Factor" is defined as the the limit of a material's capability to resist fracture through local increase in strength, plastic deformation, or other energy dissipating mechanisms.

The magnitude of the "Critical Stress Intensity Factor" is an important measure of a material's toughness. Under this concept, toughness is defined as the ability of a material to carry tensile load in the presence of notches.

Analyses to be described later show that if the relationship between nominal tensile stress, (without the presence of a crack), σ, and crack length, a, given by Eq. 5.60 is termed the "Stress Intensity Factor", K, a limiting or maximum value of K can be establihed as a basic property of most materials. In this approach:

$$K = C\sigma\sqrt{a} \qquad \text{Eq. 5.60}$$

C is a constant that is a function of a particular specimen and crack geometry. One type of geometry and load configuration is shown in Fig. 5-17. For this crack and load configuration, $C = \pi$. Other test conditions result in different values of C. This will be discussed later.

A given material will fail by tensile rupture when a particular combination of tensile stress, σ_{xf}, and crack length, a_f, produce a critical value of stress intensity factor, K_c, K_{Ic}, or K_{Id}, that represents a fracture condition. Thus:

$$K_c, K_{Ic} \text{ or } K_{Id} = C\sigma_{xf}\sqrt{a_f} \qquad \text{Eq. 5.61}$$

The stress intensity factors, K_c, K_{Ic} and K_{Id} are defined below.

Other variables that affect the critical stress intensity factor include the presence or absence of restraint of deformation normal to the plane of the primary stress field, the rate of load application, the duration of load, and the temperature of the stressed member.

Members that can freely deform normal to the stress field plane are loaded in "plane stress" and a critical stress intensity factor for plane stress, K_c, applies. Members with a small thickness perpendicular to the plane of stress are usually considered as "plane stress" cases. When deformation normal to the plane of the stress field is completely prevented, "plane strain" conditions prevail and a critical stress intensity factor for "plane strain", K_{Ic}, applies. Members that have appreciable thickness perpendicular to the plane of the stress field are considered as "plane strain" cases. Because prevention of deformation normal to the plane of the primary stress field produces tensile stresses in this direction, K_{Ic} critical stress intensity factors are lower than K_c factors. For this reason, the K_{Ic} critical stress intensity factor is usually used as the principal measure of fracture toughness.

The toughness of a material also varies with rate of load application and temperature. The critical stress intensity factor for dynamically applied load, K_{Id}, is less than K_{Ic} for most materials. Also, K_{Id} and K_{Ic} values should be related to specific temperatures or temperature ranges.

Thus, fracture mechanics shows that there are three primary factors that control the susceptibility of a structural component to brittle fracture (5.16):

- **Material toughness**, as defined by critical stress intensity fractors such as K_c, K_{Ic} or K_{Id}. In theory, these critical stress intensity factors are only applicable to linearly elastic homogeneous materials, although they find practical use in cases where some plastic deformation occurs in the vicinity of the crack tip, as well as with some composites which are not homogeneous. Much more complex elastic-plastic theories (5.16) have been developed to define the toughness of elastic-plastic materials such as mild steel and some plastics. Some of these have also been applied to composites such as reinforced plastics (5.17, 5.18).

- **Crack size**, as defined by length, a. Brittle fractures initiate from discontinuities. These can be present initially due to fabrication and handling (air voids, surface scratches, etc.), or they can result from resin crazing or micro-cracking at low levels of stress. Cracks can grow by fatigue under cyclic loads, and by stress corrosion in hostile environments.

- **Stress level.** Brittle fractures occur only as a result of tensile stresses. These may result from residual stresses caused by differential shrinkage in manufacture or fabrication, and restraint of thermal deformation in a component configuration, as well as from applied loads.

A few important results of stress analyses for members with cracks are presented below to introduce the reader to fracture mechanics concepts. This treatment is limited to homogeneous elastic materials. The further development of these concepts to account for the behavior of many actual plastics materials that are not homogeneous and/or completely elastic is not included in the scope of this elementary presentation. References given in this Section provide much more extensive treatment of fracture mechanics for actual applications.

Linear-Elastic Fracture Mechanics

Linear-elastic fracture mechanics (LEFM) provides the analyses required to relate stress field magnitude and distribution in the vicinity of a crack tip to the nominal applied tension stress (without the presence of the crack) and to the size, shape and orientation of the crack or crack-like discontinuity. As explained above, the stress intensity factor, K, represents the effect of stress field magnitude and distribution in the vicinity of the crack tip. The ability of a member to resist a given nominal stress with a given type and size of crack is determined by comparing the stress intensity factor, K_I, produced by these conditions with the critical stress intensity factor, K_{Ic}, for the material and configuration. The critical stress intensity factor represents the fracture toughness of the material. Thus, stress intensity factor, K_I, is to fracture toughness, K_{Ic}, as stress, σ is to yield or ultimate strength, σ_y or σ_u.

In LEFM, three types of relative movements of two crack surfaces are usually defined. These are shown in Fig. 5-18.

- Mode I — opening mode, where crack surfaces move away from each other. This is the most commonly investigated type of crack propagation.
- Mode II — shear mode, where two surfaces slide over each other in a direction perpendicular to the line of the crack tip.
- Mode III — tear mode, where two crack surfaces slide over each other in a direction parallel to the line of the crack tip.

Equations for stresses and displacements at any point in the vicinity of the crack tips are given in (5.16) for each of the 3 modes of relative crack surface movement with an isotropic material. See (5.18) for similiar equations for a specially orthotropic material (as defined in Sections 4.9, 6.6 and 6.7). These equations contain the stress intensity factor, K_I, K_{II} or K_{III}, for the particular mode, and are applicable to the case of plane strain (Modes I and II) where no deformation is permitted in the z direction (Fig. 5-18). The analysis shows that the magnitude of the elastic stress field can be described by the single term parameters K_I, K_{II}, K_{III}. Also, dimensional analysis and consideration of "Griffith's" analysis for crack propagation (to be discussed later in this Section), shows that $K \propto \sigma\sqrt{a}$, as given by Eq. 5.60.

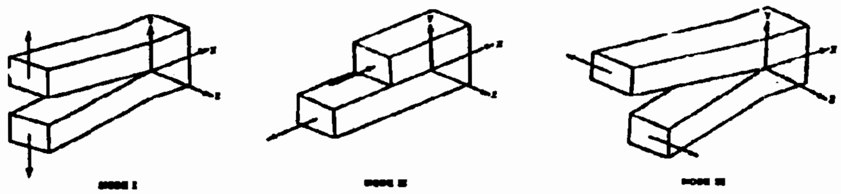

Fig. 5-18 BRITTLE FRACTURE FAILURE MODES

Relationships between the stress intensity factor for "plain strain" and various member configurations, crack orientations and shapes, and loading conditions are available in the literature (5.16, 5.17, 5.19, and 5.27). These provide numerical values for the constant C in Eq. 5.60. Values of C for some simple common configurations are given in Table 5-6. The configurations shown in the table are important because they frequently provide the basis for tests and analyses used to determine the critical stress intensity factor, K_{Ic} or K_{Id}, that defines a material's thoughness.

Correction factors given in the Table enable the designer to improve estimates of stress intensity factors for a few common practical components.

See (5.27) for a more comprehensive presentation of an approach for obtaining stress intensity factors applicable to actual components by applying appropriate correction factors that account for the effect of stress concentrations such as holes, fillets and other changes in cross section to the basic coefficients, C. The important influence of residual, stresses is also explained in (5.27).

Eq. 5.60 and the constants given in Table 5-6 apply for specially orthotropic materials (Section 4.9, 6.6 and 6.7), as well as for isotropic materials (5.17). The stress intensity factors, K_I and K_{II}, for specially orthotropic material may be used to characterize crack extension behavior and fracture in a manner that is identical to their use with isotropic material. However, as stated above, the actual stress field around a crack tip in an orthotropic material differs from that associated with isotropic materials.

Table 5-6

Coefficient, C, in Stress Intensity Equation

$$K_I = C\sigma\sqrt{a};\ K_{II} \ \& \ K_{III} = C\tau\sqrt{a}$$

Member, Crack and Load Configuration		C	Correction Factors, f for finite width plates
1. 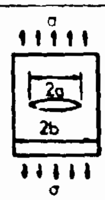	$b = \infty$	$\sqrt{\pi}$	
	b = finite	$f\sqrt{\pi}$	$f = \left(\frac{2b}{\pi a}\tan\frac{\pi a}{2b}\right)^{1/2}$
2. 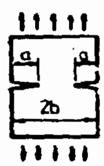	$b = \infty$	$1.12\sqrt{\pi}$	
	b = finite	$1.12f\sqrt{\pi}$	approx. the same as in 1.
	single notch and $b = \infty$	$1.12\sqrt{\pi}$	
	single notch and b = finite	$\frac{a}{b}f\sqrt{\pi}$	See (5.16)
3. 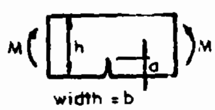		$\frac{hh^2 f}{(h-a)^{3/2}(a)^{1/2}}$	See (5.16)
4. Partial depth surface crack of elliptical shape in infinite body 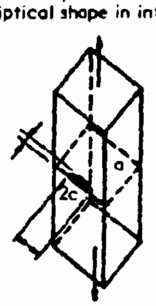		$1.12\sqrt{\frac{\pi}{f}}$	See (5.16)
5. 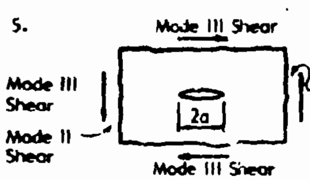	Mode I: Shear Mode II: Shear	$\sqrt{\pi}$	Note: Applies to K_{II} for shear in direction to produce mode II crack displacement and to K_{III} for shear in direction to produce mode III crack displacement.

When several types of loads such as uniform tensile loads, concentrated tensile loads, or bending loads act on a component that contains a crack, the total stress intensity factor can be obtained by adding the stress intensity factors that correspond to each load. In order for this to apply, however, each load must cause the same type of displacement of crack surfaces (i.e., all be Mode I, or all Mode II, etc.). Stress intensity factors for different modes of deformation cannot be added. One approach when both shear and tension stress fields may cause crack extension is to calculate a total energy release rate for each mode of deformation (to be described later in this Section) and to add these for each mode.

Modifications for Elastic-Plastic and Non-Homogeneous Materials

In theory, the stress intensity factor applies only to homogeneous materials that remain elastic. In application, however, the critical stress intensity factor is determined experimentally, and the concept of maintaining calculated stress intensity factors, K_I, etc. below a critical experimentally-determined stress intensity factor is generally valid for materials that develop small plastic zones around the tip. For tougher materials having larger plastic zones near the crack tip, several advanced methods are available for characterizing toughness (5.16), but space precludes their presentation here. The simple stress intensity approach developed for homogeneous elastic materials has also been applied with reasonable success to composites such as fiberglass reinforced plastics (5.17). Some of the more advanced methods devised for elastic-plastic materials have also been applied to fiberous composites with some success (5.18).

Griffith Theory of Fracture

Since Griffith's analysis (5.13) of the fracture behavior of ideally brittle materials has been widely discussed and applied, the following brief presentation is included to summarize the equations that define the onset of fracture and to show their relation to the stress intensity factor approach presented earlier in this Section. Griffith's theory is based upon the assumption that fractures will propagate in an ideally brittle material when the elastic surface energy required for the formation of new surfaces ahead of a crack is less than the elastic energy released from the stressed body when the crack extends.

Considering the infinite plate with crack shown in Fig. 5-17, for the case of "plane stress":

- Energy released by crack extension = $\frac{\pi\sigma^2 a^2}{E}$
- Elastic surface energy required to extend crack = 2 (2a γ_e), where γ_e is the elastic surface energy of the material.
- Thus:

$$\sigma \sqrt{\pi a} = (2 \gamma_e E)^{1/2} \qquad \text{Eq. 5.62}$$

The quantity $2\gamma_e$ is termed the energy release rate for the material, $\overline{G}$. Thus, for "plane stress":

$$\overline{G} = \frac{\pi\sigma^2 a}{E} = \frac{K_{Ic}^2}{E} \qquad \text{Eq. 5.63}$$

Similarly, for "plane strain":

$$\overline{G} = \frac{K_{Ic}^2 (1 - \nu^2)}{E} \qquad \text{Eq. 5.64}$$

Determination of Critical Stress Intensity Factor

Critical stress intensity factors are determined from various standard tests that have been developed to provide sufficiently accurate data about material toughness, consistent with the accuracy of data needed for design, for a reasonable cost. As in the case of other material properties, the bulk of quantitative research and testing has been done for metals. For plastics and composites, there is limited understanding of the effect of important variables like duration of load, stress corrosion in various environments, non-homogeneity of composites, etc. on the toughness of materials. Thus, there are no widely accepted standards for specimen configuration and test conditions, as have been developed for metals. However, application of fracture mechanics to plastics and composites provides a quantitative approach for assessing material toughness that should be an important tool for developing improved engineering materials, as well as for the rational use of existing materials in structural applications. See (5.20) and (5.21) for consideration of some of the problems associated with fracture toughness testing of glassy plastics, and application of fracture mechanics with such materials. See (5.17), (5.18), and (5.23) for discussion of the application of fracture mechanics with fibrous-resin composites.

Cyclic Loading and Fatigue

The strength of most plastics is reduced when critical stresses are applied as cyclic loads. Fatigue strength of plastics is discussed in Sections 2.11 and 3.7. Stress intensification at notches and discontinuities (Section 5.5) can severly reduce fatigue life compared to un-notched (flaw free) members. Cyclic loading may produce cracks at discontinuities that initially are not large enough to result in fracture, but which will propagate under continued cyclic loading until fracture finally occurs at a higher number of load cycles. Fracture mechanics provides quantitative approaches for describing the mechanisms of crack initiation and crack propagation under cyclic loads. Criteria for defining fracture behavior and a basis for predicting fatigue life can be developed with the aid of fracture mechanics. The details of such analyses are found in texts such as (5.16).

Stress-Corrosion Cracking

Hostile environments may produce delayed failure of structural components under statically applied stresses that are well below material strength in a standard test environment. Such failures are due to stress-corrosion cracking. In studies of stress-corrosion cracking, the stress intensity factor, K_I, is used to characterize the mechanical component of the crack driving force. Environmental conditions can degrade the stressed material at the tips of cracks and flaws and can cause crack extension with time under exposure until the cracks are large enough to result in fracture.

Fracture mechanics studies of the resistance of materials to stress-corrosion cracking usually are based on a critical "stress-corrosion cracking threshold" stress intensity factor for plane strain, K_{Iscc}. (5.16). This factor is determined by subjecting several precracked test specimens to a particular hositle environment at different constant stresses and at various levels of initial stress intensity factors, K_{Ii}. The highest K_{Ii} that does not produce crack extension after a long test time is the stress-corrosion cracking threshold, K_{Iscc}, for the particular material and environment. Statically loaded structural components exposed to the tested environment are expected to have an infinite life when their K_I value is less than K_{Iscc}.

Application to Design

For the designer of plastics structures, fracture mechanics provides the possibility of an important tool for the selection of appropriate materials, based on resistance to brittle fracture (toughness), and for the determination of safe design stress levels and allowable flaw sizes for given materials. The relationship of these three variobles are illustrated graphically in Fig. 5-19. The family of curves that relate nominal tensile stress at brittle fracture, σ_{xf}, to maximum flaw length, a, are similar to the curves that relate critical buckling stress, σ_{xc}, to column slenderness, L/r, (Fig. 7-3). The critical stress intensity factor, K_{Ic}, is analogous to the elastic modulus, E, in column buckling. When viewed this way, whenever the combination of tensile stress and flaw size produces a value of σ_{xf} that is less than σ_{xu}, tension or flexural member design is governed by tensile instability (brittle fracture) , just as a compression member design may be governed by compressive instability (buckling) wherever σ_{xc} is less than σ_{xu}.

Practical methods for applying the above described basic concepts of fracture mechanics to evaluation of components with common details are given in (5.27). Procedures for correcting basic stress intensity factors for various stress raisers such as holes, fillets or changes in cross section are presented and illustrated by application to practical details in steel structures.

Unfortunately, the state of the art in the application of fracture mechanics to plastics and composites has not yet made available an adequate body of reliable materials toughness parameters for use in design. Furthermore, more applied research should be undertaken to determine the extent to which LEFM can be applied to various plastics and composite materials that are of interest in structural applications. Thus, the above-described fracture mechanics approach is not yet available for widespread use by designers. Prudent part design in the absence of fracture toughness data is characterized by the elimination of all potential stress concentrating geometries, and over-design of critical dimensions to compensate for stress concentrations in the form of flaws that may develop during the service life of the structural component.

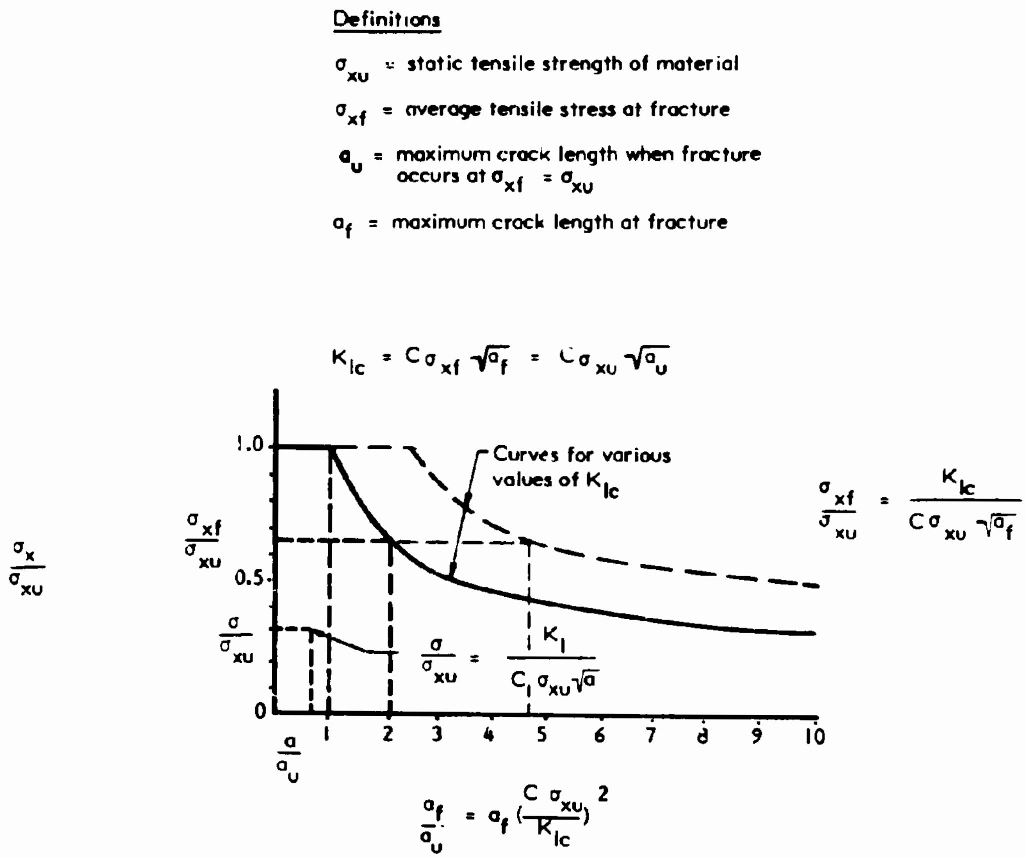

Fig. 5-19 DIMENSIONLESS RELATION BETWEEN TENSION STRESS AT FRACTURE, σ_{xf}, AND CRACK LENGTH, a_f

Hopefully, the industry will recognize the need for quantitative brittle fracture criteria and manufacturers of specific materials will undertake the research needed to demonstrate whether LEFM will characterize the toughness of their materials. Where this approach can be used, reliable values for K_{Ic}, K_{Id} and other important critical stress intensity factors that characterize the fracture toughness of specific plastics and composites must then be developed. If LEFM cannot characterize specific materials, other criteria for fracture toughness must be developed to assist designers to attain safe structural designs for members subject to axial or flexural tension.

5.9 STRUCTURAL VIBRATIONS

When a structural component or an assembly of components with a mass, $\overline{M}$, is given a certain type of small instantaneous displacement and then released, it will initially oscillate about its neutral position with a frequency, f, that is termed the "natural frequency of vibration". Frequency is measured in cycles per unit of time (usually seconds). The time required to complete one complete cycle is termed the natural period, T. The period is related to the natural frequency by:

$$T = 1/f \qquad \text{Eq. 5.65}$$

Natural frequency of idealized systems

The simplest model to illustrate this behavior is the spring supported mass shown in Fig. 5-20a. If this mass is moved an arbitrary amount y_i and released, it will oscillate in accordance with the following simple equation of motion:

$$y = y_i \cos \omega t \qquad \text{Eq. 5.66}$$

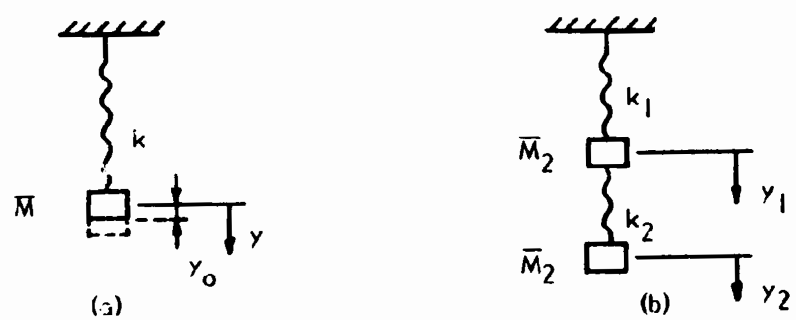

Fig. 5-20 IDEALIZED "MODELS" FOR VIBRATING SYSTEMS

ω is termed the circular natural frequency and is related to the natural frequency, f, by:

$$\omega = 2\pi f \qquad \text{Eq. 5.67}$$

f, the natural frequency is:

$$f = \frac{1}{2\pi} \sqrt{\frac{k}{M}} \qquad \text{Eq. 5.68}$$

in which k is the stiffness of the spring.

The simple structure shown in Fig. 5-20(a) is termed a "single degree-of-freedom" system, and it has only one possible mode (displacement pattern) of natural vibration and one natural frequency. The idealized structure with 2 spring supported masses shown in Fig. 5-20(b) is termed a "two degree-of-freedom" system, and it exhibits more complex vibrational behavior. It has two "modes" of free vibration, and a natural frequency for each of these modes. When the structure vibrates in one of its modes, all points vibrate in phase; that is, all points reach the maximum travel simultaneously. Texts on structural dynamics such as (5.22) present equations of motion, and both approximate and rigorous methods for determining natural frequencies and other characteristics involved in vibration analysis. Often, structural systems are approximated as one degree-of-freedom systems, and the general conclusions and methods of analysis of behavior of such systems are used for the approximate determination of vibration effects for a more complex structure.

Damping

When a member is left freely vibrating, the amplitude gradually reduces because of the inherent damping of the material and the additional damping due to friction at structural supports and connections. In viscous damping (the usual assumption), the damping force is proportional to the velocity of motion. A damping coefficient, c, is defined as:

$$c = \frac{\text{Damping force on mass}}{\text{Velocity of mass}} \qquad \text{Eq. 5.69}$$

The damping coefficient is a function of the material's characteristics, shape of structural member and arrangements of structural system, as well as other variables such as level of stress. It is difficult to measure c with great precision. The amplitude decay in one cycle of a vibrating system gives an approximate estimate of damping which is usually satisfactory for use in practical design.

Damping is generally defined in quantitative terms as a percent ratio of the amount of damping beyond which the structure does not vibrate harmonically. Thus:

$$c = \eta c_r \qquad \text{Eq. 5.70}$$

in which c_r is termed the "critical damping", and the percent of critical damping is η. For a one degree-of-freedom system, the critical damping is:

$$c_r = 2\sqrt{k\bar{M}} = 2\bar{M}\omega \qquad \text{Eq. 5.71}$$

and thus,

$$c = 2\eta\bar{M}\omega \qquad \text{Eq. 5.72}$$

Dynamic load factor

Structural vibrations occur when a member, or assembly of members is suddenly loaded or unloaded, when a structure is subject to certain types of cyclic loading or motion, or when the load varies with time. Sudden loads occur in impact and blasts; cyclic loads occur as a result of ground shaking in earthquakes, moving loads like vehicles on a bridge, machinery with parts that rotate or oscillate, forces from random wind gusts, or any loading conditions involving changes in applied forces over short time periods.

Structural vibrations often amplify the deflections and stresses produced by loads that are applied statically. In practical design, amplified stresses that result from dynamically applied loading are usually determined by multiplying the stresses caused by the design loads, as applied statically, by a dynamic load factor (DLF). In cases where dynamic loads occur because a structure is subject to motion from external effects, such as an earthquake, equivalent static forces are often determined for use with conventional static design methods.

When an applied load is varied over a time span that is less than about four times the natural period of a structural system, dynamic amplification of stresses may be significant. The magnitude of the DLF depends on the variation of applied load with time (forcing function) and the natural period of the structure. Quantitative values of DLF for various forcing functions are presented in texts on dynamics such as (5.22). Two limiting cases are useful for qualitative evaluation of certain important dynamic effects:

- An instantaneously applied load that remains on the structure produces a maximum DLF of 2.0 for a linearly elastic system without damping. Damping reduces the DLF but the reduction is usually not significant for this type of forcing function. If the "rise time" (i.e. time to reach maximum load) of a rapidly applied load is less than about one-quarter of the natural period, the DLF is essentially 2.0, the same as for an instantaneously applied load. If the "rise time" is more than about 4 or 5 times the natural period, the response is essentially static because the DLF is close to 1.0 and dynamic effects are negligible. Thus, loads with a "rise time" that is more than about 4 times the natural period are slowly applied loads.

- If a forcing function is pulsating such that its value at any time, t, may be approximated by:

$$F_t = F_1 \sin \Omega t \qquad \text{Eq. 5.73}$$

the maximum DLF is approximated by (5.22):

$$\max \text{DLF} = \pm \frac{1}{1 - (\Omega/\omega)^2} \qquad \text{Eq. 5.74}$$

It is evident from the above equations that the application of pulsating loads to structures whose natural period is close to the period of the pulsating load (forcing function) can result in very large deflections and stresses. This condition is termed "resonance". Thus, it is important to avoid vibrating loadings that may produce resonant vibration.

Approximate lowest natural frequency of actual structures

The significance of the natural frequency (or period) of a structure is evident from the above discussion of the effects of loads that vary over short time periods. The natural frequency of a single degree-of-freedom system is given by Eq. 5.68. The approximate lowest natural frequency of any structure whose dynamic behavior can be simulated by a single degree-of-freedom system can be determined using Eq. 5.68 if the stiffness, k, the effective mass, $\bar{M}_e$, and the dynamically applied forces, F_e are determined by assuming that $\bar{M}_e$ and F_e are concentrated at a single point on the structure that best represents its motion in its lowest vibration mode. For members with distributed mass and distributed dynamic forces, such as beams, this point is often the point where the deflection is maximum. In this approach:

$$k = \frac{1}{\delta_s} \qquad \text{Eq. 5.75}$$

where δ_s is the static deflection of the structure at the point of application of equivalent mass and force when the structure is subject by a unit load having the same distribution as the applied dynamic force. The effective mass, $\bar{M}_e$, can be defined in terms of the total mass, $\bar{M}$, as:

$$\bar{M}_e = c_m \bar{M} \qquad \text{Eq. 5.76}$$

Likewise, the effective force, F_e, can be defined in terms of the total distributed force, F, as:

$$F_e = c_L F \qquad \text{Eq. 5.77}$$

Procedures for determining c_m and c_L for single degree-of-freedom approximations of common structural systems are given in (5.22).

For beams, the unit load deflection, δ_s, at the point where the equivalent mass and dynamic force are assumed to be concentrated takes the form given in Table 5-1 for bending and shear deflection, with load, W = 1. Thus:

$$\delta_s = K_m \frac{L^3}{EI} + K_v \frac{L}{GA_w} \qquad \text{Eq. 5.78}$$

Values of K_m and K_v for midspan deflection are given in Table 5-1, for simply supported and rotationally fixed ended beams under concentrated and uniformly distributed loads. Substituting Eqs. 5.75, 5.76, 5.77 and 5.78 into 5.68, the lowest natural frequency for beams where shear deflection is small relative to bending deflection (the usual case except for some sandwich beams, Chapter 8) is given by:

$$f = \frac{1}{2\pi} \sqrt{\frac{c_L EI}{c_m K_m L^3 \bar{M}}} = \phi_1 \sqrt{\frac{EI}{L^3 \bar{M}}} \qquad \text{Eq. 5.79}$$

$$\phi_1 = \frac{1}{2\pi} \sqrt{\frac{c_L}{c_m K_m}} \qquad \text{Eq. 5.80}$$

Examples of midspan concentrated masses that are equivalent to combinations of concentrated or distributed mass systems and dynamically applied force systems on beams with several conditions of end restraint are given in Table 5-7. The coefficient, ϕ_1, for approximate lowest natural frequency obtained using the tabulated equivalent single midspan concentrated mass and force and the static midspan deflection for the appropriate distribution of dynamically applied force is also given in the Table for each load arrangement. Only bending deflection is included in these examples. Note that the lowest natural frequency coefficient, ϕ_1, is approximately the same for beams with different distributions of applied dynamic force, but the same mass distribution and end restraint condition (i.e. Cases 2, 6 and 7 and Cases 4 and 8 have approximately the same ϕ_1).

Approximate dynamic analysis of actual structures

Approximate methods are often used in dynamic analyses of practical structures. As alreay discussed for determining natural frequencies, the simplest methods involve idealizing a multi-degree-of-freedom structure, such as a beam or frame with distributed mass and distributed dynamically applied force, as an equivalent one degree-of-freedom system. Appropriate approximate analyses for determining dynamic response of practical structures are described in (5.22). This reference also gives design aids, such as charts of DLF for various forcing functions on single degree-of-freedom systems, and tabulations of equivalent masses, loads, and resistances for approximating response of multi-degree of freedom systems by single degree-of-freedom systems. It also gives design examples covering response of various common structural components and systems to several types of dynamic loads and resistances, including consideration of ductility and plastic behavior.

In the approach developed in (5.22), the static deflection and the static stress resultants produced by the maximum dynamically applied forces are multiplied by the maximum DLF to determine the maximum dynamic response. The static deflections and stress resultants produced by the mass loading on the structure are added to the dynamic response produced by the applied dynamic force. This approach is used for the evaluation of maximum stresses in a reinforced plastic beam in **Example 5-7.**

Note that the dynamic reactions of the actual structural member have no direct counterpart in the equivalent single degree of freedom system (i.e. equivalent spring force is not the same as the real reaction since the simplified system was selected to produce the same deflection as the actual system, rather than the same force). Methods for obtaining the maximum reactions (and, hence, the maximum shear) are given in (5.22).

Table 5-7

Equivalent Masses & Coefficient for Lowest Natural Frequency for Beams (For use in Eq. 5.78)

Dynamically Applied Force Arrangment	Mass Distribution	Equiv. Load Coeff., c_L	Equiv. Mass Coeff., c_m	Bending Stiffness Coeff., K_m (From Table 5-1)	Coeff. for Natural Frequency, ϕ_1, Eq. 5.80
1 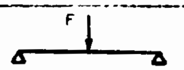	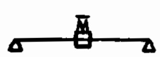	1.0	1.0	1/48	1.10
2 Same as 1		1.0	0.49	1/48	1.57
3 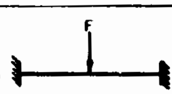	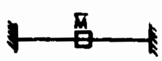	1.0	1.0	1/192	2.21
4 Same as 3		1.0	0.37	1/192	3.63
5 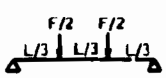	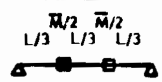	0.87	0.76	1/56.4	1.28
6 Same as 5		0.87	0.52	1/56.4	1.55
7 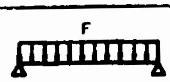		0.64	0.50	5/384	1.58
8 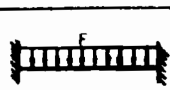	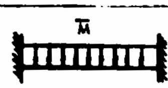	0.53	0.41	1/384	3.56

Example 5-7: Determine the lowest natural frequency and the maximum combined static and dynamic flexural stress in the beam shown in sketch "a" subject to a maximum dynamic force of 600 lbs per foot (from blast pressure) uniformly distributed over the length of the beam, if the weight on the beam is 400 lbs per foot, also uniformly distributed over the length of the beam. The section shape and properties of the beam are shown in sketch "b". (The beam is the same as the beam designed for static load in Example 7-3). The "blast pressure" forcing function that defines the variation of the 600 lbs/ft maximum applied force with time is shown in sketch "c".*

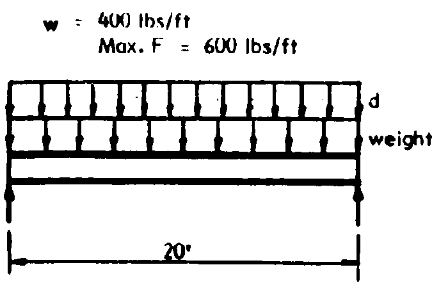

a) Beam Arrangement and Load

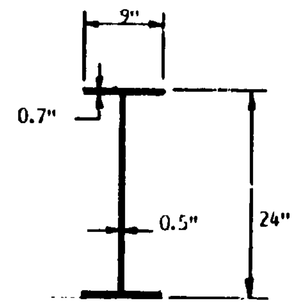

b) Beam Section

Section Properties

$I_1 = 2197 \text{ in}^4$

$S_1 = 183 \text{ in}^3$

Material Properties

$E_{11} = 1{,}400{,}000$ psi

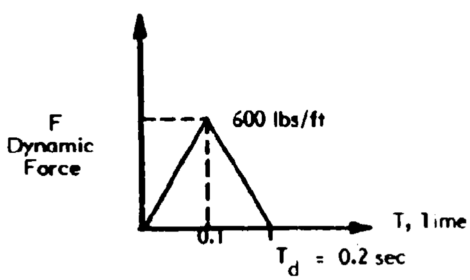

c) Dynamic Force Variation with Time

1. Natural frequency of beam with 0.4 k per ft. dead load.

$$f = \phi_1 \sqrt{\frac{EI}{L^3 \bar{M}}}; \quad E = E_{11} = 1{,}400 \text{ ksi}; \quad \text{Using inch units, } L = 20 \times 12 = 240 \text{ in.}$$

$$\bar{M} = \frac{W}{g}; \; W = 0.4 \times 20 = 8k; \; g = 386/\text{in/sec}^2; \; \bar{M} = \frac{8}{386} = 0.0207 \text{ kip-sec}^2/\text{in.}$$

$$f = \phi_1 \sqrt{\frac{1{,}400 \times 2197}{(240)^3 \times 0.0207}} = 3.28\phi_1; \quad \text{From case 7, Table 5-7, } \phi_1 = 1.58$$

---

* See note on Example 5-1, page 5-4.

Example 5-7 (continued)

$f = 3.28 \times 1.58 = 5.2$ cycles/sec; $T = \frac{1}{f} = \frac{1}{5.2} = 0.19$ sec.

2. Max. dynamic load factor, (DLF) max:

   From Fig. 2-8 in Ref. 5.22 (reproduced below) for the triangular pulse forcing function shown and T = 0.19 sec., $t_d/T = 0.2/0.19 = 0.96$: (DLF) max. = 1.5

3. Static stresses:

   Due to weight: $M_x = \frac{WL}{8} = \frac{0.4 \times 20 \times 20}{8} = 20'k$

   $\sigma_x = \frac{M}{S} = \frac{20 \times 12}{183} = 1.311$ ksi

   Due to max. forcing function: $M_x = \frac{0.6 \times 20 \times 20}{8} = 30'k$

   $\sigma_x = \frac{30 \times 12}{183} = 1.967$ ksi

4. Maximum stress = max. dynamic stress + max. static stress:

   $\max. \sigma_x = 1.967 \times (DLF) + 1.311 = 1.967 \times 1.5 + 1.311 = 4.262$ ksi

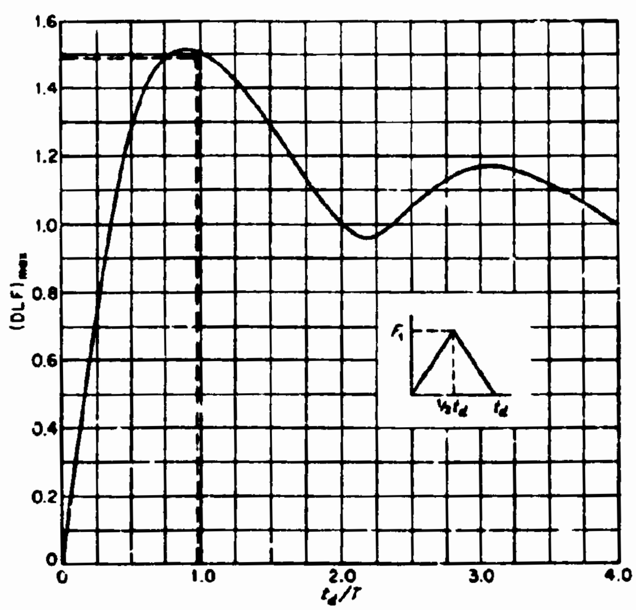

DLF from (5.22)

Note: 1 in. = 25.4 mm; 1 ft = 0.3048 m; 1 kip = 4.448 kN; 1 ft-kip = 1.356 kN-m; 1 ksi = 6.894 MPa; 1 lbf-sec^2/ft = 14.589 kg.

REFERENCES - CHAPTER 5

5.1 Norris, Wilbur and Utku, Elementary Structural Analysis, 3rd ed., New York, McGraw-Hill, 1976.

5.2 Gere, J. M., "Moment Distribution", Van Nostrand Reinhold, New York, 1963.

5.3 Conner, J., Analysis of Structural Member Systems, New York, Ronald, 1976.

5.4 Roark, R., Formulas for Stress and Strain, 5th ed., New York, McGraw-Hill, 1975. (See also 4th edition, 1965, for certain additional formulas.)

5.5 American Institute of Steel Construction, Manual of Steel Construction, 8th ed., Chicago, 1980.

5.6 Kleinlogel, A., Rigid Frame Formulas, 11th ed., New York, Unger, 1952.

5.7 Lentovich, V., Frames and Arches, New York, McGraw-Hill, 1959.

5.8. Timoshenko, S., Strength of Materials, Part I, 3rd ed., New York, Van Nostrand, 1955.

5.9 Riddell, M., and O'Toole, J., "Significant Properties of Plastics for Design", ASCE Special Publication - Structural Plastics Properties and Possibilities, Symposium on Structural Plastics, Louisville, 1969.

5.10 McGuire, W., Steel Structures, Englewood, New Jersey, Prentice-Hall, 1968.

5.11 Bethlehem Steel Co., "Torsion Analysis of Rolled Steel Sections."

5.12 Peterson, R., Stress Concentration Factors, New York, John Wiley, 1974.

5.13 Griffiths, A. A., Proc. of Int. Congr. Appl. Mech. (55) (1924).

5.14 Inglis, C., Trans. Inst. Naval Archit. (55), 219 (1913).

5.15 Irwin, G. R., Encyclopedia of Physics (6) (1958).

5.16 Rolfe, S. T. and Barsom, J. M., Fracture and Fatigue Control in Structures, Applications of Fracture Mechanics, Prentice-Hall, Englewood Cliffs, New Jersey, 1977.

5.17 Corten, H. T., "Fracture Mechanics of Composites", Chapter 9, in Volume 7, Fracture of Non-Metals and Composites, of series Fracture ed. by H. Liebowitz, Academic Press, N.Y., 1972.

5.18 Smith, G., Green A.K., and Bowyer, W. H., "The Fracture Toughness of Glass Fabric Reinforced Polyester Resins", Chapter 16 in Fracture Mechanics in Engineering Practice, ed. by P. Stanley, Applied Science Publishers, London, 1977.

5.19 Hertzberg, R. W., Deformation and Fracture Mechanics of Engineering Materials, Wiley, New York, 1976.

5.20 Margolis, R. D., Dunlap, R. W., and Markovitz, H., "Fracture Toughness Testing of Glassy Plastics", in STP 601, Cracks and Fracture, ASTM, 1976.

5.21 Berry, J. P., "Fracture of Polymeric Glasses", Chapter 2 in Volume 7, Fracture of Non-Metals and Composites, of series Fracture ed. by H. Liebowitz, Academic Press, N.Y., 1972.

5.22 Biggs, J. M., Introduction to Structural Dynamics, McGraw-Hill, 1964.

5.23 Agarwal, B. D. and Broutman, L. J., Analysis and Performance of Fiber Composites, Wiley, New York, 1980.

5.24 Saba, D. L., "Stress Concentration Around Holes in Laminated Fibrous Composites", Masters Thesis NPS-57 Bt75061, Naval Postgraduate School, Montery, CA, 1975.

5.25 Barker, R. M., Dana, J. R., Pryor, C. W., "Stress Concentrations Near Holes in Laminates", ASCE Journal of the Engineering Mechanics Division, June, 1974.

5.26 Pipes, R. B., Wetherhold, R. C., and Gillespie, J. W., Jr., "Notched Strength of Composite Materials" Journ. of Composite Materials, Vol. 13, Apr. 1979, Technomic Publishing.

5.27 Albrecht, F., and Yamada, K., "Rapid Calculation of Stress Intensity Factors", ASCE Journal of the Structural Division, February, 1977.

ASCE Structural Plastics Manual

CHAPTER 6 – FLAT PLATES AND MEMBRANES

By Frank J. Heger

TABLE OF CONTENTS

NOTATION - Chapter 6

a	long dimension of rectangular plate; diameter of circular plate
a_o	diameter of interior concentric opening in circular plate
a_i	width of support for diaphragm plate
$\bar{a}$	cross sectional area of unit width cross section
A	cross sectional area
$\bar{A}_{ij}$	in-plane stiffness of plate along axis i in direction j
b	short dimension of rectangular plate, except where noted for wide plate
b_{ij}	stiffness coefficient as defined by Eqs. along axis i in direction j
b_e	dimension of effective width of plate
c	maximum unbraced length
C_b	correction coefficient for modifying buckling coefficient for various effects of biaxial stress and edge restraint
d	distance from neutral axis to point of load application, affecting lateral stability of beam
D	flexural rigidity
D_{11}, D_{22}, or D_r	flexural rigidity in 1, 2, and radial directions
D_{ij}	flexural rigidity of plate along material axis i in direction j
D_o	flexural twisting constant as defined by Eq. 6.6
e	strain
e_x, e_y	strain in x and y directions
e_T	strain resulting from restraint of deformation due to temperature change
E, E_o	modulus of elasticity
E_v	viscoelastic modulus of elasticity (Chapters 2 and 3)
E_{11}, E_{22}, E_r, or E_θ	modulus of elasticity in 1, 2, radial, and circumferential directions

f, f_i	sag; initial sag
f_n, f_1, f_2	frequency of natural vibration in n^{th} 1^{st}, and 2^{nd} modes
F	area of vibrating membrane
g	acceleration of gravity
G	modulus of shearing rigidity
G_{12}	modulus of shearing rigidity in plane of directions 1 and 2
i	moment of inertia of unit width cross section
I	moment of inertia of cross section
k	buckling coefficient; as subscript, indicates layer number in laminated plate
k_o	coefficient for adjusting plate bending results when ν varies from 0.3. $k_o = 1.0$ when $\nu = 0.3$
k_1, k_2, k_3, k_4, k_5, k_6, k_7	coefficients in plate bending equations obtained from graphical plots of plate bending solutions
K_a, K_b, K_t	stiffness coefficient for axial, rotational and torsional edge restraints
ℓ_b	wave length of buckle
$\bar{m}$	magnification factor for deflection and moment for members subject to combined axial load and bending
m	integer
M	bending moment per unit width
M_c, M_e	maximum bending moment at center and at edge of plate
M_{cr}	bending moment which causes lateral buckling
M_o, M_a	bending moment without effect of axial load and with effect of axial load.
M_u	ultimate bending moment
M_x, M_y	bending moment in x and y directions
n	integral exponent, mode number, or integer
N	axial force per unit width

N_x, N_y	axial forces in x and y directions
N_{xy}	shear for in xy plane
N_c	axial force at edge of plate
N_h, N_v	horizontal and vertical component of axial force
N_{he}, N_{ve}	horizontal and vertical components of axial force at edge
N_{hi}, N_{hq}	horizontal component of axial force at edge, due to initial tension, and due to lateral load q
N_T	axial force due to restraint of deformation from temperature change
N_{xc}	critical buckling axial force in x direction
p_x, p_o	applied axial force per unit area
P	concentrated load
P_u	ultimate axial compression
Q	shear force per unit width
Q_a, Q_b	maximum transverse shear force on edges with lengths a and b
Q_{xz}, Q_{yz}	shear force in z direction on planes perpendicular to x and y axes
q	uniformly distributed lateral pressure
R	reaction at corner of plate
S	section modulus of cross section
V	edge reaction per unit width
V_a, V_b	maximum edge reaction on edges with lengths a and b
$\Sigma V_a, \Sigma V_b$	sum of edge reactions on edges with lengths a and b
t	thickness of plate
t_o	thickness of central portion of plate
t_k	thickness of layer, k
ΔT	change in temperature
w	deflection normal to plate

w_x, w_c	deflection at distance x from support, and at center
w_o, w_a	deflection without effect of axial load, and with effect of axial load
z_k	distance from centroid of plate to centroid of layer k
$\bar{\alpha}$	coefficient given by Eq. 6.40
α	coefficient of thermal expansion
δ_h, δ_{hi}	axial deflection of membrane edge; edge deflection caused by initial pretension
ϵ	axial strain
γ_{xy}	shear strain in x-y plane
$\bar{\gamma}$	density
λ, λ_o	dimensional ratios
λ_1, λ_2, λ_3	stiffness ratios in orthotropic plate analysis
ν, ν_1, ν_2	Poisson's ratio for isotropic materials; Poisson's ratio for materials 1 and 2
ν_{12}, ν_{21}, ν_θ, ν_r	Poisson's ratio for stress in materials directions 1 and 2 for rectangular plates and circumferential and radial directions for circular plates, orthotropic materials
ϕ_n, ϕ_1, ϕ_2	coefficients for modes n in equation for natural frequency
ψ_k	angle of principal axis of materials stiffness with plate axis, x, for layer k
ρ	mass
σ	normal stress
σ_a	axial stress
σ_b	bending stress
σ_e, σ_c, σ_d	maximum axial (in-plane) stress at edge, center, and diagonal of rectangular plate; maximum axial stress at edge and at center of circular membrane
σ_E, σ_C, σ_D	maximum combined axial and bending stress at edge, center, and diagonal of rectangular plate
σ_{eb}, σ_{cb}	maximum bending stress at edge and center of rectangular plate

σ_{mr}, $\sigma_{m\theta}$	maximum axial (in-plane) stress in radial and circumferential directions in circular plate
σ_{Tr}, $\sigma_{T\theta}$	maximum total stress in radial and circumferential directions in circular plate
σ_{ua}, σ_{ub}	ultimate axial and bending strengths for use in design (i.e., reduced for effects of time, environmental degradation and materials variation)
σ_x, σ_y	stress in directions x and y
σ_{xa}, σ_{ya}	stress in x and y directions due to axial force only
σ_{xb}, σ_{yb}	stress in x and y directions due to bending only; also used for in-plane bending stress where indicated in text
σ_{xc}, σ_{rc}, σ_{nc}	critical buckling stress in x direction on rectangular plate, in radial direction on circular plate, as shown in Fig. 6-42 on triangular plates
σ_{xcc}, σ_{xcv}	critical buckling stress corrected for biaxial stress, for creep
σ_{xc}^{o}	critical buckling axial stress without shear stress
σ_{xbc}^{o}	critical buckling in plane bending stress without shear stress
σ_{xe}	effective elastic axial stress in x direction - Fig. 6-34
σ_{xu}	ultimate stress in x direction
τ_{LT}	reduction factor for creep buckling
τ	shear stress
τ_{xy}	shear stress in x-y plane
τ_{xyc}	critical buckling shear stress in x-y plane, rectangular plate
τ_{xyc}^{o}	critical buckling shear stress without normal stress
τ_{xz}, τ_{yz}	shear stress in z direction
θ	angle of stress with x axis
θ_e	rotation at edge of plate

6. FLAT PLATES AND MEMBRANES

F. J. Heger

6.1 INTRODUCTION

Plastics structural components frequently contain elements that may be idealized as thin flat plates or membranes subject to loads perpendicular to their surfaces and to stress resultants within their planes. In a few cases, the entire component is a thin plate such as acrylic plastic window panels in separate support frames. In most cases, however, the thin plate element is a portion of a molded or formed unit that contains integral side panels, edge ribs, intermediate ribs, and the like. A very great variety of different configurations is possible.

The first step in the structural design process described in Chapter 4 is structural idealization to facilitate preliminary analysis and proportioning of a component or its key parts. Frequently, such idealization involves consideration of the individual flat plate elements that together comprise a structural component. Obviously, approximations of shape, edge support, and constants that define materials behavior are required.

The purpose of this Chapter is to assist the designer to analyze and proportion individual flat plate or membrane elements based on load, shape, edge support, and materials characteristics that commonly occur in designing plastics structures. Plate structural behavior is described and methods are presented for analyzing and designing plate components. Many design aids are presented for practical determination of maximum stresses and deflections and for evaluating buckling strength under in-plane compression. It is not the purpose of the Chapter to present the underlying theory. This is available in many of the source references given herein and in Chapter 4.

When design problems require more comprehensive solutions, solutions involving variables in shape of plate, load distribution, edge support conditions or variations in materials constants, or consideration of interactive effects between contiguous elements that cannot be bracketed by available plate idealizations, computer solutions are readily available to determine stresses and buckling strength. These usually involve either linear or non-linear finite element analysis. In recent years, finite element analysis methods and programs have become practical tools; frequently, these methods can be used in day-to-day design situations that were heretofore considered beyond the realm of practical solution. Since the details of such analyses are beyond the scope of this Manual, their use is not covered in this Chapter.

Predominant considerations in the structural behavior of thin flat plates are bending and deflection under lateral loads (normal to their plane), in-plane diaphragm stresses caused by edge loading from adjacent components, and stability (resistance to buckling) under various in-plane compression stresses. These topics are the principal subjects of this Chapter. In addition, stress analysis of unidirectional, rectangular, and circular flat membranes is covered briefly. Such elements are too thin and flexible to resist load in bending, but if proper edge support is provided, they can support load by tensile membrane stresses that develop when they deflect. Finally, natural vibration frequencies of plates and membranes are briefly discussed.

Definition of Thin Plate

This Chapter is devoted to thin plates, defined as flat structures of uniform thickness whose minimum span dimension exceeds 4 times the plate thickness, and whose minimum dimension perpendicular to this span is also at least 4 times thickness.

Limitations of Material Characteristics

Material characteristics may be uniform through the thickness (homogeneous) or they may be layered in a balanced symmetrical distribution of layers with respect to the midplane. They may be uniform in all directions (planar isotropic), or they may vary with respect to two principal perpendicular directions (planar orthotropic). In all cases, materials are assumed to behave elastically, or visco-elastically, as described in Chapters 2 and 3.

Design Considerations for Plastics

Plastic plates frequently have characteristics of behavior that offer opportunities for design optimization not available with conventional metals. Also, non-conventional aspects of their behavior often must be considered in design to avoid premature failure or unsatisfactory performance.

The following characteristics of plastics deserve special consideration when designing plate structures or components:

- Time-temperature dependent effects result in significant reductions in stiffness and in strength under long-term load and/or elevated temperature, as explained in Chapters 2 and 3.

- Thin plates often deflect in excess of half their thickness and resist a significant portion of applied lateral loads by developing in-plane or membrane stress resultants. This requires consideration of non-linear or large deflection behavior. This is particularly significant, and usually beneficial, in plates that develop restraint of in-plane edge translation.

- Stiffness and strength properties sometimes vary with direction of plate axes. Such directional characteristics of a plate material require analyses of stresses and stability that take these anisotropic properties into account. A much simplified anisotropic analysis, termed "specially orthotropic" plate analysis, is used for the following commonly occurring special materials and stress conditions:

  (1) Thin plate material has constant elastic or viscoelastic properties through its thickness, or is made up of distinct layers of materials of constant thickness and properties,

  (2) elastic properties of the constant thickness plate, or its layers, have maximum and minimum values coinciding with the two orthogonal (perpendicular) axes of symmetry of the plate,

  (3) the plate axes of symmetry are also the principal axes of stress.

  Special orthotropic plate theory is sometimes used, even where its limitations are not strictly met, as a practical approximation of the expected behavior of anisotropic plastics.

- Composites, which are mixtures of resin binder and fibrous reinforcement, have unique characteristics that, in the present state of the art, usually cannot be determined quantitatively from the individual characteristics of the resin and fiber components. In practical design, the composite is considered as a unique material with its own elastic and strength properties.

- Some layered composites are fabricated from plies having particular directional characteristics which are usually orthotropic. Analysis of plate stresses and deflections with such materials typically requires a laminated plate theory. Sometimes, however, behavior of layered materials is approximated using average elastic properties determined from testing the overall laminate. In this approach, "average stresses" are calculated from conventional "uniform thickness" plate theory, and these are compared to "average strengths," determined from test loads and average "uniform thickness" section properties.

- Most plastics and composites do not exhibit the ductile stress-strain behavior prior to rupture which is characteristic of metals and properly designed reinforced concrete. Because of their relatively low modulus of elasticity, and their usually high ratio of strength to modulus, these plastics and composites often develop relatively high strains at failure; however, they do not enjoy the beneficial redistribution of stress concentrations and other indeterminate effects that are characteristic of ductile metal structures. This non-ductile behavior requires accurate analysis of stresses resulting from restraints and environmental effects that are often ignored with metal structures. Thus, it is frequently necessary to use more accurate methods to analyze effects of loads, restraints, moisture and temperature gradients, and similar stress-producing phenomena when designing plastic and composite plate components, compared to design practice with metal plates.

In many practical design situations involving plate components, extensions or modification of conventional methods for analysis and design of metal plates are required to account for the above characteristics of plastics and composites. Significant results of the extended and modified theories are presented in the following sections to assist the designer of plastics plates to understand their behavior and to develop rational plate designs for commonly occurring component types and arrangements. Other results, particularly the equations for plate buckling, are presented in this Chapter for further use in Chapter 7 covering behavior and design of assemblies of this plates that are used as beams, columns, and ribbed flat panels.

Parameters Which Define Structural Performance

Generally, the design of plate components involves consideration of the following parameters which define structural performance:

1. **Deflections, bending moment, shear and in-plane axial stress resultants, and support reactions in laterally loaded plates.** Laterally loaded plates are plates with various shapes, edge support and restraint conditions, and load distributions, with load acting perpendicular to the plane of the

plate. Bending moments cause flexural stresses and strains that are assumed to vary linearly across the plate thickness for plates of a homogeneous material. For plates of non-homogeneous materials, such as laminated plates, strains are assumed to vary linearly across the thickness and stresses are related to strains by elastic stiffness constants for each layer of materials. In-plane axial stress resultants (membrane stresses) are significant in laterally loaded plates whose edges are held against in-plane translation, whenever deflections exceed about half the plate thickness. They must be added (algebraically) to flexural stresses. Transverse shear stresses can be significant in materials with low shear strength, in layered materials with low interlaminar strength, and in low strength "core" layers which are sandwiched between much stiffer facing materials.

2. **In-plane normal and shear stresses in diaphragm plates.** Diaphragm plates are plates with various shapes, and edge support conditions which are loaded within their own plane. These plates frequently transmit their loads to supports by in-plane bending and shear, thus, they behave as narrow deep beams. Frequently, their proportions of width-to-span require consideration of shear, bending, and transverse strains using methods of analysis termed "deep beam theory".

3. **Buckling resistance of plates subject to in-plane compressive stress.** Stress distributions of greatest interest in rectangular plates include uniaxially uniformly compressed plates, uniaxially compressed plates with linearly varying stress, diagonally compressed plates (resulting from in-plane shear), and biaxially uniformly compressed plates. The first three cases represent:

   - compressed flanges of beams, columns, and panels;
   - web bending in beams;
   - web shear in beams or facing shear in panels.

4. **Natural frequency of free vibration.** Dynamically applied loads cause responses which are greatly influenced by the natural frequency of free vibration of plates. Generally, the lowest mode is of greatest interest, but knowledge of higher modes is sometimes also necessary to evaluate dynamic behavior.

In order to evaluate the above types of structural performance, it is necessary to determine plate stiffness. Stiffness is a function of the materials properties: modulus of elasticity and Poisson's ratio, the materials directional characteristics, and the material variation through thickness (homogeneous or layered construction). It is also related to various geometrical and support parameters. Stiffness relations for plate cross sections are presented in the next Section for plates of homogeneous materials and in Section 6.7 for laminated plates.

6.2 PLATE CROSS SECTION STIFFNESS

Plate cross section stiffness is a function of materials properties and cross sectional geometry. In the equations presented in this Chapter, materials properties are assumed to be elastic and to be either isotropic or orthotropic. These terms are defined in Section 2.5, Chapter 2, with further explanations in Section 3.5 and Table 3-4 of Chapter 3 and Section 4.9 of Chapter 4.

Elastic constants define the relationship of stress to strain in a material that exhibits elastic behavior. Pseudo-elastic constants are used to relate stress and strain approximately for certain defined conditions with viscoelastic materials which exhibit time-dependent relationships between stress and strain. See Sections 3.3 and 3.5 for a discussion of the materials elastic stiffness constant: modulus of elasticity, E, and Poisson's ratio, ν. Methods for estimating elastic constants for viscoelastic plastics materials subject to various durations of loading are also given in these Sections. Elastic constants for short-term loading of some representative plastics materials are given in Section 1.5, Table 1-1, and Section 1.9, Tables 1-5 through 1-9.

Stiffness Constants for Isotropic Plates

Stiffness constants relate load to deformation. The axial stiffness constant, A, is a measure of the axial force required to produce a unit axial deformation in a plate of unit length. The flexural stiffness constant, D, is a measure of the lateral force required to produce a unit bending deflection on a plate of unit span. These stiffness constants are determined from elastic constants that define stress-strain behavior and cross sectional properties that relate force to stress.

Stres-strain relationships must account for bi-directional interactions when thin plates are stressed. For plate structures, stressed in direction x, stiffness is increased, compared to bars of similar sectional properties, because of the restraint of Poisson's deformation in the perpendicular direction y. This behavior requires stiffness and stress-strain equations for plates, that differ from equations for stiffness of narrow beams. The following stress-strain relations apply for isotropic homogeneous plates:

$$\sigma_x = \frac{E}{1 - \nu^2} e_x + \frac{\nu E}{1 - \nu^2} e_y \qquad \text{Eq. 6.1a}$$

$$\sigma_y = \frac{\nu E}{1 - \nu^2} e_x + \frac{E}{1 - \nu^2} e_y \qquad \text{Eq. 6.1b}$$

$$\tau_{xy} = G \gamma_{xy} = \frac{E}{2(1 + \nu)} \gamma_{xy} \qquad \text{Eq. 6.1c}$$

Thus, for isotropic materials, two basic independent materials constants, E, modulus of elasticity, and ν, Poisson's ratio, define stress-strain relations.

Based on the above stress-strain relations, the materials and cross sectional stiffness properties are defined in Table 6-1, part a, for plates of isotropic materials with the same cross section in all directions. The stiffness properties are given for both the more general case of non-homogeneous cross sections for later use in Chapter 8 on sandwich plates, and for the case of plates having uniform homogeneous thickness treated in this Chapter. Stiffness properties specifically organized for use with layered or laminated plates are presented in Section 6.7 of this Chapter.

Stiffness Constants for Specially Orthotropic Plates

As defined previously, the term orthotropic refers to plates whose elastic material constants have maximum and minimum values in two perpendicular directions. The orthotropic plates treated here are further limited to the special case where the two principal axes of materials properties, 1 and 2, coincide with the two principal plate axes, x and y, as shown in Fig. 6-1. These plates are termed herein "specially orthotropic."

Table 6-1

Stiffness Properties of Isotropic and Specially Orthotropic Plate Cross Sections (6.1, 6.2)

Stiffness Property			Non-homogeneous	Homogeneous, uniform thickness	Eq. No.
a. Planar isotropic plates					
In-plane axial,	$\bar{A}$	=	$\frac{E\bar{a}}{(1 - \nu^2)}$	$\frac{Et}{(1 - \nu^2)}$	6.2a
In-plane shear,	$\bar{A}_{xy}$	=	$G\bar{a} = \frac{E\bar{a}}{2(1+\nu)}$	$Gt = \frac{Et}{2(1+\nu)}$	6.2b
Transverse bending,	D	=	$\frac{EI}{(1 - \nu^2)}$	$\frac{Et^3}{12(1 - \nu^2)}$	6.3a
Transverse twisting,	D_o	=	$\frac{EI}{(1 - \nu^2)}$	$\frac{Et^3}{12(1 - \nu^2)}$	6.3b
b. Specially orthotropic plates					
In-plane axial,	A_{11}	=	$\frac{E_{11}\bar{a}_x}{1 - \nu_{12}\nu_{21}}$	$\frac{E_{11}t}{1 - \nu_{12}\nu_{21}}$	6.5a
In-plane axial,	A_{22}	=	$\frac{E_{22}\bar{a}_y}{1 - \nu_{12}\nu_{21}}$	$\frac{E_{22}t}{1 - \nu_{12}\nu_{21}}$	6.5b
In-plane axial,	$A_{12} = A_{21}$	=	$\frac{\nu_{21}E_{11}\bar{a}_x}{1 - \nu_{12}\nu_{21}}$	$\frac{\nu_{21}E_{11}t}{1 - \nu_{12}\nu_{21}}$	6.5c
In-plane axial,	A'_{12}	=	$G_{12}\sqrt{\bar{a}_x\bar{a}_y}$	$G_{12}t$	6.5d
Flexural,	D_{11}	=	$\frac{E_{11}I_x}{1 - \nu_{12}\nu_{21}}$	$\frac{E_{11}t^3}{12(1 - \nu_{12}\nu_{21})}$	6.6a
Flexural,	D_{22}	=	$\frac{E_{22}I_y}{1 - \nu_{12}\nu_{21}}$	$\frac{E_{22}t^3}{12(1 - \nu_{12}\nu_{21})}$	6.6b
Flexural,	$D_{12} = D_{21}$	=	$\frac{\nu_{21}E_{11}I_x}{1 - \nu_{12}\nu_{21}}$	$\frac{\nu_{21}E_{11}t^3}{12(1 - \nu_{12}\nu_{21})}$	6.6c
Flexural,	D'_{12}	=	$G_{12}\sqrt{I_x I_y}$	$\frac{G_{12}t^3}{12}$	6.6d

The twisting parameter for orthotropic plates is:

$$D_o = D_{12} + 2D'_{12} \qquad 6.6e$$

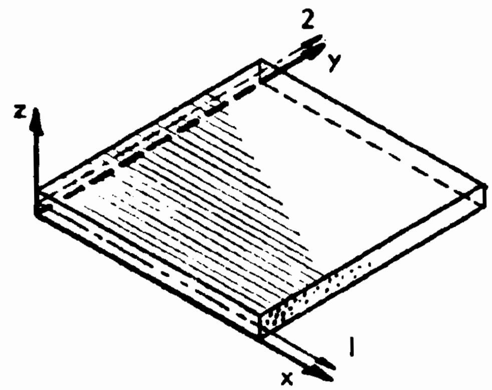

Fig. 6-1. ORIENTATION OF AXES OF PRINCIPAL STRESS AND PRINCIPAL MATERIALS STIFFNESS PROPERTIES FOR ORTHOTROPIC PLATES

The elastic stress-strain relations for "specially orthotropic" plates are (6.2):

$$\sigma_x = \frac{E_{11}\, e_x}{1 - \nu_{12}\nu_{21}} + \frac{\nu_{12} E_{22}\, e_y}{1 - \nu_{12}\nu_{21}} \qquad \text{Eq 6.4a}$$

$$\sigma_y = \frac{\nu_{21} E_{11}\, e_x}{1 - \nu_{12}\nu_{21}} + \frac{E_{22}\, e_y}{1 - \nu_{12}\nu_{21}} \qquad \text{Eq. 6.4b}$$

$$\tau_{xy} = G_{12}\, \gamma_{xy} \qquad \text{Eq. 6.4c}$$

$$\text{also } \nu_{12} = \nu_{21}\frac{E_{11}}{E_{22}} \qquad \text{Eq. 6.4d}$$

Eqs. 6.4 show that for "specially orthotropic" plates, four basic independent materials constants: E_{11}, E_{22}, moduli of elasticity in the two principal directions of orthotropicity, G_{12}, modulus of in-plane shear rigidity, and ν_{12}, Poisson's ratio for stress in direction 1, or ν_{21}, Poisson's ratio for stress in direction 2, define stress-strain relations. The two Poisson's ratios are related as given by Eq. 6.4d.

Based on the above stress-strain relations, the in-plane and flexural stiffness constants for specially orthotropic plates are defined in Table 6-1, Part b.

Some thin plates are made up of several layers of materials having different elastic and directional properties. This is characteristic of many composites. Overall flexural stiffnesses may be isotropic, quasi-isotropic, or "specially orthotropic," and may readily be determined using the elastic theory of laminated plates. See Section 6.7 in this Chapter for modifications to the above stiffness relations to cover the cases of isotropic and balanced symmetrical specially orthotropic laminated plates. Analysis of such plates is facilitated if stiffness relations are expressed in matrix notation.

Stiffness Constants for Generally Orthotropic Plates

In the special orthotropic plate case given above, the principal orthotropic axes of the material, 1 and 2, coincide with the principal plate axes, x and y (Fig. 6-1). Stiffness coefficients D_{ij} and A_{ij} are related to the principal plate axes, x and y, as given in Equations 6.4 and 6.5. See Appendix B in (6.1) for similar stiffness relations for the more general orthotropic case, where the principal axes of the material stiffness do not coincide with the plate axes. This reference also covers the case of laminated orthotropic plates that are fabricated from layers whose principal axes of materials stiffness, 1 and 2, are at an angle with the plate axes, x and y.

Application of Stiffness Relations

In-plane axial stiffenss constants are required for determining:

- deflections, stress resultants, and buckling resistance of plates with in-plane restraint of edge translation, where "large deflections" develop membrane action;
- stress resultants in "in-plane" loaded orthotropic plates;
- buckling resistance of orthotropic plates.

Flexural stiffness constants are required for determining:

- deflections of plates,

- stress resultants in plates with in-plane restraint of edge translation, where "large deflections" develop membrane action,
- stress resultants in laterally loaded orthotropic plates,
- buckling resistance of plates subject to in-plane compression.

Effect of Elastic Constants on Flexural Behavior

Both E and ν are important parameters in determining deflection of isotropic plates. Obviously they both influence all aspects of the behavior of orthotropic plates.

Bending moments and flexural stresses due to lateral loads on isotropic plates analyzed with small deflection theory do not vary with E, but they do vary with Poisson's ratio, ν. "Small deflection" isotropic plate theory solutions available in the literature for various shapes and load distributions are given for specific values of ν. Significant changes in stress may occur for other values of ν. Some approximations for estimating the effect of variations in ν are given in the next Section.

6.3 ISOTROPIC PLATES UNDER LATERAL LOAD

Plate elements frequently must be designed for resistance to lateral load. Plate thickness must be proportioned to provide the necessary load resistance without excessive stress, strain, or deflection. Plate stresses, strength and deflection depend upon the following principal variables:

- Materials properties: stress or strain limits, elastic constants, directional characteristics (isotropic or orthotropic included in this Chapter), layered construction.
- Thickness. Only "thin" plates of uniform thickness are considered in this Chapter.
- In-plane shape and dimensions between edges.
- Arrangement and location of supports.
- Restraints provided at supports: restraint of edge translation normal to plane of plate, edge rotation, and edge translation in plane of plate.
- Intensity and distribution of lateral loading.
- In-plane loads: intensity and whether tension or compression.
- Non-load effects: thermal stresses, stresses resulting from shrinkage and thermal and moisture gradients, stress caused by support deflections, built-in stresses caused by thermal effects in manufacture of laminated plates.

Structural Behavior

Lateral loads produce both flexural and membrane stresses in thin plates. These effects are shown schematically in Fig. 6-2. Membrane stresses become significant when edges are restrained from translating in the plane of the plate and when maximum deflection exceeds about half the thickness of the plate. Membrane stresses arise even when edges are not externally restrained from translating in the plane of the plate, but these do not become significant until the plate deflects enough so that it begins to behave like a shallow shell.

Solutions that take into account membrane stresses are often termed "large deflection" solutions. Large deflection effects frequently are significant in

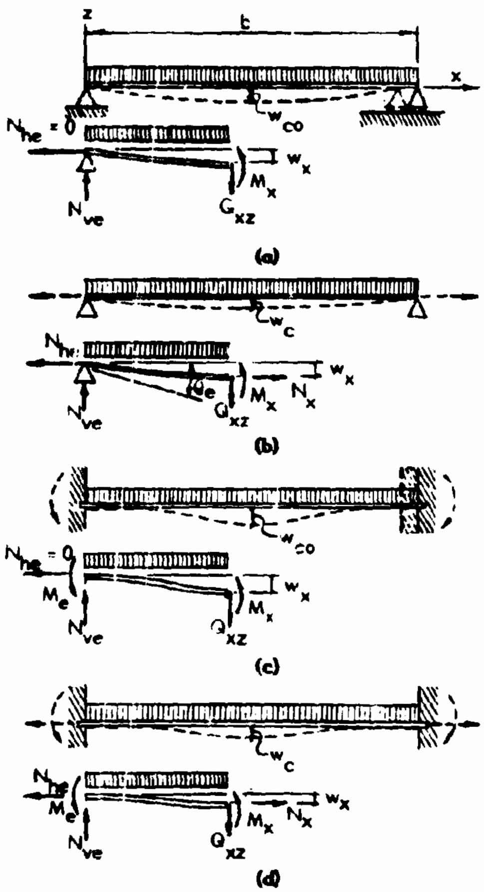

- Simply supported edges
- No restraint of in-plane translation
- Applied load resisted by shear and bending
- In-plane stresses neglected

- Simply supported edges
- Edges held to prevent in-plane translation
- Applied load resisted by bending moments, M_x, shear, Q_x, and membrane forces, N_x
- For pure membrane, $M_x = 0$, $Q_x = 0$

- Rotationally fixed edges
- No restraint of in-plane translation
- Applied load resisted by shear and bending
- In-plane stresses neglected

- Rotationally fixed edges
- Edges held to prevent in-plane translation
- Applied load resisted by bending moments, M_x, shear, Q_x, and membrane forces, N_x

Fig. 6-2 LATERALLY LOADED PLATES AND MEMBRANES WITH TYPICAL IDEALIZED LOAD AND SUPPORT ARRANGEMENTS

plastic plates because elastic moduli of plastics and many composites are much lower than elastic moduli of metals. Thus, deflections tend to be much larger in plastic plates than in comparable metal plates, and very often with plastics, deflection exceeds half the thickness. Furthermore, the membrane stresses that result from large deflection behavior usually provide a very beneficial stiffening of the plate, especially where the plate edges are held against in-plane translation. In this case, the plate resistance to effects of lateral load is non-linear; increases in load produce beneficial changes in geometry with increasing plate deflection so that stresses increase at a slower rate than load. In view of this, it is often desirable to employ "large deflection theory" in designing plastics plates.

Available Solutions for Isotropic Plates

Closed form solutions for stresses and deflections in plates under lateral load have been developed for a number of regular shapes and loadings. The state of the art is very well presented in (6.2). Most solutions are obtained for the simpler "small deflection theory" in which membrane resistance is neglected. "Large deflection" solutions are also given in (6.2) and the conditions which require consideration of the more complex "large deflection theory" are discussed.

Approximate analysis methods based on various techniques of numerical analysis have frequently been employed to obtain stresses and deflections in plates with a large variety of shapes, edge conditions, and load distributions. Older methods, such as finite differences and various grid analogies, and new finite element computer analyses have been widely used. Formulas and coefficients for deflections and stress resultants for a large number of different plate shapes, edge support conditions, and lateral load distributions are available in various published reference books.

Tabulations of solutions for plate bending moments and deflections for various conditions of load on rectangular and/or circular plates with several conditions of edge restraint are given in (6.2), (6.3), (6.4), (6.5), (6.6), (6.21), (6.22), (6.23), (6.24), (6.25), (6.26) and (6.27). See (6.3) for triangular plate solutions and (6.23) for skew plate solutions. In some cases, the tabulated solutions – (6.2), (6.3), (6.4), (6.5), (6.6), (6.21), (6.27) – include the effect of geometry changes associated with large deflections. Only a few of the tabulated solutions also include coefficients for shear and/or reactions. Solutions for some of the most common and significant cases are given later in this Section.

For the most part, tabulated solutions, based on small deflection theory, provide coefficients for determining maximum bending moment, shear, support reaction and corner reaction of a particular type or direction, and deflection at a particular location. The "small deflection" solutions typically provide the following relations between the above structural parameters and shape of plate, load, span dimension, and cross sectional stiffness:

$$M = k_1 q b^2$$

$$Q = k_2 q b$$

$$V = k_3 q b \qquad \text{Eqs. 6.7}$$

$$R = k_4 q b^2$$

$$w = k_5 \frac{q b^4}{D}$$

In some cases, flexural stresses are directly presented by dividing bending moment by section modulus. See Eq. 6.10.

The constants, k, depend on the shape of the plate and the location and direction of a structural parameter such as bending moment. The span, b, usually is the smaller span dimension for rectangular plates, and the radius or diameter for circular plates. The load, q, is usually uniformly distributed lateral pressure. However, some tabulated solutions cover concentrated loads or hydrostatic pressure distribution. Typical solutions for moments and stress resultants are usually valid only for a specific value of Poisson's ratio, ν. The cross section flexural stiffness, D, is needed for deflection calculations.

Solutions which include large deflection behavior require more complex relationships of variables as is illustrated later in this Section.

Adjustments in Tabular Solutions for Different Poisson's Ratios

Solutions given in typical tables for bending moments include Poissons Ratio, ν, as a dependent variable. Tabulated bending moment coefficients are valid only for particular values of ν. For isotropic materials, adjustments can be made to moments (small deflection theory) given for a particular Poisson's Ratio, ν_1, to obtain moments for a material with another Poisson's ratio, ν_2, with the following equations (6.3):

$$(M_x)_2 = \frac{1}{1-\nu_1^2}\left[(1-\nu_1\ \nu_2)(M_x)_1 + (\nu_2-\nu_1)(M_y)_1\right] \qquad \text{Eq. 6.8a}$$

$$(M_y)_2 = \frac{1}{1-\nu_1^2}\left[(\nu_2-\nu_1)(M_x)_1 + (1-\nu_1\ \nu_2)(M_y)_1\right] \qquad \text{Eq. 6.8b}$$

where the subscript 1 denotes values obtained in a tabulated solution for Poisson's Ratio, ν_1, and the subscript 2 denotes adjusted values for a non-tabulated Poisson's Ratio, ν_2.

Adjustment of deflection coefficients (small deflection theory) are not required with variations in ν. See (6.3) for effects of variations in ν on edge reactions, corner reactions, and twist.

Deflections and Stresses for Common Load Cases

Rectangular plates: Nomenclature, direction, and locations for maximum plate stresses shown in later figures are given in Fig. 6-3.

Midspan deflections in thin flat rectangular isotropic plates under uniformly distributed normal (lateral) pressure, with several edge support conditions, are given in Figs. 6-4, 6-5, and 6-10 (6.4).

Maximum stresses in thin flat rectangular isotropic plates with uniformly distributed normal (lateral) pressure, with several edge support conditions, are given in Figs. 6-6 to 6-10 (6.4).

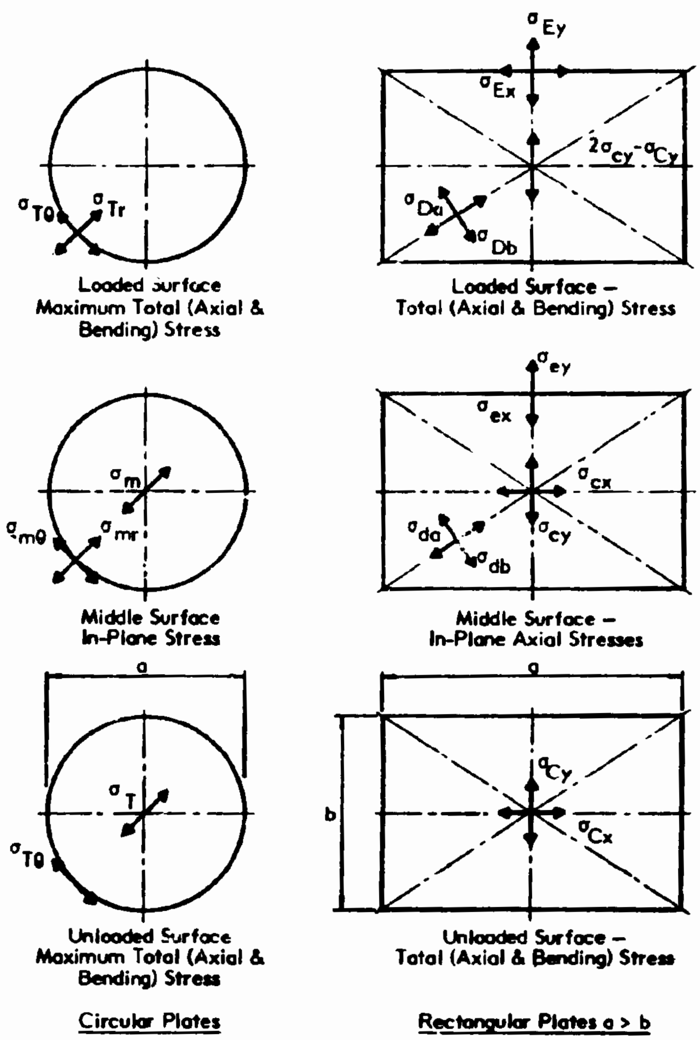

Fig. 6-3 NOTATION FOR MAXIMUM TOTAL STRESSES AND IN-PLANE STRESSES IN PLATE SOLUTIONS GIVEN IN FIGS. 6-4 TO 6-10, 6-13 TO 6-14

NOTE: These figures are adapted from graphs in "Engineering Sciences Data, Aeronautical Series, Structures Sub-Series Volume 5" (6A) by Permission of "Engineering Sciences Data Unit Ltd." London.

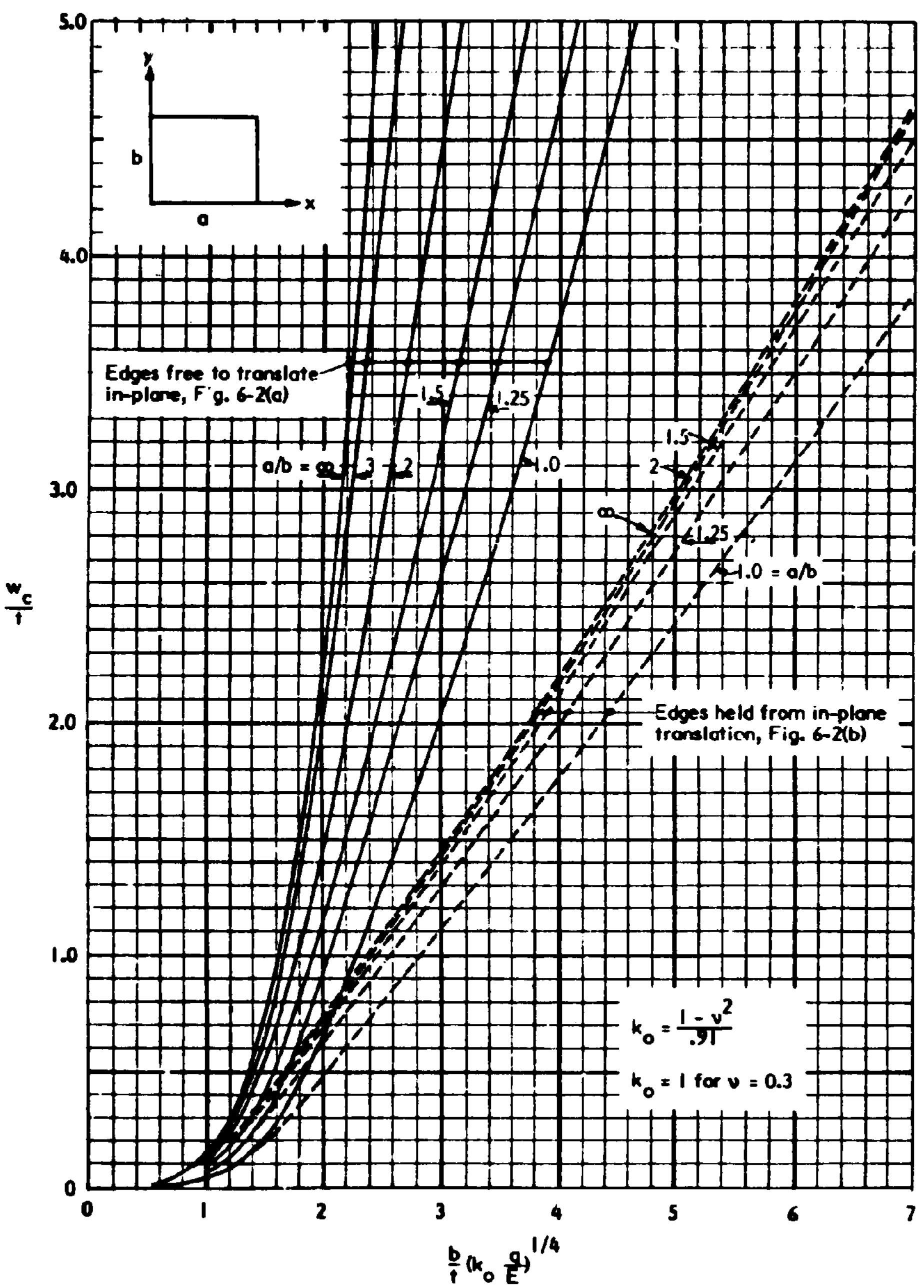

Fig. 6-4 CENTER DEFLECTIONS OF UNIFORMLY LOADED ISOTROPIC RECTANGULAR PLATES WITH EDGES FREE TO ROTATE, AND EITHER FREE TO TRANSLATE OR HELD FROM TRANSLATION IN PLANE OF PLATE (6.4)

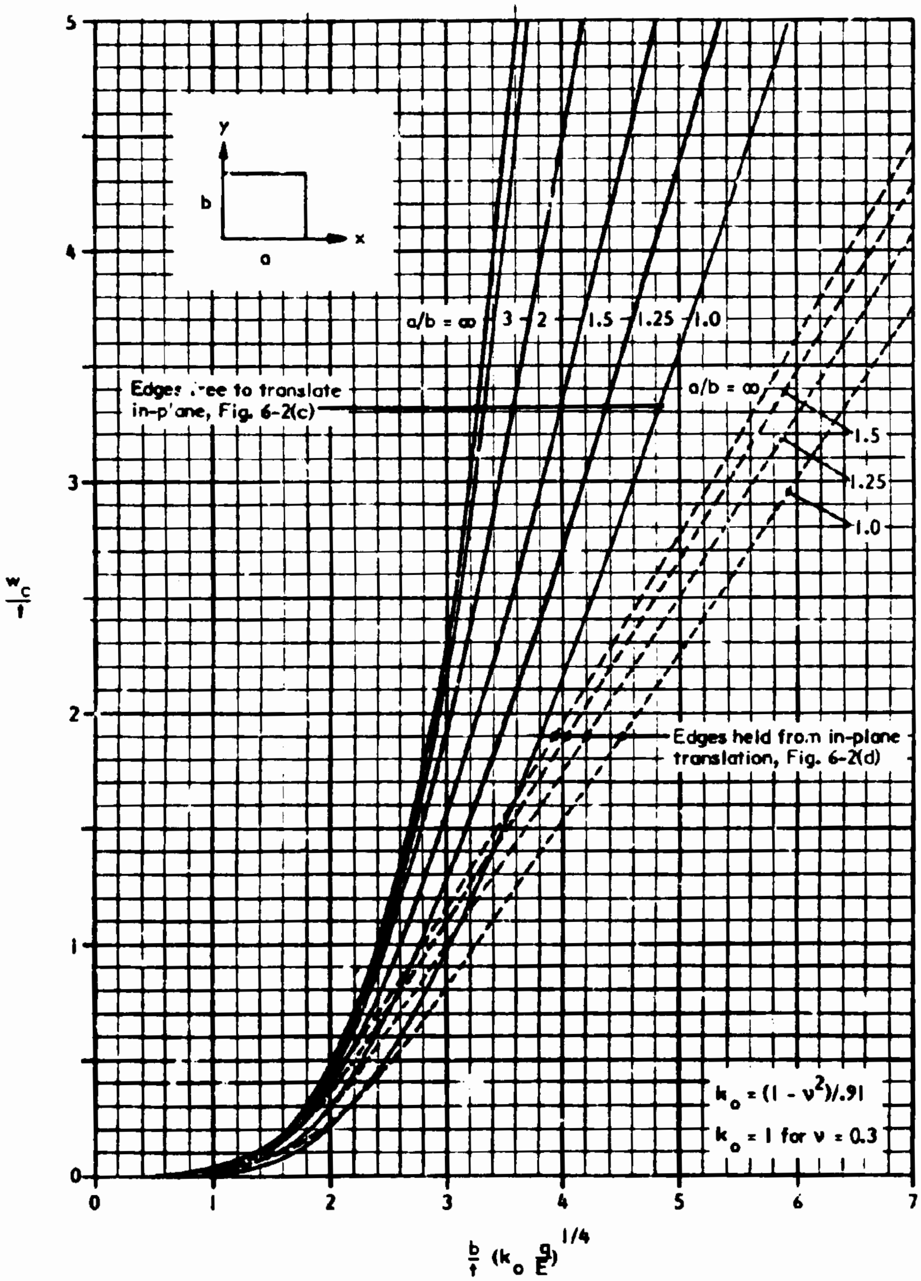

Fig. 6-5 CENTER DEFLECTIONS IN UNIFORMLY LOADED ISOTROPIC RECTANGULAR PLATE WITH EDGES FIXED AGAINST ROTATION AND EITHER FREE TO TRANSLATE OR HELD FROM TRANSLATION IN PLANE OF PLATE (6.4)

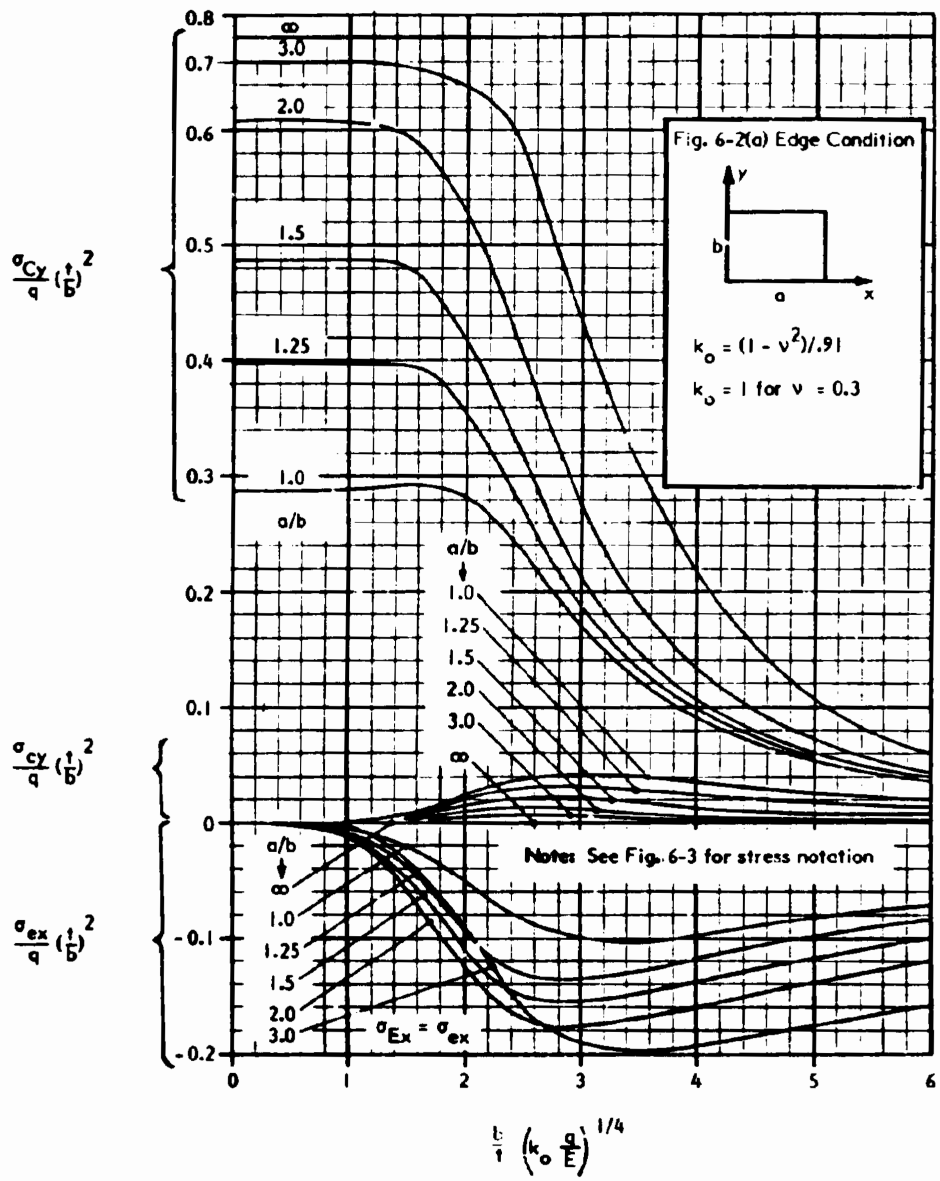

Fig. 6-6(a) MAXIMUM STRESSES IN UNIFORMLY LOADED ISOTROPIC RECTANGULAR PLATES WITH EDGES FREE TO ROTATE AND FREE TO TRANSLATE IN PLANE OF PLATE (6.4)

Note: See Fig. 6-3 for stress notation.

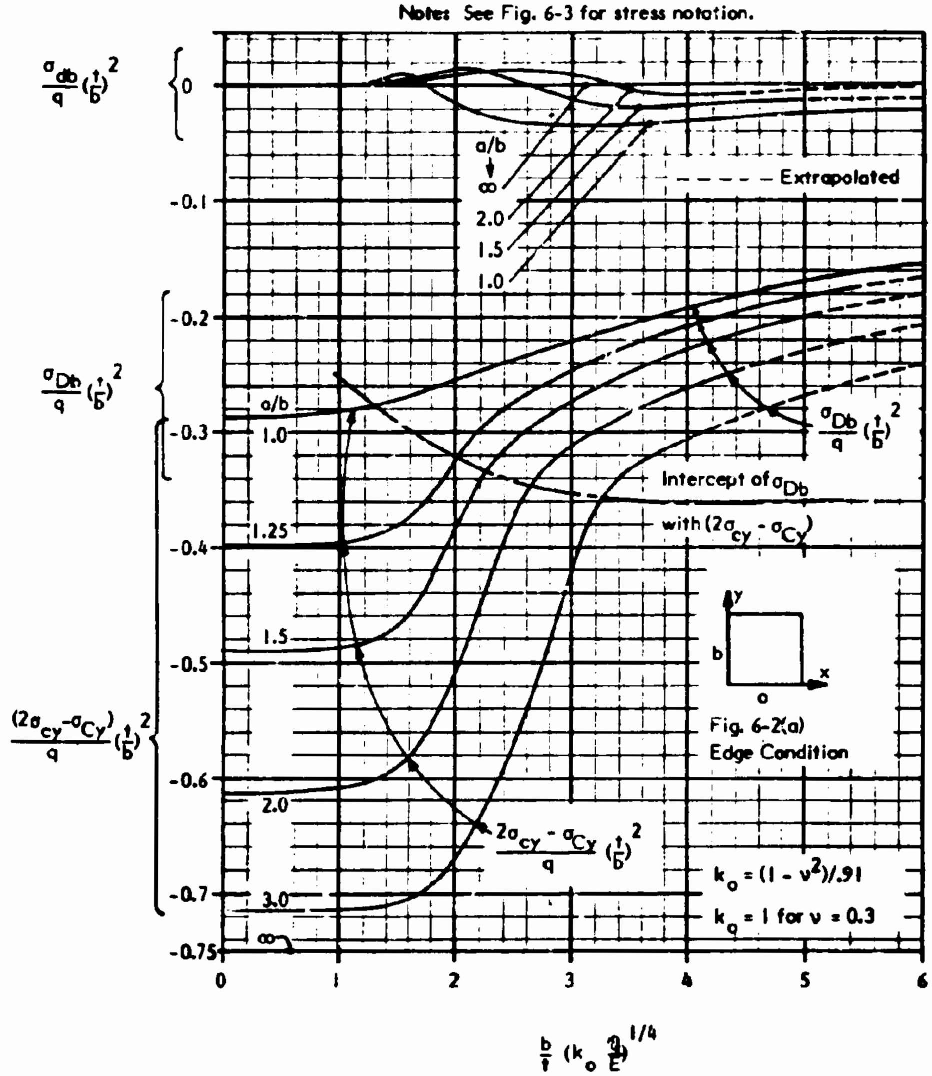

Fig. 6-6(b) MAXIMUM COMPRESSION STRESSES IN UNIFORMLY LOADED ISOTROPIC RECTANGULAR PLATES WITH EDGES FREE TO ROTATE AND FREE TO TRANSLATE IN PLANE OF PLATE (6.4)

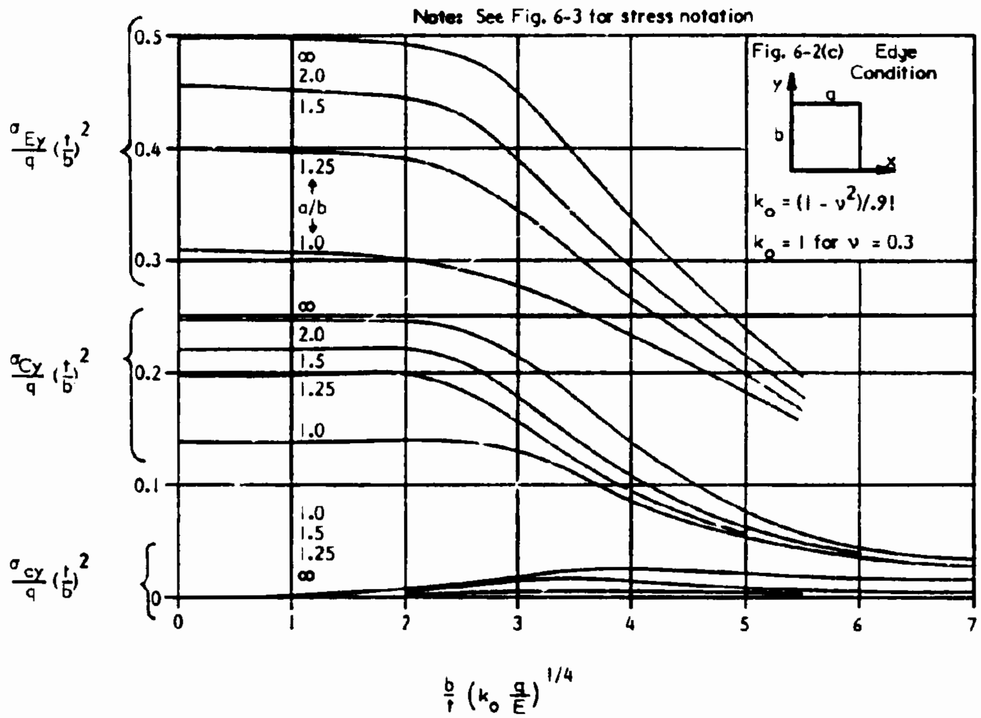

Fig. 6-7 MAXIMUM STRESSES IN UNIFORMLY LOADED ISOTROPIC RECTANGULAR PLATES WITH EDGES FIXED AGAINST ROTATION AND FREE TO TRANSLATE IN PLANE OF PLATE (6.4)

Note: See Fig. 6-3 for stress notation

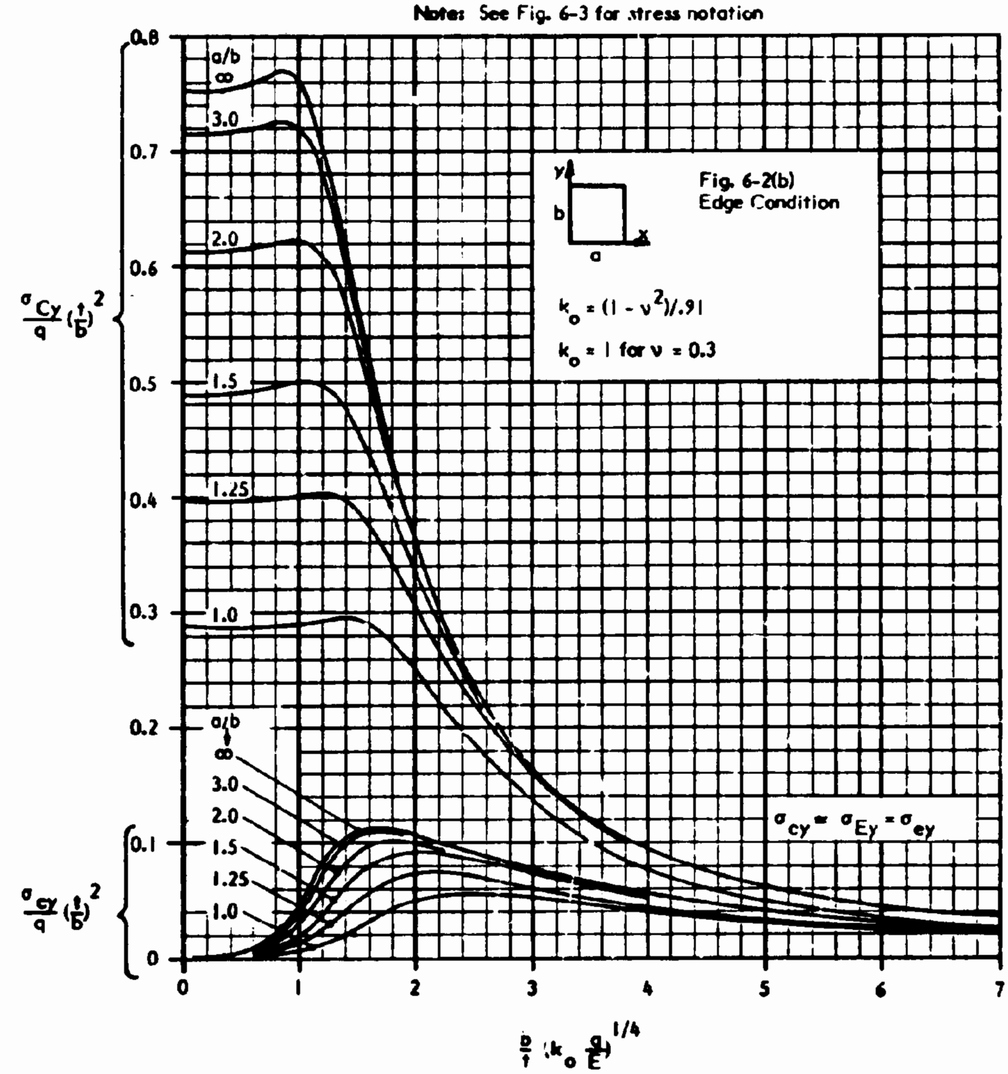

Fig. 6-8 MAXIMUM STRESSES IN UNIFORMLY LOADED ISOTROPIC RECTANGULAR PLATES WITH EDGES FREE TO ROTATE AND HELD FROM TRANSLATION IN PLANE OF PLATE (6.4)

Note: See Figure 6-3 for stress notation

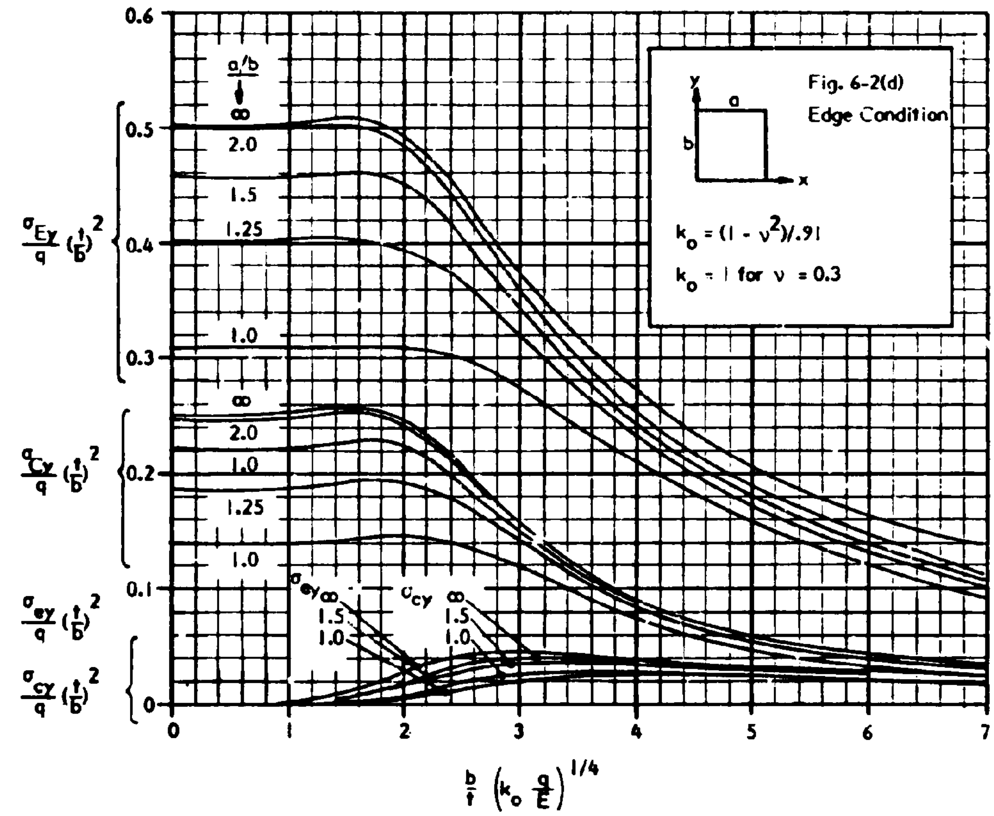

Fig. 6-9 MAXIMUM STRESSES IN UNIFORMLY LOADED ISOTROPIC RECTANGULAR PLATES WITH EDGE FIXED AGAINST ROTATION AND HELD FROM TRANSLATION IN PLANE OF PLATE (6.4)

Note: See Fig. 6-3 for stress notation.

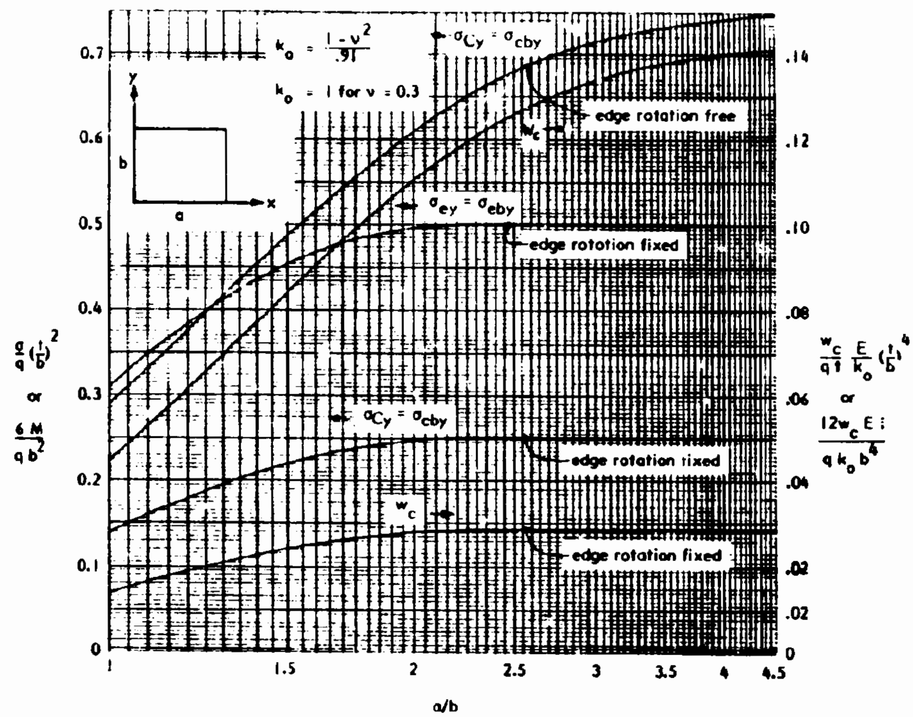

Fig. 6-10 MAXIMUM DEFLECTIONS AND STRESSES IN SMALL DEFLECTION RANGE OF UNIFORMLY LOADED ISOTROPIC RECTANGULAR PLATES WITH EDGES EITHER FREE TO ROTATE OR FIXED AGAINST ROTATION

NOTE: Effect of Restraint of Translation in Plane of Plate is Negligible in Small Deflection Range (6.4)

These are cases of frequent interest to designers of plastics components. The stresses and deflections given in Figs. 6-4 to 6-9 for various values of a/b, b/t, ν, E, and q are obtained from solutions based on "large deflection" plate theory (6.4). The thin plate theory, which is their basis, is valid for b/t greater than 20.

Stresses given in Figs. 6-6 to 6-9 are maximum total combined bending and direct stresses in the central region of the plate, σ_{Cy}, and direct membrane stresses in the middle surface, σ_{cy}, as explained in Fig. 6-3. Thus, the maximum bending stress in the central region of the plate is:

$$\sigma_{cby} = (\sigma_{Cy} - \sigma_{cy}) \qquad \text{Eq. 6.9}$$

and the maximum bending moment per unit width in the central region of the plate is:

$$M_{cy} = \frac{\sigma_{cby}\, t^2}{6} \qquad \text{Eq. 6.10}$$

When edges are held against in-plane translation, the maximum in-plane edge reaction per unit width at the center of the long edge is:

$$N_{ey} = \sigma_{ey}\, t \qquad \text{Eq. 6.11}$$

For plates which are fixed against rotation along all four edges, the maximum stress in the edge region, σ_{Ey}, and the direct membrane stress in the middle surface, σ_{ey}, are given in Figs. 6-7 and 6-9. The maximum bending stress in the edge region is:

$$\sigma_{eby} = (\sigma_{Ey} - \sigma_{ey}) \qquad \text{Eq. 6.12}$$

and the maximum bending moment per unit width in the edge region is:

$$M_{ey} = \frac{\sigma_{eby}\, t^2}{6} \qquad \text{Eq. 6.13}$$

For cases where deflections are small (less than about 0.5 t for plates which have in-plane edge restraint), and thus, where the "small deflection theory," neglecting membrane effects, provides sufficient accuracy, maximum deflections and stresses may be obtained from Fig. 6-10 (6.4). In this solution, there are no direct membrane stresses and stresses given in the Figure are bending stresses. The maximum bending moments, M_y, may be obtained using Equations 6.10 or 6.13.

Maximum shear stress resultants, Q_a and Q_b, for uniformly loaded simply supported plates analyzed by small deflection theory, are given in Fig. 6-11. Maximum edge reactions normal to the plate, V_a and V_b, are also given in Fig. 6-11. Q_a and V_a are the maximum forces per unit length resulting from load spanning in the shorter direction, and occur next to the center of the longer edge. Q_b and V_b are the maximum forces per unit length resulting from load spanning in the longer direction and occur next to the center of the shorter edge.

Because of twisting effects along the edges of the rectangular plates, the edge reactions do not equal the shears and the corners tend to lift. This lifting tendency results in concentrated uplift reactions, R, which are also given in Fig. 6-11.

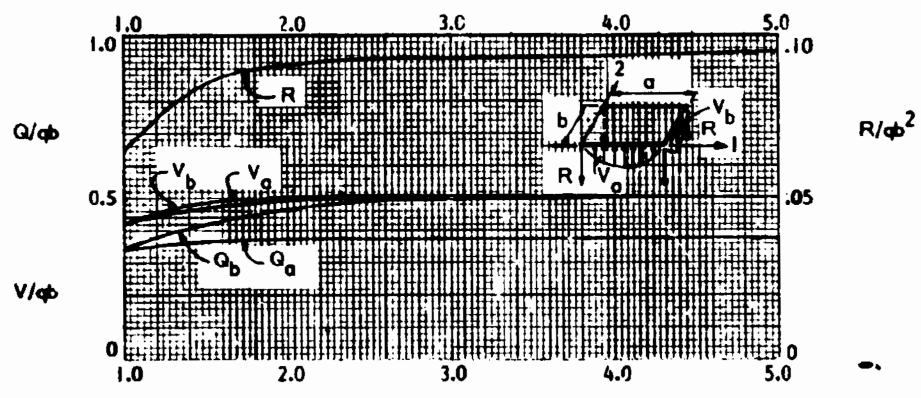

Fig. 6-11. MAXIMUM SHEAR STRESS RESULTANTS, Q_a AND Q_b, MAXIMUM REACTIONS PER UNIT LENGTH OF SIDE SUPPORT, V_a AND V_b, AND CORNER REACTIONS, R, IN UNIFORMLY LOADED, SIMPLY SUPPORTED RECTANGULAR PLATES (6.2)

Approximate total edge reactions may be estimated as follows:

For edge b, the shorter edge, distribution is approximately parabolic over the length of the edge, and:

$$\Sigma V_b = 0.7 V_b b \qquad \text{Eq. 6.14}$$

For edge a, the longer edge, distribution is assumed parabolic up to a length b/2 from each end and uniform in the central region having a length of (a - b), and:

$$\Sigma V_a = 0.7 V_a b + V_a (a - b) = V_a (a - 0.3 b) \qquad \text{Eq. 6.15}$$

The total lateral load on the plate must equal:

$$q a b = 2 \Sigma V_b + 2 \Sigma V_a - 4R \qquad \text{Eq. 6.16}$$

For plates in which large deflections are significant, the above method may be used to estimate reactions, although it will slightly overestimate maximum edge reactions and corner reactions. If necessary, a better approximation for maximum edge reactions can be obtained using the approximate method of combining small deflection and pure membrane analyses which is described in Section 6.4.

Examples 6-1 and 6-2 illustrate the use of the design aids provided in this Section to evaluate several typical rectangular plastic plate components. The significance of "large deflection" effects is shown in the examples.

Circular plates: Deflections and stresses in thin flat circular isotropic plates under uniformly distributed normal (lateral) pressure are given in Figs. 6-12 to 6-14 for cases where edges are free to translate laterally and where edges are held against lateral (in-plane) translation (6.5). These curves include "large deflection" effects which are most significant in plates with edges held against lateral translation and with higher values of (a/t). See (6.5) for additional curves for intermediate rotational edge restraint. See (6.6) for curves with increased

(Text continued on Page 6–34)

Example 6-1: Determine the maximum window size that can safely be glazed with a 1/4-inch thick acrylic plastic panel having a ratio of width to length of 1.5 and subject to a maximum uniformly-distributed wind pressure of 50 psf. Edges are simply-supported in a neoprene gasket. Maximum allowable deflection is 0.5 in. The acrylic material is considered to be isotropic, with E_o = 400,000 psi and ν = 0.3. Minimum ultimate flexural strength is 10,000 psi. Maximum allowable flexural stress during short-term wind load is 2,000 psi.* What total loads act on each edge and the corners?

Maximum size based on deflection:

$$\max \frac{w}{t} = \frac{0.5}{.25} = 2.0\ ; \qquad q = \frac{50}{144} = 0.35 \text{ psi}\ ; \qquad k_o = \frac{1-\nu^2}{.91} = \frac{1-(.3)^2}{.91} = 1.0$$

From Fig. 6-4 for edges free to translate: $\frac{b}{t}\left(k_o \frac{q}{E}\right)^{1/4} = 2.4$

thus: $\frac{b}{.25}\left(\frac{1.0 \times 0.35}{400{,}000}\right)^{1/4} = 2.40$ $\qquad$ b = 19.6 in.

a = 1.5 x 19.6 = 29.4

Check stress:

$\frac{b}{t}\left(k_o \frac{q}{E}\right)^{1/4} = 2.40$ and from Fig. 6-6(a): $\frac{\sigma_{Cy}}{q}\left(\frac{t}{b}\right)^2 = 0.333$;

$$\sigma_{Cy} = 0.35 \times 0.333 \times \left(\frac{19.6}{0.25}\right)^2 ; \quad \sigma_{Cy} = 716 \text{ psi} < 2000 \text{ psi}$$

Deflection governs design, allowable plate size is 19.6 in. by 29.4 in.

Edge Reactions: From Fig. 6-11: V_b = 0.480 x 0.35 x 19.6 = 3.29 lbs/in.

From Eq. 6.14: ΣV_b = 0.7 x 3.29 x 19.6 = 45.1 lbs

V_a = 0.486 x 0.35 x 19.6 = 33.3 lbs/in.

From Eq. 6.15: ΣV_a = 3.33 (29.4 - .3 x 19.6) = 78.3 lbs

R = 0.085 x 0.35 x 19.6^2 = 11.4 lbs

Check: Eq. 6.16: 0.35 x 19.6 x 29.4 = 201.7 lbs ;

2 x 78.3 + 2 x 45.1 - 4 x 11.4 = 201.3 lbs

201.7 $\approx$ 201.3

Note: 1 psi = 0.0069 MPa; 1 in. = 25.4 mm; 1 lbf = 4.45 N; 1 lb/in. = 0.18 N/mm

* Design loads, design criteria (such as safety factors, load factors and capacity reduction factors, etc.), and materials properties used in design examples are for illustrative purposes only. The user of this Manual is cautioned to develop his own loads, criteria and materials properties based on the requirements and conditions of his specific design project.

Example 6.2: Determine the maximum opening that can safely be covered with a 1/8-inch thick mat reinforced FRP sheet having a ratio of width to length of 1.5 and subject to a maximum uniformly distributed wind pressure of 50 psf. Edges are anchored to a stiff frame with metal screws. The edge detail can prevent the in-plane translation but does not clamp against edge rotation. Maximum allowable deflection is 0.5 in. The FRP material is considered to be isotropic, with E_o = 1,000,000 psi and ν = 0.3. Maximum allowable flexural or tensile stress during short-term wind load is taken as 3000 psi* Determine the maximum total stress and the maximum axial (membrane) and bending stress and maximum bending moment.

Maximum size, based on deflection:

$$\frac{w_c}{t} = \frac{0.5}{0.125} = 4 \qquad \frac{a}{b} = 1.5$$

From Fig. 6-4, for edges held against in-plane translation:

$$\frac{b}{t}\left(k_o \frac{q}{E}\right)^{1/4} = 6.35$$

$$\nu = 0.3 \qquad k_o = 1.0 \qquad q = \frac{50}{144} = 0.35 \text{ psi}$$

$$\frac{b}{0.125}\left(\frac{1.0 \times 0.35}{1{,}000{,}000}\right)^{1/4} = 6.35 \qquad \begin{array}{l} b = 32.6 \text{ in.} \\ a = 48.9 \text{ in.} \end{array}$$

Check stress:

$$\frac{b}{t}\left(\frac{k_o q}{E}\right)^{1/4} = 6.35 \quad \text{and} \quad \frac{a}{b} = 1.5$$

$$\text{From Fig. 6-8: } \frac{\sigma_{Cy}}{q}\left(\frac{t}{b}\right)^2 = 0.038$$

$$\text{Max. total stress: } \sigma_{Cy} = 0.35 \times 0.038 \times \left(\frac{32.6}{0.125}\right)^2 = 905 \text{ psi} \quad 3000 \text{ psi}$$

Deflection governs design, allowable plate size is 32.6 in. by 48.9 in.

$$\text{From Fig. 6-8: } \frac{\sigma_{cy}}{q}\left(\frac{t}{b}\right)^2 = 0.023$$

$$\text{Max. membrane stress} = 0.023 \times 0.35 \times \left(\frac{32.6}{0.125}\right)^2 = 548 \text{ psi}$$

Max. required safe fastener lateral strength = 548 x 1/8 = 68.5 lbs/in.

Note: 1 psi = 0.0069 MPa; 1 in. = 25.4 mm; 1 lbf = 4.45 N; 1 lbf/in. = 0.18 N/mm

* See footnote, Example 6-1, p. 29.

Note: See (6.5) for solutions for rotational edge restraint between free and fixed, $0 < K_b < \infty$

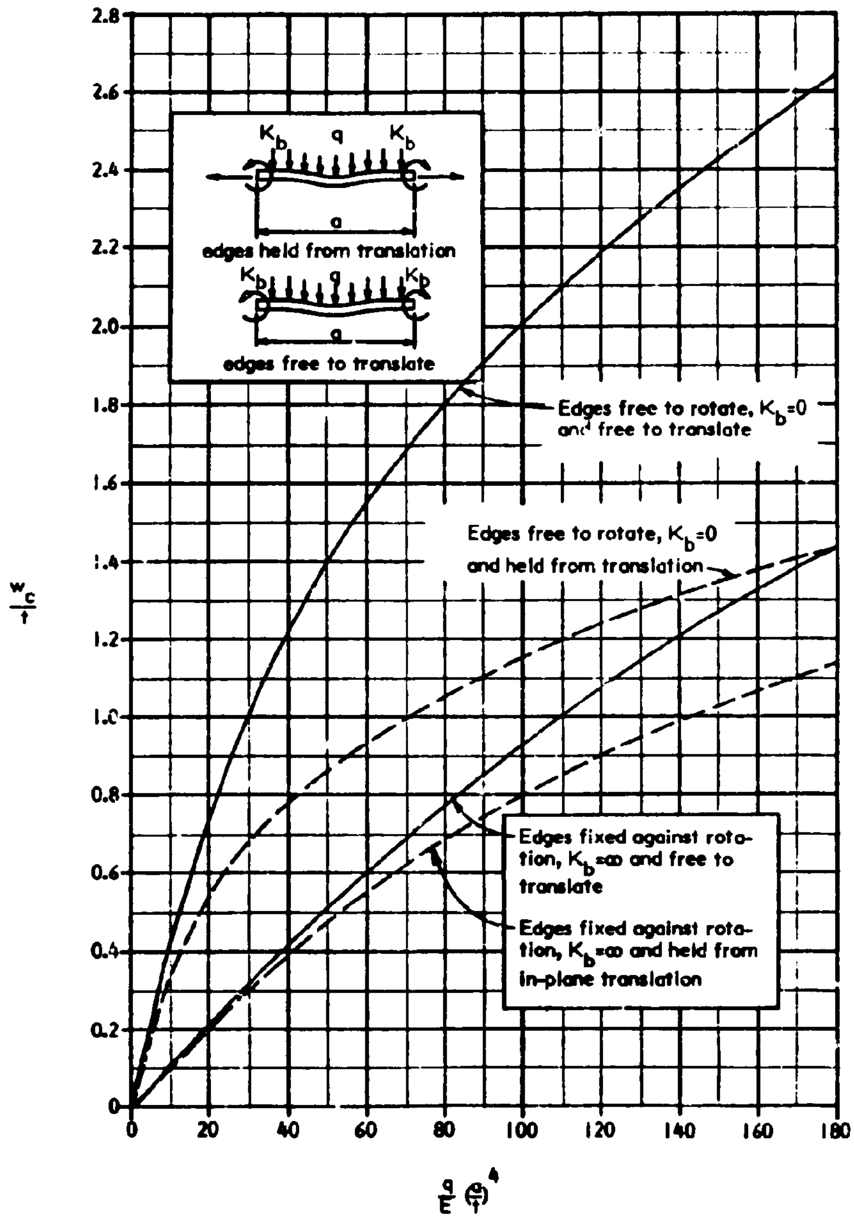

Fig. 6-12 CENTER DEFLECTIONS OF UNIFORMLY LOADED ISOTROPIC CIRCULAR PLATES WITH DIFFERENT COMBINATIONS OF EDGE RESTRAINT CONDITIONS (6.5)

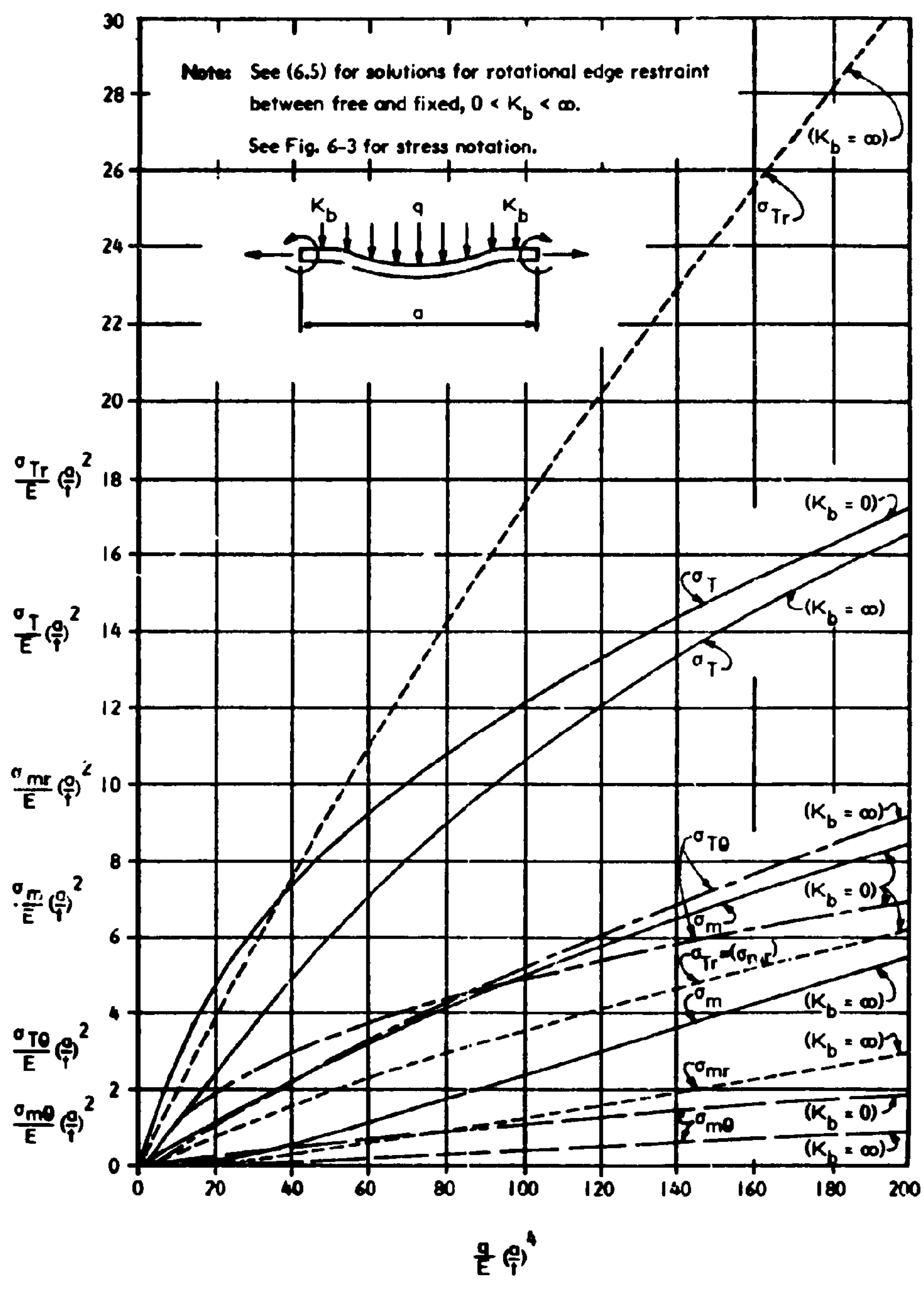

Fig. 6-13 MAXIMUM STRESSES IN UNIFORMLY LOADED ISOTROPIC CIRCULAR PLATES WITH EDGE FREE TO TRANSLATE IN PLANE OF PLATE AND EITHER FREE TO ROTATE OR FIXED AGAINST ROTATION (6.5)

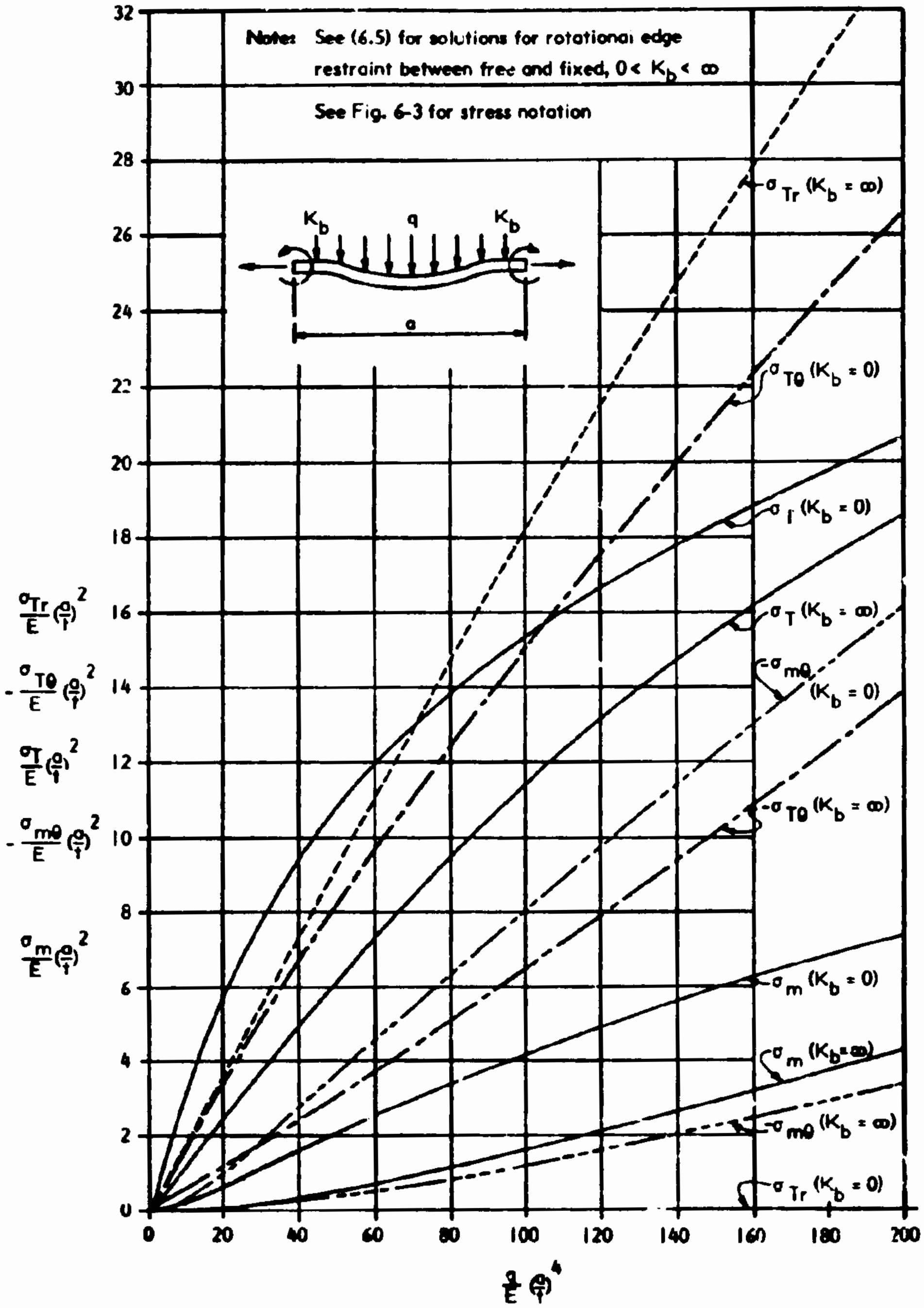

Fig. 6-14 MAXIMUM STRESSES IN UNIFORMLY LOADED ISOTROPIC CIRCULAR PLATES WITH EDGE HELD FROM TRANSLATION IN PLANE OF PLATE AND EITHER FREE TO ROTATE OR FIXED AGAINST ROTATION (6.5)

accuracy for smaller a/t values and for correction factors for stresses in plates of moderate thickness ($4 < a/t < 20$).

Triangular plates: Bending moment, deflections and reactions are given in Figs. 6-15 and 6-16 for thin flat isosceles triangular isotropic plates ($\nu = 0$) under uniformly distributed normal (lateral) pressure with simply supported and rotationally fixed edge conditions, respectively (6.3). These solutions are based on elastic "small deflection" plate theory. Thus, the total stresses equal the bending stresses, $6M/t^2$.

For plates where deflections exceed about one half the plate thickness, and where edges have translational restraint in the plane of the plate, significant membrane stresses arise which reduce bending stresses. In these plates, maximum total stress would be less than the bending stresses given by the small deflection theory. See Section 6.5 for an approximate method of estimating "large deflection" effects in thin plates with edge restraint in the plane of the plate.

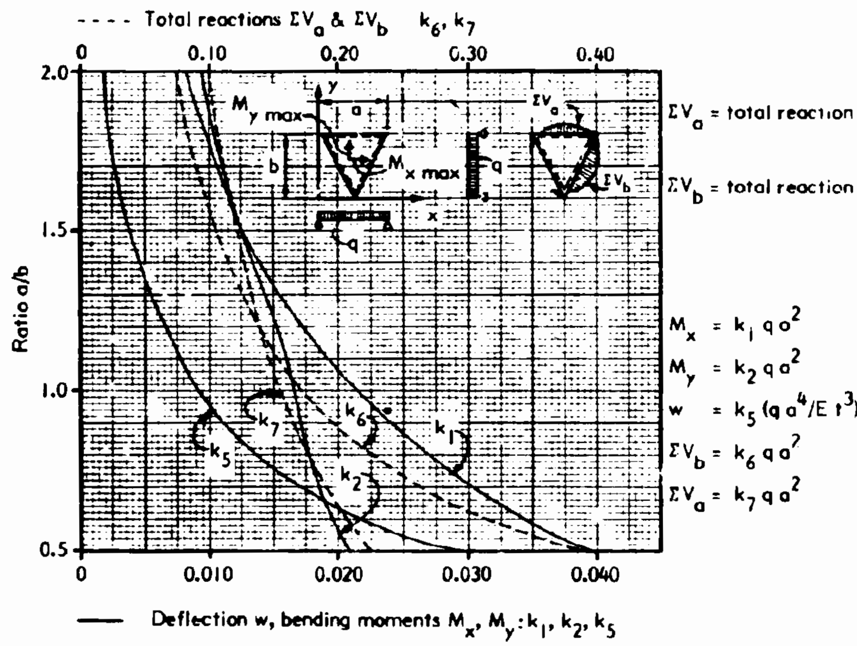

Fig. 6-15 COEFFICIENTS FOR MAXIMUM MOMENTS M, DEFLECTIONS w, AND TOTAL REACTIONS IN ISOCELES TRIANGULAR ISOTROPIC PLATES UNDER UNIFORMLY DISTRIBUTED NORMAL PRESSURE WITH SIMPLY SUPPORTED EDGES, BASED ON "SMALL DEFLECTION" PLATE THEORY (6.3)

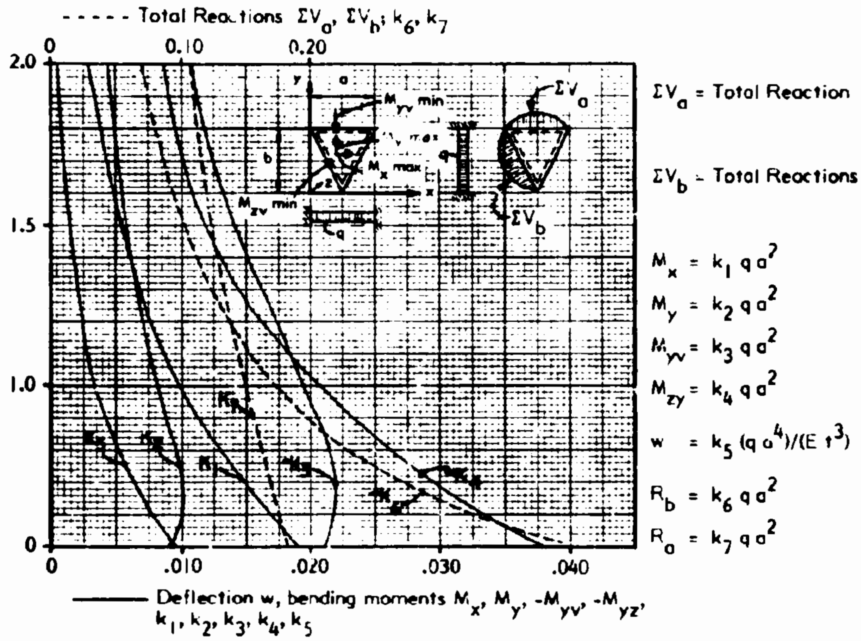

Fig. 6-16 COEFFICIENTS FOR MAXIMUM MOMENTS M, DEFLECTIONS w, AND TOTAL REACTIONS IN ISOCELES TRIANGULAR ISOTROPIC PLATES UNDER UNIFORMLY DISTRIBUTED NORMAL PRESSURE WITH ROTATIONALLY FIXED EDGES, BASED ON "SMALL DEFLECTION" PLATE THEORY (6.3)

6.4 ISOTROPIC FLAT MEMBRANES UNDER LATERAL LOAD

Plastics are sometimes used in structural applications where they behave as pure membranes under lateral load. This behavior is illustrated in Fig. 6-2 in the previous Section. The following equations for maximum deflection and stress in membranes of various shapes are useful for design of such components. In all the equations given below, the material is isotropic and elastic, bending effects are neglected, and, except where noted otherwise, the membrane is assumed to be initially flat, without slack, but with zero initial pre-tension in the plane of the membrane. The membrane is loaded by a uniformly distributed lateral pressure, q.

Long rectangular membrane, deflected to a cylindrical shape, spanning a distance, b, with membrane forces held on two opposite long edges, as shown in Fig. 6-2(b). All the equations given below are valid approximations for ratios of deflection to span of 5 percent or less. These relations may be obtained using the equations for cable tension with a sag equal to the deflection. *

Case I - Initially flat membrane, without initial tension or tautness (6.3):

$$N_{he} = 0.30 \sqrt[3]{\frac{q^2 b^2 E t}{(1-\nu^2)}} \qquad \text{Eq. 6.17}$$

$$N_{ve} = 0.5\, q\, b \qquad \text{Eq. 6.18}$$

where N_{he} and N_{ve} are the in-plane and normal edge reactions per unit length, respectively.

The membrane force in the edge region is obtained from the edge angle, θ_e:

$$\tan \theta_e = \frac{N_{ve}}{N_{he}} \quad ; \qquad N_e = \sigma_e t = \frac{N_{he}}{\cos \theta_e} \qquad \text{Eq. 6.19}$$

The membrane force at midspan is the same as N_{he}, which is given by Eq. 6.17.

---

* See for example Scalzi, J., Podolny, W. and Teng, W., "Design Fundamentals of Cable Roof Structures," published by U. S. Steel Corporation, 1969

Deflection at the center of the span is (6.3):

$$w_c = 0.41\, b \sqrt[3]{\frac{(1-\nu^2)\, q\, b}{E\, t}} \qquad \text{Eq. 6.20}$$

Case 2 - Initially flat membrane, with initial pre-tension, N_{hi}. When sag is equated to deflection of a cable with initial tension, N_{hi}, plus tension due to loading, N_{hq}, the following relation for tension due to lateral loading on a long strip of span b is obtained:

$$N_{hq} = \left[0.20\, q\, b \sqrt{\frac{E\, t}{1-\nu^2}} - N_{hi} \sqrt{N_{hq}} \right]^{2/3} \qquad \text{Eq. 6.21}$$

Eq. 6.21 may be solved by "cut and try" methods for the unknown additional in-plane edge membrane force, N_{hq}, resulting from the applied load, q. The total in-plane membrane force at the edge, N_{he}, then, is the initial pre-tension plus the additional force due to applied load:

$$N_{he} = N_{hi} + N_{hq} \qquad \text{Eq. 6.22}$$

The normal component of the edge reaction, N_{ve}, is obtained from Eq. 6.18 and the total membrane force and stress at the edge is given by Eq. 6.19.

The midspan deflection of the pre-tensioned membrane may be obtained from the additional membrane force due to applied load:

$$w_c = 0.61\, b \sqrt{\frac{N_{hq}\,(1-\nu^2)}{E\, t}} \qquad \text{Eq. 6.23}$$

Axial deformation, or elongation, of the membrane associated with pretension is:

$$\delta_{hi} = \frac{N_{hi}\, b}{E\, t} \qquad \text{Eq. 6.24}$$

Case 3 - Initially sagged membrane, with initial sag, f_i (i.e. with initial length of membrane arc greater than span, $b_i > b$), where initial sag is less than about 5 percent of the span, b.

Again, using relations between cable tension and sag *, initial sag and difference between initial length of arc and span are approximately related as follows:

$$\frac{f_i}{b} = 0.20 \frac{(b_i - b)}{b} \qquad \text{Eq. 6.25}$$

The edge reaction in the plane of the supports is:

$$N_{he} = \sqrt[3]{\left(0.625\, qb - 5\frac{f_i}{b}N_{he}\right)^2 \frac{E\,t}{(1-\nu^2)}} \qquad \text{Eq. 6.26}$$

Eq. 6.26 may be solved for N_{he} by "cut and try" methods.

As before, the normal component of the edge reaction, N_{ve}, is obtained from Eq. 6.18 and the total membrane force and stress at the edge is given by Eq. 6.19.

The additional midspan deflection, w_c, of the initially sagged membrane may be determined from the membrane edge force, N_{he}, using Eq. 6.23 above with N_{he} substituted for N_{hq}. The total final sag of the membrane is:

$$f = f_i + w_c \qquad \text{Eq. 6.27}$$

Example 6.3 illustrates the use of the above method to determine the deflection and stresses in a long rectangular plastic sheet that is assumed to behave as a pure membrane. The membrane is "pretensioned" prior to receiving lateral load. The effect of the duration of the "pretension" load is evaluated using the methods suggested in Chapter 3.

Rectangular membrane, with membrane forces held on four sides by tensile membrane reactions N_{hx}, and N_{hy}, as shown in Fig. 6-17, and $\nu = 0.3$ (6.3):

$$N_{hx} = k_1 \sqrt[3]{q^2 b^2 E\,t} \qquad \text{Eq. 6.28}$$

$$N_{hy} = k_2 \sqrt[3]{q^2 b^2 E\,t} \qquad \text{Eq. 6.29}$$

$$w_c = k_3\, b \sqrt[3]{\frac{q\,b}{E\,t}} \qquad \text{Eq. 6.30}$$

Values of k_1, k_2, and k_3 are plotted in Fig. 6-17 for a range of ratios of a/b.

---

* See footnote, p. 37.

Example 6.3: A long PE sheet, 0.1 inch thick, which has the mechanical properties given in Fig. 3-3 (Chapter 3) is supported and loaded as shown in the sketch below. This sheet is pretensioned by moving the clamped edges apart by 0.50 inches, and fixing them in that location. The lateral load is a short-term load applied 14 months (10,000 hours) after the initial application of pretension. The temperature does not vary.* Determine the maximum total membrane stress and the maximum deflection of the sheet. Neglect bending resistance. Assume $\nu = 0.3$.

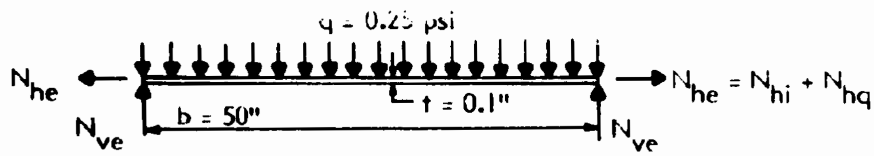

Pretension: From Eq. 6.24: $\delta_{hi} = \dfrac{N_{hi}\, b}{E\, t} = \dfrac{\sigma_i\, b}{E}$; $\sigma_i = \dfrac{E\, \delta_{hi}}{b}$

Initial Pretension: From Fig. 3-3a: E_o = 21,600 psi @ time $t_o = 0$

$$\sigma_i = 21,600 \times \frac{0.5}{50} = 216 \text{ psi}$$

Check viscoelastic limit: $\varepsilon = \dfrac{0.5}{50} = .01 < .0245$, viscoelastic limit, Fig. 3-3c.

Pretension after relaxation at time 10,000 hours:

From Fig 3-3a: E_v = 12,000 psi

$$\sigma_{10,000} = 12,000 \times 0.5/500 = 120 \text{ psi}$$

$$N_{hi} = N_{10,000} = 120 \times 0.1 = 12 \text{ lbs/in.}$$

From Eq. 6.21:

$$N_{hq} = \left(0.20 \times 0.25 \times 50 \sqrt{\frac{21,600 \times 0.1}{1 - .3^2}} - 12\sqrt{N_{hq}}\right)^{\frac{2}{3}} = \left(121.8 - 12\sqrt{N_{hq}}\right)^{\frac{2}{3}}$$

Cut and Try Solution:

Trial N_{hq}	$(121.8 - 12\sqrt{N_{hq}})^{\frac{2}{3}}$
12	18.6
17	17.3

N_{he} = 17.3 + 12 = 29.3 lbs/in. $\qquad$ $\tan\theta_o$ = 6.25/29.3 = .2133; $\theta_o = 12.0^\circ$

N_{ve} = .5 x 0.25 x 50 = 6.25 lbs/in. $\qquad$ N_e = 29.3/cos 12.0° = 30.0 lbs/in.

$$\sigma_e = 30.0/0.1 = 300 \text{ psi}$$

From Eq. 6.23: $\quad w_c = 0.61 \times 50 \sqrt{\dfrac{17.3\,(1 - .3^2)}{21,600 \times 0.1}} = 2.6$ in.

Note: 1 psi = 0.0069 MPa; 1 lb/in. = 1 N/mm; 1 in. = 25.4 mm

* See footnote, Example 6-1, p. 29.

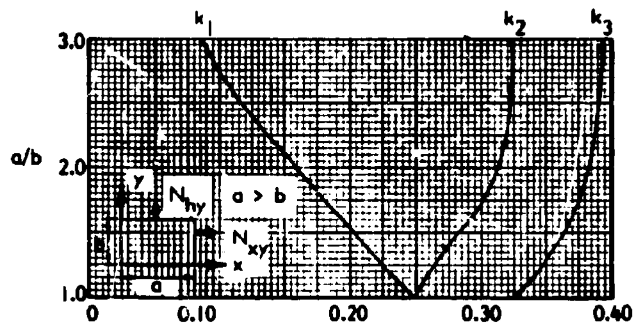

Fig. 6-17. COEFFICIENTS k_1, k_2, k_3, FOR DETERMINATION OF MAXIMUM FORCES AND DEFLECTIONS IN RECTANGULAR MEMBRANES (6.3)

Example 6.4 illustrates the use of the above equations for determining the safe load capacity of a rectangular membrane supported by a rigid, unmoving frame.

Circular membrane, with membrane force held on outer circumference (6.3):

$$\sigma_e = 0.21 \sqrt[3]{\frac{q^2 E a^2}{t^2}} \qquad \text{Eq. 6.31}$$

$$\sigma_c = 0.25 \sqrt[3]{\frac{q^2 E a^2}{t^2} \frac{(3-\nu)}{(1-\nu)}} \qquad \text{Eq. 6.32}$$

where σ_e and σ_c are the radial tension stresses at the edge and center, respectively. For the circular membrane, the membrane edge reactions are:

$$N_e = \sigma_e t$$

$$N_{ve} = 0.25\, q\, a \qquad \text{Eq. 6.33}$$

$$\sin \theta_e = \frac{0.25\, q\, a}{N_e}$$

$$N_{he} = N_e \cos \theta_e \qquad \text{Eq. 6.34}$$

Deflection at the center is:

$$w_c = 0.40\, a \sqrt[3]{\frac{q\, a}{E\, t} \frac{(1-\nu)}{(3-\nu)}} \qquad \text{Eq. 6.35}$$

Example 6.4: Determine the maximum membrane stress and the midspan deflection for the thin FRP panel of Example 6.2 if the panel is assumed to be a membrane and its bending resistance is neglected.

From Example 6.2: $a = 48.9$ in.; $b = 32.6$ in.; $t = 0.125$ in.; $E = 1 \times 10^6$ psi;
$q = 0.35$ psi

From Fig. 6-17 for a/b = 1.5: $k_1 = 0.282$; $k_2 = 0.204$; and $k_3 = 0.363$

From Eq. 6.29: $$N_{hy} = 0.282 \sqrt[3]{0.35^2 \times 32.6^2 \times 1 \times 10^6 \times 0.125} = 71.5 \text{ lb/in.}$$

$$\sigma_{cy} = \frac{71.5}{0.125} = 572 \text{ psi}$$

From Eq. 6.30: $$w_c = 0.363 \times 32.6 \sqrt[3]{\frac{0.35 \times 32.6}{1 \times 10^6 \times 0.125}} = 0.53 \text{ in.}$$

Note: 1 in. = 25.4 mm; 1 psi = 0.0069 MPa; 1 lbf/in. = 0.18 N/mm

6.5 APPROXIMATIONS FOR LARGE DEFLECTION ANALYSIS OF ISOTROPIC PLATES UNDER LATERAL LOADS

An approximate method, based on combining membrane and small deflection bending solutions, is available to determine the deflection, stresses, and reactions for plates under uniformly distributed lateral load where large deflection effects are significant (6.2). This method is best explained by first illustrating its application to a long rectangular plate with simple supports that are held against translation (i.e.: also, a plate with similar supports on two opposite sides), and then generalizing for rectangular and circular plates. The plate is loaded by a uniformly distributed lateral pressure, q. This pressure is considered as comprised of two pressures q_b and q_m, where q_b is resisted by plate bending, and q_m is resisted by membrane action and: $q = q_b + q_m$.

The center deflection of the plate, <u>considering only plate bending</u>, is (6.2):

	Long Plate	General Plate	
$w_c =$	$0.156 \dfrac{(1-\nu^2) q_b b^4}{E t^3}$		Eq. 6.36
or: $q_b =$	$\dfrac{6.4 w_c E t^3}{(1-\nu^2) b^4}$	$= \dfrac{C_1 w_c E t^3}{b^4}$	Eq. 6.36a

The center deflection of the plate, <u>considering only plate membrane action</u> as given by Eq. 6.20, is:

	Long Plate	General Plate	
$w_c =$	$0.41 \left[\dfrac{(1-\nu^2) q_m b^4}{E t}\right]^{1/3}$		Eq. 6.37
or: $q_m =$	$\dfrac{14.5 w_c^3 E t}{(1-\nu^2) b^4}$	$= \dfrac{C_2 w_c^3 E t}{b^4}$	Eq. 6.37a

Thus, considering both bending and membrane action:

Long plate: $$q = q_b + q_m = \frac{w_c E t^3}{(1-\nu^2) b^4} \left(6.4 + 14.5 \frac{w_c^2}{t^2}\right) \qquad \text{Eq. 6.38}$$

General plate: $$q = \frac{w_c E t^3}{b^4} \left(C_1 + C_2 \frac{w_c^2}{t^2}\right) \qquad \text{Eq. 6.38a}$$

In a typical design problem, the total load, q, the span dimension, b, and the material properties, E and ν are usually known, and it is desired to select a minimum plate thickness, t, that will limit maximum deflection at the center of the plate, w_c, and maximum combined bending and axial (membrane) stress, σ_c, to an allowable deflection and stress, respectively. This is accomplished by selecting a trial thickness, t, and solving Eq. 6.38 (or 6.38a) for the center deflection, w_c, by a cut and try process, or other suitable cubic equation solver. This value of w_c is then substituted into Eqs. 6.36a and 6.37a to obtain q_b and q_m. Maximum bending stresses at the center of the plate span (or at the edge for rotationally fixed edges) are then determined from "small deflection" plate theory for q_b, and direct stresses from plate membrane theory for q_m. These are obtained using the following equations:

Max. bending stress:		Long plate		General plate	
σ_{cby}	=	$0.75\, q_b\, b^2$	=	$C_3\, q_b \left(\frac{b}{t}\right)^2$	Eq. 6.39a

Membrane stress:		Long plate		General plate	
σ_{cy}	=	$0.30 \sqrt[3]{\frac{q_m^2\, b^2\, E}{(1-\nu^2)\, t^2}}$	=	$C_4 \sqrt[3]{\frac{q_m^2\, b^2\, E}{t^2}}$	Eq. 6.39b

Maximum total stress:

$$\sigma_{Cy} = \sigma_{cby} + \sigma_{cy} \qquad \text{Eq. 6.39c}$$

See Fig. 6-3 and Eq. 6.9 for stress notation.

The deflection and maximum stress coefficients in Eqs. 6.38a and 6.39, a and b, for plates with edges held against translation and ν = 0.3 are:

	a/b	C_1 Eqs. 6.36a & 6.38a		C_2	C_3 Eq. 6.39a		C_4
		Simply Supported Edges	Rotationally Fixed Edges	Eqs. 6.37a & 6.38a	Simply Supported Edges	Rotationally Fixed Edges **	Eq. 6.39b
Rectangular plates	1.0	22.6	72.7	30.0	0.29	0.31	0.25
	1.2	16.2	53.2	24.4	0.38	0.38	0.26
	1.4	13.0	44.2	22.0	0.45	0.44	0.28
	1.6	11.0	39.8	20.0	0.52	0.47	0.29
	1.8	9.8	37.4	18.0	0.57	0.49	0.30
	2.0	9.0	36.0	17.5	0.61	0.50	0.31
	∞*	7.0	35.2	16.0	0.75	0.19	0.32
Circular plates	diam = b	20.9	93.8	55.6	0.31	0.19	0.40

* long plate, or plate supported, on 2 opposite edges, at ends of b

**max. stress at edge of plate

For a material having a Poisson's Ratio, ν, that differs from 0.3, multiply the coefficient C_1 by k_o and the coefficients C_2 and C_4 by $(k_o)^{1/3}$, where k_o (1- ν)/0.91 (= 1.0 when ν = 0.3). The coefficient C_3 also varies somewhat with ν, but this may be neglected as a secondary effect.

Note that the values of C_1, C_2, C_3 and C_4, given above for a rectangular plate with an infinite ratio a/b, are the same as the coefficients given in Eqs. 6.38 and 6.39 with ν = 0.3.

Example 6.5 illustrates the use of the above method for the evaluation of the same rectangular plate that was analyzed in Example 6.2.

Alternate Method — Rectangular plate, simply supported on two opposite edges:

As an alternate to the approach used in Eq. 6.38, the following equations from (6.2) provide a convenient means for analyzing rectangular plates with supports only on two opposite sides (cylindrical bending) restrained against in-plane translation:

Let $$\bar{a} = \frac{N_{he}\, b^2}{\pi^2 D} \qquad \text{Eq. 6.40}$$

For simply supported edges (Fig. 6-2b):

$$\bar{a}(1+\bar{a})^2 = \frac{3\, w_{co}^{\;2}}{t^2} \qquad \text{Eq. 6.41}$$

Example 6.5: Determine the maximum combined membrane and bending stresses at midspan and at the edges and the midspan deflection for the thin FRP panel of Examples 6.2 and 6.4 (applied q = 0.350 psi) using the approximate method given in this Section. Compare with results obtained in the previous two examples.*

For plate bending, with a/b = 1.5, and ν = 0.3: C_1 = 12, from table after Eq. 6.39.

From Eq. 6.36a: $q_b = \dfrac{12\, w_c\, E\, t^3}{1 \times b^4} = \dfrac{12.0 \times 1{,}000{,}000 \times 0.125^3}{32.6^4}\ w_c = 0.021\ w_c$

For membrane action with a/b = 1.5, and ν = 0.3: C_2 = 21, from table after Eq. 6.39.

From Eq. 6.37a: $q_m = 21\ w_c^{\ 3}\ \dfrac{E\,t}{b^4} = \dfrac{21 \times 1{,}000{,}000}{32.6^4} \times 0.125\ w_c^{\ 3} = 2.32\ w_c^{\ 3}$

For combined action: $q = q_b + q_m$

$$q = 0.35 = 0.021\ w_c + 2.32\ w_c^{\ 3}$$

Cut and try solution:

	trial w_c	q_b $0.021\ w_c$	q_m $2.32\ w_c^{\ 3}$	$\overset{?}{=}$ q
	0.5	0.011	0.290	0.301
	0.55	0.012	0.385	0.397
	0.53	0.011	0.345	0.356
Use	0.527	0.011	0.339	0.350

Plate bending load is q_b and from above q_b = 0.011 psi.

For plate bending, a/b = 1.5 and ν = 0.3: C_3 = 0.485, from table after Eq. 6.39.

From Eq. 6.39a: $\sigma_{cby} = 0.485 \times 0.011 \times \left(\dfrac{32.6}{0.125}\right)^2 = 363$ psi

Membrane load is q_m and from above: q_m = 0.35 - 0.011 = 0.339 = 0.34 psi

For membrane action, with a/b = 1.5 and ν = 0.3: C_4 = 0.285, from table after Eq. 6.39.

From Eq. 6.39b: $\sigma_{cy} = 0.285\ \sqrt[3]{0.339^2 \times 32.6^2 \times \dfrac{1{,}000{,}000}{0.125^2}} = 567$ psi

Combined bending and membrane stress = 363 + 567 = 930 psi

Plate deflection, w_c = 0.527 in.

Note: 1 psi = 0.0069 MPa; 1 lbf/in. = 0.18 N/mm; 1 in. = 25.4 mm

* See footnote, Example 6-1, page 6-29.

w_{co} is the center span deflection when lateral load is resisted only by the bending resistance of the plate (i.e., small deflection theory).

For uniformly distributed lateral loading with simply supported edges:

$$w_{co} = \frac{5\, q\, b^4}{384\, D} \qquad \text{Eq. 6.42}$$

$\bar{\alpha}$ may be determined by a cut-and-try solution of Eq. 6.41.

The mid-span deflection is:

$$w_c = \frac{w_{co}}{(1 + \bar{\alpha})} \qquad \text{Eq. 6.43}$$

The horizontal edge reaction is equal to the membrane force at the midspan of the plate and is:

$$N_{hc} = \frac{\pi^2\, \bar{\alpha}\, D}{b^2} \qquad \text{Eq. 6.44}$$

The midspan bending moment is:

$$M_c = 0.811\, \frac{(1 - \operatorname{sech} 1.57\sqrt{\bar{\alpha}})}{\bar{\alpha}}\, M_{co} \qquad \text{Eq. 6.45}$$

M_{co} is the mid-span bending moment for simply supported edges. For uniformly distributed loading:

$$M_{co} = \frac{q\, b^2}{8} \qquad \text{Eq. 6.46}$$

When the edges are not fully held against translation and move towards each other a known or assumed amount, δ_h, the following modified relation for $\bar{\alpha}$ may be used with the above-described equations for the simply supported edge case:

$$\bar{\alpha}\,(1 + \bar{\alpha})^2\left(1 + \frac{12\, b\, \delta_h}{\pi^2\, t^2\, \bar{\alpha}}\right) = \frac{3\, w_{co}^2}{t^2} \qquad \text{Eq. 6.47}$$

When the plate has an initial curvature with initial mid-span deflection of f_i and simply supported edges, the following modified relation for $\bar{\alpha}$ applies:

$$\bar{\alpha}\,(1+\bar{\alpha})^2 = \frac{3\,(f_i + w_{co})^2}{t^2} - \frac{3\,f_i^2\,(1+\bar{\alpha})^2}{t^2} \qquad \text{Eq. 6.48}$$

If the plate has rotationally built-in and fixed edges, replace the term $(1 + \bar{\alpha})$ with $(1 + \bar{\alpha}/4)$ in the above equations 6.41, 6.47, and 6.48 for $\bar{\alpha}$. Also:

$$w_c = \frac{w_{co}}{(1 + \frac{\bar{\alpha}}{4})} \qquad \text{Eq. 6.49}$$

For uniformly distributed lateral loading with built-in edges:

$$w_{co} = \frac{q\,b^4}{384\,D} \qquad \text{Eq. 6.50}$$

$$M_e = \frac{1.216\,(1.57\sqrt{\bar{\alpha}} - \tanh 1.57\sqrt{\bar{\alpha}})}{\bar{\alpha}\,\tanh 1.57\sqrt{\bar{\alpha}}}\,M_{eo} \qquad \text{Eq. 6.51}$$

For uniformly distributed load with built-in edges:

$$M_{eo} = -\frac{q\,b^2}{12} \qquad \text{Eq. 6.52}$$

Example 6.6 illustrates the evaluation of ship plating as a long flat plate using the above approximate analysis for cases (a) where the edges are held without in-plane movement, and (b) where the supports allow a fixed inward movement. The former case is compared with results obtained using the curves of Figs. 6-4 and 6-9, with $a/b = \infty$.

Example 6.6: Determine the maximum stress and the mid-span deflection in the bottom plating of the boat hull shown below.

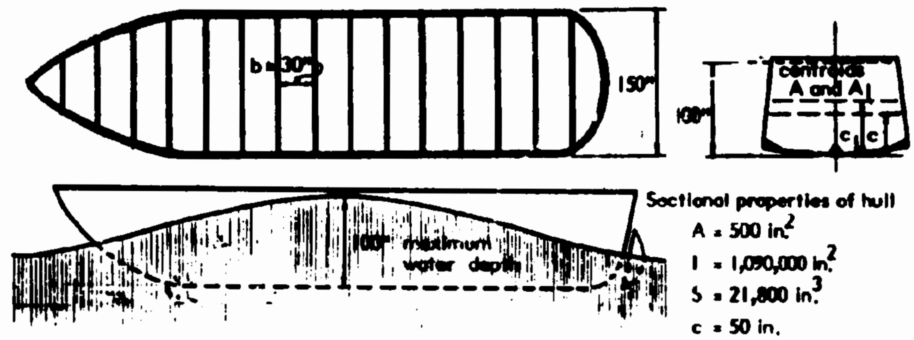

maximum "hogging" moment (i.e. hull moment with wave crest at mid-ships) = 10,000 in-lbs

The hull plating is an FRP laminate made up of a combination of mat and woven roving 0.5 inches thick. Assume that this laminate is isotropic for purposes of analysis. Initial modulus of elasticity for short time loading is 1,500,000 psi and ν is 0.3.*

(a) First assume that the frames do not move longitudinally relative to each other, thereby making the edge condition for analysis of bottom plating held against translation and fixed against rotation.

(b) Take into account relative longitudinal displacement of adjacent frames due to hull bending and reaction to membrane tension from plate action of the bottom plate under lateral pressure.

Solution:

(a) When the longitudinal movement of transverse supports is neglected, the bottom plate resists lateral fluid pressure as a plate with multiple equal spans supported on the transverse frames without edge rotation (since adjacent spans and restraints are identical) and is also held against in-plane translation. Using the approximate method for a plate essentially spanning in one direction given in this Section of the text:

$$q = 100 \times 62.4 \div 1728 = 3.61 \text{ psi}$$

$$D = \frac{1 \times 0.5^3 \times 1,500,000}{12\,(1 - .3^2)} = 17,170 \text{ lbs-in.}^2\text{/in.}$$

$$w_{co} = \frac{3.61 \times 30^4}{384 \times 17,170} = 0.44 \text{ in.}$$

Note: 1 in. = 25.4 mm; 1 in.^{2} = 645 mm^2; 1 in.^{3} = 16,387 mm^3;
1 in.^{4} = 416,231 mm^4; 1 psi = 0.0069 MPa; 1 lbf-in.^{2}/in. = 113 N-mm^2/mm;
1 lbf/in. - 0.18 N/mm; 1 in.-lbf/in. = 4.45 mm-N/mm

* See footnote, Example 6-1, p. 29.

From Eq. 6.41, modified for rotationally fixed end conditions:

$$\bar{\alpha}\left(1+\frac{\bar{\alpha}}{4}\right)^2 = \frac{3 \times 0.44^2}{0.5^2} = 2.32$$

Cut and try solution:

Trial $\bar{\alpha}$ (1)	$(1+\frac{\bar{\alpha}}{4})$ (2)	$(1) \times (2)^2 \overset{?}{=} 2.32$	
1.5	1.375	2.83	
1.3	1.325	2.28	
1.32	1.33	2.33	ok

$$w_c = \frac{0.44}{1+\frac{1.32}{4}} = 0.33 \text{ in.}$$

From Eq. 6.40: $\quad 1.32 = \dfrac{N_{he} \times 30^2}{\pi^2 \times 17{,}170}$

$N_{he} = 248.5$ lbs/in.; $\quad \sigma_{memb} = 248 \div 0.5 = 497$ psi

From Eq. 6.52: $\quad M_{eo} = -\dfrac{3.61 \times 30^2}{12} = -271$ in.-lbs/in.

From Eq. 6.51 $\quad M_e = \dfrac{1.216\,(1.57\sqrt{1.32} - \tanh 1.57\sqrt{1.32})(-271)}{1.32 \tanh 1.57\sqrt{1.32}}$

$M_e = -226$ in.-lbs/in; $\quad S = \dfrac{1 \times 0.5^2}{6} = 0.0417$

$\sigma_{eb} = \pm \dfrac{226}{0.0417} = \pm 5420$ psi

Total stress: $\quad \sigma_E = 497 + 5420 = 5917$ psi

Compare with results using direct solution, Fig. 6-9 with a/b = ∞:

$$\frac{b}{t}\left(k_o \frac{q}{E}\right)^{1/4} = \frac{30}{0.5}\left(1 \times \frac{3.61}{1.5 \times 10^6}\right)^{1/4} = 2.36$$

From Fig. 6-9 for $a/b = \infty$: $\frac{\sigma_{Ey}}{q}\left(\frac{t}{b}\right)^2 = 0.46$; $\sigma_{Ey} = 0.46 \times 3.61 \times \left(\frac{30}{0.5}\right)^2 = 5978$ psi

$$\frac{\sigma_{ey}}{q}\left(\frac{t}{b}\right)^2 = 0.04; \quad \sigma_{ey} = 0.04 \times 3.61 \times \left(\frac{30}{0.5}\right)^2 = 520 \text{ psi}$$

$$\sigma_{eb} = \sigma_{Ey} - \sigma_{ey} = 5978 - 520 = 5458 \text{ psi}$$

$$M = \sigma_{eb} S = 5458 \times \frac{0.5^2}{6} = 227 \text{ in.-lbs/in.}$$

From Fig. 6-5: $\frac{w_c}{t} = 0.65$; $\quad w_c = 0.65 \times 0.5 = 0.325$ in.

Conclude: Solutions from graphs and from approximate method are in good agreement.

(b) The hogging moment causes bending of the hull which results in relative longitudinal movement between frames. Furthermore, the membrane tension which develops in the bottom plating due to lateral load also produces a compressive reaction on adjacent longitudinal elements which tend to act as compressive bars to resist the applied membrane tension in the plating. These two effects may be taken into account by considering a cut through the bottom plate with an applied tension force N_{he} and the remainder of the longitudinal structure (having area A_l and moment of inertia I_l without the bottom plate) providing resistance to the applied bending moment and eccentrically applied N_{he}.

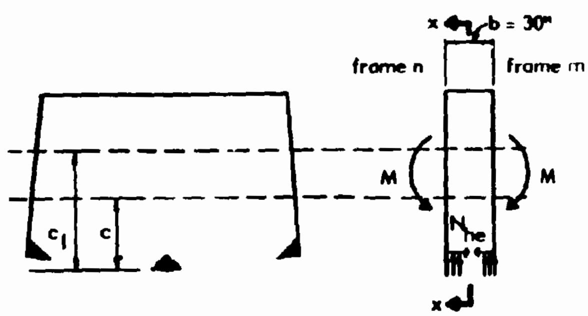

Cross Section X-X (Area A_l) Longitudinal Section

Section properties without bottom plating:

$$A_l = A - at = 500 - 150 \times 0.5 = 425 \text{ in.}$$

	Area	y	Ay	y_o	Ay_o^2	I_o
A	500	50	25,000	8.8	38,720	1,090,000
	-75	0	0	58.8	-259,412	0
A_l	425		25,000		-220,692	1,090,000

$$c_l = \frac{25,000}{425} = 58.8 \text{ in.}$$

$$I_l = 1,090,000 - 220,692 = 869,308 \text{ in.}^4$$

$$S_{l\ bot} = \frac{I_l}{c_l} = \frac{869,308}{58.8} = 14,784 \text{ in.}^3$$

Relative Longitudinal Displacement Between Frames:

$$\delta_h = \frac{b(1-\nu^2)}{E}\left[\frac{a N_{he}}{A_l} + \frac{a N_{he} c_l}{S_l} + \frac{M}{S_l(1-\nu^2)}\right]$$

$$\delta_h = \frac{30 \times 0.91}{1,500,000}\left[\frac{150 N_{he}}{425} + \frac{150 N_{he} \times 58.8}{14,784} + \frac{10,000,000}{14,784 \times 0.91}\right]$$

$$\delta_h = 18.2 \times 10^{-6}\left[0.95 N_{he} + 743\right] = (0.0173 N_{he} + 13.52)\,10^{-3}$$

From Eq. 6.40: $N_{he} = \dfrac{\pi^2 \times 17,170\,\bar{\alpha}}{30^2} = 188.3\,\bar{\alpha}$

$$\delta_h = 3.26 \times 10^{-3}\,\bar{\alpha} + 13.5 \times 10^{-3}$$

From Eq. 6.47, modified for rotationally fixed edges:

$$\bar{\alpha}\left(1 + \frac{\bar{\alpha}}{4}\right)^2\left(1 + \frac{12 \times 30\,(3.26\,\bar{\alpha} + 13.5) \times 10^{-3}}{\pi^2 \times 0.5^2}\right) = \frac{3 \times 0.44^2}{0.5^2}$$

$$\bar{\alpha}\left(1 + \frac{\bar{\alpha}}{4}\right)^2\left(0.475 + \frac{1.97}{\bar{\alpha}}\right) = 1.97\left(1 + \frac{\bar{\alpha}}{4}\right)^2(1 + 0.24\,\bar{\alpha}) = 2.32$$

$$(1 + 0.25\,\bar{\alpha})^2(1 + 0.24\,\bar{\alpha}) = 1.18$$

<u>Cut and try solution for $\bar{\alpha}$:</u>

$\bar{\alpha}$ (1)	$(1 + 0.24\,\bar{\alpha})$ (2)	$(1 + 0.25\,\bar{\alpha})$ (3)	$(2) \times (3)^2 \overset{?}{=} 1.18$
0.25	1.06	1.0625	1.19
0.24	1.0576	1.06	1.188
0.23	1.055	1.0575	1.18

$$N_{he} = \frac{0.23 \times \pi^2 \times 17,170}{30^2} = 43.3 \text{ lbs/in.}; \quad \sigma_e = \frac{43.3}{0.5} = 87 \text{ psi}$$

Stress in longitudinal elements of bottom hull, other than plate:

$$\sigma_{bot} = -\frac{10,000,000}{14,784} - \frac{150 \times 43.3}{425} - \frac{150 \times 43.3 \times 58.8}{14,784} = -676 - 15.0 - 26 = -717 \text{ psi}$$

Stress in longitudinal elements of hull if influence of bending of bottom plate on longitudinal stress is neglected:

$$\sigma_{bot} = -\frac{10,000,000}{21,800} = -460 \text{ psi}$$

Bending moment in bottom plate:

$$M_e = \frac{1.216\,(1.57\sqrt{0.23} - \tanh 1.57\sqrt{0.23})}{(0.23)\tanh 1.57\sqrt{0.23}}\, M_{eo}$$

$$M_e = 0.96\, M_{eo} = 0.96 \times 3.61 \times 30^2 \div 12 = 260 \text{ in.-lbs/in.}$$

$$\sigma_{eby} = \frac{6 \times 260}{0.5^2} = 6,240 \text{ psi}; \qquad \sigma_{Ey} = 6,240 + 87 = 6,327 \text{ psi}$$

Deflection of bottom plate:

From Equations 6.49 and 6.40:

$$w_c = \frac{3.61 \times 30^4}{384 \times 17,170\,(1 + \frac{0.23}{4})} = 0.42 \text{ in.}$$

Conclude: Strain due to hogging moment and reaction to membrane tension in bottom plates causes in-plane translation of bottom plate supports which results in a large decrease in membrane action in the bottom plating and an increase in stress in the plating resulting from the increased bending moment which accompanies the decreased membrane tension. Furthermore, the local deflection and development of membrane tension in the bottom plating reduces its effectiveness as a hull girder compression flange, resulting in an increase in longitudinal stresses in the other elements which comprise the hull girder.

Note: For purposes of simplification, the effect of deflection and membrane tension in the hull side plates has been neglected. This would cause further loss in membrane support of plate loads and further increases in plate and hull girder stresses.

6.6 ORTHOTROPIC PLATES UNDER LATERAL LOAD

Some unisotropic plastics materials can be approximated as planar orthotropic materials with stiffness properties determined as described in Section 6.2. Also grids can be evaluated as equivalent orthotropic plates as described in (6.2) and (6.3). Only a limited number of solutions for common loadings, shapes, and support conditions are available in the literature.

Deflections and Bending Moments in Common Approximations for Rectangular Plates

If an average Poisson's ratio is defined as:

$$\nu_c = \frac{\nu_{12} E_{22}}{\sqrt{E_{11} E_{22}}} = \frac{\nu_{21} E_{11}}{\sqrt{E_{11} E_{22}}}$$

then

$$D_{12} = \nu_c \sqrt{D_{22} D_{11}}$$

also, sometimes the shear stiffness, D'_{12}, may be approximated as:

$$D'_{12} = \frac{1 - \nu_c}{2} \sqrt{D_{11} D_{22}}$$

In this case, from Equation 6.6e:

$$D_o = \sqrt{D_{11} D_{22}} \qquad \text{Eq. 6.53}$$

When D_o is given by Eq. 6.53, the deflection at the center of an orthotropic plate with rigidities D_{11} and D_{22} and sides a and b is the same as the deflection of an isotropic plate with a rigidity $D = D_o$ and sides

$$a_o = a \sqrt[4]{\frac{D_o}{D_{11}}} \quad ; \quad b_o = b \sqrt[4]{\frac{D_o}{D_{22}}} \qquad \text{Eq. 6.54}$$

Using the above approximation, the deflection and bending moments at the center of a uniformly loaded, rectangular, simply supported, orthotropic plate with principal axes, 1 and 2, coinciding with the plate axes of symmetry, x and y, may be obtained using coefficients given by the curves of Fig. 6-18 and the following equations (6.2):

$$w_c = k_1 \frac{q b^4}{D_{22}} \qquad \text{Eq. 6.55}$$

$$\lambda_3 = \frac{a}{b} \sqrt[4]{\frac{D_{22}}{D_{11}}} \qquad \text{Eq. 6.56}$$

$$M_x = (k_2 + k_3 \ \nu_{21} \sqrt{\frac{D_{11}}{D_{22}}}\ ) \frac{q a^2}{\lambda_3^2} \qquad \text{Eq. 6.57}$$

$$M_y = (k_3 + k_2 \ \nu_{12} \sqrt{\frac{D_{22}}{D_{11}}}\ ) \ q b^2 \qquad \text{Eq. 6.58}$$

For isotropic plates, $D_{22} = D_{11} = D$ and $\nu_{21} = \nu_{12} = \nu$, and λ_3 is simply the ratio a/b. In this case, approximately the same results are obtained from either Fig. 6-10 or Fig. 6-18.

Direct solutions for maximum bending moments in orthotropic rectangular plates with Poisson's Ratio, $\nu_{12} = \nu_{21} = 0$, where principal axes of material stiffness coincide with plate symmetry axes, x and y, respectively, with uniformly distributed lateral load, q, and both simply supported and rotationally fixed edges are given in Figs. 6-19 and 6-20 respectively (6.3). Moments vary with $\lambda_1 = b/a \sqrt[4]{D_{11}/D_{22}}$ and with $D_o/\sqrt{D_{11} D_{22}}$, where D_o is determined using Eq. 6.6e. Moments are obtained from coefficients given in the Figures as follows:

$$M_{xc} = k_4 \, q \, a^2$$

$$M_{yc} = k_5 \, q \, b^2$$

$$M_{xe} = k_6 \, q \, a^2 \qquad \text{Eqs. 6.59}$$

$$M_{ye} = k_7 \, q \, b^2$$

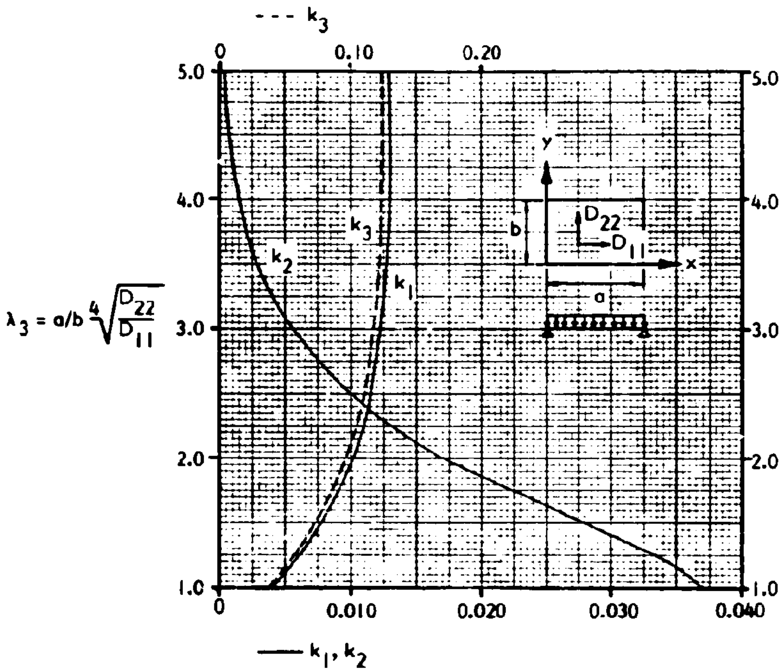

Fig. 6-18 COEFFICIENTS FOR MAXIMUM MOMENTS AND DEFLECTIONS IN SIMPLY SUPPORTED RECTANGULAR ORTHOTROPIC PLATES WHERE $D_o = \sqrt{D_{11} D_{22}}$ (SMALL DEFLECTION SOLUTION) (6.2)

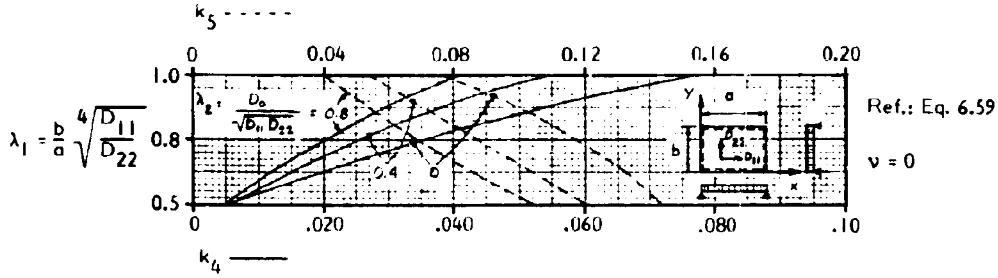

Fig. 6-19 COEFFICIENTS FOR DETERMINATION OF BENDING MOMENTS IN SIMPLY SUPPORTED RECTANGULAR ORTHOTROPIC PLATES (SMALL DEFLECTION SOLUTION) (6.3)

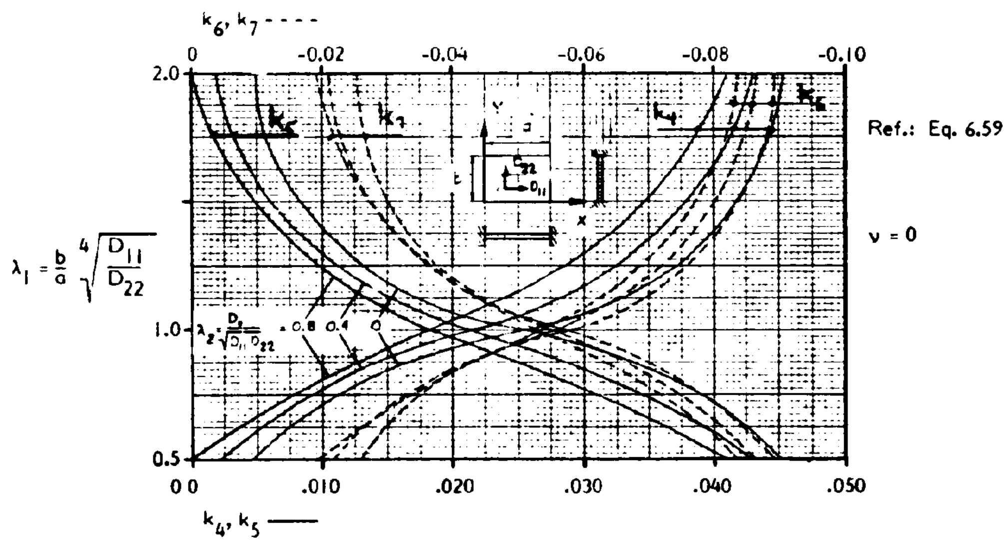

Fig. 6-20 COEFFICIENTS FOR DETERMINATION OF BENDING MOMENTS IN RECTANGULAR ORTHOTROPIC PLATES WITH ROTATIONALLY FIXED SUPPORTS (SMALL DEFLECTION SOLUTION) (6.3)

In the case of simply supported plates, the maximum moments occur at the center of the plate. In the case of rotationally fixed edges, maximum moments occur at the center of the plate and minimum (maximum negative) moments occur at the center of the fixed edge. The following approximate corrections for specific ν values may be used (6.3):

$$M_x = M_{x_o} + \nu_{21} \sqrt{\frac{D_{11}}{D_{22}}}\; M_{y_o}$$

$$M_y = M_{y_o} + \nu_{12} \sqrt{\frac{D_{22}}{D_{11}}}\; M_{x_o} \qquad \text{Eqs. 6.60}$$

where M_{x_o} and M_{y_o} are moments for $\nu = 0$ (Figs. 6-19 and 6-20).

Maximum bending stresses are:

$$\sigma_x = \frac{6\, M_x}{t^2} \;; \quad \sigma_y = \frac{6\, M_y}{t^2} \qquad \text{Eqs. 6.61}$$

When deflections determined from these small deflection solutions exceed about 0.5t, deflections and moments will be overestimated by amounts which increase with increases in flexibility. If more accurate solutions are required, it may be necessary to use a non-linear finite element analysis. See Section 4.9. Sometimes, approximate results of sufficient accuracy can be obtained by the methods suggested in the previous Section, using equations for isotropic membranes to approximate the membrane part of the problem.

Example 6-7 in the next Section illustrates the evaluation of a rectangular orthotropic plate using the curves presented in this Section for determining bending moments in each principal direction and maximum center deflection.

6.7 LAMINATED PLATES UNDER LATERAL LOADS AND INTERNAL THERMAL STRESSES

Plastics and composites are used in laminated or layered thin flat plate configurations as described in Chapters 1 to 4. Such plates are sometimes built up from layers of unidirectional composites, such as graphite or aramid reinforced epoxy, which are oriented in two or more directions to form an anisotropic layered plate (See Table 1-8, Figs. 2-12 and 4-15).

Procedures for determining stiffnesses, flexural stresses, and deflections in laminated plates are discussed below, together with a design example, to illustrate the use of laminated plate theory. Because of space limitations, the presentation is limited to specially orthotropic plates where the principal axes of each layer coincide with the plate axes, x and y, and to plates with balanced construction as shown in Fig. 6-21 and described in Sections 3.5 and 4.6.

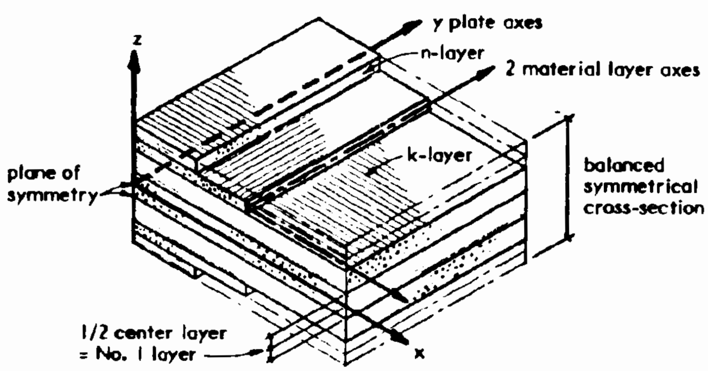

Fig. 6-21. ORIENTATION OF REFERENCE AXES FOR BALANCED SYMMETRICAL ORTHOTROPIC LAMINATED MATERIALS – PRINCIPAL AXES, 1 AND 2, OF MATERIAL STIFFNESS OF EACH LAYER ARE PARALLEL TO PLATE REFERENCE AXES, X AND Y

Presentation of the underlying theory of laminated plates is beyond the scope of this design manual. See (6.7) and (6.8) for detailed expositions of the relevant theory.

Cross Section Stiffness

In order to determine deflections, bending moments, axial thrusts, shears, twists, and reactions due to external loads on laminated plate components, it is necessary to determine the in-plane and flexural stiffnesses of the overall plate, either from direct tests on the plate, or from the elastic properties of the individual layers, if they are known. The latter approach is described in this Section.

Stiffness relationships are given in Table 3-5 of Section 3.5. They are also given in Appendix B of (6.1) for a more general case of balanced laminates where the principal axes of some of the symmetrically placed layers may be at any angle, ψ_k, with plate axis x. See also (6.9) for a more detailed and general presentation which introduces the use of matrix notation. Because of the number of components involved in the analysis, presentation is facilitated and computational work systematized by the use of matrix notation. However, because of space limitations, matrix notation will not be introduced here. See (6.1) and (6.9) for examples of the use of matrix notation for laminated plate analysis. Reference (6.1) also covers laminated plates with unbalanced construction, thermal stresses, and built-in layer stresses resulting from elevated assembly temperatures. Examples illustrating the use of the analysis procedures are included.

For a single plate consisting of an assembly of 2n layers arranged in a balanced configuration about the mid-plane, with the principal orthotropic axes of each layer coinciding with the x and y axes of the plate (Fig. 6-21), plate stiffnesses are determined using Eqs. 6.5 and 6.6 by summing the contributions from each layer, k, over the total number of layers, 2n.

The following stiffness coefficients for the kth layer, defined more extensively in (6.1), facilitate the organization of calculations, as well as use of matrix algebra, in analyzing specially orthotropic plates:

$$b_{11k} = \frac{E_{11}}{(1 - \nu_{12}\nu_{21})} \qquad \text{Eq. 6.62a}$$

$$b_{22k} = \frac{E_{22}}{(1 - \nu_{12}\ \nu_{21})} \qquad \text{Eq. 6.62b}$$

$$b_{12k} = b_{21k} = \frac{\nu_{21}\ E_{11}}{(1 - \nu_{12}\ \nu_{21})} = \frac{\nu_{12}\ E_{22}}{(1 - \nu_{12}\ \nu_{21})} \qquad \text{Eq. 6.62c}$$

$$b_{33k} = G_{12} \qquad \text{Eq. 6.62d}$$

Note that the notation 3 does <u>not</u> refer to a third axis perpendicular to plane 1-2. The analysis presented herein covers only two-dimensional thin plates, and the 33 notation is used for convenience in organizing calculations (6.1).

The stiffness coefficients for each layer, b_{ijk}, are defined by Eqs. 6.62 for layers with principal axes parallel to the plate axes, x and y. However, for layers with major axes at 90° to the x axis of the plate, it is convenient to redefine the stiffness coefficients for these layers as follows:

$$b_{11k} = \frac{E_{22}}{(1 - \nu_{12}\ \nu_{21})} \quad \text{for layers at } 90^\circ \text{ with x} \qquad \text{Eq. 6.62e}$$

$$b_{22k} = \frac{E_{11}}{(1 - \nu_{12}\ \nu_{21})} \quad \text{for layers at } 90^\circ \text{ with x} \qquad \text{Eq. 6.62f}$$

The terms in Eqs. 6.62c and d do not require modification for layers at 90° with x.

The above stiffness coefficients are used in Table 6-2 to define the basic stiffness properties for laminated specially orthotropic plate cross sections. These are similar to the properties presented previously in Table 6-1, Section 6.2, for homogeneous uniform thickness specially orthotropic plates.

Table 6-2

Stiffness Properties of Specially Orthotropic Laminated Plate Cross Sections

Stiffness Property	Balanced Symmetrical Layered Cross Section	Eq. No.
In plane, $\bar{A}_{ij}$	$2 \sum_{k=1}^{k=n} t_k b_{ijk}$	Eq. 6.63a
Flexural, D_{ij}	$2 \sum_{k=1}^{k=n} (t_k z_k^2 + i_k) b_{ijk}$	Eq. 6.63b
	$i_k = \frac{t_k^3}{12}$ *	Eq. 6.63c
	$D_{12}' = D_{33}$ for matrix notation	Eq. 6.63d

The twisting parameter is:

$$D_0 = D_{12} + 2 D_{33} \qquad \text{Eq. 6.63e}$$

* Note: For plates with thin layers, this term is often very small, relative to $t_k z_k^2$.

Flexural Stresses and Deflections

After the overall plate stiffnesses are calculated using Eqs. 6.63, bending moments in the direction of plate axes can be calculated for laterally loaded plates using the design aids given in the previous Section, or in the references at the end of this Chapter. For loading or support cases not covered by design aids, the overall stiffness constants can be used in a finite element computer analysis of the orthotropic plate (Section 4.9).

Maximum plate deflection is determined using the above mentioned design aids or computer analysis with the calculated stiffness constants.

Stresses in the various layers are then determined from the following equations:

Flexural and axial stress in x direction:

$$\sigma_{xk} = b_{11k} \left[\frac{N_x}{\bar{A}_{11}} - \frac{M_x z_k}{D_{11}} \right] \qquad \text{Eq. 6.64a}$$

Flexural and axial stress in y direction:

$$\sigma_{yk} = b_{22k} \left[\frac{N_y}{\bar{A}_{22}} - \frac{M_y z_k}{D_{22}} \right] \qquad \text{Eq. 6.64b}$$

Shear stress on x and y faces in plane of plate:

$$\tau_{xyk} = \tau_{yxk} = b_{12k} \left[\frac{N_{xy}}{\bar{A}_{12}} - \frac{M_{xy} z_k}{D_{12}} \right] \qquad \text{Eq. 6.64c}$$

The above method for determining plate stiffness and stresses in each layer of a balanced symmetrical orthotropic laminated plate is illustrated in **Example 6.7** at the end of this Section. The example also illustrates the use of Fig. 6-19 for determining bending moments and deflections in a laminated orthotropic plate.

The above method can be used for balanced laminated plates having layers at angles other than 0 degrees and 90 degrees with the plate x axis with the aid of the more complex relations for b_{ijk} given in Appendix B of (6.1) and the additional stress transformation equations given in (6.9) to obtain stresses in the principal axes direction of the layers located at an angle with the x-axis. The more general method given in (6.1) and (6.9) could easily be computerized to facilitate solution of a wide variety of laminated plate problems.

Transformed Section Method

A method commonly known as the "transformed section" method of elementary beam theory is very similar to the laminated plate theory given above for orthotropic layers balanced and with principal axes at 0 and 90 degrees to the x-axis. In the elementary "transformed section" method, however, the effects of restraint of "Poisson deformation" in plates are neglected and the effects of in-plane shear and twist are not considered. See Chapter 8 for further discussion of this elementary method for determining stiffness properties and stresses in sandwich beams and plates.

Transverse and Interlaminar Shear Stresses

Plates which transmit lateral load are subject to transverse shear forces, Q, which are proportional to the change in plate bending and twisting moments. These shear forces produce a system of equal transverse and interlaminar (between planes) shear stresses, τ_{xz} and τ_{zx} (or τ_{yz} and τ_{zy}), which vary through the thickness of the plate from a maximum at the neutral axis to zero at the surfaces. Some layered composites may have relatively low interlaminar shear strength, and thus, require more extensive investigation of the effects of shear than is needed in conventional homogeneous plates. The "rolling shear" strength used in plywood design is a familiar example of an interlaminar shear criterion.

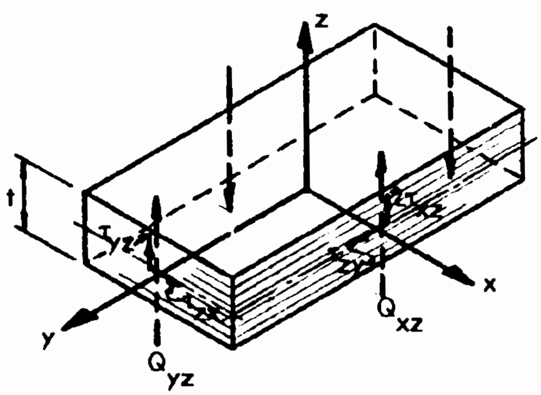

Fig. 6-22. TRANSVERSE AND INTERLAMINAR SHEAR STRESSES CAUSED BY TRANSVERSE SHEAR FORCE ON PLATE ELEMENT

Referring to Figs. 6-21 and 6-22, the maximum interlaminar shear stress occurs between layers 1 and 2 just above the neutral axis. This stress is determined from the transverse shear forces on faces of the plate perpendicular to the x and y axes, respectively, as follows:

$$\tau_{xz\ 1\text{-}2} = \tau_{zx\ 1\text{-}2} = \frac{Q_{xz} \sum_{k=2}^{k=n} t_k z_k b_{11k}}{D_{11}} \qquad \text{Eq. 6.65a}$$

$$\tau_{yz\ 1\text{-}2} = \tau_{zy\ 1\text{-}2} = \frac{Q_{yz} \sum_{k=2}^{k=n} t_k z_k b_{22k}}{D_{22}} \qquad \text{Eq. 6.65b}$$

In design, the above stresses must not exceed the transverse shear or interlaminar shear strength limits for the material. With layered composites, the interlaminar shear strength is usually much lower than the transverse shear strength, thereby dominating the shear behavior of such plates. In contrast, shear strength of a concrete member is governed by the principal diagonal tension stress resulting from the transverse and horizontal shear stresses.

Transverse shear forces also produce transverse shear deformations that are usually neglected in conventional analyses of stresses and deflections in plates. In laminated plates where some layers or interfaces have low shear stiffness, significant errors may be introduced when shear deformation is neglected. This is especially true for sandwich plates with "shear flexible" cores, as discussed in Chapter 8.

Consideration of the effects of shear deformation on plate bending moments and deflections is beyond the scope of this Chapter. See (6.8) for plots showing the significance of shear deformation with varying shear stiffness for several specific example plates. See Section 8.7 for further discussion of shear deformation in sandwich plates.

Internal Thermal Stresses

Sometimes, layered composites are assembled at temperatures which vary substantially from service temperatures, and thus are subject to significant thermal changes. If the coefficients of expansion of the various layers, α_k, are different, thermal changes will cause internal stresses within the laminate. For the symmetrical balanced constructions considered here, the following steps may be used to determine the stresses in layer, k, resulting from a temperature variation, ΔT, from the assembly temperature (6.9):

1. Determine strain in each layer, k, due to full restraint of a temperature change, ΔT (ΔT is + for temperature drop):

$$e_{Txk} = \alpha_{xk} \Delta T \; ; \; e_{Tyk} = \alpha_{yk} \Delta T \qquad \text{Eqs. 6.66}$$

2. Determine total forces, N_T, to fully restrain the plate in its assembly position:

$$N_{Tx} = 2 \sum_{k=1}^{k=n} e_{Txk} \, b_{11\,k} \, t_k \qquad \text{Eq. 6.67a}$$

$$N_{Ty} = 2 \sum_{k=1}^{k=n} e_{Tyk} \, b_{22\,k} \, t_k \qquad \text{Eq. 6.67b}$$

3. Determine stress in each layer which equals stress to fully restrain temperature strain, e_{Tk}, less stress when total holding force, N_T, is released:

$$\sigma_{xk} = b_{11\,k} \left(e_{Txk} - \frac{N_{Tx}}{\bar{A}_{11}} \right) \qquad \text{Eqs. 6.68a}$$

$$\sigma_{yk} = b_{22\,k} \left(e_{Tyk} - \frac{N_{Ty}}{\bar{A}_{22}} \right) \qquad \text{Eq. 6.68b}$$

The final total force across the thickness of a unit width section in each direction must equal zero.

Example 6.7 also illustrates the determination of thermal stresses arising from fabrication of the plate at an elevated temperature, and use of the plate at other temperatures.

Matrix methods for more complex cases involving built-in stresses in balanced symmetrical laminates with some layers at angles ψ_k with the plate axis, x, and also built-in stresses in unbalanced laminates are given in (6.9).

Other effects that may require consideration in the design of laminated composites include radial tension within and between layers in curved members, and thermal gradients across the laminate thickness. Detailed consideration of these is beyond the scope of the limited treatment of laminated plate theory in this Section. To some extent, the discussion of gradient effects in sandwich panels, which is given in Chapter 8, is relevant. Radial tension is discussed in Chapter 9.

Example 6.7: Determine the maximum short-term uniformly-distributed lateral pressure that can be applied on the plate shown in the sketch with maximum stresses and deflection within the design allowables given below. The plate is fabricated by laminating layers of unidirectional aramid and graphite-reinforced epoxy tape in a balanced symmetrical arrangement with all plies at zero or 90 degrees, arranged as shown in the cross section. Assembly temperatures differ substantially from the expected service temperature, resulting in a balanced system of internal thermal stresses in the various layers of the laminate. A maximum range of 0 to 100 degree drop from assembly temperature is to be considered in evaluating the plate in this example.*

Plate size: 24 in. x 36 in. ; Supports: Simple

Max. thermal change from assembly temperature: -100°F ; Limiting deflection: 0.2 in.

Material properties:			Aramid-epoxy	Graphite-epoxy (high modulus type)
Layer thickness:	t_k	in.	0.06	0.06
Moduli of elasticity:				
longitudinal	E_L	psi	10×10^6	25×10^6
transverse	E_T	psi	1.0×10^6	1.67×10^6
	G_{TL}	psi	0.3×10^6	0.65×10^6
	ν_L		0.30	0.30
	ν_T		0.03	0.02
Coefficient of expansion:				
longitudinal	α_{kL}	in./in./°F	-2.2×10^{-6}	0
transverse	α_{kT}	in./in./°F	32×10^{-6}	20×10^{-6}
Tension				
longitudinal	allow f_L	psi	55,000	35,000
transverse	allow f_T	psi	3,000	2,400
Compression				
longitudinal	allow f_L	psi	13,000	33,000
transverse	allow f_T	psi	12,000	12,000

Note: 1°F = 1.8°C; 1 in. = 25.4 mm; 1 psi = 0.0069 MPa;
1 in./in./°F = 1.8 mm/mm/°C; 1 lbf-in.^{2}/in. = 113 N-mm^2/mm;
1 in. kf/in. = 4450 N-mm/mm

* See footnote, Example 6-1, p. 29.

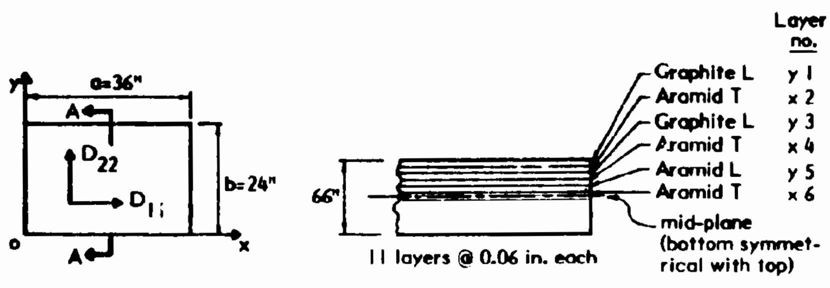

Plan

Cross Section A-A Through Laminate

Solution:

1. Determine flexural stiffness constants for the laminate: D_{11}, D_{22}, D_{12}, and D_{33}.

From Eqs. 6.63b (with $I_k = \frac{t_k^3}{12}$ considered negligible):

$$D_{11} = 2 \sum_{k=1}^{k=6} t_k z_k^2 b_{11k} \; ; \qquad D_{22} = 2 \sum_{k=1}^{k=6} t_k z_k^2 b_{22k}$$

$$D_{12} = 2 \sum_{k=1}^{k=6} t_k z_k^2 b_{12k} \; ; \qquad D_{33} = 2 \sum_{K=1}^{k=6} t_k z_k^2 b_{33k}$$

For Graphite L (G_L):
(Eqs. 6.62)

$$b_{22} = \frac{25 \times 10^6}{1 - 0.3 \times 0.02} = 25.15 \times 10^6 \text{ psi}$$

$$b_{11} = \frac{1.67 \times 10^6}{1 - 0.3 \times 0.02} = 1.68 \times 10^6 \text{ psi}$$

$$b_{12} = \frac{0.02 \times 25 \times 10^6}{1 - 0.3 \times 0.02} = 0.503 \times 10^6 \text{ psi}$$

or

$$b_{12} = \frac{0.3 \times 1.67 \times 10^6}{1 - 0.3 \times 0.02} = 0.503 \times 10^6 \text{ psi}$$

$$b_{33} = 0.65 \times 10^6$$

For Aramid T (A_T):
(Eqs. 6.62)

$$b_{22} = \frac{1 \times 10^6}{1 - 0.3 \times 0.03} = 1.01 \times 10^6 \text{ psi}$$

$$b_{11} = \frac{10 \times 10^6}{1 - 0.3 \times 0.03} = 10.09 \times 10^6 \text{ psi}$$

$$b_{12} = \frac{0.3 \times 1.0 \times 10^6}{1 \times 0.3 \times 0.03} = 0.303 \times 10^6 \text{ psi}$$

$$b_{33} = 0.3 \times 10^6 \text{ psi}$$

For Aramid L (A_L): (Eqs. 6.62)

$$b_{22} = \frac{10 \times 10^6}{1 - 0.3 \times 0.03} = 10.09 \times 10^6 \text{ psi}$$

$$b_{11} = \frac{1 \times 10^6}{1 \times 0.3 \times 0.03} = 1.01 \times 10^6 \text{ psi}$$

b_{12} and b_{33} same as A_T.

Table (a)

Layer No.	t	z_k	tz_k^2 $(\times 10^{-3})$	D_{22} $b_{22k}tz_k^2$ $(\times 10^3)$	D_{11} $b_{11k}tz_k^2$ $(\times 10^3)$	D_{12} $b_{12k}tz_k^2$ $(\times 10^3)$	D_{33} $b_{33}tz_k^2$ $(\times 10^3)$
1 G_L	.06	.30	5.40	136	9	2.7	3.5
2 A_T	.06	.24	3.46	3	35	1.0	1.0
3 G_L	.06	.18	1.94	49	3	1.0	1.3
4 A_T	.06	.12	0.86	1	9	0.3	0.3
5 A_L	.06	.06	0.22	2	0	0.1	0.1
6 A_T	.06	0	0	0	0	0.0	0.0
			11.88	191	56	5.1	6.2
				x 2	x 2	x 2	x 2
				382	112	10.2	12.4

$D_{22} = 382 \times 10^3$ lbs-in.^{2}/in.; $D_{11} = 112 \times 10^3$ lbs-in.^{2}/in.

From Eq. 6.63e: $D_o = D_{12} + 2\,D_{33} = (10.2 + 2 \times 12.4) \times 10^3 = 35 \times 10^3$ lbs-in.^{2}/in.

2. Analysis for Bending Moment - use Fig. 6-19

$$\lambda_1 = \frac{b}{a}\sqrt[4]{\frac{D_{11}}{D_{22}}} = \frac{24}{36}\sqrt[4]{\frac{112}{382}} = 0.49 \approx 0.5$$

$$\lambda_2 = \frac{D_o}{\sqrt{D_{11}D_{22}}} = \frac{35}{\sqrt{382 \times 112}} = 0.17$$

From Fig. 6-19: $k_4 = 0.006$; $k_5 = 0.132$

From Eq. 6.59: $M_{xc} = 0.006 \times q \times 36^2 = 7.78\,q$ in.-k/in. for $\nu = 0$

$M_{yc} = 0.132 \times q \times 24^2 = 76.0\,q$ in.-k/in.

Correction for $\nu \neq 0$: Use Eq. 6.60 and a weighted average for ν as follows:

$$\text{av. } \nu_{21} = \frac{\Sigma \nu_{21} t_k z_k}{\Sigma t_k z_k} \; ; \qquad \text{av. } \nu_{12} = \frac{\Sigma \nu_{12} t_k z_k}{\Sigma t_k z_k}$$

Layer No.	$t_k z_k$	$\nu_{21} t_k z_k$	$\nu_{12} t_k z_k$
1 G_L	.0180	.0054	.0005
2 A_T	.0144	.0003	.0043
3 G_L	.0108	.0032	.0003
4 A_T	.0072	.0001	.0022
5 A_L	.0036	.0011	.0001
6 A_T	0	0	0
	.0540	.0101	.0074

$$\text{Av. } \nu_{21} = \frac{.0101}{.054} = 0.19 \; ; \qquad \text{av. } \nu_{12} = \frac{.0074}{.054} = 0.14$$

From Eq. 6.60: $M_{xc} = 7.78\ q + 0.19 \sqrt{\frac{112}{382}}\ 76.0\ q = 15.6\ q$

$$M_{yc} = 76.0\ q + 0.14 \sqrt{\frac{382}{112}}\ 7.78\ q = 78.0\ q$$

Average Bending Stresses in Each Layer:

x direction, Eq. 6.64a: $\sigma_{xk} = \frac{b_{11k} z_k M_{xc}}{D_{11}} = \frac{15.6\ q}{112 \times 10^3}\ b_{11k} z_k$

y direction, Eq. 6.64b: $\sigma_{yk} = \frac{b_{22k} z_k M_{yc}}{D_{22}} = \frac{78.0\ q}{382 \times 10^3}\ b_{22k} z_k$

Table (b)

Layer No.	z_k (in.)	$10^{-6} b_{22k}$	$10^{-6} b_{11k}$	$\frac{\sigma_{yk}}{q}$ (psi)	$\frac{\sigma_{xk}}{q}$ (psi)
1 G_L	0.30	25.15	1.68	1532	70
2 A_T	0.24	1.01	10.09	49	337
3 G_L	0.18	25.15	1.68	920	42
4 A_T	0.12	1.01	10.09	25	168
5 A_L	0.06	10.09	1.01	123	8
6 A_T	0	1.01	10.09	0	0

Thermal Stresses

Assume that Modulus of Elasticity and Coefficient of Thermal Expansion have the average values given above over the full range of variation in temperature. Assume that the thermal change is a long-term effect which reduces the effective moduli E_L to 80% of values given in the table above and E_T to 50% of short-term values given above.

Strain in each layer from full restraint of movement after temperature change, T.

Eqs. 6.65: $e_{Txk} = \alpha_{xk} \times 100$; $e_{Tyk} = \alpha_{yk} \times 100$

Axial stiffness of laminate:

Eq. 6.63a: $A_{11} = 2 \sum_{k=1}^{k=6} t_k b_{11k}$; $A_{22} = 2 \sum_{k=1}^{k=6} t_k b_{22k}$

Force on laminate if fully restrained from thermal movement:

Eq. 6.66: $N_{Tx} = 2 \sum_{k=1}^{k=6} e_{Txk} b_{11k} t_k$; $N_{Ty} = 2 \sum_{k=1}^{k=6} e_{Tyk} b_{22k} t_k$

Thermal stresses in layers:

Eq. 6.67: $\sigma_{xk} = b_{11k}\left(e_{Txk} - \frac{N_{Tx}}{A_{11}}\right)$; $\sigma_{yk} = b_{22k}\left(e_{Txk} - \frac{N_{Ty}}{A_{22}}\right)$

Table (c)

Layer No.	t_k	b_{22k} ($\times 10^6$)	b_{11k} ($\times 10^6$)	A_{22} $t_k b_{22k}$ (10^6)	A_{11} $t_k b_{11k}$ ($\times 10^6$)	α_{yk} ($\times 10^{-6}$)	α_{xk} ($\times 10^{-6}$)	N_{Ty} $e_{Tyk} b_{22k} t_k$	N_{Tx} $e_{Txk} b_{11k} t_k$	$e_{Tyk} - \frac{N_{Ty}}{A_{22}}$ ($\times 10^{-6}$)	σ_{yk}	$e_{Txk} - \frac{N_{Tx}}{A_{11}}$ ($\times 10^{-6}$)	σ_{xk}
1 C_L	.06	.8 x 25.15	.5 x 1.68	1.207	0.050	0	20.0	0	100.0	- 45	- 905	1978	1662
2 A_T	.06	.5 x 1.01	.8 x 10.09	0.030	0.484	32.0	-2.2	96.0	-106.5	3155	1593	- 242	-1953
3 C_L	.06	.8 x 25.15	.5 x 1.68	1.207	0.050	0	20.0	0	100.0	- 45	- 905	1978	1662
4 A_T	.06	.5 x 1.01	.8 x 10.09	0.030	0.484	32.0	-2.2	96.0	-106.5	3155	1593	- 242	-1953
5 A_L	.06	.8 x 10.09	.5 x 1.01	0.484	0.030	-2.2	32.0	-106.5	96.0	- 265	-2139	3178	1605
6 A_T	.03	.5 x 1.01	.8 x 10.09	0.015	0.242	32.0	-2.2	48.0	- 53.0	3155	1593	- 242	-1953
				2.973	1.340			133.5	30.0				
				x 2	x 2			x 2	x 2				
				5.946	2.680			267.0	60.0				

Thermal stresses greatly reduce the allowable stresses available for lateral load, particularly in the transverse direction. The allowable lateral pressure, q, is determined using the σ/q ratios calculated in Table (b) and the difference between allowable material stress and thermal stress (Table (c)) for the various layers and lateral directions of material axis:

Transverse - Aramid

$$\frac{\sigma_y}{q} = 49 \; ; \qquad q = \frac{3000 - 1593}{49} = 29 \text{ psi}$$

Transverse - Graphite

$$\frac{\sigma_x}{q} = 70 \; ; \qquad q = \frac{2400 - 1662}{70} = 10.5 \text{ psi}$$

Longitudinal - Graphite

$$\frac{\sigma_y}{q} = 1532 \; ; \qquad q = \frac{33{,}000 - 905}{1532} = 21 \text{ psi}$$

Longitudinal - Aramid

$$\frac{\sigma_x}{q} = 337 \; ; \qquad q = \frac{13{,}000 - 1{,}978}{337} = 33 \text{ psi}$$

Thus, Transverse Graphite in outer layer governs and allowable lateral pressure (short term) = 10.5 psi.

6.8 ISOTROPIC DIAPHRAGMS

Thin plates that transmit applied loads to edge supports with all forces acting in their mid-planes are often referred to as diaphragms. A state of plane stress exists in such plates. A plate loaded in this way is shown in Fig. 6-23. In order to evaluate the structural adequacy of such a plate, it is necessary to determine the maximum tension and compression stresses, and their directions. These are compared to the material strength for the conditions of use (stress duration, temperature, and other environmental conditions) and the required safety factors. Also compression stress is evaluated based on stability considerations, as described in the next Section.

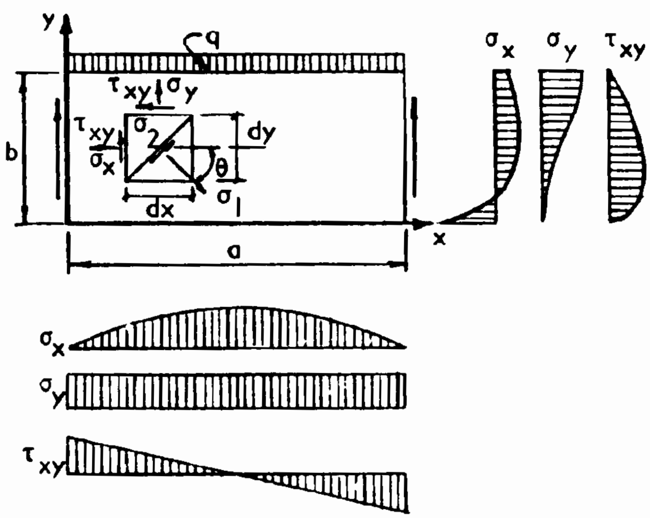

Fig. 6-23. **DIAPHRAGM PLATE – LOADS, SUPPORTS AND STRESS VARIATIONS**

Examples of plates where diaphragm stresses may be significant include floor and roof slabs and shear walls which distribute wind and seismic loads in buildings, bearing walls on intermittent supports, and webs of I or boxed shaped beams and deep girders.

Maximum tension and compression are "principal stresses." They may be determined, by first determining the general plane stress state at any point in the diaphragm, σ_x, σ_y, and σ_{xy}. Principal stresses, σ_m and σ_n are then:

$$\sigma_{m,n} = 0.5\,(\sigma_x + \sigma_y) \pm 0.5\sqrt{(\sigma_x - \sigma_y)^2 + 4\,\tau_{xy}^2} \qquad \text{Eq. 6.69a}$$

and their directions (principal axes) from the x-axis, $\theta_{m,n}$ are:

$$\tan 2\,\theta_{m,n} = \frac{2\,\tau_{xy}}{\sigma_x - \sigma_y} \qquad \text{Eq. 6.69b}$$

In some common cases of diaphragm plates, maximum values of σ_x and σ_y occur at locations where shear, τ_{xy}, is zero. In such locations, σ_x and σ_y are the principal stresses and no further calculations are required.

Determination of diaphragm stresses

In the general case of a diaphragm with arbitrary shape, loads and boundary conditions, stresses can readily be determined using elastic finite element analysis. See Section 4.9 and the related references in Chapter 4. Often, however, diaphragm elements of components can be idealized with shape, loading, and support conditions for which tabulations of maximum stresses are available in reference handbooks.

Available solutions for isotropic plates: Diaphragm plates are often loaded and supported such that they behave as deep beams. Stresses in deep beams are significantly influenced by the distribution of in-plane shear and bearing stresses at boundaries, as well as by the location of the points of application of external in-plane loadings. Furthermore, shear deflection cannot be neglected relative to flexural deflection in deep beams. Because of this, magnitude and distribution of stress is significantly altered from results of conventional beam theory in continuous, or other "indeterminant" deep beams.

For statically determinate simply supported diaphragm plates, in-plane stresses differ substantially from stresses determined with conventional beam theory when the span of the diaphragm, a, is less than about twice the depth, b. For continuous diaphragm plates, because of the additional rotational displacement over the supports resulting from shear deflection, in-plane stresses differ substantially from stresses determined with conventional beam theory when the span of the diaphragm is less than about three times the depth, b.

Graphs for determining maximum longitudinal stresses, σ_x, in common loading cases are given below. Tables of coefficients for maximum stresses in other loading and support cases are given in (6.3). See (6.10) for more detailed discussion of solutions for continuous deep beams.

For rectangular diaphragm plates having proportions of length to depth (a/b in Fig. 6-23) greater than about 1.5 for cantilever spans, 2.0 for simple spans, and 3.0 for fixed ended or continuous spans, in-plane stresses may usually be determined with sufficient accuracy by considering the diaphragm as a rectangular beam whose cross sections deform as a linear plane (plane sections remain plane after deformation) during bending. In this case:

$$\text{max. } \sigma_x = \frac{6\, M_{\text{in-plane}}}{t\, b^2} \qquad \text{Eq. 6.70a}$$

$$\text{max. } \tau_{xy} = \frac{1.5\, Q_{\text{in-plane}}}{t\, b} \qquad \text{Eq. 6.70b}$$

Diaphragm stresses in common loading cases: Maximum in-plane stresses for some common idealizations of rectangular diaphragm plates are given in Figs. 6-24 (a), (b), and (c)(6.3), 6-26, and 6-27 (6.10). Deflections are given in Fig. 6-25 (6.3).

Example 6.8 illustrates the use of these curves for determining maximum stresses in a diaphragm which behaves as a deep beam.

Stresses at selected points in an equilateral triangular diaphragm are given in Fig. 6-28 (6.3). Stresses in the vicinity of a short length of uniform load along one edge of an infinite plate are given in Fig. 6-29 (6.3).

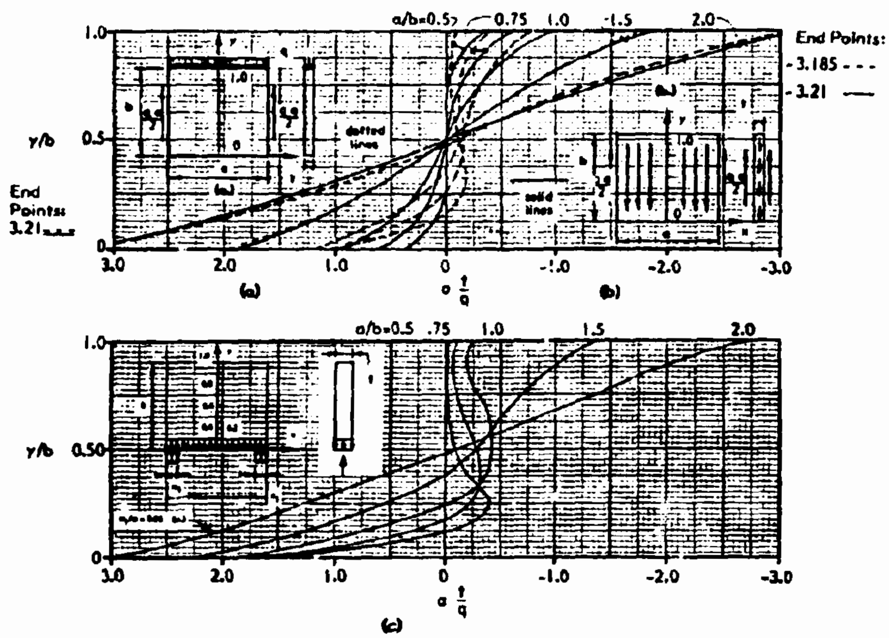

Fig. 6-24 VARIATION OF MIDSPAN σ_x WITH y/b FOR UNIFORMLY LOADED, SIMPLY SUPPORTED RECTANGULAR DIAPHRAGM PLATE (6.3)

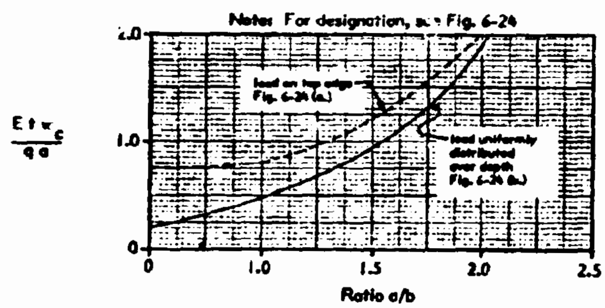

Fig. 6-25 MAXIMUM MIDSPAN DEFLECTION AT TOP OF UNIFORMLY LOADED, SIMPLY SUPPORTED RECTANGULAR DIAPHRAGM PLATES (6.3)

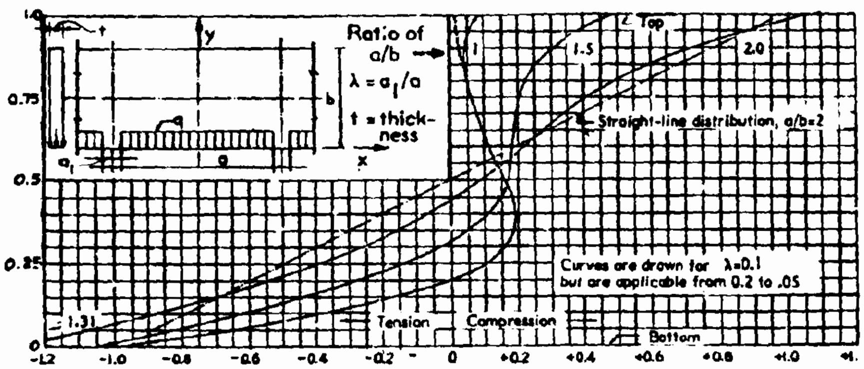

(a.) σ_x at Midspan

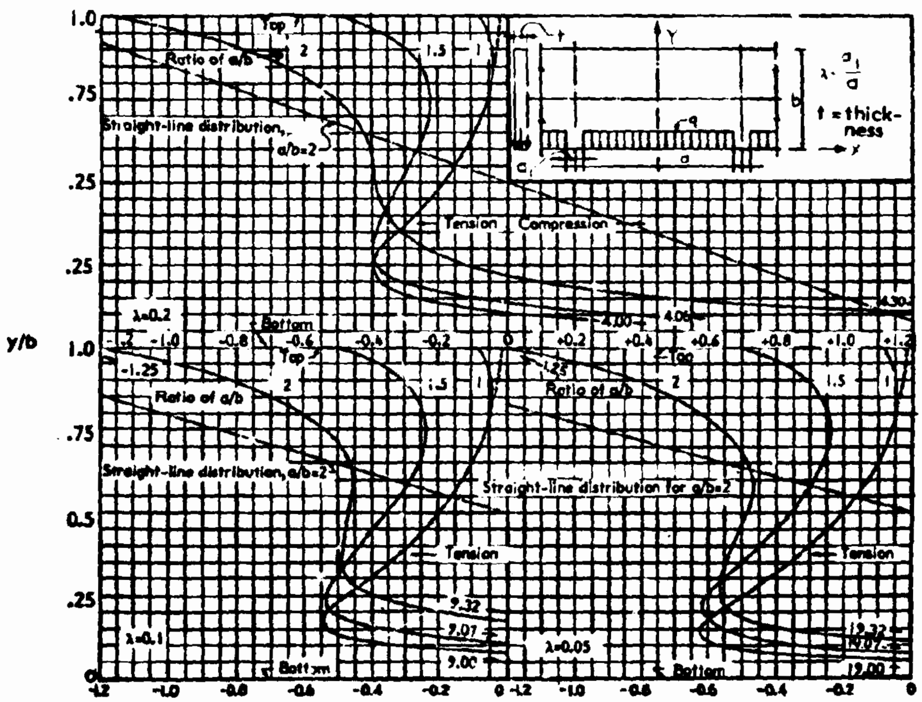

(b.) σ_x Over Support for ε = 0.05, 0.1, 0.2

Fig. 6-26 VARIATION IN σ_x WITH y/b FOR UNIFORMLY LOADED CONTINUOUS DIAPHRAGM PLATES WITH EQUAL SPANS (6.10)

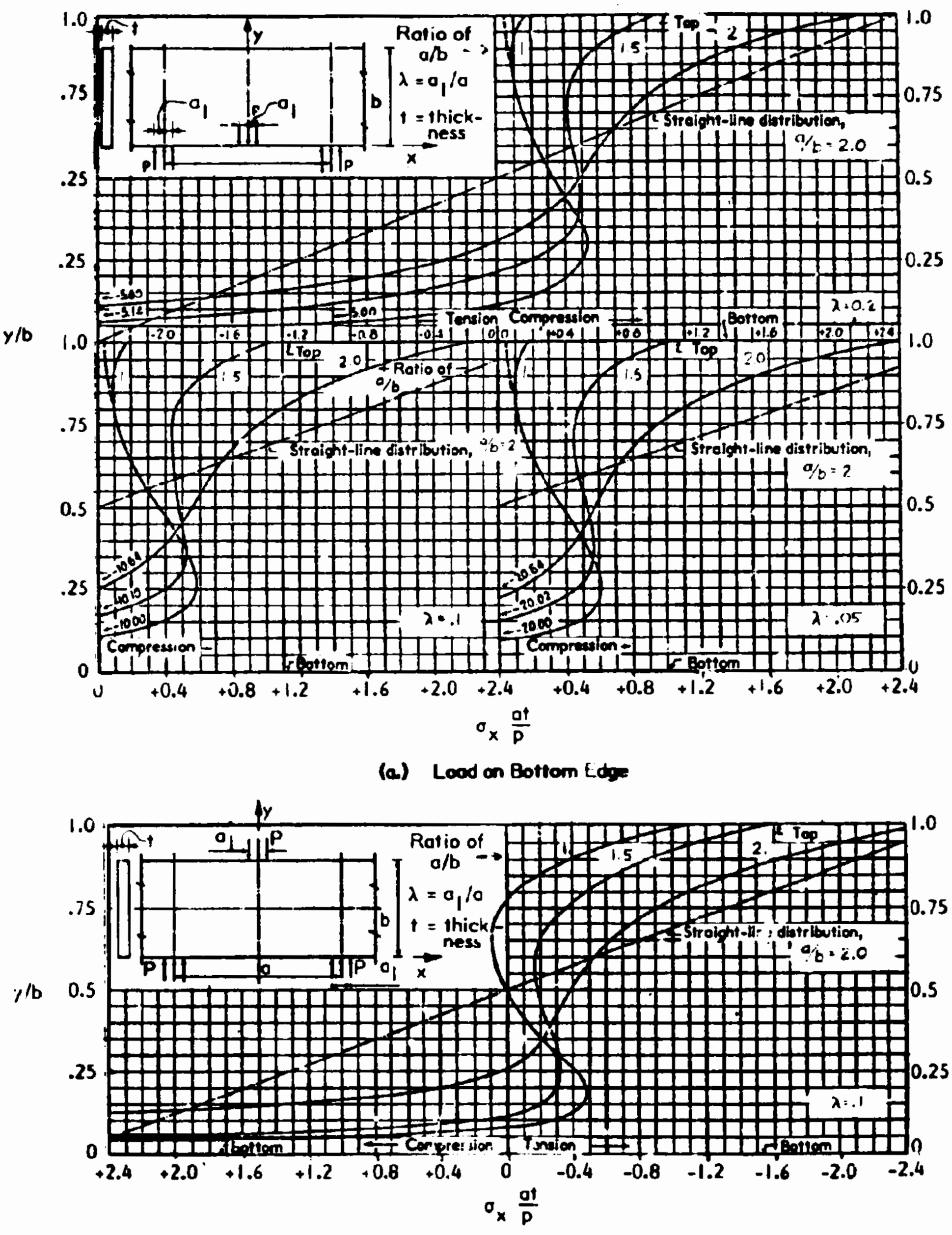

(a.) Load on Bottom Edge

(b.) Load on Top Edge

Fig. 6-27 VARIATION IN σ_x WITH y/b FOR MIDSPAN CONCENTRATED LOADING AT THE TOP AND BOTTOM EDGES OF CONTINUOUS DIAPHRAGM PLATES (6.10)

Example 6.8: Determine the required wall thickness of the equipment mount shown in the sketch. The mount is to be fabricated from a mat reinforced compression-molded FRP laminate having the following initial in-plane strength properties:

Tension:	12,000 psi
Compression:	20,000 psi
Shear:	8,000 psi
Compressive, tensile, or flexural modulus of elasticity	1,200,000 psi

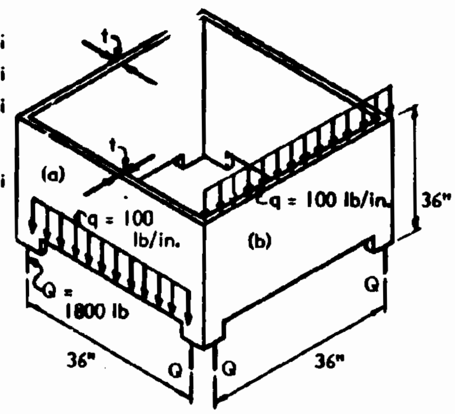

Assume that the load is long term. Allow for degradation in ultimate strength due to long term load, environmental conditions, and fabrication variation, and minimize resin micro-cracking by designing for a usable long-term ultimate strength of 25 percent of the above values. Then use a load factor of 2.0 to obtain the design load based on the above reduced ultimate strengths. Assume that modulus of elasticity reduces to 80% of its original value due to creep and degradation. Use a load factor of 2.5 for failure by instability.*

(a) Assume that the load is uniformly distributed along the bottom edge with an intensity of 100 lbs/in.

(b) Assume that the load is uniformly distributed along the top edge with an intensity of 100 lbs/in.

Solution: (a) Idealize the diaphragm as a simply supported deep beam loaded on its lower edge, and determine maximum longitudinal stresses at midspan from Fig. 6.24 (c).

Tension - strength, a/b = 1.0:

$$\max \frac{\sigma_x t}{q} = 1.85$$

$$\text{allowable } \sigma_x = 0.25 \times 12{,}000/2 = 1500 \text{ psi}$$

$$\text{required } t = \frac{1.85 \times 100}{1500} = 0.12 \text{ in.}$$

Note: 1 psi = 0.0069 MPa; 1 lbf/in. = 0.18 N/mm; 1 in. = 25.4 mm.

* See footnote, Example 6-1, p. 29.

Compression - strength, a/b = 1.0:

$$\max \frac{\sigma_x t}{q} = 0.40$$

max. allowable σ_x =0.25 x 20,000/2 = 2,500 psi

$$\text{required } t = \frac{0.40 \times 100}{2,500} = 0.016 \text{ - does not govern.}$$

Compression - stability, a/b = 1.0:

Equate compression stress along the top edge at ultimate to critical buckling stress from Eq. 6.72a in the next Section, with k ≈ 2.08 from Case II, Table 6-5. Case II is used to represent the parabolic build-up of compression due to varying bending moment along the span length.

$$\frac{-0.4 \times 100 \times 2.5}{t} = \frac{-2.08\ \pi^2 \times 1,200,000 \times 0.8\ t^2}{12\,(1 - 0.3^2) \times 36^2}$$

t^3 = 0.072 ; required t = 0.42 in.

Stability governs required thickness.

(b) For stresses in a simply supported deep beam loaded along its top edge, use Fig. 6-24(a):

Tension - strength, a/b = 1.0:

$$\max. \frac{\sigma_x t}{q} = 1.20$$

$$\text{required } t = \frac{1.20 \times 100}{1500} = 0.08 \text{ in.}$$

Compression - stability, a/b = 1.0

$$\max \frac{\sigma_x t}{q} = 0.75$$

$$\frac{-0.75 \times 100 \times 2.5}{t} = \frac{-2.08\ \pi^2 \times 1,200,000 \times 0.8\ t^2}{12\,(1 - 0.3^2) \times 36^2}$$

t^3 = 0.135 in.^{3} ; t = 0.51 in.

Result: Use t = 0.51 in. minimum thickness, as governed by stability in compression when loaded along the top edge under a uniformly distributed edge load.

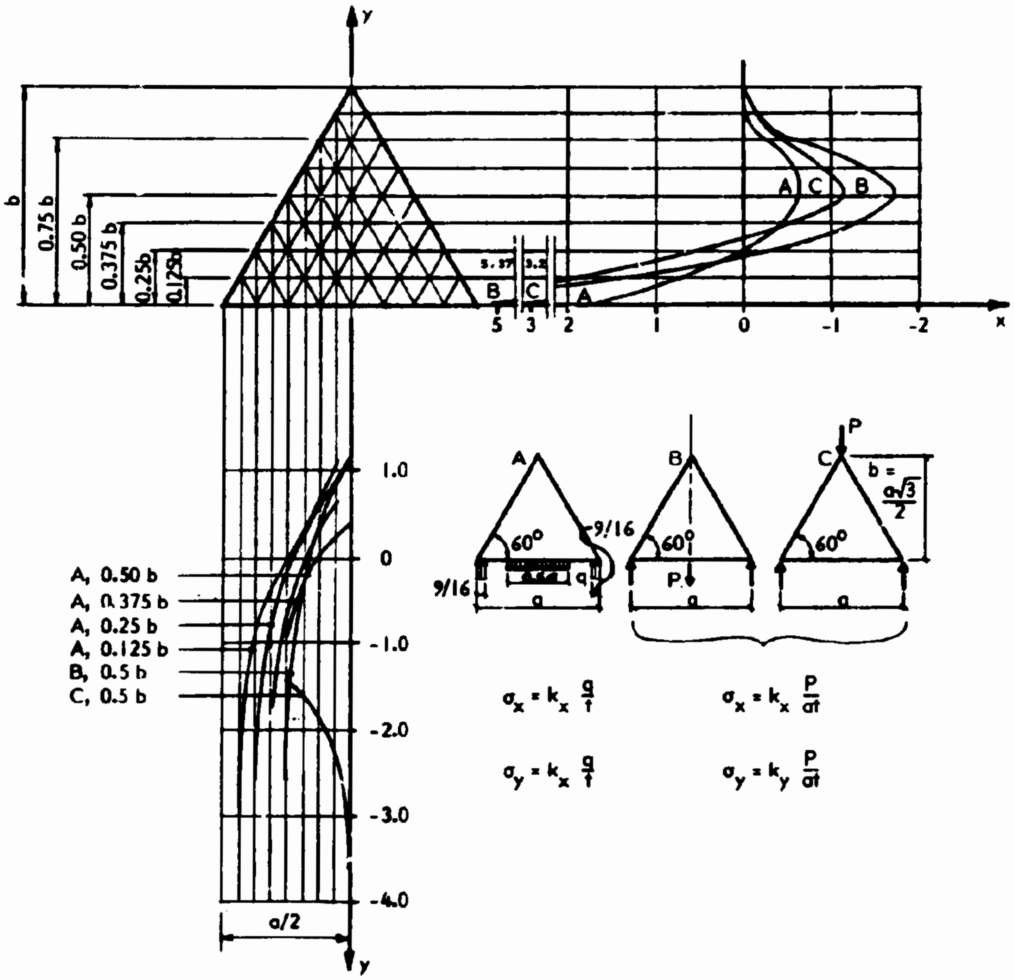

Fig. 6-28 STRESSES IN EQUILATERAL TRIANGULAR DIAPHRAGM UNDER VARIOUS LOADS (6.3)

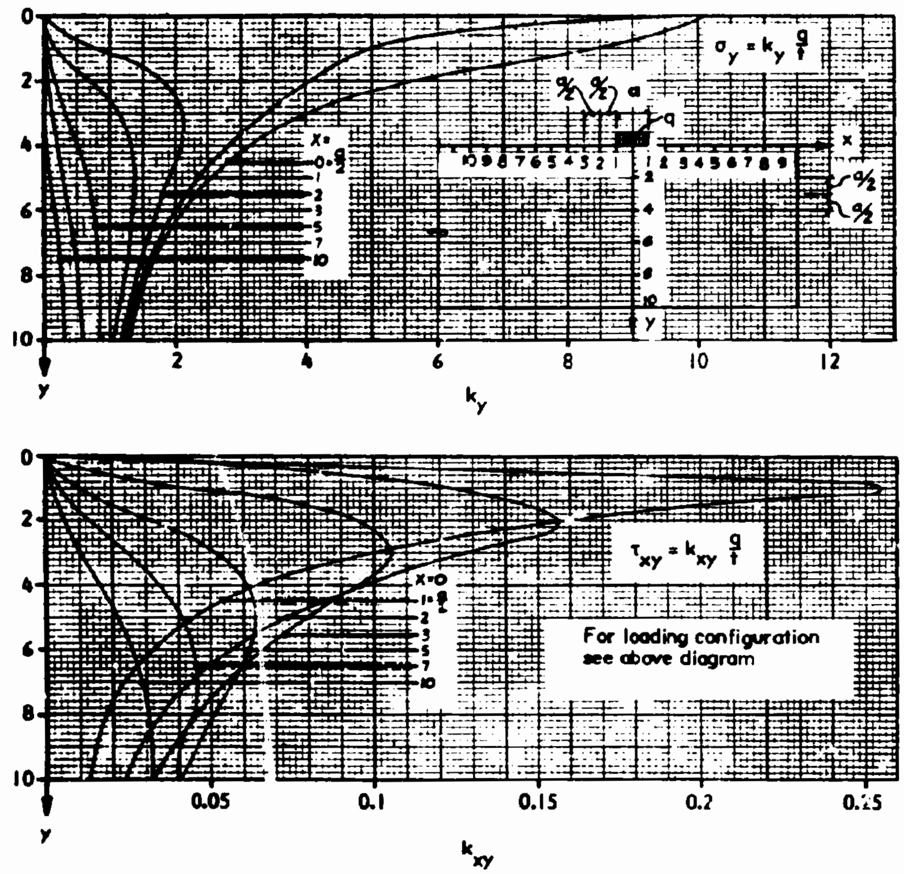

Fig. 6-29 STRESSES σ_y AND τ_{xy} IN INFINITE PLATE FROM EDGE FORCE, q, DISTRIBUTED ON LENGTH, a (6.3)

6.9 STABILITY OF ISOTROPIC PLATES

Plate elements often comprise flat portions of thin walled structural members such as I-shaped, box, channel, angle, or hat-shaped sections, and stressed skin, ribbed or hollow core panels. These assemblies of plates function as beams, columns, walls, diaphragms, roofs, floors, covers, stiffeners, and the like. In such members, the plates may serve as flanges or webs that are stressed in uniform or varying in-plane compression. They also may function as webs stressed in shear or diagonal compression. These thin compression elements are subject to local buckling as plates with various conditions of edge restraint.

The overall behavior and design of members comprised of assemblies of plates is presented in Chapter 7. Determination of the stability of their local plate elements is essential for analysis and design of the overall member. Buckling criteria for isotropic flat plates are presented in this Section and for orthotropic flat plates in the next Section.

General Behavior

When a thin plate is loaded in compression within its own plane, it is subject to sudden buckling, or lateral deflection at a stress that depends upon its stiffness, and this stress is often less than the limiting compressive strength of the material. While this initial buckling causes a usually undesirable rippling in the plate, it does not always result in catastrophic failure. For example, when buckling occurs in a longitudinally compressed rectangular plate at a stress below the yield stress or proportional limit of the material, the effective stiffness of a plate that is supported along its longitudinal edges is reduced after buckling. In this case, the longitudinal stresses near the plate edges increase more rapidly than the load, while the stresses in the buckled central portion increase less rapidly or decrease. The plate has "post buckling" strength that depends upon the ratio of initial buckling stress to material strength and the geometry of the plate as well as its edge restraints. In the case of thin plates with edge supports that restrain lateral or in-plane movement, the post-buckling strength can be quite significant due to the transverse membrane action that supports the plate as it buckles.

Stability of Long Rectangular Plates

Long rectangular plates subject to longitudinal compression, and having one or both of the longer edges supported perpendicular to their plane, with various rotational and in-plane edge restraints, are common cases of interest for buckling analysis. Transverse edges are also usually supported, but these will not influence the plate stability if the plate is sufficiently long. A long plate under uniaxial compression, with all edges simply supported, will buckle into a series of waves having half-wavelengths about equal to plate width (Fig. 6-30a). This means that the minimum buckling stress in the long simply-supported plate with uniaxial load is about the same as the buckling stress in a square simply-supported plate. If the long plate has longitudinal edges clamped against rotation, the half-wavelength will be about two-thirds of the plate width.

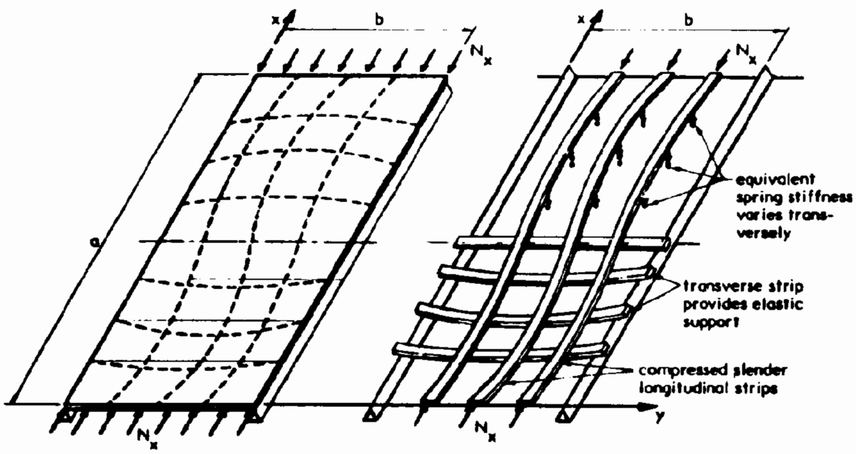

(a) Long Rectangular Plate

(b) Analogous Longitudinal Strips Supported by Elastic Stiffness of Transverse Strips Acting as Spring Supports

Fig. 6-30. BUCKLING OF LONG RECTANGULAR PLATES UNDER UNAXIAL COMPRESSIONS

A useful analogy is to consider the longitudinally compressed long rectangular plate as comprised of longitudinal strips, or thin compressed bars, that obtain lateral support against buckling perpendicular to the plane of the plate from the elastic stiffness of transverse strips (Fig. 6-30b). However, because of the variation in stiffness that occurs transversely, quantitative results for plate stability cannot be obtained from direct application of the theory of compressed bars on an elastic foundation, because the appropriate foundation modulus cannot be defined in a simple way. Nevertheless, the analogy is an aid to a physical understanding of how buckling resistance develops in plates.

Rectangular Plates in Direct Stress

When a rectangular plate is subject to a compressive stress resultant N_x in its own plane (Fig. 6-30a), the elastic buckling resistance is (6.15):

$$N_{xc} = \frac{k \pi^2 D}{b^2} \qquad \text{Eq. 6.71}$$

k is a buckling coefficient that depends on edge support conditions, the plate proportions, a/b, and the variation of N_x over the plate width b. In terms of stress and plate thickness, Eq. 6.71 becomes:

$$\sigma_{xc} = \frac{k \pi^2 E}{12(1-\nu^2)} \left(\frac{t}{b}\right)^2 \qquad \text{Eq. 6.71a}$$

k has minimum values for those ratios of a/b that result in buckling of the plate in an integral number of half-wavelengths in the x-direction, with lengths equal to the critical half-wavelength of buckle. For example, as was indicated previously, the critical half-wavelength is b for a uniformly compressed rectangular plate with simple edge supports (Fig. 6.30a). Consequently, for plate lengths, a, greater than b, the minimum value of $k = 4.0$ is frequently used for determination of critical buckling stress, and plates with this loading and edge condition are considered "long" when $a \geq b$. The maximum error in this assumption is an underestimate of buckling stress by 12 percent at $a = 1.4b$. The error is only 4 percent at $a = 2.45$ b, with minimum values of k falling in between the above a/b ratios.

Minimum values of the buckling coefficient, k, for use with Eqs. 6.71 or 6.71a are presented in Table 6-3 for common cases of edge restraint and in-plane stress distribution. See (6.11) for solutions for critical buckling stress in many other rectangular plate arrangements with different combination of edge restraint conditions and loading distributions. Most of these are refinements to the values for k given in Table 6-3.

Table 6-3

BUCKLING COEFFICIENTS FOR LONG ISOTROPIC PLATES SUPPORTED ON THREE OR FOUR SIDES UNDER LONGITUDINAL COMPRESSION

(Source 6.14)

			Minimum Buckling Coefficient,* k					
					Top Edge Free		Bottom Edge Free	
Case	Loading	Ratio of Bending Stress to Uniform Compression Stress	Unloaded Edges Simply Supported	Unloaded Edges Fixed	Bottom Edge Simply Supported	Bottom Edge Fixed	Top Edge Simply Supported	Top Edge Fixed
1	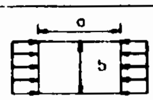	0.0 (pure compression)	4.0	6.97	0.45**	1.33	0.45**	1.33
	(min. a/b for long plate)		(1.0)	(0.6)	(5.+)**	(1.5)	(5.+)	(1.5)
2	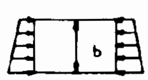	0.50	5.8					
3	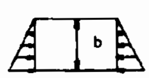	1.00	7.8	13.6	0.57	1.61	1.70	5.93
4		2.00	11.0					
5	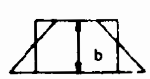	5.00	15.7					
6		∞ (pure bending)	23.9	39.6	0.85	2.15		
	(min. a/b for long plate)		(0.6)					

* Values given are based on plates having loaded edges simply supported and are conservative for plates having loaded edges fixed.

** A more accurate value of k for plates with one longitudinal support free and the other simply supported with a/b 0.7 is (6.11): $k = 0.45 + (b/a)^2$.

Example 6.9 and Example 6.11, which are given later in this Section, illustrate the use of Eq. 6.71a to establish proportions of flange plates that will develop the full compressive strength of the walls of hollow tubular sections without local buckling. This is discussed further in Chapter 7.

In cases where the plate is not laterally supported along its longitudinal (unloaded) edges (Fig. 6-31), or for wide plates where b is much greater than a, the critical buckling stress resultant and stress are given by Euler's Formula and are as follows (6.15):

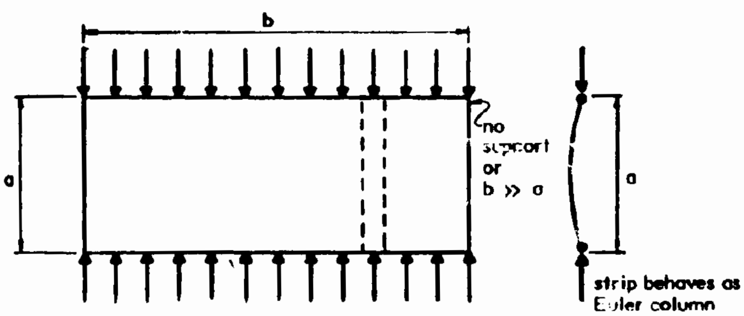

Fig. 6-31. BUCKLING OF WIDE PLATES UNDER UNIAXIAL COMPRESSION

$$N_{xc} = \frac{k \pi^2 D}{a^2} \qquad \text{Eq. 6.72}$$

or
$$\sigma_{xc} = \frac{k \pi^2 E}{12(1-\nu^2)} \left(\frac{t}{a}\right)^2 \qquad \text{Eq. 6.72a}$$

Values of the buckling coefficient, k, for various conditions of end restraint and application of compression force, N_{xc}, are given in Table 6-4. Values of k for additional conditions are given in (6.11).

When edges are held in the plane of the plate, longitudinal compression produces transverse compression due to restraint of Poisson expansion. This results in some reduction in the buckling coefficient. A buckling coefficient correction factor, C_b, to be applied to k = 4, the coefficient for uniaxial compression on

Table 6-4

Buckling Coefficients for Wide Isotropic Plates or Plates Supported Only on Transverse Edges Under Uniform Longitudinal Compression (6.11)

Case	Plate Loading	Support Restraint	Buckling Coefficient, k (Eq. 6.72, 6.72a)
7	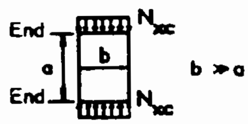	Pin ends	1.0
8		Clamped ends	4.0
9		One end pinned opposite end clamped	2.0
10	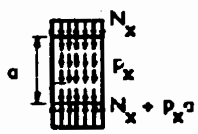	pin ends	$\frac{1.69}{1 + 1.30 \frac{N_x}{p_x}} + 1.0$
11	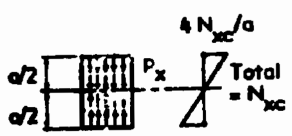	pin ends	2.08
12	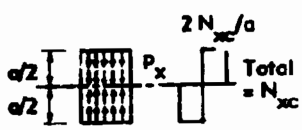	pin ends	3.19
13	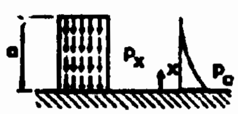	cantilever $p_x = p_o(1 - \frac{x}{a})^n$ $N_{xc} = \frac{p_o a}{n+1}$ n = 0 n = 1 n = 2 n = 3	 0.79 1.63 2.77 4.18

long plates with simple support of longitudinal edges is given in Fig. 6-32 (6.12). The correction factor for simply-supported edges and varying amounts of restraint of in-plane edge movement, K_a, is given on the left side of the Figure and is to be applied to $k = 4.0$ for use in Equations 6.71 and 6.71a.

When longitudinal edges are also restrained against rotation, the correction factor increases with increasing edge restraint, K_b, as shown in the main part of the Figure. The asymptote values given on the right side of the Figure are for fully clamped edges. The "corrected" critical buckling stress, σ_{xcc}, is (6.12):

$$\sigma_{xcc} = \frac{4\, C_b\, \pi^2 E}{12\,(1-\nu^2)} \left(\frac{t}{b}\right)^2 \qquad \text{Eq. 6.71b}$$

For a given amount of rotational restraint, the correction factors that reduce elastic buckling coefficients when restraint of in-plane translation is provided have little practical significance, since restraint of in-plane translation substantially increases the post-buckling strength of the plate. This type of restraint develops the plate's membrane resistance to large lateral deflection, but since this effect is non-linear, it does not enhance the initial buckling resistance.

Biaxial stress conditions also have significant influence on plate buckling strength. Correction factors, C_b, for various ratios of uniform transverse tension or compression stress to uniform longitudinal compressive buckling stress on a plate with simply supported edges are given in Fig. 6-33 (6.12). Note that in the curves given in the Figure, the longitudinal stress term, σ_{xc}, in the transverse stress ratio, σ_y / σ_{xc}, is obtained from Eq. 6.71a. These factors are multiplied by $k = 4$ in Equations 6.71 or 6.71a to obtain critical buckling stresses in the longitudinal direction, as given in Eq. 6.71b above. See (6.12) for similar curves for plates with other edge conditions.

Effect of Creep

Creep in plastics subject to long-duration stress was discussed in Chapters 2 and 3. The use of a reduced modulus of elasticity, termed the viscoelastic modulus, was recommended to account for creep. In the linear range, the viscoelastic modulus depends on the duration of stress. In the case of a plate, stress

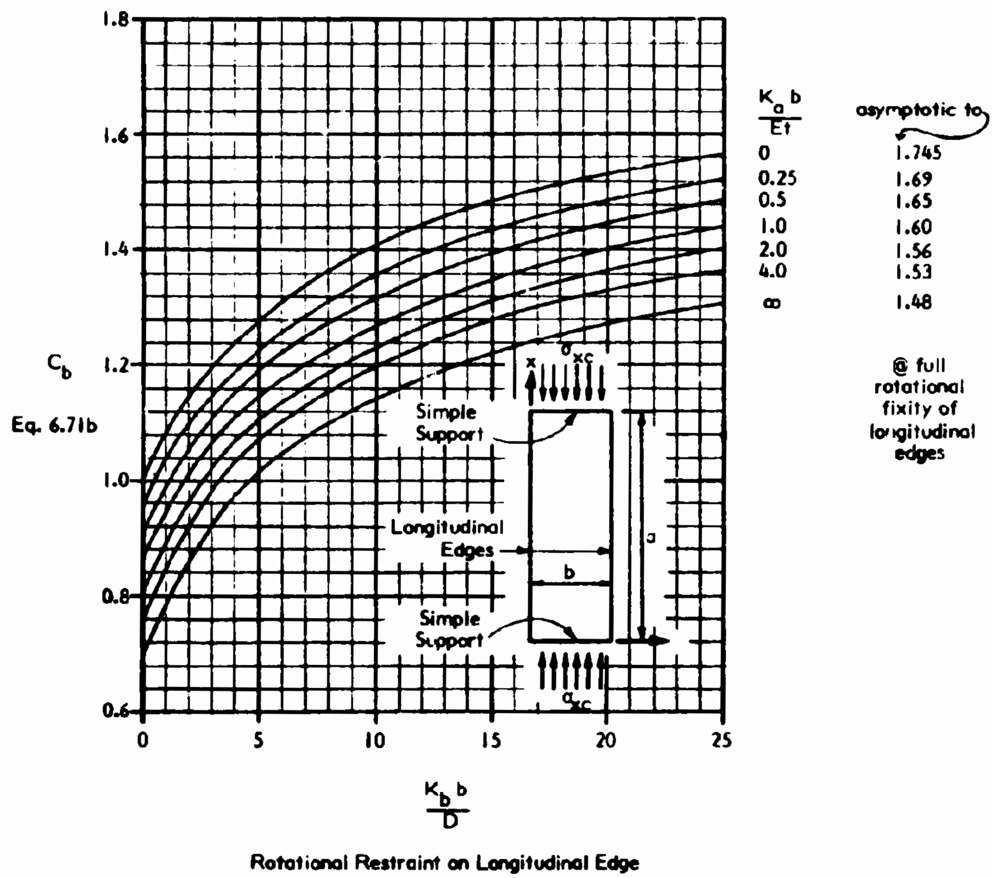

$$K_a = \left(\frac{\text{in-plane edge force}}{\text{unit displacement x unit edge length}}\right) \; ; \; K_a = \left(\frac{\text{edge bending moment}}{\text{unit angle x unit edge length}}\right)$$

Fig. 6-32 CORRECTION FACTORS TO k = 4.0 FOR DETERMINATION OF k IN EQS. 6.71 FOR VARIOUS CONDITIONS OF LONGITUDINAL EDGE SUPPORT IN UNIAXIAL COMPRESSED LONG PLATES (6.12)

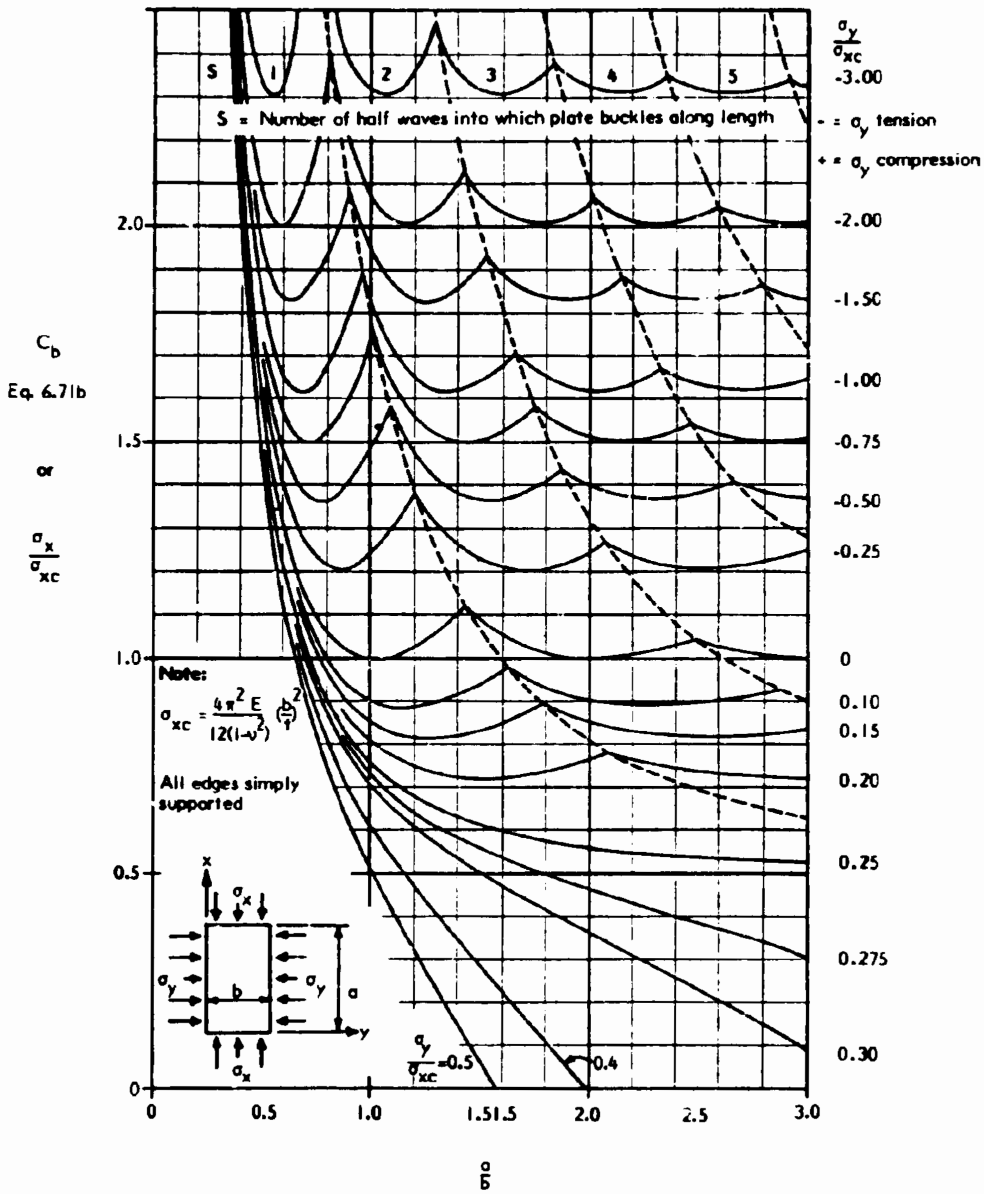

Fig. 6-33. CORRECTION FACTORS TO k = 4.0 FOR DETERMINATION OF k IN EQS. 6.71 FOR VARIOUS BIAXIAL LOADING CONDITIONS IN SIMPLY SUPPORTED COMPRESSED PLATES (6.12)

intensity, and perhaps duration, frequently is greater in, say the x direction than in the y direction. Since the buckling strength of a longitudinally loaded rectangular plate, for example, is largely determined by the transverse flexural stiffness, a question arises about the proper modulus of elasticity to use in the plate buckling equations. The following modification factor is derived from an approach suggested by Bleich (6.13) for metal plates loaded beyond their proportional limits:

$$\tau_{LT} = \frac{E_{v\ \text{longitudinal}}}{E_{o\ \text{transverse}}} \qquad \text{Eq. 6.73}$$

Modify σ_{xc} (or N_{xc}, from the previously given formulas for elastic buckling of rectangular plates as follows:

$$\sigma_{xcv} = \sigma_{xc}\sqrt{\tau_{LT}} \qquad \text{Eq. 6.74}$$

The approach suggested above is semi-empirical in concept, and thus, should be confirmed or adjusted using plate buckling tests on specific plastics materials.

Example 6.9 illustrates the calculation of the maximum buckling stress in a compressed plate which is a component of a rectangular tube column fabricated from a plastic material exhibiting the creep characteristics determined in Chapter 3, Fig. 3-2.

Post Buckling Strength of Rectangular Plates in Direct Stress

When the critical buckling stress is less than the yield strength or proportional limit strength of the material, the ultimate strength of a thin plate may exceed its buckling strength. After initial buckling occurs in a rectangular plate subject to uniform uniaxial compression and supported along each longitudinal edge, stresses decrease in the central area of maximum buckle deflection, and they increase in the strips adjacent to the longitudinal supports (Fig. 6-34). At the collapse condition, two strips adjacent to the longitudinal support, having a width b_e, as shown in Fig. 6-34, are considered to carry the entire plate load at a stress equal to the ultimate usable compressive strength of the plate material (first damage, or yield strength).

Example 6.9: Determine the minimum thickness required to develop the full ultimate compressive strength without local buckling of a hollow 10-in.-square tubular compression member extruded of PVC plastic having the viscoelastic properties given in Fig. 3-2. (a) Assume short-term loading, 0.1 hours or less; (b) assume long-term loading, 100,000 hours. *

Solution: (a) From Fig. 3-2 for 0.1 hour duration of loading, $E_v \approx E_o = 550,000$ psi and maximum usable stress, $\sigma_v = 4,500$ psi. Assume "hinged" edge condition for longitudinal edges because adjacent sides can buckle alternately inward and outward, as shown in the sketch.

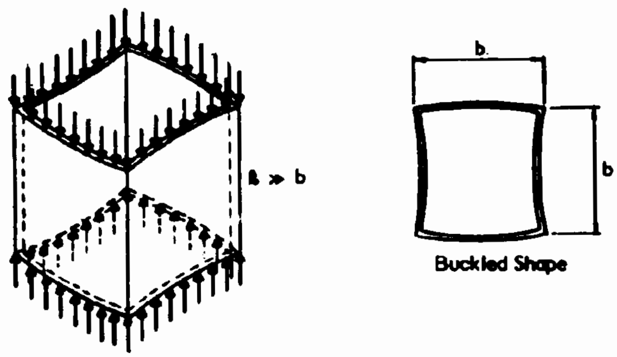

From Eq. 6.71a with k = 4.0 for hinged edges:

$$\sigma_{xc} = \sigma_v = 4,500 = \frac{4.0 \times \pi^2 \times 550,000}{12\,(1 - .3^2)} \left(\frac{t}{10}\right)^2$$

t = 0.476 in. (use min. t = 0.48 in.)

(b) From Fig. 3-2 for 100,000 hour duration of loading, E_v is reduced because of creep and the maximum usable stress is also reduced because of reduction in long-term ultimate strength. Thus, $E_v = 300,000$ psi and $\sigma_v = 2,300$ psi.

First, using isotropic buckling theory:

$$\sigma_{xc} = \sigma_v = 2,300 = \frac{4.0 \times \pi^2 \times 300,000}{12\,(1 - .3^2)} \left(\frac{t}{10}\right)^2$$

t = .46 in.

Note: 1 psi = 0.0069 MPa; 1 in. = 25.4 mm

* See footnote, Example 6-1, p. 29.

Comment: The buckling theory for isotropic materials may produce an overly conservative evaluation of the buckling strength of a uniaxial compressed plate, depending on the effect of duration of load on the flexural rigidity transverse to the direction of compression. If we assume that buckling resistance is governed by short-term modulus of elasticity transverse to the direction of load, the plate buckles as an orthotropic plate and we can use the following solutions:

(1) Simplified Solution: From Eqs. 6.73 and 6.74 with:

$$\tau = \frac{E_{v\ long.}}{E_{o\ transv.}} = \frac{300{,}000}{550{,}000} = 0.55$$

$$\sigma_{xcv} = 2{,}300 = \frac{4.0 \times \pi^2 \times 550{,}000\ \sqrt{.55}}{12\,(1 - .3^2)} \left(\frac{t}{10}\right)^2$$

$t = .40$ in.

(2) Application of orthotropic buckling equation given in the next Section:

From Eq. 6.89 with: $D_{11} = \dfrac{E_v \times t^3}{(1 - \nu_{12}\,\nu_{21})\,12}$; $D_{22} = \dfrac{E_o \times t^3}{(1 - \nu_{12}\,\nu_{21})\,12}$

$$D_o = D_{12} + 2D'_{12} \approx \sqrt{D_{11}\,D_{12}}$$

$$\sigma_{xc} = \frac{2\pi^2}{b^2\,t} \times 2\sqrt{D_{11}\,D_{12}} = \frac{4\pi^2\ t^2\sqrt{E_v\,E_o}}{12\,(1 - \nu_{12}\,\nu_{21})\,10^2}$$

$$\sigma_{xcv} = \frac{4\pi^2\ t^2\ E_o}{12\,(1 - \nu_{12}\,\nu_{21})\,10^2}\sqrt{\frac{E_v}{E_o}}$$

This is the same as the above simplified expression if $\nu_{12} = \nu_{21}$.

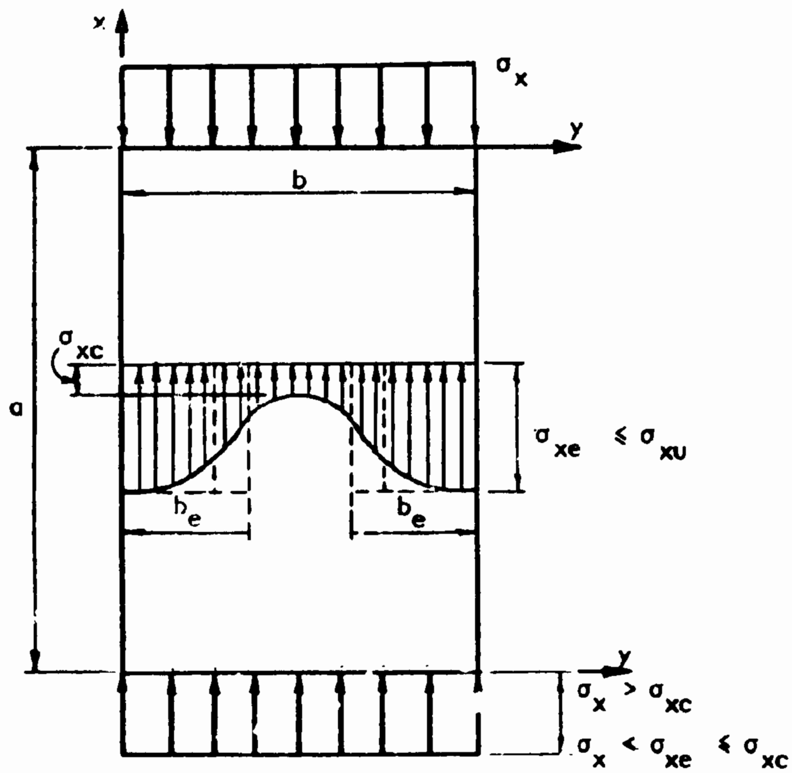

Fig. 6-34. POST BUCKLING STRESSES IN THIN PLATES WITH SUPPORT ALONG BOTH LONGITUDINAL EDGES

The following semi-empirical relations have been developed (6.14) for effective post-buckling strength of thin metal plates simply supported along longitudinal edges (refer to Fig. 6.34):

$$\frac{b_e}{b} = \sqrt{\frac{\sigma_{xc}}{\sigma_{xe}}} \left(1.0 - 0.22 \sqrt{\frac{\sigma_{xc}}{\sigma_{xe}}} \right) \qquad \text{Eq. 6.75}$$

σ_{xc} is determined from Eq. 6.71a with the appropriate value of k for a plate supported along two longitudinal edges.

$$\sigma_{xe} = \frac{N_x b}{t\, b_e} \qquad \text{Eq. 6.76}$$

$$\sigma_x = \frac{N_x}{t} = \sqrt{\sigma_{xc}\,\sigma_{xe}}\ (1.0 - 0.22\sqrt{\frac{\sigma_{xc}}{\sigma_{xe}}}) \qquad \text{Eq. 6.77}$$

In practical design, σ_{xe} and b_e are determined by cut and try solution of the above equations whenever $\sigma_{xu} > \sigma_{xc}$.

For a plate supported along only one longitudinal edge:

$$\frac{b_e}{b} = 1.19\sqrt{\frac{\sigma_{xc}}{\sigma_{xe}}}\ (1 - 0.30\sqrt{\frac{\sigma_{xc}}{\sigma_{xe}}}) \qquad \text{Eq. 6.78}$$

σ_{xc} is determined from Eq. 6.71a with the appropriate value of k for a plate supported along only one longitudinal edge.

$$\sigma_x = \frac{N_x}{t} = 1.19\sqrt{\sigma_{xc}\,\sigma_{xe}}\ (1 - 0.30\sqrt{\frac{\sigma_{xc}}{\sigma_{xe}}}) \qquad \text{Eq. 6.79}$$

The coefficients in the above Eqs. 6.75 to 6.79 are not greatly affected by the restraint conditions along longitudinal edges and use of the above relations is appropriate for all types of restraint at supported edges. Of course, σ_{xc} will vary with the type of edge restraint.

No data are available to evaluate whether the above relations are suitable for use with plastics materials. Tests on thin plates under direct compression should be conducted for each specific material of interest.

Combined Direct Compression and Lateral Load

Plates are frequently subject to combined direct compression forces and lateral loads, requiring consideration of interaction effects. An example is ship bottom plating which serves as a portion of the hull girder flange and also resists substantial hydrostatic pressure. The following approximate interaction relations are extremely useful for practical design:

1. **Elastic buckling stress:** Unlike a slender column, the presence of lateral load in combination with direct thrust does not reduce the elastic buckling strength of a plate (6.13). On the contrary, some increase in buckling

strength may occur if the shape of the deflection curve produced by lateral load differs significantly from the shape of the lowest mode buckle.

2. **Deflection due to lateral load:** Deflection due to lateral load is increased by the presence of compressive axial force and is decreased by the presence of tensile axial force. This increased (or decreased) deflection is determined by a magnification factor, $\overline{m}$, as follows (6.13):

$$w_a = \overline{m}\, w_o \qquad \text{Eq. 6.80}$$

where $$\overline{m} = \frac{1}{1 - \dfrac{\sigma_{xa}}{\sigma_{xc}}} \qquad \text{Eq. 6.81}$$

and $\sigma_{xa} \leq \sigma_{xu}$; $\sigma_{xa} \leq \sigma_{xc}$

$$w_o \leq \frac{t}{2}$$

3. **Bending moment and stress due to lateral load:** In a similar way, bending moment is increased by the presence of compressive axial force and decreased by the presence of tensile axial force, as follows (6.13):

$$M_a = \overline{m}\, M_o \qquad \text{Eq. 6.82}$$

$$\sigma_x = \sigma_{xa} + \overline{m}\, \sigma_{xb}$$

$$\sigma_y = \overline{m}\, \sigma_{yb} \qquad \text{Eqs. 6.83}$$

The same limitations to σ_{xa} and w_o as described above for deflection also apply to the use of the magnification factor for moment.

Example 6.10 illustrates the determination of combined axial and bending stress in a box-shaped cross section used for corrosion resistant ducting that supports both internal pressure and axial load on the side walls.

Rectangular Plates in Shear

Under a state of pure shear stress in a thin plate (Fig. 6-35), compressive and tensile principal stresses (Eq. 6.69) equal to the shear stress are directed at ± 45

Example 6.10: Determine the required wall thickness of the FRP duct section shown in the sketch. The duct is to be designed for the combined effect of an internal pressure of 3 psi and equipment supported on the wall which produces a line load on each side wall of 300 lbs/in. These loads should be considered "long term". The FRP laminate to be used for the duct wall is alternate layers of mat and woven roving glass reinforcement with polyester resin. The structural properties of the overall laminate are as follows:

tensile strength	15,000 psi
flexural strength	22,000 psi
compressive strength	24,000 psi
flexural modulus of elasticity	1,500,000 psi

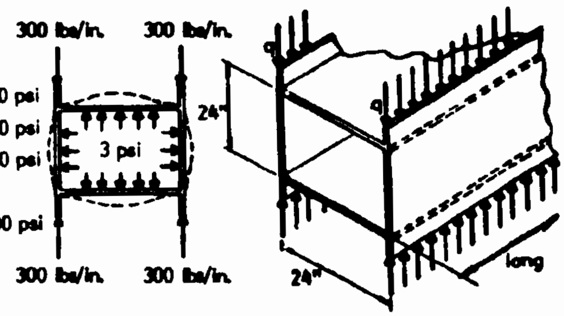

Assume that the effective modulus of elasticity is reduced to 80% of the above value for long-term load. Assume that the usable ultimate long-term strength is one-fourth the above values, including allowance for tolerances in fabrication, effect of long-term load and environmental degradation. Apply a "load factor" of 2 to the above design loads for "ultimate strength" design, except use a load factor of 3 for the case of stability due to axial load alone. *

<u>Solution:</u> The duct wall spans 24 inches as a long plate with edges rotationally fully fixed by the balancing effect of pressure on the adjacent wall (see sketch). Each side wall is subject to the combined effects of bending plus axial compression. The symmetrical application of internal pressure on the adjacent walls of the square duct results in rotational fixity at the edges of the plate.

The effect of axial load without internal pressure must also be considered. In this case, the side walls which support axial load must be considered as pin ended struts, since there is no effect of balancing pressure on adjacent sides to provide fixity.

Ultimate Bending Moment: $M_u = \frac{2qb^2}{12} = \frac{2 \times 3 \times 24^2}{12} = 288$ in.-lbs/in.

Ultimate Axial Compression: $P_u = 2\,(-300 + \frac{qb}{2}) = 2\,(-300 + \frac{3 \times 24}{2}) = -528$ lbs/in.

Ultimate Design Stresses:

Flexure:	σ_{ub}	$= 22{,}000 \div 4 = 5{,}500$ psi
Compression:	σ_{ua}	$= 24{,}000 \div 4 = 6{,}000$ psi
Tension:	σ_{ua}	$= 15{,}000 \div 4 = 3{,}750$ psi

Note: 1 psi = 0.0069 MPa; 1 in.-lbf/in. = 4.45 mm-N/mm; 1 lbf/in. = 0.18 N/mm; 1 in. = 25.4 mm

* See footnote, Example 6-1, p. 29.

Trial Thickness: Assume moment magnification factor increases moment by 10%, or decreases usable flexure strength to 5,000 psi.

Then: $\frac{P_u}{A} + \frac{M_u}{S} = \sigma_u$

$$\frac{-528}{t} - \frac{6 \times 288}{t^2} = -5{,}000$$

$$5{,}000\, t^2 - 528\, t - 1{,}728 = 0$$

$$t = \frac{528 \pm \sqrt{528^2 + 4 \times 5{,}000 \times 1{,}728}}{2 \times 5{,}000} = .64 \text{ in.}$$

Try: $t = 0.75$ in.

$$\sigma_{xa} = \frac{-528}{0.75} = -704 \text{ psi}$$

From Eq. 6.72a for clamped edges: $\sigma_{xc} = \frac{4\pi^2 \times 1{,}500{,}000 \times .8}{12\,(1 - .3^2)} \left(\frac{.75}{24}\right)^2 = -4{,}236$ psi

Magnification factor: $m = 1 - \frac{\sigma_{xa}}{\sigma_{xc}} = 1 - \frac{704}{4{,}326} = 0.83$

Bending Stress: Ult. $\sigma_{xb} = \frac{M_u}{m\,S} = \frac{6 \times 288}{.83 \times (.75)^2} = 3{,}701$ psi

Axial Stress: Ult. $\sigma_{xa} = \frac{-528}{.75} = -704$ psi

Interaction Relation: $\frac{\sigma_{xa}}{\sigma_{xc}}$ or $\frac{\sigma_{xa}}{\sigma_{ua}} + \frac{\sigma_{xb}}{\sigma_{ub}} \leq 1.0$

$$\frac{704}{4{,}236} + \frac{3{,}701}{5{,}500} \leq 1$$

$$.17 + .67 = .84 < 1 \qquad \text{O.K.}$$

Check case of axial load only on side walls considered as <u>pin ended</u> struts with load factor = 3.

$$\sigma_{xa} = 704 \times 3/2 = 1{,}056 \text{ psi}$$

$$\sigma_{xc} = \frac{1.0 \times \pi^2 \times 1{,}500{,}000 \times .8}{12\,(1 - .3^2)} \left(\frac{.75}{24}\right)^2 = -\,1{,}059 \text{ psi}$$

$$\frac{\sigma_{xa}}{\sigma_{xc}} = \frac{1{,}056}{1{,}059} \approx 1.0 \qquad \text{O.K.}$$

Use 0.75 in. thick duct side walls

Note: Top and bottom walls could be sized for bending plus tension, if desired, as follows:

$$\text{trial } t = \sqrt{\frac{6 \times 288}{(5{,}500-100)}} = .57 \text{ in.}$$

The magnification effect of tension in the top and bottom plates allows a further reduction in wall thickness:

Try: $t = 0.56$ in.

$$\sigma_{xa} = \frac{2 \times 2 \times 24}{.56 \times 2} = 86 \text{ psi}$$

$$\sigma_{xc} = \frac{4 \times {}^2 \times 1{,}500{,}000}{12\,(1 - .3^2)} \left(\frac{.56}{24}\right)^2 = 2{,}952 \text{ psi}$$

$$m = 1 + \frac{86}{2{,}952} = 1.029$$

$$\sigma_b = \frac{6 \times 288}{1.029 \times 0.56^2} = 5{,}355 \text{ psi}$$

$$\frac{86}{3{,}750} + \frac{5{,}355}{5{,}500} \leq 1$$

$$0.023 + 0.974 = 0.997 < 1 \qquad \text{O.K.}$$

degrees to the x axis respectively. The limiting shear stress that results in elastic buckling in the direction of diagonal compression is (6.14):

$$\tau_{xycr} = \frac{k_{xy} \pi^2 E}{12(1-\nu^2)} \left(\frac{t}{b}\right)^2 \qquad \text{Eq. 6.84}$$

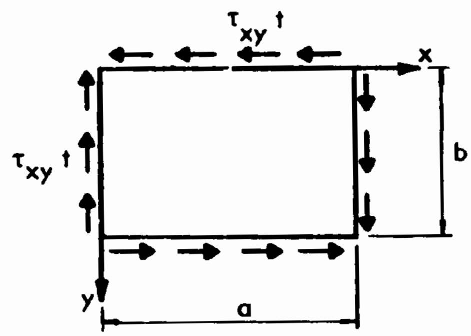

Fig. 6-35. PURE SHEAR LOAD ON RECTANGULAR PLATES

The buckling coefficient, k_{xy}, depends on the aspect ratio, b/a, and the conditions of edge restraint. The following equations may be used to determine k_{xy} for plates with $b < a$ (6.14):

Simply supported edges:

$$k_{xy} = 5.34 + 4\left(\frac{b}{a}\right)^2 \qquad \text{Eq. 6.85}$$

All edges clamped:

$$k_{xy} = 8.98 + 5.60\left(\frac{b}{a}\right)^2 \qquad \text{Eq. 6.86}$$

Equations 6.84 and 6.85 are frequently used to evaluate elastic stability of thin webs of plate girders, where a is the spacing of stiffeners and b is the depth of the girder, except that a and b are reversed where stiffeners are closer than the depth of the girder.

Example 6.11 illustrates the use of Eqs. 6.84 and 6.85 to establish proportions of web plates in box sections that will develop the full shear strength of the web without local buckling in shear. This is discussed further in Chapter 7.

Stiffened girder webs have significant post-buckling strength. After buckling occurs in the direction of diagonal compression, the web behaves like a truss with diagonal tension (tension field) in the web and compression in the stiffening ribs which extend between flanges. This is discussed in Chapter 7.

Rectangular Plates in Combined Shear and Uniaxial Compressive or In-Plane Bending Stress

The critical buckling stress (for both shear and direct stress) is reduced when a plate is subjected to the combined effects of shear and uniaxial compressive or in-plane bending stress (Fig. 6-36). For such cases, the critical buckling stresses can be closely approximated with the following interaction formulas (6.13)(6.15):

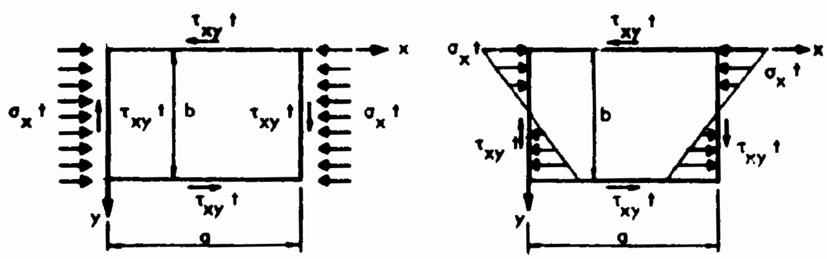

(a) Uniaxial compression stress (b) In-place bending stress

Fig. 6-36. COMBINED SHEAR AND UNIAXIAL COMPRESSION OR IN-PLANE BENDING STRESSES ON RECTANGULAR PLATES

Example 6.11: Determine the minimum thicknesses of web and flange in the FRP box section beam shown in the sketch to develop the full ultimate web shear strength and flange compressive strength without local wall buckling. Assume that the material is isotropic and that the web and flange plates are long relative to their widths with longitudinal edges pinned.*

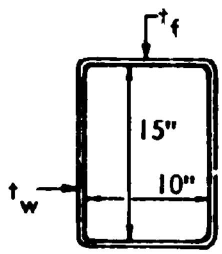

Material Properties

E = 1,200,000

ult. compression strength = 16,000 psi

ult. shear strength = 8,000 psi

Solution:

Web: From Eq. 6.82: $k = 5.34 + .4\,(15/\infty)^2 = 5.34$

From Eq. 6.81: $$\tau_{xzc} = 8{,}000 = \frac{5.34\,\pi^2 \times 1{,}200{,}000}{12\,(1-.3^2)}\left(\frac{t_w}{15}\right)^2$$

$t_w = 0.56$ in.

Flange: From Eq. 6.71a and Table 5-3:

$$\sigma_{xc} = 16{,}000 = \frac{4.0\,\pi^2 \times 1{,}200{,}000}{12\,(1-.3^2)}\left(\frac{t_f}{10}\right)^2$$

$t_f = 0.61$ in.

Comment: For wall thicknesses greater than given above, the ultimate strength of a beam using this box section is governed by material strength; for wall thicknesses less than these values, ultimate strength is governed by local wall buckling, which is a function of the stiffness rather than of the strength of the material.

Note: 1 psi = 0.0069 MPa; 1 in. = 25.4 mm

* See footnote, Example 6-1, p. 29.

Combined shear and uniform compression (Fig. 6-36a), where a/b > 1.0:

$$\left(\frac{\tau_{xy}}{\tau^{o}_{xyc}}\right)^{2} + \frac{\sigma_x}{\sigma^{o}_{xc}} = 1 \qquad \text{Eq. 6.87}$$

When a/b < 1.0, the above formula is very conservative and more accurate relations are given in (6.13).

Combined shear and pure in-plane bending (Fig. 6-36b); where a/b > 1.0:

$$\left(\frac{\tau_{xy}}{\tau^{o}_{xyc}}\right)^{2} + \left(\frac{\sigma_{xb}}{\sigma^{o}_{xbc}}\right)^{2} = 1 \qquad \text{Eq. 6.88}$$

Eqs. 6.87 and 6.88 may be combined into one three-part interaction equation when all three types of stress occur simultaneously (6.14).

Rectangular Plates Without Lateral Support Along Compressed Longitudinal Edges

Sometimes, as in Example 6.9 in Section 6.8, a diaphragm plate transfers load as a "deep beam" without lateral support along the compressed edge, as shown in Fig. 6-37. In such plates, a conservative estimate of critical buckling stress may be obtained by considering that a strip of unit width along the compressed edge (or other location of maximum compression) behaves as a slender strut between points of lateral support. The critical buckling stress in such a strip is given by Eq. 6.72a. The buckling coefficient, k, reflects the end restraint conditions and the variation in build-up of compression stress over the unsupported length. This approach neglects the additional resistance which can be provided by adjacent strips which are stressed to lower levels. Mobilization of this additional resistance brings into play the torsional stiffness of the plate.

If the span-depth ratio of the diaphragm plate exceeds about two, a more accurate determination of buckling stress may be obtained from the theory of lateral-torsional buckling of rectangular beams (6.15). For this case, the critical buckling stress at the laterally unsupported compression edge of a diaphragm

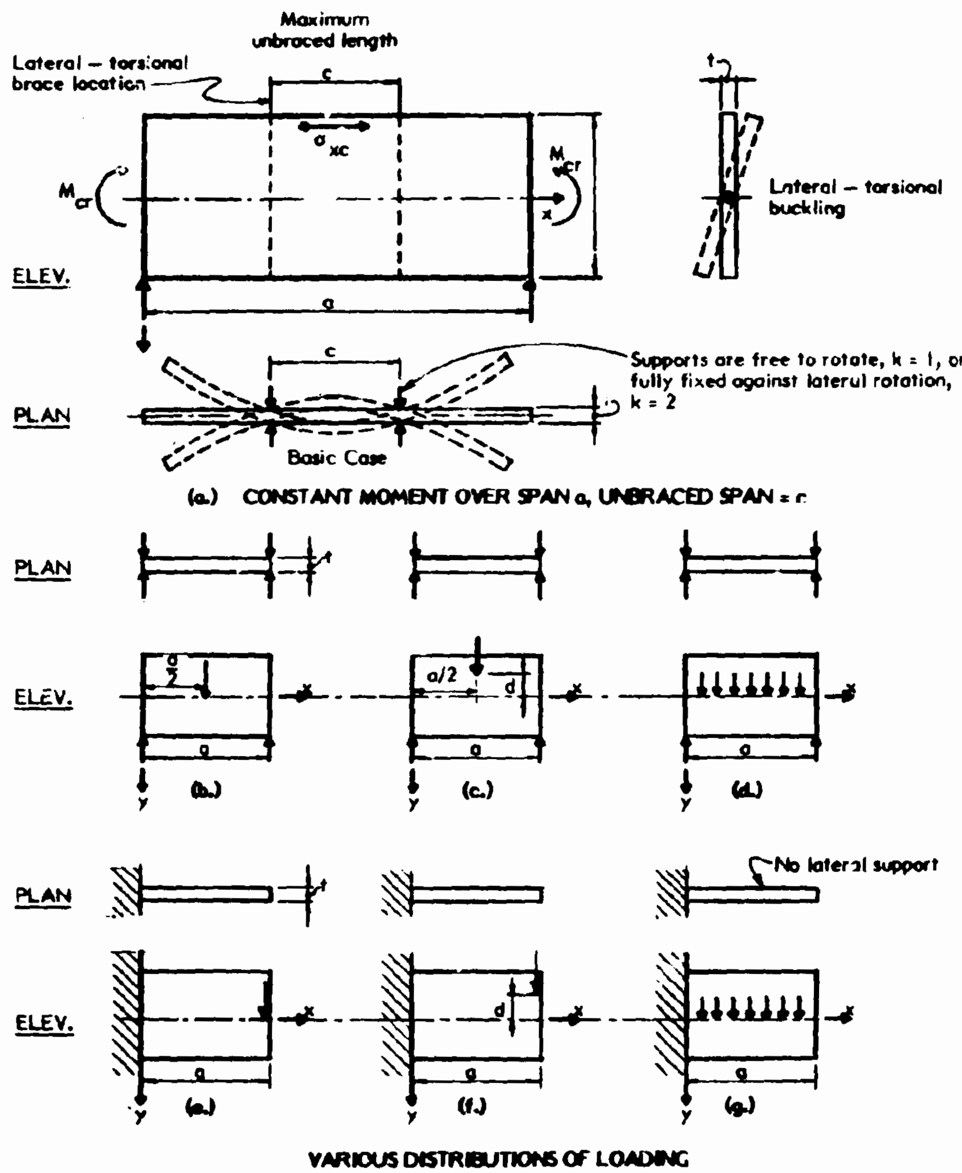

Fig. 6-37 LATERAL-TORSIONAL BUCKLING OF DIAPHRAGM PLATES WITHOUT CONTINUOUS SUPPORT ALONG LONGITUDINAL EDGES a/b > 2

plate of thickness, t, depth, b, span, a, and laterally unsupported length, c, subject to various loading distributions and conditions of restraint at supports, as shown in Fig. 6-37, is (6.15):

$$\sigma_{xc} = \frac{k\pi}{c}\frac{t^2 E}{b}\sqrt{\frac{(1 - 0.63\frac{t}{b})}{2(1+\nu)}} \qquad \text{Eq. 6.89}$$

The buckling coefficient, k, varies for different distributions of loading on the diaphragm plate, for different locations of load application relative to the centroidal x axis, and for different types of restraint at the points of lateral support. Some values of k for the commonly occurring load and restraint conditions shown in Fig. 6-37 are given in Table 6-5.

The value k = 1.0 for pure bending without restraint of rotation at points of lateral restraint may often be used to establish practical design limits for buckling because it conservatively approximates the other conditions with reasonable accuracy in most cases.

The above solution is based upon twisting of the plate as a rigid body, neglecting transverse bending of the plate which reduces its torsional rigidity. This could result in an overestimate of the buckling stress, depending on the a/b and b/t ratios of the diaphragm plate.

Circular Plates

The critical buckling stress on the perimeter of a radially compressed circular plate (Fig. 6-38) is (6.11):

$$\sigma_{rc} = \frac{4k\pi^2 D}{a^2 t} \qquad \text{Eq. 6.90}$$

or

$$\sigma_{rc} = \frac{k\pi^2 E}{3(1-\nu^2)}\left(\frac{t}{a}\right)^2 \qquad \text{Eq. 6.90a}$$

The following values of k apply to various cases of support restraint:

Table 6-5

Buckling Coefficients for Narrow Rectangular Beams With a/b > 2, Subject to In-Plane Bending (6.11) (6.15)

Loading Distribution	Buckling Coefficient, k, in Eq. 6.89	
	lateral restraint at indicated spacing without lateral rotational fixity	lateral restraint at indicated spacing with full lateral rotational fixity
1. Pure bending in plane of plate - Fig. 6-37(a) with lateral unbraced length = c	1.0	2.0
2. In-plane concentrated load at mid-span, applied at centroidal x axis - Fig. 6-37(b), simple supports in-plane span a, lateral support span a	1.35	2.12
3. Same as 2, except load is applied at distance d above centroidal x axis Fig. 6-37 (c), or -d below.	$1.35\left(1-1.74\frac{d}{a}\sqrt{\frac{(1+\nu)}{2(1-0.63\frac{t}{b})}}\right)$	-
4. Uniformly distributed load applied at centroidal x-axis - Fig. 6-37(d), simple supports in plane span a, lateral support span a	1.13	-
5. Concentrated load at end of cantilever, applied at centroidal x axis - Fig. 6-37(e), no in-plane or lateral support at point of load application	n.a.	1.28
6. Same as 5, except load is applied at d above centroid axis, Fig. 6-37 (f) or -d below	n.a.	$1.28\left(1-\frac{d}{a}\sqrt{\frac{(1+\nu)}{2(1-0.63\frac{t}{b})}}\right)$
7. Uniformly distributed load on cantilever, applied at centroidal x-axis - Fig. 6-37 (g), no in-plane or lateral support at cantilever end	n.a.	2.05

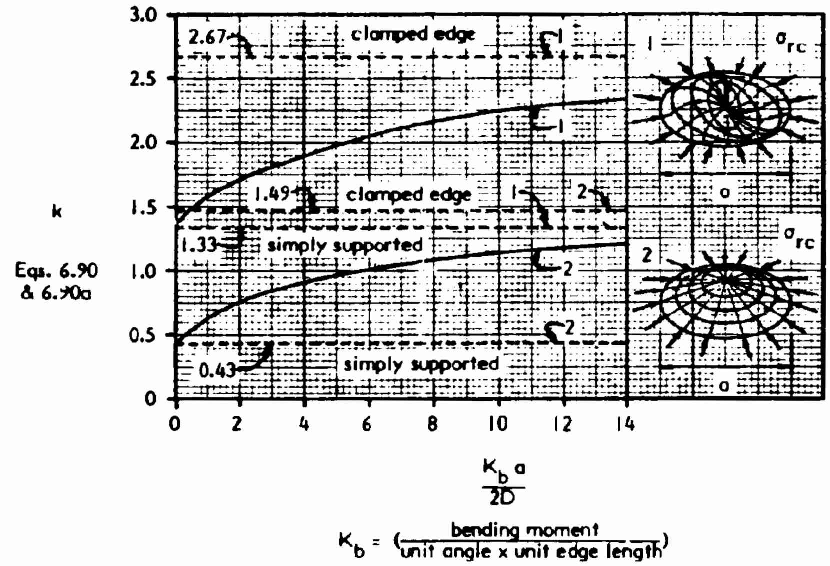

Fig. 6-38 BUCKLING COEFFICIENTS k FOR CIRCULAR ISOTROPIC PLATE WITH ROTATIONALLY RESTRAINED EDGES (6.11)

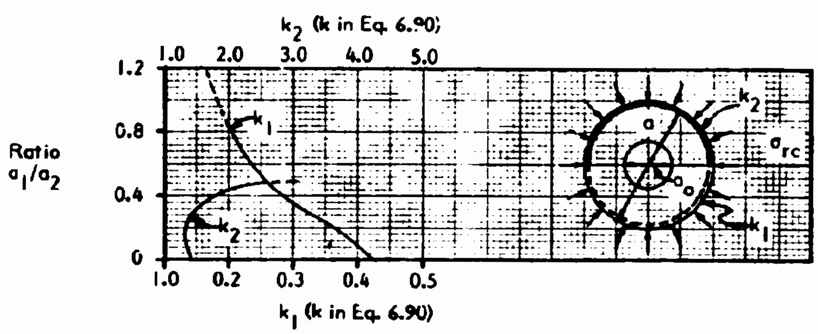

Fig. 6-39 BUCKLING COEFFICIENTS FOR ANNULAR ISOTROPIC PLATES WITH SIMPLY SUPPORTED (k_1) OR CLAMPED OUTSIDE EDGES (k_2) – INTERNAL BOUNDARY FREE IN BOTH CASES (6.11)

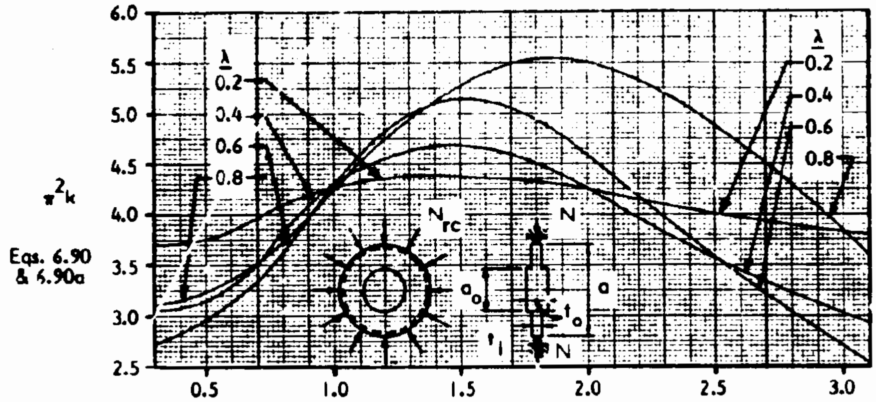

Simply Supported Edges

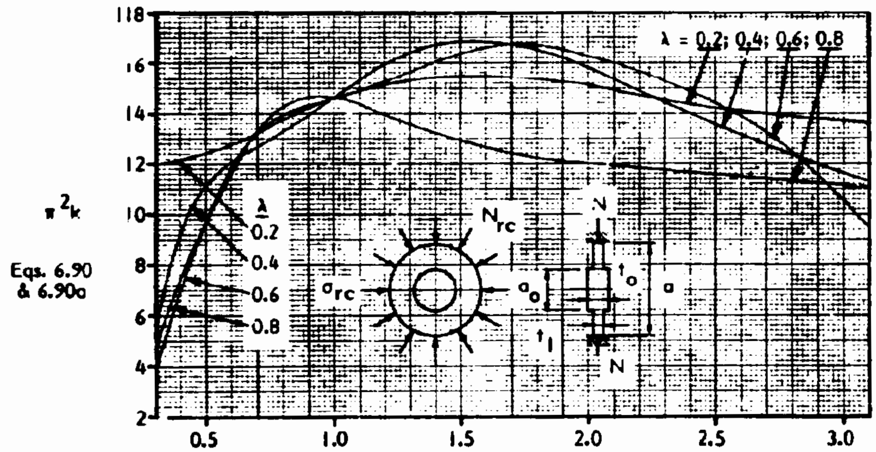

Clamped Edges

$$\lambda = \frac{a_o}{a} \; ; \; t = t_i \left(1 - \lambda^2 + \frac{t_o}{t_i} \lambda^2\right)$$

Fig. 6-40 BUCKLING COEFFICIENTS FOR CIRCULAR ISOTROPIC PLATES WITH ANNULAR THICKENING (6.11)

For simply supported edges: k = 0.426

For clamped edges: k = 1.49

For elastically supported edges: See Fig. 6-38

For simply-supported or clamped plate with unsupported annular openings: See Fig. 6-39

For simply supported plates and clamped plates with annular thickening: See Fig. 6-40

For an elliptical plate with boundaries clamped: See Fig. 6-41

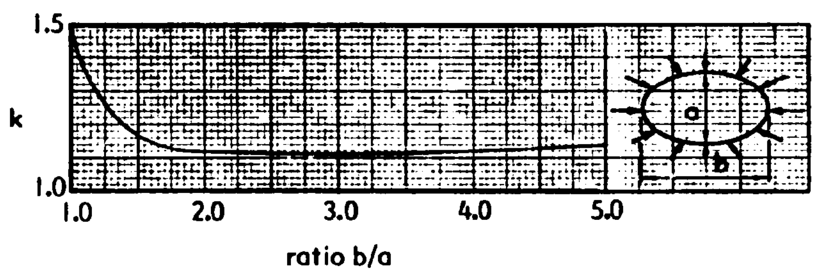

Fig. 6-41. BUCKLING COEFFICIENT FOR ELLIPTICAL PLATE WITH CLAMPED EDGES (6.11)

See (6.11) for buckling of circular plates under partial external radial compression, external radial compression with boundary partially simply supported and partially clamped, various cases involving support of an annular opening normal to plate, various circular sectoral plates, and buckling of plates with compression applied radially at internal boundaries of annular openings and combined with radial compression on external boundaries.

Triangular and Polygonal Plates

The critical buckling stress on the perimeter of equally stressed triangular plates (Fig. 6-42) is as follows (6.11):

$$\sigma_{nc} = \frac{k \pi^2 E}{12(1-\nu^2)} \left(\frac{t}{a}\right)^2 \qquad \text{Eq. 6.91}$$

For equilateral triangle with simply supported edges (Fig. 6-42a): $k = 4.0$

For right angled isosceles triangular plate with simply supported edges (Fig. 6-42b): $k = 5.0$

See (6.11) for buckling of many other polygonal plates under various conditions of shape, proportions, edge loads, and edge restraint.

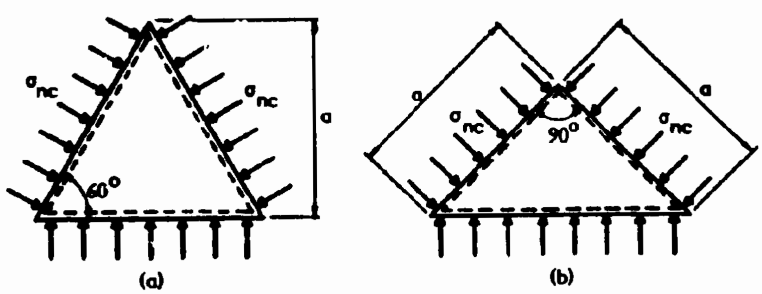

Fig. 6-42. DIRECT STRESS ON SIMPLY SUPPORTED TRIANGULAR PLATES

6.10 STABILITY OF ORTHOTROPIC PLATES

When plate materials are not isotropic, stability relations become much more complex. Only a few basic cases involving buckling of specially orthotropic rectangular plates are presented here. In these plates, the principal plate axes, principal axes of materials stiffness and axes of principal stress (except in pure shear case given below) all coincide.

Uniform Uniaxial Compression

For the basic case of uniaxial compression on a simply supported rectangular plate stressed in the x direction (Fig. 6-43a), the critical buckling stress resultant is (6.11)(6.18)(6.19):

$$N_{xc} = \frac{2\pi^2}{b^2}\left(\sqrt{D_{11} D_{22}} + D_3\right) \qquad \text{Eq. 6.92}$$

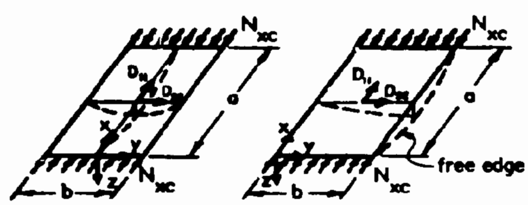

(a) Plate simply supported along all four edges

(b) Plate with one edge free, others simply supported

Fig. 6-43. BUCKLING OF PLATES IN UNIAXIAL COMPRESSION

For single thickness plates, the critical buckling stress is:

$$\sigma_{xc} = \frac{N_{xc}}{t} \qquad \text{Eq. 6.92a}$$

For specially orthotropic, laminated plates, the critical buckling stress in layer k, with its stiffness properties referenced to direction 1 in the x direction, is:

$$\sigma_{xck} = \frac{N_{xc}\, b_{11k}}{\bar{A}_{11}} \qquad \text{Eq. 6.92b}$$

also $N_{xc} = 2 \sum_{1}^{n} \sigma_{xck} t_k$ Eq. 6.92c

The half-wavelength of buckle, ℓ_b, is:

$$\ell_b = b \sqrt[4]{\frac{D_{11}}{D_{22}}} \qquad \text{Eq. 6.93}$$

See Eq. 6.6 for D_o. For an isotropic plate $D_{11} = D_{22} = D$ and $D_o = D(1 - \nu^2)/(1 + \nu) + \nu D = D$; thus, σ_{xc} is the same as given in Eq. 6.71a. Also the half-wavelength of buckle is b.

Equations 6.92 and 6.93 only apply for plates whose length, a, equals or exceeds ℓ_b. See (6.16) for buckling coefficients for smaller a/b ratios.

Example 6.12 illustrates the determination of critical local buckling stress in a rectangular tube column fabricated from the orthotropic laminate whose stiffness was calculated in Example 6.7.

When the longitudinal plate edges are rotationally fixed, the critical buckling stress is (6.16):

$$\sigma_{xc} = \frac{4.52}{b^2} \frac{\pi^2}{t} \left(\sqrt{D_{11} D_{22}} + \frac{D_o}{1.84} \right) \qquad \text{Eq. 6.94}$$

$$\ell_b = 0.67\, b \sqrt[4]{\frac{D_{11}}{D_{22}}} \qquad \text{Eq. 6.95}$$

Equations 6.94 and 6.95 apply only for plates whose length, a, equals or exceeds ℓ_b.

When information about the in-plane shearing rigidity of the specially orthotropic material is not available to calculate D_o, an estimate of the effect of the differing stiffness in the 1 and 2 directions on the buckling stress in the x-direction can be obtained by modifying the buckling formulas for isotropic plates as follows:

Example 6.12: Determine the local wall buckling compressive stress under short term load in a square tube section constructed with the laminate whose stiffness properties were determined in Example 6.7 and whose cross section dimensions are shown in the sketch: *

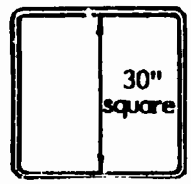

Solution:

From Example 6.7:

Flexural Stiffness:	Longitudinal:	D_{22}	$= 382 \times 10^3$ lbs-in.^{2}/in.
	Transverse:	D_{11}	$= 112 \times 10^3$ lbs-in.^{2}/in.
Twisting Stiffness:		D_o	$= 35 \times 10^3$ lbs-in.^{2}/in.

From Eq. 6.89, modified for a laminated plate:

$$N_{yc} = \frac{2\pi^2}{b^2}\left(\sqrt{D_{22}D_{11}} + D_o\right)$$

$$= \frac{2\pi^2}{30^2}\left(\sqrt{382 \times 10^3 \times 112 \times 10^3} + 35 \times 10^3\right) = 5304 \text{ lbs/in.}$$

In each layer: $\sigma_{yck} = \dfrac{N_{yc}\, b_{22k}}{\bar{A}_{22}}$

$$\bar{A}_{22} = \Sigma\, t\, b_{22} = 0.06\,(25.15 + 1.01 + 25.15 + 1.01 + 10.09) \times 2 \times 10^6 + 0.06 \times 1.01 \times 10^6 = 7.55 \times 10^6$$

Graphite, longitudinal: $\sigma_{yck} = \dfrac{5{,}304 \times 25.15 \times 10^6}{7.55 \times 10^6} = 17{,}670$ psi

Aramid, longitudinal: $\sigma_{yck} = \dfrac{5{,}304 \times 10.09 \times 10^6}{7.55 \times 10^6} = 7{,}089$ psi

Aramid, transverse: $\sigma_{yck} = \dfrac{5{,}304 \times 1.01 \times 10^6}{7.55 \times 10^6} = 710$ psi

Check total load:

Graphite, L:	17,670 x 0.06 x 4 layers =	4,240 lbs/in.
Aramid, L:	7,089 x 0.06 x 2 layers =	851
Aramid, T:	710 x 0.06 x 5 layers =	213
		5.304 lbs/in.

Note: 1 lbf-in.^{2}/in. = 113 N-mm^2/mm; 1 lbf/in. = 0.18 N/mm; 1 psi = 0.0069 MPa

* See footnote, Example 6-1, p. 29.

1. Use E_{22} (or D_{22}) in isotropic formulas to determine $\sigma_{xc\ isotropic}$. Direction 1 lies along the x axis.

2. Modify buckling stress as follows:

$$\sigma_{xc\ ortho} = \sigma_{xc\ isotropic} \sqrt{\frac{E_{11}}{E_{22}}} \qquad \text{Eq. 6.96}$$

This is the same relation that was suggested in a previous Section to account for creep in buckling of isotropic plates under long-term loads.

Two other conditions of practical importance are the cases of uniaxial compression with one edge at y = b free and the other edge at y = 0 either simply supported or fixed as shown in Fig. 6-43(b). These cases are limiting conditions in the local buckling of an outstanding flange of an I or C shaped beam.

The following equations for the approximate critical buckling stress in specially orthotropic plates with one unloaded edge free are given in (6.18)(6.19). These were developed for homogeneous plates of uniform thickness, and are given for the above two limiting conditions of edge restraint:

(a) edge at y = b free and at y = 0 simply supported:

$$\sigma_{xc} = \frac{\pi^2}{b^2 t} \left[D_{11} \left(\frac{b}{a}\right)^2 + \frac{12}{\pi^2} D'_{12} \right] \qquad \text{Eq. 6.97}$$

for a very long plate, where a/b is large:

$$\sigma_{xc} = G_{12} \left(\frac{t}{b}\right)^2 \qquad \text{Eq. 6.98}$$

For this edge condition, the half wave length of buckle equals the length of the plate, a. This is similar to the isotropic plate buckling conditions given in Case 4, Table 6-3.

(b) edge at y = b free and at y = 0 fixed:

$$\sigma_{xc} = \frac{\pi^2}{b^2 t}\left[\left(0.935\sqrt{D_{11}\,D_{12}} - 0.656\,D_{12} + 2.082\,D'_{12}\right)\right] \quad \text{Eq. 6.99}$$

For this edge condition, the half wave length of buckle is:

$$\ell_b = 1.46\,b\,\sqrt[4]{\frac{D_{11}}{D_{12}}} \quad \text{Eq. 6.100}$$

See Chapter 7 for a design example showing the application of the above equations for design of composite beam flanges.

Effect of Shear Deformation in Laminated Plates

Buckling relations become very complex when transverse (interlaminar) shear deformation is not neglected, as it is in the classical buckling relations presented above. Buckling stresses, including transverse shear deformation, for uniformly compressed specially orthotropic rectangular plates with loaded edges simply supported and unloaded edges: (a) simply supported, (b) clamped, and (c) one simply supported and one free, are given in (6.8), but the equations are too cumbersome to present here. Plots comparing buckling stress including shear deformation with stresses neglecting it are also given in (6.8) to illustrate conditions when shear deformation may be significant. These may occur when $E_{11}\,t/G_{13}\,b > 2$, where the direction of the buckling stress is in the materials direction 1. See Chapter 8 for further discussion relative to consideration of shear deformation in the buckling of sandwich panels.

Pure In-Plane Bending

For in-plane stresses distributed across the plate width b in pure bending (Fig. 6-44), with varying degrees of edge restraint from torsional rigidity of a flange, the critical buckling stress is (6.11):

$$\sigma_{xc} = \frac{k\,\pi^2 D_{11}}{b^2 t} \quad \text{Eq. 6.101}$$

The buckling coefficient k is obtained from the curves given in Fig. 6-44.

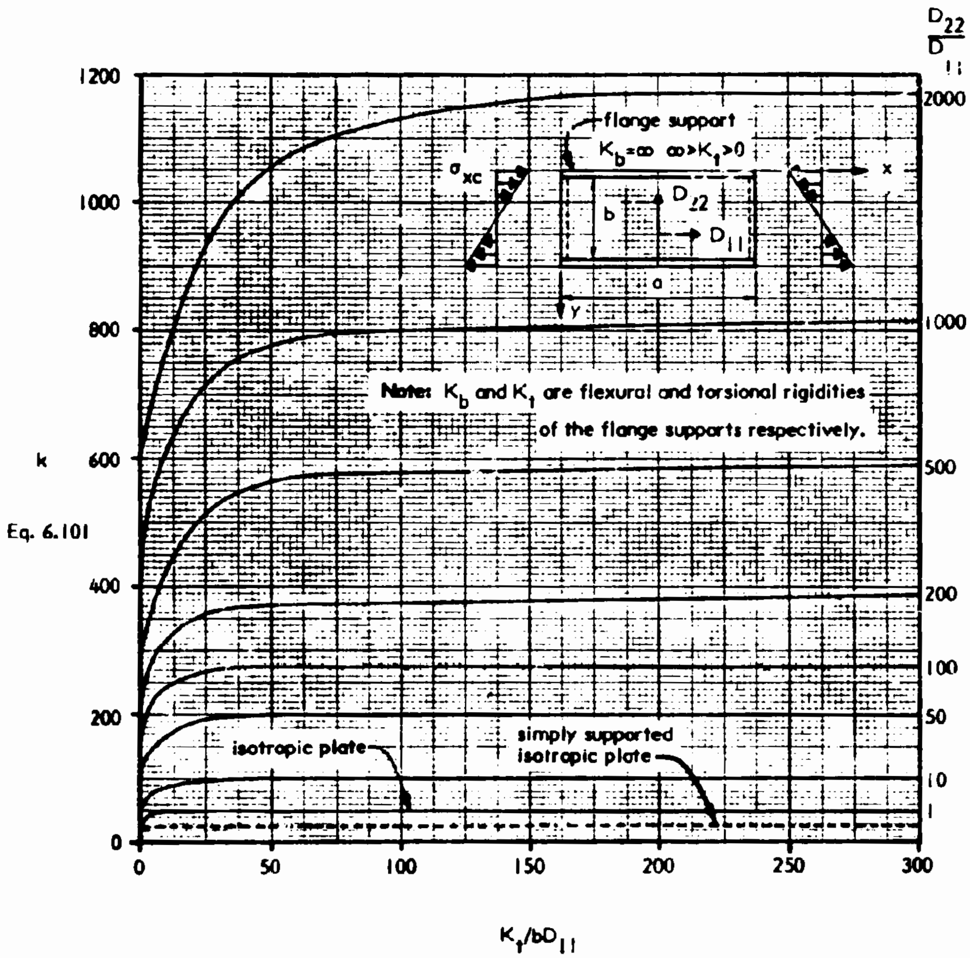

Fig. 6-44 BUCKLING COEFFICIENTS FOR RECTANGULAR ORTHOTROPIC PLATE IN PURE BENDING (6.11)

Pure Shear

For pure shear stresses on a simply supported rectangular plate (Fig. 6-45), the critical buckling stress is (6.11):

$$\tau_{xyc} = \frac{4\,k_{xy}\,(D_{11}\,D_{22}^{3})^{1/4}}{b^2\,t} \qquad \text{Eq. 6.102}$$

The buckling coefficient k_{xy} is obtained from the curves in Fig. 6-45.

See (6.11) for several other cases of rectangular plates in pure shear. See (6.17) for the critical buckling stresses in shear for long plates with various degrees of rotational restraint on the longitudinal edges. These solutions are useful for determining shear buckling of orthotropic webs of plate girders whose flanges provide varying degrees of rotational restraint. However, the solution given by Equation 6.102 above may be used in many cases where the rotational restraint from the flanges is low, or is neglected.

Combined Shear and Direct Stress

The interaction equations 6.87 and 6.88 suggested in the previous Section for buckling of isotropic plates may be used to obtain a tentative estimate of the stability of an orthotropic plate under combined loading. Tests should be conducted to confirm the applicability of these relations.

Circular Plates

The critical buckling stress for a circular orthotropic plate with uniform radially applied edge loads and with orthotropic axes of material arranged radially and circumferentially is (6.11):

$$N_{rc} = \frac{4\,k\,D_r}{a^2} \qquad \text{Eq. 6.103}$$

See Fig. 6.46 for values of k for a range of ratios of $\sqrt{E_\theta / E_r}$.

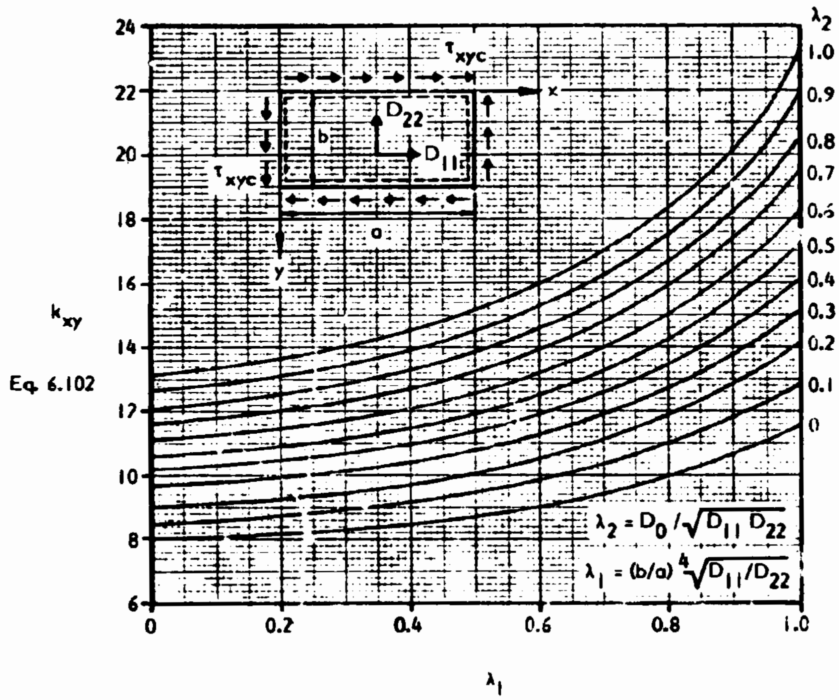

Fig. 6-45 BUCKLING COEFFICIENTS FOR RECTANGULAR SIMPLY SUPPORTED ORTHOTROPIC PLATES IN PURE SHEAR (6.11)

k

Eq. 6.103

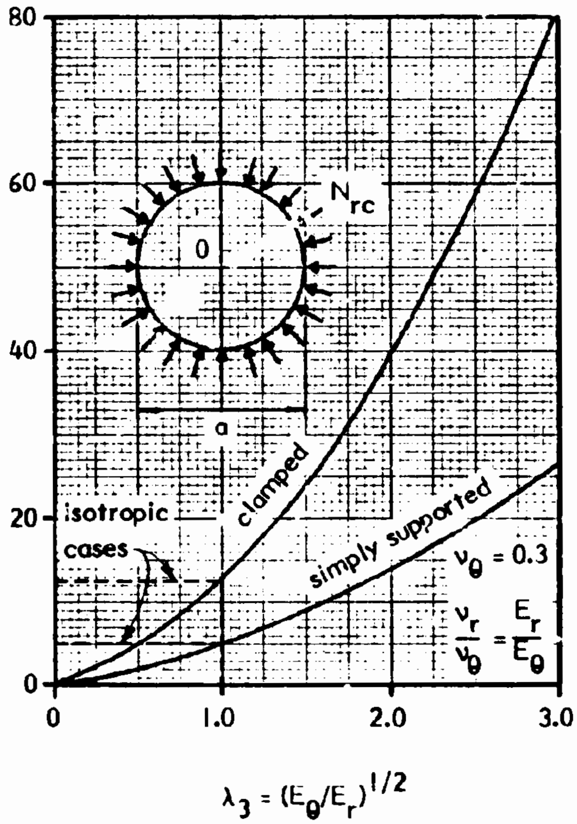

Fig. 6-46 BUCKLING COEFFICIENTS FOR SIMPLY SUPPORTED OR CLAMPED CIRCULAR ORTHOTROPIC PLATES (6.11)

6.11 NATURAL FREQUENCIES OF PLATES AND MEMBRANES

In problems of investigation or design involving transversely loaded plate elements subjected to dynamically applied loading or support motion, the natural frequencies of free harmonic vibration of the plates must first be determined. Generally, the lowest natural frequency is of greatest interest, but sometimes higher modes must also be investigated. See (6.3) and (6.20) for tabulated formulas for natural frequencies of transversely loaded rectangular, circular, triangular, and miscellaneous shaped plates with various conditions of edge restraint. Some common cases are presented here based on equations given in these references. These equations are fairly accurate "upper bound" approximations for the lowest and second mode natural frequencies of the indicated plate types.

Rectangular Isotropic plates

The natural frequencies of rectangular plates supporting a uniformly distributed mass ρ on a unit area are given by the following relation (6.3):

$$f_n = \frac{\phi_n}{a^2}\sqrt{\frac{D}{\rho}} \qquad \text{Eq. 6.104}$$

for a plate loaded only by its own weight, where $\rho = \frac{\bar{\gamma} t}{g}$:

$$f_n = \frac{\phi_n}{a^2}\sqrt{\frac{E\,t^2\,g}{12\,(1-\nu^2)\,\bar{\gamma}}} \qquad \text{Eq. 6.104a}$$

The frequency coefficient ϕ_n in the above Equations varies with the mode and with the edge support conditions. See (6.3) for values of ϕ_n for the two lowest modes of vibration for rectangular plates with various edge restraints. For two common cases, where $\lambda_o = a/b$:

Simply supported edges:

First mode: $\phi_1 = 1.57\,(1 + \lambda_o^2)$ Eq. 6.105

Second mode: (use lowest)

$$\phi_2 = 6.28\,(1 + 0.25\,\lambda_o^2)$$

$$\phi_2 = 1.57\,(1 + 4\,\lambda_o^2)$$

Eqs. 6.106

Rotationally fixed edges:

First mode: $\phi_1 = 1.57\sqrt{5.14 + 3.13\,\lambda_o^2 + 5.14\,\lambda_o^4}$ Eq. 6.107

Second mode: (use lowest) $\phi_2 = 9.82\sqrt{1 + 0.298\,\lambda_o^2 + 0.132\,\lambda_o^4}$

$\phi_2 = 1.57\sqrt{5.14 + 11.65\,\lambda_o^2 + 39.06\,\lambda_o^4}$ Eq. 6.108

When the plate is subject to in-plane tensile or compressive forces, N_x and N_y, the natural frequencies are modified. In-plane tensile forces (+N) increase the natural frequency and compressive forces (-N) reduce it. Compressive forces equal to the plate buckling load reduce the natural frequency to zero. The following equation is a fairly accurate "upper bound" estimate of the natural frequency of a plate with simply supported edges subject to in-plane forces N_x and N_y (6.20).

$$f_n = \frac{1.57}{a^2\sqrt{\rho}}\sqrt{\left\{D\left[m^2 + n^2\left(\frac{a}{b}\right)^2\right]^2 + N_y\, a^2\left(\frac{m}{\pi}\right)^2 + N_x\, a^2\left(\frac{n}{\pi}\right)^2\left(\frac{a}{b}\right)^2\right\}} \quad \text{Eq. 6.109}$$

where a, b, x, y, N_x, and N_y are directed as shown in Fig. 6-47, and m and n are integers which define mode frequencies.

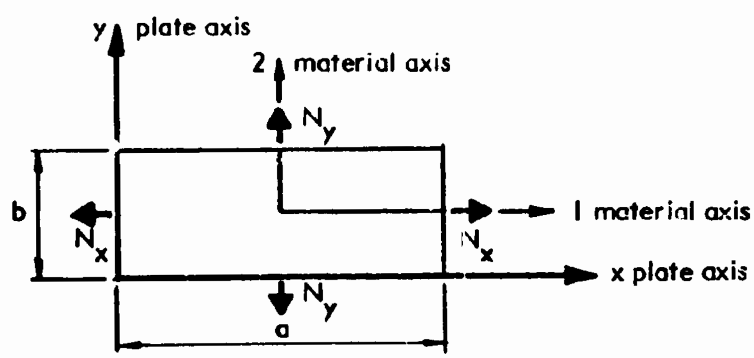

Fig. 6-47. ORIENTATION OF PLATE AXES, MATERIAL AXES AND PLATE EDGE DIMENSIONS

The lowest, or first mode occurs when $m = n = 1$, except in certain cases where $a \neq b$ and N_x is negative and approaches N_{xc}. Other modes must be determined by cut and try substitution of various values of m and n. When $N_x = N_y = 0$, the above equation reduces to Eq. 6.104 and Eqs. 6.105 or 6.106, using the appropriate values of m and n.

When the amplitude of vibration exceeds about half the plate thickness, the plate is stiffened significantly by the changes in its shape, and its natural frequency increases. An approximate determination of the increased non-linear natural frequency, relative to the frequencies given above for "small deflections," is given by the curves in Fig. 6-48. The ratio of linear frequency to nonlinear frequency for various ratios of vibration amplitude to plate thickness is given for limiting ratios of a/b and several conditions of edge restraint.

The greatest effect of stiffening due to "large deflection" shape changes occurs with simply supported edges that are held against lateral translation (Curves 2 in the Figure). For this case, the ratio of linear to non-linear frequency does not vary significantly with a/b. The other edge conditions given in the Figure are Curve 1 for simply supported edges, not held against in-plane translation, Curve 3 for clamped edges, not held against in-plane translation, and Curve 4 for clamped edges, held against in-plane translation.

Rectangular "Specially Orthotropic" Plates

The natural frequencies of rectangular specially orthotropic plates supporting a uniformly distributed mass ρ on a unit area are given by the following relation for plates with all edges simply supported (6.20):

$$f_n = \frac{1.57}{a^2\sqrt{\rho}} \sqrt{D_{11}\, m^4 + 2\,D_o\, m^2 n^2 \left(\frac{a}{b}\right)^2 + D_{22} n^4 \left(\frac{a}{b}\right)^4} \qquad \text{Eq. 6.110}$$

where a, b, and materials axes 1 and 2 are directed as shown in Fig. 6-47, and m and n are integers which define mode frequencies. The lowest or first mode frequency occurs when $m = n = 1$. The second mode frequency is the lowest of the results from Eq. 6.110 with $m = 2$, $n = 1$, or with $m = 1$, $n = 2$. Higher mode frequencies are obtained with various combinations of integral values of m and n.

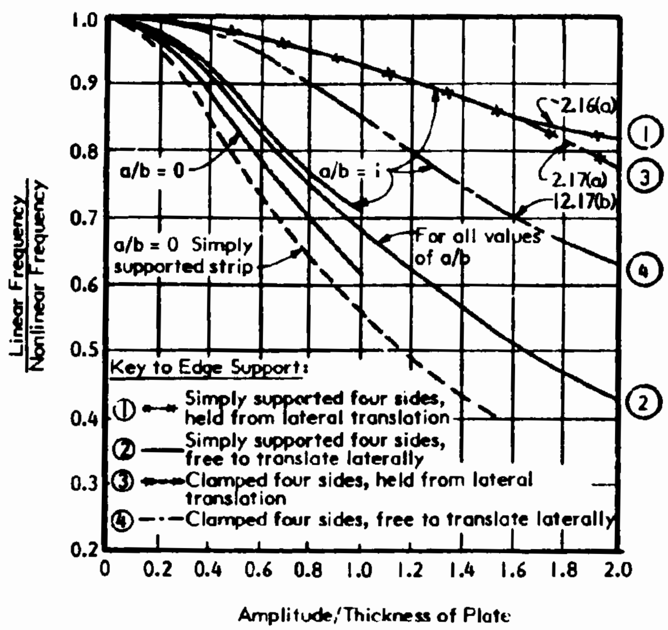

Fig. 6-48 RATIO OF LINEAR TO NONLINEAR FREQUENCY AS A FUNCTION OF AMPLITUDE/THICKNESS RATIO FOR LARGE DEFLECTIONS OF RECTANGULAR PLATES (6.20)

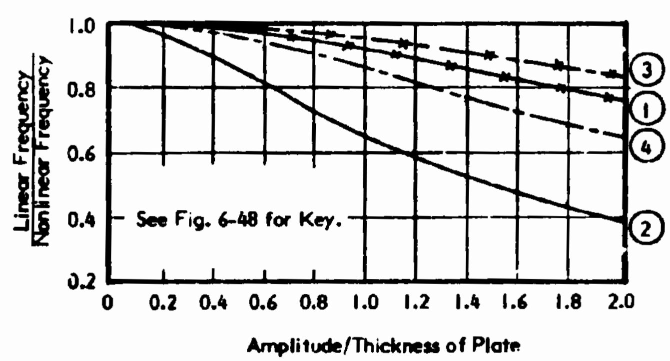

Fig. 6-49 RATIO OF LINEAR TO NONLINEAR FREQUENCY AS A FUNCTION OF AMPLITUDE/THICKNESS RATIO FOR LARGE DEFLECTIONS OF CIRCULAR PLATES (6.20)

Eq. 6.110, with appropriate values of m and n, reduces to Eq. 6.104 and Eqs. 6.105 or 6.106, for the first and second mode frequencies of isotropic simply supported rectangular plates ($D_{11} = D_{22} = D_o = D$). It also reduces to Eq. 6.109 with N = 0.

Circular Plates

The lowest natural frequency of a simply supported, transversely loaded circular plate is (6.3):

$$f_1 = \frac{\pi}{a^2} \sqrt{\frac{D}{\rho}} \qquad \text{Eq. 6.111}$$

An approximate determination of the increased nonlinear natural frequency which occurs when the plate undergoes large deflections is given by the curves of Fig. 6-49. The ratio of linear frequency to nonlinear frequency for various ratios of vibration amplitude to plate thickness is obtained using Curve 1 for simply supported edges, not held against in-plane translation, and Curve 2 for simply supported edges held against in-plane translation. Curves 3 and 4 give the same information for circular plates with clamped edges.

Triangular Plates

The lowest natural frequency of a simply supported, transversely loaded right triangular plate with two perpendicular sides of length, a, is (6.3):

$$f_1 = \frac{7.85}{a^2} \sqrt{\frac{D}{\rho}} \qquad \text{Eq. 6.112}$$

See (6.20) for many more plate edge proportions and support conditions.

Membranes

The lowest natural frequency of various membranes stretched with a uniform edge tension force per unit length, N, and having the shapes listed below, is (6.3):

$$f_1 = \frac{k}{2\pi} \sqrt{\frac{Ng}{Fq}} \qquad \text{Eq. 6.113}$$

F is the area of the membrane

g is the acceleration due to gravity

q is the uniformly distributed transverse pressure

k is a coefficient which depends on the shape of the membrane. For some common shapes, k is:

	k	
Circle	4.26	
Square	4.44	
Equilateral triangle	4.77	
60° sector of circle	4.62	
Semicircle	4.80	
Rectangle	$\pi\sqrt{\frac{b}{a}\left[1+\left(\frac{a}{b}\right)^{2}\right]}$	$a > b$

Example 6.13 illustrates the use of the above equations to determine the lowest natural frequency of several rectangular plates, such as might be used in plastic glazing and screen wall panels, respectively. Excessive wind-induced vibration may occur in such panels if the frequency of wind gusts approaches the natural frequency of the plates. This is not likely in the first plate in the example, but may occur for the first mode vibration of the second example plate.

An exhaustive summary of available solutions for natural frequencies, mode shapes, nodal lines, and amplitude coefficients in plates of various types is presented in (6.20). Information provided covers many different shapes of plates, conditions of edge restraint, behavior of anisotropic plates and plates of variable thickness. Relations for effects of in-plane load, "large deflections," and transverse shear deflection on the natural frequency of certain types of plates are also included.

Example 6.13: Determine the two lowest natural frequencies of the plates in (a) Example 6.1 and (b) Example 6.2. Use specific gravity of thermoplastic materials given in Table 4-4, and FRP given in Table 1-6. *

(a) Solution: Specific gravity of acrylic = 1.17

From Eqs. 6.102 and 6.103 with $\lambda_o = 1.5$

First Mode: $\phi_1 = 1.57\,(1 + 1.5^2) = 5.10$

Second Mode: $\phi_2 = 6.28\,(1 + 0.25 \times 1.5^2) = 9.81$ Use

or $\phi_2 = 1.57\,(1 + 4 \times 1.5^2) = 15.7$

From Eq. 6.101a:

$$f_1 = \frac{5.10}{29.4^2}\sqrt{\frac{400{,}000 \times 0.25^2 \times 32.2}{12(1-0.3^2)\times 1.17\times 0.036}} = 7.81 \text{ cps}$$

$$f_2 = \frac{9.81}{5.10} \times 7.81 = 15.01 \text{ cps}$$

(b) Solution: Specific gravity of mat reinforced polyester = 1.4

Using equations for plates with small deflections:

From Eqs. 6.102 and 6.103 with $\lambda_o = 1.5$ and from part (a) above: $\phi_1 = 5.1$; $\phi_2 = 9.81$

From Eq. 6.97a:

$$f_1 = \frac{5.1}{48.9^2}\sqrt{\frac{1{,}000{,}000 \times 0.125^2 \times 32.2}{12(1 - 0.3^2) \times 1.4 \times 0.036}} = 2.04 \text{ cps}$$

$$f_2 = \frac{9.81}{5.1} \times 2.04 = 3.92 \text{ cps}$$

The natural frequencies determined for small deflections will increase as the plate stiffens when it is subjected to sufficiently high loads to cause appreciable deflection. At the maximum design deflection of 1/2 in. the amplitude/thickness ratio is 4.0. If the approximate curve for any value of a/b in Fig. 6-48 is extrapolated to the above amplitude/thickness ratio, the estimated lowest natural frequency is:

$f_1 = 2.04/0.2 \approx 10.$

* See footnote, Example 6-1, p. 29.

Chapter 6 – REFERENCES

6.1 Engineering Sciences Data Unit, "Stiffness of laminated flat plates," Item No. 75002, Jan. 1975, Structures Sub-series, Vol. 8, London.

6.2 Timoshenko, S. and Woinowsky-Krieger, S., Theory of Plates and Shells, 2nd Edition, McGraw-Hill, 1959.

6.3 Bares, R., Tables for the Analysis of Plate, Slabs, Diaphragms Based on the Elastic Theory, Bauverlag, Wiesbaden, 1969.

6.4 Engineering Sciences Data Unit, "Elastic direct stresses and deflections for flat rectangular plates under uniformly distributed normal pressure," Item No. 71013, May 1971, Structures Sub-series, Vol. 5, London.

6.5 Engineering Sciences Data Unit, "Elastic Stresses and Deflections for Flat Circular Plates With D/t > 20 Under Uniform Pressure," Item No. 65003, Sept. 1965, Structures Sub-series, Vol. 5, London.

6.6 Engineering Sciences Data Unit, Elastic Stresses and Deflections for Flat Circular Plates with D/t > 4 Under Uniform Pressure," Item No. 65002, Sept. 1965, Structures Sub-series, Vol. 5, London.

6.7 Ashton, J. E., and Whitney, J. M., Theory of Laminated Plates, Technomic, Stamford, Connecticut, 1970.

6.8 Vinson, J.R., and Chou, T.W., Composite Materials and Their Use in Structures, Wiley, New York, 1975.

6.9 Engineering Sciences Data Unit, "Stress analysis of laminated flat plates," Item No. 74039, Feb. 1975, Structures Sub-series, Vol. 8, London.

6.10 Portland Cement Association, "Design of Deep Girders," No. ST 66, 1944,

6.11 Column Research Committee of Japan, Handbook of Structural Stability, Corona, Tokyo, 1971.

6.12 Engineering Sciences Data Unit, "Buckling of flat isotropic plates under uniaxial and biaxial loading," Item No. 72019, Sept. 1976, Structures Sub-series, Vol. 2, London.

6.13 Bleich, F., Buckling Strength of Metal Structures, McGraw-Hill, New York, 1952.

6.14 Structural Stability Research Council, Guide to Stability Design Criteria for Metal Structures, 3rd Edition, Ed. by B. G. Johnston, Wiley, New York, 1976.

6.15 Timoshenko, S. and Gere, Theory of Elastic Stability, 2nd Edition, McGraw Hill, 1961.

6.16 Engineering Sciences Data Unit, "Buckling of thin flat orthotropic plates under uniaxial compression," Item No. 71015, Sept. 1971, Structures Sub-series, Vol. 8, London.

6.17 Engineering Sciences Data Unit, "Buckling of long flat orthotropic plates in shear," Item No. 74005, Feb. 1975, Structures Sub-series, Vol. 8, London.

6.18 Haaijer, G., "Plate Buckling in the Strain-Hardening Range," Paper No. 2968, Transactions of ASCE, 1959.

6.19 Haaijer, G. and Thurlimann, B. "Inelastic Buckling in Steel," Paper No. 3023, Transactions of ASCE, 1960.

6.20 Leissa, A. W., Vibration of Plates, NASA Report SP-160, 1969.

Additional references for tabulations of plate bending formulas:

6.21 Engineering Sciences Data Unit, "Elastic stresses and deflections for flat square plates under uniformly distributed normal pressure." Item No. 70001, April 1970, Structures Sub-series, Vol. 5, London.

6.22 Erturk, I. N., Zwei-, drei- und vierseitig gestutzte Rechteckplatten, Verlag von Wilhelm Ernst & Sohn. Berlin, Munchen, 1965.

6.23 Schliecher, C., Wegener, B., Continuous Skew Slabs, Tables for Statical Analyses, VEB Verlag fur Bauwesen, Berlin, 1971.

6.24 Stiglat, K., Wippel, H., Platten, Verlag von Wilhelm Ernst & Sohn. Berlin, Munchen, 1966.

6.25 Roark, R. J., Young, W. C., Formulas for Stress and Strain, Fifth edition, McGraw-Hill, 1975.

6.26 Griffel, W., Plate Formulas, Frederick Ungar Publishing, 1968.

6.27 Engineering Sciences Data Unit, "Elastic Stresses and deflections for long flat rectangular plates under uniformly distributed and linearly varying normal pressure." Item No. 69018, September 1969. Structures Sub-series, Vol. 5, London.

ASCE Structural Plastics Design Manual

CHAPTER 7 - BEAMS AND AXIALLY STRESSED MEMBERS

By Frank J. Heger

TABLE OF CONTENTS

NOTATION - Chapter 7

a	see Fig. 7-7 & Fig. 7-12
A	cross sectional area
A_e, A'_e	effective cross sectional areas after local buckling of compressed plate
A_b	area of brace member
A_f	area of one flange of thin-wall beam
A_n	area of net section
A_n, A_m	area of plates n and m, respectively, (Fig. 7-25)
A_{top}, A_{bot}	effective area of top and bottom flanges of a box section
A_w	area of web between inside of flanges of thin-wall beam
b, b_f, b_w,	width; width of flange; width of web
b_c	distance defined after Eq. 7.85
b_e	effective width of local plate in post buckling state, or for resistance to concentrated load, or for corrected flange stress because of shear lag
b'_e	effective flange width for corrected deflection because of shear lag
b_s	longitudinal spacing between transverse stiffeners; also, width of substitute panel in shear lag analysis
c	dimension in Fig. 7-12

c_f maximum transverse deflection of thin flange caused by curvature produced by longitudinal stress

C_b, C_c, C_1 coefficients in buckling equations

C_m reduction factor in equations for effect of combined bending and axial compression

C_w warping constant

d, d_w depth of section, depth of web

d dimension in Fig. 7-12

D_f transverse flexural rigidity of flange

e distance from shear center to centroid along 1-1 axis of symmetry

E, E_T elastic modulus, tangent modulus

E_L elastic modulus in longitudinal direction

E_v, E_{vT} viscoelastic modulus (Chapters 2 and 3), viscoelastic tangent modulus

E_x elastic modulus in x direction

E_b elastic modulus of brace member

G shear modulus

G_{xy} shear modulus in x-y plane

I moment of inertia of cross section

I_1, I_2 moment of inertia about axes 1 and 2, respectively, in member cross section

I_{le}	effective moment of inertia after local buckling of compressed plate element, or as reduced by shear lag
I_s	moment of inertia of web stiffener about the plane of the web; centroidal moment of inertia of support element for stiffened plate
J	torsion constant for cross section
k	plate buckling coefficient; width defined in Fig. 7-7
k_{mn}, k_{nm}	stress distribution factors given by Eqs. 7.89 and 7.90
K	effective length coefficient for buckling of columns
K_m	coefficient for bending deflection of beams
K_s	spring stiffness of braces
K_t	stress concentration factor
L	member length
M	bending moment
M_f	lateral bending moment on each flange of I section caused by torque
M_{xuI}	ultimate design bending moment at a point along reference axis x in a plane perpendicular to centroidal axis I-I
n	width of bearing (Fig. 7-7)
N	axial force per unit width
N_n	maximum axial thrust at fold line n in folded plate

$N_x^{\bullet}$ axial force in x direction

N_{xc} critical buckling load on centrally loaded column

N_{xcF1}, N_{xcT} critical elastic buckling load in flexure about axis 1, and in torsion, respectively

N'_{xu} ultimate axial force in x direction

p numerical value given by Eq. 7.63; uniformly distributed load intensity normal to surface of folded plate

p_y uniformly distributed load intensity on horizontal projection of folded plate

P applied load

P_{e2} Euler buckling load for weak direction

q uniformly distributed load normal to beam axis

q_r radial load on thin flange due to curvature with longitudinal stress

q_{sn} shear flow at fold line n in folded plate

Q form factor for local buckling

Q_s form factor for local buckling of unstiffened plate

Q_a, Q'_a form factor for local buckling of stiffened plates where post buckling strength is considered

r, r_o radius of gyration; polar radius of gyration

r_1, r_2 — radius of gyration about strong axis 1-1 and weak axis 2-2, respectively

r_{1e} — radius of gyration about axis 1-1, based on effective section properties

r_s — polar radius of gyration about shear center

R_u — concentrated load or reaction normal to beam axis

S — section modulus of cross section

S_1, S_2 — section modulus with respect to centroidal axes 1 and 2, respectively, in member cross section

S_{1e} — effective section modulus after local buckling of compressed plate element, or as reduced by shear lag

t, t_f, t_w — thickness; thickness of flange; thickness of web;

T — torque (twisting moment)

V — transverse shear force

T_s — portion of total torque resisted by torsionally induced shear stresses

V_f — lateral shear on each flange of I section caused by torque

V_{xu1} — ultimate transverse shear force at point along x axis for bending about centroidal axis 1-1

W — total uniformly distributed load

x — distance in direction of x axis, from a reference point

β	flexural-torsion constant defined by Eq. 7.24
δ, δ_0	deflection, initial deflection
Δ	lateral deflection of frame
ν	Poisson's ratio
ψ	a function defined by Eq. 7.75
σ	normal stress
σ_n	normal stress at fold line n in folded plate
σ_x, σ_{xav}	stress in x direction, average normal stress
σ_{xb}	bending stress in flange caused by torque
σ_{xc}, σ_{yc}	ultimate buckling normal stress in x direction, and in y direction
σ_{xce}	elastic buckling normal stress in x direction
σ_{xu}, σ_{yu}	reduced ultimate strength of material (normal stress) in x direction, and in y direction
τ	shear stress
τ_f	shear stress in flange caused by bending resistance to torque
τ_s, τ_{sf}, τ_{sw}	shear stress caused by torsional resistance to torque, same in flange, same in web
τ_x, τ_{xm}	shear stress at point along x axis, and maximum shear stress at this point

τ_{xc} ultimate shear stress that produces buckling at a point along x axis

τ_{xu} reduced ultimate shear strength of material at a point along x axis

7. BEAMS AND AXIALLY STRESSED MEMBERS

F.J. Heger

7.1 INTRODUCTION

Plastics may be formed to obtain tension members, columns, beams, ribbed panels, and other beam-like components that have efficient sections for resisting direct thrust and bending. These sections are usually rectangular or circular hollow tubular shapes, or I, , T, hat, or other open thin wall shapes that are assemblies of thin plate elements. Such shapes may be formed by extrusion, or other processes as described in Chapter 1. Glass or other fiber reinforcements are used in larger and more significant structural members. Fiberglass reinforced polyester members made by the pultrusion process are described in Chapter 1. Reinforced plastic tubular sections and ribs are also fabricated by filament winding, spray up, hand layup, compression molding and other suitable processes.

Design methods for plastic and reinforced plastic structural members that resist axial forces and bending are provided in this Chapter. These members are usually termed "columns or struts" when they resist primarily compressive thrust, "ties", or tension members, when they resist tensile thrust, and "beams" when they resist transverse loads that produce bending. Members subject to combined compression and bending are often termed "beam-columns". Flat panels having ribs spanning in one direction behave essentially as columns, beams or beam-columns, with each rib and its adjacent plate acting as a repetitive structural member. Other components, or assemblies of components, that behave like beams include large stressed skin components such as aircraft bodies, box beams, ISO-type cargo containers, vehicle bodies, and folded plate sections.

Equations and methods of analysis are presented for designing columns, beams and ribbed panels considering axial strength and stability, bending strength, twisting strength, lateral-torsional stability, stability of local plate elements, and deflection. These methods are based on conventional elastic theory for bending and buckling of bars in which a basic assumption is that "plane sections before bending remain plane after bending." Certain modifications are introduced when needed for members with wide flanges, deep webs, and other special considerations. Since some plastics and reinforced plastics do not have isotropic elastic properties, design considerations for members with orthotropic elastic properties are included.

Many of the design recommendations presented in this Chapter are based on design practice for metal members. Design procedures and formulas for metal members have evolved from theoretical formulations of structural behavior that account for fundamental materials properties such as elastic modulus and yield strength. Often these may also be used for other materials, such as plastics, and the theoretical relations required for designing beams and axially stressed members are presented and discussed in this Chapter, or elsewhere in this Manual. However, implementation of accurate design methods for metal members has required over 50 years of careful structural research to determine significant parameters that govern structural behavior. Important examples are residual stresses that reduce the effective elastic modulus in buckling when stresses exceed about one-half to two-thirds the yield strength, and inelastic resistance to buckling that permits plastic deformation without buckling in some members. Residual stresses are introduced by the manufacturing process, and inelastic behavior is affected by the ductility and post yield performance of the material. The same type of comprehensive research has yet to be done for plastics and reinforced plastic structural members.

The experience gained in developing design practice for metal members should provide a large headstart toward the development of a proven design practice for the various plastics and composite materials that are useful for structural applications. However, as has already been discussed in Chapters 2 and 3, plastics are much more sensitive to variations in temperature and duration of load than metals and, unlike common metals, some plastics and reinforced plastics have elastic properties that are anisotropic (i.e., vary with direction of stress relative to materials property axes). Futhermore, each plastics material and manufacturing method will have its own characteristics relative to residual stresses, manufacturing tolerances and inelastic behavior near ultimate strength. Thus, design practice for metal members may require significant modifications beyond those required due to differences in fundamental materials properties in order to provide an accurate basis for design of plastics. Further research is needed to investigate the effects of the above factors on the behavior of plastic structural members. Until this is completed, design approaches and tentative recommendations of specific design procedures presented in this Chapter, as well as elsewhere in this book, based on theoretical concepts that have been proven for metal members, will provide useful interim design methods. They should also assist the designer to understand the fundamental structural behavior involved in member design, and they may help the plastics industry to define the type of applied research that is needed for rational prediction of structural behavior and design of members.

The design practice that has evolved for cold-formed steel structural members (7.1) provides the most comprehensive model for design recommendations for structural plastics because of its extensive coverage of local and overall buckling of thin-walled sections. Also, the cold-formed steel design specification has an excellent commentary that describes the basis of the design recommendations in terms of fundamental material properties such as E and σ_y, where possible. Another excellent description of the basis for many of the design provisions for compression in the structural, cold-formed steel and aluminum specifications is found in (7.2). These are the primary sources for design recommendations for local plate buckling, column buckling and lateral buckling of beams given in this Chapter. However, modifications to account for orthotropic properties of plate elements are included in the buckling relations presented later in this Chapter. The designer should recognize that tests on specific structural plastics are especially needed to develop the "effective section" concept of post buckling resistance of thin, stiffened plate elements and to define the effect of local element and overall member buckling when elastic buckling stresses exceed about one-half to two-thirds of the ultimate strength. This is explained in the relevant sections of this Chapter.

7.2 TENSION MEMBERS

Members subject to direct tensile axial stress without significant bending are used as ties, struts, braces, hangers, and chords and diagonals in trusses. These members must be designed to have adequate strength, and also some level of control of deformations. The member requires a minimum net cross sectional area, A_n, that is determined as follows:

$$\text{req'd } A_n = \frac{N_{xu} K_t}{\sigma_{xu}} \qquad \text{Eq. 7.1}$$

The stress concentration factor, K_t, is determined for the worst type of discontinuity envisioned for the member. (See Section 5.5.) Stress may be amplified adjacent to holes for connections, variations in the dimensions of the cross section, notches, threads, or other discontinuities. If the expected discontinuity produces an eccentricity between the net section at the discontinuity and the line of action of the applied load, this may be taken into account in the K_t value, or the combined bending and axial stress on the net section may be determined using Eq. 5.23, and this stress amplified by a suitable lower K_t value.

The material strength, σ_{xu}, should be reduced, if the applied load is a long term load, or a cyclic load, or if elevated temperatures, and exposure to aggressive environments are expected. The reduced strength should then be multiplied by a suitable capacity reduction factor (< 1.0) that allows for variations in the strength of production materials to obtain σ_{xu}. If the material has low toughness (i.e., is brittle), and/or if significant flaws may be introduced during material production, or component fabrication, the material strength should be based on fracture toughness requirements. Quantitative procedures for this are not well developed. See Section 5.8 for a summary of fracture toughness concepts.

The design load should be multiplied by an appropriate load factor (> 1.0), as discussed in Chapters 3 and 4, to obtain the required ultimate load, N_{xu}. In selecting a load factor, the designer should consider whether accidental eccentricity in load application may increase stresses above the nominal axial stress. Alternatively, the designer may include an accidental eccentricity in the design criteria and design the member for combined bending and direct stress, as explained in Section 7.5

The total elongation of tension members is determined from Eq. 5.28. See (5.1) for elementary methods for determining the deflection of assemblies of axially loaded members such as trusses and bracing. In determining axial deformation, the time-dependent viscoelastic modulus is used to account for the expected duration of load, service temperature and other environmental conditions. This is discussed in detail in Chapters 2 and 3.

The design of a thermoplastic hanger strap for a hung storage tank, including the stress concentration effect caused by connection holes, is illustrated in Example 7-1.

Example 7-1: Design a Polycarbonate thermoplastic strap hanger to support each end of a water storage tank that hangs from the roof structure of a railroad car as shown. Lateral loads are taken by a second system of straps. Assume that bolts are 5/8 in. diameter. Weight supported by each U strap is 1,000 lbs. Assume that the material has a minimum tensile strength of 8,000 psi, and a minimum compressive strength of 12,000 psi for bolt bearing. Use a capacity reduction factor of 0.3 in tension and 0.5 in compression for establishing the maximum long term strength, as well as the strength under repetitive loading. Use a load factor of 2.0 to obtain the design ultimate load.*

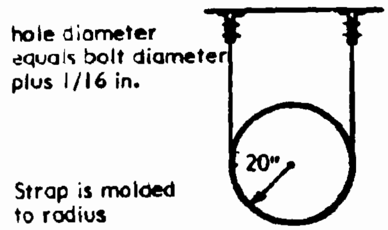

1. Thickness required for bolt bearing with 6 - 5/8 in diameter bolts:

   Reduced ultimate compression strength 0.5 x 12,000 = 6,000 psi;

   Ultimate design load, $2P_u$ = 1,000 x 2.0 x 1.50* = 3,000 lbs.

   (*Note: load is increased 50 percent for impact.)

   $\sigma_{uc} t\ a = 2P_u$, where σ_{uc} = bolt bearing strength = 6000 psi

   min. $t = \dfrac{3000}{6{,}000 \times 5/8 \times 6} = 0.14$ in.; Try a 1/4 in. (0.25) thick strap.

2. Trial width required at section with hole: hole diameter a = .625 + .063 = .69 in.;

   Estimate stress concentration factor, $K_t = 2.8$

   Reduced ultimate tension strength, $\sigma_{ut} = 0.3 \times 8{,}000 = 2{,}400$ psi

   $\sigma_{ut} = \dfrac{P_u K_t}{(b - a)t_{ut}}$; $(b - 0.69) = \dfrac{3{,}000 \times 2.8}{2 \times 0.25 \times 2{,}400} = 7.0$; trial b = 7.69 in.

3. Calculate stress concentration factor, K_t, for net section stress. Try b = 7.5:

   Eq. 5.49: $K_t = 2 + (1 - \frac{.69}{7.5})^3 = 2.75$

4. Determine minimum width, b, for section at hole:

   min $b = \dfrac{3{,}000 \times 2.75}{2 \times 0.25 \times 2{,}400} + 0.69 = 7.56$ in.; Could use 1/4 in. x 8 in. strap. $A = 2.\ in^2$.

5. Alternate design with 1/2 in. thick material:

   Trial b = 4 in. & $K_t = 2 + (1 - \frac{0.69}{4})^3 = 2.57$; min. $b = \dfrac{3{,}000 \times 2.57}{2 \times 0.50 \times 2{,}400} + 0.69 = 3.90$

   Use 1/2 in. x 4 in. strap. Bolt bearing will be lower with this alternate design

6. Bearing pressure under strap on tank wall: T = 1000/2 = 500 lbs

   From Eq. 9.1: $\dfrac{T}{\text{width}} = pr$, $p = \dfrac{500}{20 \times 4} = 6.25$ psi

Note: 1 psi = 6.895 KPa; 1 in. = 25.4 mm; 1 lbf = 4.45N

* Design loads, design criteria (such as safety factors, load factors, and capacity reduction factors, etc.), and materials properties used in design examples are for illustrative purposes only. The user of this Manual is cautioned to develop his own loads, criteria and materials properties based on the requirements and conditions of his specific design project.

7.3 CENTRALLY LOADED COLUMNS

Columns and other compression members are centrally loaded when the line of action of an applied load coincides with the centroidal axis of the member. Eccentricity between the applied load and the centroidal axis results in bending stress in addition to axial stress. Behavior under combined bending and axial load is treated later in Section 7.5

As in the case of tension members, design of columns involves proportioning for both adequate strength and control of axial deformation. The presence of stress concentrations may also require consideration when determining the strength of compression members, and the stress concentration factors described in Section 5.5 may also be applied to compression members. There are more situations in practical design, however, where compression members can be arranged without holes or changes in cross section, as compared to tension and bending members.

Buckling or instability is frequently a critical consideration in the design of compression members. Buckling occurs when either local or overall member stiffness is inadequate to prevent large deflections when a slight lateral force is applied or when slight deviations in member straightness exist. This behavior is illustrated in Section 5.7, where the buckling resistance of an idealized compression member is derived. As is shown below, buckling considerations greatly influence the level of compression stress that can be allowed in the design of a column.

Strength

The compressive strength of the material is the highest compressive stress that can be used in the design of a short centrally loaded column. Similar to a tension member, the minimum section area of a centrally loaded column, as governed by material strength, is given by Eq. 7.1. The guidelines for establishing tensile capacity given earlier also apply to compressive capacity. However, except for very short columns, or columns having significant stress concentrations, the full compressive strength of the column material can seldom be mobilized, because compression stress must be maintained below the materials' compressive strength, σ_{xu}, to provide safety against buckling. Furthermore, small flaws and brittle fracture usually are not design considerations for compression elements.

As for tension members, axial shortening of a centrally loaded column is determined from Eq. 5.28. The same considerations given for tension members also influence the selection of elastic modulus, E, for control of deformation in compression members.

Buckling

Members that are subject to compressive thrust must have adequate stiffness to safely resist failure by buckling. The following types of buckling must be considered:

1. Local buckling of thin parts of a section comprised of an assembly of thin plates (i.e. flanges, and webs of tubes and I sections)
2. Lateral bending (flexural buckling) of overall member
3. Twisting (torsional buckling) of overall member
4. Combined flexural-torsional buckling of overall member.

Local buckling of thin plate elements may limit the maximum stress that can be developed in a short column that has adequate resistance to overall buckling. Since plastic columns frequently are comprised of thin plate elements, consideration of local buckling of plate elements is important. Equations for buckling of thin longitudinally compressed plates are given in Section 6.9 for isotropic materials, and in Section 6.10 for orthotropic materials.

For stresses in the elastic range, the local buckling stress in the plate elements that comprise typical thin-walled sections (Fig. 5-2) are given by Eq. 6.71a in Section 6.9 for isotropic materials. The longitudinally compressed plate elements are considered to be "long plates" and buckling coefficients are presented in Table 6-3. Various idealized conditions of edge restraint are assumed along longitudinal edges. Most commonly, a conservative assumption that edges are simply supported is made. Sometimes the buckling coefficient is increased slightly to reflect some edge restraint provided by adjoining members, or a special analysis can be made that accounts for the restraint provided by adjacent plates in the member cross section. Buckling relations for orthotropic plates are given in Section. 6.10.

It is useful to classify local plate elements as "stiffened" or "unstiffened". A plate that can support additional axial load after initial elastic buckling (See Section 6.9) is termed "stiffened", while a plate whose maximum strength can not exceed its initial elastic buckling strength is termed "unstiffened". Unstiffened plates are usually plates with only one longitudinal edge supported, such as outstanding flanges, while stiffened plates have both longitudinal edges supported.

A value of k = 0.5 in Eq. 6.71a is suggested in (7.1) for unstiffened outstanding flanges of channels, I sections and similar sections, when such flanges are subject to uniform compression. For plates that are supported on each longitudinal edge (stiffened plates), k = 4.0 is used when edges are assumed to be simply supported and plates are subject to uniform in-plane compression stress across their width. Values of k for other conditions of restraint and for plates where in-plane stress varies linearly across the width are given in Table 6-3 and in Figs. 6-32 and 6-33. See Section 6.10 for orthotropic plates.

When stiffened plates are supported by an element of limited width such as the "lip" of a stiffened channel (Fig. 7-1), the supporting element must have sufficient in-plane stiffness to support the stiffened plate. For isotropic materials, the following relations for minimum moment of inertia, I_s, about the centroid of support elements, (derived from requirements for cold-formed metal members), may provide a suitable guide for design with plastics (7.1)(7.3):

Edge stiffener (Fig. 7-1):

$$I_s \geq 2.0\, t^4 \quad (\frac{b}{t})^2 - \frac{0.19E}{\sigma_{xu}} \quad \geq \quad 10t^4 \qquad \text{Eq. 7.2}$$

Intermediate stiffener-centrally located (Fig. 7-1):

$$I_s \geq 4.0\, t^4 \quad (\frac{b}{t})^2 - \frac{0.19E}{\sigma_{xu}} \quad \geq \quad 20t^4 \qquad \text{Eq. 7.3}$$

Intermediate stiffener - not centrally located (Fig. 7-1):

$$I_s = 4.0\,t^4 \left[\sqrt{\left(\frac{b_1}{t}\right)^2 - \frac{0.19E}{\sigma_{xu}}} + \sqrt{\left(\frac{b_2}{t}\right)^2 - \frac{0.19E}{\sigma_{xu}}} \right] \qquad \text{Eq. 7.4}$$

The applicability of these relations to plastics should be checked by tests with specific materials.

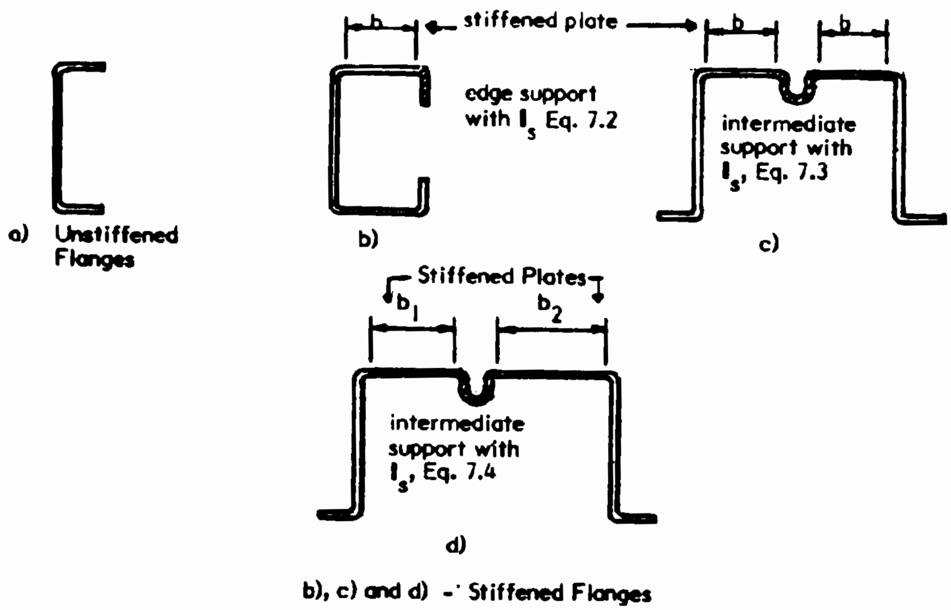

Fig. 7-1 ARRANGEMENT OF SUPPORT ELEMENTS FOR STIFFENED PLATES

In design practice for unstiffened cold-formed steel members (7.1), when σ_{xc} obtained from elastic buckling theory (Eq. 6.71a), exceeds $0.65\,\sigma_{xu}$ (σ_{xu} = yield strength in the case of steel members), the critical buckling stress in the metal members, σ_{xc}, is reduced, as shown in Fig. 7-2. If σ_{xc} obtained using the elastic relations for local buckling, Eq. 6.71a, is designated, σ_{xce}, then the reduced σ_{xc} in the transition region is:

$$\sigma_{xce} > 0.65\,\sigma_{xu}: \quad \sigma_{xc} = 1.3\,\sigma_{xu}\left(1 - 0.4\sqrt{\frac{\sigma_{xu}}{\sigma_{xce}}}\right) \leq \sigma_{xu} \qquad \text{Eq. 7.5}$$

This reduction is used because for stresses above about 0.65 σ_{xu}, effects of residual stresses and tolerances in flatness reduce the actual buckling load that unstiffened plates can carry, as shown by tests of the buckling strength of metal members. For plastics, it is uncertain whether the reduced buckling stress given by Eq. 7.5 should be used instead of the elastic buckling stress (Eq. 6.71a) since the residual stress state, flatness in manufacture and inelastic properties near ultimate are different than in metal members. However, since in Eq. 7.5, σ_{xc} is reduced over the elastic buckling stress when $\sigma_{xce} >$ 0.65 σ_{xu}, Eq. 7.5 is tentatively recommended for design with plastics.

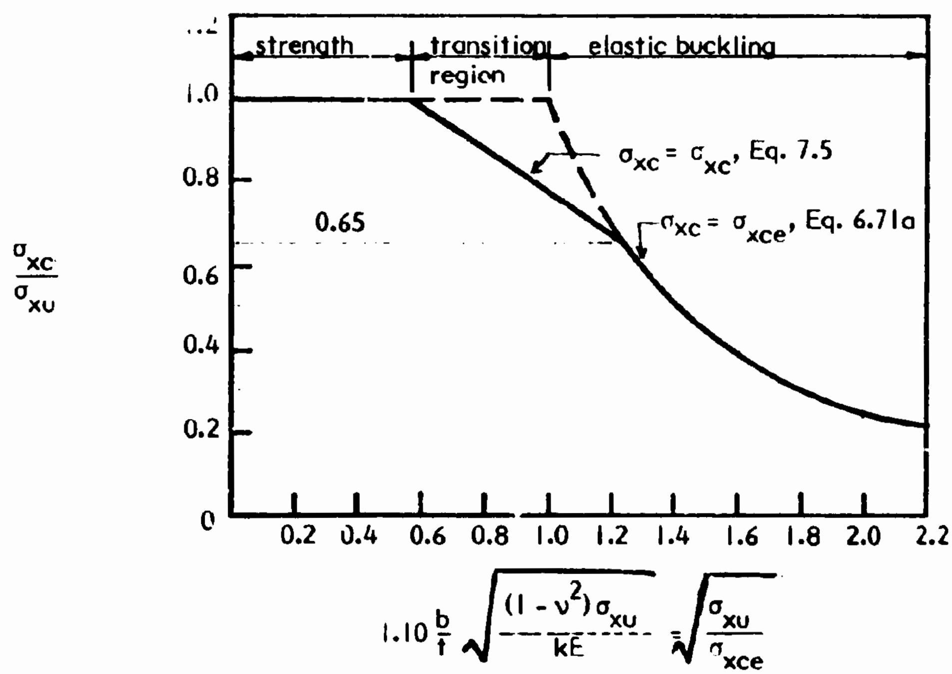

Fig. 7-2 VARIATION OF LOCAL BUCKLING STRESS σ_{xc}/σ_{xu} WITH (b/t)

For convenience in design, a form factor, Q, is used to relate the local bucking stress, σ_{xc}, to the material strength, σ_{xu} (7.2). This form factor is determined as follows:

(1). For unstiffened plate elements, or for stiffened elements where the post buckling strength of the plates is neglected:

$$Q = Q_s = \frac{\sigma_{xc}}{\sigma_{xu}} \leq 1.0 \qquad \text{Eq. 7.6}$$

where, for isotropic materials, σ_{xc} is obtained from Eqs. 7.5 and 6.71a with k coefficients from Table 6-3 for the plate component in a column section that has the lowest local buckling strength, based on idealized conditions of longitudinal edge restraint. If the rotational stiffness at longitudinal edge supports can be established, Eq. 6.71b with C_b correction factor for edge stiffness given in Fig. 6-33 can be used. Eqs. 6.92a, 6.94, 6.97 or 6.98, together with Eq. 7.5, should be used for determining σ_{xc} with orthotropic materials.

(2). For a thin-walled member made up only of stiffened plate elements that are allowed to buckle locally (if they can still support load after buckling), the form factor is:

$$Q = Q_a = \frac{A_e}{A} \leq 1.0 \qquad \text{Eq. 7.7}$$

The effective area, A_e, of the above member for resisting compression as a short column is the sum of the products of the effective widths, b_e, times the thickness of each stiffened plate. The effective width, b_e, after initial elastic buckling may be obtained from Eq. 6.75 by letting $\sigma_{xe} = \sigma_{xu}$. For a stiffened plate of isotropic material supported on two longitudinal edges, the effective width, b_e, may be obtained directly using the following relation, derived from Eq. 6.75 with $\sigma_{xe} = \sigma_{xu}$:

$$b_e = 1.9t\sqrt{\frac{E}{\sigma_{xu}}}\left(1 - \frac{0.145}{(b/t)}\sqrt{\frac{E}{\sigma_{xu}}}\right) \leq b \qquad \text{Eq. 7.8}$$

The more general Eq. 6.75 with $\sigma_{xe} = \sigma_{xu}$ should be used to calculate b_e for orthotropic materials and for other types of local plate elements.

The effective area, then, is:

$$A_e = \Sigma b_e t \qquad \text{Eq. 7.9}$$

Eq. 6.75 (and thus, Eq. 7.8) was developed based on tests of thin metal plates that are ductile. Furthermore, as previously discussed, local buckling is influenced by residual stresses that exist after fabricating operations such as cold-forming, and hot-rolling for steel shapes, or extruding, molding, and casting for plastics. Thus, tests are required to verify that specific plastics materials can sustain post buckling loads without damage or fracture. This verification is needed for both reinforced plastics which are not ductile, and for thermoplastics where stresses beyond the viscoelastic limit are undesirable.

The effective width of plates that do not buckle locally at a stress less than σ_{xu}, (Eq. 7.5) is taken as their full width, b.

(3). For a thin-walled compression member comprised of a combination of stiffened plates that buckle locally at a stress below the buckling strength of the unstiffened plates in the section, stiffened plates that do not buckle locally, and unstiffened plates that buckle at a stress, $\sigma_{xc} < \sigma_{xu}$, the maximum compressive stress in a short column is limited to the lowest local buckling stress in the unstiffened plates, σ_{xc}. The effective area of the column section is denoted A_e' and is determined by summing the thickness times the effective width of each partially buckled stiffened plate, based on $\sigma_{xe} = \sigma_{xc}$ (for the lowest buckling strength of the unstiffened elements), instead of σ_{xu} in Eq. 6.75, plus the full area of all unstiffened elements. Thus, if b_e' is the above described effective width of stiffened plates that buckle initially at a stress below σ_{xc} and b is the width of the other elements which have not buckled at the lowest buckling stress of the unstiffened elements:

$$A_e' = \Sigma b_e' t + \Sigma bt \qquad \text{Eq. 7.10}$$

The partial form factor that accounts for local buckling of some of the stiffened plates at a stress below σ_{xc} then becomes:

$$Q_a' = \frac{A_e'}{A} \leq 1.0 \qquad \text{Eq. 7.11}$$

Also, the partial form factor that accounts for a maximum stress level $\sigma_{xe} < \sigma_{xu}$ is Q_s, given by Eq. 7-6 with σ_{xe} = lowest σ_{xc} for unstiffened plates. Thus, the form factor for the column sections having both stiffened plates that buckle locally, stiffened plates that do not buckle locally, and unstiffened plates is:

$$Q \quad = \quad Q_a' Q_s \;=\; \frac{A_e'}{A}\;\frac{\sigma_{xc}}{\sigma_{xu}} \;\leq\; 1.0 \qquad \text{Eq 7.12}$$

where σ_{xc} is the lowest critical buckling stress of the unstiffened elements and A'_e is the effective area to develop σ_{xc}, rather than σ_{xu}.

Specific tests should be made to confirm both the ability of a thin stiffened plate to support load after initial elastic buckling and the method for determining the effective width, b_e. If test data is not available, the form factor, Q, should be determined using Eq. 7.6 with the lowest σ_{xc} for all the plates in the cross section, both stiffened and unstiffened. This will usually result in a conservative estimate of the form factor.

For very short compression members, the form factor is applied to the maximum stress in Eq. 7.1:

$$\text{req'd } A \quad = \quad \frac{N_{xu}}{Q\sigma_{xu}} \qquad \text{Eq. 7.13}$$

For longer compression members, Eq. 7.13 gives the minimum cross section area required for adequate local buckling resistance. In this case, however, larger values of req'd A may be necessary, as explained later.

Structural steel specifications given in (5.5) establish design rules for b/t ratios that will result in Q = 1.0. When Q = 1.0, the full design strength of the material can be developed, whenever other buckling or deflection criteria do not restrict the maximum design stress. This can result in desirable simplifications in design specifications, but buckling provisions may in some cases be overly conservative.

Some examples of b/t and d/t limits to develop a maximum material strength, σ_{xu}, are given in Table 7-1. These are derived by letting σ_{xc}, from Eq. 6.71a, =

Table 7-1

Maximum Width-to-Thickness Ratios to Prevent Local Buckling Below the Material Design Strength

Type of Stress	Type of Plate Element and Longitudinal Edge Support, Isotropic Materials	Maximum Width-to-Thickness Ratio to Prevent Local Buckling at σ_{xu} or τ_{xu}	
Uniform compression	Flange 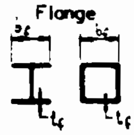	$\frac{b_f}{t_f} = C_b \sqrt{\frac{E}{\sigma_{xu}(1-\nu^2)}}$	Eq. 7.14a
Uniform compression and pure in-plane bending	Web 	$\frac{d_w}{t_w} = C_b \sqrt{\frac{E}{\sigma_{xu}(1-\nu^2)}}$	Eq. 7.14b
In-plane shear	Web	$\frac{d_w}{t_w} = C_b \sqrt{\frac{E}{\tau_{xu}(1-\nu^2)}}$	Eq. 7.14c

			C_b
1.	Uniform Compression	Flange with one edge free, the other simply supported. Used for I and □ shapes	0.6
2.	Uniform Compression	Flange with one edge free the other clamped	1.0
3.	Uniform Compression	Column flange, or web with both edges simply supported. Used for □ and [shapes	1.8
		Beam Flange, some edge conditions	$0.9\sqrt{5.2 + 0.16\frac{b_f}{d_w}} \leq 2.37$
4.	Uniform Compression	Column flange, or web, with both edges clamped	2.4
5.	Pure in-plane bending	Web, with both edges simply supported. Used for Web of [shapes*	4.4
6.	Pure in-plane bending	Web, with both edges clamped*	5.7
7.	Pure in-plane shear	Web, without stiffeners (i.e. long web), with both edges simply supported. Used for web of [shape*	2.1
8.	Pure in-plane shear	Web, without stiffeners, with both edges clamped*	2.7

*Notes: Average of 5. and 6. and of 7. and 8., used for webs of I and □, when flange is thicker than web. If flange is flexible, use 5. and 7.

σ_{xu}. The d/t ratios that are given for in-plane bending and shear of beam webs are explained in Section 7.4. The limiting b/t and d/t ratios given in the Table are for isotropic plate elements with the idealized conditions of edge restraint noted. Similar ratios for orthotropic plate elements may be obtained by letting $\sigma_{xc} = \sigma_{xu}$ in the buckling equations in Section 6.10. When these ratios are used as maximum limits in design specifications, local buckling will not govern the strength of a section.

Overall flexural buckling. A slender column may experience large lateral deflections, and become unstable under a central load, termed the critical load, that is less than the capacity governed by material strength (Eq. 7.13). When the critical load is applied to the columns, any slight deviation in straightness, or any small lateral force, will produce an unlimited amplified bending moment, $N_{xc}\ \Delta$ (Fig. 7-3), a condition of flexural instability. This type of behavior is described conceptually in Section 5.7 for a very simplified and idealized type of compression member in which flexibility is modeled by a concentrated single spring at mid-height. In the Euler bucking theory, the same conceptual approach is applied to more practical centrally loaded columns where the stiffness, EI, is constant over the column length (Fig. 7-3). In this case, the critical buckling load is:

$$N_{xc} = \frac{\pi^2 EI}{(KL)^2} \qquad \text{Eq. 7.15}$$

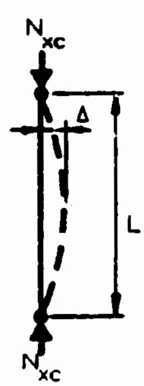

Pin End: K = 1.0

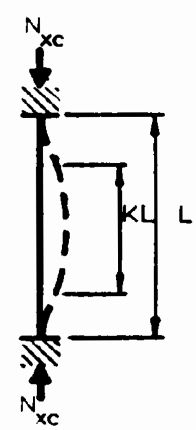

Restrained End: K = 4.0 for full fixity

Fig. 7-3 FLEXURAL BUCKLING OF SLENDER COLUMN

K is an effective length coefficient that is determined by the conditions of end restraint. For the basic case of pin ends, K = 1.0. For other end restraints, K may vary from 0.5 to infinity. The effective length coefficient, K, may be determined from the buckling coefficient, k, given in Table 6-4, as follows:

$$K = \frac{1}{k} \qquad \text{Eq. 7.16}$$

It is useful for design purposes to combine Eqs. 5.20, 5.6 and 7.15, obtaining:

$$\sigma_{xc} = \frac{\pi^2 E}{(\frac{KL}{r})^2} \qquad \text{Eq. 7.17}$$

KL is the effective unbraced length in the direction of buckling, while r is the radius of gyration (Eqs. 5.6 or 5.7) for bending in that direction. The lowest value of σ_{xc} will be obtained for buckling in the direction with the highest ratio, KL/r.

E is the elastic modulus for bending in the direction of lowest σ_{xc} for materials with a linear stress-strain behavior. If E is not constant, the tangent modulus, E_T, for the stress level, σ_{xc}, should be used in Eqs. 7.15 or 7.17 (7.2). For plastics, the elastic modulus used in buckling calculations should reflect the maximum duration of load and the range of temperature and exposure conditions expected for a particular component design. Usually, the lowest viscoelastic modulus for the range of expected design conditions can be used so long as σ_{xc} remains below the viscoelastic limit (Chapters 2 and 3).

A non-dimensional plot for Eq. 7.17, divided by σ_{xu} is given in Fig. 7-4 (Curve 2). However, curves 3, 4 and 5 are more representative of the actual test behavior of steel and aluminum columns, where buckling capacity is lowered by modulus reduction at higher stresses, residual stresses and accidental eccentricities caused by deviations in column straightness (7.2). Similar curves should also apply to plastic columns, although their shapes might vary somewhat, depending upon specific stress-strain relations, residual stresses from fabrication, and eccentricities of the part.

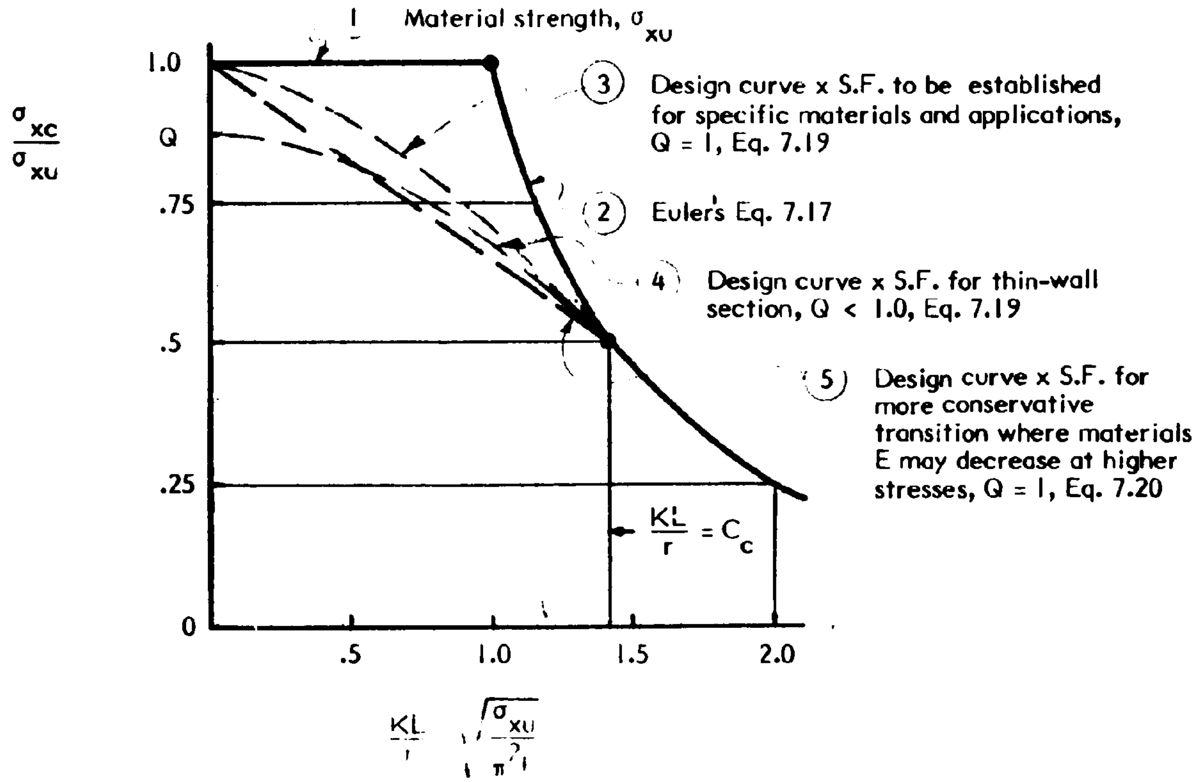

Fig. 7-4 MAXIMUM STRESS FOR CENTRALLY LOADED COLUMNS GOVERNED BY FLEXURAL BUCKLING

In the absence of test data for columns of specific plastic materials, shape, fabrication process, and arrangement, the approach used for steel columns may be used as a trial approximation for plastics materials that essentially exhibit a linear stress-strain relation up to σ_{xu}. In this approach, the maximum stress is reduced below σ_{xc} given by Eq. 7.17 whenever:

$$\frac{KL}{r} < C_c = \sqrt{\frac{2\pi^2 E}{\sigma_{xu}}} \qquad \text{Eq. 7.18}$$

Eq. 7.17 gives $\sigma_{xc} = 0.5\sigma_{xu}$ when $KL/r = C_c$. For lower values of KL/r, σ_{xc} is determined from the following semi-empirical equation, giving a parabolic transition of stress from the Euler stress at $\sigma_{xc} = 0.5\sigma_{xu}$ to σ_{xu} at $KL/r = 0$:

For $\frac{KL}{r} < C_c$ (given by Eq. 7.18):

$$\sigma_{xc} = \sigma_{xu} - \frac{(\sigma_{xu})^2}{4\pi^2 E}\left(\frac{KL}{r}\right)^2 \qquad \text{Eq. 7.19}$$

This equation, divided by σ_{xu} is plotted in non-dimensional form as Curve 3 in Fig. 7-4.

For column sections where the form factor, $Q < 1.0$, $Q\sigma_{xu}$ should be substituted for σ_{xu} in Eqs. 7.18 and 7.19 (7.1). Curve 4 in Fig. 7-4 shows this case.

An alternate approach that is more conservative, and perhaps appropriate for materials with an elastic modulus that decreases significantly at stresses approaching σ_{xu}, is to use a straight line increase in σ_{xc} from $0.5\sigma_{xu}$ to σ_{xu}. This results in the following equation:

For $\frac{KL}{r} < C_c$ (given by Eq. 7.18):

$$\sigma_{xc} = \sigma_{xu} - \frac{(\sigma_{xu})^{3/2}}{2\pi \quad 2E}\left(\frac{KL}{r}\right) \qquad \text{Eq. 7.20}$$

This equation, divided by σ_{xu}, is plotted in non-dimensional form as Curve 5 in Fig. 7-4. Again, for column sections with $Q < 1.0$, $Q\sigma_{xu}$ should be substituted for σ_{xu} in Eqs. 7.18 and 7.20.

Torsional buckling may occur at a lower critical load than the flexural buckling load given by Eq.7.15 for certain types of doubly symmetric thin wall cross sections having low torsional stiffness. Torsional buckling does not prove critical with the tubular and I shaped sections that are commonly used as centrally compressed columns. However, it may govern the critical load for a cruciform shaped section and it contributes to the reduced torsional-flexural buckling resistance of open thin-walled sections that are not doubly symmetric, as explained below.

The torsional buckling resistance is (7.4):

$$N_{xc} = \frac{1}{r_o^2}\left(GJ + \frac{\pi^2 E C_w}{(KL)^2}\right) \qquad \text{Eq. 7.21}$$

The torsional constant, J, was defined previously in Section 5.4 and the warping constant, C_w, will be defined later in Section 7.4. The polar radius of gyration, r_o, is given in Table 5-4.

For a cruciform shape, the term in Eq. 7.21 containing C_w, (i.e. the warping resistance), is negligible and the following approximation for the critical torsional buckling stress is valid (7.4):

$$\sigma_{xc} = \frac{E}{2(1+\nu)} \left(\frac{t}{b}\right)^2 \qquad \text{Eq. 7.22}$$

This stress is approximately the same as the critical local buckling stress for a longitudinally compressed plate with one longitudinal edge free and the other simply supported, (7.4). Furthermore, for cruciform columns that are long relative to their width, flexural buckling (Eqs. 7.17, 7.19 or 7.20) may result in a lower buckling strength. Thus, since the torsional buckling stress is the same as the local buckling stress, the same procedure for determining the maximum design stress may be used for these torsionally flexible sections, as was given previously to determine whether local buckling or flexural buckling governs maximum strength.

Torsional-flexural buckling may be critical for thin-wall open sections with unsymmetrical and singly symmetrical configurations, such as angles and some channels with thin wide flanges. In this type of buckling, coupling of the flexural and torsional modes of buckling reduces the critical load below the load calculated for either mode independently. The elastic torsional-flexural buckling strength of centrally loaded compression struts with a singly symmetric section, such as channel, hat or I with unequal flanges, is (7.1):

$$N_{xc} = \frac{1}{2\beta} \left[N_{xcF1} + N_{xcT} - \sqrt{(N_{xcF1} + N_{xcT})^2 - 4\,\beta N_{xcF1} N_{xcT}} \right] \qquad \text{Eq. 7.23}$$

N_{xcF1} is the elastic flexural buckling strength about the axis of symmetry (axis 1-1, Fig. 5-4), obtained using Eq. 7.15, and N_{xcT} is the elastic torsional buckling strength, obtained using Eq. 7.21. β is a cross sectional property as follows:

$$\beta = 1 - (e/r_s)^2 \qquad \text{Eq. 7.24}$$

where e is the distance from the shear center to the centroid along the 1-1 axis (Table 5-5, x_o-x_o axis) and r_s is the polar moment of inertia of the cross section about the shear center:

$$r_s = \sqrt{r_1^2 + r_2^2 + e^2} \qquad \text{Eq. 7.25}$$

A "centrally loaded" (without bending) member of the above type must have the thrust load applied through the shear center. If thrust is applied elsewhere on the section, the member will be subject to combined bending and axial load (Section 7.5).

The critical elastic buckling stress for torsional-flexural buckling of singly symmetric sections is:

$$\sigma_{xce} = \frac{N_{xc}}{A} \; ; (N_{xc} \text{ from Eq. 7.23}) \qquad \text{Eq. 7.26}$$

When $\sigma_{xce} > 0.5\,\sigma_{xu}$ the elastic value of σ_{xce} obtained using Eqs. 7.26 and 7.23 should be reduced to provide a transition between elastic flexural-torsional buckling and short column strength. A transition similar to curve 3 in Fig. 7-4 is obtained with the following equations (7.1):

$$\sigma_{xce} > 0.50\,\sigma_{xu}\text{:} \quad \sigma_{xc} = \sigma_{xu} - \frac{\sigma_{xu}^2}{4\sigma_{xce}} \qquad \text{Eq. 7.27}$$

$$\sigma_{xce} < 0.50\,\sigma_{xu}\text{:} \quad \sigma_{xc} = \sigma_{xce} \qquad \text{Eq. 7.28}$$

Torsional-flexural buckling of singly symmetric sections involves deformation by twisting about the shear center and bending about the axis of symmetry (usually the strong axis). Thus, only members, or portions of members, that are free to deform this way need to be checked for torsional-flexural buckling.

Flexural buckling involves bending about the weak axis of the section (usually axis 2-2), with a member length that is free to deform about that axis. For a centrally loaded column with a singly symmetric section, the permissible column load is the lessor of the buckling load for flexural buckling about the weak axis (usually 2-2), as given by Eqs. 7.15 - 7.20, and the buckling load for torsional-flexural buckling by twisting about the shear center and bending about the axis of symmetry, as given by Eq. 7.23.

With thin-wall sections when the form factor Q < 1.0, the term σ_{xu} in Eq. 7.27 should be multiplied by the form factor, Q, as described previously for flexural buckling.

For single angles, buckling resistance can usually be approximated by the lower of the buckling stresses given by Eq. 7.22 for torsional buckling or Eqs. 7.17, 7.19 or 7.20 for flexural buckling about the weak axis. A typical plot of the critical stress vs. length is given in Fig. 7-5. Flexural buckling is determined with reference to each of the principal axes 1-1 and 2-2. The weak axis is usually 2-2. Again, a transition region should be included as shown in the Figure.

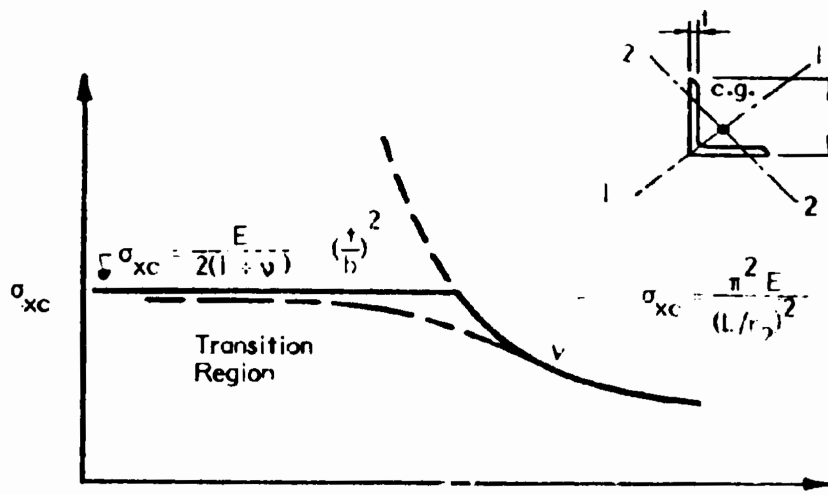

Fig. 7-5 BUCKLING STRESS IN SINGLE ANGLE

See (7.3) or (7.4) for additional torsional-flexural buckling relations for open thin wall sections that do not meet the limitations discussed above. The subject is considered again in Sections 7.4 and 7.5 with reference to the stability of laterally unsupported beams and of columns under combined bending and direct stress, respectively.

Summary of Design Procedure for Centrally Loaded Plastic Columns.

The above described aspects of column behavior are reflected in the following procedure for the design of centrally loaded plastic compression members.

(1) Select a plastic material, a trial column cross section and a manufacturing process. Establish design criteria: loads, duration of loading, service temperature and other environmental conditions, and restraint condition at ends of column.

(2) Determine material constants for use in design. These are:

E — Use E_{xT} at $0.5\sigma_{xu}$, as a trial value, or establish plot of E_x vs. σ_x. For time-dependent considerations, use E_{vxT} at 0.5 times the viscoelastic limit stress (or at another appropriate stress) for the longest time duration required for design, or establish plot of E_{vxT} vs. σ_x. If material is orthotropic, stiffness properties in direction 2-2 will also be required for determining local buckling strength.

σ_{xu} — Use the appropriate strength limit for the specific materials, load duration, and environmental conditons. Frequently, for unreinforced plastics, this will be the viscoelastic limit stress for the design time-temperature-exposure conditions. For reinforced plastics, it may be either the first damage strength, or the rupture strength, again taking into account the time-temperature-exposure design conditions.

See Chapter 3 for further discussion of structural properties for use in design.

(3) Select load and strength reduction factors for use in comparing required strength with provided strength:

- Multiply design load by a load factor (greater than 1.0) that allows for overloads, inaccuracies in analysis, etc., to obtain required ultimate capacity
- Multiply materials properties, E and σ_{xu}, by capacity reduction factors (less than 1.0) that allow for variations in structural properties to obtain the reduced material properties for use in design. Different capacity reduction factors may be used for E and σ_{xu}.

(4) Determine the form factor, Q, for thin wall sections, based on Eq. 7.12, and the appropriate local buckling relations (equations in Chapter 6). Use E for the appropriate local buckling stress level.

(5) For Q = 1.0 with doubly symmetric sections, calculate:

$$C_c = \sqrt{\frac{2\pi^2 E}{\sigma_{xu}}} \qquad \text{Eq. 7.18}$$

For Q < 1.0, use:

$$C'_c = \frac{C_c}{Q} \qquad \text{Eq. 7.18a}$$

(6) If $KL/r \geq C_c$ (C'_c for $Q < 1.0$), determine compressive strength, σ_{xc}, from Eq. 7.17.

If $KL/r \leq C_c$ (C'_c for $Q < 1.0$), determine compressive strength, σ_{xc}, from Eqs. 7.19 or 7.20. If $Q < 1.0$, replace σ_{xu} in the above equations with $Q\sigma_{xu}$.

In general, Eq. 7.20 will give lower estimated strengths than Eq. 7.19 and is more appropriate for materials with a non-linear stress-strain relation (i.e. when E_T reduces for stress above $0.5\sigma_{xu}$). However, an accurate determination of critical strength in the transition zone, where $KL/r < C_c$, requires experimental verification of centrally loaded plastic column behavior with specific plastic materials and column configurations.

(7) Determine:

$$\max N_{xc} = \sigma_{xc} A \geq \text{req'd } N_{xu} \qquad \text{Eq. 7.29}$$

$$\text{If } Q < 1.0, \max N_{xc} = \sigma_{xc} A_e \text{ or } \sigma_{xc} A'_e \qquad \text{Eq. 7.29a}$$

A_e, or A'_e, are determined from Eqs. 7.9, or 7.10, respectively

(8) With singly symmetric sections, use Eqs. 7.26 or 7.27 to determine maximum N_{xc} for lengths of sections that are free to twist and to bend about the symmetry axis 1-1. Also, check to determine if N_{xc} is more critical by Eq. 7.15 for buckling about the weak axis 2-2. For single angle members use Eqs. 7.22 and 7.15. For members with general unsymmetrical sections, see (7.1).

(9) Limit the maximum slenderness ratio, KL/r:

$$\max. \frac{KL}{r} = 200 \qquad \text{Eq. 7.30}$$

Use the highest value of KL/r for the section. This arbitrary limit has been traditionally used in structural steel practice to preclude the design of members that meet theoretical requirements for buckling resistance, but that are excessively slender from a practical standpoint.

(10) Intermediate bracing may be used to increase buckling resistance by reducing the slenderness ratio, KL/r, about either or both principal axes. To be effective, such bracing must provide strength and stiffness that is adequate to prevent excessive distortion of the column at the brace point,

thereby forcing the column to buckle in the shape of a higher mode, with the maximum buckle length equal to the unbraced length. (7.5).

Brace stiffness. The required minimum stiffness for an intermediate brace in a direction perpendicular to the main member depends on the out-of-straightness of the column and the number of intermediate brace points. Minimum brace stiffness is recommended in (7.4) as:

$$\text{min. req'd } K_s = \frac{4\,N_{xc}}{L} \qquad \text{for a column with one intermediate brace} \qquad \text{Eq. 7.31a}$$

$$\text{min. req'd } K_s = \frac{8\,N_{xc}}{L} \qquad \text{for a column with two, or more intermediate braces} \qquad \text{Eq. 7.31b}$$

Where K_s is the spring stiffness of the brace (i.e. the brace force that produces a unit axial displacement in the brace), L is the length of the column between braced points, and N_{xc} is the buckling load, $\sigma_{xc}A$, for the main member with length, L. For a strut brace with length L_b, area Ab and elastic modulus Eb:

$$K_s = \frac{Ab\,Eb}{L_b} \qquad \text{Eq. 7.32}$$

Brace strength. The requirements for minimum strength of intermediate bracing depend on the out-of-straightness of the main member and the stiffness of the brace. Typical rules for minimum bracing strength are discussed in (7.4). Required strength of braces range between one and three percent of the buckling strength of the braced main member. The higher brace strengths are needed when bracing stiffness is near the minimum requirements, while the lower values are appropriate for stiff bracing systems and main members with low deviations from straightness (L/500 or less, where L is the length between brace points). A minimum brace strength of two per cent of the compressive capacity of the main member is often used as a practical design requirement.

The above design procedure is used in **Example 7-2** to determine the design capacity of a centrally loaded tubular reinforced plastic column.

7.4 BEAMS

As discussed in Chapter 5, beams support transverse loads by a combination of bending, shear and sometimes torsion. Beam sections in the form of rectangles, thin wall tubes, I-sections, channels, hat sections, T-sections, Z-sections, and many shapes of open corrugations or closed ribs in flat panels, are commonly found in plastics structural components. Considerable simplification in analysis and design is possible when the beam has at least one longitudinal plane of symmetry and when the load axis is aligned with an axis of symmetry of the cross section. Except for a few special cases to be discussed later, the design procedure that follows is limited to the above types of sections and load axes.

Example 7-2: Determine the maximum long term axial compression thrust load that can be safely applied to the fiberglass reinforced plastic column shown in the sketch. Service temperature is 0° to 100°F. Assume that the column is pin ended, and has the tubular section shown in the sketch. This section is made by a pultrusion process that produces the following ultimate strength and stiffness properties based on standard short term tests: longitudinal compression: 25,000 psi, elastic moduli: E_{11} = 2,000,000 psi; E_{22} = 1,000,000 psi; G = 450,000 psi, Poisson's Ratios: ν_{12} = 0.36; ν_{21} = 0.18*

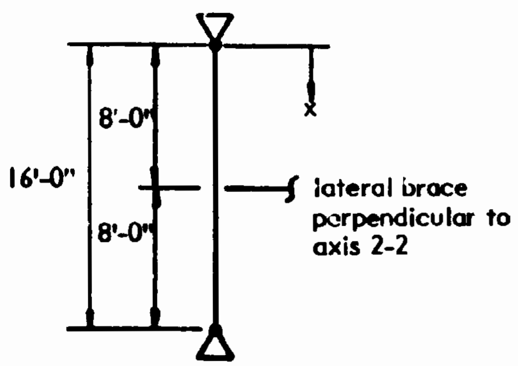

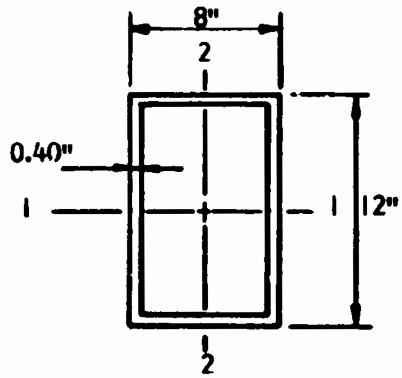

Column Section

1. Section properties from Table 5-3, Case 9:

$$A = 2 \times 0.40\,(7.6 + 11.6) = 15.36\ \text{in.}^2$$

$$I_1 = \frac{0.40 \times 11.6^2}{6}(11.6 + 3 \times 7.6) = 308.6\ \text{in.}^4$$

$$I_2 = \frac{0.40 \times 7.6^2}{6}(7.6 + 3 \times 11.6) = 163.3\ \text{in.}^4$$

2. Reduced material properties to allow for long term load effects and manufacturing variations: Capacity reduction factor 0.5 for ultimate compressive strength, and 0.7 for elastic moduli; Thus:

$$\sigma_{xu} = 0.5 \times 25{,}000 = 12{,}500\ \text{psi};\ E_{11} = 0.7 \times 2{,}000{,}000 = 1{,}400{,}000\ \text{psi}$$

$$E_{22} = 0.7 \times 1{,}000{,}000 = 700{,}000\ \text{psi}$$

3. Load factors for ultimate strength: Multiply the design load by a load factor of 2.5 to account for variation in applied load, accidental bending, and differences between analytical models and real behavior.

4. Local buckling stress: Eq. 6.92 for long plate with "pinned" longitudinal edges gives;

$$\sigma_{xc} = \frac{2\pi^2}{t\,b^2}\left(\sqrt{D_1 D_{22}} + D_o\right);$$ b is the maximum inside width of plate elements = 11.2 in.

Eq. 6.6 a, b: $D_{11} = \dfrac{1{,}400{,}000 \times 0.4^3}{12(1 - 0.36 \times 0.18)} = 7{,}984;\ D_{22} = \frac{1}{2} D_{11} = 3992$

* See note on Example 7-1, page 7-5.

Example 7-2 (continued)

Eq. 6.6c: $D_{12} = \nu_{21} D_1 = 0.18 \times 7984 = 1437$

Eq. 6.6d: $D_{12}' = \frac{315{,}000(0.4)^3}{12} = 1{,}680$

Eq. 6.6e: $D_o = 1437 + 2 \times 1680 = 4797$

$$\sigma_{xc} = \frac{2\pi^2}{0.40 \times 11.2^2} \left(\sqrt{7{,}984 \times 3992} + 4797 \right) = 4108 \text{ psi}$$

If we neglect post buckling strength of the plates in the column:

Eq. 7.6: $Q = \frac{\sigma_{xc}}{\sigma_{xu}} = \frac{4108}{12500} = 0.33 < 0.65$ no need to consider transition for local buckling.

5. Slenderness factor, C_c, for column buckling:

Eq. 7.18: $C_c = \sqrt{\frac{2\pi^2 E_{11}}{Q\sigma_{xu}}} = \sqrt{\frac{2\pi^2 \times 1{,}400{,}000}{0.33 \times 12{,}500}} = 81.8$

6. Column buckling stress, σ_{xc}:

radius of gyration:

$r_1 = \sqrt{\frac{I_1}{A}} = \sqrt{\frac{308.6}{15.36}} = 4.48$ in.; $r_2 = \sqrt{\frac{I_2}{A}} = \sqrt{\frac{163.3}{15.36}} = 3.26$

column has "pin" ends; thus, K = 1.0

$\frac{KL_1}{r_1} = \frac{1.0 \times 16 \times 12}{4.48} = 42.9$ governs; $\frac{KL_2}{r_2} = \frac{1.0 \times 8 \times 12}{3.26} = 29.4$

$KL_1/r_1 < C_c$; thus, use either Eq. 7.19 or 7.20 to determine σ_{xc}. In the absense of buckling test results, the more conservative Eq. 7.20 will be used.

$$\text{Eq. 7.20: } \sigma_{xc} = Q\,\sigma_{xu} - \frac{(Q\sigma_{xu})^{3/2}}{2\pi\sqrt{2E}} \left(\frac{KL}{r}\right)$$

$$= 0.33 \times 12{,}500 - \frac{(0.33 \times 12{,}500)^{3/2} \times 42.9}{2\sqrt{2 \times 1{,}400{,}000}} = 3044 \text{ psi}$$

7. Column design load

Eq. 7.29: $N_{xc} = 3044 \times 15.36 = 46{,}756$ lbs

Max. design axial load, $P = \frac{N_{xc}}{L.F.} = \frac{46{,}756}{2.5} = 18{,}702$ lbs

Example 7-2 (continued)

Alternate design with consideration of post buckling strength of stiffened plate elements:

4a. Local buckling stress:

Eq. 6.75: $\frac{b_e}{b} = \sqrt{\frac{\sigma_{xc}}{\sigma_{xu}}} \left(1 - 0.22 \sqrt{\frac{\sigma_{xc}}{\sigma_{xu}}}\right)$

long sides: $\frac{\sigma_{xc}}{\sigma_{xu}} = \frac{4180}{12,500} = 0.33; \sqrt{0.33} = 0.574$

$\frac{b_e}{b} = 0.574 (1 - 0.22 \times 0.574) = 0.50; b_e = 0.50 \times (12 - 2 \times 0.4) = 5.60$ in.

short sides: $\sigma_{xc} = \frac{2\pi^2}{0.40 \times 7.2^2} (\sqrt{7,984 \times 3,992} + 4797) = 9940 = \sigma_{xce}$

$\frac{\sigma_{xce}}{\sigma_{xu}} = \frac{9940}{12,500} = 0.79 > 0.65\, \sigma_{xu}$

Reduced σ_{xc} for transition, Eq. 7.5:

$\sigma_{xc} = 1.3\, \sigma_{xu} \left(1 - \frac{0.40}{\sqrt{\sigma_{xce}}} \sqrt{\sigma_{xu}}\right) = 1.3\, \sigma_{xu} \left(1 - \frac{.40}{\sqrt{.79}}\right) = 0.715\, \sigma_{xu} = 8937$ psi

$\sqrt{\frac{\sigma_{xc}}{\sigma_{xu}}} = 0.715 = 0.85; \frac{b_e}{b} = 0.85 (1 - 0.22 \times 0.85) = 0.69; b_e = 0.69 (8.0 - 2 \times 0.4) = 4.97$ in.

Effective area and Q: $A_c = 5.60 \times 0.4 \times 2 + 4.97 \times 0.4 \times 2 + 0.4 \times 0.4 \times 4 = 9.10$ in.^{2}

Eq. 7.7: $Q = \frac{A_e}{A} = \frac{9.10}{15.36} = 0.59$

5a. Slenderness factor:

$$C_c = \sqrt{\frac{2\pi^2 \times 1,400,000}{.59 \times 12,500}} = 61.2 > \frac{KL}{r}$$

6a. Column buckling stress:

$$\sigma_{xc} = 0.59 \times 12,500 - \frac{(0.59 \times 12,500)^{3/2} \times 42.9}{2\pi \sqrt{2 \times 1,400,000}} = 4791 \text{ psi}$$

7a. Column design load:

$N_{xc} = 4791 \times 15.36 = 73,590$ lbs

Max. design load, $P = \frac{73,590}{2.5} = 29,436$ lbs

Conclusion: the buckling load with the alternate solution is 57% larger than the buckling load that neglects post buckling strength. Note, however, that the key relation for post buckling strength, Eq. 6.75, has not be checked experimentally with the type of orthotropic fiberglass reinforced plastic material being used in this example design.

Note: 1 psi = 6.895 KPa, 1 in. = 25.4 mm, 1 in.^{2} = 645.2 mm^2, 1 in.^{4} = 416,233 mm^4, 1 ft = 0.305 m, 1° C = ($^\circ$F - 32)/1.8, 1 lbf = 4.45 N

The design of beams made from plastics must consider the following:

- Strength in both bending and shear must be adequate to safely support the design loads.

- When thin wall sections are used, width-thickness ratios of compression elements must be proportioned to avoid premature local buckling of flanges and webs, or reduced stresses governed by local buckling must be used in design.

- Thin webs must be designed to avoid premature local buckling, and must not be overstressed or locally buckled by concentrated loads and reactions.

- When compression flanges are laterally unbraced, either lateral-torsional stiffness must be adequate to preclude premature failure by lateral-torsional buckling, or distance between points of lateral bracing must be limited to avoid this type of buckling.

- Stiffness must be adequate for deflection control.

- When flexural members have very thin compression elements that are allowed to buckle elastically prior to reaching maximum design strength, the change in section properties and the loss in flexural stiffness must be taken into account in practical design.

- The loss in effective cross section properties that occurs due to shear lag when thin beam flanges are very wide relative to span length must be considered.

- The flange curling that results from beam curvature in beams with thin flanges and flanges with a high width to thickness ratio sometimes should be considered.

Practical design approaches that recognize the above behavior are presented below. Limited consideration is given to the design of beams having unsymmetrical sections and to the design of beams subject to torsion. References are given for more complete treatment of these more complex subjects.

Flexural Strength

Beams are designed for flexural strength based on the elastic beam theory (Section 5.4). The validity of this engineering theory has been investigated for application to conventional I-shaped beam sections fabricated with pultruded FRP structural composites (7.25). Test results presented in this reference confirm that the theory provides stresses and deflections that agree closely with calculated values.

Section modulus must be adequate to resist the bending moment, M_{xu} which is usually applied about the strong axis, I-I, of the beam section.

$$\text{req'd min. } S_I = \frac{M_{xuI}}{\sigma_{xu}} \qquad \text{Eq. 7.33}$$

σ_{xu} is the reduced ultimate strength, including the capacity reduction factors described previously for tension members and columns. For solid materials, σ_{xu} should be the bending strength. This may differ from both the tensile and compressive strengths of the material because of the stress gradient in test samples. See Chapters 2 and 3. For thin wall sections, σ_{xu} should be the tensile strength of the tension flange and the compressive strength of the compression flange. For some materials and design applications, the fracture toughness considerations described in Section 5.8 should be taken into account when selecting the limiting value of σ_{xu} for tension elements in beams.

S_I is the required minimum section modulus with respect to either the extremity of the tension flange or the compression flange, whichever gives the more critical requirement. See Table 5-2 in Chapter 5 for methods of calculating S, and see Table 5-3 for expressions for determining S for some common regular shapes. Also values of S for standard shapes like wide flange beams and tubes are often given in handbooks prepared by manufacturers or trade associations (1.9) (5.5).

M_{xuI} is the maximum design moment in a plane perpendicular to section axis I-I, multiplied by the load factor, as explained previously.

When a beam is subjected to bending about both principal axes, the resulting combined stresses on a trial section are determined using Eq. 5.23. The maximum combined stress must be less than σ_{xu}.

The reduced sectional properties of the net section should be used to calculate stresses when holes or other discontinuities exist near points of maximum moment. Furthermore, the calculated stress adjacent to these discontinuities, σ_x, should then be multiplied by a suitable stress concentration factor, K_t, as explained in Section 5.5, and the increased stress, $\sigma_x K_t$, must be less than σ_{xu}.

Local Buckling of Compression Flanges

For thin wall sections, the capacity of the compression flange may be limited by local buckling, rather than by the compressive strength of the flange materials. Two conditions are considered for practical design:

(1) The maximum compressive stress is limited to the local buckling stress of the flange. In this case:

$$\text{req'd } S_l = \frac{M_{xul}}{\sigma_{xc}} \qquad \text{Eq. 7.34}$$

As discussed in the previous Section, the critical local buckling stress, σ_{xc}, may be determined using the local plate buckling equations given in Sections 6.9 and 6.10. Buckling coefficients for isotropic materials are given in Table 6-3 for various stress distributions and longitudinal edge conditions. Case I is used for flanges subject to uniform compression. Buckling equations and coefficients for orthotropic materials are given in Section 6.10. Equations and coefficients given in Sections 6.9 and 6.10 include the important cases of uniformly compressed plates with one edge free, and the other simply supported, corresponding to outstanding flanges of I or [shapes, and both edges simply supported, corresponding to the flanges of □ or ⊓⊔ shapes.

For rectangular tube sections, and hat sections or lipped sections where the compression flange having a width b_f is supported on each side by webs of depth d_w (Fig. 5-2), the web provides edge restraint that increases the buckling coefficient for the compression flanges of such members. For these sections, the critical buckling stress is:

$$\sigma_{xc} = \frac{k\pi^2 E}{12(1-\nu^2)\left(\frac{b_f}{t}\right)^2} \qquad \text{Eq. 7.35}$$

where (7.6):

$$k = 5.2 + 0.16\frac{b_f}{d_w} \le 6.97 \qquad \text{Eq. 7.36}$$

When $\sigma_{xc} > 0.65\,\sigma_{xu}$, the same reduction in σ_{xc} below the elastic value given by Eq. 7.35 that was explained previously for columns (Eq. 7.5 and Fig. 7-2) is appropriate.

(2) For stiffened flanges only, the flange may be allowed to buckle elastically. Since a stiffened flange exhibits post-buckling strength, the actual area of the flange is reduced to an effective area, as explained previously for local buckling of stiffened elements in columns. The maximum compressive strength of the flange is taken as the effective area times the material compressive strength. The "effective" cross section properties are determined based on the "effective" width of the compression flange (Eqs. 6.75 or 7.8) and:

$$\text{req'd } S_{le} = \frac{M_{xul}}{\sigma_{xu}} \qquad \text{Eq. 7.37}$$

The relation between S_{le} and S_l must be determined by a "cut and try" calculation of b_e of the compression flange and S_{le}, using trial section proportions. The effective section is usually symmetrical about only the 2-2 axis, and the effective moment of inertia, I_{le}, and effective section modulus, S_{le}, for the compression flange may be determined as explained in Section 5.3.

The first condition, Eq. 7.34, is used for all beams with unstiffened compression flanges and for designs with stiffened flanges when local buckling is not to be permitted. It is the more conservative of the two conditions and the simpler criterion to use in design, since it requires only a substitution of σ_{xc} for σ_{xu} in the equations given previously for required section modulus.

The second condition, Eq. 7.37, may be needed for design economy where the b/t ratio of the compression flange is large, resulting in a low ratio of σ_{xc}/σ_{xu}. In this case, it may be desirable to use the post buckling strength of a stiffened element. As noted previously for columns, the equations for effective width of local plate elements in the post buckling range given in Section 6.9 were developed for metal members, and they should be verified, or modified as required, for use with plastics. Also, design for the second condition is complicated because the behavior of the beam in the post buckling range is non-linear as the effective compression area changes with stress level. This results in reductions in effective section modulus S_{le}, moment of inertia, I_{le}, area, A_e, and radius of gyration, r_{le}, as stress level increases above the initial buckling stress. However, the section properties can readily be determined for the effective compression flange area that exists under the full materials strength σ_{xu} (Eq. 6.75 with $\sigma_{xe} = \sigma_{xu}$, or Eq. 7.8) and the limiting ultimate strength can be examined on this basis.

Limiting width-thickness ratios required to prevent local buckling at stresses below σ_{xu} (Q = 1.0) can be established by setting $\sigma_{xc} = \sigma_{xu}$ in the equations for local buckling of various types of compressed plates. This approach is used in structural steel specifications. Limiting width-thickness ratios for certain plate elements that frequently occur in beam members are given in Table 7-1 for isotropic materials. As was discussed earlier for columns, these width-thickness ratios can be used to establish proportions of thin walled cross sections that can be stressed to their ultimate strengths without buckling. The use of limiting width-thickness ratios in practical design is illustrated in Example 7-3, given later in this Section under the heading "Design Procedure for Beams". However, proportions based on this approach may not provide economical sections, compared to thinner "stiffened" flanges that have adequate post buckling strength.

Shear Strength

Maximum shear stress resultants often occur at points where normal stresses caused by bending are low. In this case, the interaction of shear and bending effects need not be considered, and shear effects can be examined independently from bending, as discussed below.

Shear strength is adequate when the maximum shear stress, determined using Eqs. 5.31, or 5.32, is less than the shear stength of the material. The material's shear strength is the "interlaminar" shear strength for layered materials in sections with planes of layers parallel to the plane of horizontal shear (axis of bending), or it is the "in-plane" shear strength for thin wall webs with their plane perpendicular to the axis of bending. In some sections, it may be necessary to investigute in-plane shear stresses in one part of a cross section and interlaminar shear stresses in another part. This is illustrated in Example 7-3, given later.

Design of Webs

In sections such as I, □, or ⅃L, the web carries the major portion of the shear stress resultant applied to the section. For many practical beams, the web is subject to almost "pure shear" (i.e. shear without normal stress) at sections of maximum shear, and to pure, in-plane flexural normal stresses at sections of maximum bending. However, in some cases, the web must be designed to resist combined in-plane bending and shear, or even combined in-plane thrust, bending, and shear. Design considerations for webs include in-plane shear strength, in-plane flexural or axial strength, in-plane shear buckling, in-plane flexural or axial buckling, and local strength and buckling resistance at concentrated loads and reactions. Webs may also be stressed in shear due to torsion, but this will be considered separately.

Web thickness must be adequate to resist the maximum shear stress resultant that acts in the plane of the web. For the thin-wall sections described above, the approximate Eq. 5.32 for shear stress in a flexural member may be recast as:

$$\text{req'd min. } t_w = \frac{V_{xul}}{\tau_{xu}\, d_w} \qquad \text{Eq. 7.38}$$

τ_{xu} is the reduced in-plane shear strength of the web, d_w is the depth of the web between insides of flanges, t_w is the total required thickness of all webs that are in the plane of bending, and V_{xul} is the maximum design shear force mutipled by a load factor. If torsion produces additional shear stresses, these must be included when determining web thickness. This is discussed later.

Web buckling in shear. If the ratio, d_w/t_w, is too great at the section of maximum shear (Section 1-1 in Fig. 7-6), the web may fail by buckling at a stress below the shear strength, τ_{xu}. The local buckling strength of the web in pure shear is given by Eq. 6.84 for isotropic webs and Eq. 6.102 for orthotropic webs. Replace b with d_w in these equations. See Table 7-1 for the d_w/t_w ratios that give τ_{xc} equal τ_{xu} for isotropic materials.

Use τ_{xc} in place of τ_{xu} in Eq. 7.38, whenever τ_{xc} is less than τ_{xu}. Alternatively, τ_{xc} may be increased by adding transverse web stiffeners at the proper longitudinal spacing, a, to make τ_{xc} equal τ_{xu} in Eqs. 6.84 or 6.102. Longitudinal stiffeners may also be used to reduce the effective unsupported depth, d_w. The design of stiffeners is presented later.

Web buckling in flexure. If the ratio d_w/t_w is too great at the section of maximum compressive bending stress (Section 2-2 in Fig. 7-6), the web may fail by buckling due to in-plane flexure. For isotropic materials, the local buckling stress at the compression extremity is given by Eq. 6.71a with the coefficient for Case 6 in Table 6-3. For orthotropic materials, use Eq. 6.101, with the coefficient from Fig. 6-44.

If σ_{xc} is less than the maximum web compression that occurs when the adjacent flange is fully stressed, the web thickness should be increased to permit efficient use of the adjacent flange material. Since, for thin flanges and and deep webs in doubly symmetric beams, the maximum web compression stress is nearly equal to the adjacent flange stress, in many cases the maximum d_w/t_w ratio will be the ratio that develops σ_{XU} without buckling of the web. If the flange is considered to provide partially fixed rotational restraint of the web, the maximum d_w/t_w to preclude flexural buckling of a thin isotropic web before the maximum in-plane strength of the material is developed is:

$$\max.\ d_w/t_w = 5.0\sqrt{\frac{E}{\sigma_{XU}(1-\nu^2)}} \qquad \text{Eq. 7.39}$$

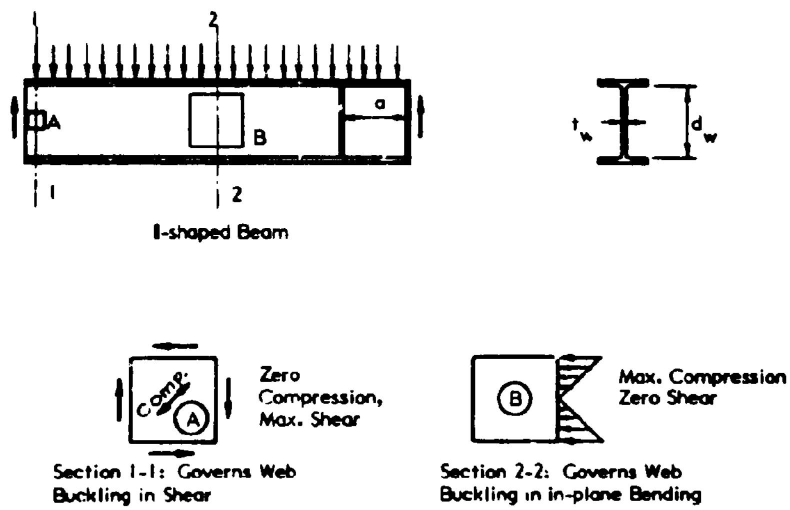

Fig. 7-6 WEB BUCKLING DUE TO SHEAR AND IN-PLANE BENDING

See Table 7-1 for d_w/t_w ratios for the basic conditions of zero and fixed rotational restraint from the flanges.

The above web slenderness is greater than proportions used in most practical webs. However, a larger overall depth of web may be obtained by providing a longitudinal stiffener in the compression region of the web. The buckling stress will then depend on the d/t ratios between the compression flange and the stiffener, and the tension flange and the stiffener. For isotropic materials, it will be given by Eq. 6.71a, with coefficient from the appropriate cases in Table 6-3 (using the appropriate stress variations between stiffener and each of the flanges).

Web buckling in combined shear and flexure. When high shear and in-plane compression due to flexure occur at the same section, the web thickness selected based on the previously discussed criteria should be checked for adequacy under the combined effects of shear and in-plane compression, as described in Section 6.9. The interaction equation, Eq. 6.88, may be used for this check. If this equation gives a ratio summation greater than 1.0, the web thickness must be increased. This will increase the critical shear and in-plane flexure buckling stresses while at the same time decreasing the actual shear stresses. Alternatively, web stiffeners may be added to increase either the shear buckling or the flexural buckling stresses, as required.

Web stiffeners. When τ_{xc} is less than τ_{xu}, or σ_{xc} is less than σ_{xu} in the web, it may be advantageous to increase these critical buckling stresses to allow the use of the full material strength by providing transverse or longitudinal stiffeners. If used at all, transverse web stiffeners are usually only applied in regions of high shear stress to increase the shear buckling strength of the web. However, the maximum d_w/t_w ratio usually cannot exceed the ratio given by Eq. 7.39, the limiting ratio for flexural buckling of the web.

To be effective, stiffeners must be properly spaced, and they must not deform excessively as they support the thin web. This requires that they have sufficient lateral moment of inertia, I_s, about the plane of the web. When the stiffeners and web are isotropic with the same E, the minimum required I_s is (7.4):

$$I_s = 0.34\, d_w^4 \left(\frac{t_w}{b_s}\right)^3 \qquad \text{Eq. 7.40}$$

I_s is the minimum required moment of inertia of the stiffener about the plane of the web, and b_s is the longitudinal spacing of stiffeners.

When the web is braced by both longitudinal (horizontal) stiffeners, located between 0.2 and 0.25 d_w from the compression flange, and transverse (vertical) stiffeners spaced at b_s, the minimum lateral moment of inertia of the longitudinal stiffener should be (7.4):

$$I_s = d_w t_w^3 \left[2.4 \left(\frac{b_s}{d_w}\right)^2 - 0.13 \right] \qquad \text{Eq. 7.41}$$

The required moment of inertia of the transverse stiffener should continue to be given by Eq. 7.40.

Web crippling. When localized bearing loads are applied to thin webs by concentrated loads or reactions, the loads or reactions may produce significant transverse compression stresses in the web. This stress state is shown in Fig. 7-7 The web must be checked for adequate strength and resistance to local buckling, sometimes called crippling. If the web provides the entire transverse resistance to the concentrated forces shown in the Figure, web thickness must be adequate to meet the following transverse strength and buckling requirements (7.4):

Strength:

$$\sigma_{yu} \geq \underset{\text{Interior Bearing}}{\frac{R_u}{t_w (n + 2k)}} \quad \text{or} \geq \underset{\text{End Bearing}}{\frac{R_u}{t_w (n + k)}} \qquad \text{Eq. 7.42}$$

where n and k are shown in Fig. 7-7.

Buckling resistance:

$$\sigma_{yc} = \frac{\pi^2 E}{12 (1 - \nu^2)} \left(\frac{t_w}{d_w}\right)^2 \left(2 + \frac{4 d_w^2}{a^2}\right) \qquad \text{Eq. 7.43}$$

Buckling resistance, as given by Eq. 7.43, shall be greater than the following transverse stress in the web (Fig. 7-7):

$$\sigma_{yc} \geq \sigma_y = \underset{\text{Interior Bearing}}{\frac{R_u}{t_w d_w}} \quad \text{or,} \quad = \underset{\text{End Bearing}}{\frac{R_u}{t_w (0.5 d_w + n)}} \qquad \text{Eq. 7.44}$$

and for uniformly distributed load:

$$\sigma_{yc} \geq \sigma_y = \frac{q}{t_w} \qquad \text{Eq. 7.45}$$

The above equations are used for structural steel sections, and are believed to be conservative, but should be considered as highly tentative for application to thin plastic webs. Extensive tests of cold-formed steel members provide the basis for the empirical web crippling criteria used for cold-formed sections (7.1). Because the latter criteria do not include variables for basic materials parameters, they are not useful for design of plastics members with thin webs. Tests of specific materials and typical bearing configurations are required for accurate evaluation of web crippling and local buckling at bearings with thin-walled plastics sections.

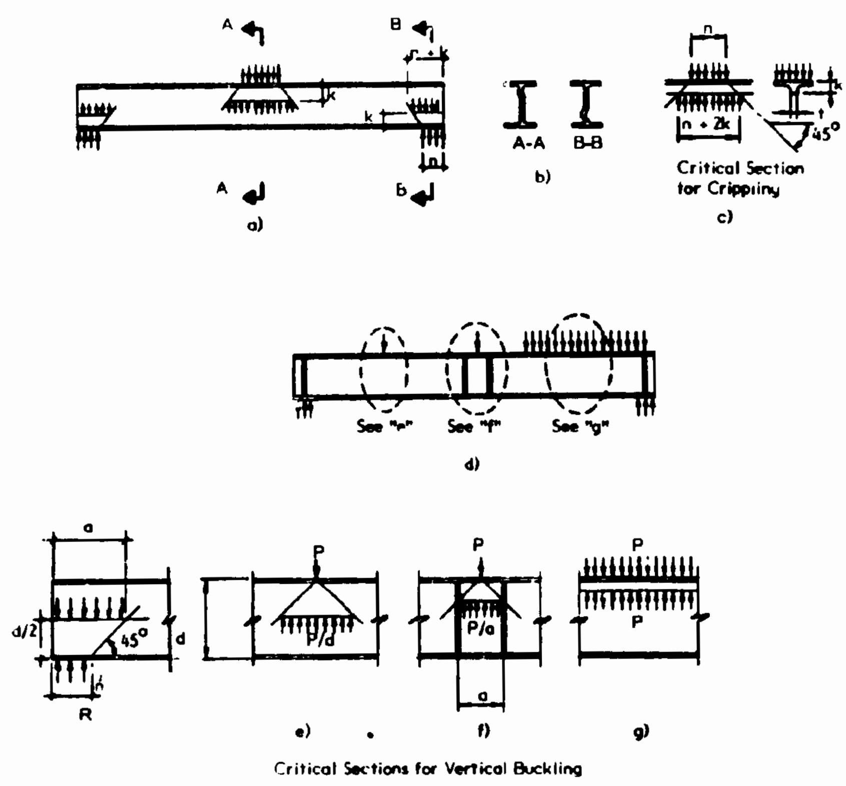

Fig. 7-7 CRITICAL SECTIONS FOR WEB CRIPPLING AND VERTICAL BUCKLING

Lateral buckling

In most practical design cases, beams are supported against lateral deformation by plates or other local components that transfer load to the beam. In such cases, the beam can deform only in one direction, usually the direction of the load. There are situations, however, where beams have no lateral support or bracing over part or all of their span. Sometimes, such laterally unbraced beams can buckle at a lower load than the load that develops the full flexural or shear strength of the beam.

Fig. 7-8 shows a beam in pure bending, simply supported and also held against tipping at both ends. The top flange is in uniform compression, tending to buckle laterally like a column in its unsupported direction. The bottom flange is in tension and tends to remain straight. As a consequence, during buckling the entire cross section rotates as the top flange moves laterally and the bottom flange remains straight. Both the resistance of the top flange to lateral bending and the resistance of the cross section to twisting are mobilized as the beam resists lateral buckling. Thus, a more accurate, but less commonly used, description of this behavior is **lateral-torsional buckling.**

Lateral-torsional buckling seldom limits the load resistance of unbraced beams having closed thin-wall sections or stocky solid sections such as a round or square shapes. However, open thin-wall shapes are torsionally flexible, and when unbraced, they are prone to buckling in the lateral-torsional mode.

The lateral-torsional buckling resistance of an unbraced beam with an open thin walled cross section derives from its lateral bending stiffness, from its torsional stiffness, and from its warping stiffness. Warping involves bending of thin wall elements (such as flanges) as the angle of twist of the beam changes along its length. This is shown in Fig. 7-8. This behavior is discussed again later in this Section under the heading, **Torsion.**

Equations are given below for the critical bending moment that causes lateral-torsional buckling of beams with the following limitations:

- materials are isotropic and elastic

- beam cross sections are doubly symmetric
- loads are applied at the centroid of the cross section, which is also the center of twist of a doubly symmetric section.
- loads are directed along the weak axis, perpendicular to the strong axis. They produce only bending, or bending and flexural shear, about the strong axis.

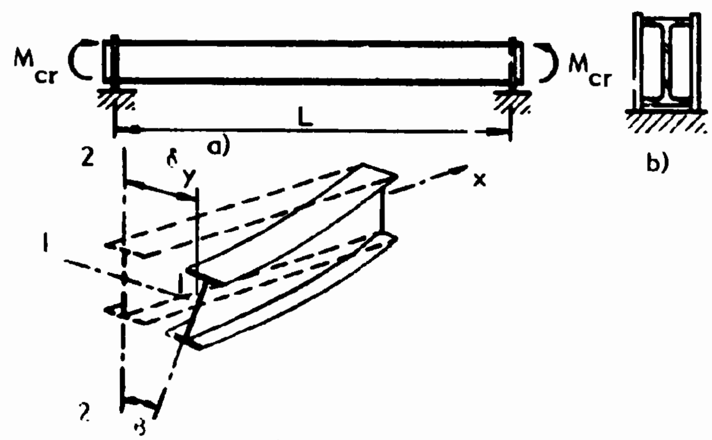

c)

Fig. 7-8 LATERAL-TORSIONAL BUCKLING OF UNBRACED BEAM

The basic equation for critical buckling flexural stress is (7.2):

$$\sigma_{xc} = \frac{C_1}{S_1} \sqrt{M_{xc}^2 + \frac{d^2}{4} P_{e2}^2} \qquad \text{Eq. 7.46}$$

where

$$M_{xc} = \frac{\pi}{KL} \sqrt{E I_2 G J} \qquad \text{Eq. 7.47}$$

For open thin-wall sections, such as I sections, P_{e2} is the Euler column load for buckling in the weak direction, and is:

$$P_{e2} = \frac{\pi^2 E I_2}{(KL)^2} \qquad \text{Eq. 7.48}$$

For rectangular solid or tubular sections, P_{e2} is taken as zero. Thus, for these types of sections, M_{xc} is the critical buckling moment under applied moment that is constant over the unbraced length.

C_1 is a coefficient that depends on load distribution and end conditions, and K is the effective length factor (see Section 7.3) for column buckling in the weak (2-2) plane of bending. Values of C_1 and K for common load cases and end conditions are given in Table 7-2. If a beam has intermediate lateral supports, the lateral buckling coefficient, C_1, is approximated by:

$$C_1 = 1.75 + 1.05\,(M_1/M_2) + 0.3\left(\frac{M_1}{M_2}\right)^2 \leq 2.3 \qquad \text{Eq. 7.49}$$

Table 7-2

Lateral Buckling Coefficients for Beams with Various Load and Support Arrangements

Loading and end restraint* about x-axis	Bending-moment diagram	End restraint* about y-axis	K	C_1
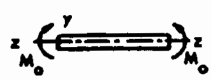		None	1.0	1.0
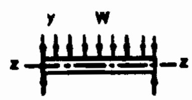		None Full	1.0 0.5	1.13 0.97
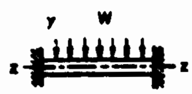		None Full	1.0 0.5	1.30** 0.86**
		None Full	1.0 0.5	1.35 1.07
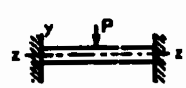		None Full	1.0 0.5	1.70 1.04
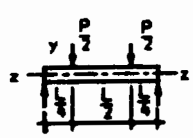		None	1.0	1.04

* All beams are restrained at each end against rotation about the x-axis and displacement in the y and z directions. Loads applied at beam centroidal axis.

** Critical Stress based on center moment (WL/24).

where M_1 and M_2 are the moments at each end of a segment between brace points, and $M_1 < M_2$; M_1/M_2 is positive for reverse curvature bending and negative for single curvature bending. Thus, if M is constant between two brace points, $M_1 = -M_2$ and $C_1 = 1.0$.

Equations for determining the section properties, S_1, I_2, and J are given in Section 5.3. Also, for isotropic materials, the modulus of shearing rigidity, G = $E/2\,(1+\nu)$.

Simplifications of Eq. 7.46 are usually used for practical design. For example, in structural steel practice, sections have significant torsional rigidity because thickness of flanges and webs is not "thin." For these types of symmetrical I beams with $S_1 = 2I_1/d$; $I_2 = 2tb^3/12$, $J = 2bt_f^3/3$, when $(d/4\ P_{e2})^2$ is small compared to M^2_{xc}, $\nu = 0.3$, with isotropic materials, and $K = 1.0$ for simple support of flange bending about the weak axis:

$$\sigma_{xc} = 0.65\, C_1\, E\, \left(\frac{bt_f}{L\,d}\right) \qquad \text{Eq. 7.50}$$

In another simplification, applicable for very deep I sections, and sections with very low torsional rigidity (with "thin" flanges and webs), the entire resistance to lateral buckling is assigned to the lateral buckling resistance of the top flange.

$$\sigma_{xc} = \frac{C_1\, \pi^2 E}{\left(\frac{KL}{r_2}\right)^2} \qquad \text{Eq. 7.51}$$

This is further simplified with a rectangular compression flange of width b to:

$$\sigma_{xc} = \frac{0.8\, C_1\, E}{(KL/b)^2} = \frac{C_1\, \pi^2\, E\, d\, I_2}{(KL)^2\, S_1} \qquad \text{Eq. 7.52}$$

In cases where it is not clear whether Eq. 7.50 or 7.51 (or 7.52) should be applied, the highest buckling stress obtained with either of these equations governs. Other equations for approximate critical buckling stress are given in (7.1) and (7.2).

The lateral-torsional buckling resistance of closed thin wall sections, such as rectangular tubes, is obtained from the critical buckling moment M_{xc} given by Eq. 7.47 (7.2), and the buckling stress is:

$$\sigma_{xc} = \frac{C_l\, M_{xc}}{S_l} \qquad \text{Eq. 7.53}$$

In design practice for cold-formed steel beams (7.1), the lateral buckling stress given by the above Eq. 7.52 is reduced when $\sigma_{xc} > 0.55\,\sigma_{xu}$. The reasons for this are the same as already discussed for buckling of centrally compressed columns and local buckling of thin-walled plate elements. The following reduction equations represent the basis of design requirements given in (7.1): Let $\sigma_{xce} = \sigma_{xc}$ for elastic buckling using Eq. 7.52 (or σ_{xc} in Eqs. 7.46, 7.50, 7.51 or 7.53 could also be used):

$$\text{For } \left(\frac{KL}{b}\right)^2 \geq \frac{1.4\, C_l\, E}{\sigma_{xu}} : \sigma_{xc} = \sigma_{xce} \qquad \text{Eq. 7.54a}$$

$(\sigma_{xc} < 0.55\,\sigma_{xu})$

$$\text{For } \left(\frac{KL}{b}\right)^2 \text{ betw. } \frac{1.4\, C_l\, E}{\sigma_{xu}} \;\&\; \frac{0.3\, C_l\, E}{\sigma_{xu}} : \sigma_{xc} = 1.1\sigma_{xu} - \frac{\sigma_{xu}^2}{3.2\,\sigma_{xce}} \qquad \text{Eq. 7.54b}$$

$$\text{For } \left(\frac{KL}{b}\right)^2 < \frac{0.3\, C_l\, E}{\sigma_{xu}} : \sigma_{xc} = \sigma_{xu} \qquad \text{Eq. 7.54c}$$

Design practice for structural steel (5.5) does not incorporate the above reduction equations. Rolled steel beams derive most of their resistance to lateral buckling from the St. Venant torsion resistance of their flanges, and Eq. 7.50 usually best approximates the resistance of such shapes. Neglect of the other terms in Eq. 7.46 may compensate for the simplifying omission of reduction factors when $\sigma_{xc} > 0.55\,\sigma_{xu}$.

The lateral-torsional buckling resistance of beams having thin rectangular cross sections (Fig. 6-37) is given by Eq. 6.89, with coefficients for the loading cases of Fig. 6-37 given in Table 6-5. These are useful for determining the strength of plates that behave like beams with a compressed unsupported edge due to in-plane flexure. (Such plates are termed diaphragms in Chapter 6.)

When loads are applied at the top flange, instead of at the centroid of a beam section, buckling resistance is slightly reduced. Conversely, when loads are applied at the bottom flange, buckling resistance is larger than given by the preceeding equations. These refinements are presented in (7.2). Generally, they are not taken into account in practical design; thus, the more complex lateral buckling equations with these refinements are not included here.

Lateral buckling solutions for beams with singly symmetric or with unsymmetrical cross sections are given in (7.1) (7.2) and (7.4); since the use of such sections is not common, these more complex solutions also are not given here. When an unbraced beam is designed with a singly symmetric cross section, a compression flange with increased lateral stiffness is frequently used. An example is an I section with the outer edges of the compression flange turned down (or a channel added to the compression flange). Eq. 7.51 usually provides a suitable approximation of the buckling stress in this type of beam. However, the radius of gyration, r_2, should be for the compression flange only.

When lateral buckling resistance is inadequate, the designer may select a beam section with improved lateral and/or torsional stiffness, or he may reduce the unbraced length by using bracing at intermediate points along the span of the beam. The bracing must be effective in preventing lateral deflection of the compression flange, and torsional rotation of the beam cross section, and it must limit the unbraced length of the beam to obtain adequate levels of critical buckling stress, as given by the preceeding equations. Effective bracing arrangements are generally one of the following two types, shown schematically in Fig. 7-9:

- The Type I system supports the compression flange by a lateral system that prevents significant lateral deflection. The minimum required strength and stiffness of this type of bracing system is that required to stabilize the compression force in the beam when its compression side is considered as a column.

  The methods given in Section 7.3 for minimum requirements of column bracing may then be applied to obtain conservative estimates of the required strength and stiffness of the bracing system. Each lateral support should be designed for two percent of the total compression force at that brace point in the laterally braced beam (7.2). When compression flange bracing is provided by a continuous diaphragm that is elastic, approximate methods for determining the usually very low minimum required strength and stiffness are discussed in (7.4).

- The Type 2 system prevents twisting of the entire cross section at the brace points. Rigid diaphragms are provided between two parallel beams. This bracing system is effective without any system for increasing the lateral strength and stiffness of the top chord (7.7). Each diaphragm should be designed to resist a minimum shear force of two percent of the total compressi flange force at the brace point and the same shear applied in the opposite direction at the tension flange. See Fig. 7-9. These forces must be balanced by small upward and downward loads on the adjacent beams as shown in the Figure.

Another arrangement of some interest in design is the case where lateral support is provided at the tension flange, instead of at the compression flange. This is not an efficient location for lateral support, but sometimes the improvement in lateral buckling resistance afforded by available lateral restraint on the tension side requires consideration in practical design. Some examples of flexural members with this type of cross section are shown in Fig. 7-10.

In general, when the tension flange is braced and compression flange unbraced the compression flange behaves like a compressed strut laterally supported by a continuous elastic foundation. The foundation stiffness is the stiffness provided by the web and tension flange against lateral translation and torsional rotation. This behavior is complex and simple relations are not available to predict the buckling strength of the flange. See (7.1) or (7.3) for an approximate procedure.

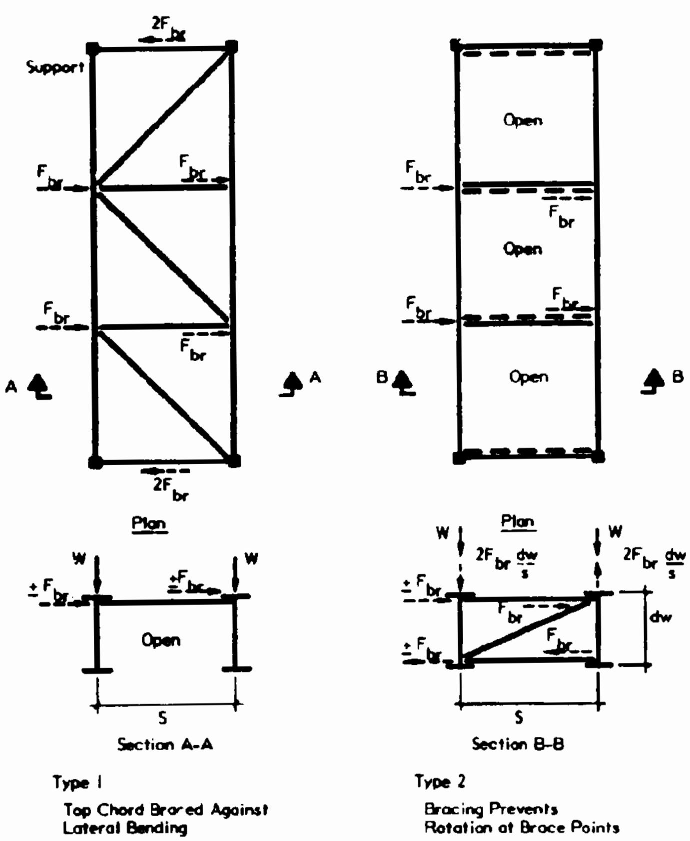

Fig. 7-9 EFFECTIVE LATERAL BRACING SYSTEMS

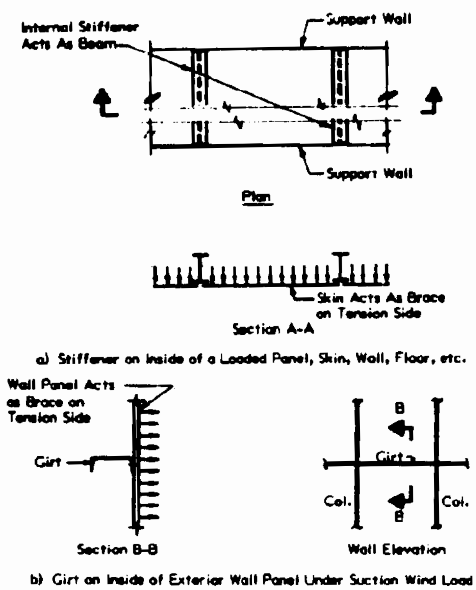

Fig. 7-10 LATERAL BRACING ON TENSION SIDE OF BEAM

Deflection

Because the elastic and viscoelastic moduli of plastics are low, deflection is frequently a critical design criterion. Performance criteria often limit maximum deflection under service load to avoid unsatisfactory appearance, distress in attached non-structural components, flutter in wind, leakage at weather seals and excessive movement at joints. Typical limits range from L/180 or less for visual acceptance to L/400, or less, for adequate rigidity for resistance to certain vibratory motion.

Beam deflection results from both flexural and shear deformation. Except for beams with sandwich constructions having low density cores, or for beams that have large depth to span ratios, shear deflection is small compared to bending deflection, and is usually neglected. Only bending deflection is considered here. Shear deformation of sandwich beams is presented in detail in Chapter 8.

A general expression for curvature produced by bending moment is given in Section 5.4. The integration of curvature, together with boundary conditions at supports, gives the slope at any point along the beam axis caused by bending. Then, the integration of slope, together with boundary conditions at supports, gives the deflection at points along the beam axis. See (5.8) for the derivation and solution of the differential equation for the deflection of elastic beams, based on Eq. 5.29, the basic elastic curvature relation.

In practical calculations, slopes and deflections of beams are often determined using the **conjugate beam analogy**. This simple method is explained in Section 5.4 and illustrated in Fig. 5-5. It may be used effectively whenever the bending moment diagram has first been determined.

The maximum bending deflection occurs at a point of zero slope or at a boundary. A general expression for the maximum bending deflection in the plane of the loads for a member with a constant cross section over the length, L, and symmetric about the load plane is:

$$w = \frac{K_m WL^3}{E I_l} \qquad \text{Eq. 7.55}$$

The bending deflection constant, K_m, varies with the distribution of total load, W, on the beam and with end-support and end-fixity conditions. Values of K_m for some common load and end support conditions are given in Table 5-1 in Chapter 5. See also Table 8-3 in Chapter 8. The elastic modulus in Eq. 7.55 is the modulus in the longitudinal direction. See Section 5.3 and Tables 5-2 and 5-3 for methods and equations for determining I.

See (5.1), (5.3), and (5.8) for general methods for determining deflection of beams and rigid frames and (5.4) and (5.5) for tables giving formulas for deflection and coefficients for maximum deflection.

When beams with thin flanges are designed to allow local buckling at loads below the design load, based on the "effective width" concept that was explained previously, the moment of inertia decreases in the region of high moment where the effective width is less than the actual width. In this case, the beam stiffness, EI, is variable over the beam length as shown in Fig. 7-11. Stiffness depends on stress level and behavior is non-linear. An accurate determination of deflection, if needed, can be obtained using a computer analysis for beams with variable stiffness. An upper limit of deflection can be obtained by taking the smallest effective moment of inertia at the section of maximum moment as a constant I, or a better estimate can be obtained with some weighted average between the I of the gross section and the I of the effective section at the location of highest stress.

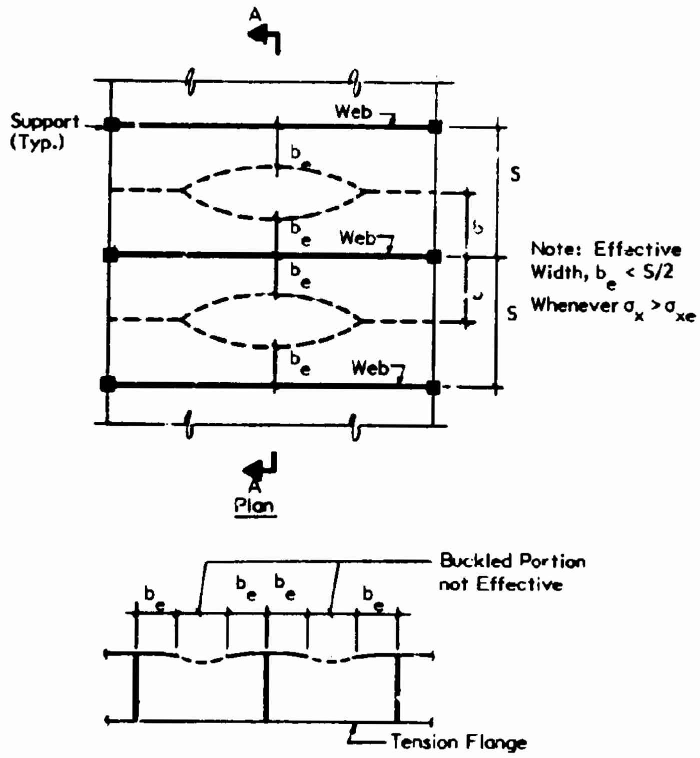

Fig. 7-11 EFFECTIVE WIDTH VARIATION WITH MAXIMUM STRESS

Design procedure for beams

The design procedure for beams is similar to the step by step summary given at the end of Section 7.3 for centrally loaded columns. Of course, the equations for bending strength and lateral stability of unbraced compression flanges presented earlier in this Section are used instead of the equations for compression strength and stability given in the summary for columns. Also, additional considerations involving shear strength and stability, local stresses at reactions and concentrated loads and deflection frequently are important with beam members. These are described in detail in the preceding paragraphs.

When standardized structural members are available, manufacturers usually develop tables of section properties such as section modulus, S, and moment of inertia, I, and members that have the required S and I properties may be selected directly with the aid of such information. However, when the designer has to determine his own proportions for members, a procedure for selecting trial proportions, based on approximate relations for S_l and I_l, is useful. Trial proportions for designing thin-wall I and rectangular tube sections can be established as follows:

1. Determine maximum flange b_f/t_f and web d_w/t_w ratios that permit ${}_{xu}$ in these members without local buckling. Also, determine maximum d_w/t_w that permits ${}_{xu}$ in the web. See Table 7-1.

2. Determine minimum required area of web, A_w (i.e., $t_w d_w$), from Eq. 7.38. Select a trial depth and web thickness that provides A_w and the deepest section that has d_w/t_w less than the limiting value for buckling, or that provides practical proportions for the beam.

3. Determine the required minimum section modulus, S_l, from Eq. 7.33.

4. Determine a trial area of each flange to obtain the required section modulus from the following approximate relation:

$$\text{trial } A_f^* = \frac{S_l}{(d_w + t_f)} - \frac{A_w}{6} \qquad \text{Eq. 7.56}$$

5. Determine the required minimum moment of inertia, I_l, from Eq. 7.55.

6. Determine a trial area of each flange to obtain the required moment of inertia from the following approximate relation:

$$\text{trial } A_f^* = \frac{2I_l}{(d_w + t_f)^2} - \frac{A_w}{6} \qquad \text{Eq. 7.57}$$

7. If a greater flange area is required for I_l, than S_l, it may be more economical to use a deeper section, if permitted by functional requirements and manufacturing limits.

---

*Note: See steps 6.2 and 6.3 in Example 7-3 for derivation of these equations.

8. Establish a width and thickness of flange that develops the flexural strength required with the governing flange area. If S_l governs, the b_f/t_f ratio must be limited to develop σ_{xu} without local buckling of the flange. If I_l requires a larger flange area, the permissible b_f/t_f ratio can be increased, since σ_x will be less than σ_{xu}. After trial proportions are selected, check that the maximum flexural compressive stress under the factored design load is equal to, or less than, the reduced ultimate strength of the material, σ_{xu}, or the maximum buckling strength, σ_{xc}, whichever is less.

9. Check the adequacy of web thickness and bearing length for bearing strength and stability at concentrated reactions and loads.

10. If the compression flange is not laterally braced, check the member for adequate resistance to lateral-torsional buckling. If resistance is not adequate, provide appropriate lateral bracing.

Application of the beam design procedure is illustrated in Example 7-3. Also, the flexural behavior of the same beam under a dynamically applied load from blast pressure is illustrated in Example 5-7.

A few additional considerations for special cases involving plates that behave like beams, beams with thin and wide flanges, and beams subject to torsion are given in the remainder of this Section.

One-way plates as beams

Plates that are supported on opposite edges and span in one direction are essentially wide beams. The methods for analysis and design of beams presented above may also be applied to such plates. However, the effective stiffness of the plate as a beam is increased because contraction and expansion of the "wide beam" due to the Poisson effect is restrained. The increased stiffness is taken into account by replacing the elastic modulus, E, in the equations above by $E/(1 - \nu^2)$. This is discussed in detail in Chapter 6.

When plates spanning in one direction are subject to concentrated loads (Fig. 7-12), shear and bending effects result in directions both parallel to and perpendicular to the direction of the span. The maximum stresses occur at the load, but significant bending in the direction of the span extends longitudinally along the plate, distributing the concentrated load effects to adjacent strips.

Example 7-3 — Beam Design: Design a beam to support a uniformly distributed long term load of 1 kip per ft. over a span of 20 ft. Service temperature range is 0^o to 100^oF. Limit maximum deflection to L/200. Design the beam for full lateral support and determine the maximum spacing, and the minimum strength and stiffness of lateral bracing that will develop full lateral support. Also determine the minimum length of bearing support required if the beam is supported by direct bearing at its ends.*

Use a fiberglass reinforced plastic I-shaped section manufactured by the pultrusion process with the same longitudinal and transverse properties as the tubular column section used in Example 7-2. Material properties based on standard short-time tests are:

> longitudinal compression: 25,000 psi; longitudinal tension: 30,000 psi; elastic moduli: E_{11} = 2,000,000 psi; E_{22} = 1,000,000 psi; G_{12} = 450,000 psi: Poisson's Ratios: ν_{12} = 0.36; ν_{21} = 0.18; web shear, in-plane: 10,000 psi; flange shear, interlaminar: 3,000 psi; transverse compression: 15,000 psi

1. "Reduced" material properties to allow for long term load effects and manufacturing variations: ϕ = 0.5 for compression, 0.4 for tension, 0.7 for elastic moduli and 0.3 for in-plane and interlaminar shear strength.

1.1 Compression: σ_{xu} = 0.5 x 25,000 = 12,500 psi

1.2 Tension: σ_{xu} = 0.4 x 30,000 = 12,000 psi (governs bending)

1.3 Elastic Moduli: E_{11} = 0.7 x 2,000,000 = 1,400,000 psi;

E_{22} = 0.7 x 1,000,000 = 700,000 psi; G_{12} = 0.7 x 450,000 = 315,000 psi

1.4 Web in-plane: σ_{xu} = 0.3 x 10,000 = 3000 psi

1.5 Flange interlaminar shear: σ_{xu} = 0.3 x 3000 = 900 psi

1.6 Transverse compression on web: σ_{yu} = 0.5 x 15000 = 7,500 psi.

2. Load factor for ultimate strength:

Multiply the design load, w = 1 kip/ft., by a load factor = 2.0 to allow for overload, inaccuracy in support arrangement and load application, and differences between analytical models and real behavior.

3. Determine required section modulus, S_I

Table 5-1, Case Ia: Max. $M_{xuI} = \frac{w_u L^2}{8} = \frac{2 \times 1 \times 20^2}{8} = 100'^k$

Eq. 7.33a: req'd $S_I = \frac{100{,}000 \times 12}{12{,}000} = 100 \text{ in.}^3$

4. Determine required moment of inertia, I,

Table 5-1, Case Ia: max. $_I = \frac{5 w L^4}{384 EI_I} = \frac{L}{200}$

---

* See note on Example 7-1, page 7-5.

Example 7-3 (continued)

Thus req'd $I_I = \frac{1000\, w\, L^3}{384\, E} = \frac{1000 \times 1000 \times 20^3 \times 144}{384 \times 1{,}400{,}000} = 2143 \text{ in.}^4$

5. Determine minimum ratios of flange width to flange thickness, b_f/t_f, and web width to web thickness, d_w/t_w to develop ultimate flexural compression strength of 12,000 psi and ultimate shear strength of 3000 psi, respectively:

5.1 Flange - to develop ultimate compression strength (based on conservative assumption of pinned edge at web):

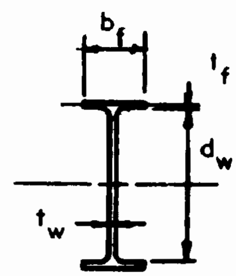

$A_f = b_f\, t_f$

$A_w = d_w\, t_w$

Eq. 6.98: $\left(\frac{b_f}{2t_f}\right)^2 = \frac{G_{12}}{\sigma_{xc}}$; $\sigma_{xc} = \sigma_{xu} = 12{,}000$ psi

$\max \frac{b_f}{2t_f} = \sqrt{\frac{315{,}000}{12{,}000}} = 5.1$

5.2 Web - to develop full 12,000 psi flexural stress at flange:

Eq. 6.101: $\frac{d_w^{\,2}\, t_w}{D_{11}} = \frac{k\,\pi^2}{\sigma_{xc}}$

Eq. 6.6a: $D_{11} = \frac{1{,}400{,}000\, t_w^3}{12(1 - 0.36 \times 0.18)} = 124{,}800\, t_w^3$

Fig. 6-44: for $\frac{D_{22}}{D_{11}} = 0.5$: estimate $k = 20$; $\max \frac{d_w}{t_w} = \pi \sqrt{\frac{20 \times 124{,}800}{12{,}000}} = 45$

5.3 Web - to develop full 3000 psi reduced ultimate shear strength:

Eq. 6.102: $\frac{d_w^2\, t_w}{(D_{11}\, D_{22}^{\,3})^{1/4}} = \frac{4\, k_{xy}}{\tau_{xyc}}$

Eq. 6.6b: $D_{22} = \frac{700{,}000\, t_w^{\,3}}{12(1 - 0.36 \times 0.18)} = 62{,}400\, t_w^{\,3}$

Fig. 6-45 & Eq. 6.6c: $D_{12} = {}_{21}\, D_{11} = 0.18 \times 124{,}800\, t_w^{\,3} = 22{,}500\, t_w^{\,3}$

Eq. 6.6d : $D'_{12} = \frac{G_{12}\, t_w^{\,3}}{12} = \frac{315{,}000}{12}\, t^3 = 26{,}250 t_w^{\,3}$

Eq. 6.6e: $D_0 = D_{12} + 2D'_{12} = (22{,}500 + 2 \times 26{,}250) t_w^{\,3} = 75{,}000 t_w^{\,3}$

$\lambda_2 = \frac{D_o}{\sqrt{D_{11}\, D_{22}}} = \frac{75}{\sqrt{124.8 \times 62.4}} = 0.84$; $\lambda_1 = 0$ for long plate; Fig. 6-45: $k_{xy} = 12$

$\max. \left(\frac{d_w}{t_w}\right) = \frac{4 \times 12 \times (124{,}800 \times 62{,}400^3)^{1/4}}{3{,}000} = 34.5$

6. Select trial I section with $b_f/t_f \le 6$, $d_w/t_w \le 45$, $S_I \ge 100$ and $I_I \ge 2143$.

Example 7-3 (continued)

6.1 Trial web design with depth = 24 in.: d_w = 22 in.; $t_w = \frac{22}{45}$ - 0.50 in.; A_w = .50 x 22 = 11 in.^{2}

6.2 Trial flange design for strength, based on S:

$$S \quad A_f(d_w + t_f) + \frac{A_w d_w}{6} \text{ and } (d_w + t_f) \quad d_w$$

Eq. 7.56: Trial $A_f \quad \frac{S}{(d_w + t_f)} - \frac{A_w}{6}$; estimate t_f = 1.0

Trial $A_f = \frac{100}{23} - \frac{11}{6} = 2.51$ in.^{2}

6.3 Trial flange design for stiffness, based on I

$$I \quad \frac{A_f (d_w + t_f)^2}{2} + \frac{A_w d_w^{\ 2}}{12} \text{ and } (d_w + t_f) \approx d_w$$

Eq. 7.57: Trial $A_f = \frac{2I}{(d_w + t_w)^2} - \frac{A_w}{6}$

Trial $A_f = \frac{2 \times 2143}{23^2} - \frac{11}{6}$ - 6.3 in.^{2} (governs)

6.4 Trial Section: Depth = 24 in.; b_f = 9 in., $t_f = \frac{6.3}{9}$ = 0.70. in.

d_w = 24 - 2 x .70 = 22.6 in., t_w = 0.5 in.

$\frac{b_f}{2t_f} = \frac{9}{2 \times .70}$ = 6.4 > 5.2 but may be acceptable because stiffness, rather than strength, governs design.

$\frac{d_w}{t_w} = \frac{22.6}{0.5} = 45.2 \approx 45$

6.5 Check properties and stresses:

$I = 9 \times .70 \times \frac{(23.10)^2}{2} + \frac{0.5 \times 22.7^3}{12}$ = 2162 in.^{4} > 2143 o.k.;

$S = \frac{2162}{12}$ = 180 in.^{3} > 100 o.k.

req'd $\sigma_{xc} = \frac{100 \times 12}{180}$ = 6667 psi; furn. $\sigma_{xc} = \frac{315,000}{(6.4)^2}$ = 7690 psi, o.k.

7. Check adequacy of web for shear:

7.1 Table 5-1, Case 1a: max $V_{xu1} = \frac{w_u L}{2} = \frac{2 \times 1 \times 20}{2}$ = 20k

7.2 Eq. 7.58: req'd min. $t_w = \frac{20,000}{3000 \times 22.6}$ = 0.30 < 0.50 furn., o.k.

$\tau_{xyu} = \frac{0.3}{0.5} \times 3000$ = 1800 psi

Example 7-3 (continued)

7.3 Check for buckling in shear:

Eq. 6.102: $\tau_{xyc} = \dfrac{4 \times 12 \times (124{,}800 \times 62{,}400^3)^{1/4}}{(45.8)^2 \times 0.5} = 3396$ psi, with "hinged" edges

o.k.

8. Check maximum interlaminar shear in flange. Assume thickness of inside layer of longitudinal fibers is 0.03 in. and calculate maximum horizontal (interlaminar) shear on plane a-a:

$\bar{Q}_{sy} = 9 \times 0.67 \times (12.0 - 0.33) = 70.4$ in.^{3}

Eq. 5.30: $\tau_x = \dfrac{20{,}000 \times 70.4}{9 \times 2197} = 71.2$ psi $<$ 900 psi, o.k.

9. Determine minimum length of bearing based on web crippling and local web buckling at supports.

9.1 Table 5-1, Case 1a: $R_u = \dfrac{2. \times 1. \times 20}{2} = 20\text{k}$

9.2 Eq. 7.42: Req'd $(n + k) = \dfrac{R_u}{\sigma_{yu}\, t_w} = \dfrac{20{,}000}{7500 \times 0.5} = 5.33$ in.

If a 1/2 in. fillet is used, k = 0.75 in., and required bearing length n = 5.33 - 0.75 = 4.58 in

9.3 Try 5 in. bearing length:

"a" for local buckling $= (5 + \frac{h}{2}) = (5 + \frac{24}{2}) = 17$ in.

$\sigma_{yu} = \dfrac{20{,}000}{0.5 \times 17} = 2353$ psi

9.4 Eq. 7.43*: $\sigma_{yc} = \dfrac{\pi^2 E_{22}}{12(1 - \nu_{12}\,\nu_{21})} \left(\dfrac{t_w}{d_w}\right)^2 \left(2 + \dfrac{4\, d_w^2}{a^2}\right)$

$\sigma_{yc} = \dfrac{\pi^2 \times 700{,}000}{12(1 - .36 \times .18)} \left(\dfrac{0.5}{22.7}\right)^2 \left(2 + \dfrac{4 \times 22.7^2}{17^2}\right) = 2{,}728$ psi $>$ 2353 o.k.

* Note: Since $E_{11} \gg E_{22}$, it is conservative to use isotropic buckling equations with E_{22}

9.5 Use 6 in. minimum length of bearing, allowing 1.4 in. for tolerance.

10. Minimum spacing of lateral supports:

10.1 Approx. check with Eq. 7.50: $\sigma_{xc} = 0.65\, C_1 E_{11} \dfrac{b_f t_f}{Ld}$ & take $C_1 = 1.0$

$\sigma_{xc} = 0.65 \times 1{,}400{,}000 \times \dfrac{9 \times 0.7}{L \times 24} = \dfrac{238{,}875}{L}$; max. $L = \dfrac{238{,}875}{\sigma_{xc}}$

Example 7-3 (continued)

$$\text{req'd } \sigma_{xc} = \frac{M_u}{S} = \frac{100 \times 12}{183} = 6557 \text{ psi; max. } L = \frac{238{,}875}{6557} = 36.4 \text{ in.}$$

10.2 Approx. check with Eq. 7.52: $\sigma_{xc} = \dfrac{0.8\, C_1\, E_{11}}{(KL/b)^2} = \dfrac{0.8 \times 1.0 \times 1{,}400{,}000}{L^2/9^2}$

$$\text{max. } L = 9\sqrt{\frac{0.8 \times 1{,}400{,}000}{6557}} = 117.6 \text{ in.}$$

10.3 Try a 10 ft. unbraced length (one brace at midspan), and use Eq. 7.46 for critical buckling stress:

$$\text{Eq. 7.46:} \quad \sigma_{xc} = \frac{C_1}{S_1} \sqrt{M_{xc}^2 + \frac{d^2}{4} P_{e2}^2}$$

$$\text{Eq. 7.47:} \quad M_{xc} = \frac{\pi}{KL}\sqrt{EI_2\, G\, J}$$

$$I_2 = \frac{0.7 \times 9^3}{12} \times 2 = 85.05 \text{ in.}^4; \quad J = \frac{9 \times 0.7^3 \times 2}{3} + \frac{22.6 \times 0.5^3}{3} = 3.00 \text{ in.}^4$$

$$M_{xc} = \frac{\pi}{1 \times 120}\sqrt{1{,}400{,}000 \times 85. \times 315{,}000 \times 3.0} = 277{,}625 \text{ in-lbs.}$$

$$\text{Eq. 7.48:} \quad P_{e2} = \frac{\pi^2 EI_2}{(KL)^2} = \frac{\pi^2 \times 1{,}400{,}000 \times 85.}{(120)^2} = 81{,}561 \text{ lbs}$$

From Eq. 7.49 with : $M_1 = 0$: $C_1 = 1.75$

$$\text{Eq. 7.46:} \quad \sigma_{xc} = \frac{1.75}{183}\sqrt{(277{,}625)^2 + \frac{24^2}{4} \times 81{,}561^2} = 9729 \text{ psi} > 6557 \text{ psi o.k.}$$

Conclusion: One brace at midspan and one at each support are adequate.

10.4 Min. brace stiffness, K_{bs}, (Section 7.3): Eq. 7.31a: min. $K_{bs} = \dfrac{4\, N_{xc}}{L}$

$$N_{xc} = (A_f + A_w/6)\, \sigma_{xc} = \left(9 \times 0.7 + \frac{22.6 \times 0.5}{6}\right) 9729 = 80{,}000 \text{ lbs}$$

$$\text{min. } K_{bs} = \frac{4 \times 80{,}000}{120} = 2667 \text{ lbs/in.}$$

10.5 Min. brace strength, N_{bu}, (Section 7.3): min. N_{bu} = 0.02 x 80,000 = 1600 lbs.

Note:

1 in. = 25.4 mm, 1 in^2 = 645 mm^2, 1 in^3 = 16.387 mm^3, 1 in^4 = 416,231 mm^4, 1 ft = 0.3048 m, 1 lbf = 4.448N, 1 Kip = 4.448 KN, 1 ft-k = 1.356 KN-m, 1 in-lb = 0.113 N-m, 1 lb/in = 0.175 N/mm, 1 Kip/ft = 14.59 KN/m, 1 psi = 6.895 KPa, $^oC = (^oF - 32)/1.8$

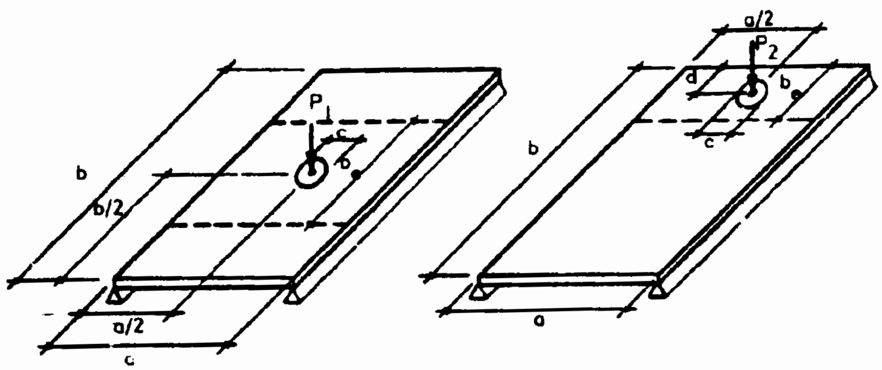

a) Central Concentrated Load b) Off-Center Concentrated Load

Fig. 7-12 EFFECTIVE WIDTH FOR CONCENTRATED LOAD ON ONE-WAY SPAN PLATE

The entire concentrated load is assumed to be carried by a strip of the plate having an "effective width", b_e, whose maximum flexural normal stress, σ_{xe}, uniformly distributed over width, b_e, is equal to the maximum flexural normal stress in the plate, σ_x.

The following equations for approximating the effective width are useful (5.4):

1. Concentrated load on central circular area of diameter c (Fig. 7-12a):

$$b_e = 0.58a + 4c \qquad \text{Eq. 7.58}$$

2. Concentrated load on mid-span off-center circular area of diameter c, located a distance, d, from nearest edge of plate (Fig. 7-12b):

$$b_e = 0.29a + 2c + d \qquad \text{Eq. 7.59}$$

but not greater than b_e in Eq. 7.58.

See (7.8) or (7.9) for more accurate and comprehensive procedures for determining stress resultants caused by concentrated loads on plates.

Shear lag in wide flanges of beams

When the flange of a beam is wide relative to its span length, shear deformation produces a non-uniformity in the distribution of bending stresses over the width of the flange that can be significant. Eq. 5.30 gives the shear stresses in the flange of an I or box type beam shown in Fig. 7-13. The shear deformation associated with these stresses results in the distribution of flexural stresses shown in the same Figure.

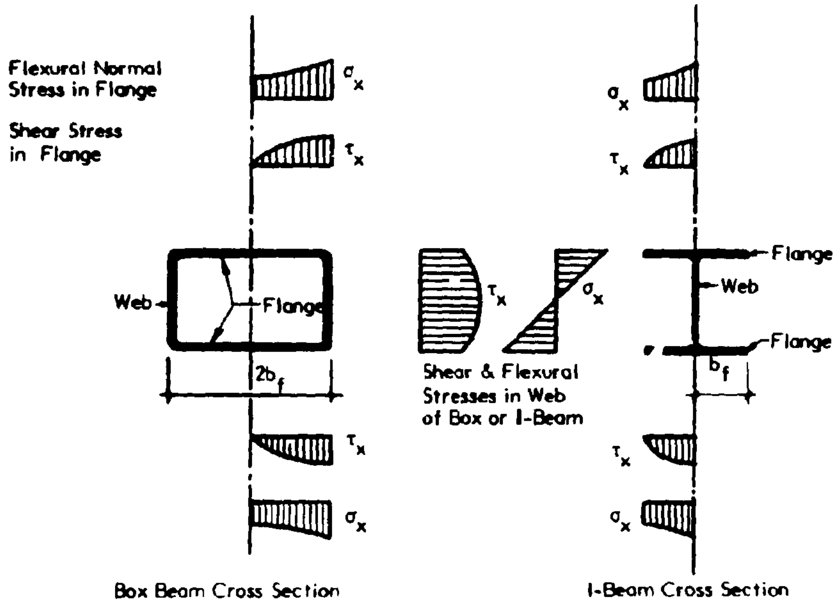

Fig. 7-13 SHEAR LAG IN I OR BOX BEAMS WITH WIDE FLANGES

Shear lag can be taken into account in design by using an "effective width," similar in concept to the effective width used in the post buckling behavior or thin stiffened compression flanges. The bending capacity of a beam having the effective flange width, b_e, uniformly stressed to σ_{xm} is equal to the bending capacity of the actual beam having a maximum flange stress, σ_{xm}, at the flange location adjacent to the web.

Graphs giving an effective reduced flange width, b_e, that accounts for shear lag in simply supported, continuous and cantilever box or I-shaped beams are provided in Fig. 7-14. The graphs in Fig. 7-14a give the effective width, b_e, that is needed for calculating an effective section modulus at the section of maximum moment in the above types of beams. Maximum flange stress is:

$$\sigma_{xm} = \frac{M_{xI}}{S_{Ie}} \qquad \text{Eq. 7.60}$$

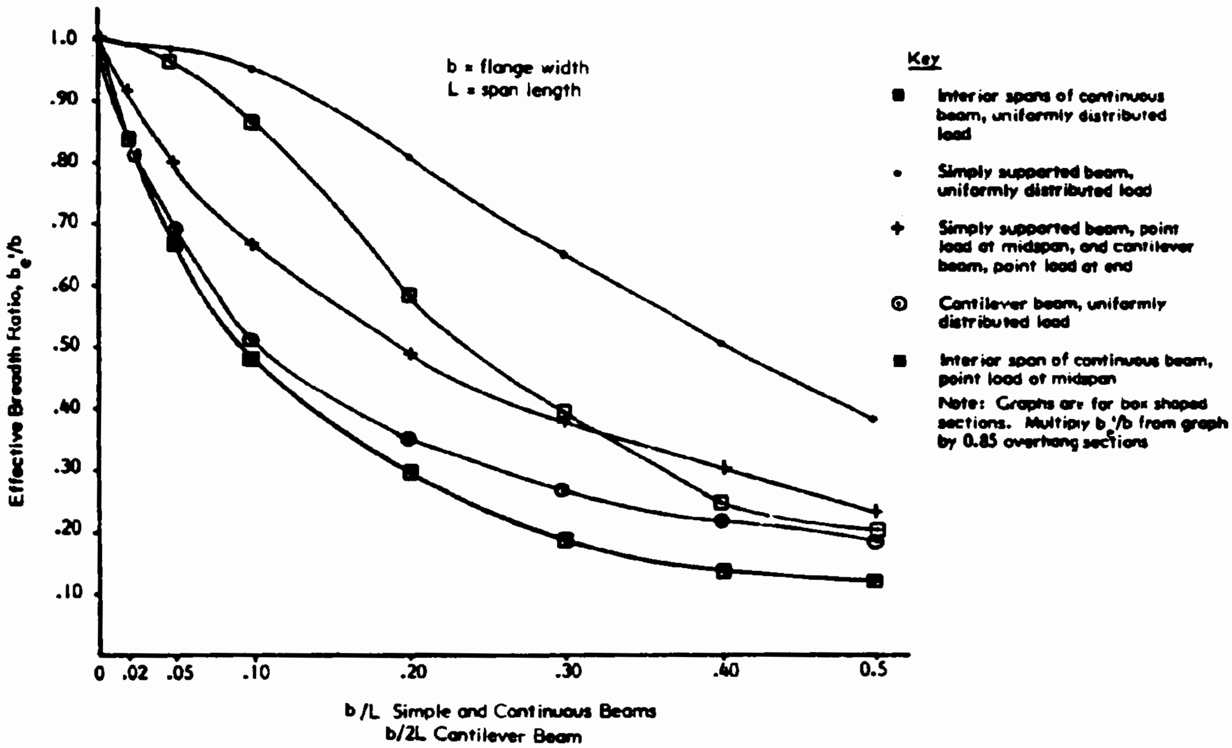

Fig. 7-14(a) EFFECTIVE BREADTH RATIOS FOR SHEAR LAG AT SECTIONS OF MAXIMUM MOMENT

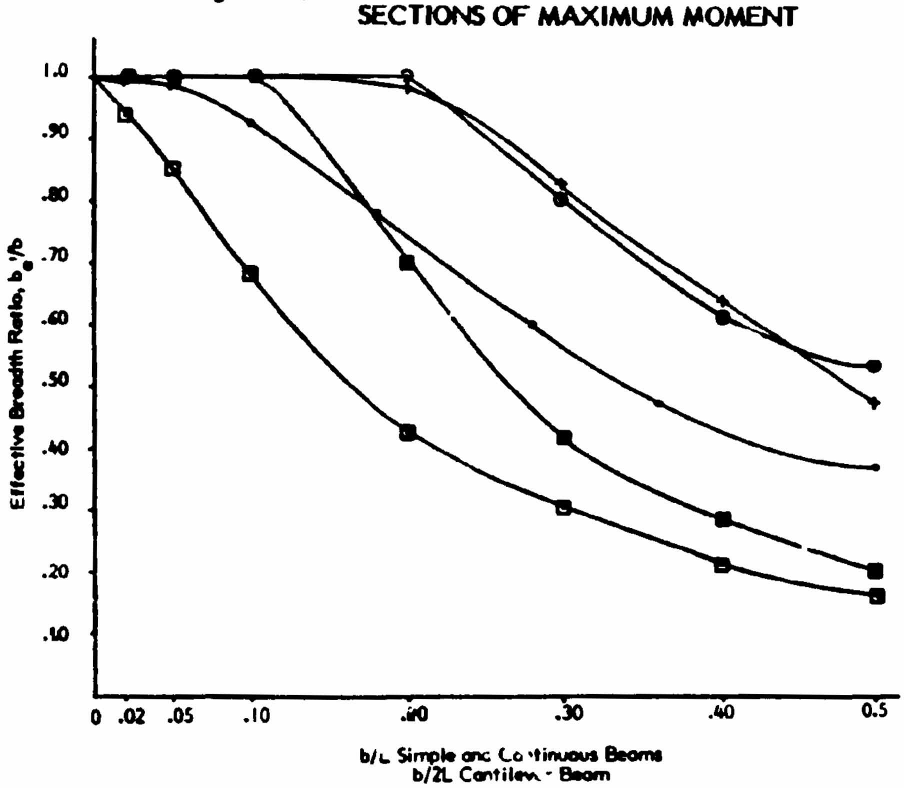

Fig. 7-14(b) AVERAGE EFFECTIVE BREADTH RATIOS FOR SHEAR LAG AT SECTIONS FOR DEFLECTION CALCULATIONS

The following equation provides an estimate of flexural stress, σ_x, at any point in the flange width a distance y from the web (7.10):

$$\sigma_x = \sigma_{xm} \quad (\frac{y}{b})^4 - K(1 - \frac{y}{b})^4 \qquad \text{Eq. 7.61}$$

where: σ_{xm} = maximum stress adjacent to web;

$K = (5b_e/b - 1)/4$ for flanges that extend between webs (box sections);

$K = (4.25\ b_e/b - 1)/4$ for flanges that overhang the web.

The graphs in Fig. 7-14(b) give the average effective width, b'_e, that is needed for calculating an average moment of inertia, I_e, to be used for calculating midspan deflection with equations given in Table 5-1.

The graphs in Figs. 7-14 a and b, show that consideration of shear lag becomes more important (i.e., effective width reduces) as the ratio of span to flange width reduces, and as the load distribution becomes more concentrated at the section of maximum moment. The amount of shear lag also varies with the ratio of G/E and with the quantity, $m = 3I_w + I_f/I_w + I_f$, where I_w and I_f are moments of inertia of web and flanges, respectively, about the neutral axis of the beam.

The results presented in the graphs were developed in shear lag studies of composite steel and concrete box girders (7.10). Thus, they are most valid for members with isotropic materials and with proportions similiar to the box and I girders used in the investigation reported in (7.10).

See also (7.3) for a summary of effective widths for shear lag, as determined by various investigators for cantilever and simply supported beams with various load distributions.

Flange curling

When a beam with thin wide flanges bends, the flanges curl inward toward the neutral axis because the radial components of the curved flange tension and compression forces cause transverse bending (see Section 9.2). This behavior is illustrated in Fig. 7-15 for doubly symmetric thin wall I and ▯ sections.

The average radial component, q_r, of the longitudinal flange force, $\sigma_{xav}\, t_f$, that results from the flexural curvature of the beam is (7.3):

$$q_r = \frac{\sigma_{xav}\, t_f}{E_x\, I/M} = \frac{2\sigma^2_{xav}\, t_f}{E_x\, d} \qquad \text{Eq. 7.62}$$

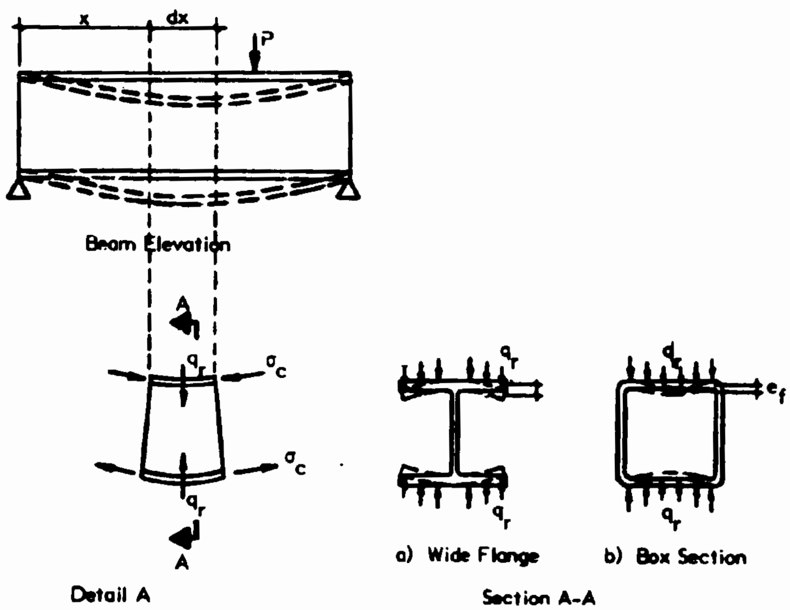

Fig. 7-15 WIDE FLANGE CURLING DUE TO CURVATURE OF DEFLECTED BEAM

The transverse deflection of the curled flange (Fig. 7-15) of thin-wall I and sections under the distributed radial load, q_r, is:

$$c_f = \frac{K_m q_r\, b_f^4}{D_f} = 24\, K_m\, (1 - \nu_f^2)\left(\frac{\sigma_{xav}}{E_x\, E_{yf}}\right)^2 \frac{b_f^4}{t_f^2\, d} \qquad \text{Eq. 7.63}$$

The bending deflection coefficient, K_m, is given in Table 5-1 for beams under uniformly distributed load with various support arrangements. The uniformly loaded cantilever beam case should be used for curling of an I beam, giving K_m

= 1/8. Uniformly loaded beams with simply supported ends, and with rotationally fixed ends represent limits for the flange of a box section, with the actual K_m dependent on the amount of end restraint provided by the web. K_m equal to 2/384 to 2.5/384 is probably a reasonable approximation for many practical box shapes. E_x is the elastic modulus for axial stress in the longitudinal direction, while E_{yf} is the transverse elastic modulus of the flange in flexure. The flange stress σ_{xav} is the average stress at the mid-depth of the flange caused by the design loads on the beam.

Aesthetic considerations or other performance criteria may require a limitation on c_f. If a maximum value for c_f is established, the width or thickness or the flange in the thin-wall beam can be adjusted, if necessary, to limit c_f. Generally, the radius of curvature in primary bending is large enough so that the resulting transverse stresses due to curling are small. In the case of curved thin wall beams, however, the radius of curvature may be such that both transverse stresses and deflections are significant, and constitute a primary design consideration. This is discussed in Section 9.2.

Torsion

Torsion of shafts was discussed in Section 5.4, along with equations for determining the resulting shear stresses. However, as noted in that section, support conditions may prevent the free warping that occurs when non-circular cross sections are subject to twist. When warping of a thin-walled section is prevented, torsionally induced shear stresses are reduced, but additional bending and shear stresses are produced by the lateral bending that results from warping restraint. Bending due to warping restraint is most significant in the torsional resistance of beams having open thin wall cross sections (i.e. I, L, C, J, JL). Also the relative importance of warping restraint increases as the beam span decreases.

The torsional deformation of an open thin-wall section is illustrated in Figs. 5-8 and 7-8 given previously. The first figure illustrates how torsion is resisted by shear stresses developed individually in each rectangular element of the open cross section and by lateral bending stresses that arise in the flange elements as the top and bottom flanges deflect laterally in opposite directions during twist.

These bending stresses must be added to stresses that arise from primary bending in the planes of the applied loads to obtain the maximum bending stresses that occur at the tips of the flanges.

Closed thin-wall sections: From a design viewpoint, a member that is subject to significant torque should be provided with a torsionally efficient section, such as a closed thin-wall (i.e. tubular) shape. For members with these sections, the equations presented in Section 5.4 for the shear stresses caused by primary torsion provide a sufficiently accurate basis for design, and the longitudinal stresses and torsional resistance that develop from warping restraint can be neglected as very small in all but unusually short members.

When designing a beam with a tubular section for combined bending and torsion, the combined web shear stresses must be kept below the in-plane shear strength of the material. They must also be less than the critical shear buckling stress as discussed previously. (See **Design of webs,** this Section). Also, thin flange elements must be checked for local buckling under combined shear and axial compression. Eq. 6.87 may be used for this check. The design of a beam with a tubular cross section subject to combined bending and torsion is illustrated in Example 7-5 given later.

Open thin wall sections generally provide inefficient resistance to torsional moments. Nevertheless, their widespread use as efficient bending members, and the need to consider situations where loads are sometimes applied eccentrically, producing twisting as well as bending, occasionally requires the determination of torsionally induced stresses in members with open thin wall sections.

The theory for torsion of open thin wall sections is somewhat complex. See, (7.3), (7.4) (7.6) (7.11) and (7.12) for theoretical development of the theory and for explanations of its use, including concise presentations of equations for stress and deformation. See (7.11) for extensive design aids such as a table of warping constants and function charts for determining stress and deformation in many common loading and support arrangements. See (7.12) for an extensive treatment of torsion in many types of members.

To illustrate the practical evaluation of torsional effects in members with open thin wall sections, equations are presented below for the simplified basic case of a beam with an I-shaped section (doubly symmetric), and having flanges that are rotationally fixed in lateral bending at one end (full warping restraint). The beam is subject to a constant torque, T, over its length, L. Fig. 5-8b illustrates the arrangement and torsional behavior of this structure while Fig. 5-8a shows that same beam subject to uniform twist when the ends of the flanges are free to rotate (warp). The following step-by-step procedure can be used to determine maximum stresses caused by the torque, T, for the case where warping is restrained (Fig. 5-8b):

1. Determine warping constant, C_w

$$C_w = \frac{I_2 d^2}{4} \qquad \text{Eq. 7.64}$$

   The warping constants for standard metal shapes are given in handbooks such as (5.5) and (7.11).

2. Let $p^2 = \frac{G J}{E C_w}$ Eq. 7.65

3. Determine the bending moment and shear force induced in the flange by lateral deformation during twist. Also determine the portion of the total torque, T, resisted by torsionally induced shear, T_s. Only the case of constant torque, T, over a length, L, as shown in Fig. 5-8, b and c, is given here. See (7.11) for solutions to cases with different variations of torque along the beam length and various conditions of end restraint of lateral deformation.

   3.1 Flange Bending: $$M_f = -\frac{T}{p d} \frac{\sinh p (L - x)}{\cosh p L} \qquad \text{Eq. 7.66}$$

   3.2 Flange Shear: $$V_f = \frac{T}{d} \frac{\cosh p (L - x)}{\cosh p L} \qquad \text{Eq. 7.67}$$

   3.3 Torque taken by torsional shear:

$$T_s = T \left[1 - \frac{\cosh p (L - x)}{\cosh p L} \right] \qquad \text{Eq. 7.68}$$

4. Determine the maximum lateral bending and shear stresses induced by M_f and V_f acting on each of the flanges and T_s acting on the assembly of flange and web plates. (See Fig. 5-8e, f and g for illustration of stresses).

4.1 $\quad \max.\ \sigma_{xb} = \pm \dfrac{M_{f\,max}}{S_f} = \dfrac{6T \tanh pL}{p\,d\,t_f\,b_f^2}$ Eq. 7.69

This stress occurs at the tips of flanges at the fixed support.

4.2 $\quad \max.\ \tau_f = \dfrac{3}{2}\ \dfrac{V_{f\,max}}{A_f} = \dfrac{3}{2}\ \dfrac{T}{d\,t_f b_f}$ Eq.7.70

This stress occurs at the junction of flange and web at the fixed support.

4.3 $\quad$ max τ_s in flange:

$$\max.\ \tau_{sf} = \frac{t_f\,T_{s\,max}}{J} = \frac{t_f\,T}{J} \qquad \text{Eq. 7.71}$$

$$\text{where } J = \frac{2\,b_f\,t_f^3}{3} + \frac{d_w\,t_w^{\,3}}{3} \qquad \text{Eq. 7.72}$$

This stress occurs along the outside surfaces of the flange at the point of load application.

4.4 $\quad$ max τ_s in web:

$$\max\ \tau_{sw} = \pm \frac{t_w\,T}{J} \qquad \text{Eq. 7.73}$$

This stress occurs along the outside surfaces of the web at the point of load application.

The above case also applies to a beam of length 2L with a concentrated torque applied at mid-span, and flange ends simply supported (no rotational fixity) with respect to lateral bending (Fig. 5-8c). In this case, warping is restrained at midspan because of symmetry, and behavior is the same as a cantilever with its built-in end at mid-span of the actual beam subject to one half the total midspan torque (i.e., the torque transmitted to each support).

The above procedure is used in **Example 7-4** to determine the stresses in an I-shaped beam subject to combined torsion and bending. Local buckling resistance under the combined stress state is also investigated in this example.

Beams curved in plane

Beams loaded perpendicular to their plane of curvature are subject to combined torsion and bending. **Example 7-5** illustrates the determination of bending and torsional stresses in a curved beam of this type having a tubular section that resists torsion efficiently. See (7.13) for detailed treatment of this type of member.

Example 7-4: Determine the maximum bending and shear stresses in the I-beam designed in Example 7-3, if the loads shown below are applied to the beam. Determine if these stresses exceed the safe strength of the beam, based on the material properties, capacity reduction factors and load factors given in Example 7-3 and the criteria given in the text for resistance to lateral and local buckling.

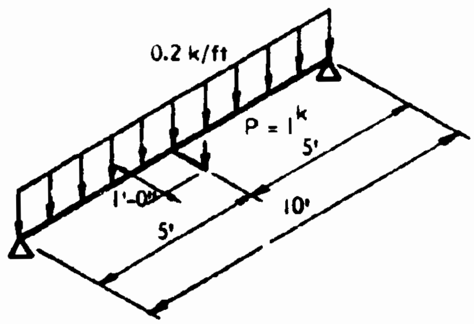

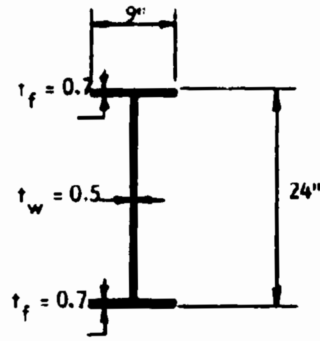

$\bar{I}_1 = 2191 \text{ in}^4 \quad S_1 = 183 \text{ in}^3$

$I_2 = 85 \text{ in}^4 \quad J = 3.0 \text{ in}^4$

1. Midspan bending moment:

Table 5-1: $M_x = 0.2 \times \frac{10^2}{8} + \frac{1 \times 10}{4} = 2.5 + 2.5 = 5.0'k$

$V_x = 0.2 \times 5 + 1 \times 0.5 = 1.5k$

2. Bending stress - vertical loads: Eq. 7.23: $\sigma_x = \frac{M_{xu1}}{S_1} = \frac{5.0 \times 2 \times 12}{183} = 0.66$ ksi

3. Shear stress - vertical load

Eq. 5.30: $\tau_w = \frac{V_{xu1}\bar{Q}_{s1}}{b\,\bar{I}_1}$; $Q_s = 0.70 \times 9 \times (12 - 0.35) + \frac{0.5 \times 11.3^2}{2} = 105.3 \text{ in}^3$

$\tau_w = \frac{1.5 \times 2 \times 105.3}{0.5 \times 2191} = 0.29$ ksi

4. Torsional effects

4.1 Torque: $T_{xu} = \frac{1 \times 1 \times 2}{2} = 1.'k$, constant between midspan and supports

4.2 Constants:

Eq. 7.64: $C_w = \frac{85 \times 24^2}{4} = 12{,}240$

Eq. 7.65: $p^2 = \frac{GJ}{E\,C_w} = \frac{315{,}000 \times 3.0}{700{,}000 \times 12{,}240} = 0.00011$; $p = 0.0105$

4.3 Maximum flange bending stress due to warping resistance of flanges:

Eq. 7.69: $\sigma_{xb} = \frac{6\,T \tanh pL}{p\,d\,t_f\,b_f^2}$; $pL = 0.0105 \times 5 \times 12 = 0.63$; $\tanh pL = 0.5581$

$\sigma_{xb} = \frac{6 \times 1.0 \times 12 \times .5581}{0.0105 \times 24 \times 0.7 \times 9^2} = 2.81$ ksi, at midspan

---

* See note on Example 7-1, page 7-5.

Example 7-4 (continued)

4.4 Maximum flange shear caused by lateral bending of flange:

Eq. 7.70: $\tau_f = \frac{3}{2}\frac{T}{d\,t_f\,b_f} = \frac{3 \times 1.0 \times 12}{2 \times 24 \times .7 \times 9} = 0.12$ ksi, at midspan

4.5 Maximum flange shear caused by twist:

Eq. 7.71: $\tau_{sf} = \pm\frac{t_f\,T}{J} = \frac{0.7 \times 1.0 \times 12}{3} = 2.80$ ksi, max. at supports

4.6 Maximum web shear caused by twist:

Eq. 7.72: $\tau_{sw} = \pm\frac{t_f\,T}{J} = \frac{0.5 \times 1.0 \times 12}{3} = 2.00$ ksi

5. Combined stresses

5.1 Bending at midspan: max. $\sigma_x = 0.66 + 2.81 = 3.47$ ksi

5.2 In-plane shear at supports: Flange: $\tau_f = 0.12 + 2.80 = 2.92$ ksi

Web: $\tau_w = 0.29 + 2.00 = 2.29$ ksi

6. Adequacy, based on material properties and section given in Example 7-3.

6.1 Bending: Use interaction equation similiar to Eq. 7.80 for combined axial and bending, for reduction in ultimate strength caused by lateral buckling effects.

$$\frac{\sigma_b \text{ (bending from vertical load)}}{\sigma_{xc} \text{ (lateral buckling resistance)}} + \frac{\sigma_{\text{bending from twist}}}{\sigma_{xu}\left(1 - \frac{\sigma_b}{\sigma_{xc}}\right)} \leq 1.0$$

With lateral support at ends only, $C_l = 1.0$, lateral buckling resistance is:

$$\sigma_{xc} = \frac{238.9}{L} = \frac{238.9}{10 \times 12} = 2.00 \text{ ksi (from Example 7-3)}$$

$$\frac{0.66}{2.00} + \frac{2.81}{12.0\left(1 - \frac{0.66}{2.00}\right)} = 0.33 + 0.35 = .68 < 1.0 \text{ o.k.;}$$

Conclusion: Normal stress, σ_x, caused by bending is not excessive.

6.2 Flange shear: $\tau_f = 2.92$ ksi max. at supports < 3.0 ksi in-plane web shear strength given in Example 7-3, o.k. in shear

6.3 Web shear: $\tau_w = 2.29$ ksi max. at supports < 3.0 ksi, in-plane web shear strength, o.k.

6.4 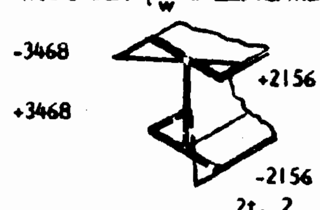

Local buckling of compression flange: Use Eq. 6.98 for buckling stress in orthotropic plate, uniformly stressed across width, as conservative approximation for flange of this beam with stress distribution shown in sketch:

Eq. 6.98: $\sigma_{xc} = G_{12}\left(\frac{2t_f}{b_f}\right)^2 = 315\left(\frac{2 \times .7}{9}\right)^2 = 7.62 \text{ ksi} > 3.47 \text{ ksi o.k.}$

---

1 in. = 25.4 mm, 1 in.^{2} = 645 mm^2, 1 in.^{3} = 16,387 mm^3, 1 in.^{4} = 416,231 mm^4, 1 ft = 0.3048 m, 1 Kip = 4.448 N, 1 ft-k = 1,356 KN-m, 1 k/ft = 14.59 KN/m, 1 ksi = 6.895 MPa

Example 7-5: Determine the bending and torsional stresses in the curved cantilever beam shown in the sketch subject to a tip load perpendicular to the plane of the curved portion of the member. Use the same FRP material properties and load factors as used for Examples 7-2 and 7-3. Neglect weight of beam.

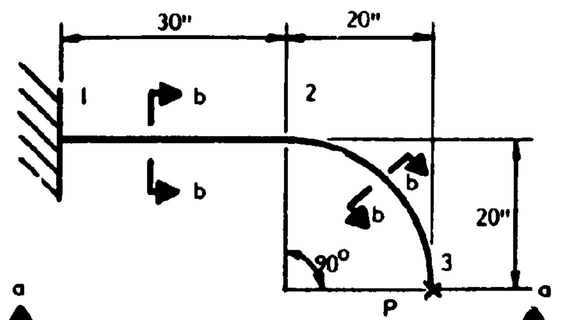

Plan

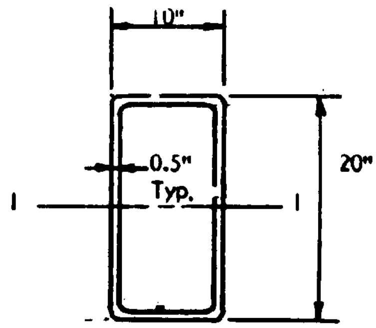

Section b-b

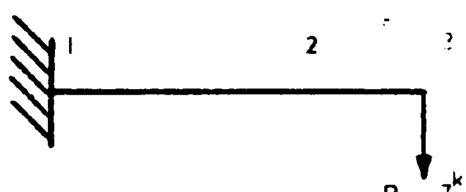

Elevation a-a

(Same as beam in Example 5-4)

From Example 5-4: $I_1 = 1521\ in^4$; $S_1 = 156\ in^3$; $A = 29\ in^2$

1. Maximum bending moment, normal stress, shear force and flexural shear stress:

$M_{xu} = 50\,P \times \overline{LF} = 50 \times 7 \times 2. = 700$ in-k; $V_{xu} = P \times \overline{LF} = 7 \times 2 = 14.0$ k

$$\sigma_x = \frac{M_{xu}}{S_1};\ \sigma_x = \frac{700}{156} = 4.5 \text{ ksi}$$

$$\tau_x = \frac{V_{xu}\,\overline{Q}_{sy1}}{bI_1};\ \overline{Q}_{sy1} = 0.5 \times 10\,\frac{19.5}{2} + 0.5 \times 2 \times \frac{19}{2} \times \frac{19}{4} = 93.9 \text{ in}^3$$

$$\tau_x = \frac{14 \times 93.9}{2 \times 0.5 \times 1521} = 0.9 \text{ ksi}$$

2. Maximum torsion moment and shear stress

$T_{xu} = 20P \times \overline{LF} = 20 \times 7 \times 2.0 = 280$ in-k

$$\text{Eq. 5.37: } \tau_x = \frac{T_{xu}}{2A_p t} = \frac{280}{2 \times 9.5 \times 19.5 \times 0.5} = 1.5 \text{ ksi}$$

3. Combined torsional and flexural shear:

$\tau_x = 1.5 + 0.9 = 2.4$ ksi at mid-height of web

4. Check adequacy, based on materials strength, or local buckling, whichever governs.

See note on Example 7-1, page 7-5.

Example 7-5 (continued)

Eq. 6.6a: $D_{11} = \dfrac{1400 \times 0.5^3}{12(1 - 0.36 \times 0.18)} = 15.6$; $D_{22} = 1/2\, D_{11} = 7.8$

Eqs. 6.6e, 6.6 c and 6.6d: $D_o = D_{12} + 2D'_{12} = \dfrac{0.18 \times 1{,}400 \times 0.5^3}{12(1 - 0.36 \times 0.18)} + \dfrac{2 \times 315 \times 0.5^3}{12} = 9.37$

$\sigma_{xc} = \dfrac{2\pi^2}{0.5 \times 9^2}\ (15.6 \times 7.8 + 9.37) = 9.94$ ksi $< \sigma_{xu} = 12.5$ ksi; Use σ_{xc}

4.2 Flange - shear buckling stress, τ_{xyc}

Eq. 6.102: $\tau_{xyc} = \dfrac{4k_{xy}(D_{11}\, D_{22}^3)^{1/4}}{b^2\, t}$;

Fig. 6-45: $\lambda_1 = (\frac{b}{a})\ \ D_{11}/D_{22} = 0$; $\lambda_2 = D_o/\ \ D_{11}\, D_{22} = \dfrac{9.37}{15.6 \times 7.8} = 0.85$

$k_{xy} = 12.2$;

$\tau_{xyc} = \dfrac{4 \times 12.2\,(15.6 \times 7.8^3)^{1/4}}{9^2 \times 0.5} = 11.2$ ksi $> \tau_{xyu} = 3$ ksi; use τ_{xyu}

4.3 Flange adequacy in combined shear and bending, Eq. 6.87:

$(\frac{1.5}{3.0})^2 + \frac{4.5}{9.9} \leq 1.0$; $0.25 + 0.45 = 0.70 < 1.0$, o.k.

4.4 Web - normal buckling stress, σ_{xc}

Eq. 6.101: $\sigma_{xc} = \dfrac{k\pi^2 D_{11}}{b^2\, t}$; Fig. 6-44: k 20 for $D_{22}/D_{11} = 0.5$

$\sigma_{xc} = \dfrac{20\,\pi^2 \times 15.6}{19^2 \times 0.5} = 17.0$ ksi $> \sigma_{xu} = 12.5$ ksi; Use $\sigma_{xu} = 12.5$ ksi

4.5 Web - shear buckling stress, τ_{xyc}:

k_{xy} from 4.2 above;

Eq. 6.102: $\tau_{xyc} = \dfrac{4 \times 12.2\,(15.6 \times 7.8^3)^{1/4}}{19^2 \times 0.5} = 2.5$ ksi $< \tau_{xyu} = 3.0$ ksi; Use τ_{xyc}

4.6 Web adequacy in combined shear and normal stress; Eq. 6.88:

$(\frac{2.4}{2.5})^2 + (\frac{4.5 \times 9.5}{12.5 \times 10})^2 \leq 1.0$: $0.92 + .12 = 1.04$ 1.0. o.k.; close enough

Conclusion: Since the flange is understressed, a slightly wider and shallower tube would be more efficient because the torsional effects are more significant than the flexural effects.

Note: 1 psi = 6.895 KPa; 1 in. = 25.4 mm; 1 lbf = 4.45 N
1 in. = 25.4 mm, 1 in^2 = 645 mm^2, 1 in^3 = 16,387 mm^3, 1 in^4 = 416.231 in^4, 1K = 4.448 KN, 1 in-K = 113 N-m, 1 Ksi = 6.895 MPa

See note on Example 7-1, page 7-5.

7.5 BEAM - COLUMNS

Beam-columns are subject to combined bending and axial compression. As shown previously in Section 5.7, when axial compression is applied to a member already bent (laterally deflected) as a result of bending stress and/or initial crookedness, these initial deflections are eccentricities that produce more deflection due to the applied compression force. As a result, stresses increase non-linearly as axial load increases. A simple method for estimating the magnified bending moment caused by axial load, involves the determination of a "magnification factor," as defined in Section 5.7. The estimated maximum bending moment is determined from the calculated moment, M_{xo}, and axial thrust, N_x, obtained in a linear analysis:

$$M_{max} = M_{xo} + N_x \delta_o \left[\frac{1}{1 - \frac{N_x}{N_{xc}}} \right] \qquad \text{Eq. 7.74}$$

In this equation, δ_o is the maximum lateral deflection in a member of length L caused by initial crookedness and/or an applied bending moment, M_{xo}, based on linear analysis. N_{xc} is the Euler buckling load for a pin ended member, and N_x is the applied load.

The term $(1 - N_x/N_{xc})$ is called the "magnification" or "amplification" factor, since it provides a simple multiplier for determining the approximate effect of the non-linear magnification of initial crookedness, eccentricities in the application of axial load, and deflections due to lateral loads as calculated using linear elastic analysis.

Eq. 7.74 is written in more convenient form by defining (5.5) (7.2):

$$\psi = \frac{{}_oN_{xc}}{M_{xo}} - 1 \qquad \text{Eq. 7.75}$$

Thus:

$$M_{max} = M_{xo} \frac{(1 + \psi \frac{N_x}{N_{xc}})}{(1 - \frac{N_x}{N_{xc}})} \qquad \text{Eq. 7.76}$$

Maximum deflections of beams with several conditions of end restraint, end moments and transverse loads are given in Table 5-1. When these deflections, and the related Euler column buckling loads, N_{xc}, (Eq. 7.15) are applied to Eq. 7.76, values may be obtained for ψ. These are given in Table 7-3 for some common load cases. This Table shows that $\psi = 0$ for the case of equal end moments of the same sign, producing single curvature with constant moment over the length of the member. Also, this is the largest value of ψ, since ψ is negative for the other cases. In view of this, the term in the numerator of Eq. 7.76 is called the "Reduction Factor", C_m, where:

$$C_m = 1 + \psi \frac{N_x}{N_{xc}} \qquad \text{Eq. 7.77}$$

Table 7-3

Reduction Factor for Combined Bending and Axial Load

Case	ψ	C_m
1. 	0	1.0
2. 	−0.4	$1 - 0.4\frac{\sigma_{xa}}{\sigma_{xae}}$
3. 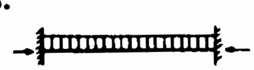	−0.4	$1 - 0.4\frac{\sigma_{xa}}{\sigma_{xae}}$
4. 	−0.2	$1 - 0.2\frac{\sigma_{xa}}{\sigma_{xae}}$
5. 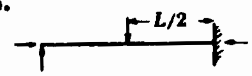	0.3	$1 - 0.3\frac{\sigma_{xa}}{\sigma_{xae}}$
6. 	−0.2	$1 - 0.2\frac{\sigma_{xa}}{\sigma_{xae}}$

* Applied for C_{m1} and σ_{xa1e} when 1-1 is axis of bending and for C_{m2} when 2-2 is axis of bending

Values of C_m for common cases are also given in Table 7-3. Thus, the following modified version of Eq. 7.75 will be used in the design equations presented later:

$$M_{max} = M_{xo} \frac{C_m}{(1 - \frac{N_x}{N_{xc}})} \qquad \text{Eq. 7.78}$$

If it is desired to include an additional amount of deflection, δ_{oi}, for initial crookedness, this may be done using Eq. 7.75. However, as a design simplification, no initial crookedness is included for the determination of ψ used in structural steel design practice (7.2).

The common cases where end moments are unequal are not included in Table 7-3 because they involve theoretically complex relations for ψ. An approximate approach given in (7.2) greatly simplifies the calculation of C_m for this important case (Fig. 7-16, a or b), giving the following practical approximation:

$$C_m = 0.6 + 0.4 \frac{M_1}{M_2} \text{, but not less than } 0.4 \qquad \text{Eq. 7.79}$$

where M_1 is the numerically smaller end moment, and M_1/M_2 is positive for members bent in single curvature (Fig. 7-16(a)), and negative for members bent in double curvature (Fig. 7-16(b)).

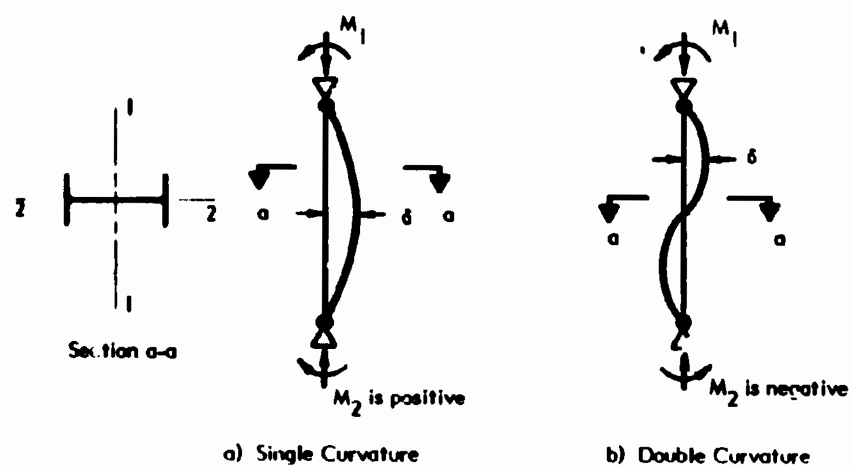

Fig. 7-16 SINGLE AND DOUBLE CURVATURE OF BEAM-COLUMNS

Bending combined with axial compression implies the absence of lateral support in at least the plane of bending. The beam-column may, or may not, have lateral support in the direction perpendicular to the plane of bending. An accurate determination of the behavior of a laterally unsupported beam-column is complex (7.4). The same is true for a member subject to axial compression combined with biaxial bending. An approach based on a simple **interaction formula** has proved to give a conservative approximation of the effects of combined bending and axial compression that is very useful for practical design. The generalized form of an interaction equation for members such as those shown in Fig. 7-16 is (7.2) (7.4):

$$\frac{\sigma_{xa}}{Q\sigma_{xac}} + \frac{C_{m1}\,\sigma_{xb1}}{Q\,\sigma_{xb1c}\left(1-\frac{\sigma_{xa}}{\sigma_{xa1e}}\right)} + \frac{C_{m2}\,\sigma_{xb2}}{Q\,\sigma_{xb2u}\left(1-\frac{\sigma_{xa}}{\sigma_{xa2e}}\right)} \leq 1.0 \quad \text{Eq. 7.80}$$

where σ_{xa} = axial design stress times load factor, $Q\,\sigma_{xac}$ = axial strength in compression (including any reduction for local buckling), based on Fig. 7-4 for buckling in weak direction (usually axis 2-2), σ_{xb1} = bending design stress about 1-1 axis times load factor, $Q\sigma_{xb1c}$ = bending strength about 1-1 axis (including any reduction for lateral and/or local buckling), σ_{xa1e} = axial Euler buckling stress (Eq. 7.17) when laterally unsupported normal to 1-1 axis, C_{m1} = reduction factor for bending about 1-1 axis, σ_{xb2} = bending design stress about 2-2 axis times load factor, $Q\sigma_{xb2e}$ = bending strength about 2-2 axis, σ_{xa2e} = axial Euler buckling stress (Eq. 7.17) when laterally unsupported normal to 2-2 axis and C_{m2} = reduction factor for bending about 2-2 axis. If the member is not subject to bi-axial bending, the third term in Eq. 7.80 is not required.

Because the reduction factor, C_m, may be as low as 0.4, it often is necessary to check the effects of combined stress at joints where no amplification of bending can occur (except in frames subject to sidesway). In this case, neither the axial strength, σ_{xau}, nor the bending strength, σ_{xbu}, need be reduced for lateral buckling. Any reduction due to local buckling is taken into account in the determination of the Q factor. Thus, the interaction formula becomes:

$$\frac{\sigma_{xa}}{Q\sigma_{xau}} + \frac{\sigma_{xb1} + \sigma_{xb2}}{Q\sigma_{xbu}} \leq 1.0 \qquad \text{Eq. 7.81}$$

Design of members subject to combined bending and axial stress usually requires an initial or trial design, based on the designer's judgement about the interaction of axial stress and bending. The factored ultimate stresses obtained with this design, σ_{xa}, σ_{xb1}, σ_{xb2}, must be investigated using both Eqs. 7.80 and 7.81. **Example 7-6** illustrates the investigation of a linear member subjected to combined bending and axial stress resultants.

When members form part of a frame in which joints may deflect laterally, design for combined bending and axial load becomes more complex. The behavior of laterally and vertically loaded rigid frames and slender braced frames (Fig. 7-17(a) and (b)) exemplifies the non-linear increase in deflection and bending that occurs due to interaction of effects produced by these loads (Section 5.6). Lateral load produces lateral deflection of joints. The product of vertical load, P_v, and lateral joint deflection, Δ, produce additional bending in rigid moment frames (Fig. 7-17(a)) and additional axial load in "pin jointed" braced frames (Fig. 7-17(b)). These effects are significant in certain slender or flexible structures but methods for their determination are beyond the scope of this Design Manual. See (7.14) for a comprehensive presentation of a practical approximate method for determining $P_v\Delta$ effects.

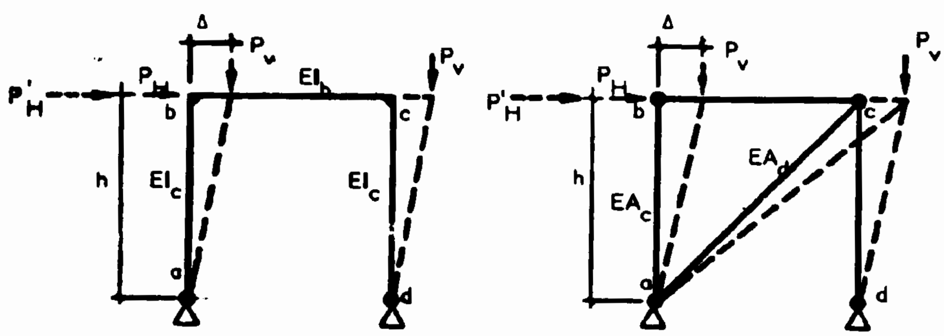

a) Rigid Frame

Additional Moment at b and c = $P_v\Delta$

b) Braced Frame

$P_v\Delta$ Effect is Equivalent to Effect of an Additional Lateral Load Applied at b, where $P'_H = 2P_v\Delta/h$

Fig. 7-17 ADDITIONAL STRESS RESULTANTS DUE TO FRAME DEFLECTION

Example 7-6: Determine the maximum design axial compressive load that can be applied to the beam shown in the sketch. The fiberglass reinforced plastic materials are the same as for the beam in Example 7-3. The design beam load applied perpendicular to axis 1-1 is 500 lbs per ft. The beam is laterally braced at midspan. The beam section is shown in Section a-a.*

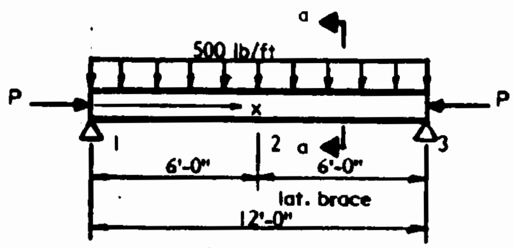

Elevation

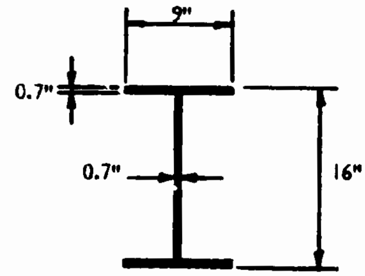

Section a-a

1. Reduced ultimate strength and stiffness properties (See Example 7-3):

σ_{xu} = 12,500 psi (compression); τ_{xu} = 3,000 psi

E_{11} = 1,400,000 psi; E_{22} = 700,000 psi; G_{12} = 315,000 psi

$\nu_{12} = 0.36$; $\nu_{21} = 0.18$

2. Section properties:

$$A = 0.7 \times 9 \times 2 + 0.7 \times (16 - 1.4) = 22.82 \text{ in}^2$$

$$I_1 = 0.7 \times 9 \times 7.65^2 \times 2 + \frac{0.7 \times 14.6^3}{12} = 918.9 \text{ in}^4; \; S_1 = \frac{918.9}{8} = 115 \text{ in}^3$$

$$I_2 = \frac{.7 \times 2 \times 9^3}{12} + \frac{14.6 \times .7^3}{12} = 85.5 \text{ in}^4$$

$$r_1 = \sqrt{\frac{I_1}{A}} = \sqrt{\frac{918.9}{22.82}} = 6.35 \text{ in}; \; r_2 = \sqrt{\frac{85.5}{22.82}} = 1.94 \text{ in.}$$

2.1 Bending. Use load factor of 2.0

$$M_u = \frac{0.5 \times 12^2 \times 2.}{8} = 18.0'\text{k} \times 12 = 216 \text{ "-k}; \; \max \sigma_{xb1} = \frac{216}{115} = 1.88 \text{ ksi}$$

3. Determine the form factor, Q, for local buckling under axial compression alone: This may be governed by either the local buckling resistance of the flanges or the web.

Flange: $\frac{b_f}{2t_f} = \frac{9}{2 \times .70} = 6.4$

---

* See note on Example 7-1, page 7-5.

Example 7-C (continued)

Eq. 6.98: $\sigma_{xc} = \frac{G_{12}}{(b_f/2t_f)^2} = \frac{315,000}{(6.4)^2} = 7,690$ psi; $Q = \frac{7690}{12,500} = 0.615$

Web - for uniform compression: Eqs. 6.92 and 6.92a: $\sigma_{xc} = \frac{2\pi^2}{b^2 t}(\sqrt{D_{11} D_{22}} + D_o)$

$$\sigma_{xc} = \frac{2\pi^2}{(14.6)^2 \times 0.7} (0.7^3 \sqrt{124,800 \times 62,400} + 75,000 \times 0.7^3)$$

Note: See Example 7-3 for calculation of D_{11}, D_{22} and D_o

$\sigma_{xc} = 7,396$ psi 7,400 psi; Use $Q = \frac{7,400}{12,500} = 0.59$

Post buckling strength of the web is not used because web must also carry shear and bending from lateral load.

4. Ultimate axial compression strength: K = 1.0 for simply supported ends, with respect to both 1-1 and 2-2 axes; L_1 = 12 ft.; L_2 = 6 ft.

$$\frac{KL_1}{r_1} = \frac{12 \times 12}{6.35} = 22.7; \quad \frac{KL_2}{r_2} = \frac{6 \times 12}{1.94} = 37.1$$

Eq. 7.18a: $C'_c = \sqrt{\frac{2\pi^2 E}{Q\sigma_{xu}}} = \sqrt{\frac{2\pi^2 \times 1,400,000}{7,400}} = 61.$

Note: $Q\sigma_{xu} = 0.59 \times 12,500 = 7,400$ psi

When $\frac{KL}{r_2} < C'_c$, use Eq. 7.20 for transition zone (Fig. 7-4, curve 5):

$$\sigma_{xac} = Q\sigma_{xu} - \frac{(Q\sigma_{xu})^{1.5}}{2\pi\sqrt{2E}} \left(\frac{KL}{r_2}\right) = 7,400 - \frac{(7,400)^{1.5} \times 37.1}{2\pi\sqrt{2 \times 1,400,000}} = 5154 \text{ psi}$$

5. Ultimate bending compression strength, based on lateral buckling resistance, material compression strength, or local buckling resistance.

Eq. 7.50: $\sigma_{xblc} = 0.65\, C_1 E_{11} \frac{b_f t_f}{L d} \leq Q\sigma_{xu}$

With brace at midspan ($M_2 = M_{max}$ and $M_1 = 0$), from Eq. 7.39: $C_1 = 1.75$

$\sigma_{xblc} = 0.65 \times 1.75 \times 1,400,000 \times \frac{9 \times 0.7}{72 \times 16} = 8708$ psi $> Q\sigma_{xu} = 0.615 \times 12,500$ psi $= 7700$

Use $Q\sigma_{xbu}$ = 7.7 Ksi

6. Bending amplification factor (Eq. 7.80):

Amplification factor for bending about axis 1-1 in Eq. 7.80 is $(1 - \sigma_{xa}/\sigma_{xalc})$. σ_{xale} is the Euler buckling stress about axis 1-1, and is obtained using Eq. 7.17.

Example 7-6 (continued)

Eq. 7.17: $\sigma_{xale} = \dfrac{\pi^2 E_{11}}{(L/r_1)^2} = \dfrac{\pi^2 \times 1{,}400{,}000}{(22.7)^2} = 26{,}815 \text{ psi} = 26.8 \text{ ksi}$

Note: Use Euler stress even if $\sigma_{xale} > \sigma_{xu}$

also, σ_{xa} is the axial stress, P_u/A: $\sigma_{xa} = P_u/22.8$

Thus, amplification factor $= 1 - \dfrac{P_u}{22.8 \times 26.8} = 1 - \dfrac{P_u}{611}$

7. Bending reduction factor, C_{m1} (Eq. 7.80): Table 7-3, Case 1; $C_{m1} = 1.0$

8. Determination of P_u, based on interaction equation, Eq. 7.80

$$\frac{\sigma_{xa}}{\sigma_{xac}} + \frac{C_{m1}\,\sigma_{xb1}}{\sigma_{xb1c}\left(1 - \dfrac{\sigma_{xa}}{\sigma_{xale}}\right)} = 1.0; \quad \frac{P_u}{22.8 \times 5.154} + \frac{1.0 \times 1.88}{7.7(1 - P_u/611)} = 1.0$$

$$\frac{P_u}{117.5} + \frac{0.244}{(1 - P_u/611)} = 1.0$$

Cut and Try Solution:

P_u kips	$(1 - P_u/611)$	$P_u/117.5$	$0.244/(1 - P_u/611)$	$\Sigma = 1.0$	
85	0.861	0.723	.283	1.006	
84	0.863	0.715	.283	.998	1.00

Result: Maximum ultimate axial thrust that can be added = 84k. Using a load factor of 2.0, the maximum design axial thrust is 42k.

Note:

1 in. = 25.4 mm, 1 in^2 645 mm^2, 1 in^3 = 16,387 mm^3, 1 in^4 = 416,231 mm^4, 1 ft = 0.3048 m, 1 Kip = 4.448 KN, 1 in-k = 113 N-m, 1 ft-k = 1.356 KN-m, 1 lbf/ft = 14.59 N/m, 1 psi = 6.895 KPa, 1 Ksi = 6.895 MPa

7.6 RIBBED PANELS

When plastics are used for flat components that resist transverse loads, configurations comprised of corrugated shapes or flat sheets with ribs are often used. See Figs. 4-4, 4-5 and 4-6 in Section 4.4 for typical panels with various types of open corrugations, solid ribs or closed hollow ribs. Most of these panel types have a system of ribs that span between support members along ends of the panel. Such panels are designed as one-way spanning beams. Panels may be simply supported by members located at panel ends, or they may be multiple span continuous beams supported by members located at intermediate points in the panel length.

Design considerations are the same as previously described in Section 7.4 for beams having open thin-wall sections or tubular sections. These include panel flexural strength based on tension and compression strength of the respective tension and compression flanges, in-plane bending and shear strength of the web, in-plane and interlaminar shear strength of the flanges, local buckling of both the compression flange and the web, and panel deflection. If a ribbed flat panel is used to support axial load as a column or bearing wall, design procedures given in Section 7.3 should be followed.

The section properties of a common type of corrugated panel formed of undulating circular arcs of equal radii are given in Fig. 7-18 as a function of the pitch-depth ratio, as defined in the Figure. This chart facilitates the rapid calculation of section properties for this type of corrugated panel.

When a concentrated load is applied at a single rib, or at a point between two ribs, on a panel with multiple ribs, the load effects are distributed partly to the directly loaded ribs and partly to ribs beyond the loaded ribs. The analysis required for an accurate determination of the load distribution between ribs is complex and beyond the scope covered here. Studies developed for bridge decks (7.8) (7.9) provide some useful approximate procedures for obtaining load distribution between the transverse ribs. Also, as explained in Chapter 6, the ribbed panel can be considered to be an orthotropic plate; in this approach stress resultants may be determined using charts or tables provided in references given in Chapter 6. Sometimes, it is sufficiently accurate for design to consider that the entire concentrated load is carried by the loaded rib, or ribs, with no distribution of load effects to adjacent ribs. This assumption is most applicable to ribbed panels with thin facings that do not have "distribution ribs" running perpendicular to the primary ribs spanning between panel supports.

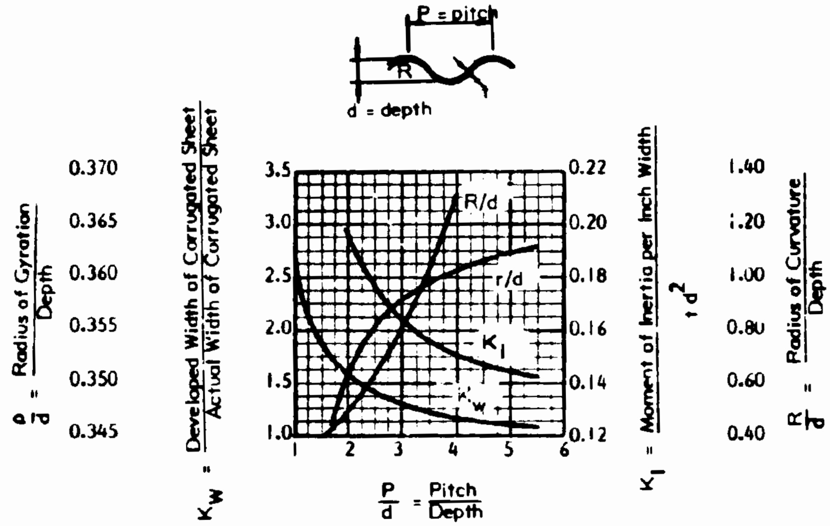

Fig. 7-18 SECTION PROPERTIES OF PANELS WITH CIRCULAR ARC CORRUGATION (7.15)

The design of a single-span corrugated wall panel with circular arc corrugations is illustrated in Example 7-7. The design of a single span flat panel with hollow ribs that forms the deck of a marine floating dock is illustrated in Example 7-8.

7.7 LARGE BOX AND T-BEAMS

When structural plastics are considered for large structural componenets, a "box type" configuration, comprised of wide ribbed or sandwich panel flanges integral with deep webs, is often an efficient structure that can be economically fabricated. Such a member is shown in Fig. 7-19a. A few examples in existing usage include footbridges in sewage plants, floating docks and walkways at Marinas, freezer truck bodies, cargo containers, and aircraft bodies.

If the wide flanges or covers of a box beam with multiple webs occur only on one side of the webs, the overall cross section is a T configuration instead of a box as shown in Fig. 7-19b. Large structures with "box" or "T" configurations often behave as beams and their design is based on the methods and criteria given above in Section 7.4. However, flange components may first have to be designed as local bending members, spanning transversley between webs. This is illustrated in Example 7-8 in Section 7.6.

Example 7-7: Determine the required thickness of a transparent acrylic plastic corrugated sheet wall panel with a pitch of 5 inches and a depth of 2 inches to safely span 60 inches (simply supported) under a short-term (wind) design load of 20 lbs per sq. ft. (suction or pressure). Limit the maximum service load deflection to span length divided by 120 (i.e., 0.5 in.) Assume the following minimum test properties for the acrylic material:*

Tension Strength	9,000 psi
Compression Strength	11,000 psi
Flexural Strength	12,000 psi
Elastic modulus	400,000 psi

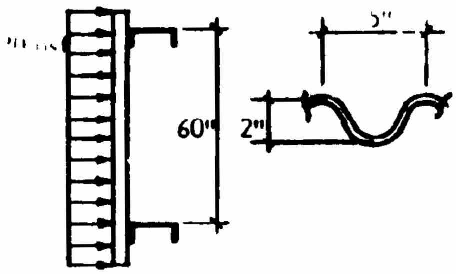

1. Reduced ultimate strength and stiffness: Assume capacity reduction factors for wind load as 0.3 for tension, 0.4 for flexure, 0.5 for compression and 0.9 for elastic modulus. The lower capacity reduction factors for tension and flexure are selected because acrylics tend to behave as brittle materials.

   Use load factor of 2.5

2. Bending strength:

   $M_{xu} = \frac{20 \times 5^2 \times 2.5}{8} = 156$ ft-lbs/ft or in-lbs/in, where 2.5 is the load factor

   Required section modulus, S_l: Eq. 7.33: $S_l = \frac{M}{\sigma_{xu}} = \frac{156}{.3 \times 9000}$ ** $= 0.058$ in^3/in

   Thus, $I_l = S_l \, d/2 = 0.058 \times 1.0 = 0.058$ in^4/in

** Note: "tension" rather than "flexure" governs, because the full thickness of the sheet is stressed at the maximum tension stress at the trough at midspan. In this formulation, the variation in stress over the thickness of the sheet is neglected for thin sheets.

From Fig.7-18 for pitch/depth ratio = 5/2 = 2.5: $I_l = 0.180 \, t \, d^2$; thus:

$$\text{req'd } t = \frac{I_l}{.180 \times d^2} = \frac{0.058}{0.180 \times 2 \times 2} = 0.081 \text{ in.}$$

3. Bending deflection: On one inch wide strip: $W = 20 \times \frac{60}{144} = 8.33$ lbs/in. width

   Table 5-1: $\delta_m = \frac{5WL^3}{384EI} = \frac{5 \times 8.33 \times 60^3}{384 \times .9 \times 400{,}000 \times 0.058} = 1.122$ in.

   allow $\delta_m = \frac{L}{120} = \frac{60}{120} = 0.50$ in.

   Increase thickness to $t = \frac{1.122}{0.50} \times 0.081 = 0.182$ in., since I_l increases linearly with t

* See note on Example 7-1, page 7-5.

Example 7-7 (continued)

4. Local buckling resistance: furn $S_I = 2I_I/d = 2 \times 0.180 \times 0.182 \times 2^2/2.0 = 0.131\ in^3/in$

max. req'd $\sigma_x = \frac{156}{0.131} = 1190 \quad 1200$ psi

Conservative approximate buckling strength is given by buckling resistance of cylindrical shell under longitudinal compression (Section 9.10):

Fig 7-18: radius of curvature, R = 0.65d for pitch/depth = 2.5; R = 0.65 x 2 = 1.30 in.

Eq. 9.74 $\quad \sigma_{xc} = \frac{C\,E\,t}{R} = \frac{k_o\,k_n\,E\,t}{R}$

Fig. 9-25 for bending with $R/t = \frac{1.30}{.182} = 7.14$: $k_n \doteq 0.85$

Also for isotropic materials with $\nu = 0.3$; $k_o = 0.6$

$$\sigma_{xc} = \frac{0.6 \times 0.85 \times 0.9 \times 400{,}000 \times 0.182}{1.3} = 25{,}700 \text{ psi} > 1200 \text{ psi}$$

Local buckling does not govern

5. Use a thickness of 3/16 in. with a corrugation having 5 in pitch and 2 in. depth center to center of sheet.

From Fig. 7-18, the required width of equivalent flat sheet is $K_w = 1.45$ times the laying width of corrugated sheet plus any required side laps. Area of sheet section = 1.45t x (laying width + side laps).

---

1 in = 25.4 mm, 1 in^3/in = 645 mm^3/mm, 1 in^4 = 16,387 mm^4/mm. 1 ft-lbf/ft = 4.448 N-m/m, 1 in-lbs/in = 4.448 N-mm/mm, 1 lbf/in = 0.175 N/mm, 1 psi = 6.895 KPa, 1 lbf/ft^2 = 47.88 Pa

Example 7-8: Design a deck panel that spans 6 ft. (simply supported) and provides a walkway for floating slipways in a small boat marina. Transverse and longitudinal sections through the walkway showing the required deck panel are:*

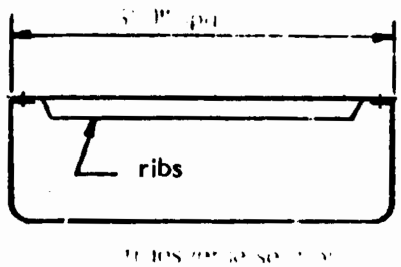

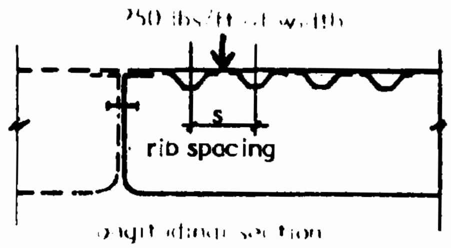

Assume the following design loads: Uniformly distributed: 100 lbs/sq.ft. (includes panel weight)
Line: 250 lbs/ft (See longitudinal section)

Use a fiberglass reinforced plastic laminate with alternate layers of mat and woven roving and polyester resin. Assume the following mechanical properties, based on short time tests in wet environment:

Tension Strength: 20,000 psi; Compression and Flexural Strength: 25,000 psi;

Shear Strength (in-plane): 6,000 psi; Shear Strength (interlaminar): 1,500 psi;

Elastic Moduli: $E_{11} = E_{22} = 1{,}500{,}000$ psi; $G_{12} = 450{,}000$ psi;

Poisson's ratio: $\nu_{12} = \nu_{21} = 0.2$

Use the rib arrangement shown in the sketch at the right. The rib is layed up wet over a cardboard core whose contribution to strength, stiffness and local buckling resistance is neglected.

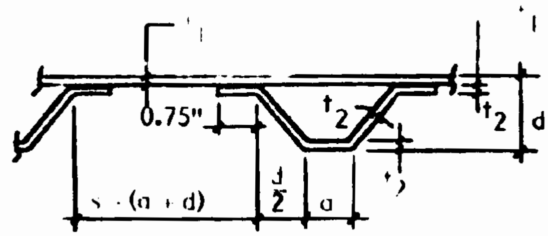

1. Use the following capacity reduction factors, ϕ, for reduced ultimate strength properties and service stiffness properties (design loads are applied intermittently over a long period of time): Tension, Compression, flexure and in-plane shear: ϕ = 0.5; Interlaminar shear strength: ϕ = 0.3; Elastic Moduli: ϕ = 0.8

2. Use a load factor of 1.7

3. Determine thickness, t_1, of deck sheet, and clear spacing between ribs.

3.1 Try t_1 = 0.3 in. Let clear span between supports = s' = s - (a + d). Line load will govern local flexural stresses, transverse direction, between ribs.

---

* See note on Example 7-1, page 7-5.

Example 7-8 (continued)

$P_u = \frac{250 \times 1.7}{12} = 35.4$ lbs/in. width

3.2 Check strength criteria:

applied $M_u \approx \frac{P_u \times s'}{5} = \frac{35.4 \times s'}{5} = 7.08\, s'$ in-lbs/in

Note: Coefficient 1/5 allows for effects of some end fixity.

Flexural strength, $\sigma_{xu} = 0.5 \times 25{,}000 = 12{,}500$ psi

$S_l = \frac{b\, t_l^2}{6} = \frac{1 \times 0.3^2}{6} = 0.015\ \text{in}^3/\text{in.}$

allowed max. $M_u = \sigma_{xu} S_l = 12{,}500 \times 0.015 = 187.5$ in-lbs/in

max. allowed clear span: $7.08\, s' = 187.5;\ s' = 26.5$ in

3.3 Check deflection criteria:

Table 5-1: Assume end restraint results in deflection midway between simply supported and fixed end cases.

$\delta_m = \frac{K_m P s'^3}{EI}$; $P = 250/12 = 20.8$ lbs/in. at midspan; $K_m = (\frac{1}{48} + \frac{1}{192}) \times \frac{1}{2} = 0.013;$

$E = 0.8 \times 1{,}600{,}000 = 1{,}280{,}000$ psi; $I = \frac{b\, t_l^3}{12} = \frac{1 \times 0.3^3}{12} = 0.00225\ \text{in}^4$

allow $\delta_m = \frac{\text{span}}{300} = \frac{s'}{300}$ to avoid excessively "soft" feel

$\frac{s'}{300} = \frac{.013 \times 20.8\, s'^3}{1{,}280{,}000 \times 0.00225} = \frac{0.094\, s'^3}{1000}$; max $s' = \sqrt{\frac{10}{.094 \times 3}} = 5.95 \quad 6$ in.

Conclusion: If deck sheet is 0.3 in thick, clear distance between ribs should not exceed 6 in.

4. Determine center to center rib spacing and rib dimensions:

4.1 Try ribs at 12 inches on center: Either line load or uniformly distributed load may govern design. Ribs span 6 ft. as simply supported beams

$P_u = 250 \times 1.0 \times 1.7 = 425$ lbs.; $W_u = 100 \times 1.0 \times 6.0 \times 1.7 = 1020$ lbs.

Since distributed load, W_u, is more than twice concentrated line load, P_u, W_u will govern design.

4.2 Strength criteria:

applied $M_u = \frac{1020 \times 6. \times 12}{8} = 9{,}180$ in-lbs/rib

if we can develop full strength of laminate: $\sigma_{xu} = 0.5 \times 20{,}000 = 10{,}000$ psi

Example 7-8 (continued)

Eq. 7.33: req'd $S_1 = \frac{M_u}{\sigma_{xu}} = \frac{9180}{10,000} = 0.92\ in^3/rib$

4.3 Stiffness criteria

$\frac{L}{300} = \frac{5}{384}\frac{WL^3}{EI}$; req'd $I = \frac{3.91\ WL^2}{E} = \frac{3.91 \times 600 \times 72^2}{1,280,000} = 9.50\ in^4/rib$

4.4 Rib dimensions, using trial approximations

(1) Initial estimate of proportions and section properties:

Compression flange area = $0.3 \times 12 = 3.6\ in^2$

If effective tension flange area $\approx 0.2 \times$ compression flange $= 0.2 \times 3.6 = 0.7\ in^2$

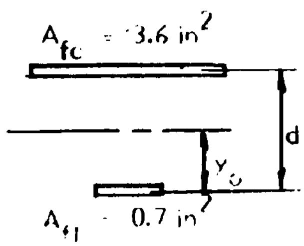

Trial c.g., $y_o = \frac{3.6d}{3.6 + 0.7} = 0.84d$

Trial $I_1 = 3.6 \times (.16d)^2 + 0.7 \times (0.84d)^2 = 0.586d^2$

Trial min. $S_1 = \frac{0.586d^2}{.84d} = 0.7d = 0.92$; trial d = 1.31 in.

Trial min. $I_1 = 0.586\ d^2 = 9.50$; trial d = 4.0 in.

(2) Limiting width-thickness ratio of deck sheet to preclude local buckling with d = 4 in. & I = 9.50 in^4/ft:

top $S = \frac{9.50}{0.16 \times 4} = 14.8\ in^3/rib$; $\sigma_x = \frac{9,180}{14.8} = 620$ psi

Eq. 6.71a: $\sigma_{xc} = \frac{k\pi^2 E}{12(1-\nu^2)}\left(\frac{t}{b}\right)^2 = 620$; $k = 4.0$

$\max\left(\frac{b}{t}\right) = \sqrt{\frac{4\pi^2 \times 1,280,000}{620 \times 12(1 - 0.2^2)}} = 84.1$; if t = 0.3, max b = 25.2 in o.k.

Use max. (a + d) = 6 in., as governed by transverse stiffness, d = 4 in., a = 2 in.,

(3) if tension flange A = 0.7 in^2: $0.7 = (1.12d \times 2/6 + a)\,t_2$

$0.7 = (0.37 \times 4 + 2)t_2$; min $t_2 = \frac{0.7}{3.49} \approx 0.20$ in.

Try $t_2 = 0.25$ in.

Example 7-8 (continued)

(4) Trial proportions of rib and section properties:

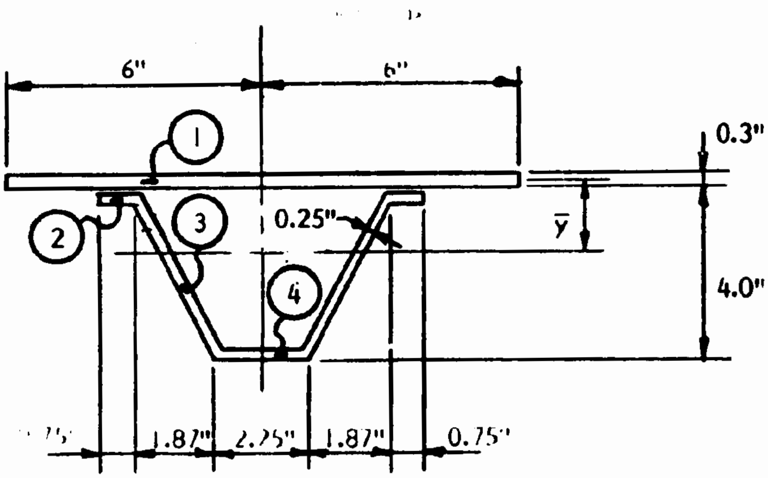

Segment	Area		A in^2	y in	Ay in^3	Ay_o^2 in^4	I_o		
1	0.3 x 12	=	3.60	0.	0.	3.82	$3.6 \times .3^2/12$	=	0.03
2	0.25 x 0.75 x 2	=	.38	0.27	0.10	0.22	negl.		
3	0.25 x 1.12 x 4 x 2	=	2.24	2.15	4.82	2.81	$2.24 \times 4^2/12$	=	2.99
4	0.25 x 2.	=	.50	4.	2.00	4.41	negl.		
			6.72		6.92	11.26			3.02
									11.26
									14.28

$\bar{y} = \frac{6.92}{6.72} = 1.03$ in.; $I_o = 14.28$ in^4 9.50

t_2 may be reduced to about .25 x 9.5/14.3 = .17 in and the above calculation for section properties repeated.

Local buckling will not govern bottom flange which is in tension, nor webs which are o.k. by inspection, since stresses are low because of the rib depth required for stiffness.

---

1 in = 25.4 mm, 1 in^2 = 645 MM^2, 1 in^3 = 16,387 mm^3, 1 in^3/in = 645 mm^3/mm, 1 in^4 = 416,231 mm^4, 1 in^4/ft = 1,365,587 mm^4/m, 1 ft = 0.3048 m, 1 lbf = 4.448 N, 1 lbf/in = 0.175 N/mm, 1 lbf/ft = 14.59 N/m, 1 in-lbs/in = 4.448 N-mm/mm, 1 psi = 6.895 KPa, 1 lbf.ft^2 = 47.88 N/m^2, 1 in-lbf = 113 N-mm

Sometimes, the proportions of large box and T beams require consideration of effects that are normally neglected in the elementary theory of flexure used for practical design of most bending members. The elementary theory is based on the assumption that "plane sections before bending remain plane after bending". By this assumption, shear strain is neglected. However, shear strain causes important modifications of the distribution and magnitude of normal and shear stress when either the depth, or the width, of a box section is large relative to the span of the box beam.

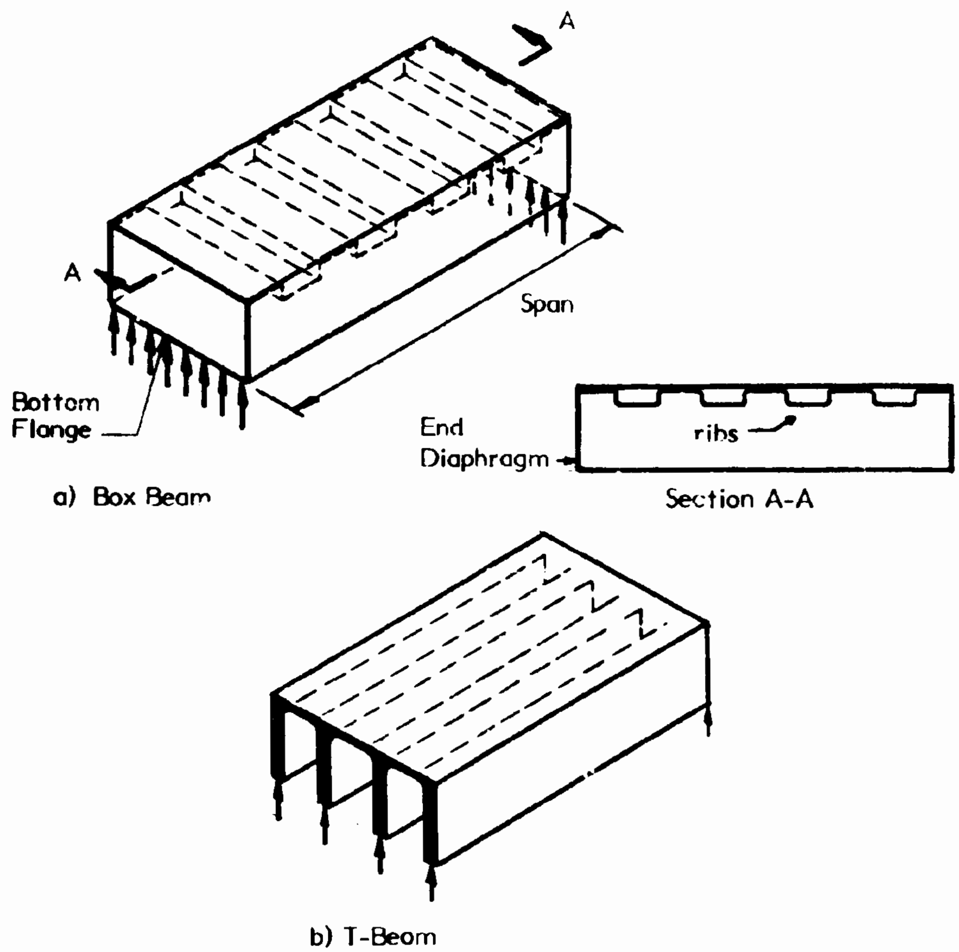

Fig. 7-19 BOX AND T-BEAMS

Box T or beams that have span to web depth ratios that are less than about 1 to 2 (for simple spans) or span to flange width ratios that are less than about 5 for uniform load and 8 for concentrated load (for simple spans) should probably be analyzed by methods that account for effects of shear strain. This can be done using finite element analysis with element stiffnesses that account for both axial and shear deformation. Also, the above span-to-depth, and span-to-width, ratios are based on isotropic materials having a Poisson's Ratio, ν, of 0.3. Significant differences may be expected with orthotropic materials and with materials with a low in-plane shear modulus, G.

Solutions for stresses in deep rectangular isotropic beams are given in Section 6.8. These are not applicable to deep beams with flanges, but indicate the general nature of the effects of low span-depth ratios. In deep beams, the effectiveness of the flange is reduced and rough design could be based on the web only behaving as a rectangular diaphragm plate.

The modification in flange normal stress caused by shear deformation in wide flanges is usually called **shear lag**. This is discussed in Section 7.4. Again, the approximations given in that section apply only to beams with isotropic materials and $\nu = 0.3$. Shear lag in members with wide flanges is usually taken into account by using a reduced flange width, termed the "effective" flange width.

The "effective flange width" is the flange width of an equivalent beam with uniform flange stress having the same maximum flange stress, or mid-span, deflection, as the maximum flange stress in the actual beam with non-uniform flange stress caused by shear lag. See Fig. 7-14 for graphs giving effective flange width/actual flange width ratios as a function of span/flange width ratio's for simply supported and cantilever box and I-beams subject to uniformly distributed load or concentrated loads at midspan or one-third span. Fig. 7-14(a) gives the effective width, b_e, for calculating effective section modulus for determining maximum flange stress at the section of maximum moment, while Fig. 7-14(b) gives the effective width, b'_e, for calculating the average moment of inertia for determining mid-span deflection.

The design of a large box section beam with a wide flange is presented in **Example 7-9.** An effective flange width is determined using the above method to account for shear lag.

Example 7-9: Develop a prototype design for the entrance canopy roof shown in the sketch as a transparent glass reinforced polycarbonate plastic cantilevered box beam.*

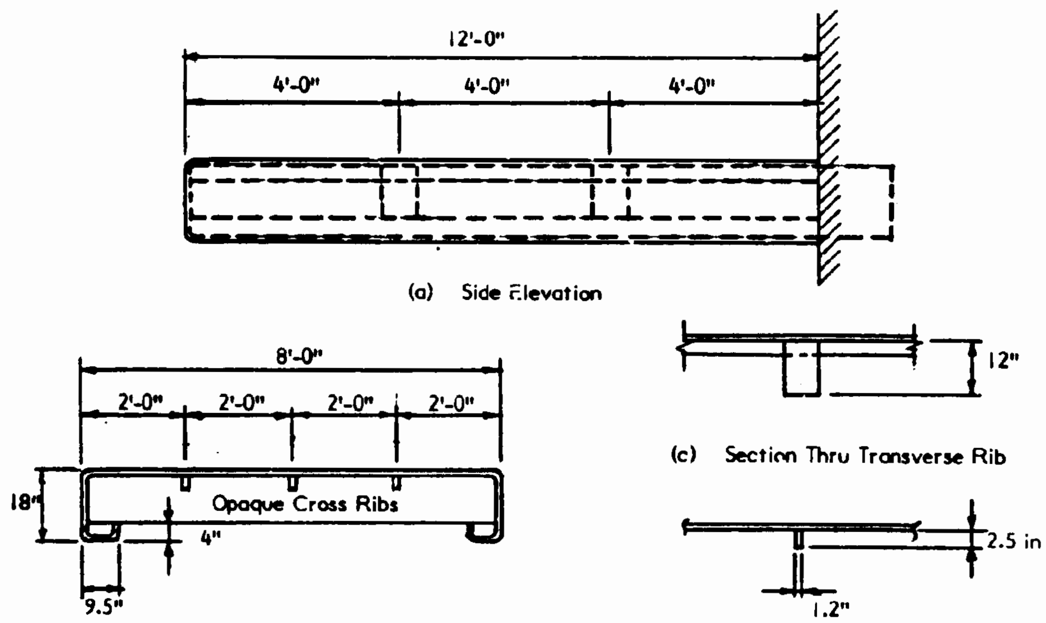

(a) Side Elevation

(b) Transverse Section

(c) Section Thru Transverse Rib

(d) Section Thru Longitudinal Rib

Design loads are 100 psf at the wall, varying linearly to 50 psf at tip, for drifted snow and dead load of structure, and 15 psf for net wind uplift. Assume the following materials properties, based on short time tests: tensile strength = 12,000 psi, flexural strength = 15,000 psi, compressive strength = 12,000 psi, in-plane shear strength = 8,000 psi, initial elastic modulus = 800,000 psi, Poisson's ratio = 0.35. Limit the tip deflection to 1.5 in. under maximum design snow load, and the deflection of ribs and deck sheet to 0.5 in.

1. Use capacity reduction factors for snow load of 0.5 for tension and shear, 0.6 for local flexure and for compression, and 0.8 for initial elastic modulus. Multiply the above values by 1.2 for wind load.

   Thus, for snow load: σ_{xu} in tension = 0.5 x 12,000 = 6,000 psi; σ_{xu} in local flexure = 0.6 x 15,000 = 9,000 psi; σ_{xu} in compression = 0.6 x 12,000 = 7,200 psi, σ_{xu} for in-plane shear = 0.5 x 8,000 = 4,000 psi; E = .8 x 800,000 = 640,000 psi.

   Use a load factor of 2.0 for strength under snow and wind loads.

2. Determine top skin thickness for 3 longitudinal ribs equally spaced at 24 inches.

2.1 Establish trial thickness for deflection control with the aid of Figs. 6-4 and 6-5. Estimate that edge restraints are midway between rotationally fixed and pinned, and also about midway between "edges held" and "edges free to translate."
$\frac{a}{b} = \frac{48}{24} = 2.0$; $\frac{w_c}{t} = \frac{0.5}{t}$; In bay closest to wall, load averages (100 + 83) ÷ 2 ÷ 144 = 0.64 psi

---
* See note on Example 7-1, page 7-5.

Example 7-9 (continued)

Poisson's index, $k_o = \frac{0.35}{0.30} = 1.17$; $(k_o \frac{q}{E})^{1/4} = (\frac{1.17 \times 0.64}{640{,}000})^{1/4} = \frac{1}{30.4}$

Try $t = 0.3$ in.; for $\frac{w_c}{t} = \frac{0.50}{0.30} = 1.67$ and $a/b = 2.0$ in Figs. 6-4 & 6-5 for average of edge support cases in these Figures:

req'd $\frac{b}{t} = (k_o \frac{q}{E})^{1/4} = (2.1 + 3.3 + 2.8 + 3.6) \div 4 = 2.95$

$\frac{24}{t} \times \frac{1}{30.4} = 2.95$; $t = \frac{24}{30.4 \times 2.95} = 0.27$ in.; Use trial sheet thickness = 0.30 in.

2.2 Check strength: First try 1 in. wide simple beam strip as a conservative approximation.

$M_u = \frac{0.64 \times 2.0 \times 24^2}{8} = 92$ lbs/in.: $S = \frac{1 \times t^2}{6} = \frac{0.3^2}{6} = 0.015$ in^3

$\sigma_x = \frac{92}{0.015} = 6133$ psi   9,000 psi

Actual maximum stress wil be substantially less because of two-way bending and membrane action. A more accurate check could be made using Figs. 6-6 to 6-9 for "large deflection" plate analysis. However, since $\sigma_x < 9{,}000$ psi above, there is no need for this.

3. Design longitudinal ribs for 1.2 inch trial width. (4 - 0.3 in thick strips laminated vertically, see Sketch d.) Span = 48 in between transverse ribs.

3.1 Strength: End span has maximum moment.

Approx. $M_u = \frac{184 \times 2.0 \times 4 \times 48}{8} = 8{,}832$ in-lbs; where 2.0 is the load factor for ultimate.

Req'd $S = \frac{8832}{6000} = 1.47$ in^3

Note: 6000 psi tensile strength is used instead of 9000 psi flexure; bottom lamination is mostly in tension.

if we neglect flange of "T" section: $S = \frac{bh^2}{6}$ and $b = 1.2$ in.

req'd $h^2 = \frac{6 \times 1.47}{1.2} = 7.36$; $h = 2.71$ in.

Try $h = 2.5$ in and consider an effective T-flange width of 8t on each side of stem.

	A	y	Ay	y_o	Ay_o^2	I_o	
6 x 0.3	= 1.8	0	0	0.87	1.36	neglect	= 0
2.5 x 1.2	= 3.0	1.40	4.20	0.53	.84	$1.2 \times 2.5^3/12$	= 1.56
	4.8		4.20		2.20		1.56
					1.56		

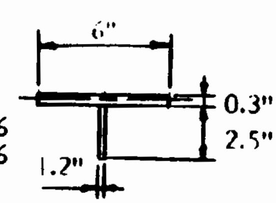

$\bar{y} = \frac{4.20}{4.8} = 0.88$ in.; $I_o = 3.76$ in^4; min $S = \frac{3.76}{1.78} = 2.11$ 1.47 o.k.

3.2 Check deflection - End span:

Approx. $\delta_m = \frac{1}{2} \times \frac{5}{384} \frac{WL^3}{EI} = \frac{1}{2} \times \frac{5 \times 184 \times 4 \times 48^3}{384 \times 640{,}000 \times 3.76} = 0.22$ in.   o.k.

Example 7-9 (continued)

4. Transverse ribs: Assume glued laminated wood used. Design is not presented for lack of space.

5. Design of Main Box Beam: (Use one side of symmetry line.)

5.1 Ultimate loads:

$w_{1u} = 50 \times 1.0 \times 2.0 \text{ (load factor)} = 100 \text{ psf}; \quad w_{2u} = 100 \times 1.0 \times 2.0 = 200 \text{ psf}$

$P_{1u} = (50 \times 3 \times 2 + 17 \times \frac{3}{2} \times \frac{4}{3}) \times 2.0 = 668 \text{ lbs}$

$P_{2u} = (50 \times 3 \times 2 + 17 \times \frac{3}{2} \times \frac{8}{3} + 67 \times 3 \times 2 + 17 \times \frac{3}{2} \times \frac{4}{3}) \times 2.0 = 1608 \text{ lbs}$

$P_{3u} = (67 \times 3 \times 2 + 17 \times \frac{3}{2} \times \frac{8}{3} + 83 \times 3 \times 2 + 17 \times \frac{3}{2} \times \frac{4}{3}) \times 2.0 = 2004 \text{ lbs}$

5.2 Maximum ultimate shear & moment - stress resultants:

$V_u = 100 \times 12 + 100 \times \frac{12}{2} + 668 + 1608 + 2004 = 6080 \text{ lbs}$

$M_u = 100 \times 12 \times \frac{12}{2} + 100 \times \frac{12}{2} \times \frac{12}{3} + 668 \times 12 + 1608 \times 8 + 2004 \times 4 = 38{,}496 \text{ ft-lbs}$

5.3 Required Section Modulus, Web Area for Shear and Moment of Inertia:

Upper flange in tension: req'd $S_1 = \frac{M_u}{\sigma_{xu}} = \frac{38{,}496 \times 12}{6000} = 77 \text{ in}^3$

Lower flange in compression: req'd $S_1 = \frac{38{,}496 \times 12}{7200} = 64 \text{ in}^3$

Web in shear: req'd $A_w = \frac{V_u}{\tau_{xu}} = \frac{6080}{4000} = 1.5 \text{ in}^2$

Deflection limit: Cantilever beam not included in Table 5-1. Use Ref. (5.5), cases 18 and 19. For service loads:

$$\delta_m = \frac{WL^3}{15EI} + \frac{WL^3}{8EI}$$

$$\delta_m = \frac{50 \times 4 \times 12/2 \times 12^3 \times 12^3}{15 \times 640{,}000 \text{ I}} + \frac{50 \times 3 \times 11 \times 12^3 \times 12^3}{8 \times 640{,}000 \text{ I}} = 1.5 \text{ in.}$$

$$1.5 = \frac{373}{I} + \frac{962}{I} = \frac{1335}{I}; \quad \text{min. } I = 890 \text{ in}^4$$

5.4 Trial Proportions - Try to maintain 0.3 in constant thickness so that shape can be thermoformed. Section modulus for bending strength, or moment of inertia for bending stiffness will govern by inspection.

(1) Maximum width of lower flange to develop compressive σ_{xu} without local buckling.

$$\frac{b_f}{t_f} = C_b \sqrt{\frac{E}{\sigma_{xu}(1 - \nu^2)}}; \quad C_b \text{ from Case 3 in Table 7-1} = 1.8, \text{ as trial value}$$

$$\frac{b_f}{t_f} = 1.8 \sqrt{\frac{640{,}000}{7{,}200(1 - .35^2)}} = 18.1$$

Example 7-9 (continued)

Max. width of bottom flange to develop 7200 psi in compression:

$b_f = 0.3 \times 18.1 = 5.4$ in.

(2) Maximum depth of web to develop compressive σ_{xu} without local buckling:

C_b from Table 7-1 = 4.4; $d_w = 5.4 \times 4.4/1.8 = 13.2$ in.

(3) Maximum depth of edge return for inner edge of bottom flange to develop compressive σ_{xu} without local buckling - assume uniform compression.
C_b from Case I in Table 7-1 = 0.6. $b_f = 5.4 \times 0.6/1.8 = 1.8$ in.

Min. stiffness to brace inner edge of bottom flange:

Eq.7.2: $I_s = 2.0\, t^4 \sqrt{(\frac{b}{t})^2 - \frac{0.19E}{\sigma_{xu}}} = 2.0 \times 0.3^4 \sqrt{(\frac{5.5}{0.3})^2 - \frac{0.19 \times 640}{7.2}} = 0.29\ \text{in}^4$

Determine I_s about centroid of 2 in. trial lip plus 2 in. radius section;

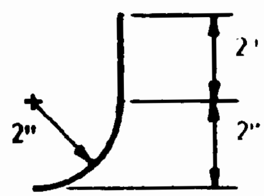

Lower limit for $I_s = 0.3 \times 4^3/12 = 1.6\ \text{in}^4$

No need to calculate accurate value for I_s.

(4) Try the following section:

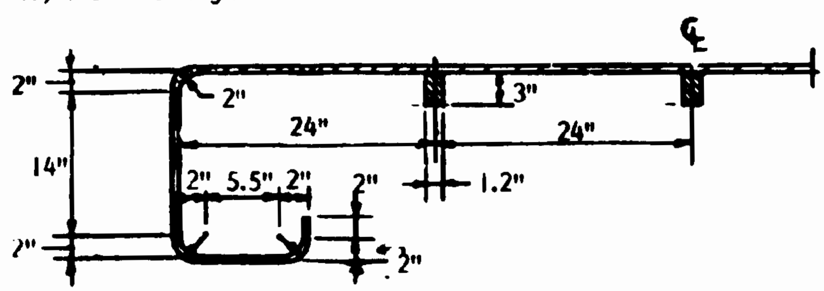

(5) Estimate effective properties of beam including correction for shear lag in top flange.

Effective Top flange area, as reduced due to shear lag.

(a) For maximum flange tension:

From Fig. 7-14(a) for b/2L = 8/2 x 12 = 0.33

and using 0.8 times a cantilever beam with uniformly distributed load case as an approximation for our case of combined uniform and triangular (drift) distribution:

$b_e = 0.8 \times 0.25b = 0.20b$

Example 7-9 (continued)

The factor 0.8 is used because the triangular portion of the load produces a sharper build-up of moment near the root of the cantilever than in the uniformly distributed case, causing more lag in developing flexural normal stress in portions of the flange away from the edge.

Thus, take effective area of half the top flange, A_{Top}, for maximum stress as $(A_w/6 + b_e t_f/2 + b_e/b \times 1.5\ A_{stringer}$

$$A_{Top} = \frac{0.3 \times 18}{6} + \frac{0.20 \times 96 \times 0.3}{2} + 0.20 \times 1.5 \times 1.2 \times 3 = 4.8\ \text{in.}^2$$

(b) For deflection:

From Fig. 7-14(b) for $b/2L = 0.33$ and using the same cantilever beam case described above for flange stress: $b'_e = 0.8 \times 0.74b = 0.59b$

Thus, take effective area of half the top flange, A_{Top} for deflection as:

$$A'_{Top} = 0.9 + \frac{0.59 \times 96 \times 0.3}{2} + 0.59 \times 1.5 \times 1.2 \times 3 = 12.6\ \text{in.}^2$$

Bottom Flange Area:

$$A_{Bot} = \frac{A_w}{6} + b_1 t + b_2 t \quad \frac{0.3 \times 18}{6} + 0.3 \times 9.5 + 0.3 \times 2 = 4.4\ \text{in.}^2$$

Section Properties - Stress

$$\text{Centroid, } \bar{y} = \frac{4.8 \times (17\pm)}{9.2} = 8.87 \text{ in up from c.g. bot. flange.}$$

$$I_{ie} \quad 4.8 \times (17 - 8.9)^2 + 4.4 \times 8.9^2 = 663.5\ \text{in}^4$$

$$S_{leTop} = \frac{663.5}{8.6} = 77.1\ \text{in}^3 \approx \text{req'd } 77\ \text{in}^3$$

$$S_{leBot} = \frac{663.5}{9.4} = 70.5\ \text{in}^3 > \text{ req'd } 64\ \text{in}^3$$

Section Properties - Deflection:

$$\text{Centroid} - \bar{y} = \frac{12.6 \times (17\pm)}{17.0} = 12.6 \text{ in. up from c.g. bot. flange}$$

$$I'_{le} = 12.6 \times (17 - 12.6)^2 + 4.4 \times 12.6^2 = 942.5\ \text{in}^4 < \text{req'd } 1182\ \text{in}^4$$

Section may be overly flexible since estimated effective I is only about 80% of the required I.

A prototype should be built and tested since approximations have been used in the analysis and design of the prototype. Thickness could be increased to $1.2 \times 0.3 = 0.36$ in. or allowable deflection could be increased by 20%, if necessary, based on tests on the prototype. An additional longitudinal rib could be added in lieu of thickening the sheet. The prototype design will be continued using the previous section.

5.5 Check for web buckling:

$$\text{Av. shear stress } \tau_x = \frac{V_u}{A_w} = \frac{6080}{0.3 \times (14+)} = 1444 \approx 1450 \text{ psi}$$

Example 7-9 (continued)

To develop this stress: Table 7-1

$$\frac{d_w}{t_w} = C_b\sqrt{\frac{E}{\tau_{xc}(1-\nu^2)}}\ ;\ C_b = 2.1;\ \text{min. } t_w = \frac{14}{2.1\sqrt{\dfrac{640{,}000}{1450\,(1-.35^2)}}} = 0.30$$

o.k.

6. Checks for wind uplift loading case:

6.1 Ultimate loads and stress resultants.

To save space, only the check for overall bending of the box shape will be presented here.

Net w_{1u} = 15 x 1.0 x 2.0 = 30 plf.; P_{1u} = 15 x 3 x 2 x 2.0 = 180 lbs

P_{2u} = 2 x P_{1u} = 360 lbs.; P_{3u} = P_{2u} = 360 lbs

V_u = 30 x 12 + 180 + 360 + 360 = 1260 lbs

M_u = 30 x 12 x 12/2 + 180 x 12 + 360 x 8 + 360 x 4 = 8640 ft-lbs

6.2 Effective width of top flange in buckling. Treat flange as an outstanding flange of channel, with remainder of flange toward inside assumed as locally buckled. Determine maximum effective b_f, for various trial values of maximum stress. Use Case 1 in Table 7-1.

If $S_{top} \approx 40$ in^3, trial $\sigma_x = \dfrac{8640 \times 12}{40} = 2592$ psi

$$b_f = t_w C_b\sqrt{\frac{E}{\sigma_x(1-\nu^2)}} = 0.3 \times 0.6\sqrt{\frac{640{,}000 \times 1.2}{2592\,(1-.35^2)}} = 3.3 \text{ in.}$$

Estimate A_e for top flange = $\dfrac{.3 \times 18}{6}$ + .3 x (3.3 + 2) = 2.5 in^2

6.3 Section Properties: A_{Top} = 2.5 in^2; A_{Bot} = 4.4 in^2

Centroid: $\bar{y} = \dfrac{2.5 \times (17\pm)}{6.9}$ = 6.16 in. up from c.g. bot. flange

I_1 2.5 x 10.84^2 + 4.4 x 6.15^2 = 461 in^4

$S_{1top} = \dfrac{461}{11.3}$ = 41 in^3; $S_{bot} = \dfrac{461}{6.6}$ = 70 in^3

S_{1top} furnished is slightly larger than the assumed value of 40 in^3. Thus, shape is o.k. for wind load, as governed by local buckling of the top flange.

---

1 in. = 25.4mm, 1 in^2 = 645 mm^2, 1 in^3 = 16387mm^3, 1 in^4 = 416.231mm^4, 1 in^{-1} = 0.04mm^{-1}, 1 ft = 0.3048m, 1 lbf = 4.448N, 1 lbf/in = 0.175N/mm, 1 psi = 6.895 KPa, 1 psf = 47.88 N/m^2, 1 in-lbf = 113 N-mm, 1 ft-lbf = 1.356 N-m.

Shear and normal stresses in the vicinity of large flange openings, and open joints, can be estimated based on shear lag approximations developed for analysis of aircraft structures. Space precludes the inclusion of a quantitative presentation here, but numerous cases are covered in (7.16).

7.8 FOLDED PLATE STRUCTURES

Methods of analysis and design previously presented for plates and beams may also be applied to more complex structures such as "folded plate" structures. Folded plate structures are assemblies of plates of rectangular, triangular or other shapes that behave overall as beams, portal frames, arches or shells. Some typical configurations with rectangular plates are shown in Fig. 7-20. Configurations with triangular and trapazoidal shapes are shown in Fig. 7-21.

Stresses in some folded plate structures can be determined with acceptable accuracy by applying the elementary beam theory (Eq. 7-33) to the overall cross section of the plate assembly. In this "beam method", the overall section properties are determined using the methods given in Section 5.3 and 7.4. Assemblies of plates whose lengths are large relative to their dimensions of cross section (i.e. thin-wall beam sections, ribbed panels, etc.), and assemblies of large plates whose fold lines deflect identically (i.e. interior bays of roof shown in Fig. 7-20c), can be analyzed as beams.

The following more elaborate procedure may be used to determine transverse bending stresses in assemblies of large plates and to determine longitudinal stresses in structures with "pinned" connections along fold lines which do not deflect identically (exterior bay of roof shown in Fig. 7-20c). For procedures covering structures with monolithic joints that have varying deflections at fold lines, see (7.17), (7.18) or (7.19). For a more comprehensive review of methods of analysis for folded plate structures, see (7.20).

Procedure for analysis of folded plates (7.17)

1. Replace actual structure with equivalent compound structure comprised of transversely loaded plates (slab structure), and plate system loaded "in-plane" at fold lines as shown in Fig. 7-22.

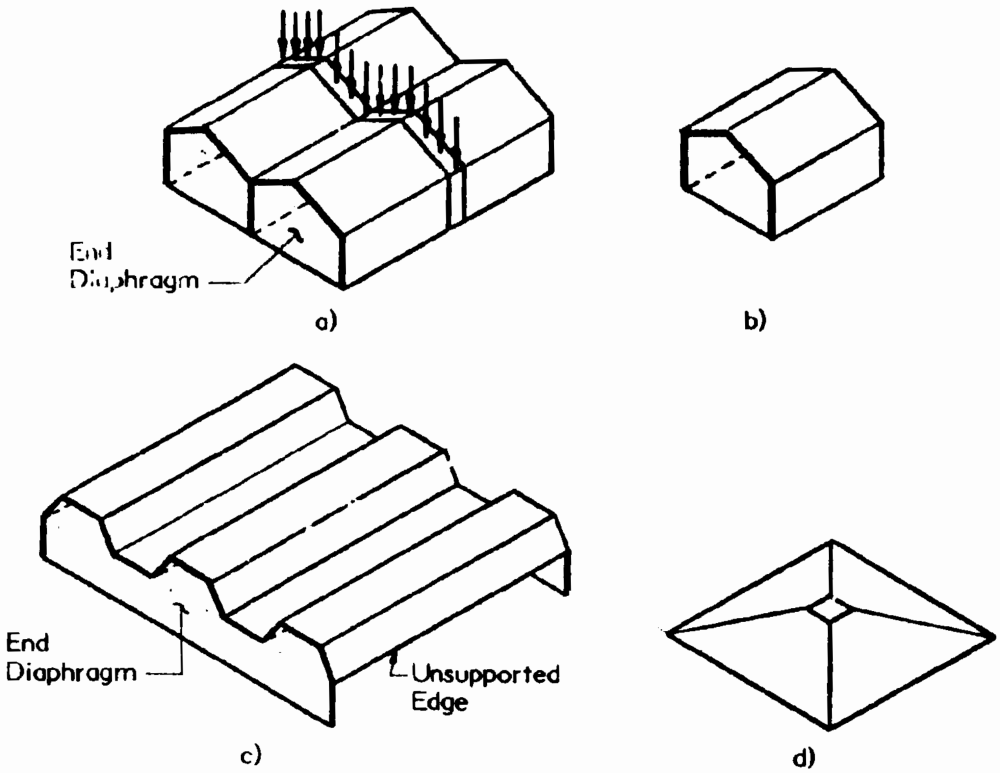

Fig. 7-20 FOLDED PLATE CONFIGURATIONS

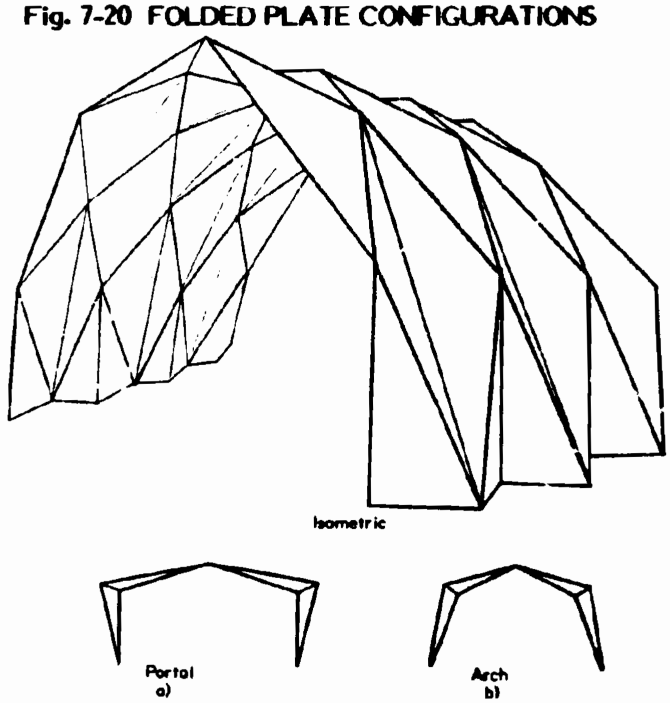

Fig. 7-21 FOLDED PLATE FRAMES AND ARCHES FORMED FROM TRIANGULAR PLATES

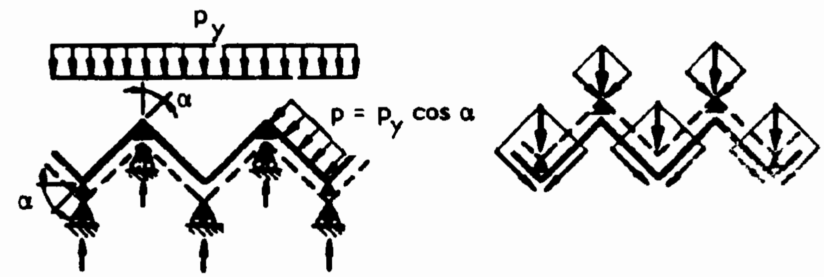

a) Slab b) Plates

Fig. 7-22 FOLDED PLATE SECTION AS A COMPOSITE OF SLAB AND PLATE STRUCTURE

2. Analyze "slab structure" as one way plate, spanning between fold lines with lateral loads (Fig. 7-22a):

$$p = p_y \cos \alpha \qquad \text{Eq. 7.82}$$

If the "slab structure" is monolithic with adjacent plates at fold lines, assume for this part of the analysis that "slab structure" supports do not have relative deflection and analyze a unit width strip of "slab structure" as a continuous beam on unyielding supports at the fold lines. If "slab structure" is not monolithic with adjacent plates at fold lines (pin ended), differential deflections of "slab structure" at fold lines do not produce changes in "slab structure" moments. Determine "slab structure" reactions at fold lines and maximum transverse bending moments at governing sections of "slab structure".

3. Apply slab reactions at fold lines as ridge reactions on system of longitudinal plates, as shown in Fig. 7-22b. Resolve these ridge reactions into plate loads by determining their components in the planes of the two intersecting plates at a ridge.

4. Temporarily assume that each plate is independent from its neighbors (Fig. 7-23a). Calculate in-plane flexural and shear stresses due to the in-plane components of the ridge reactions. Use elementary beam theory (Eq. 5.25) to determine normal stresses along the edges (free edge stresses).

5. Apply equal and opposite shear loads along each edge where adjacent plates intersect to equalize normal (longitudinal) stresses in contiguous plates. This is shown in Fig. 7-23b. Shear loads are given the same longitudinal distribution as the "free edge" flexural stresses. Their summation produces a thrust stress resultant with a line of action along the edge. The maximum thrust occurs at the location of maximum free edge stresses. This thrust stress resultant produces correction normal stresses that vary linearly across the plate (Fig. 7-23b).

   The correcting normal stresses can be determined using a stress distribution procedure that is similar to "moment distribution". In this procedure the "free edge stresses" are equivalent to fixed ended moments in

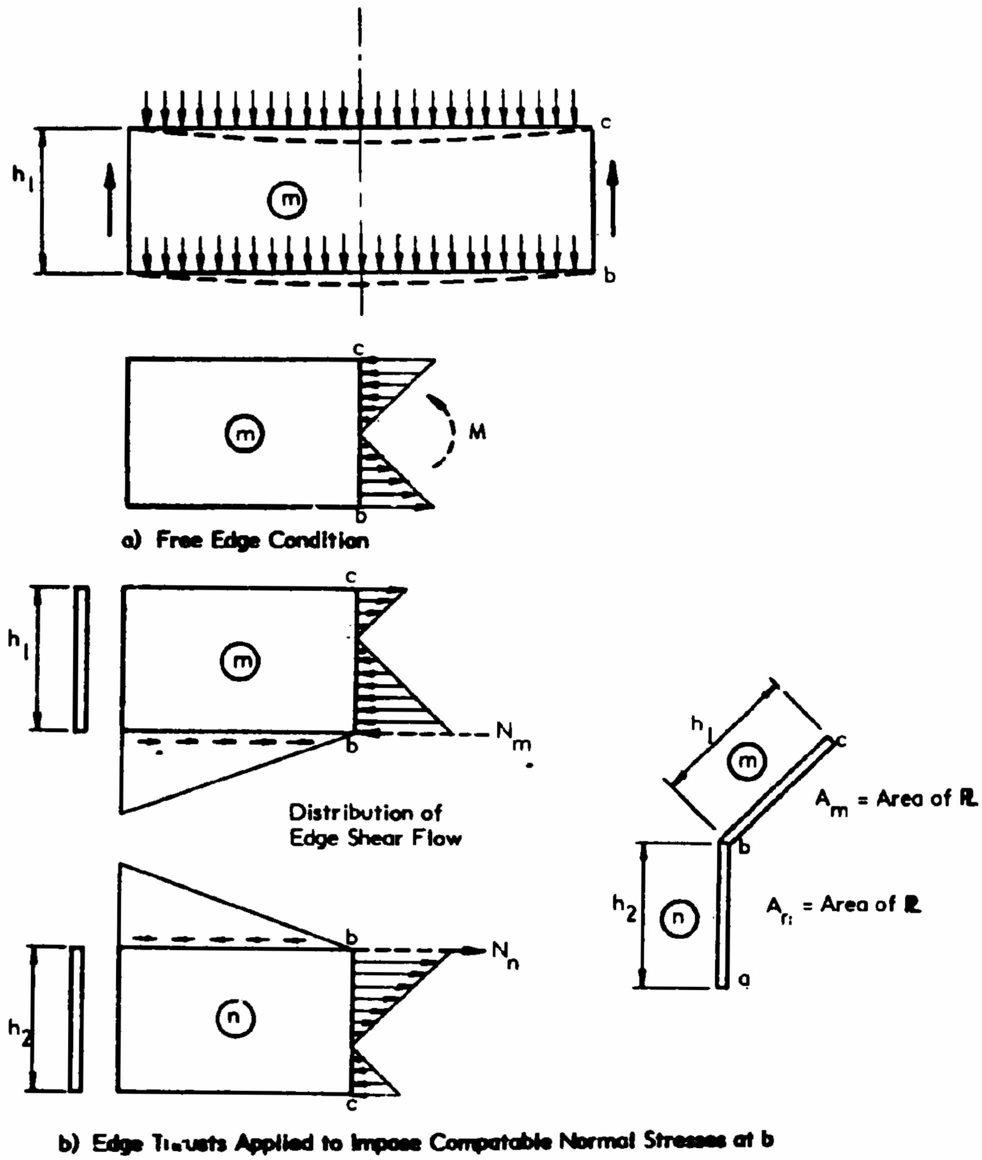

Fig. 7-23 EDGE SHEARS APPLIED AT JOINTS TO FORCE COMPATABILITY OF LONGITUDINAL STRESSES IN FOLDED PLATE STRUCTURES

"moment distribution". For rectangular plates, the stress distribution factors at each fold line, m-n, are:

$$k_{mn} = \frac{A_n}{A_n + A_m} \qquad \text{Eq. 7.83}$$

$$k_{nm} = \frac{A_m}{A_n + A_m} \qquad \text{Eq. 7.84}$$

See Fig. 7-23 for notation. The stress distribution factor, k_{mn} is the normal stress that must be imposed at the m-n edge of plate m by the axial thrust resultant, N_m, to remove a 1 psi difference in free edge normal stress between adjacent edges of plates m and n. For rectangular plates, the carry over factors for stress correction at edges opposite joint n-m are 1/2. See Example 7-10 given later for an illustration of the stress distribution process.

The magnitude of the applied shear loads is determined so that the combined "free edge" normal stress plus the correcting normal stress in each plate at a fold line are equal.

6. Determine thrust stress resultants required to obtain equal longitudinal stresses at fold lines: These are determined from the final stresses calculated in Step 5 above, starting from a free boundary, using the following equation.

$$N_n = N_{n-1} + \frac{(\sigma_{n-1} + \sigma_n) A_n}{2} \qquad \text{Eq. 7.85}$$

7. Determine shear forces per unit length (shear flow) at fold lines and maximum shear in the plane of the plate. The sum of the shear force along the fold lines to the point of maximum normal stress is equal to the maximum fold line thrust N_n, and the shear flow at a fold line has the same distribution along the length of the plate as the plate shear stress resultant in the free edge plate (Step 4). Thus, for a plate system with uniformly distributed load, the maximum shear flow is at the end of the longitudinal span and its magnitude is:

$$\max q_{sn} = \frac{4 N_n}{L} \qquad \text{Eq. 7.86}$$

The shear flow (shear stress times thickness) in a rectangular plate is determined by adding the corrective edge shears and the free edge plate shears. The maximum shear flow in a rectangular plate is either the shear flow at one of the edges, or the shear flow within the plate given by:

$$q_s = \frac{3}{2}\frac{V_o}{h_n} + \frac{q_{sa} + q_{sb}}{4} + \frac{h}{12}\,\frac{(q_{sa} - q_{sb})^2}{2V_o + h_n (q_{sa} + q_{sb})} \qquad \text{Eq. 7.87}$$

The notation used in Eq. 7.93 and the variation in shear over the height of the plate is shown in Fig. 7-24.

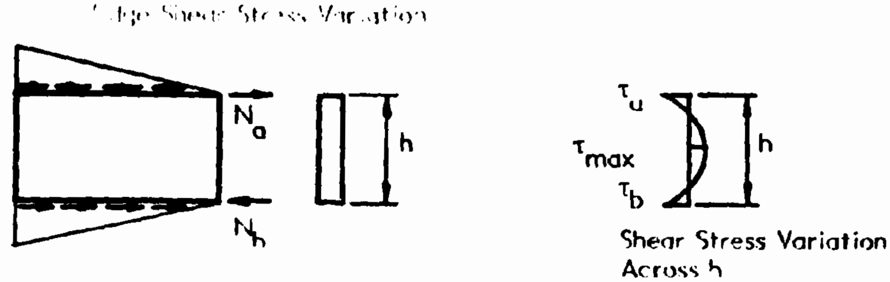

Fig. 7-24 SHEAR STRESSES IN FOLDED PLATE STRUCTURES

Resistance to local buckling of plate elements may be investigated using the plate buckling equations given in Chapter 6. See also (7.21) and (7.22) for a more comprehensive consideration of buckling of folded plate structures, including test results and an extensive bibliography of additional references.

The design of a folded plate roof with sandwich plates and pin joints using the above procedure is given in **Example 7-10.** The stress distribution method outlined above is used to obtain the final longitudinal stresses in the various plates of the structure. The maximum shear stresses at fold lines and within plates are also determined. The longitudinal stresses obtained in the interior plates of the example structure are compared with stresses at the same location obtained using the "beam method".

The procedure given above can be extended to cover structures with monolithic joints whose fold lines deflect differentially. Space does not permit a detailed consideration of such cases. See (7.17) for a comprehensive treatment of this problem. This type of structure is also analyzed in (7.18) and (7.19).

Results of tests of two aluminum faced plastic core folded sandwich panel roof structures are presented in (7.23). Experimentally determined behavior correlates well with behavior predicted by folded plate theory.

Structural configurations that require complex analyses with the above approaches can probably be analyzed more efficiently and accurately using finite element computer analysis. Existing general purpose programs such as ANSYS, NASTRAN or STARDYNE can readily handle such problems. These are discussed in Chapter 4.

Example 7-10: Design a steel faced, polyurethane foam core sandwich panel folded plate roof having the arrangement shown in the sketch. (Refer also to Chapter 8).*

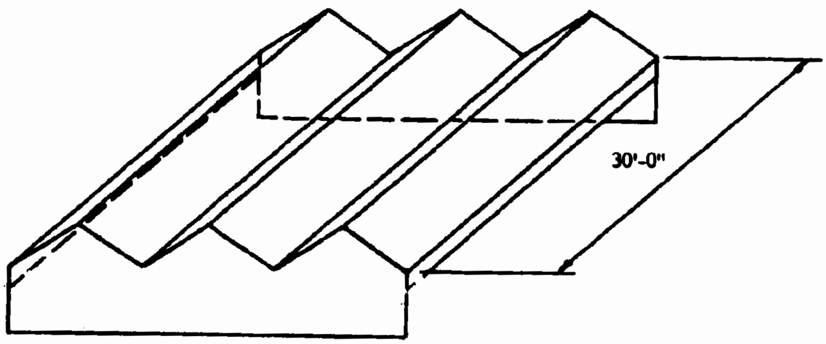

Solid End Walls or Stiff Transverse Beam

Sketch of Typical Structural Arrangement

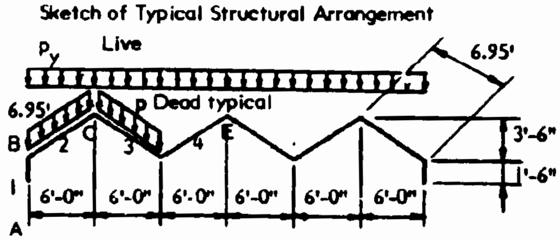

Typical Section

Properties of materials:

Facings - steel: E = 30,000,000 psi; tensile, compressive and flexural yield strength = 30,000 psi

Core - polyurethane foam, 2.5 lbs/cu.ft. min.; density: G = 500 psi, E = 1,500 psi, tensile strength = 25 psi, compressive strength = 20 psi and shear strength = 20 psi.

1. Capacity reduction factors: Use 0.9 for strength and 1.0 for E for steel and 0.6 for strengths and 0.8 for E and G for foam core. Thus: Steel; E = 30 x 10^6 psi, σ_{xu} = 0.9 x 30,000 = 27,000 psi; Foam core: E = 0.8 x 1,500 = 1,200 psi, G = 0.8 x 500 = 400 psi, σ_{xu} = .6 x 25 = 15 psi in tension, σ_{xu} = .6 x 20 = 12 psi in compression and σ_{xu} = .6 x 20 psi = 12 psi in shear.

2. Load Factor: Use a load factor of 1.6

---

* See note on Example 7-1, page 7-5.

Example 7-10 (continued)

3. Trial Design of Sandwich Elements:

Plate 1: 18 ga. steel skins, polyurethane foam plastic, 2 in. core:

t_f = .0478 in., A_f = .0478 x 2 x 12 = 1.15 in^2/ft.; A_c = 2 x 12 = 24 in^2/ft.

Plates 2, 3 & 4: 22 ga. steel skins, 2 in. foam plastic core:

t_f = .0299 in., A_f = 0.0299 x 2 x 12 = 0.72 in^2/ft; I = 0.72 x 1.015^2 = 0.74 in^4/ft; S = 0.74/1.03 = 0.72 in^3/ft.; A_c = 2 x 12 = 24 in^2/ft.

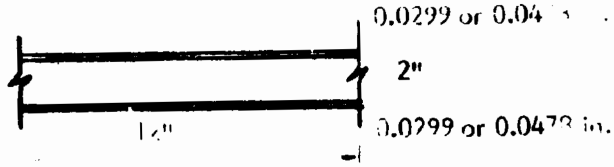

4. Load components:

Normal to Plate	Snow	$30\left(\frac{6.}{6.95}\right)^2$	=	22.45
	Dead	$4.3\left(\frac{6}{6.95}\right)$	=	3.75
	Total	p	=	26.2 psf
Equivalent on Horizontal Projection	Snow	30	=	30
	Dead	$4.3\left(\frac{6.95}{6}\right)$	=	5
	Total	p_y	=	35 psf

5. Slab Analysis - Pinned Joints - For service loads:

$$\text{Slabs BC, CD, DE:} M = \frac{w_v l_h^2}{8} = 35 \times \frac{6^2}{8} = 158 \text{ lbs/ft.}$$

$$V = \frac{w_v l_h}{2} = 35 \times \frac{6}{2} = 105 \text{ lbs/ft.}$$

Check Flexure Stress:

$$\sigma = \frac{158 \times 12}{0.72} = 2600 \text{ psi; Ultimate } \sigma_x = 2600 \times 1.6 = 4160 \text{ psi} < 27{,}000 \text{ psi}$$

Check local buckling (face wrinkling):

$$\text{Eq. 8.107: } \sigma_{wr} = 0.5(E_f E_c G_c)^{1/3} = 0.5(30 \times 10^6 \times 1200 \times 400)^{1/3} = 12{,}150 \text{ psi} > 4160 \text{ psi}$$

Secondary bending of sandwich section facings is discussed in Chapter 8. It can be shown by the analysis given in Chapter 8 that for the very thin facings of this beam, secondary bending stresses are negligible.

Example 7-10 (continued)

Check shear in core:

$$\tau_{cu} = \frac{V_u}{A_c} \; ; \; V_u = 26.2 \times 6.95/2 \times 1.6 = 146 \text{ lbs/ft.}$$

$$\tau_{cu} = \frac{146}{2 \times 12} = 6.1 \text{ psi} < 12 \text{ psi} \quad \text{o.k.}$$

Check Deflection:

$$\text{Eq. 8.27:} \quad w = \frac{5PL^3}{384D_m} + \frac{PL}{8D_v}$$

$$D_m = \frac{30 \times 10^6 \times 0.74}{(1 - 0.3^2)} = 24{,}395{,}600 \text{ lbs-in}^2; \; D_v = 2 \times 12 \times 400 = 9600 \text{ lbs}$$

$$w = \frac{5 \times 26.2 \times \overline{6.95}^{\,4} \times 1728}{384 \times 24{,}395{,}600} + \frac{26.2 \times \overline{6.95}^{\,2} \times 12}{8 \times 9600} = 0.056 + .198 = 0.253 \text{ in.}$$

$$w_{allow} = \frac{L}{300} = \frac{6.95 \times 12}{300} = 0.28 \text{ in.} \quad \text{o.k.}$$

6. Plate Analysis:

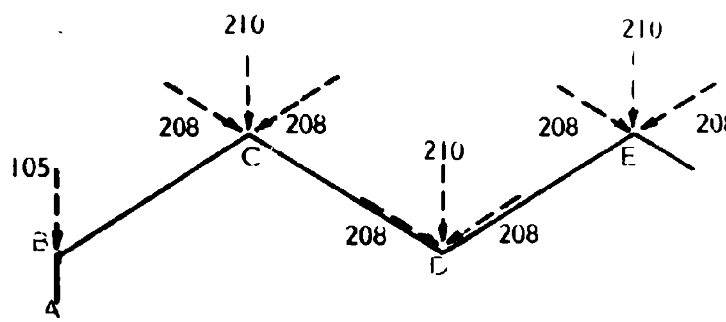

To find plate components of the vertical reaction of 2V = 2 x 105 = 210 lb/ft @ C, D & E:
$w_{PL} = 210 \times 1/2 \times 6.95/3.5 = 208$ lbs/ft

Plate 1: "Free Edge" Stresses:

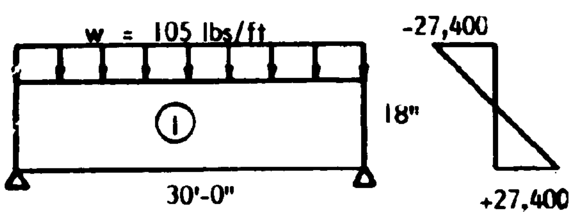

$$M = 105 \times \frac{\overline{30}^2}{8} = 11{,}800 \text{ lbs}$$

$$S = \frac{0.0478 \times 2 \times \overline{18}^2}{6} = 5.16 \text{ in}^3$$

$$\sigma = \frac{M}{S} = \frac{11{,}800 \times 12}{5.16} = 27{,}400 \text{ psi}$$

Example 7-10 (continued)

Plate 2: Free Edge Stresses:

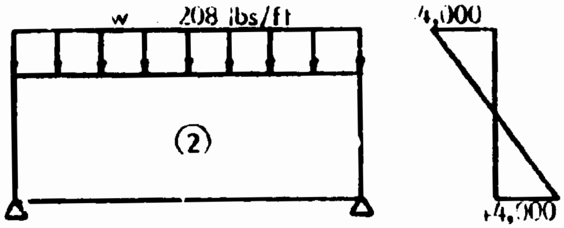

$$M = 208 \times \frac{30^2}{8} = 23{,}400 \text{ lbs}$$

$$S = \frac{.0299 \times 2 \times (6.95 \times 12)^2}{6} = 70 \text{ in}^3$$

$$\sigma = \frac{23{,}400 \times 12}{70} = 4000 \text{ psi}$$

Plate 3 & 4: Free Edge Stresses:

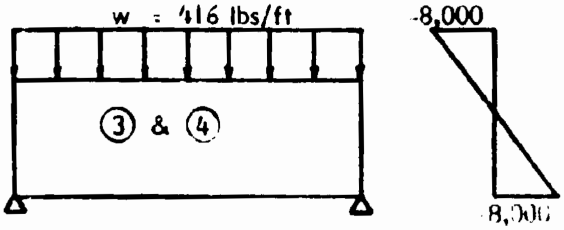

Load is twice plate 2 load; thus

$$\sigma = 2 \times 4000 = 8000 \text{ psi}$$

7. Correction of Edge Stresses to Equalize Strains of Abutting Edges:

Typical Computation for Correction Stresses Resulting from Restraint of Adjacent Plates

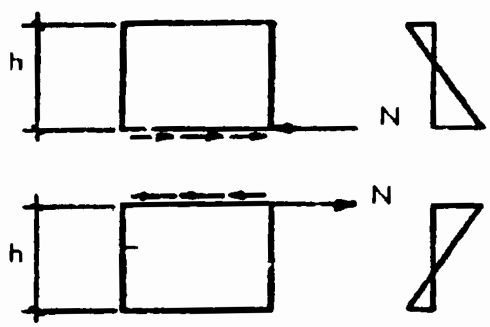

$$\sigma_t = -\frac{N}{bh} + \frac{N\,h/2}{bh^2/6} = -\frac{N}{bh} + \frac{3N}{bh} = \frac{2N}{A}$$

$$\sigma_c = -\frac{N}{bh} - \frac{3N}{bh} = -\frac{4N}{A}$$

$$\sigma_t = \frac{4N}{A}$$

$$\sigma_c = -\frac{2N}{A}$$

Stress Distribution Factors:

$$k_{12} = \frac{A_2}{A_1 + A_2}$$

$$k_{12} = \frac{5.0}{1.73 + 5.0} = 0.74$$

$$k_{21} = \frac{1.73}{5.0 + 1.73} = 0.26$$

$$k_{23} = \frac{5.0}{5.0 + 5.0} = 0.50 = k_{32} = k_{34} = k_{43}$$

Carry Over Factor:

- 1/2 for all spans

Example 7-10 (continued)

Stress Distribution:

1.73		5.0		5.0		5.0		Area (in^2)
0	.74	.26	.50	.50	.50	.50	0	Distribution Factor
$-\frac{1}{2}$		$-\frac{1}{2}$		$-\frac{1}{2}$		$-\frac{1}{2}$		Carry Over Factor
+27.4	-27.4 +23.2	+4.0 -8.2	-4.0 -2.0	-8.0 +2.0	+8.0	+8.0	-8.0	Free Edge Stress Distribution
-11.6	+.7	+1.0 - .3	+4.1 -2.0	+2.1	-1.0 + .5	- .5		Carry Over Distribution
- .4	+.7	+1.0 - .3	+ .1 - .2	- .2 + .1	-1.0 + .5	- .5	+ .2	Carry Over Distribution
- .4	+ .1	+ .1	+ .1 - .2	- .2 + .1	- .1 + .1		+ .2	Carry Over Distribution
+15.0	-2.7	-2.7	-4.1	-4.1	+7.0	+7.0	-7.6	Total - Final Stresses

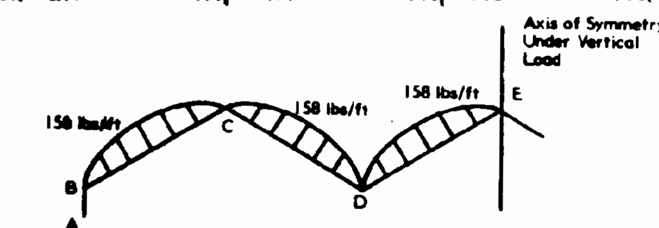

Slab Moments
(Multiply by 1.6 for ultimate)

Plate Stresses
(Multiply by 1.6 for ultimate)

Maximum ultimate plate stress = 15,000 x 1.6 = 24,000 psi tension < 27,000 psi; 7.6 x 1.6 = 12,160 psi compression $\approx$ 12,150 psi.

8. Conclusion: Strength is adequate, as governed by tensile strength of facings, local buckling compressive strength of facings, and shear strength of core.

Example 7-10 (continued)

9. Check Overall Buckling of Sandwich Plates:

Eq. 6.71: $N_{xc} = \frac{k\pi^2 D}{b^2}$; $\sigma_{xc} = \frac{N_{xc}}{2t_f}$ & k from Table 6-3

Check plate 2: In-plane uniform compression, $\sigma_x = \frac{4.1 + 2.7}{2} = 3.4$ ksi

and bending = 4.1 - 3.4 = 0.7 ksi

Ratio = $\frac{.7}{3.4}$ = 0.20; estimate k = 4.0 + .5 = 4.5

Stiffness D is greatly reduced by shear deformation of core. Based on the ratio of shear to bending deflection calculated in the plate analysis of step 5 above, use $D_{eff.}$ = 24,395,600 x .056/.253 = 5,400,000 lbs-in2.

$$\sigma_{xc} = \frac{4.5\ \pi^2\ 5,400,000}{2 \times .0299 \times (6.95 \times 12)^2} = 577,000 \text{ psi} \gg 1.6 \times 4,100 \text{ psi}$$

Conclusion: Buckling of sandwich plates under in-plane longitudinal compressive stress will not limit resistance of structure.

10. Maximum plate shear (in plane of facings) may be determined using equations given in text. Calculations for plate shear and development of connection details are omitted due to lack of space.

11. Alternate Approximate Analysis Using Beam Method

11.1 Interior bay

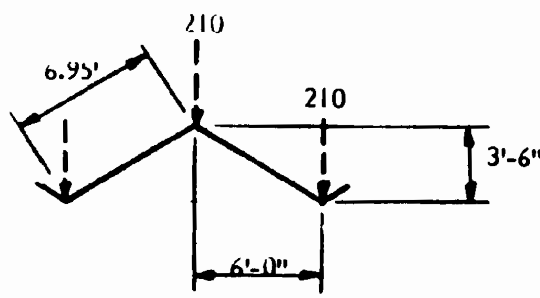

$A = 0.72 \times 6.95 \times 2 = 10.0 \text{ in}^2$

$I_o = 10.0 \times 42^2/12 = 1471 \text{ in}^4$

$S' = 1471/21 = 70 \text{ in}^3$

$M = \frac{210 \times 2 \times 30^2 \times 12}{8} = 567,000$ in-lbs

$\sigma_x = \frac{567,000}{70.0} = 8,093$ psi

Example 7-10 (continued)

11.2 Exterior bay

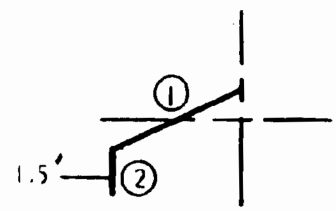

		A	y	Ay	y_o	Ay_o^2	I_o	
1		5.00	0	0	7.7	296	1471/2	= 735
2	1.15 x 1.5 =	1.73	30	51.8	22.3	860	$1.73 \times 18^2/12$	= 47
		6.73		51.8		1156		782
						782		

$\bar{y} = 51.8/6.73 = 7.7$ in. $\qquad I_o = \quad 1938\ \text{in}^4$

$S_{top} = \dfrac{1938}{28.7} = 67.5\ \text{in}^3$; $S_{bot} = \dfrac{1938}{31.3} = 61.9\ \text{in}^3$

$M = 567{,}000 \times 1/2 = 283{,}500$

top $\sigma_x = \dfrac{283{,}500}{67.5} = 4200$ psi; bot. $\sigma_x = \dfrac{283{,}500}{61.9} = 4580$ psi

Compare the above results with stresses shown in sketch given in Step 7.

Conclusion: "Beam Method" is fairly accurate for interior bay, but is extremely inaccurate for bottom plate of end bay.

---

1 in = 25.4mm, 1 in^2 = 645mm^2, 1 in^2/ft = 2117mm^2/m, 1 in^3 = 16,387mm^3, 1 in^3/ft = 53763mm^3/m, 1 in^4 = 416.231mm^4, 1 ft = 0.3048m, 1 lbf = 4.448 N, 1 lbs/ft = 14.59 N/m, 1 psf = 47.88N/m^2, 1 psi = 6.895 KPa, 1ksi = 6.895 MPa, 1 in-lbs = 113 N-mm, 1 lbs-in^2 = 2870 N-mm^2.

The "beam method" may also be used to obtain approximate estimates of plate stresses for many irregular assemblies of plates that comprise folded beam, frame and arch-like structures (Figs. 7-20e). This is discussed in (7.24). Approximate methods are also given in (7.21) for determining plate deflections and moments in thin folded plates without edge supports, where deflections often are large enough to require consideration in the analysis. Several forms of folded plate structures with triangular plates (Fig. 7-20, d, Fig. 7-21) are discussed in (7.24), and design examples using approximate analyses are given.

CHAPTER 7 - REFERENCES

7.1 "Specification for the Design of Cold-Formed Steel Structural Members, 1980 Edition," and "Commentary on the 1980 Edition of the Specification. . .", American Iron and Steel Institute, Washington, 1980.

7.2 Johnston, B., (Ed.), Guide to Stability Design Criteria for Metal Structures, 3rd ed., New York, Wiley, 1976.

7.3 Wei-Wen Yu, Cold-Formed Steel Structures: Design-Analysis-Construction, New York, McGraw-Hill, 1973.

7.4 McGuire, W., Steel Structures, Englewood, N.J., Prentice-Hall, 1968.

7.5 Winter, F., "Lateral Bracing of Columns and Beams," Journal of Structural Division, ASCE, Vol. 4, No. 572, March 1958.

7.6 Walker, A.C., (Ed.), Design and Analysis of Cold-Formed Sections, New York, Wiley, 1975.

7.7 Timoshenko & Gere, Theory of Elastic Stability, 2nd ed., New York, McGraw-Hill, 1961.

7.8 Cusens, A., and Pama, R., Bridge Deck Analysis, London, Wiley, 1975.

7.9 Hendry, A., and Jaeger, L., The Analysis of Grid Frameworks and Related Structures, London, Chatto and Windus, 1958.

7.10 Moffatt, K., and Dowling, P., "British Shear Lag Rules for Composite Girders," Journ. of Struct. Div., ASCE, Vol. 104, ST7, July 1978, p. 1123.

7.11 Bethlehem Steel Co., Torsion Analysis of Rolled Steel Sections, New York, 1963.

7.12 Kollbrunner, C., and Basler, K., Torsion in Structures, Berlin, Springer-Verlag, 1969.

7.13 Heins, C., Bending and Torsional Design in Structural Members, Lexington, MA, Heath, 1975.

7.14 LeMessurier, W., "A Practical Method of Second Order Analysis/Parts 1 and 2, AISC Engineering Journal, Vol. 13, No. 4, 1976, and Vol. 14, No. 2, 1977.

7.15 Sechler, E., and Dunn, L., Airplane Structural Analysis and Design, New York, Dover, 1963.

7.16 Kuhn, Paul, Stresses in Aircraft and Shell Structures, McGraw-Hill, New York, 1956.

7.17 Yitzaki, D., Prismatic and Cylindrical Sheel Roofs, Haifa, Israel, Haifa Science 1958.

7.18 Simpson, H., "Design of Folded Plate Roofs", ASCE Journal of the Structural Division, January 1958.

7.19 Portland Cement Association, "Direct Solution of Folded Plate Concrete Roofs", Advanced Eng. Bulletin 3, Chicago, 1960.

7.20 Iffland, J., "Folded Plae Structures," Journal of the Structural Division, ASCE, January 1979.

7.21 Swartz, S. E., and Rosebraugh, V. H., "Local Buckling of Long-Span Folded Plates," Journal of the Structural Division, ASCE, May 1975.

7.22 Swartz, S. E., and Rosebraugh, V. H., "Local Buckling of Long-Span Concrete Folded Plates," Journal of the Structural Division, ASCE, October 1976.

7.23 Fazio, P., "Failure Modes of Folded Sandwich Panel Roofs," Journal of the Structural Division, ASCE, May 1972.

7.24 Benjamin, B.S., Structural Design with Plastics, New York, Van Nostrand Reinhold, 1969.

7.25 Johnson, J. E., Lee, J. W., Dupuis, R. M., "Structural Behavior of Reinforced Plastic Beam Shapes", Proceedings of ASCE Specialty Conference on Selection, Design and Fabrication of Composite Materials for Civil Engineering Structures, ASCE, Nov. 1972, New York.

ASCE Structural Plastics Design Manual

CHAPTER 8 – FLAT SANDWICH STRUCTURES

By Richard E. Chambers

TABLE OF CONTENTS

NOTATIONS – Chapter 8

a	span length in a two-span panel; longer side of rectangular plate; general dimension
$\bar{a}$	width of bearing
A	transformed area of cross section
A_c	transformed area of core
A_f	transformed area of faces
$\bar{A}$	in-plane or axial stiffness
A_v	effective shear area
b	width of sandwich beam; unit width of sandwich plate; shorter side of rectangular plate.
b_i	width of "i" face
c	thickness of sandwich core; indicates "core" when used as a subscript.
C_c	cost per unit volume of core material
C_f	cost per unit volume of face material
C_p	cost per unit surface area of sandwich panel
d	distance between neutral axes of sandwich faces.
d'	diameter of circle inscribed within hexagon or square of honeycomb cell
D	stiffness
D_m	bending stiffness
D_{mx}, D_{my}	bending stiffness in x and y directions respectively
D_{mf}	total bending stiffness of faces, about their own neutral axes
D_{mfi}	bending stiffness of the "i" face
D_v	shear stiffness
D_{vx}, D_{vy}	shear stiffness in x and y directions respectively

NOTATIONS (continued)

E	elastic modulus
E_c	elastic modulus of the core
E_e	effective elastic modulus
E_f	elastic modulus of the faces
E_i	elastic modulus of the "i" element in the transformed section
E_o	tangent modulus of a viscoelastic plastic subjected to constant strain rate
E_r	reference elastic or viscoelastic modulus for use in the transformed section
E_v	viscoelastic modulus
f	indicates "faces" when used as a subscript
F	ultimate strength
F_{uc}	ultimate compression strength
F_{uL}	long-term ultimate strength
F_{uS}	short-term ultimate strength
F_{ut}	ultimate tensile strength
F_{uv}	ultimate shear strength
G	shear modulus of rididity
G_c	shear modulus of rigidity of sandwich core
G_{cx}, G_{cy}	shear modulus of rigidity of the core in the x and y directions respectively
i	integer designating layers in sandwich composite
I	moment of inertia
I_c	moment of inertia of core
I_f	moment of inertia of both faces about their own neutral axes
I_o	moment of inertia of both faces about neutral axis of the cross section of the whole sandwich.

NOTATIONS (continued)

k	buckling coefficient
K_i	coefficient for stresses and deflection in orthotropic sandwich
K_m	coefficient for deflection due to moment
K_v	coefficient for deflection due to shear
L	span length
$\overline{LF}$	load factor
m	cost coefficient for direct optimum cost design
M	bending moment on beam; bending moment per unit width (bending stress resultant) or plate
M_x, M_y	bending stress resultants on faces indicated by subscripts
M_p	primary bending moment applied to transformed section
M_s	secondary bending moment applied to sandwich faces
n_i	modular ratio of element "i" in transformed section of beam or column
n_i'	modular ratio of element "i" in transformed section of plate
N	direct force per unit width (direct stress resultant)
N_x, N_y, N_z	direct force per unit width in x, y and z directions, respectively.
N_{xy}	shear stress resultant applied in the plane of sandwich
NA	neutral axis
P	concentrated load; or total load applied to sandwich beam
P_{cr}	critical buckling load
P_{crv}	critical column buckling load governed by initial eccentricities
P_e	Euler buckling load
P_v	buckling load governed by shear rigidity of core

NOTATIONS (continued)

q	uniform load per unit length or area
q_p	primary component of uniform load
q_s	secondary component of uniform load acting on faces
Q	shear force on beam
Q_p	primary component of shear on sandwich beam having shear-flexible core
Q_s	secondary component of shear acting on faces of sandwich beam having shear-flexible core
Q_x, Q_y	shear force per unit width (stress resultant) transverse to plane of sandwich plate
$\bar{Q}_i$	first moment of an element "i" about the neutral axis of the cross section
$\bar{Q}_{NA}$	first moment of all elements about the neutral axis of the cross section
S	section modulus
S_f	section modulus on face
$\overline{SF}$	safety factor
t	thickness of one face in sandwich having equal faces; indicates "tension" when used as a subscript.
t_i	thickness of i face in sandwich having unequal faces
T	temperature
T_{xz}, T_{yz}	twisting stress resultants in planes designated by superscript
u	indicates "ultimate" when used as a subscript
v	indicates "shear" when used as a subscript

NOTATIONS (continued)

w	total deflection of sandwich plate
w_a	allowable deflection of sandwich beam
w_e	total deflection of sandwich plate with "effective" properties
w_s	secondary component of deflection along face
w_m	deflection of sandwich beam or plate due to moment
w_o	initial eccentricity or lateral displacement of column centerline
w_p	primary component of deflection of sandwich beam or plate
w_v	deflection of a sandwich beam or plate due to shear
x	in-plane axis of sandwich plate; distance from centerline along span of beam
X	distance from support along span of beam
y	in-plane axis of sandwich plate
z	axis of plate normal to plane
z_{ef}	distance from neutral axis to extreme fiber
z_i	distance from neutral axis to "i" face centroid
z_i'	distance from reference axis to "i" face centroid
$\bar{z}$	distance from reference axis to neutral axis
α	coefficient of thermal expansion; shear deformation
Δ	change
ϵ	strain
ϵ_i	strain in "i" face
ν	Poisson's ratio
ν_f	Poisson's ratio of faces
$_i$	Poisson's ratio of "i" faces
ϕ_i	coefficients for sandwich beam with shear flexible core

NOTATIONS (continued)

σ	stress
σ_{cr}	critical buckling stress
σ_i	stress in "i" face
σ_L	long-term stress
σ_S	short-term stress
σ_{wr}	critical stress for face wrinkling
τ	shear stress
τ_u	ultimate shear stress
θ	shear flexibility coefficient for beams
$\bar{\theta}$	shear flexibility coefficient for plates

CHAPTER 8 - FLAT SANDWICH STRUCTURES

Richard E. Chambers

8.1 Introduction

The state of the art in the analysis and design of structural sandwich panels is well advanced. Early theory was developed mostly for "stressed-skin" wood construction, and it has been refined and extended over the years as sandwich construction has been used in a wide range of structural applications, including those as diverse as doors for residences, and components for aerospace vehicles. Several texts and handbooks are available which provide theoretical treatment of a wide variety of sandwich arrangements, under various load and support conditions (8.1, 8.2, 8.3, 8.4, 8.5).

Typical structural sandwich constructions have lightweight cores that are significantly less stiff and less rigid than the faces. Structural analysis and design of sandwich constructions must account for the effects of such cores. This is especially important in this Manual on plastics, since low density plastic foam cores, or plastics in other configurations that have low shear rigidity, are frequently used in sandwich constructions for reasons of low weight, low cost, and high thermal resistance.

The objective of this Chapter is to present significant considerations in the structural analysis and design of sandwich components that are fabricated, in whole or in part, from plastics. The Chapter deals with flat sandwich panels subjected to transverse and in-plane forces, and to loads developed while panels are restrained against thermal, shrinkage, or other dimensional changes. Panels having cores that are flexible relative to their faces are considered in detail because many plastic cores have low rigidity. Design examples are developed to illustrate implementation of key concepts, including direct design for minimum cost. While this Chapter is devoted to flat sandwich panels, the concepts presented are also applicable to curved sandwich shells and rings which are treated in Chapter 9.

8.2 Components of Sandwich Construction

A structural sandwich is a composite that is comprised of two faces, separated by and connected to a structural core that is less stiff and less dense (Section 1.10). The faces and core are usually connected by an adhesive that provides structural continuity across the panel depth (Fig. 8-1). In some special constructions, a separate adhesive layer is not needed because faces and core are integrally formed. Plastics may comprise all or part of a typical structural sandwich panel, since they may be used for either or both faces, for the core, and for the adhesive.

Faces

The primary structural role of the faces of a sandwich panel is to carry tensile, compressive, flexural, and shear stress resultants that act parallel to the plane of the panel. Faces may also serve to distribute localized loads and reactions to the softer and weaker core. Typical forms of faces are shown in Fig. 8-2a; any of these types of faces may be fabricated from plastics, as well as from other sheet materials.

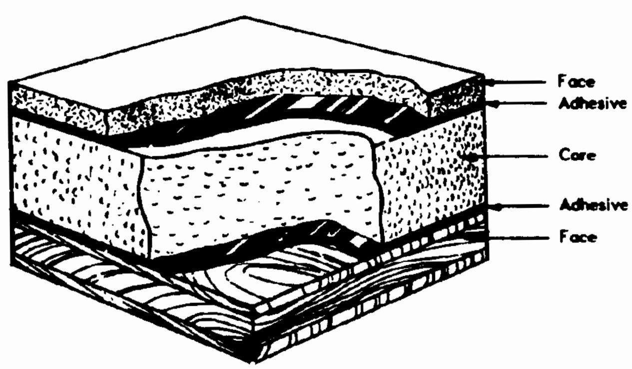

Fig. 8-1 GENERAL ARRANGEMENT OF SANDWICH CONSTRUCTION

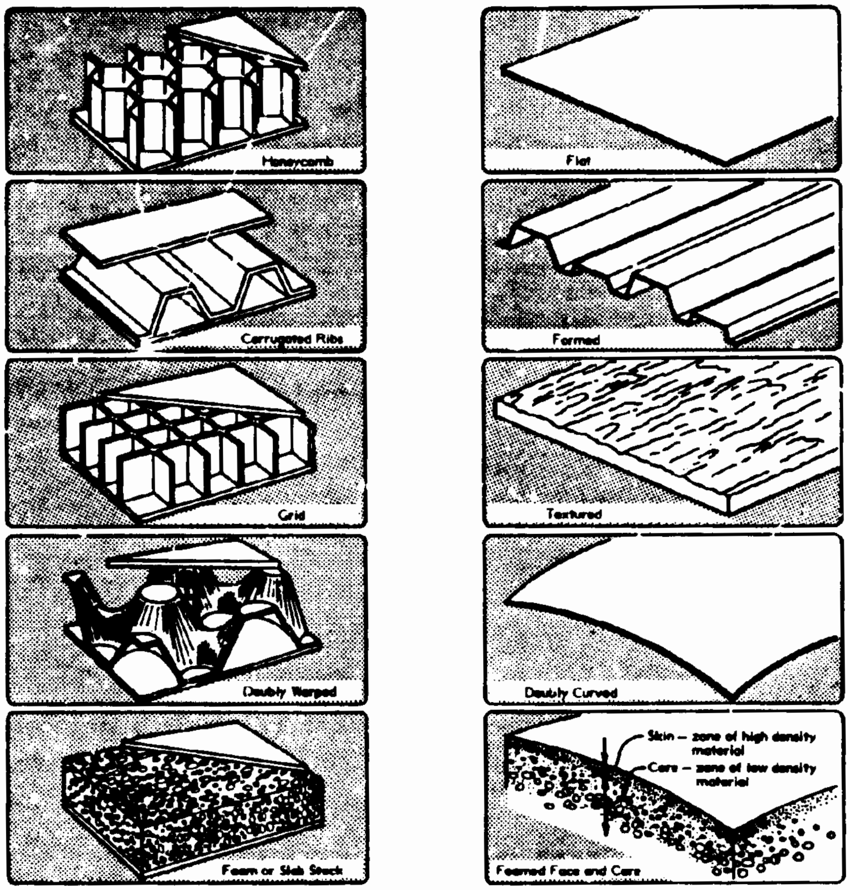

a. Sandwich Faces b. Sandwich Cores

Fig. 8-2 TYPICAL ELEMENTS OF SANDWICH CONSTRUCTION

In addition to their structural role, the faces may provide non-structural attributes such as texture or color, and resistance to weather, flame spread, fire, heat, abrasion, erosion, skidding, water and moisture, chemicals, radiation, and biological attack.

Cores

The core of a sandwich panel separates the two faces and holds them in a stable position. It provides the shear load path between faces, it stabilizes the faces against buckling, and, together with the faces, it carries loads that are applied normal to the plane of the panel. Typical types of sandwich cores are shown in Fig. 8-2b. Cores are usually fabricated from plastics, although they may also be manufactured from other materials such as metal, gypsum, foamed cement, wood particle board, or end-grain balsa. Honeycomb cores may be fabricated from resin impregnated paper, or from reinforced plastic or metal if structural performance requirements are stringent.

The sandwich core may also provide thermal or acoustical resistance, and occasionally fire resistance or visual effects.

Face/Core Interface

The primary structural role of the face/core interface in sandwich construction is to transfer transverse shear stresses between faces and core, to stabilize the faces against buckling away from the core, and to carry loads applied normal to the panel surface. For the most part, the faces and core of sandwich constructions that contain plastics are connected by adhesive bonding. In some special cases, such as truss-core pipe, for example (Fig. 4-6), faces and core are formed together during the extrusion process, resulting in an integral homogeneous connection between the components. Fasteners are seldom used to connect faces and core because they may allow erratic shear slippage between faces and core or buckling of the faces between fasteners; also, they may compromise other attributes such as waterproofing integrity and appearance.

8.3 Design Criteria for Sandwich Construction

The formulation of design criteria for plastic-based sandwich structures, must include both the unique characteristics introduced by sandwich construction, and the special behavior introduced by plastics. This is discussed below.

Overall Component Stiffness

The overall stiffness provided by the interaction of the faces, the core, and their interfaces, must be sufficient to meet deflection and deformation limits set for the structure. Overall stiffness of the sandwich component is also a key consideration in design for general instability of elements in compression (Fig. 8-3a).

In most typical sandwich constructions, the faces provide primary stiffness under in-plane shear stress resultants, (N_{xy}), direct stress resultants (N_x, N_y), and bending stress resultants (M_x, M_y) (Fig. 8-4). Furthermore, and as important, the adhesive and the core provide primary stiffness under normal direct stress resultants (N_z), and transverse shear stress resultants (Q_x, Q_y). Resistance to twisting moments (T_{xz}, T_{yz}), which is important in certain plate configurations, is provided by the faces.

Local Buckling

The stiffness of the face and core elements of a sandwich composite must be sufficient to preclude local buckling of the faces. This local buckling can take either of two forms (Fig. 8-3). Local crippling occurs when the two faces buckle in the same mode (anti-symmetric). Local wrinkling occurs when either or both faces buckle locally and independently of each other. Local wrinkling can occur under either axial compression (Fig. 8-3c), or bending compression (Fig. 8-3b). Resistance to local buckling is developed by an interaction between face and core which depends upon the stiffness of each.

General Instability

General instability, or overall buckling, of sandwich components subjected to in-plane compression (Fig. 8-3a) may be a governing limit state. In sandwich construction, buckling resistance depends on both the flexural rigidity of the faces and the shear rigidity of the core. Core shear deformation reduces the buckling resistance as calculated by typical handbook formulas, which are based on flexural rigidity alone.

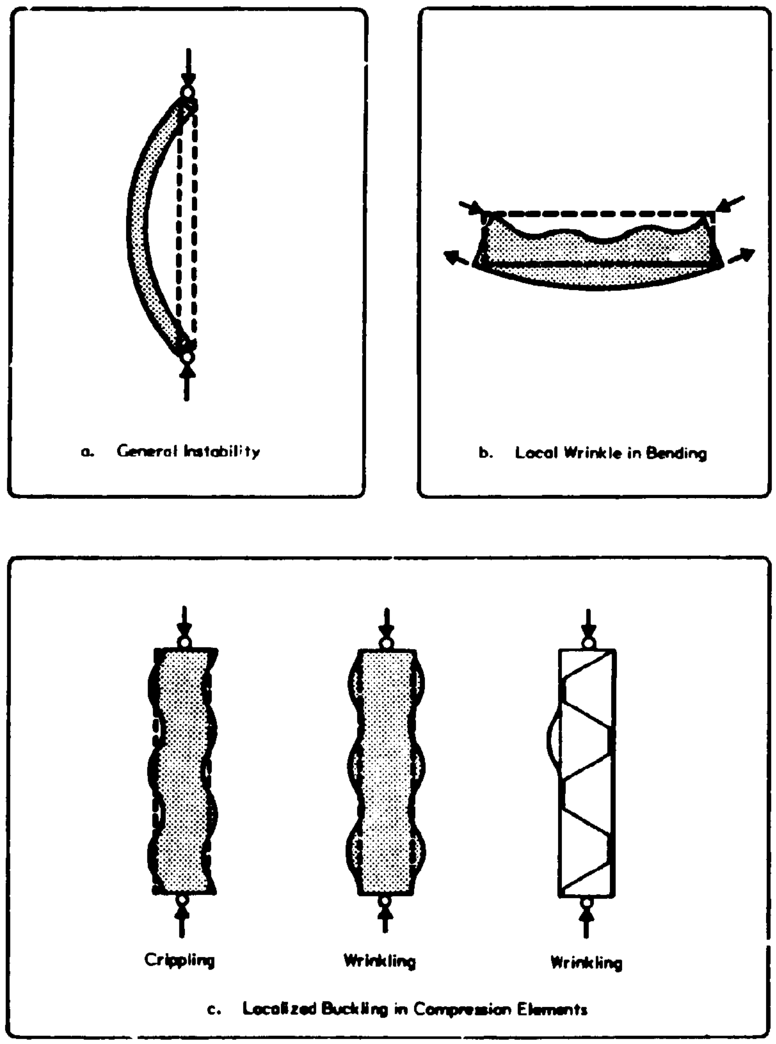

Fig. 8-3 BUCKLING MODES IN SANDWICH CONSTRUCTION

Strength of the General Panel

The structure must have sufficient strength to resist direct (in-plane) and transverse stress resultants without rupture or buckling. In most sandwich constructions, the faces are designed to resist direct stress and shear stress resultants applied in the plane of the panel and bending stress resultants acting across the panel (Fig. 8-4). Capacity of faces may be limited by either material strength or resistance to local buckling.

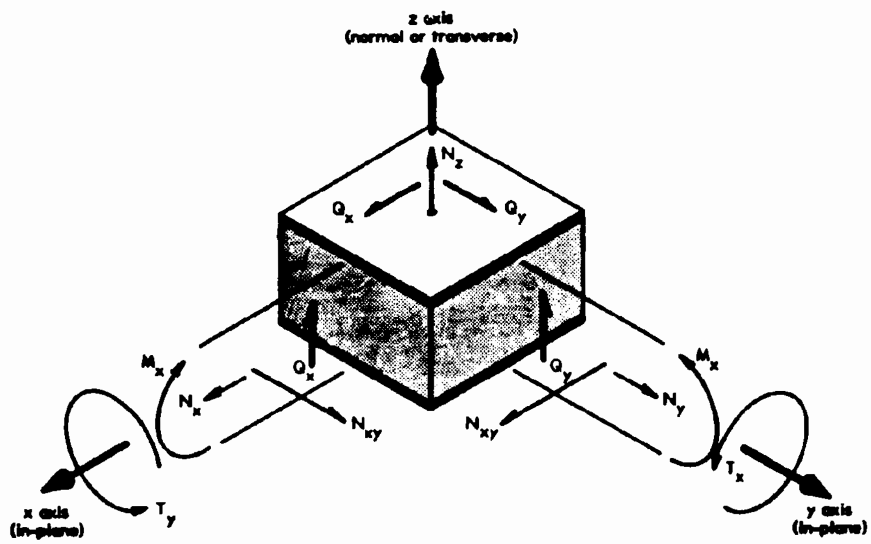

Note: For the orthotropic materials considered herein, the natural material axes 1, 2 and 3 are always aligned with the member axes shown.

Fig. 8-4 COORDINATE SYSTEM AND STRESS RESULTANTS

The core and adhesive are designed to resist transverse shear and normal compressive and tensile stress resultants. These elements must also have sufficient tension and compression strength and stiffness to restrain the face against local buckling, since during local buckling the face tends both to indent and to pull away from the core.

Characteristics of the Core

The properties of the core, and especially the relative properties of core and faces, have significant effect on the structural behavior of sandwich constructions. The key characteristics of the sandwich core are delineated below:

In-Plane Stiffness—Soft and Stiff Cores: If either the elastic or the viscoelastic modulus of the core in the plane of the panel is very low relative to that of the faces, the core is termed **soft** herein. As compared to a stiff core, a soft core does not contribute significantly to either the in-plane or the bending stiffnesses of the cross section. Usually, the in-plane bending and stiffnesses of soft cores are neglected; stiffness properties in other directions are usually assumed to be finite.

The majority of commonly used core materials (honeycombs, low density plastic foams, and balsa), when used with stiff faces (steel, aluminum, wood, FRP), possess relatively low in-plane stiffness. Thus, the emphasis of the analyses presented herein is on constructions having soft cores.

Shear Stiffness— Shear-Flexible and Shear-Rigid Cores: A **shear-flexible** core has a transverse shear stiffness that is low enough to result in shear deformations that are significant relative to bending deformations. A **shear-rigid** core has a shear stiffness that is high enough to render shear deformations negligible compared to bending deformations. Since low-density plastic foam cores for sandwich constructions usually provide low shear rigidity compared to the flexural rigidity of the sandwich, behavior of panels having shear-flexible cores will be discussed subsequently.

Resistance to Localized Loads

The structure must sustain localized effects due to concentrated loads, reactions, attachments, or at other discontinuities in the panels (Fig. 8-5 and Section 8.7). Localized loads are frequently the source of panel failures, and in many instances, they are the result of faulty design. Sometimes, however,

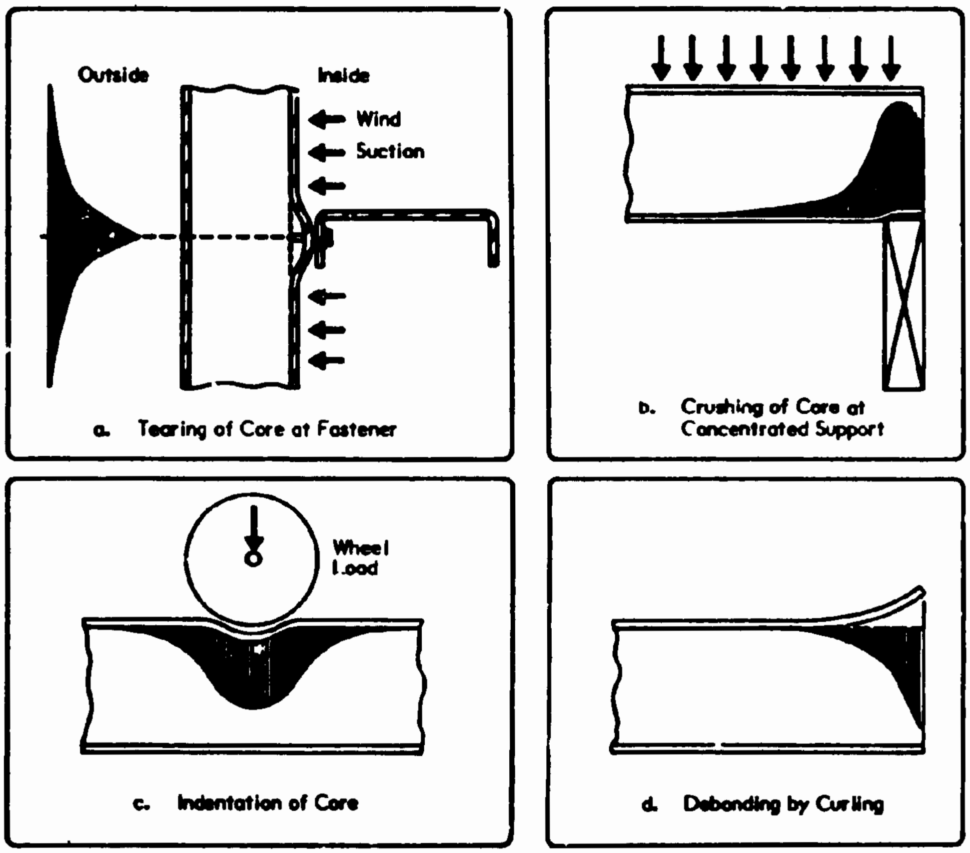

Note: Shaded areas indicate schematic stress distribution in core.

Fig. 8-5 EFFECTS OF LOCALIZED NORMAL LOADS localized connections are a necessary compromise, and they require detailed evaluation. The effects of such localized loads are difficult to estimate accurately by calculation, and evaluation by tests is usually required. Local stiffeners, or reinforcing elements, end and edge closures, and the like, usually proved the most suitable load paths for normal loads that are applied locally.

Volume Changes due to Environmental Exposure and Curing

Panel elements may be subjected to stresses and strains due to causes other than external loads. Moisture, temperature, curing or cooling shrinkage, and expansion and contraction due to exposures to chemical environments may create strains and warping in the panel. Furthermore, large cumulative movements and rotations may require special detailing at connections to prevent rupture of sealants at panel edges. Finally, very substantial stresses can result when internal strains are restrained by either the supporting structure or by the geometry of the component itself. This will be discussed in more detail in Section 8.10.

Compatibility

Compatibility among the various materials used in a sandwich composite, as well as compatibility with the environment to which they are exposed, are important, but frequently overlooked, design considerations. The chemical and physical compositions of all materials should be compatible initially, and this compatibility should be preserved for the life of the product in its environment.

While compatibility is not considered further herein, a few examples drawn from experience are cited here to emphasize the importance of this criterion. An adhesive that shows high levels of adhesion at room temperature may cleave cleanly from its adherend on impact, or at low stress levels, when temperatures are below freezing. An oil-based plasticizer may leach from the thermoplastic compound used in the face or core, and ultimately destroy what was initially a sound adhesive bond. A "blowing" agent may dissipate from a plastic foam core and alter its thermal resistance or cause significant shrinkage effects. An alkaline ingredient may leach from a cementitious face, and chemically degrade an adhesive that is not resistant to alkalies. When an element is made from plastic, the presence of heat, stress, and other aggressive environments may help to accelerate or aggravate some of the above degradation processes.

8.4 Section Properties for Beams and Columns

Inherently, the elastic, or viscoelastic, modulus of the core and faces of a structural sandwich are different; the moduli of the two faces may be different as well. Thus, section properties of sandwich cross sections, required for the analysis of beams and columns, are determined from **transformed section theory.** Application of this theory is well developed, as it is used in the determination of section properties of reinforced concrete, plywood, laminated and stressed-skin timber construction, and composite concrete/steel design; it is treated only briefly herein.

Analysis of Transformed Section

The following procedure is used in the determination of transformed section properties of sandwich beams and columns that are comprised of elastic elements. Modifications to account for both viscoelastic behavior and plate behavior will be discussed subsequently.

a) A reference elastic modulus, E_r, is selected for convenience of calculation. This is usually taken as the elastic modulus of one of the faces. The reference modulus is arbitrarily taken herein as the modulus of the bottom face of the cross section, as drawn; that is $E_r = E_1$. Another appropriate criterion is that the reference modulus is that of the face having the higher modulus. The reference modulus becomes the effective modulus of the whole cross-section for purposes of determining stiffness and deformation of the section under transverse bending and under in-plane loads.

b) The whole width of the beam cross section may be used in calculations. However, for sandwich constructions having a continuous cross-section, selection a unit width usually proves convenient. When elements of the cross-section are not uniform in depth or thickness, as in the case of a corrugated face, the width might be taken as the wave-length of the corrugation. Whatever the choice of reference width, it is referred to here as the **actual** width.

c) The modular ratio n is determined for each element of the cross-section. This is the ratio of the actual elastic modulus, E_i, of the element to the reference modulus.

$$n_i = \frac{E_i}{E_r} \qquad \text{Eq. 8.1}$$

This relationship is modified to account for the effects of plane strain conditions in Section 8.5 for columns in compression, and Section 8.7 for wide beams and plates in bending.

d) The actual width of each element of the cross section is multiplied by the modular ratio, n_i, to obtain the **transformed** width. The new cross-section is the **transformed section.**

Once the above transformations are accomplished, the section properties of the transformed section are obtained directly by established methods for isotropic sections having variable width (Table 8-1).

Time-Dependent Section Properties: The time-dependent behavior of linear viscoelastic plastics is readily taken into account in the determination of time-dependent section properties of the sandwich cross-section. The elastic component, E_o, of the viscoelastic modulus, E_v, is used in place of E_i, if short-term stresses and strains are applied. If long-term sustained loads or strains are anticipated, the appropriate value of the variable time-dependent viscoelastic modulus, E_v, is used in place of E_i (see Section 3.3). When the modulus changes with shifts in temperature, the temperature-dependent modulus is required.

For constructions that contain plastics displaying time-dependent behavior, it may prove convenient to select the reference modulus as that of an element of the cross section which demonstrates elastic (non-time-dependent) behavior. If all elements are viscoelastic, the criteria for selecting the reference viscoelastic modulus are as given in a) above for the elastic modulus. In any event, the modular ratio, n_i, will normally vary with time unless the moduli of all elements of the cross section demonstrate the same relative decay with time (i.e. all materials have the same creepocity. See Available Estimates of Viscoelastic Response, Section 3.3).

Table 8-1
Section Properties of Beam and Column Sandwich Cross-Sections *

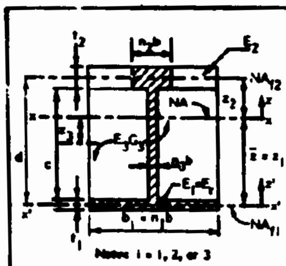

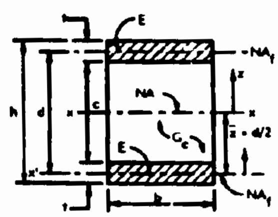

PROPERTY	a. Unequal Faces with Stiff or Soft Core	b. Equal Faces with Soft Core ($E_1 = E_2 = E$)		EQ.
	Thick or Thin Faces	Thick Faces	Thin Faces	
Area	$A = A_f + A_c$	$A = A_f$	$A = A_f$	8.2 a, b
Faces	$A_f = n_1 A_1 + n_2 A_2 = n_1 bt_1 + n_2 bt_2$	$A_f = 2bt$	$A = 2bt$	8.3 a, b
Core	$A_c = n_3 bc$; $A_c = 0$ for soft core	$A_c = 0$	$A_c = 0$	8.4 a, b
Axial Stiffness	$\bar{A} = AE_r = AE_1$	$\bar{A} = AE$	$\bar{A} = AE$	8.5 a, b
Neutral Axis	$\bar{z} = \frac{n_i A_i z_i'}{\bar{A}} = z_1$	$\bar{z} = \frac{d}{2}$	$\bar{z} = \frac{d}{2}$	8.6 a, b
Moment of Inertia				
Total	$I = I_o + I_f + I_{oc} + I_c$	$I = I_o + I_f$	$I = I_o$	8.7 a, b, c
Faces about NA of Section	$I_o = n_1 A_1 z_1^2 + n_2 A_2 z_2^2$	$I_o = \frac{btd^2}{2}$	$I_o = \frac{btd^2}{2}$	8.8 a, b
Faces about their own NA	$I_f = I_{f1} + I_{f2} = \frac{n_1 bt_1^3}{12} + \frac{n_2 bt_2^3}{12}$	$I_f = I_{f1} + I_{f2} = \frac{bt^3}{6}$	$I_f = 0$	8.9 a, b, c
Core about NA of Section	$I_{oc} = n_3 A_3 z_3^2 = 0$ (for soft core)			8.10 a, b
Core about its own NA	$I_c = \frac{1}{12} n_3 b c^3 = 0$ (for soft core)			8.11 a, b
Bending Stiffness				
Primary	$D_m = E_r I = E_1 I$	$D_m = EI$	$D_m = EI$	8.12 a, b
Faces	$D_{mf} = E_r I_f = E_1 I_f$	$D_{mf} = EI_f$	$D_{mf} = 0$	8.13 a, b
Section Modulus in Bending				
Extreme Fibers	$S_i = \frac{I}{n_i (z_i + 0.5\,t_i)}$	$S = \frac{I}{(\bar{z} + 0.5\,t)} = \frac{2I}{h}$	$S = \frac{I}{\bar{z}} = \frac{2I}{d} = btd$	8.14 a, b, c
At z	$S_z = \frac{I}{n_i z}$	$S_z = \frac{I}{z}$	$S = \frac{I}{\bar{z}} = \frac{2I}{d} = btd$	8.15 a, b, c
One Face	$S_{fi} = \frac{2 I_{fi}}{n_i t_i}$	$S_f = \frac{2 I_f}{t}$	$S_f = 0$	8.16 a, b, c
Shear Properties				
First Moment about Neutral Axis	$Q_1 = n_1 A_1 z_1$ (Face 1 only) $Q_2 = n_2 A_2 z_2$ (Face 2 only)	$Q_1 = A_1 z_1 = Q_{NA}$	$Q_1 = Q_{NA}$	8.17 a, b
	$Q_{NA} = n_1 A_1 z_1 + \frac{1}{2} n_3 b \left[z_1 - \frac{t_1}{2}\right]^2$	$Q_2 = -Q_1$	—	8.18 a, b
For Soft Core ($n_3 = 0$)	$Q_{NA} = Q_1 = Q_2$	$Q_{NA} = \frac{btd}{2} = \frac{I_o}{d}$	$Q_{NA} = \frac{btd}{2} = \frac{I_o}{d}$	8.19 a, b
Effective Shear Area	$A_v = \frac{bI}{Q_i}$ or $\frac{bI}{Q_{NA}}$	$A_v = \frac{bI}{Q_{NA}} = \frac{bdI}{I_o}$	$A_v = bd = \frac{bd^2}{c}$	8.20 a, b, c, d
Shear Stiffness	$D_v = A_v G$	$D_v = A_v G$	$D_v = A_v G$	8.21

* See Sections 8.5 and 8.7 for modifications of section properties to account for plate behavior

Characteristics of the Transformed Section: The following are important characteristics of the transformed section, particularly as they pertain to sandwich structures.

- The **strain** in any element of the transformed section is the same as that in the actual section.
- The **stress** in the transformed section is a pseudo stress which must be transformed to the actual stress by multiplying the psuedo stress by the modular ratio, n_i. This transformation is included in formulas for section modulus, Eqs. 8.16a, 8.17a, and 8.18a.
- In the general case of a layered cross-section, a rigorous solution for the shear stiffness of the transformed section would account for the different shear stiffnesses of the individual layers. For the special case of sandwich structures, the transverse shear stiffness of the faces is usually much greater than that of the core. Hence, only the core is considered in computation of shear deformation; shear deformation in the faces is assumed negligible.
- The shear stress on the core and adhesive layer is the shear stress calculated for the actual width of these elements.

Equations for determining section properties for typical sandwich beam and column cross-sections having varying degrees of complexity are given in Table 8-1. The section properties in bending for the whole transformed section are appropriate for elementary analyses of constructions having shear-rigid cores. The other expressions for the components of moment of inertia and bending stiffness (e.g. I_o, I_f, D_{mf}, etc.) are needed in the analysis of sandwich panels having shear-flexible cores. This is discussed in more detail in Sections 8.6 to 8.8.

Example Calculations

Example 8-1 illustrates calculations for section properties of a simple cross section having thin faces and a plastic honeycomb core. Because the faces are thin and identical, and the core is "soft", the calculations are simple and straightforward.

Example 8-1: Transformed Section Properties of a Sandwich Beam Having Thin Equal Faces *

Determine the section properties of a sandwich beam having the cross-section shown below. Assume that the 12 in. width of the beam is small enough that plate action can be neglected (See Section 8.7):

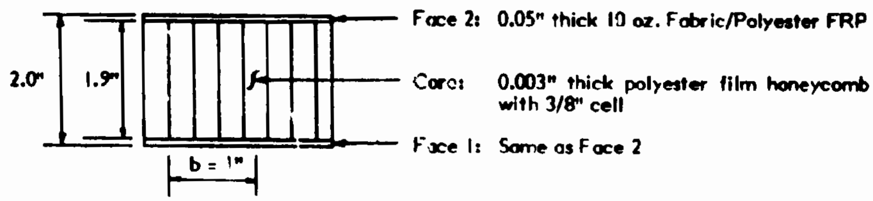

1. **Materials Properties** (in direction of span)

Properties (psi)	Faces (Table 1-6)	Core (8.2)
Elastic Modulus, E_i	2.2×10^6 psi	Neglect
Shear Modulus, G_c	Assume = ∞	5,000 psi

2. **Calculations:** Follow Table 8-1b for thin faces. Use unit width of b = 1.0 in., $E_r = E_1 = 2.2 \times 10^6$, $d = 2.0'' - t_f = 2.0 - 0.05 = 1.95$ in., $c = 2.0 - 2\,t_f = 2.0 - 0.1 = 1.90$ in.

$$A = A_f = 2\,t_f = 2 \times 0.05 \times 1 = 0.10 \text{ in./in.}$$

$$\bar{A} = AE = 0.10 \times 2.2 \times 10^6 = 0.22 \times 10^6 \text{ in.}^2\text{/in.}$$

$$\bar{z} = \frac{d}{2} = \frac{1.95}{2} = 0.975 \text{ in. (mid-depth)}$$

$$I = I_o = \frac{btd^2}{2} = \frac{1 \times 0.05 \times 1.95^2}{2} = 0.095 \text{ in.}^4\text{/in.}$$

$$D_m = EI = 2.2 \times 10^6 \times 0.095 = 0.209 \times 10^6 \text{ lb-in./in.}$$

$$S = btd = 1 \times 0.05 \times 1.95 = 0.0975 \text{ in.}^3\text{/in.}$$

$$\bar{Q}_{NA} = \frac{I_o}{d} = \frac{0.095}{1.95} = 0.049 \text{ in.}^3\text{/in.}$$

$$A_v = bd = 1 \times 1.95 = 1.95 \text{ in.}^2\text{/in.}$$

$$D_v = A_v G = bd\,G = 1 \times 1.95 \times 5{,}000 = 9{,}750 \text{ psi}$$

Note: 1 in. = 25.4 mm; 1 psi = 6.9 kPa; 1 in.^{4}/in. = 16,387 mm^4/mm

---

* Design loads, design criteria (such as safety factors, load factors, capacity reduction factors, etc.) and material properties used in design examples are for illustrative purposes only. The user of this Manual is cautioned to develop his own loads, criteria and materials properties based on the requirements and conditions of his specific design project.

Example 8-2 illustrates calculations for section properties of a more complicated sandwich beam with dissimilar faces. The tabular arrangement for calculations organizes hand calculations for more complicated constructions and it provides a convenient array for checking purposes. Other formats are more suitable for computer use (8.4).

The calculations for the sandwich construction of Example 8-2 show that the core does not contribute significantly to the axial and bending stiffness, in this example. As is typical for soft cores, A_c and I_c are both small. Whether or not the core is shear-flexible will be determined in Section 8.6.

Any time-dependent changes in modulus will usually result in a shift in the neutral axis, and a change in area, stiffness, and moment of inertia of the transformed section. Example 8-3 illustrates these changes in properties of the structural cross-section, for a sandwich panel with one viscoelastic face. Note that for sandwiches having soft cores and thin faces, the section modulus remains unchanged, even though the neutral axis shifts significantly. This, of course, is the expected result since the two faces carry the applied moment by statics.

Example 8-4 illustrates the calculation of section properties for a cross section having one corrugated face.

8.5 Members Under Axial Load

Once the neutral (or centroidal) axis and section properties of the transformed section have been established, stresses, strains and displacements occurring under axial in-plane loads applied at the neutral axis are readily calculated from the following relationships:

Example 8-2: Transformed Section Properties of a Sandwich Panel Having Dissimilar Faces*

Determine the section properties of the sandwich construction shown below. Assume that the 12 in. width of beam is small enough that plate action can be neglected (See Section 8.7).

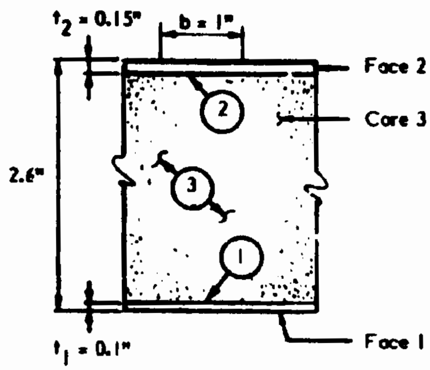

Actual Section

(total width = 12 in.)

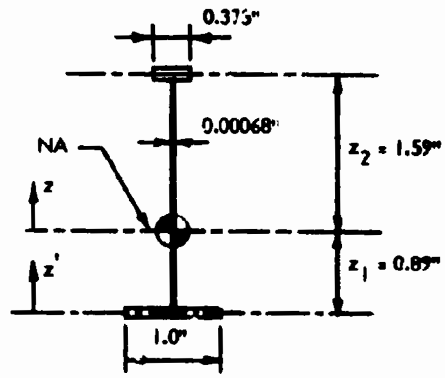

Transformed Section

$E_r = 2.2 \times 10^6$psi

1. Material Properties – Short Term

Element	Face 1	Face 2	Core 3
Material	10 oz FRP	Mat FRP	2.5 pcf PU Foam
Reference	(Table 1 - 6)	(Table 1 - 6)	(8.6)
Elastic Modulus, E_i, psi	2.2×10^6	0.82×10^6	1,500
Shear Modulus, G_c, psi	∞	∞	500
Tensile Strength, F_{ut}, psi	24,000	11,000	25
Compression Strength, F_{uc}, psi	21,000	22,000	20
Shear Strength, F_{uv}, psi	–	–	20

* See Footnote, Example 8-1.

Example 8-2 continued

2. Section Properties

Properties	Unit	Face 1	Face 2	Core 3	Total
E_i	10^6 psi	$2.2 = E_r$	0.82	0.0015	—
G_c	10^6 psi	—	—	0.0005	—
n_i	—	1.0	0.373	0.00068	—
$n_i b_i$	in.	1.0	0.373	0.00068	—
t_i	in.	0.1	0.15	2.35	—
$n_i A_i = n_i b_i t_i$	in.^{2}/in	0.1	0.056	0.00165	0.156 *
z_i'	in.	0	2.48	1.23	—
$n_i A_i z_i'$	in.^{3}/in	0	0.139	0.00197	0.139 *
$\bar{z} = \dfrac{\Sigma n_i A_i z_i'}{\Sigma n_i A_i}$	in.	0.89	—	—	—
$z_i = -\bar{z} + z_i'$	in.	- 0.89	1.59	0.34	—
$I_o = \Sigma n_i A_i z_i^2$	in.^{4}/in.	0.0792	0.142	—	0.221
$I_f = \Sigma n_i b\, t_i^3/12$	in.^{4}/in.	0.000083	0.00010	—	0.000183
$I_{oc} = n_3 b z_3^2$	in.^{4}/in.	these steps are omitted for soft cores *		0.000079	—
$I_c = n_3 b c^3/12$	in.^{4}/in.			0.00074	—
$I = I_o + I_f$	in.^{4}/in.	—	—	—	0.221 *
$D_m = E_r I = E_1 I$	lb-in.^{2}/in.	—	—	—	486,000
$D_{mi} = E_r I_f$	lb-in.^{2}/in.	—	—	—	403
z (extreme fiber)	in.	0.94	1.66	1.51	—
$S = \dfrac{I}{n_i z}$	in.^{3}/in.	0.235	0.357	636	—
$S_{fi} = \dfrac{2 I_{fi}}{n_i t_i} = \dfrac{b_i t_i^2}{6}$	in.^{3}/in.	0.00167	0.00375	—	—
$Q_{NA} = n_1 A_1 z_1$ or	in.^{3}/in.	- 0.089 **	—	—	—
$= n_2 A_2 z_2$				0.089 **	—
$A_v = \dfrac{b I}{Q_{NA}}$	in.^{2}/in.	—	—	2.48	—
$D_v = A_v G_c$	lb/in.	—	—	1240	—

Notes: * Core stiffness neglected. If not, $n_i A_i = 0.158$ in.^{2}/in., $n_i A_i z_i' = 0.141$ in.^{3}/in., and $I = 0.222$ in.^{4}/in.

** Checks as equal for soft core

1 in. = 25.4 mm; 1 psi = 6.9 kPa; 1 lb = 2.2 Kg

Example 8-3: Time Dependent Section Properties of a Sandwich Plate Panel Having Elastic and Viscoelastic Faces *

Determine the short-term and long-term section properties in bending for a sandwich panel having aluminum and PVC faces, and a soft core, as described below:

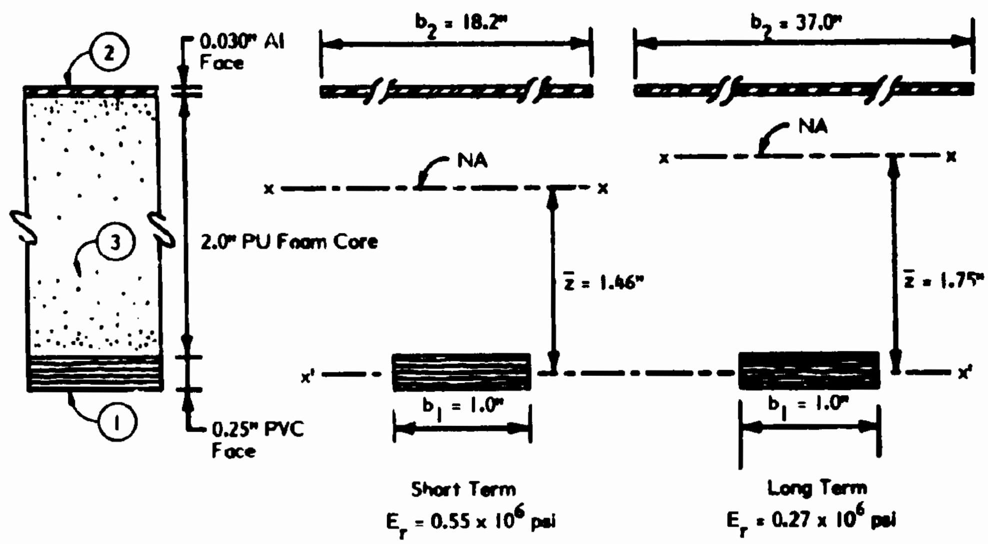

Actual Section **Time-Dependent Transformed Sections**

Solution: Establish E_r as the viscoelastic modulus E_v of PVC. Assume short-term modulus $E_o = 0.55 \times 10^6$ psi, and since $R \simeq 2$ (Table 2-2) the long-term modulus $E_v = 0.55 \times 10^6/2 = 0.27 \times 10^6$ psi. Take E of aluminum as 10×10^6 psi, and assume that this modulus is not time dependent. Assume, G, of foam is 500 psi short-term and 250 psi long-term. Use format of Example 8-2, and neglect in-place stiffness of core since it is soft. Neglect effects of Poisson's ratio.

---

* See Footnote, Example 8-1.

Example 8-3 continued

I. Section Properties

Properties	Unit	Short Term Face 1	Short Term Face 2	Short Term Total	Long Term Face 1	Long Term Face 2	Long Term Total
E	10^6 psi	$0.55 \times E_r$	10	—	$0.27 \times E_r$	10	—
n_i	–	1.0	18.2	—	1.0	37.0	—
$n_i b_i$	in.	1.0	18.2	—	1.0	37.0	—
t_i	in.	0.25	0.03	—	0.25	0.03	—
$n_i A_i$	in.^{2}/in.	0.25	0.546	0.80	0.25	1.11	1.36
z_i'	in.	0	2.14	—	0	2.14	—
$n_i A_i z_i'$	in.^{3}/in.	0	1.17	1.17	0	2.38	2.38
$\bar{z}$	in.	<u>1.46</u>	—	—	<u>1.75</u>	—	—
z_i	in.	- 1.46	0.68	—	- 1.75	0.39	—
I_o	in.^{4}/in.	0.533	0.252	0.785	0.766	0.169	0.935
I_f	in.^{4}/in.	0.0013	small	0.0013	0.0013	small	0.0013
I	in.^{4}/in.	—	—	0.786	—	—	0.936
D_m	lb-in.^{2}/in.	—	—	430,000	—	—	253,000
D_{mf}	lb-in.^{2}/in.	—	—	720	—	—	350
z_{ef}	in.	1.58	0.695	—	1.87	0.405	—
S_{top}	in.^{3}/in.	—	0.062 *	—	—	0.062 *	—
S_{bot}	in.^{3}/in.	0.497 *	—	—	0.500 *	—	—
Q_{NA}	in.^{3}/in.	- 0.365 *	+ 0.371 *	—	- 0.438 *	+ 0.433 *	—
A_v	in.^{2}/in.	2.15 *	—	—	2.14 *	–	—
D_v	lb/in.	1075	—	—	535	—	—

Notes: * Checks as equal on same row

1 in. = 25.4 mm; 1 psi = 6.9 kPa; 1 lb = 2.2 Kg

Example 8-4: **Section Properties of a Steel-Faced Foam-Core Sandwich Panel Having One Corrugated Face** *

Determine the section properties of the sandwich panel described below for long-term loading conditions. Neglect effects of Poisson's ratio as being small since top sheet is corrugated (See Section 8.7).

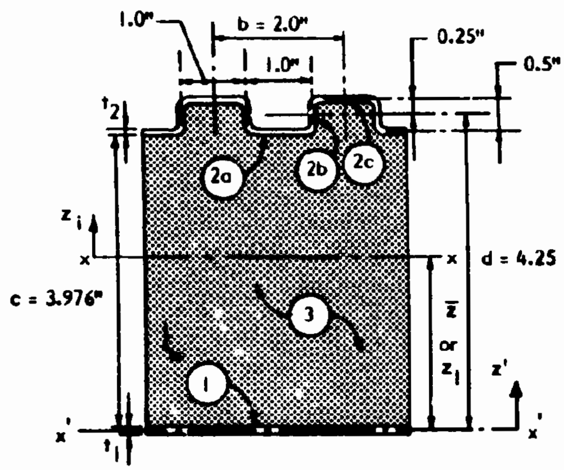

Actual Section

1. Materials Properties

Element	Faces 1 & 2	Core 3	
Material	24 Ga. Steel (t = 0.024")	2.5 pcf PU foam	
Loading Time	Any	Short-Term	Long-Term
Elastic Modulus E_i (psi)	29×10^6	—	—
Shear Modulus G_c (psi)	–	500	250
Min. Yield or Ultimate Strength			
Tension Yield (psi)	36,000	—	–
Tension Ultimate (psi)	58,000	—	—
Compression Ultimate (psi)	—	20	7
Shear Ultimate (psi)	—	20	7
Note: 1 in. = 25.4 mm; 1 psi = 6.1 kPa; 1 pcf = 81.5 kg/m^3			

* See Footnote, Example 8-1.

Example 8-4 continued

2. Section Properties (b = 2 in.)

Properties	Unit	Elements of Cross Section					Total
		Face 1	Face 2			Core 3	
			2a	2b	2c		
$E_i \times 10^6$ psi	29	29	29	29	—	—	—
G_c (long-term)	psi	—	—	—	—	250	—
n_i	—	1	1	1	1	—	—
b_i	in.	2	1.024	0.048	1.024	2	—
t_i	in.	0.024	0.024	0.476	0.024	3.976	—
A (see Eq. 8.2a)	in.^{2}	0.048	0.025	0.023	0.025	—	0.121
z_i'	in.	0	4	4.25	4.5	—	—
$n_i A_i z_i'$	in.^{3}	0	0.10C	0.098	0.113	—	0.311
z_i	in.	-2.57	1.43	1.68	1.93	—	—
I_o (see Eq. 8.8a)	in.^{4}	0.317	0.051	0.065	0.093	—	0.526
I_{f1} (see Eq. 8.9a)	in.^{4}	2.3×10^{-6}	—	—	—	—	2.3×10^{-6}
I_{f2} (see Eq. 8.7a) *	in.^{4}	—	0.00154	0.00043	0.00154	—	—
I_f	in.^{4}	—	—	—	—	—	0.0035
$I = I_o + I_f$	in.^{4}	—	—	—	—	—	0.530
$D_m = E_i\, I \times 10^{-3}$	lb-in.^{2}	—	—	—	—	—	15,370
$D_{mfi} = E_i\, I_f \times 10^{-3}$	lb-in.^{2}	0.067	44.7	12.5	44.7	—	102.0
$S_i = \dfrac{I}{n_i (z_i \pm 0.5\, t_2)}$	in.^{3}	0.205	0.374	—	0.273	—	—
$S_{f1} = \dfrac{0.167\, b_i\, t_i'^2}{n_i}$	in.$^3\times10^{-3}$	0.192	—	—	—	—	—
$S_{f2} = \dfrac{2\, I_f}{n_i (0.5 + t_2)}$	in.^{3}	—	0.0134	—	0.0134	—	—
$Q_{NA} = n_i A_i z_i$	in.^{3}	-0.123	—	—	—	—	—
$A_v = \dfrac{b\, I}{Q_{NA}}$	in.^{2}	—	—	—	—	8.618	—
$D_v = A_v G_c$	lb	—	—	—	—	2012	—

Note: 1 in. = 25.4 mm; 1 psi = 6.9 kPa; 1 lb = 2.2 Kg

* Since the corrugated face in itself resembles key features of a sandwich (thin faces separated by a core or thin web), it is a special case of Table 8-1a, and Eq. 8.7a for I is used to determine I_{f2} here.

Table 8-2

Stress, Strain and Stiffness Relationships for Members under Axial Load

Relationship	Compression Element: Columns and Struts	Compression Element: Plates (Plane Strain)	Eq.
Area, A	$\Sigma n_i A_i$	$\Sigma n_i A_i$	8.2a
Stiffness, $\bar{A}$	$\Sigma n_i A_i E_i = AE_r$	$\Sigma n'_i A_i E_i = AE_r$	8.22 a, b
Stress, σ_i	$\frac{n_i P}{\bar{A}}$	$\frac{n'_i P}{\bar{A}}$	8.23 a, b
Strain, ε	$\frac{P}{\bar{A}}$	$\frac{P}{\bar{A}}$	8.24

Note: If b = 1, P = N

The term n'_i in the above relationships is defined as follows:

$$n'_i = \frac{1}{1 - \nu_i^2}\left(\frac{E_i}{E_r}\right) = \frac{n_i}{1 - \nu_i^2} \qquad \text{Eq. 8.25}$$

In effect, n'_i reflects the increase in axial stiffness in cases where lateral movements due to the Poisson effect are restrained. Such conditions occur in axially loaded plates subjected to plane strain conditions.

Bending stiffness is important in the evaluation of the behavior of columns and plates subjected to loads that are eccentric from the neutral axis, and for evaluating buckling capacity. Bending stiffness is discussed in Sections 8.6 and 8.7.

As illustrated in Example 8-3, certain arrangements of viscoelastic plastics in sandwich cross sections with dissimilar faces may result in very significant shifts in the neutral axis with time under stress and strain. This means that an axial load applied initially at the centroid will gradually become eccentric with respect to the shifting neutral axis. When this occurs, the load is no longer purely axial, and the resulting additional bending effects should be taken into account. When the material stress is within the viscoelastic limit, this can be considered a linear problem, independent of stress level. If the viscoelastic limit is exceeded (which is not recommended), the neutral axis shift would become a function of both stress level and time, and the analysis becomes non-linear.

See Section 8.8 for stability of sandwich members under axial load. Example 8-7, in Section 8.8, illustrates the evaluation of a sandwich member under axial load.

8.6 Beams

Two approaches to the analysis of sandwich beams are presented herein. An elementary theory, which is appropriate for constructions having **shear-rigid cores**, is presented first. It is merely an extension of well established concepts based upon conventional beam theory. A more rigorous theory, which is appropriate for constructions having **shear-flexible cores**, is presented subsequently.

Elementary Theory (Shear-Rigid Cores)

Sandwich structures having shear-rigid cores are very efficient, because the rigid core provides an effective load path to carry shear from one face to the other. Hence, direct or membrane stress resultants are mobilized in the faces to provide high strength and stiffness. As in any efficient bending structure, such as a truss, the objective is to maximize direct stress and minimize bending stress in all elements.

Elementary bending theory, based on plane sections remaining plane after bending, applies to sandwich beams that have adequate core shear rigidity. In this case, beams can be analyzed by conventional transformed-section theory, as described below.

Deflection: In the elementary theory, the total deflection is the sum of the deflection due to bending of the transformed section and the deflection due to shear deformation of the core (Fig. 8-6).

$$w = w_m + w_v \qquad \text{Eq. 8.26}$$

where

w = total deflection

w_m = bending deflection of transformed section under total load

w_v = shear deflection of core under total load

In essence, the bending deflection is that of a beam having a finite bending stiffness and a core having infinite shear rigidity; the shear deflection is that of a beam having an infinite bending stiffness and a finite shear rigidity of the core.

For certain simple support and loading cases, the combined maximum bending and shear deflection for beams with span length, L, can be found by using properties of the transformed section in conjunction with the following equation (8.7):

$$w = \frac{K_m P L^3}{D_m} + \frac{K_v P L}{D_v} \qquad \text{Eq. 8.27}$$

where

P = total load on beam

K_m = deflection coefficient for moment (Table 8-3)

K_v = deflection coefficient for shear (Table 8-3)

The first term on the right of Eq. 8.27 is the conventional beam-theory formula for the deflection of elastic beams due to bending, as typically found in handbooks. The second term accounts for shear deflection, and is generally less readily available. Values of the coefficients are given in Table 8-3 for a number of loading and support conditions.

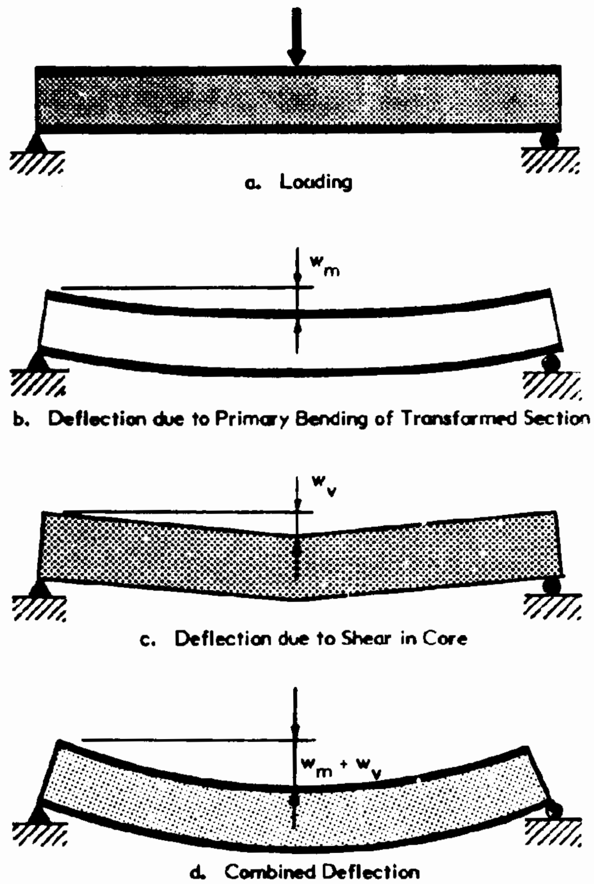

Fig. 8-6 COMPONENTS OF DEFLECTION OF CENTRALLY LOADED SANDWICH BEAM

Table 8-3

Coefficients for Bending and Shear Deflection of Sandwich Beams for Use in Eq. 8.27 (8.7)

Beam Type	Loading Conditions	Location of Deflection	Coefficients Bending K_m	Coefficients Shear K_v
Simply Supported	Uniformly Distributed	Midspan	5/384	1/8
	Concentrated at Midspan	Midspan	1/48	1/4
	Concentrated at Both Quarter Points	Midspan Quarter Points	11/768 1/96	1/8 1/8
Both Ends Fixed	Uniformly Distributed	Midspan	1/384	1/8
	Concentrated at Midspan	Midspan	1/192	1/4
Cantilever	Uniformly Distributed	Free End	1/8	1/2
	Concentrated at Free End	Free End	1/3	1

Non-Symmetric Loads: Shear deflection in a sandwich beam may lead to significant amplification of deflection when loads or support conditions are unsymmetrical. An example this is shown in Fig. 8-7. Physical reasoning (and theory) shows that the shear forces in span AB do not produce vertical deformation and that the shear deformation in that span is merely the lateral displacement of the original square a-b-c-d into a rhombus, creating an angle change of α_1. The shear deformation within the cantilevered portion BC, then, must be taken relative to α_1. Thus, the vertical shear deflection of point C is $(\alpha_1 + \alpha_2) \times BC$.

Indeterminate Support Conditions: When shear deformations become significant in indeterminate structures, handbook formulas based only on bending stiffness

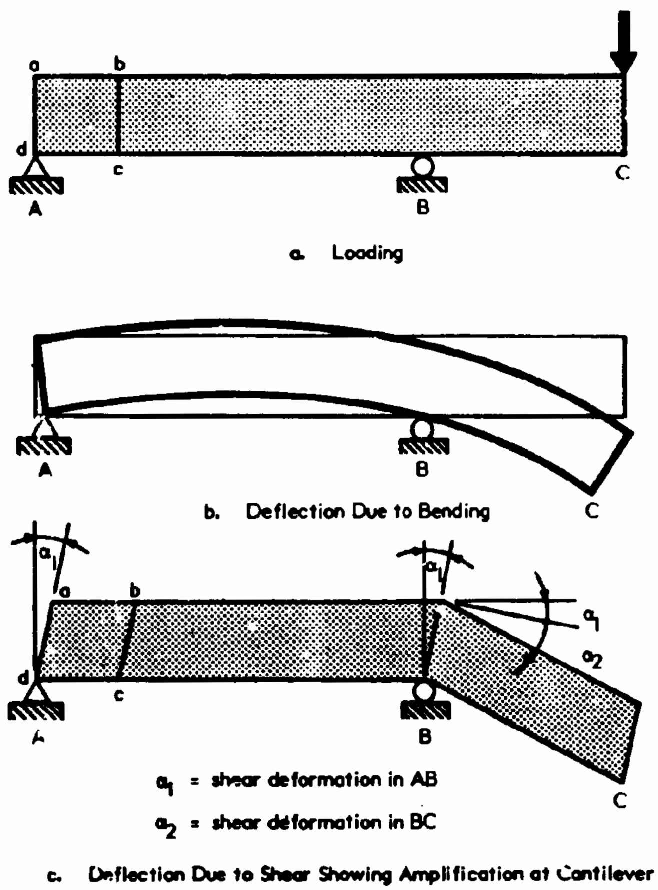

Fig. 8-7 BENDING AND SHEAR DEFLECTION COMPONENTS IN A BEAM WITH CANTILEVERED OVERHANG

may produce large errors in the calculation of reactions, shears, moments, and deflections due to bending. Therefore, shear deflections should be included when determining redundant reactions in such structures. Example 8-5 illustrates such a calculation for a two-span panel subjected to uniform load. The results of this example are used in the numerical example given in Section 8.11.

Viscoelastic Properties: When viscoelastic plastic materials are used for either the faces or the core of a sandwich panel, the time-dependent transformed-section properties which are derived from the appropriate viscoelastic modulus should be used in the calculation of deflections. The stress levels occurring in the various viscoelastic sandwich elements should be checked to verify that they are below the viscoelastic limits for the material in each element.

Stresses: With the properties of the transformed section established, bending and shear stresses are readily calculated using conventional beam theory for a cross-section of variable width. Characteristic bending and shear stress distributions, together with elementary formulas for determining actual stress levels, are given in Fig. 8-8, for several cases as follows:

(a) Thick faces and a stiff and shear-rigid core. This corresponds to the most general cross section having uniform thickness (See also Table 8-1a). The rigid core in this case carries a portion of the applied bending moment and the shear stress in the core varies with distance from the neutral axis.

(b) Thick faces and axially soft, but shear-rigid, core. As discussed earlier, this case allows some simplification, since the soft core does not carry significant bending stress. The core shear stress is essentially uniform. While the soft core does not contribute significantly to bending capacity, the stresses in the core should never be neglected out of hand, since most soft cores are very weak compared to the faces. Note that the approximate Eq. 8.38b is conservative by 8% or less for practical sandwich constructions where t/d is less than 0.5.

(c) Thin faces and axially soft, but shear-rigid, core. The faces are sufficiently thin to permit the simplifying assumption that there is a negligible stress gradient between the neutral axis of the face and the extreme fibers of the section.

Example 8-5: Derivation of Reactions, Moments and Shears in a Two-Span Beam Subjected to Uniform Load *

1. **Structural Arrangement**

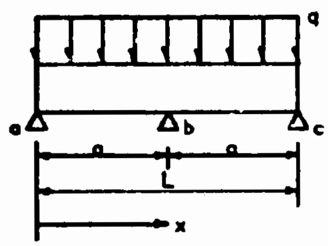

2. **Determine Deflection due to Uniform Load with Redundant Support R_{bL} Removed**

$$w_b = \frac{K_m P L^3}{D_m} + \frac{K_v P L}{D_v} \qquad \text{Eq. 8.27}$$

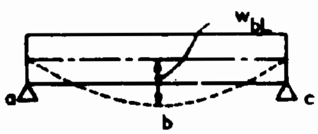

for uniform load (Table 8-3)

$K_m = 5/384;\ K_v = 1/8;\ P = qL = 2qa$

$$w_{bL} = \frac{qa^2}{2}\ \frac{5a^2}{12D_m} + \frac{1}{D_v} \qquad \text{Eq. 8.38}$$

3. **Determine Restoring Deflection with Redundant Support Reaction Acting Alone**

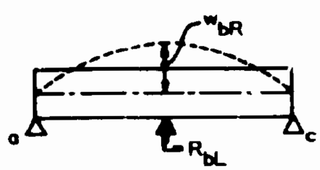

for concentrated load at midspan (Table 8-3)

$K_m = 1/48;\ K_v = 1/4;\ P = R_{bL}$

$$w_{bR} = -\frac{R_{bL}\,a}{2}\left[\frac{a^2}{3D_m} + \frac{1}{D_v}\right] \qquad \text{Eq. 8.29}$$

4. **Solve for R_{bL} by Setting Deflection at b = 0**

$$w_{bL} + w_{bR} = 0;\ R_{bL} = q\,a\left[\frac{\frac{5a^2}{12D_m} + \frac{1}{D_v}}{\frac{a^2}{3D_m} + \frac{1}{D_v}}\right] \qquad \text{Eq. 8.30}$$

---

* See Footnote, Example 8-1.

Example 8-5 continued

5. End Reactions R_{aL} and R_{cL}

$$-q\ (2a) + R_{bL} + R_{aL} + R_{cL} = 0$$

$$R_{aL} = R_{cL} = \frac{-R_{bL} + 2\,qa}{2} \qquad \text{Eq. 8.31}$$

6. Moment in Span ab

$$M_{ab} = R_{aL}x - \frac{qx^2}{2}; \text{ at midspan, } x = \frac{a}{2}, \text{ and}$$

$$M = R_{aL}\frac{a}{2} - \frac{q\,a^2}{8} \qquad \text{Eq. 8.32 a, b}$$

7. Moment at b (x = a)

$$M_{bL} = R_{aL}a - q\frac{a^2}{2} \qquad \text{Eq. 8.33}$$

8. Shears at a and b

$$V_{aL} = R_{aL}\ ;\ V_{bL} = R_{aL} - q\,a \qquad \text{Eq. 8.34a, b}$$

9. Deflection at Midspan ab

Superimpose two loading cases on span a b. Case A is deflection of simply supported uniformly loaded beam (Eq. 8.27) moment M_{bL} not acting. Case B is deflection (in opposite direction) of simply supported beam with no load, and acted upon by M_{bL} (8.14) at b. (Note: M_{bL} is negative.)

$$w_L = w_A + w_B$$

$$w_L = \left[\frac{K_m\,Pa^3}{D_m} + \frac{K_v\,Pa}{D_v}\right]_A + \left[\frac{M_{bL}\,a^2}{16\,D_m}\right]_B$$

$$K_m = 5/384,\ K_v = 1/8 \text{ (Table 8-3)},\ P = q\,a$$

$$w_L = \frac{1}{8}\,q\,a^2\left[\frac{5a^2}{48\,D_m} + \frac{1}{D_v}\right] + \frac{M_{bL}\,a^2}{16\,D_m} \qquad \text{Eq. 8.35}$$

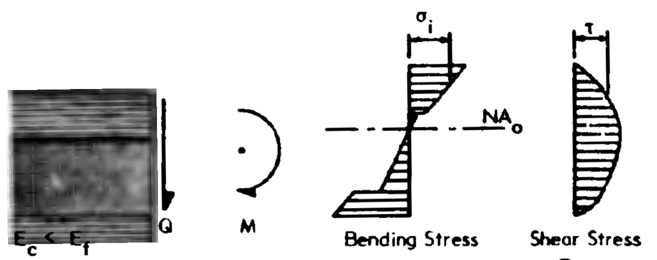

$\sigma_i = \frac{M}{S_i}$ (Eq. 8.36) $\quad \tau = \frac{Q\bar{Q}}{bI}$ (Eq. 8.32)

a. Thick faces – axially stiff and shear-rigid core

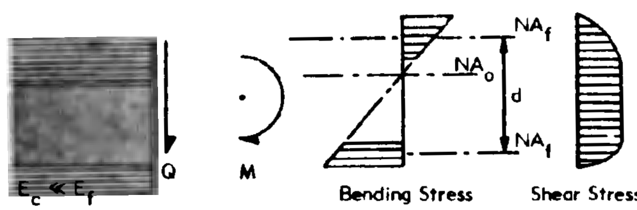

$\sigma_i = \frac{M}{S_i}$ $\quad \tau = \frac{Q\bar{Q}_f}{bI} \quad \frac{Q^*}{bd}$ (Eq. 8.38a, b)

* for t_i/d 0.5, see text

b. Thick faces – axially soft and shear-rigid core

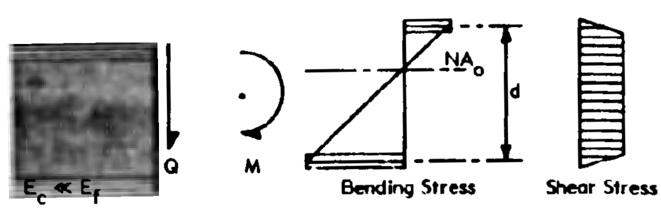

$\sigma = \frac{M}{S}$ (Eq. 8.39) $\quad \tau = \frac{Q}{bd}$ (Eq. 8.40)

c. Thin faces – axially soft and shear-rigid core

Fig. 8-8 BENDING AND SHEAR STRESS DISTRIBUTION IN SANDWICH BEAMS HAVING SHEAR-RIGID CORES

In all of the above cases, it is implicit that plane sections before bending remain plane after bending. This is only valid for shear-rigid cores. The important effects introduced by shear-flexible cores are discussed below.

Analysis for Shear-Flexible Cores

The term shear-flexible, as used herein, defines a relative condition in which the core provides a low shear rigidity compared to the flexural stiffness of the faces. Sandwich panels having shear-flexible cores do not behave in accordance with conventional beam theory. Shear deformations and deflections become significant, and conventional elementary theory described earlier may fail to predict behavior within suitable limits. Such limits will be discussed subsequently.

Sandwich constructions which have shear-flexible cores are not efficient beams. The shear-flexible core is only partially effective in carrying shear from one face to the other, and hence, resistance to bending by direct or membrane stress resultants in the faces may not be fully mobilized. The result is that the faces carry a larger share of the load in bending about their own neutral axes than is indicated from elementary theory. In the extreme, lacking help from the core, the two faces may carry all of the load as separate beams, spanning between reactions, independent of the core.

While it is the objective of structural design to develop efficient primary structures, there are other criteria that may require a compromise in this design objective, and lead to structural arrangements where the core acts in a shear-flexible manner. Examples are as follows:

- The use of low density foamed plastics may be desirable for reasons of weight, thermal resistance, or cost. Such cores frequently have very low shear rigidity compared to the faces, as well as in comparison with other cores available for sandwich construction, such as honeycombs made from metal or plastic-impregnated paper. For example, the long-term visco-elastic shear modulus of a low density plastic foam may be as low as 200 psi — such cores prove to be shear-flexible in most practical sandwich constructions.

- Faces may be corrugated, ribbed, or exceptionally thick for aesthetics, stability against local buckling, and many other reasons. Furthermore, the modulus of elasticity of some advanced-fiber reinforced plastics facings may be very high, and approach that of metals. Thus, the bending stiffness of faces may be high, relative to the shear rigidity of many practical cores.

Thus, in view of the above, there may be many practical cases where the shear-flexible core condition exists, and the application of rigorous theory may be required.

Description of Analysis: The analysis for shear-flexible cores employs differential equations to enforce compatibility between the bending and shear deflections of the transformed section, and the bending deflection of the faces, along the full length of the beam. In the elementary theory, summing the shear and moment deflections to obtain the total deflection neglects the resistance to deflection offered by the secondary bending of the faces. Therefore, the deflection of the member according to the refined theory will generally be less than that calculated from the elementary theory, but the faces stresses will be greater because the secondary bending is less efficient than the primary bending in resisting loads. Using the refined theory, the total deflection (w) is the sum of the primary (w_p) and secondary bending deflections, where the secondary bending deflections are the same as the shear deflections, (w_s).

The following expressions describe the components of loads and transverse shear and moment stress resultants at any point along the beam length assumed in the refined theory:

$$q = q_p + q_s \qquad \text{Eq. 8.41}$$

$$Q = Q_p + Q_s \qquad \text{Eq. 8.42}$$

$$M = M_p + M_s \qquad \text{Eq. 8.43}$$

In each case, the subscript "p" indicates the component carried by the full transformed section (Fig. 8-9a). The subscript "s" denotes the component carried by shear and bending in the faces, over and above that which occurs in the transformed section (Fig. 8-9b).

The total deflection (w) is as follows:

$$w = w_p + w_s \qquad \text{Eq. 8.44}$$

where w_p = primary bending deflection of transformed section due to primary shear stress resultants (Q_p)

w_s = secondary deflection

= deflection of core due to primary shear stress resultants (Q_p)

= deflection of faces bending about their own neutral axes due to secondary shear stress resultants (Q_s)

Consideration of both statics and compatibility of deflections leads to the following differential equations (8.3):

$$-Q_p = D w_l''' = E I_o w_p''' + E I_f w_p''' \qquad \text{Eq. 8.45}$$

from which

$$Q_p'' - \frac{4\theta^2 Q_p}{L^2} = -\frac{4\theta^2 Q}{L^2} \qquad \text{Eq. 8.46}$$

and

$$w_s' = Q_p\left(\frac{L^2}{4\theta^2}\right) \qquad \text{Eq. 8.47}$$

where

$$\theta = \frac{L}{2}\left[\frac{AGI}{E_f I_o}\right]^{1/2} = \frac{L}{2}\left[\frac{D_v I}{D_{mf} I_o}\right]^{1/2} \approx \frac{L}{2}\left[\frac{D_v}{D_{mf}}\right]^{1/2} \qquad \text{Eq. 8.48a, b, c}$$

Primes denote differentiation with respect to x, the distance along beam length.

In any particular problem in which the total shear, Q, is a given function of, x, Eq. 8.46 can be solved for Q_p. The quantities M_p, w_p, and q_p may be obtained by integration and differentiation. The slope, w_s', can be obtained from Eq. 8.47, and the quantities M_s, w_s, and q_s are obtained by subsequent integration and differentiation. Eq. 8.41 to 8.45 and suitable boundary conditions are needed to effect the above solutions.

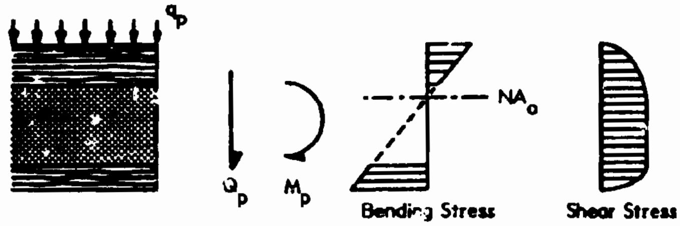

a. Distribution under Primary Bending and Shear on Transformed Section – Axially Soft and Shear-Rigid Cores

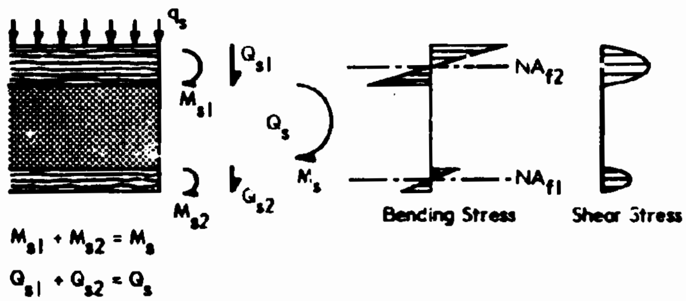

b. Distribution under Secondary Bending and Shear on Facings

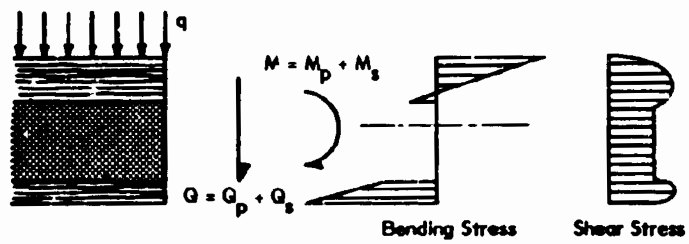

c. Net Distribution under Applied Moment and Shear

Fig. 8-9 BENDING AND SHEAR STRESS DISTRIBUTION IN SANDWICH BEAMS HAVING SHEAR-FLEXIBLE CORES

In essence, in the analysis for shear-flexible cores, the total shear (Q) and the total moment (M) acting on any cross section are divided into two components, as described below and shown in Fig. 8-9:

- The **primary** shear (Q_p) and moment (M_p) stress resultants act on the full transformed section in exactly the same way as shown earlier for the elementary theory in Fig. 8-8. (Compare Figs. 8-8b and 8-9a.)
- The **secondary** shear (Q_s) and moment (M_s) stress resultants act only on the faces (Fig. 8-9b). These secondary stress resultants cause the faces to bend about their own neutral axis. This bending of faces, which is over and above the bending imposed on the transformed section by the primary stress resultants, is neglected in the elementary analysis.

Numerical Solutions: The analysis for shear-flexible cores is general and can be applied to any loading condition (8.3, 8.8). Only the simpler cases of simply supported beams loaded with a uniformly distributed load or concentrated loads are presented herein. Of course, by symmetry and superposition, these cases can be readily altered to handle both cantilever and continuous beams. Numerical solutions for other load and support cases must be derived from the general differential equations as given in (8.3, 8.5, 8.8), and summarized from (8.3), below:

Equations giving numerical results for the analysis of shear-flexible cores, are given for certain load and support conditions in Table 8-4. Relations are given for deflections, moments, and shears at any point along the beam length. Equations for maximum values are also given. Note that the origin (x = 0, or X = 0) is different for different loading cases.

Effects of θ: The shear flexibility coefficient, θ, Eq. 8.48 has a strong influence on the magnitude of the deflection, moments, and shears, calculated in accordance with the theory for shear-flexible cores. The magnitude of the shear flexibility coefficient, θ, depends upon the span, the ratio of shear rigidity of the core to the flexural stiffness of the faces, and the ratio of I to I_o. Since $(I/I_o)^{1/2}$ is usually close to one, even for relatively thick faces, its effect on θ is negligible. (See Table 8-1 for definition of I and I_o.) Hence, for a given span, θ

Table 8-4

Deflections, Moments and Shears in Sandwich Beams Having Flexible Cores (as derived from 8.3, 8.5 and 8.8)

Loading Condition	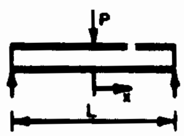	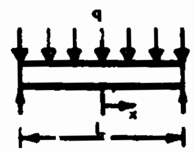	
	GENERAL EXPRESSIONS		Equation
Deflection (relative to midspan)	$w = \frac{PL\,x^2}{24\,D_m}\left(3 - \frac{2x}{L}\right) + \frac{PL}{4D_v}\left(\frac{I_o}{T}\right)^2$ $\left[\frac{2x}{L} - \frac{1}{\theta}\left(\sinh\frac{2\theta x}{L} + \tanh\theta\left(1 - \cosh\frac{2\theta x}{L}\right)\right)\right]$	$w = \frac{qL^2x^2}{48\,D_m}\left(3 - \frac{2x^2}{L^2}\right) + \frac{qL^2}{8D_v}\left(\frac{I_o}{T}\right)^2\left[\frac{4x^2}{L^2} + \frac{2}{\theta^2}\frac{1}{\cosh\theta}\left(1 - \cosh\frac{2\theta x}{L}\right)\right]$	8.49a, b
Bending Moment			
Total	$M = \frac{P}{2}\left(\frac{L}{2} - x\right)$	$M = q\left(\frac{L^2}{8} - \frac{x^2}{2}\right)$	8.50a, b
Primary	$M_p = M - M_s$	$M_p = M - M_s$	8.45
Secondary	$M_s = \frac{PL}{4\theta}\left(\tanh\theta\cosh\frac{2\theta x}{L} - \sinh\frac{2\theta x}{L}\right)$	$M_s = \frac{qL^2}{4\theta^2}\left(1 - \frac{\cosh\frac{2\theta}{L}}{\cosh\theta}\right)$	8.51a, b
Shear			
Total	$Q = \frac{P}{2}$	$Q = qx$	8.52a, b
Primary	$Q_p = Q\left(1 - \cosh\frac{2\theta x}{L} + \tanh\theta\sinh\frac{2\theta x}{L}\right)$	$Q_p = \frac{qL}{2}\left(\frac{2x}{L} - \frac{\sinh\frac{2\theta x}{L}}{\theta\cosh\theta}\right)$	8.53a, b
Secondary	$Q_s = Q - Q_p$	$Q_s = Q - Q_p$	8.44
	MAXIMUM VALUES		
Midspan Deflection	$w = \frac{PL^3}{48\,D_m} + \frac{PL}{4D_v}\left(\frac{I_o}{T}\right)^2\phi_1$	$w = \frac{5\,qL^4}{384\,D_m} + \frac{qL^2}{8D_v}\left(\frac{I_o}{T}\right)^2\phi_3$	8.54a, b
Bending Moment			
Primary @ x = 0	$M_p = M\phi_1$	$M_p = M\phi_3$	8.55a, b
Faces @ x = 0	$M_s = M(1 - \phi_1)$	$M_s = M(1 - \phi_3)$	8.56a, b
Total @ x = 0	$M = M_p + M_s = \frac{PL}{4}$	$M = M_p + M_s = \frac{qL^2}{8}$	8.57a, b
Shear			
Primary @ x = L/2	$Q_p = \frac{P}{2}\phi_2$	$Q_p = \frac{qL}{2}\phi_1$	8.58a, b
Faces	$Q_s = \frac{P}{2}$ (@ x = 0)	$Q_s = \frac{qL}{2}(1 - \phi_1)$ (@ x = L/2)	8.59a, b

COEFFICIENTS

$$\phi_1 = 1 - \frac{\tanh\theta}{\theta} \qquad \phi_2 = 1 - \frac{1}{\cosh\theta} \qquad \phi_3 = 1 - \frac{2}{\theta^2}\left(1 - \frac{1}{\cosh\theta}\right) \qquad \text{8.60a, b, c}$$

$$\theta = \frac{L}{2}\left(\frac{AG\,I}{EI_f\,T_o}\right)^{1/2} = \frac{L}{2}\left(\frac{D_v\,I}{D_{mf}\,T_o}\right)^{1/2} = \frac{L}{2}\left(\frac{D_v}{D_{mf}}\right)^{1/2} \qquad \text{8.48a, b, c}$$

$$\text{for } \theta \geq 5,\quad \phi_1 = \frac{\theta - 1}{\theta},\quad \phi_2 = 1,\quad \phi_3 = \frac{\theta^2 - 2}{\theta^2} \qquad \text{8.61a, b, c}$$

Table 8-4 (continued)

Deflections, Moments and Shears in Sandwich Beams Having Flexible Cores (as derived from 8.3, 8.5 and 8.8)

Loading Condition

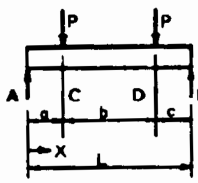

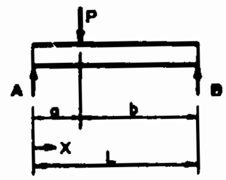

GENERAL EXPRESSIONS

			Equation
Deflection	For Midspan Deflection see **Maximum Values** below.		
Bending Moment			
Total	$M = \frac{P(L-a)X}{L}$	$M = PX\ (@\ 0 < X < a);\ M = Pa\ (@\ a < X < a+b)$	8.62a, b, c
Primary	$M_p = M - M_s$	$M_p = M - M_s$	8.45
Secondary: $(0 < X < a)$	$M_s = M \frac{L}{(L-a)}\left[\frac{\sinh\left[2\theta(1-\frac{a}{L})\right]\sinh\left[2\theta\frac{X}{L}\right]}{2\theta\frac{X}{L}\sinh 2\theta}\right]$	$M_s = M\frac{\cosh\left[\theta(1-\frac{2a}{L})\right]\sinh\left[2\theta\frac{X}{L}\right]}{2\theta\frac{X}{L}\cosh\theta}$	8.63a, b
$(a < X < a+b)$	$M_s = M\frac{L}{a}\frac{\sinh\left[2\theta(1-\frac{X}{L})\right]\sinh\left[2\theta\frac{a}{L}\right]}{2\theta(1-\frac{X}{L})\sinh 2\theta}$	$M_s = M\frac{\cosh\left[\theta(1-\frac{2X}{L})\right]\sinh\left[2\theta\frac{a}{L}\right]}{2\theta\frac{a}{L}\cosh\theta}$	8.64a, b
Shear			
Total	$Q_A = \frac{P(L-a)}{L};\ Q_B = \frac{Pa}{L}$	$Q_A = -Q_B;\ Q_{CD} = -Q_{DC} = 0$	8.65a, b, c
Primary $(0 < X < a)$	$Q_p = Q_A\left[1 - \frac{L}{(L-a)}\frac{\sinh\left[2\theta(1-\frac{a}{L})\right]\cosh\left[2\theta\frac{X}{L}\right]}{\sinh 2\theta}\right]$	$Q_p = P\left[1 - \frac{\cosh\left[\theta(1-\frac{2a}{L})\right]\cosh\left[2\theta\frac{X}{L}\right]}{\cosh\theta}\right]$	8.66a, b
$(a < X < a+b)$	$Q_p = Q_B\left[1 - \frac{L}{a}\frac{\sinh\left[2\theta\frac{a}{L}\right]\cosh\left[2\theta(1-\frac{X}{L})\right]}{\sinh 2\theta}\right]$	$Q_p = P\left[\frac{\sinh\left[2\theta\frac{a}{L}\right]\sinh\left[\theta(1-\frac{2X}{L})\right]}{\cosh\theta}\right]$	8.67a, b
Secondary	$Q_s = Q - Q_p$	$Q_s = Q - Q_p$	8.44

MAXIMUM VALUES

Midspan Deflection	$w = \frac{PaL^2}{16D_m}\left[1 - \frac{4}{3}\left(\frac{a}{L}\right)^2\right] + \frac{Pa}{2D_v}\left(\frac{I_o}{T}\right)^2\phi_4$	$w = \frac{PaL^2}{8D_m}\left[1 - \frac{4}{3}\left(\frac{a}{L}\right)^2\right] + \frac{Pa}{D_v}\left(\frac{I_o}{T}\right)^2\phi_5$	8.68
Bending Moment			
Primary	$M_p = M\phi_4\ (@\ X = a)$	$M_p = M\phi_5\ (@\ X = a),\ M_p = M\phi_6\ (@\ X = L/2)$	8.69a, b, c
Faces	$M_s = M(1-\phi_4)\ (@\ X = a)$	$M_s = M(1-\phi_5)\ (@\ X = a),\ M_s = M(1-\phi_6)\ (@\ X = L/2)$	8.70a, b, c
Total	$M = M_p + M_s = \frac{P(L-a)a}{L}\ (@\ X = a)$	$M = M_p + M_s = Pa\ (@\ X = a);\ M_p + M_s = Pa\ (@\ X = L/2)$	8.71a, b, c
Shear			
Primary	$Q_p = \frac{Pb}{L}\phi_7\ (@\ X = 0),\ Q_p = -\frac{Pa}{L}\phi_8\ (@\ X = L)$	$Q_p = P\phi_9\ (@\ X = 0)$	8.72a, b, c
Faces	$Q_s = \frac{Pb}{L}\ (@\ X = a)$	$Q_s = P\ (@\ X = a)$	8.73

COEFFICIENTS

$\phi_4 = 1 - \frac{L}{(L-a)}\frac{\sinh\left[2\theta(1-\frac{a}{L})\right]\sinh\left[2\theta\frac{a}{L}\right]}{2\theta\frac{a}{L}\sinh 2\theta}$	$\phi_7 = 1 - \frac{L}{(L-a)}\frac{\sinh\left[2\theta(1-\frac{a}{L})\right]}{\sinh 2\theta}$	8.74a, b
$\phi_5 = 1 - \frac{\cosh\left[\theta(1-\frac{2a}{L})\right]\sinh\left[2\theta\frac{a}{L}\right]}{2\theta\frac{a}{L}\cosh\theta}$	$\phi_8 = 1 - \frac{L}{a}\frac{\sinh\left[2\theta\frac{a}{L}\right]}{\tanh 2\theta}$	8.75a, b
$\phi_6 = 1 - \frac{\sinh\left[2\theta\frac{a}{L}\right]}{2\theta\frac{a}{L}\cosh\theta}$	$\phi_9 = 1 - \frac{\cosh\left[\theta(1-\frac{2a}{L})\right]}{\cosh\theta}$	8.76a, b

$$\theta = \frac{L}{2}\left(\frac{AG\,I}{EI_f T_o}\right)^{1/2} = \frac{L}{2}\left(\frac{D_v I}{D_{mf} T_o}\right)^{1/2} \quad \frac{L}{2}\left(\frac{D_v}{D_{mf}}\right)^{1/2} \qquad \text{8.48a, b, c}$$

$$\text{for } \theta > 5:\ \phi_4 = 1 - \frac{1}{4\theta\frac{a}{L}(1-\frac{a}{L})};\quad \phi_7 = 1 \qquad \text{8.77a, b}$$

depends on D_v/D_{mf}, and Eq. 8.48c can be used for most practical sandwich structures.

The magnitude of the shear flexibility coefficient, θ, governs the relative importance of secondary face bending. This is illustrated in Fig. 8-10 which shows the distribution of primary and secondary shear and moments along the length of a centrally loaded, simply supported sandwich beam, for a range of θ = 1 to ∞. Following are significant results shown in the Figure:

- The faces carry the full shear near the center of the span for all values of θ. In the elementary analysis it is assumed that the core carries the full shear for the whole length of the beam.
- As θ decreases, faces carry an increasing share of the total shear over substantial portions of the beam.
- As θ decreases, an increasing share of the total moment in the central portion of the beam is carried by the faces in secondary bending about their own neutral axes. At $\theta = 3$ for example, the faces carry about 25% of the total midspan moment.

With θ equal to about 5 or greater, tanh θ = 1 for all practical purposes, and simplified coefficients, ϕ, are given in Table 8-4 for this case. Further simplifications for two common cases are:

for concentrated loads at midspan	$M_{s\,max} = \frac{M_{max}}{\theta}$; $\theta \geq 5$	Eq. 8.78
for uniformly distributed loads	$M_{s\,max} = \frac{2\,M_{max}}{\theta^2}$; $\theta \geq 5$	Eq. 8.79

As θ increases further, the share of the total moment carried by the faces in secondary bending about their own axes decreases rapidly and the primary transformed section carries most of the total moment. The structure thus becomes a more efficient composite, and the behavior approaches that assumed in elementary theory. However, even though M_s decreases to small values with increases in θ, face stresses may still be significant, since the section modulus of thin faces is small.

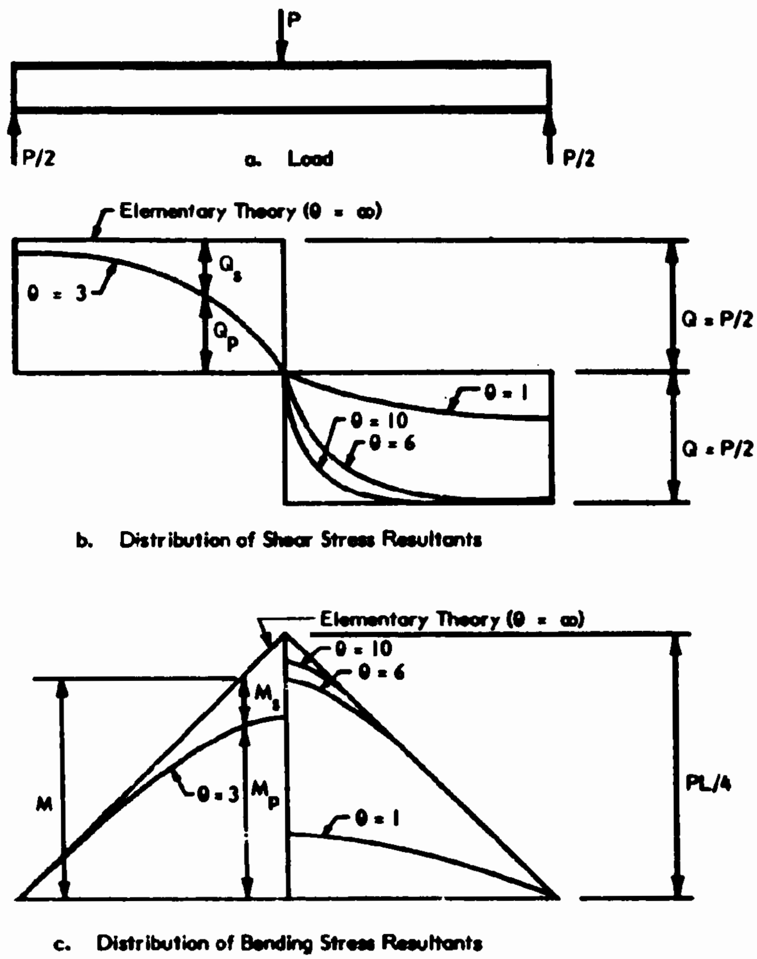

Fig. 8-10 DISTRIBUTION OF MOMENTS AND SHEARS IN SIMPLY-SUPPORTED SANDWICH BEAMS HAVING SHEAR-FLEXIBLE CORES

Effects of Concentration of Load: In the analysis for shear-flexible cores, concentrated loads are assumed to be applied as line or knife-edge loads. In practical structures, concentrated loads are actually distributed locally over a finite width. Whether it is important to account for the actual width of the load can be determined by comparing this width to the distance over which the secondary bending moment from the knife-edge load decays to a small value.

For a knife-edge load applied at midspan of a simply supported sandwich beam, the bending moment decays to p% of its maximum value at a distance, $(2x)_d$, defined by the following relationship:

$$(2x)_d = 0.408 \left[\frac{t^3 E_f}{d G_c}\right]^{1/2} \log_e \left(\frac{100}{p}\right) \qquad \text{Eq. 8.78}$$

This equation, derived from Eqs. 8.48 and 8.51a, holds only for relatively thin faces where the problem of large face stresses resulting from knife-edge loads is most critical, and for values of θ greater than about 5. The calculation of the distance $(2x)_d$ is illustrated in connection with a practical design in Fig. 8-11, which will be discussed in more detail later.

In application, if the actual width of the load is on the order of $(2x)_d$, it can be divided into a number of knife-edge loads distributed over the actual width. The effects of each concentrated load are then superimposed to determine the maximum moment under the load.

Effects of Overhangs at Beam Ends: For simplicity, equations given in Table 8-4 pertain to beams without overhangs at supports. The effects of overhangs, which are unloaded, are fairly small, and such overhangs are not usually encountered in practical framing. However, flexural test coupons of sandwich constructions are usually significantly longer than the test span, and the effects of the overhanging ends should be considered in interpreting test results. Equations which account for the effects of overhangs on centrally loaded and uniformly loaded beams are given in (8.3).

Application of the Analysis for Shear-Flexible Cores: The following procedure is used to analyze sandwich cross sections having shear-flexible cores:

- Section properties and bending stiffness of both the transformed section and the faces, and shear stiffness of the core, are calculated using equations given in Table 8-1.
- The equations given in Table 8-4 are used to determine the shear-flexibility coefficient θ, deflections, and the primary, secondary, and total bending moments.
- The primary moment, M_p, is applied to the transformed section of the whole cross-section, and primary bending stresses are calculated in the same fashion as described previously for the elementary theory.
- The secondary face moment, M_s, is applied to Faces 1 and 2 in proportion to the ratio of bending stiffness of the respective faces, D_{mf1}, and D_{mf2} to the total bending stiffness of both faces ($D_{mf1} + D_{mf2}$). The moments so calculated, M_{s1} and M_{s2}, are then divided by the section modulus of each respective face (about its own neutral axis) to obtain secondary face stresses.
- The stresses due to the primary and secondary moments are added to obtain the total stresses in the faces.
- The primary shear stress resultants are calculated from equations given in Table 8-4. These are then divided by the shear area, Table 8-1, to obtain shear stresses in the core, and in the adhesive bond as appropriate.
- The secondary shear stress resultants which act on the faces may be calculated from equations given in Table 8-4. The shear stresses are then calculated for each face from elementary beam theory. These stresses are seldom critical in practical sandwich constructions.
- If concentrated loads have a width on the order that given by Eq. 8.78, the load can be divided into a number of knife-edge loads, as discussed earlier, to provide a refined estimate of maximum secondary moment on the faces (see above, Effects of Concentration of Load).

Example 8-6 illustrates the calculations required to analyze for secondary bending effects in an unbalanced, metal-faced, sandwich beam having one corrugated face and a plastic foam core. In this example, maximum combined face stress caused by primary and secondary bending of the stiff corrugated face is 6,133 psi (42.4 MPa). As is shown, elementary theory, which neglects the flexibility of the core, would have given a total stress of 3,436 psi (24.1 MPa)

Example 8-6: Evaluate Foam Core Sandwich Beam with One Face Corrugated *

Determine adequacy of the steel-faced panel for which section properties were determined in Example 8-4. Span is 100 in., and the long-term design load is 30 psf. Use Load Factor of 1.8. Deflection Limit is L/200.

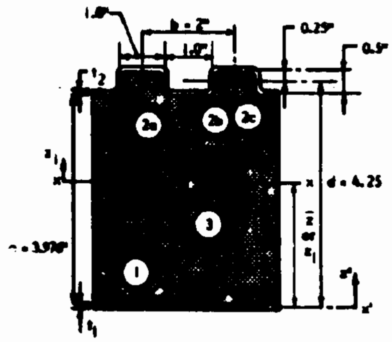

Actual Section
(from Example 8-4)
(Use 2 in. wide repeating strip)

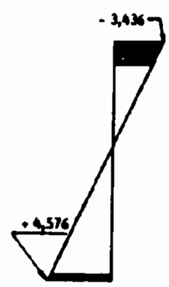

Stress Distribution Transformed Section Analysis

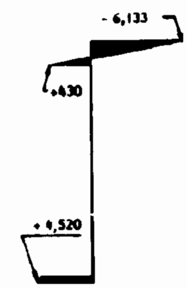

Stress Distribution Shear-Flexible Core Analysis

1. **Design Load** (b = 2 in.) $q = \frac{30 \times 2}{144} = 0.417$ lb/in. (unfactored)

2. **Coefficients** (See Example 8-4 for section properties and Table 8-4 for equations)

$$\theta = \frac{L}{2}\left[\frac{D_v I}{D_{mf} I_o}\right]^{0.5} = \frac{100}{2}\left[\frac{2012 \times 0.530}{102 \times 10^3 \times 0.526}\right]^{0.5} = 7.1$$

for $\theta > 5$ use Eq. 8.61a, c, Table 8-4.

$$\phi_3 = \frac{\theta^2 - 2}{\theta^2} = \frac{7.1^2 - 2}{7.1^2} = 0.96 \text{ for moment and deflection}$$

$$\phi_1 = \frac{\theta - 1}{\theta} = \frac{7.1 - 1}{7.1} = 0.86 \text{ for shear}$$

---

* See Footnote, Example 8-1.

Example 8-6 continued

3. **Ultimate Bending Moment** (LF = 1.8)

$$M = \frac{1}{8} q L^2 \times LF = \frac{1}{8} \times 0.417 \times 100^2 \times 1.8 = 938 \text{ lb-in.}$$

4. **Determine Primary and Secondary Moments:**

Primary: $M_p = \phi_3 M = 0.96 \times 938 = 900$ lb-in.

Secondary: $M_s = M - M_p = 938 - 900 = 38$ lb-in.

Secondary moment is assigned to faces in proportion to their bending stiffness.

$$M_{s1} = \frac{D_{mf1}}{D_{mf}} \times M_s = \frac{0.067}{102.0} \times 38 = 0.025 \text{ lb/in.}$$

$$M_{s2} = \frac{D_{mf2}}{D_{mf}} \times M_s = \frac{102 - 0.067}{102.0} \times 38 = 38 \text{ lb/in.}$$

5. **Maximum Stresses in Faces at Midspan:**

Face 1:	Primary (tension)	$f_{p_1} = \frac{M_p}{S_1} = \frac{900}{0.205} = +4{,}390$ psi	
	Secondary	$f_{s_1} = \frac{0.025}{0.192 \times 10^{-3}} = \pm \underline{130}$ psi	Total = +4,520 psi and + 4,260 psi
Face 2: (Element 2a)	Primary (compression)	$f_{p_{2a}} = \frac{M_p}{S_{2a}} = \frac{900}{0.374} = -2{,}406$ psi	
	Secondary (tension)	$f_{s_{2a}} = \frac{M_{s2}}{S_{f2}} = \frac{38}{0.0134} = +\underline{2{,}836}$ psi	Total = + 430 psi
Face 2: (Element 2c)	Primary (compression)	$f_{p_{2c}} = \frac{M_p}{S_{2c}} = \frac{900}{0.273} = -3{,}297$ psi	
	Secondary (compression)	$f_{s_{2c}} = -f_{s_{2a}} = -\underline{2{,}836}$ psi	Total = -6,133 psi (Maximum)

Example 8-6 continued

6. Check Above Stresses Against Elementary Theory
(neglectiing shear-flexible-core behavior)

Maximum face stress, Element 2c, is $f_2 = M/S_{2c} = 938/0.273 = -3,436$ psi. This is only 56% of total stress (-6,133 psi) from the above analysis. Maximum stress in bottom face is $f_1 = 938/0.205 = 4,576$ which is almost the same as f_{p1} above.

7. Maximum Core Shear Stress

$$Q_p = Q\phi_1 \times LF = \frac{qL}{2}\phi_1 \times LF = \frac{0.417 \times 100 \times 0.86 \times 1.8}{2} = 32.3 \text{ lb}$$

$$f_v = \frac{Q}{A_v} = \frac{32.3}{8.618} = 3.75 \text{ psi}$$

8. Deflection (Unfactored Load)

$$w = \frac{5qL^4}{384\,D_m} + \frac{qL^2}{3\,D_v}\left(\frac{I_o}{I}\right)^2 \phi_3$$

$$= \frac{5 \times 0.417 \times 100^4}{384 \times 15,370 \times 10^3} + \frac{0.417 \times 100^2}{8 \times 2012}\left(\frac{0.526}{0.530}\right)^2 \times 0.96$$

$$= 0.0353 + 0.245 = 0.280 \text{ in.} < 0.5'' = L/200 \text{ ok.}$$

Note that shear deflection is about 87% of the total deflection.

9. Evaluate Stress and Deflection Levels

Steel Faces: The steel faces, having a minimum yield strength of 36,000 psi and ultimate strength of 58,000 psi (Example 8-4) are safe by inspection since maximum stress is 6,133 psi in compression and 4,520 psi in tension. Stability of the upper face against wrinkling must be evaluated by test since analytical expressions for buckling of corrugated faces restrained by core are not available (see Section 8.8).

Foam Core: The maximum long-term shear stress in the foam core, which includes a load factor of 1.8, is 3.75 psi. This compares to a minimum long-term strength of 7 psi (Example 8-4). This provides a margin of safety of 7/3.75 = 1.87 between minimum ultimate short-term strength and factored stress. Equivalent capacity reduction factor is 1/1.87 = 0.54 which appears reasonable.

Deflection: The section meets deflection criteria.

Note: 1 in. = 25.4 mm; 1 psi = 6.9 kPa; 1 in.^{4}/in. = 16,387 mm^4/mm that is only about 56% of the maximum stress determined by the present more rigorous method. Furthermore, the difference would increase with shorter spans, shallower sections, more shear-flexible cores, or deeper corrugations.

Comparison of Elementary and Rigorous Theories

In certain cases, the elementary and rigorous theories may produce widely different estimates of stresses and deflections. The error involved in using the simplified appoach increases with the following:

- Decrease in span.
- Decrease in core shear rigidity relative to bending stiffness of faces about their own neutral axis.
- Increase in bending stiffness of faces relative to stiffness of the overall transformed section.
- More concentrated distribution of load

Fig. 8-11 provides a quantitative comparison of the results of elementary and rigorous theories, as affected by core shear stiffness and span-depth ratio. The figure shows the critical span-depth ratios where secondary stresses are equal greater than 10% of primary stresses for two loading conditions and a simply supported span. The critical span/depth ratio is a function of the face-thickness-to-panel-depth ratio and the face-modulus-to-core modulus ratio. The graphs in the figure indicate the following for L/d = 10 to 50, which is a practical range of span/depth ratios for most sandwich constructions:

- The concentrated loading condition (Fig. 8-11a) results in critical span/depth ratios that are substantially higher than for uniform loads, and well into or above the practical range of L/d = 10 to 50. The secondary stresses are greater than 10% of the primary stress for most practical designs for concentrated loads.
- For uniform loads (Fig. 8-11b) and a shear-rigid core with E_f/G_c less than about 100, L/d_{cr} is below the practical range of L/d for most facing thicknesses; secondary face stresses are less than 10% of the primary stresses in such cases.

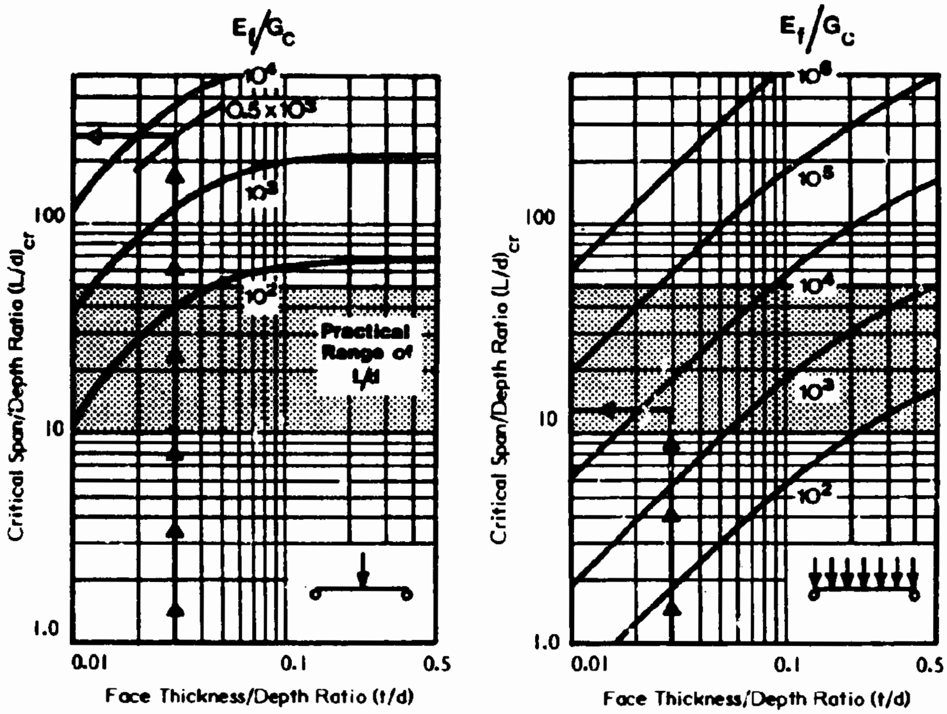

a. Critical Span/Depth Ratio for Concentrated Load

b. Critical Span/Depth Ratio for Uniformly Distributed Load

Note: 1. If actual value of L/d is less than $(L/d)_{cr}$, use of shear-flexible core theory is indicated, depending upon actual level of acceptable error.

2. Graphs are for uniform and symmetrical cross sections.

Illustration of Chart Use: Find span/depth ratio below which further analysis for shear-flexible cores is required to restrict errors in face stress to 10% or less. Sandwich has 0.06 in. FRP faces ($E_f = 2.5 \times 10^6$ psi) and a 2 in. thick, 2.5 pcf polyurethane foam core (G_c = 500 psi). Calculate t/d = 0.03, $E_f/G_c = 5 \times 10^3$. Find L/d_{cr} = 12 for uniform loads and 270 for concentrated loads. Calculate θ_{cr} = 42 for uniform loads and 954 for concentrated loads (Eqs. 8.78 and 8.79).

Also calculate decay distance for concentrated knife edge load, using Eq. 8.78, with p = 10%:

$$(2x)_d = 0.816 \left[\frac{0.06^3 \times 2.5 \times 10^6}{500 \times 2.0}\right]^{1/2} \log_e \left(\frac{100}{10}\right) = 1.4 \text{ in.}$$

Therefore, if actual load width is on the order of 1.4 in. or greater, consider distributing load over a finite width.

Fig. 8-11 CRITICAL SPAN/DEPTH RATIO BELOW WHICH ELEMENTARY THEORY PRODUCES FACE STRESS ERRORS OF 10% OR GREATER

The illustrative example shown in Fig. 8-11 indicates that secondary stresses are less than 10% of primary stresses for uniform loads at span/depth ratios of 12 or greater. For concentrated knife-edge loads, however, secondary stresses are greater than 10% of primary stresses for all spans up to $(L/d)_{cr} = 270$, which includes the range of practical spans.

For concentrated loads, the example also shows that secondary face stresses can be significant even when faces are quite thin, and when the secondary moment is small compared to the maximum moment. In this case, according to Eq. 8.78, $M_{s\ max} = M_{max}/\theta = M_{max}/954 \doteq 0.001\ M_{max}$. Or, the secondary moment is only one thousandth of the maximum moment applied to the cross section.

8.7 Bending and Shear in Sandwich Plates

The analysis and design of sandwich plates is in many respects similar to that of solid plates which were covered in detail in Chapter 6. This section deals principally with special considerations which arise in sandwich plates where the core is soft, and perhaps shear flexible and orthotropic as well.

Section Properties of Sandwich Plates

As in the case for solid plates, the stiffness of the sandwich plate is greater than that of a narrow beam of column due to restraints of Poisson's deformations, introduced by boundary conditions or shape of the structure. This increase in stiffness can be accounted for by the modified modular ratio, n'_i, as defined earlier:

$$n'_i = \frac{1}{1-\nu_i^2}\left(\frac{E_i}{E_v}\right) = \frac{n_i}{1-\nu_i^2} \qquad \text{Eq. 8.25}$$

The term n'_i is used in place of n_i, in relationships for section properties, such as are given in Table 8-1a. For relationships given in Table 8-1b, c that are derived for sandwiches with equal faces ($E_1 = E_2 = E = E_r$), it is implicit that $n_i = 1$.

Substituting, n'_i, for the implied, n_i, in appropriate stiffness relationships results in the following:

$$D_m = n'_i EI = \frac{EI}{1 - \nu^2} \qquad \text{Eq. 8.79}$$

This equation is identical in form to Eq. 6.2a given in Chapter 6 for solid plates.

The increase in plate bending stiffness over that of a beam is a result of the restraint of warpage or anticlastic curvature transverse to the span direction. For example, in solid plates, subjected to cylindrical bending on a simple span, this restraint is developed by internal shears and moments near the unsupported edges of the plate. In the case of sandwich plates, the internal shears are carried by the core which is, relatively, very much less shear rigid than in a solid plate – significant shear deformation is expected. Hence, a sandwich plate must be significantly wider than a solid plate in order for the full restraint of anticlastic curvature to develop. Hence, the use of n'_i in place of n_i is accurate only for very wide sandwich plates.

In light of the above and the fact that ν^2 is usually a small term, the effect of Poisson's ratio may safely be neglected in most practical designs. In such instances the formulas of Table 8-1, may be used without replacing, n_i with n'_i. Of course, if in a particular design, neglecting the effects of Poisson's ratio leads to an unconservative result, the use of n'_i in place of n_i is indicated.

If one or both faces of a sandwich panel are corrugated, the local bending transverse to the corrugation direction normally relieves the effects of transverse moments required to restrain anticlastic curvature. In this case, there is no justification for the use of n'_i unless the faces are very thick. If corrugated faces are thick, special study is required.

Isotropic Sandwich Plates

An "isotropic" sandwich plate is constructed from layers of isotropic or planar isotropic materials, and properties are isotropic only in the plane of the plate.

Simply Supported Rectangular Sandwich Plates: When an isotropic sandwich plate is simply supported, bending moments, torsional moments, shears, and also bending deflections are the same as those which occur in a simply supported solid isotropic plate having a uniform thickness. The principal difference in behavior between a simply supported isotropic sandwich plate and its solid isotropic homogeneous plate counterpart is shear deflection. While the analyses for shear deflection of sandwich plates is considerably more complex, the concept is similar to that discussed earlier for sandwich beams. That is, the total deflection is assumed to be the sum of the bending deflection (with infinite shear rigidity assumed) and the shear deflection (with infinite bending rigidity assumed).

Fig. 8-12 gives non-dimensional coefficients for shear and bending deflections, and shear and bending stress resultants for simply supported isotropic rectangular sandwich plates under uniform lateral load. As expected from the above discussion, the maximum bending stress resultant (M_x), and the bending deflection are the same as those shown in Fig. 6-10, and the shear stress resultants are the same as those given in Fig. 6-11; they are given here only for completeness of the present figure.

Rectangular Sandwich Plates with Clamped Edges: In the case of uniformly loaded rectangular sandwich plates having clamped edges, the bending deflection and the shear and bending stress resultants are not the same as for an equivalent isotropic plate. Rather, these values depend upon the plate shear-flexibility parameter, $\bar{U}$, where

$$\bar{U} = \frac{b^2 D_v}{\pi^2 D_m} \qquad \text{Eq. 8.80}$$

This plate shear flexibility parameter is similar in many respects to the shear flexibility parameter for beams, discussed earlier, and defined by Eq. 8.49. Dimensionless coefficients for three limiting values of $\bar{U}$ are given in Table 8-5.

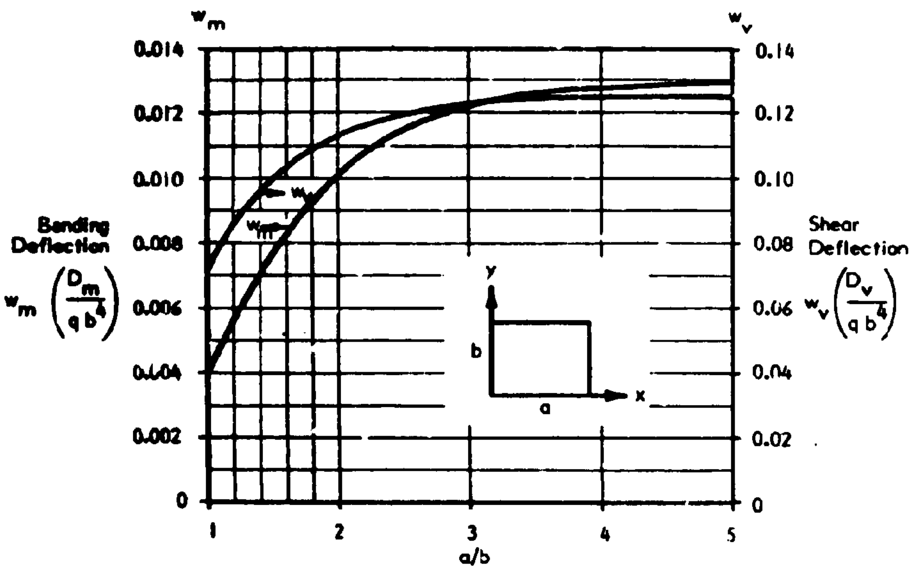

a. Deflection at Center of Plate

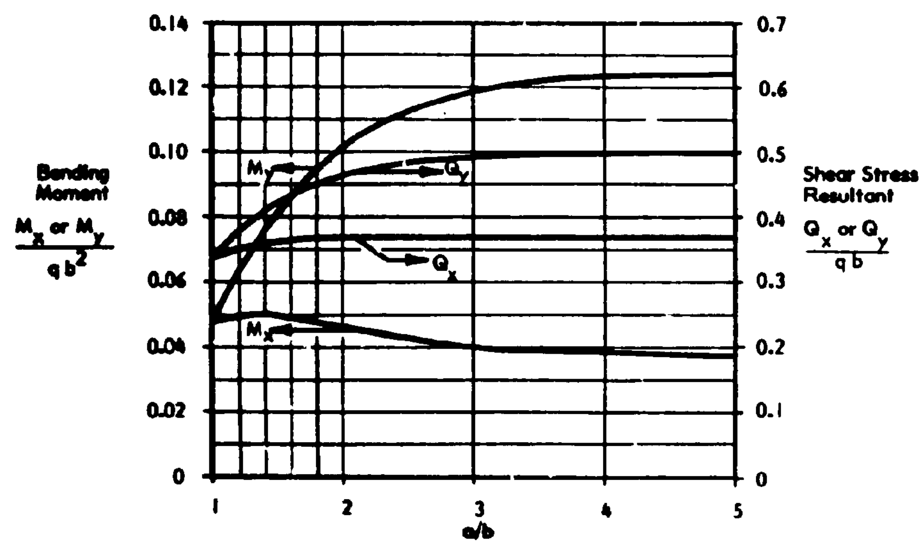

b. Shear at Midlength of Edges, and Moments at Center of Plate

Fig. 8-12 DEFLECTIONS, SHEARS AND MOMENTS IN UNIFORMLY LOADED ISOTROPIC SANDWICH PLATE HAVING SIMPLY SUPPORTED EDGES (ADAPTED FROM 8.5)

Table 8-5

Coefficients for Maximum Deflection and Moment for Clamped Square Sandwich Plate Under Uniform Load (8.5)

$\bar{\theta}$	$w \dfrac{D_m}{q a^4}$ *	$\dfrac{M}{q a^2}$ *
∞	0.00126	0.0513
4	0.00325	0.0410
0	∞	0.0347

* Maximum bending stress resultant occurs at middle of each edge. Maximum deflection is at center of the plate.

Circular Sandwich Plates: Circular sandwich plates which are symmetrically loaded and simply supported behave in the same manner as circular homogeneous isotropic plates, except that the shear deflection, w_v, must be added to the bending deflection w_m. The equations for maximum shear deflection and bending deflection at the center of a plate of diameter a, and subjected to a uniform load, q, are given below (8.5):

total deflection	$w = w_m + w_v$	Eq. 8.26
for simply-supported edge	$w_m = \dfrac{5 + \nu}{1024 (1 + \nu)} \dfrac{q a^4}{D_m}$	Eq. 8.81
for clamped edges	$w_m = \dfrac{q a^4}{1024 D_m}$	Eq. 8.82
for either edge conditon	$w_v = \dfrac{q a^2}{64 D_v}$	Eq. 8.83

The equations for the moment component of deflection given above are identical to those for homogeneous plates.

Approximate Methods: Relationships derived for conventional, homogeneous, uniform plates can be modified to give approximate moments and deflections for isotropic sandwich plates. The following procedure has been proposed to adapt conventional plate formulas, for homogeneous solid sections in which shear rigidity is assumed infinite, to the case of layered sandwich construction where core shear rigidity has a finite value (8.1):

1. Calculate "effective properties" of the sandwich plate for use in conventional formulas for homogeneous isotropic plates, as follows:

   General:

$$t_e = 3.46 \left[\frac{(1 - \nu^2)\, D_m}{\bar{A}} \right]^{1/2} \qquad \text{Eq. 8.84}$$

$$E_e = \frac{\bar{A}}{t_e} \qquad \text{Eq. 8.85}$$

   For thin equal faces and soft but shear-rigid core:

$$t_e = 1.73d \qquad \text{Eq. 8.86}$$

$$E_e = \frac{1.16\, t_f E_f}{d} \qquad \text{Eq. 8.87}$$

   Thus, an isotropic sandwich plate having a bending stiffness D_m, and an in-plane stiffness $\bar{A}$, is identical in stiffness to a homogeneous isotropic plate having a thickness t_e, and a modulus of elasticity, E_e.

2. Calculate w_e, the maximum bending deflection of the equivalent homogeneous plate simply supported at its edges, with loads applied normal to the plate, using appropriate formulas for an homogeneous isotropic plate having the geometry of the actual plate, and having thickness t_e, and elastic modulus, E_e.

3. Calculate actual approximate upper-bound maximum deflection of the sandwich plate, to account for the finite shear rigidity of the core:

$$w_u = w_e \left(1 + 20 \frac{D_m}{D_v b^2}\right) \cong w_e \left(1 + \frac{2}{\theta}\right) \qquad \text{Eq. 8.88a, b}$$

   Since w_u is an upper-bound value, the actual maximum deflection, w, will lie between w_u and w_e. Thus, w is an estimated value.

4. Calculate the bending and shear stress resultants using equations for the homogeneous isotropic plate having the geometry of the actual plate. For

plate solutions based on small deflection theory, which is usually the only case of interest for practical sandwich structures, stress resultants, (not stress), depend only on plate geometry, load, and boundary conditions, and are independent of thickness. Many handbooks (e.g. 8.15) give solutions for plates in terms of stress rather than stress resultants. In such cases, and for small deflections only, stresses can be converted to stress resultants by setting t = 1, and multipling the resulting bending stress by 6 and the shear stress by 2/3.

The stress resultants determined by the above procedures do not account for the extra face-bending effects associated with shear-flexible cores, such as was determined for beams in the shear-flexible core analysis described in Section 8.6. This is discussed further below:

Shear-Flexible Cores: The effects of shear-flexible cores, discussed in Section 8.6 for beams, also occur in plates. There are no practical rigorous solutions available for the analysis plates having shear-flexible cores. The following approach for determining the approximate maximum stress due to primary and secondary bending effects, may prove useful in some cases.

a) Consider a free-body strip of the plate as a beam.

b) Determine the ratio of maximum bending stress (primary plus secondary) to primary bending stress, using methods given in Section 8.6.

c) Determine the primary bending stress in the actual sandwich plate by the methods discussed in this Section.

d) Estimate the maximum stress in the plate by multiplying the primary stress in the plate determined in Step c above by the ratio obtained in Step b above.

Since the plate is being modeled as a beam, Fig. 8-11 may also be used to estimate when secondary bending effects are significant by estimating approximate critical span-depth ratios.

The accuracy of the above approach depends on load distribution, geometry, and cross-sectional proportions and materials properties and the like. Depending on the specific design problem, more accurate analysis and tests may be required.

Orthotropic Sandwich Plates

The faces or the core of a sandwich structure may be orthotropic. Numerical solutions for orthotropic sandwich plates are very limited, mainly because of the complexity of the analysis problem. Equations for deflections and bending stress resultants for uniformly loaded rectangular plates having either simply-supported or clamped edges, with principal directions of orthotropic faces and cores aligned with edges are given in (8.1) but they are complex and cumbersome to use. Furthermore, expressions for shear stress are not provided in this reference.

The following equations may be used to determine maximum deflections and stress resultants for the case of a uniformly loaded, simply supported rectangular sandwich plate having thin but dissimilar isotropic faces and an orthotropic core with the principal axes of the core aligned with the edges (8.2).

deflection $w = K_1 \left(\frac{1}{E_1 t_1} + \frac{1}{E_2 t_2}\right) \frac{q b^4}{d^2}$ Eq. 8.89

face stress $\sigma_{y1} = K_2 \frac{q b^2}{d t_1}$; $\sigma_{y2} = \frac{K_2 q b^2}{d t_2}$ Eq. 8.90a, b

core shear stress $\tau_x = K_{3x} q \frac{b}{d}$; $\tau_y = K_{3y} q \frac{b}{d}$ Eq. 8.91a, b

Values of coefficients K_1 to K_3 are plotted in Fig. 8-13 to 8-15. These coefficients vary with aspect ratio of the plate, with the degree of orthotropicity of the core, as defined by $R = G_{cy}/G_{cx}$, and also with $\bar{Q}$. The values of G_{cy}/G_{cx} range from 0.4 to 2.5, which is typical of many available honeycomb cores.

More generally, a reasonable approximation of maximum stresses and deflections may be obtained, provided the plate elements are not strongly orthotropic, by analyzing the orthotropic plate as an isotropic sandwich plate having the following properties (8.5):

Coefficient K_1 for use in Eq. 8.89

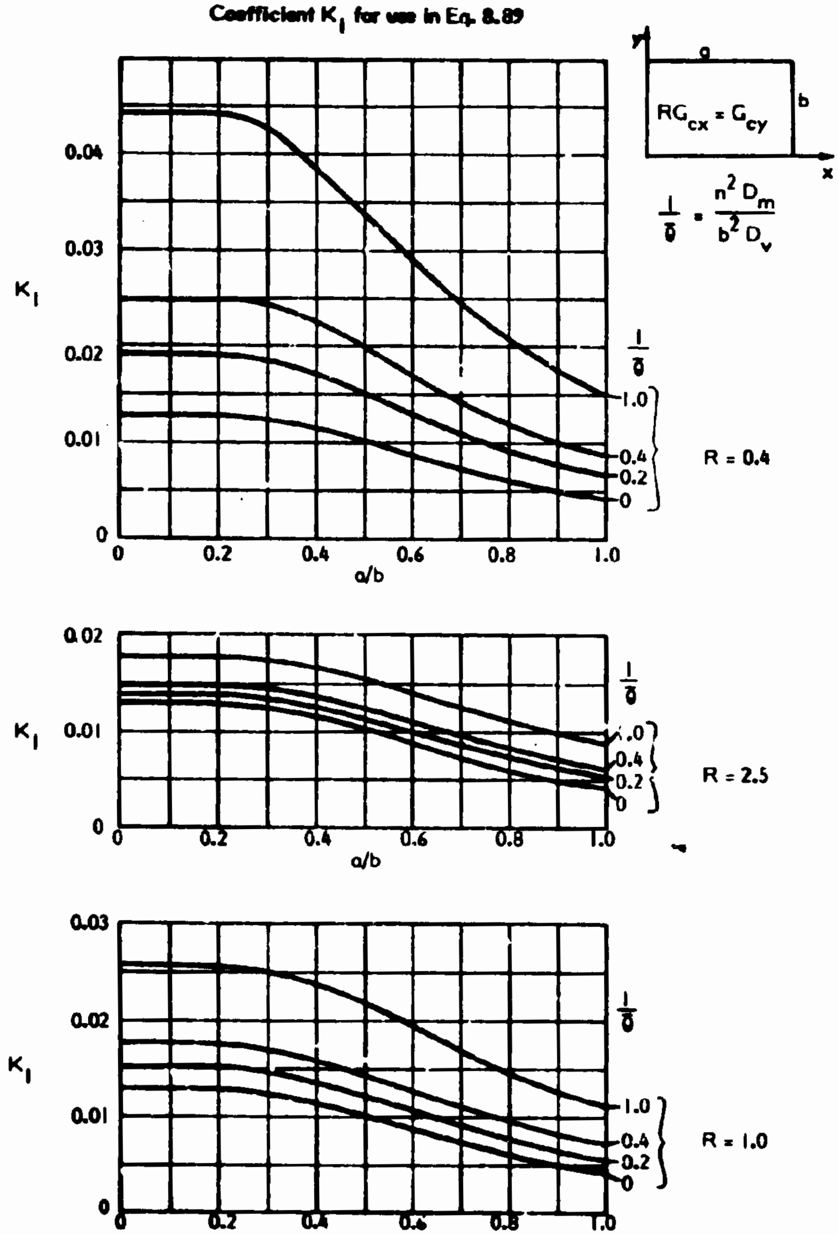

Fig. 8-13 COEFFICIENTS FOR MAXIMUM DEFLECTION IN SANDWICH PLATES WITH ISOTROPIC FACES AND ORTHOTROPIC CORE (8.2)

Coefficient K_2 for use in Eq. 8.90

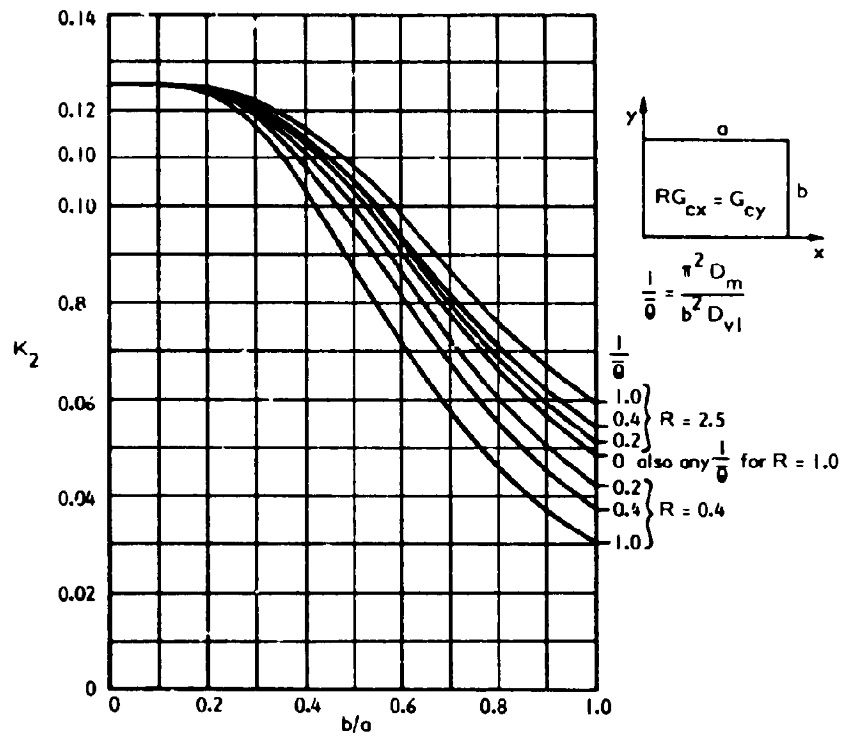

Fig. 8-14 COEFFICIENTS FOR MAXIMUM STRESS AT THE CENTROID OF EACH FACE IN SANDWICH PLATE HAVING ISOTROPIC FACES AND ORTHOTROPIC CORE (8.2)

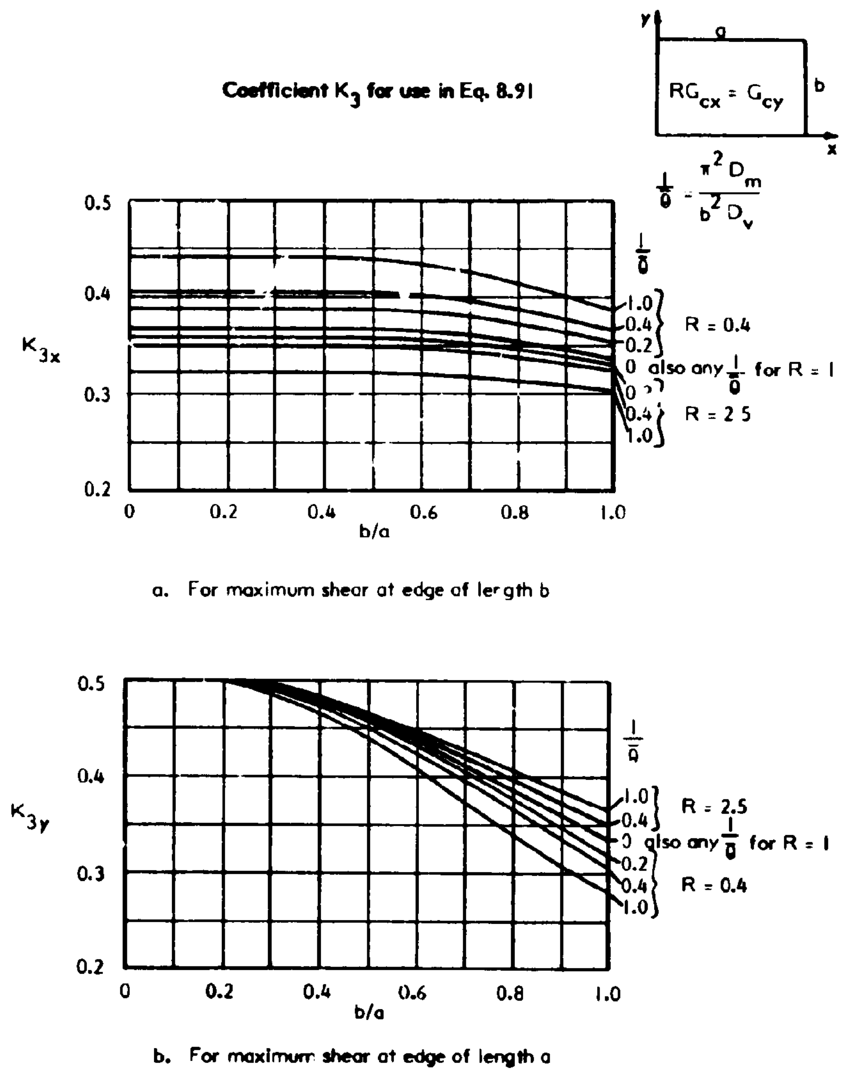

a. For maximum shear at edge of length b

b. For maximum shear at edge of length a

Fig. 8-15 COEFFICIENTS FOR CORE SHEAR STRESS IN SANDWICH PLATES WITH ISOTROPIC FACES AND ORTHOTROPIC CORE (8.2)

$$\text{for } \frac{a}{b} = 1: D_m = \frac{1}{2}(D_{mx} + D_{my}),\ D_v = \frac{1}{2}(D_{vx} + D_{vy}) \qquad \text{Eq. 8.92a, b}$$

$$\text{for } \frac{a}{b} \geq 3: D_m = D_{my}, \qquad D_v = D_{vy} \qquad \text{Eq. 8.93a, b}$$

The accuracy of this approximation diminishes if D_{my} is significantly less than D_{mx}, but this is usually neither a common nor an efficient condition in practical structures.

Stresses Caused by Localized Loads

When concentrated loads are applied normal to a sandwich panel, localized bending stresses are produced in the face(s) of the panel, and shear and tension or compression stresses are developd in the core. These effects are usually maximum at or near the point of load application, and can cause significant stresses, as discussed in Section 8.3.

Relationships for stresses developed under two simple cases of localized loads are given in Figs. 8-16 and 8-17. Fig. 8-16 is for the case of a local circular load applied to the face in regions away from the edges of a wide sandwich beam or sandwich plate. Fig. 8-17 is for a line load applied near the edge of a panel. In both cases the face and core stresses resulting from overall bending and shear should be superimposed on these local stresses to obtain the total stresses in the component.

Overall, effects of localized loads such as local stresses due to peeling at the face-core interface, and the usual very low strength of sandwich cores, combine to render most analyses as highly approximate. Tests of the effects of localized loads are frequently a necessary part on any detailed evaluation.

8.8 Stability of Sandwich Elements in Compression

Both general instability of sandwich columns, struts and compression panels, and local instability of compression faces of sandwich structures are important limit states, and are considered in this Section.

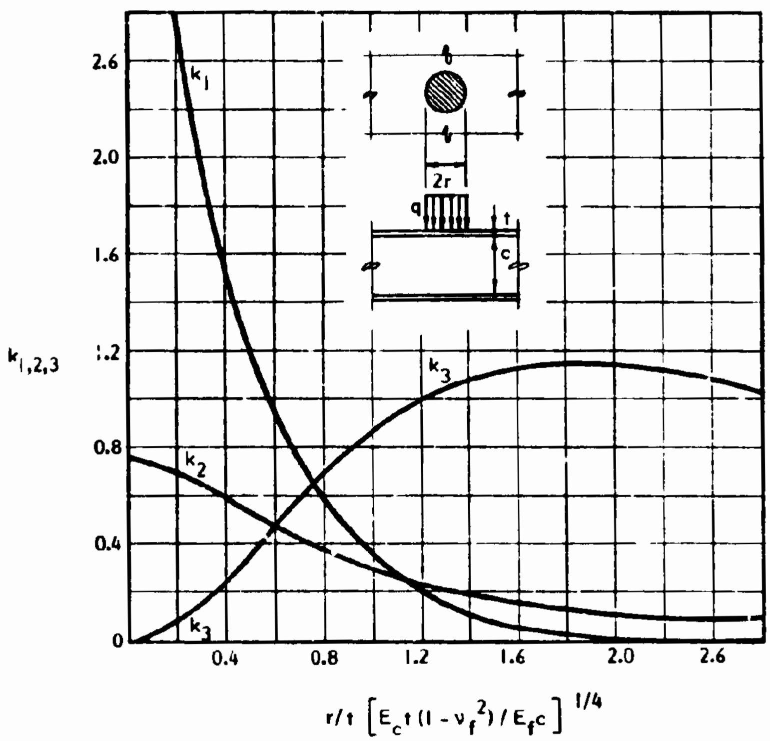

Stresses in loaded face:

Extreme fiber, bending	$\sigma_f = k_1 q (r/t)^2$	Eq. 8.94
Shear	$\tau_f = k_2 q r/t$	Eq. 8.95

Stress in Core:

Compression (or Tension) normal to plane	$\sigma_c = k_3 q$	Eq. 8.96

Fig. 8-16 MAXIMUM STRESSES DUE TO CONCENTRATED LOAD APPLIED TO SANDWICH FACE (8.9)

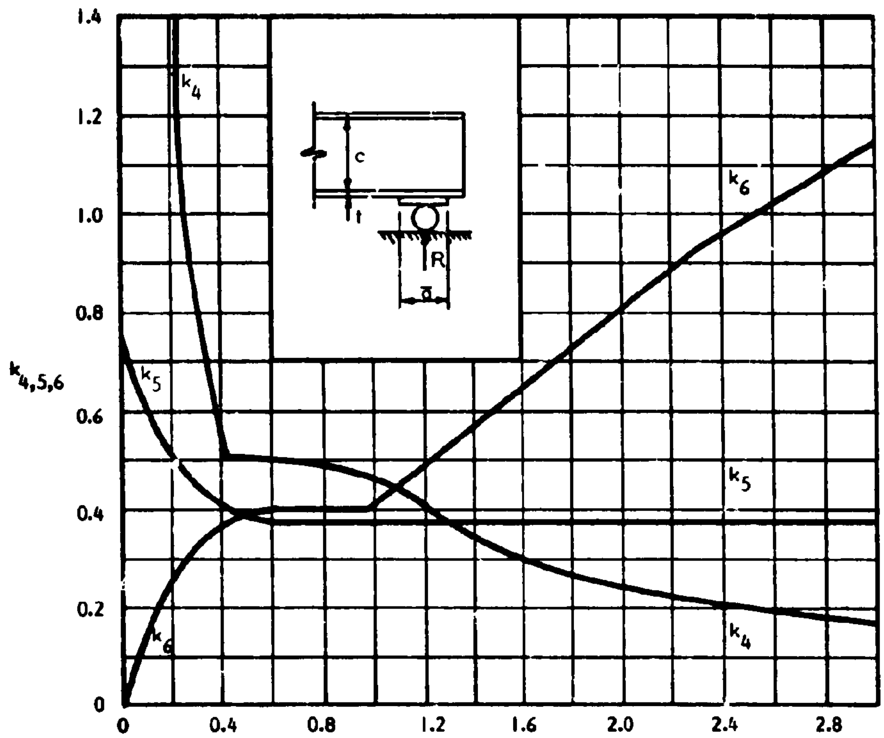

$\bar{a}/t \left[E_c t (1-\nu_f^2)/E_f c\right]^{1/4}$

Stresses in loaded face:

Extreme fiber, bending	$\sigma_f = k_4 R\bar{a}/t^2$	Eq. 8.97
Shear	$\tau_f = k_5 R/t$	Eq. 8.98

Stress in Core:

Compression (or Tension) normal to plane	$\sigma_c = k_6 R/\bar{a}$	Eq. 8.99

Fig. 8-17 MAXIMUM STRESSES DUE TO CONCENTRATED LINE LOAD APPLIED TO SANDWICH FACE NEAR PANEL EDGE (8.9)

Buckling of Columns and Struts

During the process of buckling, a simple pin-ended column loaded in compression deflects laterally in bending. The curvature that develops during this deflection produces both an eccentricity of the load relative to the axis of the column, and a shear component transverse to the column axis. In most conventional compression members the distortions due to shear stress are small enough to be neglected. In sandwich construction, however, shear deformations may reduce buckling capacity significantly from loads calculated from classical Euler theory. The following equation gives the buckling load for sandwich compression members that experience significant shear deformations in addition to bending deformation during the buckling process (8.5):

$$\frac{1}{P_{cr}} = \frac{1}{P_e} + \frac{1}{P_v} \qquad \text{Eq. 8.100}$$

It can be shown that the critical buckling load associated with shear deformation only, is the same as the shear stiffness of the column (8.5); thus:

$$P_v = D_v \qquad \text{Eq. 8.101}$$

Thus, Eq. 8.100 can be written

$$\frac{1}{P_{cr}} = \frac{1}{P_e} + \frac{1}{D_v} \qquad \text{Eq. 8.102}$$

where $P_e = \dfrac{k\,\pi^2 D_m}{L^2} = \begin{cases}\text{critical Euler buckling load} \\ \text{for column with infinite shear} \\ \text{stiffness and finite bending} \\ \text{stiffness}\end{cases}$ Eq. 8.103

$D_v = P_v = \begin{cases}\text{critical buckling load for column} \\ \text{with finite shear stiffness and} \\ \text{infinite bending stiffness, and} \\ \text{with buckling made either sym-} \\ \text{metrical or anti-symmetrical} \\ \text{with respect to column midlength}\end{cases}$

k = buckling coefficient depending upon column end conditions (See Table 6-4)

These simple relationships yield results which are identical to more complicated exact solutions for the general case where the buckling mode is either symmetrical or anti-symmetrical about column mid-length. Such buckling modes occur in axially-loaded columns which have both ends pinned, both ends clamped, or both ends clamped with one end free to translate. The equation also results in values which are only slightly unconservative for several practical sandwich constructions in which one end is pinned and the other end is clamped, with both ends held against translation (8.5). More rigorous methods are available for such cases where the buckling mode is neither symmetrical nor anti-symmetrical about mid-length (8.5).

Calculations for determining the critical buckling load of a simple pin-ended column are given in Example 8-7 at the end of this Section. For the column examined, shear deformations reduce the Euler buckling load by 27%.

For materials which display elastic-plastic behavior, the secant modulus of rigidity should be used in the determination of D_v, as well as D_m. In the case of plastics, the time-dependent viscoelastic modulus should be used in place of the elastic modulus, provided that stresses are held below the viscoelastic limit (Chapter 3).

Effects of Initial Eccentricities: When significant initial eccentricities are built into a sandwich column which has either a weak core or a weak adhesive bond, the column may fail by rupture of the core at a load which is lower than the critical buckling load given by Eq. 8.100. For an axially loaded column that is clamped at each end and held against translation, the critical load P_{crv}, governed by the shear strength τ_u, of either the core or the adhesive, whichever is lower, is as follows (8.5):

$$P_{crv} = \frac{\tau_u A_v L}{4 w_o} \quad ; \quad \text{if } k L \leq \pi \qquad \text{Eq. 8.104}$$

$$P_{crv} = \frac{\tau_u A_v L}{4 w_o} \sin \frac{kL}{2} \; ; \quad \text{if } k L > \pi \qquad \text{Eq. 8.105}$$

where $k = \left[\dfrac{P D_v}{(D_v - P) D_m}\right]^{1/2}$ Eq. 8.106

w_o = initial eccentricity or lateral displacement of column centerline

The critical load is determined by trial and error to test for the equality, $P = P_{crv}$.

When plastics are used as the core of a sandwich panel, appropriate values of time-dependent strength as well as modulus should be used in the evaluation of the effects of initial eccentricities.

Buckling of Plates Under In-Plane Compression

Conceptually, isotropic sandwich plates or panels with isotropic faces and cores buckle under in-plane compression in a manner similar to isotropic homogeneous plates (Section 6.9). As in the case of sandwich columns, core shear deformation reduces the buckling strength of sandwich plates from classical solutions that are based on bending stiffness alone.

Buckling resistance of uniaxially compressed, simply supported sandwich plates having isotropic faces and an orthotropic core may be determined from Eq. 6.71, together with the buckling coefficients given in Figs. 8-18a and 8-18c. These Figures, together with Figure 8-18b for isotropic cores, show how the buckling resistance varies as the ratio of core shear rigidity in each principal direction, $R = G_{cy}/G_{cx}$, varies from 0.4 to 2.5. This range of R values is typical of the core characteristics of honeycomb core materials.

Buckling resistance of uniaxially compressed, simply supported, sandwich plates having isotropic faces and an isotropic core may be determined from Eq. 6.71 and the buckling coefficients given in Fig. 8-18b. The coefficient, $\bar{U}$, represents the ratio of shearing to bending stiffness. The figure shows that changes in this ratio can have significant influence on buckling strength. Equations for buckling

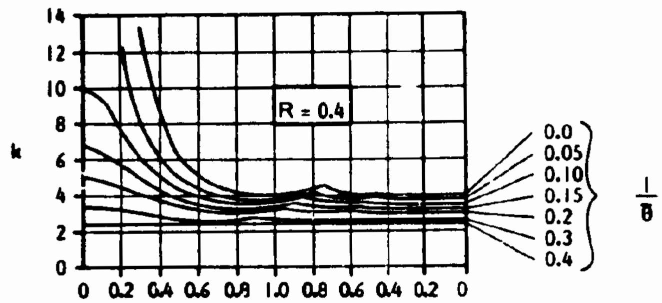

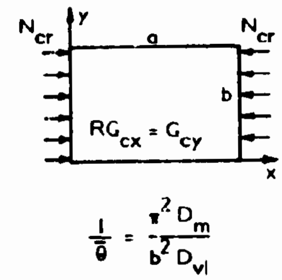

a. Isotropic faces and core orientation in x direction

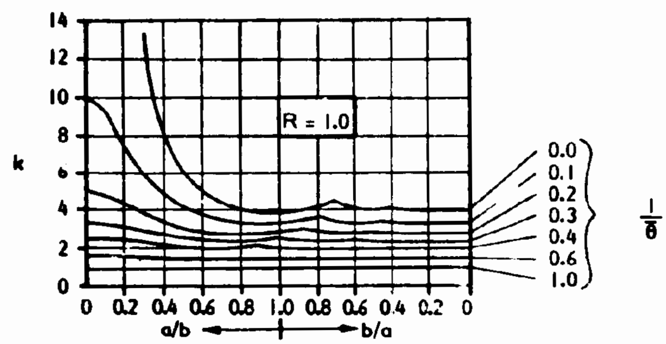

b. Faces and core both isotropic

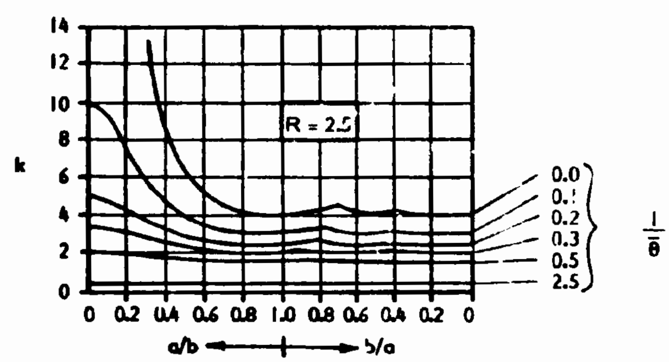

c. Isotropic faces and core orientation in y direction

Fig. 8-18 BUCKLING COEFFICIENTS FOR EQ. 6.71 FOR SIMPLY SUPPORTED ORTHOTROPIC SANDWICH PLATES UNDER UNIFORM EDGE COMPRESSION (8.10)

resistance of isotropic sandwich plates for some other loading and support conditions are available (8.5 and 8.11).

Equations are also available to determine buckling resistance of sandwich plates having orthotropic elements for a variety of other loading conditions, support arrangements, and plate geometries (8.1, 8.2, 8.5, 8.10). Discrete, but somewhat cumbersome, equations are available for rectangular plates having principal orthogonal axes of the faces and core parallel to the plate edges (8.1).

The corrugated core sandwich configuration is a practical but special case of a sandwich plate having an orthotropic core. Analysis for overall instability, and local instability of thin web and face elements, though somewhat cumbersome, are available (8.1, 8.2, 8.5, 8.10, 8.11).

Face Wrinkling and Local Instability

Face wrinkling may be a critical limit state when compression faces are thin and flexible and the core has a low shear modulus, and also a low compression modulus normal to the plane of the face. Face wrinkling is a form of instability associated with short wave length ripples as opposed to the general instability discussed above. Wrinkling may take the form of either symmetrical or antisymmetrical buckling of both faces of compression members, or in the case of a sandwich plate or beam in bending, the compression skin may buckle while the tension skin remains taut (Fig. 8-3).

The following semi-empirical equation gives a conservative lower bound for the face stress at the onset of local face buckling with a continuous core material. This equation is derived from an analysis of a large number of test results on a variety of sandwich members with thin face materials and continuous cores (8.5, 8.12).

$$\sigma_{wr} = 0.5 \ (E_f E_c G_c)^{\frac{1}{3}} \qquad \text{Eq. 8.107}$$

The modulus, E_c, in this case is either the elastic or viscoelastic modulus of the core for homogeneous cores, or the elastic or viscoelastic modulus normal to the faces for orthotropic cores such as honeycombs or end-grain balsa.

Theoretical equations are also available that are intended to account for the effects of waviness of the faces on face wrinkling strength (8.2, 8.3, 8.5). A knowledge of the magnitude of the initial waviness amplitude is required for use in such equations. However, measured values of initial waviness do not provide suitable predictions of skin wrinkling stresses, and empirical values of initial waviness must be assumed for proper correlation between theoretical results and actual test values. Hence, in general, these equations are of limited practical use in predicting critical wrinkling stress a priori. Furthermore, Eq. 8.107 has been found to provide reasonably good lower-bound predictions of skin wrinkling stresses independent of surface waviness characteristics (8.12). Overall, this suggests that wrinkling stress is best established by Eq. 8.107 and then verified by test as appropriate, and especially when cores are shear flexible and weak.

Example 8-7 illustrates the calculation for critical wrinkling stress for a plastic-based sandwich column. For the member examined, wrinkling stress is about three times the critical stress for overall buckling. If the panel were significantly shorter than assumed in the example, wrinkling stress might govern (See also Example 8-11).

The effects of biaxial stress on the critical wrinkling stress have been examined, with the following conclusions (8.5):

$$\text{If} \quad \frac{\sigma_y}{\sigma_x} < \left(\frac{G_{cy}}{G_{cx}}\right)^{\frac{1}{3}}, \ \text{then } \sigma_x = \sigma_{cr}, \qquad \text{Eq. 8.108}$$

$$\text{If} \quad \frac{\sigma_y}{\sigma_x} > \left(\frac{G_{cy}}{G_{cx}}\right)^{\frac{1}{3}}, \ \text{then } \sigma_y = \sigma_{cr}, \qquad \text{Eq. 8.109}$$

$$\text{If} \quad \frac{\sigma_y}{\sigma_x} = \left(\frac{G_{cy}}{G_{cx}}\right)^{\frac{1}{3}}, \ \text{then } \sigma_x = \sigma_{xcr} \text{ and } \sigma_y = \sigma_{ycr}. \qquad \text{Eq. 8.110}$$

Example 8-7: Capacity of a Sandwich Column Loaded in Axial Compression *

Determine the short-term ultimate load capacity of a pin-ended sandwich column 10 inches wide and 8'-4" long, and having the cross section shown in Example 8-2. Load is applied at the neutral axis.

1. Compression Strength (Eq. 8.23a)

Let P_u = ultimate load capacity governed by compression strength.

$$\sigma_i = \frac{n_i P}{A} \quad \text{or} \quad P_u = \frac{A\sigma_i}{n_i} = \frac{A F_{uc}}{n_i}$$

From Example 8-2: Face 1: $n = 1, F_{uc} = 21{,}000$ psi

Face 2: $n = 0.373, F_{uc} = 22{,}000$ psi

Core: $n = 0.00068, F_{uc} = 20$ psi

$\Sigma n_i A_i = A = 0.156$ in.^{2}/in. $(E_r = E_i)$

Capacity: Face 1: $P_u = \dfrac{0.156 \times 21{,}000}{1} = 3{,}276$ lb/in. (governs)

Face 2: $P_u = \dfrac{0.156 \times 22{,}000}{0.373} = 9{,}200$ lb/in.

Core: $P_u = \dfrac{0.156 \times 20}{0.00068} = 4{,}588$ lb/in.

2. General Instability (Eq. 8.102)

$$\frac{1}{P_{cr}} = \frac{1}{P_e} + \frac{1}{D_v}; \quad \text{and} \quad P_e = \frac{k\pi^2 D_m}{L^2}$$

k = 1 for pin-ended column (Table 6-4):

D_m = 486,000 in./lb, D_v = 1,240 in./lb (Example 8-2)

$$P_e = \frac{\pi^2 \times 486{,}000}{100^2} = 480 \text{ lb/in.}$$

$$P_{cr} = \frac{1}{\frac{1}{480} + \frac{1}{1{,}240}} = 346 \text{ lb/in.}$$

---

* See Footnote, Example 8-1.

Example 8-7 continued

3. **Local Wrinkling** (Eq. 8.107)

$$\sigma_{cr} = 0.5 \left(E_f E_c G_c\right)^{\frac{1}{3}} = 0.5 \left(1500 \times 500 E_f\right)^{\frac{1}{3}} = 45.4 E_f^{\frac{1}{3}}$$

$$P_{cr} = \sigma_{cr} \frac{A}{n_i} = \frac{45.4 E_f^{1/3} \times 0.156}{n_i} = \frac{7.08 \ E_f^{1/3}}{n_i}$$

Face 1: $E_1 = 2.2 \times 10^6$ psi; $P_{cr} = \dfrac{7.08 (2.2 \times 10^6)^{1/3}}{1} = 921$ lb/in.

Face 2: $E_2 = 0.82 \times 10^6$ psi; $P_{cr} = \dfrac{7.08 (0.82 \times 10^6)^{1/3}}{0.373} = 1777$ lb/in.

4. **Conclude**

Ultimate load on column is 346 lb/in. as governed by general instability. Total short term ultimate load is 346 lb/in. x 10 in. = 3460 lbs. Note that low shear stiffness of core reduced Euler load of 480 lb/in. to 346 lb/in., a reduction of 27%.

Note: 1 psi = 0.0069 MPa; 1 in. = 25.4 mm; 1 lb = 0.454 kg

In essence, these equations indicate that the critical wrinkling stress is unaffected by biaxiality of stress.

When thin faces are supported by honeycomb cores with large cells, they may wrinkle or dimple in or out of the voids in the cells. The critical face buckling stress for such honeycomb cores is (8.5):

$$\sigma_{cr} = k \ E \ (\frac{t}{d'})^2 \qquad \text{Eq. 8.111}$$

where

d' = diameter of circle inscribed within hexagon or square of honeycomb cell (Fig. 8.2b)

k = 3 for hexagonal cells, and for square cells with stress applied parallel to the sides

k = 2.5 for square cells with stress applied parallel to the diagonal of the square grid

When the sandwich consists of thin faces applied to a corrugated or other discontinuous core, a number of modes of local buckling must be considered. That is, either the face or the core may buckle independently or simultaneously. Furthermore, if the face is attached to the core only locally, as with fasteners or rivets, the elements may buckle between fasteners. Some guidance for determining the local buckling resistance of such sandwich panels with corrugated cores is given in (8.2, 8.11).

8.9 Optimum Design to Minimize Cost or Weight

The structural arrangement of sandwich construction offers unique opportunities to mix and tailor materials and cross-section proportions to meet structural design criteria. For cost-effective design, economic comparisons between combinations of different materials in a sandwich structure must be made. Such comparisons should be based on sandwich proportions that vary for each combination of materials, and that reflect the minimum combined cost of the core and facings. Simplified relations which can be used for these economic analyses are presented in this Section. If weight rather than cost is to be optimized, unit weight may be substituted directly for unit cost in the ensuing discussion and equations.

The following are the principal simplifications and assumptions used in the derivation of minimum cost relations that are presented subsequently:

- The faces are identical and thin and secondary bending effects due to shear-flexible cores are negligible.
- The costs of adhesive, other bonding or fastening processes, and surface finishes are not included in the analysis.
- The core is assumed to be "soft," as defined in Section 8.4.
- The unit cost per volume of skins and faces does not vary with thickness.

The validity of the above assumptions may have to be investigated in more detail, once initial proportions are established. Equations in Table 8-1h give section properties for sandwich sections that meet the criteria described above.

Cost Effective Proportions for Components in Bending

In sandwich components such as wall, roof, or floor members designed to support normal loads in bending , cross-section proportions are usually governed by a required moment of inertia, section modulus, and core area. These section properties may be satisfied by infinite combinations of facing and core thicknesses. However, only one set of proportions provides the required section properties at minimum cost. A procedure for determining the minimum cost of panels that have the required section properties is developed below. For simplicity, the procedure is developed for a beam strip of unit width (i.e. b = 1).

Panel Cost: The cost per unit surface area, C_p, of a sandwich panel meeting the assumptions given earlier, is expressed as follows:

$$C_p = 2\,t\,C_f + c\,C_c \qquad \text{Eq. 8.112}$$

where

C_f = cost per unit volume of face material

C_c = cost per unit volume of core material

This expression will be used below in the development of relationships for minimum cost panels.

Criterion I – Moment of Inertia Governs: In a specific design situation, stiffness requirements may dominate the design problem and govern sandwich proportions. Thus, Criterion I results in a cross section that provides the required moment of inertia, I*, at minimum cost. The resulting section is adequate only if its section modulus, S, and shear area, c, are also adequate for the specific requirements of the application (i.e. $S \geqq S^*$, and $c \geqq c^*$). Equations satisfying Criterion I are developed below.

The total material cost per unit surface area of the panel is obtained in terms of I* and unit costs of materials, by combining Eqs. 8.7c and 8.112 for a unit width of section (b = 1):

$$C_p = (2\,C_f - C_c)\,t + C_c\,\left(\frac{2\,I^*}{t}\right)^{1/2} \qquad \text{Eq. 8.113}$$

Differentiating this equation with respect to t, and setting the result equal to 0, gives the face thickness required for minimum panel cost, in terms of I* and the unit costs of materials. Expressions for the core thickness and the total panel cost can then be readily determined. Resulting relationships for situations where I* governs design ($S \geq S^*$, and $c \geq c^*$) are as follows:

$$t = \left[\frac{C_c^{\,2}\, I^*}{2\,(2\,C_f - C_c)^2}\right]^{\frac{1}{3}} \qquad \text{Eq. 8.114}$$

$$c = \left(\frac{4\,C_f}{C_c} - 3\right)\,t \qquad \text{Eq. 8.115}$$

$$S = td \simeq t\,(c + 2t) = S_{min} \qquad \text{Eq. 8.14c}$$

$$= \left(\frac{4\,C_f}{C_c} - 3\right)\,\left[\frac{C_c^{\,2}\, I^*}{2\,(2\,C_f - C_c)^2}\right]^{\frac{2}{3}} \qquad \text{Eq. 8.116}$$

$$\min.\ C_p = \text{cost of faces} + \text{cost of core} \qquad \text{Eq. 8.112}$$

$$= 2\,t\,C_f + \left(\frac{4\,C_f}{C_c} - 3\right) t\,C_c \qquad \text{Eq. 8.117}$$

$$= 2.38 \left[C_c^{\,2}\ (2\,C_f - C_c)\ I^*\right]^{1/3} \qquad \text{Eq. 8.117a}$$

$$\cong 2\,t\,C_f + 4\,t\,C_f \quad (\text{if } C_f/C_c \gg \tfrac{3}{4}) \qquad \text{Eq. 8.117b}$$

Eq. 8.117b shows that for a cross section proportioned for moment of inertia at minimum cost, the faces comprise one-third of the panel cost, and the core comprises two-thirds of the panel cost. This is true for many practical panels where the cost per unit volume of the face material is significantly greater than that of the core (i.e. $C_f/C_c \gg \frac{3}{4}$).

Criterion 2 — Section Modulus Governs: In contrast to the above, situations can arise where strength requirements dominate the design problem, and govern sandwich proportions. Thus, Criterion 2 results in a cross section which provides the required section modulus, S^*, at minimum cost. The resulting section is adequate only if its moment of inertia, I, and shear area, c, are also adequate for the specific requirements of the application (i.e. $I \geq I^*$, and $c \geq c^*$). Equations for Criterion 2 are developed below.

The total material cost per unit surface area of the panel is obtained in terms of, S^*, and unit costs of materials, by combining Eqs. 8.14c and 8.112:

$$C_p = (2\,C_f - C_c)\,t + C_c\left(\frac{S^*}{t}\right) \qquad \text{Eq. 8.118}$$

By reasoning similar to that described above for Criterion 1, the following relationships can be derived for situations where S^* governs design ($I \geq I^*$, and $c \geq c^*$):

$$t = \left[\frac{C_c\,S^*}{2\,C_f}\right]^{1/2} \qquad \text{Eq. 8.119}$$

$$c = \frac{2\,C_f\,t}{C_c} = \left[\frac{2\,C_f\,S^*}{C_c}\right]^{1/2} \qquad \text{Eq. 8.120}$$

$$I = \frac{t\,d^2}{2} = \frac{t\,(c+t)^2}{2} \qquad \text{Eq. 8.7 c}$$

$$= \left(1 + \frac{C_c}{C_f}\right)\left[\frac{C_f\,S*^3}{2\,C_c}\right]^{1/2} \qquad \text{Eq. 8.121}$$

$$\text{min. } C_p = \text{cost of faces + cost of core} \qquad \text{Eq. 8.112}$$

$$= 2\,t\,C_f + \frac{2\,C_f\,t\,C_c}{C_c}$$

$$= 2\,t\,C_f + 2\,t\,C_f \qquad \text{Eq. 8.122}$$

$$= (8\,C_f\,C_c\,S*)^{1/2} \qquad \text{Eq. 8.123}$$

Eq. 8.122 shows that for a cross section proportioned to obtain minimum cost of materials for a given section modulus, the total materials cost is divided equally between the faces and the core.

Criterion 3 – Moment of Inertia and Section Modulus Satisfied Simultaneously:

In certain cases, a cross section that provides the required moment of inertia, I*, and the required section modulus, S*, simultaneously, also provides the minimum panel cost. In order to be adequate, the cross-section proportioned in accordance with Criterion 3 must also provide adequate shear area (i.e. $c \geq c*$). Equations for Criterion 3 are developed below.

Proportions that provide section properties in accordance with Criterion 3, are as derived from Eqs. 8.7c and 8.14c for reasonably thin faces:

$$c = \frac{2\,I*}{S*} - \frac{S*^2}{S\,I*} \approx \frac{2\,I*}{S*} \text{ (for thin faces)} \qquad \text{Eq. 8.124}$$

$$t = \frac{S*^2}{2\,I*} \qquad \text{Eq. 8.125}$$

Thus, substituting Equations 8.124 and 8.125 into 8.112, results in the following panel cost:

$$C_p = \frac{S^{*2}}{2 I^*} (2 C_f - C_c) + \frac{2 I^*}{S^*} C_c \qquad \text{Eq. 8.126}$$

This equation gives the panel cost directly from the minimum required section properties. As will be explained later, it may provide the minimum panel cost as well, depending on the relative magnitude of S* and I* and unit costs, and providing $c \geq c^*$, for a given design situation.

Criterion 4 — Shear Area, c*: In addition to the requirements for bending section properties, the cross section must also provide sufficient core thickness, c* or greater, to develop required shear strength. This serves as a final check on the strength capacity of the cross-section meeting the other criteria given above.

Graphical Determination of Governing Criteria: A graphical presentation of both required and cost-effective proportions demonstrates, quantitatively, which of the above criteria governs in a given design situation. Fig. 8-19 presents such graphs for a specific set of I*, S*, and c* requirements, which will be used in a numerical solution in Example 8-8. The following are key elements shown in Fig. 8-19.

- The curves in Fig. 8-19 define section proportions which satisfy the required values of I*, S*, and c*. The shaded portions of the curves define the bounds over which proportions are governed by S* by I*, and by c*, respectively.

- The dashed straight-lines are contours of constant panel unit cost. The minimum-cost cross section occurs at the point of tangency of the cost contour and the I* and S* curves.

- The points of tangency, as obtained by Criteria 1, 2 and 3, are marked on Fig. 8-19. For this specific set of criteria, these happen to points occur on

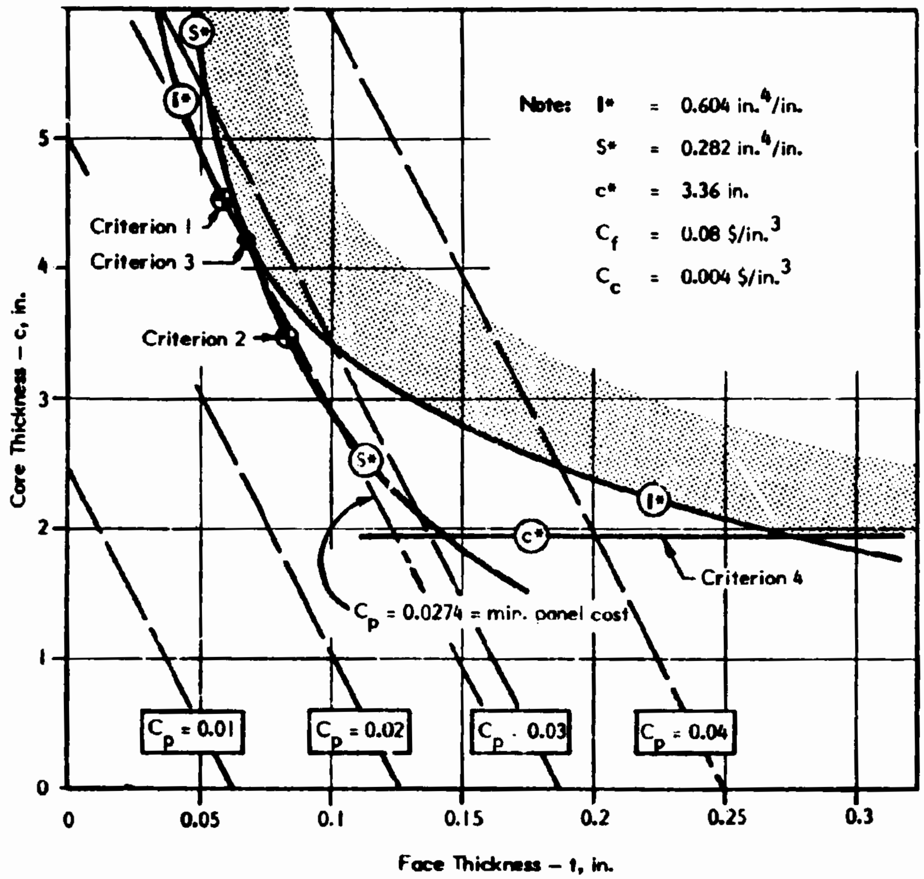

Fig. 8-19 CRITERIA FOR SELECTING MINIMUM-COST BEAM CROSS SECTION FOR EXAMPLE 8-8

approximately the same contour ($C_p \cong$ 0.027 \$/in.^{2}), but this is not the general rule.

- Both Criterion 1 and Criterion 2 fail to provide the minimum panel cost because, in each instance, the alternate requirement for section properties is not satisfied. For example, for the same depth, the Criterion 1 thickness (and cost) must be increased to provide the needed S*. The result is similar for I* and Criterion 2.

- Criterion 3, by definition, satisfies both section modulus and moment of inertia requirements. And, it is the only point on the shaded boundary that meets both criteria. Hence, it provides the minimum cost (i.e. tangent to the left-most cost contour). The minimum cost is C_p = 0.0274 \$/in.^{3}

- Criterion 4 forms a fourth bound on cross-section proportions, which is the minimum depth required for shear strength. Core depth provided by the above criteria must be greater than c* in order to meet the shear strength criterion.

For the specific set of design criteria examined above, Criteria 1, 2, and 3 all produce similar minimum panel costs since they lie on approximately the same C_p contour. However, they produce significantly different minimum cost proportions. In this instance, Criterion 3 prevails, since it satisfies both section modulus and moment of inertia criteria.

Clearly, the minimum cost solution examined above is not subject to generalization. Depending upon shifts in the relative magnitude of I* and S* and c* in a specific design situation, or a change in slope of the cost contours, as dictated by the relative unit cost of face and core materials, either Criterion 1 or Criterion 2 could govern in bending. Furthermore, if the core is especially weak, Criterion 4 might prove to govern as a result of shear strength considerations.

Detailed Design Procedure: While the above graphical approach is useful in understanding how the governing criterion is selected, a direct numerical design procedure is useful in determining optimum designs. The following procedure provides a direct approach to the determination of minimum-cost panels, for a specific application:

a) Determine the required section properties I^* and S^*, and the minimum core thickness, c^*, required for shear strength.

b) Solve for the section modulus furnished by the Criterion 1 cross section (Eq. 8.116). If $S \geq S^*$, Criterion 1 provides the minimum-cost cross section as governed by I^*. If $S < S^*$, the Criterion 1 cross section is not adequate and is rejected.

c) If from the above, $S < S^*$, solve for the moment of inertia furnished by the Criterion 2 cross section (Eq. 8.121). if $I \geq I^*$, Criterion 2 provides the minimum-cost cross section as governed by S^*. If $I < I^*$, the Criterion 2 cross section is not adequate and is rejected.

d) If Steps b and c result in rejection of Criterion 1 and 2, Criterion 3 yields the minimum-cost bending cross section.

e) Once the criterion which produces the minimum-cost bending cross-section is established from Steps b through d above, the core depth provided, c, should be compared to, c^*, in accordance with Criterion 4. If this criterion is satisfied, the face and core thickness and the panel cost can be obtained by the appropriate equations for the governing bending criterion given earlier.

f) If Criterion 4 requirements are not met, the core depth must be increased to provide the required strength. The face thickness can be diminished, while still satisfying I^* and S^*, as core depth is increased (Eq. 8.7a, b and 8.14a, b, c). Alternately, a stronger or stiffer core may be needed to provide a cost-effective design.

g) Finally, the selected section should be checked for other governing criteria such as shear deflection.

Example 8-8 illustrates the procedure for determining cost effective proportions of a sandwich wall panel.

Direct Determination of Required Moment of Inertia

When designing a conventional beam or column for stiffness, the moment of inertia required to limit beam deflection or provide column stability can be calculated directly for a given beam or column span and load distribution. Usually, this cannot be done for a sandwich beam or column because it is necessary to account for the effects of core shear deformation.

In Example 8-8 an estimate was made that core shear deflection would be about 25% of bending deflection. Based on this, the required moment of inertia, I*, was increased from that due to bending alone in the wall panel, to compensate for the increased deflection due to shear. However, for a sandwich beam or column proportioned for minimum cost of panel and face materials based on Criteria 1 or 3, a direct determination of I*, which accounts for core shear effects in addition to bending, can be formulated as follows:

Bending Plus Shear Deflection in Beams: Solving Eqs. 8.27 and 8.115 simultaneously yields the following expression for I* if Criterion 1 pertains

$$I^* - \frac{K_v PL}{mG_c w_a} (I^*)^{2/3} = \frac{K_m PL^3}{E w_a} \qquad \text{Eq. 8.127}$$

where

w_a = allowable deflection

$$m = \left(\frac{4C_f}{C_c} - 3\right) \left[\frac{C_c^{2}}{2(2C_f - C_f)^2}\right]^{1/3} \qquad \text{Eq. 8.128}$$

for K_v and K_m, see Table 8-3.

Example 8-8: Optimum-Cost Panel Design *

Determine minimum-cost proportions for a sandwich wall panel that spans 8 feet, and has fiberglass-mat-reinforced polyester faces of equal thickness, and an extruded polystyrene structural foam core.

1. Design Criteria

Wind load	q	= 40 psf = 0.28 psi
Safety Factor on Strength (Typical Basis - see section 3.4)	$\overline{FS}$	= 5
Deflection limit	w_a	= L/150 = 0.64 in.

2. Material Properties (short-term)

	Face (mat)	Core (foam) (8.13)
Cost ($/in.^{3})	C_f = 0.08	C_c = 0.004
Ultimate Tensile Strength (Tension Governs)	F_{ult} = 10,000 psi	—
Ultimate Shear Strength	—	F_{vu} = 35 psi
Design Strength ($\overline{FS}$ = 5)	F_{td} = 2,000 psi	F_{vd} = 7 psi
Modulus of Elasticity	E_f = 1×10^6 psi	E_c = 1,500 psi
Modulus of Rigidity	—	G_c = 1,000 psi

3. Required Properties

Determine Minimum Allowable Stress, F:

Tension:

$$F_{td} = 2000 \text{ psi}$$

Wrinkling of Face:

$$F_{crd} = 0.5\ (E_f\, E_c\, G_c)^{1/3} \times \frac{1}{\overline{FS}} \qquad \text{Eq. 8.107}$$

$$= 0.5\,(1 \times 10^6 \times 1{,}500 \times 1{,}000)^{1/3} \times \frac{1}{5} = 1{,}144 \text{ psi} < 2{,}000 \text{ psi} = F_{td}$$

Use F = 1,144 psi as governed by face wrinkling.

---

* See Footnote, Example 8-1.

Example 8-8 continued

Required Section Modulus, S*:

$$S^* = \frac{M}{F} = \frac{qL^2}{8F} = \frac{0.28 \times 96^2}{8 \times 1,144} = 0.282 \text{ in.}^3/\text{in.}$$

Required Moment of Inertia, I*:

$$I^* = \frac{5\,q\,L^4}{384\,E_f \times w_a} = \frac{5 \times 0.28 \times 96^4}{384 \times 1 \times 10^6 \times 0.64} = 0.483 \text{ in.}^4/\text{in. for bending only}$$

Try adding 25% to moment of inertia required for bending to compensate for shear deflection. Therefore, try $I^* = 0.604$ in.^{4}/in. as first cut.

Required Minimum Core Thickness for Shear, c*:

$$A_v = c^* = \frac{qL}{2F_{vd}} = \frac{0.28 \times 96}{2 \times 7} = 1.92 \text{ in.}$$

4. **Determine Applicable Criterion for Minimum Cost Proportions:**

Section Modulus Furnished by Criterion 1:

$$S = \left(\frac{4\,C_f}{C_c} - 3\right)\left[\frac{C_2^{\,2}\,I^*}{2\,(2\,C_f - C_c)^2}\right]^{2/3} \qquad \text{Eq. 8.116}$$

$$= \left(\frac{4 \times 0.08}{0.004} - 3\right)\left[\frac{0.004^2 \times 0.604}{2\,(2 \times 0.08 - 0.004)^2}\right]^{2/3}$$

$$= 0.262 < 0.282 \text{ in.}^3/\text{in.} = S^*. \text{ Criterion 1 is invalid.}$$

Moment of Inertia Furnished by Criterion 2:

$$I = \left[\frac{C_f\,S^{*3}}{2\,C_c}\right]^{1/2} = \left[\frac{0.08 \times 0.282^3}{2 \times 0.004}\right]^{1/2} \qquad \text{Eq. 8.121}$$

$$= 0.474 < 0.604 \text{ in.}^4/\text{in.} = I^*. \text{ Criterion 2 is invalid.}$$

Conclude: Since neither Criterion 1 or 2 satisfies both S* and I*, Criterion 3 governs the bending cross-section.

Example 8-8 continued

5. **Proportions and Cost for Criterion 3**

$$c = \frac{2\,I^*}{S^*} - \frac{S^{*2}}{2\,I^*} = \frac{2 \times 0.604}{0.282} - \frac{0.282^2}{2 \times 0.604} \qquad \text{Eq. 8.124}$$

$$= 4.28 - 0.066 = 4.21 \text{ in.}$$

Note that the second term is small for thin faces.

$$t = \frac{S^{*2}}{2I^*} = \frac{0.282^2}{2 \times 0.604} = 0.066 \text{ in.} \qquad \text{Eq. 8.125}$$

$$C_p = 2 \times 0.066 \times 0.08 + 4.21 \times 0.004 \qquad \text{Eq. 8.112}$$

$$= 0.0106 + 0.0168 = 0.0274 \text{ \$/in.}^2 = 3.95 \text{ \$/ft}^2$$

6. **Check Criterion 4:**

From Criterion 3, $c = 4.21$ in. $>$ 1.92 in. $= c^*$. OK

7. **Check accuracy of 25% increase in moment of inertia.** Check assumption as to compensation for shear deflection in step 3.

$$w = \frac{K_m PL^3}{D_m} + \frac{K_v PL}{D_v}\,; \; K_m = \frac{5}{384},\; K_v = \frac{1}{8} \text{ (Table 8-3)} \qquad \text{Eq. 8.27}$$

$$= \frac{5\,(0.28 \times 96)\,96^3}{384 \times 1 \times 10^6 \times 0.604} + \frac{(0.28 \times 96)\,96}{8 \times 1{,}000 \times 4.21}$$

$$= 0.512 + 0.077 = 0.59 \text{ in.} < 0.64 \text{ in.} = w_a \text{ (within 8.5\%)} \qquad \text{OK}$$

Refine by second trial with I^* reduced by about 7%, if desired.

8. **Conclusion**

Minimum cost panel which meets design criteria has 4.21 in. core and 0.066 in. faces. Panel cost is \$3.95/sq ft plus cost of bonding adhesive.

If Criterion 3 governs, solving Eqs. 8.27 and 8.124 results in the following expression for I*:

$$I^* = \frac{PL}{w_a}\left[\frac{K_m L^2}{E} + \frac{K_v S^*}{2a}\right] \qquad \text{Eq. 8.129}$$

In application, Eq. 8.127 is used when evaluating Criterion 1, and Eq. 8.129 is used when evaluating Criterion 3.

Column Buckling Including Effects of Shear Deflection: Solving Eqs. 8.102 and 8.117a yields the following expression for I*:

$$I^* - \left(\frac{P}{mG_c\,\overline{SF}}\right) I^{*2/3} = \frac{L^2 P}{k\,\pi^2 E\,\overline{SF}} \qquad \text{Eq. 8.130}$$

where

P = design axial load

$\overline{SF}$ = safety factor against buckling

for k see Table 6-4.

After determining I* from Eq. 8.130, it is used in conjunction with Eqs. 8.113 to 8.115 to find optimum proportions and minimum cost. Independent checks are then made to verify whether the compression strength of the materials is adequate.

8.10 Temperature and Moisture Movements and Other Volume Changes

Structural plastics may display significant dimensional or volume changes when subjected to moisture and temperature changes. Plastics may also undergo significant volume changes such as permanent or transient swelling and shrinkage in chemical environments, permanent shrinkage on exposure to UV, and aging shrinkage that may develop with time and which is accelerated by elevated temperature. These volume changes and associated linear expansions and contractions can cause significant distortions in sandwich panels that are free to move and significant stresses in panels that are restrained. While the effects of temperature are used herein to illustrate these important effects, the principles developed may be applied in the analysis for the effects of moisture movements, curing and aging shrinkage, or volume changes resulting from other environmental exposures.

Warping and Changes in Length.

When opposing faces of an unrestrained panel undergo different volume changes, a strain differential is imposed across the thickness of the panel. The unrestrained panel warps to a curvature having a radius:

$$R = \frac{d}{\varepsilon_2 - \varepsilon_1} \qquad \text{Eq. 8.131}$$

where

$\varepsilon_1, \varepsilon_2$ = unit dimensional change or strain occurring on opposite faces.

From a practical standpoint, this change in dimension is usually taken from a reference condition such as that at the completion of manufacture, or at the time of installation. For unit dimensional changes that do not vary over the length of the panel, curvature is constant along the length, and in effect, is analogous to the curvature in a panel which is subjected to equal bending moments at its ends. The deflection normal to the plane of the panel at its mid-length resulting from this curvature is:

$$w = \frac{(\varepsilon_2 - \varepsilon_1) L^2}{8d} \qquad \text{Eq. 8.132}$$

The term $(\varepsilon_2 - \varepsilon_1)$ is the magnitude of the in-plane strain differential caused by differential volume changes of the two faces. In the case of a uniform temperature change which is uniform across the face:

$$\varepsilon_i = \alpha_i \, \Delta T_i \qquad \text{Eq. 8.133}$$

where

ε_i = strain due to thermal expansion of i face

σ_i = coefficient of thermal expansion of the "i" face

ΔT_i = temperature change in the "i" face from reference condition

In addition to causing bowing, a strain gradient imposed across the panel results in a change in its overall length. The magnitude of the change is:

$$\Delta L = \frac{(\varepsilon_1 + \varepsilon_2) L}{2} \qquad \text{Eq. 8.134}$$

Joint sealants and other details at panel ends, and holes at fasteners, should be designed to accommodate such movements which can be significant in long panels. Example 8-9 illustrates the calculation of deflection and length change for an unbalanced panel subjected to a temperature change that is constant throughout the panel depth.

Stresses Due to the Restraint of Warping

Sandwich panels that are continuous for several spans may be supported by primary framing at intermediate points along the panel length. When different strain gradients are imposed on opposite faces of such panels, reactions develop to prevent deflection at the supports. These reactions cause moments and shears in the panels. Since shear stresses and deformations may be significant in sandwich structures, they must be included in the calculation of stresses, deformations and reactions for this indeterminant structure.

The derivation of expressions for moments, shears, and reactions in a sandwich panel that is continuous over two equal spans, and that is subjected to a temperature gradient, is given in Example 8-10 (8.14). The example shows that maximum support reactions and associated panel shears and moments depend on both the flexural stiffness of the panel and shear rigidity of the core. Furthermore, thermally induced reactions may increase or decrease as panel span increases, and moments generally increase as the span increases. While this example is developed for a temperature differential across the panel, the general approach is valid for other sources of differential volume changes in the faces, such as moisture gradients.

Example 8-9: **Bowing in an Unbalanced Sandwich Beam Subjected to Uniform Temperature Change** *

Determine the magnitude of warping and shrinkage in the Aluminum/PVC panel shown in Example 8-3, at a temperature of 25°F. The panel is 10 feet long and it was flat when manufactured at 75°F.

1. **Panel Properties**

Panel depth to centroids of facings, d = 2.14 in.

Panel Length = 10 ft x 12 = 120 in.

Coefficient of Thermal Expansion: Aluminum $\sigma_1 = 12.8 \times 10^{-6}/^{o}F$

PVC $\sigma_2 = 30 \times 10^{-6}/^{o}F$

2. **Maximum Deflection at Mid-Length**

$$w = \frac{(\epsilon_2 - \epsilon_1)L^2}{8d}$$

$$\epsilon_1 = \alpha_1 \Delta T_1 = 12.8 \times 10^{-6} (-50) = -0.640 \times 10^{-3} \text{in./in.}$$

$$\epsilon_2 = \alpha_2 \Delta T_2 = 30 \times 10^{-6} \times (-50) = -1.50 \times 10^{-3} \text{in./in.}$$

$$w = \frac{(-1.50 + 0.64) \times 120^2}{8 \times 2.14} = 0.723 \text{ in.}$$

3. **Length Change**

$$\Delta L = \frac{(\epsilon_1 + \epsilon_2) L}{2}$$

$$= \frac{(-0.65 - 1.50) \times 10^{-3} \times 120}{2} = 0.129 \text{ in.}$$

4. **Conclude:** The 10 foot long Aluminum/PVC sandwich panel, manufactured at 75°F, warps about 3/4 in. and shrinks about 1/8 in. when it is exposed to a temperature of 25°F.

---

* See Footnote, Example 8-1.

Example 8-10: Derivation of Reuctions, Moments, Shears and Deflection in a Two-Span Panel Subjected to a Temperature Gradient Across Its Thickness (8.14) *

1. Structural Arrangement (For Temperature Change, each face)

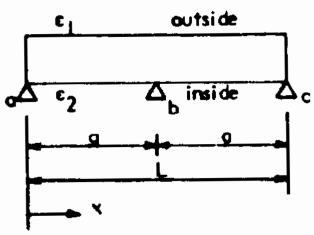

$$\epsilon_1 = \alpha_1 \ \Delta T_1$$

$$\epsilon_2 = \alpha_2 \ \Delta T_2 \qquad \text{Eq. 8.133}$$

2. Determine Thermal Deflection with Redundant Support at b Removed

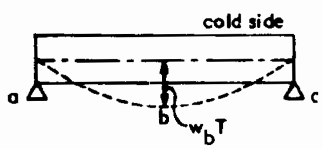

$$w_{bT} = \frac{(\epsilon_2 - \epsilon_1) L^2}{8d} \qquad \text{Eq. 8.132}$$

$$w_{bT} = \frac{(\alpha_2 \ \Delta T_2 - \alpha_1 \ \Delta T_1)(2a)^2}{8d} = \frac{(\alpha_2 \ \Delta T_2 - \alpha_1 \ \Delta T_1)\, a^2}{2d} \qquad \text{Eq. 8.135}$$

3. Determine Restoring Deflection with Redundant Support Reaction Acting Alone

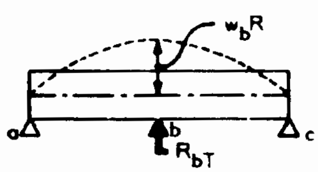

$$w_{bR} = \frac{K_m R_{bT} L^3}{D_m} + \frac{K_v R_{bT} L}{D_v} \qquad \text{Eq. 8.27}$$

For concentrated load at midspan (Table 8-2): $K_m = 1/48; \ K_v = 1/4$

$$w_{bR} = \frac{R_{bT}\, a}{2} \left[\frac{a^2}{3 D_m} + \frac{1}{D_v} \right] \qquad \text{Eq. 8.136}$$

---

* See Footnote, Example 8-1.

Example 8-10 (continued)

4. Solve for R_{bT}, by Equating Restoring Deflection to Thermal Deflection at b

$$w_{bT} = w_{bR} \; ; \; R_{bT} = \frac{(\alpha_2 \, \Delta T_2 - \alpha_1 \, \Delta T_1)\, a}{d \left[\frac{a^2}{3 D_m} + \frac{1}{D_v} \right]} \qquad \text{Eq. 8.137}$$

5. End Reactions R_{aT} and R_{cT}

$$R_{aT} + R_{bT} + R_{cT} = 0 \quad \text{(upward positive)}$$

by symmetry

$$R_{aT} = R_{cT} ; \quad R_{aT} = R_{cT} = -\frac{R_{bT}}{2} \qquad \text{Eq. 8.138}$$

6. Moment at b

$$M_{bT} = R_{aT} a = \frac{-R_{bT} a}{2} \qquad \text{Eq. 8.139}$$

7. Moment in Span ab, at distance x

$$M_x = R_{aT} x \qquad \text{Eq. 8.140}$$

8. Shears at a, b and c

$$V_{aT} = R_{aT} ; \; V_{cT} = -R_{cT} ; \; V_{bT} = R_{bT}/2 \qquad \text{Eq. 8.141a, b, c}$$

9. Deflection at Midspan of ab

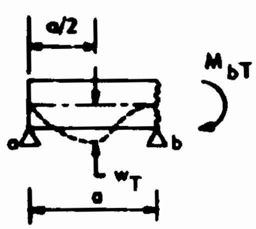

$$w_T = \frac{(\epsilon_2 - \epsilon_1)\, a^2}{8d} + \frac{M_{bT}\, a^2}{16 D_m} \qquad \text{Eq. 8.142}$$

Design of connections between the panel and its supports should include uplift reactions that result from gradients. In addition, local crushing at compressive reactions must be evaluated. (See Section 8.7).

8.11 Panel Subjected to Wind Load and Temperature Gradients

Both plastics materials and sandwich construction are used extensively in insulated structures such as cooler, freezer, and other refrigerated buildings, arctic buildings, ISO-type freight containers for multi-modal transport, and truck bodies. Foamed plastics are used frequently for the cores of such structures, and in some cases, faces are manufactured from fiberglass reinforced plastic, as well.

The concluding example in this Chapter, Example 8-11, presents an analysis of an all-plastic insulating sandwich panel for use in insulated buildings. The example is based on design criteria developed for an installation for the Alaskan North Slope at Prudhoe Bay, and an extension of analytical procedures used in their structural evaluation (8.14).

Example 8-11 demonstrates the analysis and evaluation of wind and thermal stresses in a restrained two-span panel subjected to temperature gradient. It also illustrates many of the concepts introduced in this Chapter and elsewhere in this Manual, and the numerous considerations involved in a comprehensive design of a structural sandwich component. The following is a commentary on key elements of the evaluation.

1. **Design Criteria:** Temperature and wind conditions are estimates for the the Prudhoe Bay region. The maximum wind load is assumed to occur either with or without the temperature differential acting.

Load factors (LF) are assigned with the purpose of increasing loads or stresses to account for the potential for overloads, and other unknowns related to the loads and the analysis, as is done in structural design with conventional structural materials. See Section 3.2, 4.2 and 4.10.

Example 8-11: Evaluation of Wall Panel for Arctic Exposure *

Determine structural adequacy of an exterior two-span sandwich wall panel for arctic buildings. Design criteria include 30 psf wind load and -60°F outdoor temperature in winter. Use 0.1 in. thick mat-reinforced plastic faces on 4 in. thick, 2.5 pcf PU foam core (t = 0.1 in. d = 4.1 in.)

1. Design Criteria

Span: 2 @ 10 ft. (120 in.)

Temperature: Installation at 50°F,
T_1 = - 60°F outside in winter,
T_2 = 70° F inside.

Wind load: q = 30 psf
= 0.21 psi, inward or outward

Load Factors: 1.7 on wind
1.4 on thermal gradient

Capacity Reduction Factor (CRF): 0.60 for FRP faces;
0.40 for foam core.

Maximum Deflection: Span/150 = 120/150 = 0.80 in.

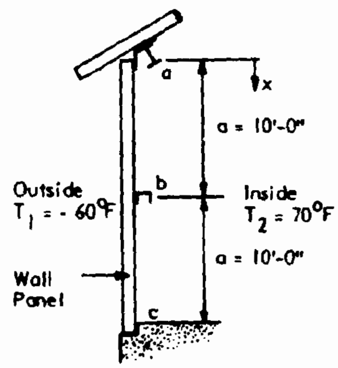

Wall Section

2. Materials Properties

Element	Properties	Units	Short Term Property	Reduction Factor for 10 yr Duration of Stress	Long Term Property
Faces	E_f	psi	0.8×10^6	2	0.4×10^6
	ν_f	–	0.3	–	0.3
	F_{ut}	psi	11,000 **	3	3670 **
	F_{uc}	psi	22,000	3	7340
		1/°F	15×10^{-6}	–	15×10^{-6}
Core	E_c	psi	2500	2	1250
	G_c	psi	800	2	400
	F_{uv}	psi	25	3	8.3

** Use tensile strength for flexural tension strength (See "Flexural Strength," Section 3.6)

* See Footnote, Example 8-1.

Example 8-11 continued

3. Design Stresses — Ultimate Strength Approach

Establish reduced ultimate design strengths to be compared later to factored stresses due to loads.

a. Multiply typical ultimate strengths in 1. above by Capacity Reduction Factor to obtain reduced ultimate design strength:

Properties		Short Term	Long Term
Tension:	F_{utr}	$0.6 \times 11{,}000 = 6{,}600$ psi	$0.6 \times 3670 = 2{,}200$ psi
Compression:	F_{ucr}	$0.6 \times 22{,}000 = 13{,}200$ psi	$0.6 \times 7{,}340 = 4{,}400$ psi
Shear:	F_{uvr}	$0.4 \times 25 = 10.0$ psi	$0.4 \times 8.3 = 3.3$ psi

Tension strength governs ultimate strength of faces.

b. Check strength governed by face wrinkling (Eq. 8.109). Use CRF = 0.6.

Wrinkling Stress		Short Term	Long Term
Ultimate:	F_{cr}	$0.5\,(0.8 \times 10^6 \times 2{,}500 \times 800)^{1/3}$	$0.5\,(0.4 \times 10^6 \times 1{,}250 \times 400)^{1/3}$
		5,850 psi	2,925 psi
Reduced:	F_{crr}	$0.6 \times 5{,}850 = 3{,}510$ psi	$0.6 \times 2{,}930 = 1{,}760$ psi

Failure by face wrinkling in compression governs design of faces.

c. Summary — Final reduced ultimate design strengths:

	Short Term (psi)	Long Term (psi)
Face ultimate strength F_{utr} (tension)	6,600	2,200
Face wrinkling strength F_{crr} (compression)	3,510	1,760
Core strength F_{uvr} (shear)	10	3.3

Example 8-11 continued

4. **Section Properties:** Refer to Table 8-1:

Properties	Units	Short-Term Property	Reduction Factor for Duration of Stress	Long-Term Property
$I = I_o = td^2/2$	$in.^4/in.$	0.84	—	0.84
$D_m = E_f I/(1 - \nu^2)$	$in.^2$-lb/in.	0.74×10^6	2	0.37×10^6
$S = td$	$in.^3/in.$	0.41	—	0.41
$I_f = t^3/6$	$in.^4/in.$	0.00017		0.00017
$D_{mf} = E_f I$	$in.^2$-lb/in.	133.3	2	66.7
$S_{f1} = S_{f2} = t^2/6$	$in.^3/in.$	0.0017		0.0017
$A_c = d^2/c$	$in.^2/in.$	4.2	—	4.2
$D_v = A_c G_c$	lb/in.	3360	2	1680
Coefficients (from Table 8-4):				
$\theta = \frac{2a}{2}\left(\frac{D_v}{D_{mf}}\right)^{1/2}$	—	602	—	602
$\phi_1 = \frac{\theta - 1}{\theta}$	—	0.9983	—	0.9983
$\phi_2 = 1$		1.000		1.000
$\phi_3 = \frac{\theta^2 - 2}{\theta^2}$	—	0.9999	—	0.9999

Example 8-11 continued

5. Stress Analysis for Wind Effects

Use short-term properties for wind. See Example 8-5 for equations.

Reactions:

$$R_{bL} = qa \left[\frac{5a^2}{12 D_m} + \frac{1}{D_v}\right] + \left[\frac{a^2}{3 D_m} + \frac{1}{D_v}\right] \qquad \text{Eq. 8.30}$$

$$= 0.21 \times 120 \left[\frac{5 \times 120^2}{12 \times 0.74 \times 10^6} + \frac{1}{3360}\right]$$

$$+ \left[\frac{120^2}{3 \times 0.74 \times 10^6} + \frac{1}{3360}\right] = 31.2 \text{ lb/in.}$$

$$R_{aL} = \frac{-R_{bL} + 2aq}{2} = \frac{-31.2 + 2 \times 120 \times 0.21}{2} = 9.6 \text{ in.-lb/in.}$$

Moment, M', at center reaction at b: due to wind load, W, acting on full span 2a:

$$M'_{bL} = \frac{W(2a)^2}{8} = \frac{0.21 \times 240^2}{8} = 1{,}512 \text{ in.-lb/in.}$$

Moment at b due to reaction R_{bL}:

$$M''_{bL} = \frac{R_{bL}(2a)}{4} = -\frac{31.2 \times 240}{4} = -1{,}872 \text{ in.-lb/in.}$$

Net Moment at b:

$$M_{bL} = M'_{bL} + M''_{bL} = 1512 - 1872 = -360 \text{ in.-lb/in.}$$

Note: A check shows that moments at midspan of span a are less than M_{bL}.

Example 8-11 continued

Bending Stresses: Distribute moments between faces and transformed section in accordance with Table 8-4. M' is distributed as for a beam under uniform load; M" is distributed as for beam under concentrated central load.

$$\sigma_{bLp} = \frac{M'_{bL}\,\phi_3}{S} + \frac{M''_{bL}\,\phi_1}{S}$$

$$= \frac{1512 \times 0.9999}{0.41} - \frac{1872 \times 0.9983}{0.41} = -871 \text{ psi} \quad \text{(primary stress on transformed section)}$$

$$\sigma_{bLf} = \frac{M'_{bL}\,(1-\phi_3)}{2\,S_{fi}} + \frac{M''_{bL}\,(1-\phi_1)}{2\,S_{fi}}$$

$$= \frac{1512 \times 0.0001}{2 \times 0.0017} - \frac{1872 \times 0.0017}{2 \times 0.0017} = -892 \text{ psi} \quad \text{(secondary face-bending stress)}$$

$$\sigma_{bL} = f_{bLp} + f_{bLf} = -871 - 892 = -1{,}763 \text{ psi}$$

Note: Secondary stresses are approximately equal to the primary stresses.

Shear Stress @ b:

$$\tau_L = \frac{R_{bL}\phi_2}{2d} = \frac{31.2 \times 1}{2 \times 4.1} = 3.8 \text{ psi}$$

6. **Stress Analysis for Thermal Effects** (Refer to Example 8-10 for equations):

Panel was flat when fastened on building at T = + 50°F which is taken as reference temperature.

$$\epsilon_1 = \alpha_1\,\Delta T_1 = 15 \times 10^{-6} \left[-60 - (+50)\right] = -1.65 \times 10^{-3} \text{ in./in.}$$

$$\epsilon_2 = \alpha_2\,\Delta T_2 = 15 \times 10^{6} \left[+70 - (+50)\right] = +0.30 \times 10^{-3} \text{ in./in.}$$

$$\epsilon_2 - \epsilon_1 = +0\,3 \times 10^{-3} - (-1.65 \times 10^{-3}) = +1.95 \times 10^{-3} \text{ in./in.}$$

Example 8-11 continued

Short-Term Thermal Effects

Reactions:

$$R_{bT} = \frac{(\alpha_2 \Delta T_2 - \alpha_1 \Delta T_1)\, a}{\left[d \dfrac{a^2}{3 D_m} + \dfrac{1}{D_v}\right]} \qquad \text{Eq. 8.137}$$

$$= \frac{(+\,1.95 \times 10^{-3})\, 120}{4.1 \left[\dfrac{120^2}{3 \times 0.74 \times 10^6} + \dfrac{1}{3360}\right]} = +8.4 \text{ lb/in.}$$

$$R_{aT} = \frac{R_{bT}}{2} = -4.2 \text{ lb/in.}$$

Moments:

Total Moment: $M_{bT} = R_{aT} a = -4.2 \times 120 = -504$ in.-lb/in.

Primary Moment: $M_{bTp} = M_{bT}\, \phi_1 = M_{bT} \times 1 = -504$ in.-lb/in.

Secondary Moment: $M_{bTf} = M\,(1 - \phi_1) = -504\,(1 - 0.9983) = 0.857$ in.-lb/in.

Bending Stresses:

$$\sigma_{bTp} = \frac{M_{bTp}}{S} = -\frac{504}{0.41} = -1{,}229 \text{ psi}$$ (primary stress on transformed section)

$$\sigma_{bTf} = \frac{M_{bTf}}{S_f} = \frac{0.857}{0.0033} = -\,260 \text{ psi}$$ (secondary face-bending stress)

$$\sigma_{bT} = \sigma_{bTp} + \sigma_{bTf} = -1229 - 260 = -1{,}489 \text{ psi}$$

Note: Secondary stresses are only about 20% of primary stresses for this case.

Shear Stress @ b:

$$\tau_T = \frac{R_{bT}\, \phi_3}{2\,d} = \frac{+\,8.4 \times 0.9999}{2 \times 4.1} = +\,1.02 \text{ psi}$$

Example 8-11 continued

Long-Term Thermal Effects

Since stiffness properties D_{m}, D_{mf}, and D_{v} are proportional to E_{f} and G_{c} respectively, and since the latter moduli both decrease by a factor of 2 for stresses of long duration, long-term reactions, moments, and stresses are one-half of the short-term values calculated above. These reduced values are reflected in the table below, for the long-term (thermal) loading condition.

7. Evaluate Stresses

Loading Condition	Element	Mode*	Wind Stresses: Load Factor	Wind Stresses: σ_L	Wind Stresses: F_{ur}	Thermal Stresses: Load Factor	Thermal Stresses: σ_T	Thermal Stresses: F_{ur}	Interaction: $\frac{\sigma_L \times LF}{F_{ur}} + \frac{\sigma_T \times LF}{F_{ur}}$
Wind (W)	Face	B		871	3510		—	—	0.42
	Face	R	1.7	1763	6600	—	—	—	0.45
	Core	R		3.8	10		—	—	0.65
Short-Term Thermal (TS)	Face	B		—	—		1229	3510	0.49
	Face	R	—	—	—	1.4	1489	6600	0.32
	Core	R		—	—		1.02	10	0.14
Long-Term Thermal (TL)	Face	B		—	—		615	1760	0.49
	Face	R	—	—	—	1.4	745	2200	0.47
	Core	R		—	—		0.50	3.3	0.21
Wind + Short-Term Thermal (W + TS)	Face	B		871	3510		1229	3510	0.91
	Face	R	1.7	1763	6600	1.4	1469	6600	0.77
	Core	R		3.8	10		1.02	10	0.79
Wind + Long-Term Thermal (W + TL)	Face	B		871	3510		615	1760	0.91
	Face	R	1.7	1763	6600	1.4	745	2200	0.93
	Core	R		3.8	10		0.50	3.3	0.86

* B = Ultimate strength controlled by buckling of compression face
R = Ultimate strength controlled by rupture of face or core

Example 8-11 continued

8. **Calculate Deflections** (Load Factor = 1.0) midspan between a & b

Maximum deflection is inward due to temperature gradient and wind load.

$$w = M\left[\frac{5a^2}{48D_m} + \frac{1}{D_v}\right] + \frac{(\epsilon_2 - \epsilon_1)\,a^2}{8d} + \frac{(M_{bL} + M_{bT})\,a^2}{16\,D_m} \qquad \text{Eqs. 8.35 \& 8.142}$$

$$M = 0.125\,qa^2 = 0.125 \times 0.21 \times 120^2 = 378 \text{ in.-lb/in.}$$

$$w = 378\left[\frac{5 \times 120^2}{48 \times 0.74 \times 10^6} + \frac{1}{3360}\right]$$

$$+ \frac{1.95 \times 10^{-3} \times 120^2}{8 \times 4.1} + \frac{(-360\ -504)\,120^2}{16 \times 0.74 \times 10^6}$$

$$= 0.88 + 0.86 - 1.05 = 0.69 \text{ in.} < 0.80 \text{ in. Max. OK}$$

Conclude: Panel meets wind and thermal stress criteria with 7% margin (i.e. maximum interaction = 0.93). The most severe loading condition is face wrinkling under wind load combined with long-term thermal stress.

A load factor of 1.7 is assigned to wind load, as is frequently used in building design. This factor accounts for inaccuracies in determining pressure distributions, uncertainties of gust magnitude, wind velocities which may exceed the design value, and inaccuracies in analysis. Most building codes allow a reduction in wind load when combined with other loads to an equivalent load factor of 1.33. This reduction is not taken here because, unlike most conventional building structures, wind is the principal loading on the panel.

A lower load factor of 1.4 is assigned to temperature effects, as is conventionally used in building design. This load factor reflects the probability that the design temperature is near the minimum value, and that significantly lower temperatures are improbable. As is the case of wind load, some building codes allow a reduction in temperature stress when combined with other load effects. This reduction is not taken here because temperature stress is also a primary loading for a panel in the arctic environment.

Capacity reduction factors (CRF) are assigned to account for mode and consequences of failure under the imposed loads, the possiblity of low strength material being present at a point of maximum stress, and similar uncertainties. A CRF of 0.6 (equivalent to a partial factor of safety of 1 / 0.6 = 1.7) is assigned to the FRP faces, since they are to be made by a reasonably well controlled process with good reproductibility and under adequate levels of quality control. A CRF of 0.4 (equivalent to a partial factor of safety of 1 / 0.4 = 2.5) is assigned to the shear strength of the foam, recognizing that this material is to be foamed in place and that orientation in cell structure and variations in density may produce significant variations in strength from the assumed ultimate values. A higher value of CRF of 0.6 is assigned to face wrinkling strength recognizing that modulus varies less then strength, and the chance of the face and core having lowest modulus values of the same point in the structure is remote.

2. **Materials Properties:** The short-term strength and elastic or viscoelastic moduli are reduced to account for long durations of stress and strain which may occur during the winter when the temperature differential is imposed for long periods. The reduction factors of 2 on modulus and 3 on strength are established

in consideration of R values shown in Table 2-2 and discussed in Chapter 3, stress rupture data as is shown in Figure 1-20 for fiberglass reinforced plastics, and HDB data on thermoplastics, as in Table 3-3. In the present state of the art in characterization of structural plastics behavior, these are judgment factors, since long-term effects on properties or specific formulations of polyurethane foam are essentially unknown. However, if the materials had been characterized as described in Tables 3-8 and 3-9, the level of confidence in this evaluation would be greatly improved. Furthermore, knowledge of strain limits would then be available to provide a rational design approach that would be more consistent with the criteria, based on time-dependent properties of plastics developed in Chapter 3.

3. **Design Strengths:** In some other parts of this Manual, a working stress approach has been used for simplicity of presentation. An ultimate strength design approach is used for this example because it represents the more advanced state of the art in practical design.

The reduced ultimate design strength in tension governs strength design at 6,600 psi, short-term, and 2,200 psi, long-term. This is compared later in the analysis to the maximum extreme fiber stresses in the faces.

As noted in Chapters 2 and 3, the flexural strength of unreinforced and reinforced plastics, obtained in standard tests, is usually greater than either the strength under uniaxial tension or compression. If "first damage" theory is accepted, first damage should occur at a strain which is independent of flexural tension or in-plane tension stress mode. Furthermore, flexural strength varies with thickness of the material and span-to-depth ratio (as does wood), whereas tensile strength is less sensitive to thickness. There are enough uncertainties about the variations in flexural strength with test sample geometry, to render the use of flexural strength obtained via standard test methods of questionable value. Thus, the lower value of tension or compression strength is used in this example as an indication of flexural strength as well. Of course, if full-scale prototype tests were conducted, this rationale could be modified to reflect the actual results. Possibly an approach, where the interaction between the higher flexural strength and the lower uniaxial strength are accounted for, is applicable. Such an approach is taken later in the analysis for the evaluation of combined short-term and long-term strength. Such interaction approaches need verification by test to provide a sound basis for such a rule.

The reduced ultimate face wrinkling compressive stress of 3,510 psi short-term and 1,760 psi long-term is lower than the reduced ultimate design strength in tension. However, the face-wrinkling strength is compared, later in the analysis, to the average compression stress in the face, not to the combined compression and bending stress that governs in strength evaluation. The compression stress resultant is used, because as discussed in Chapter 6, the buckling of a plate depends mostly on the in-plane compression stress, and is independent of the magnitude of flexural stress.

4. **Section Properties:** Determination of section properties includes the calculation of moment of inertia and section modulus of the faces, in addition to the overall stiffness and strength properties of the transformed section, in anticipation of the possibly significant effects of shear flexible cores as discussed in Section 8.6. The shear flexibility coefficient, θ, and values of, ϕ, are needed for this analysis.

5. **Stress Analysis for Wind Loads:** Maximum wind loads act only for brief periods, and hence, the analysis for wind considers only short-term behavior. The analysis for stresses and moments derived in Example 8-5, that accounts for the effects of shear deformation in the core is used to determine stress resultants and reactions.

6. **Stress Analysis for Thermal Loads:** Thermal loads near maximum are expected to be applied for long periods during winter. In this case, the effects of both the initial short-term thermal load, and the long-term (assumed indefinite) thermal loading must be considered.

The bending stresses arising from the temperature differential (1,489 psi) are somewhat higher than those due to wind load (1,248 psi). This demonstrates that thermal stress is a significant limit state for sandwich panels used in insulated buildings.

7. **Evaluation of Stresses:** The table given in this part of the example summarizes the various loading conditions considered in the analysis, and the load factor criteria set for the project. The stresses shown are the unfactored stresses resulting from design loads. The strengths shown are the reduced ultimate design strengths which were established in Step 3 of the calculations.

The combined effects of short-term wind and long-term thermal loads present a special problem in evaluation since the ultimate strength varies with load duration. An interaction approach is introduced herein. Interaction relationships are frequently used in conventional structural design in cases where different stress modes are governed by different strength criteria. In effect, if the following condition is met, the structure is assumed to meet the design criteria:

$$\frac{\text{maximum wind stress}}{\text{reduced short-term strength}} + \frac{\text{maximum thermal stress}}{\text{reduced long-term strength}} \leq 1$$

$$\frac{\sigma_S \, LF_1}{F_{uS}} + \frac{\sigma_L \times LF_2}{F_{uL}} \leq 1 \qquad \text{Eq. 8.143}$$

where F_{uS} = short-term ultimate strength
F_{uL} = long-term ultimate strength.

In this example, the above criterion is met. The highest combined stress (wind plus long-term thermal load, results in an interaction factor of 0.93, which is 7% below the safe value as predicted by this criterion.

In view of previous discussions (Retention of Short-Term Properties after Sustained Loadings, Section 2.8, and Examples 3-8 and 3-9, Section 3.4), the use of a limiting strain approach would permit an evaluation of behavior strength behavior under loads of mixed duration that reflects better the behavior of plastics. Implementation of this approach awaits the characterization of key structural properties for both face and core materials along the lines proposed in Tables 3-8 and 3-9.

REFERENCES

8.1 ANC-23 Bulletin, Sandwich Construction for Aircraft, Part II, Materials Properties and Design Criteria, U. S. Depts. of the Air Force, Navy, and Commerce, 2nd Edition, 1955.

8.2 Structural Sandwich Composites, MIL-HDBK-23A, U. S. Dept. Defense, Washington, D. C. 20025, 30 December 1968.

8.3 Allen, H. G., Analysis and Design of Structural Sandwich Panels, Pergamon Press, Oxford.

8.4 Hartsock, J. A., Design of Foam-Filled Structures, Technomic Publishing Co., Inc., Stamford, CT 06901, June 1968.

8.5 Plantema, F. J., Sandwich Construction, John Wiley & Sons Inc., New York, 1966.

8.6 Landrock, A. H., Polyurethane Foams. Technology, Properties and Applications, Plastics Technical Evaluation Center, Picatinny Arsenal, Dover, NJ 07801, January 1969.

8.7 Schwartz, R. T. and Rosato, D. V., "Structural Sandwich Construction," Composite Engineering Laminates, A. G. H. Dietz, Ed., The M. I. T. Press, Massachusetts Institute of Technology, Cambridge, MA, 1969.

8.8 Rshanizyn, A. R., Theory of Composite Structural Bars, Stroyis dat, U.S.S.R., 1948.

8.9 Recommendations for Design and Stress Analysis of Plastic Structures, Central Research Institute of Building Structures (ZNIISK), Moscow, 1969.

8.10 Column Research Committee of Japan, Handbook of Structural Stability, Corona, Tokyo, 1971.

8.11 Engineering Sciences Data Unit Ltd., Sandwich Panels, Aeronautical Series, Structures Sub-Series, Volume 3, London.

8.12 Hoff, N. J., "The Strength of Laminates and Sandwich Structural Elements," Chapter 1, Engineering Laminates, A. G. H. Dietz, Ed., John Wiley & Sons Inc., New York, NY, 1949.

8.13 Sandwich Panel Construction with Styrofoam Brand Plastic Foam, Dow Chemical U.S.A., Midland, Michigan, 1979.

8.14 Heger, F. J., "Thermal Gradient Deflections and Stresses in Structural Sandwich Insulating Panels," Proceedings of ASCE Cold Regions Specialty Conference, Anchorage, Alaska, May 1978.

8.15 Roark, R. J., Formulas for Stress and Strain, 4th Edition, McGraw-Hill Book Co., New York, NY, 1965.

ASCE Structural Plastics Design Manual

CHAPTER 9 – THIN RINGS AND SHELLS

By Frank J. Heger

TABLE OF CONTENTS

NOTATIONS - Chapter 9
(See Table 9-9 for notations used in equations for analysis and design of buried pipe in Section 9.14)

a	governing dimension in shell geometry, dimension of hypar edge along x axis
$\bar{a}$	cross sectional area of unit width cross section
a_θ, $a_{\theta n}$	section area per unit width in θ direction; above plane n, Fig. 9-4(d)
a_f	area of unit width of sandwich shell for transformed section with facings E
A, A_θ	cross sectional area, section area in circumferential direction
$\bar{A}_1$, $\bar{A}_2$	in-plane stiffness of shell in direction of principal radii of curvature, R_1 and R_2
$\bar{A}_x$, $\bar{A}_\theta$	in-plane stiffness of shell in x and θ directions
$\bar{A}_{x\theta}$	shear stiffness in x-θ plane
b, c	width and half depth cross section dimensions
b	governing dimension in shell geometry, radius of circle of revolution in torus; dimension of hypar edge along y axis
b_x	component of width in x direction
B	coefficient in stress concentration equation
c	governing dimension in shell geometry, rise of hypar in z direction
c_M, c_N c_V, c_w	coefficients for bending, thrust, shear, and radial deflection
c_r, c_s	coefficient for maximum radial and shear stresses
C	buckling coefficient
C_f, C_c	unit volume cost of facing and core materials in sandwich shell
C, C_0, C_1 C_x, C_y	coefficients
d	largest distance between ribs in spherical shell
D_1, D_2	flexural stiffness in directions of principal radii of curvatures, R_1 and R_2

D_r	flexural stiffness in radial direction
D_x, D_ϕ, D_θ	flexural stiffness in x, ϕ, and θ directions
$D'_{x\theta}$	twisting stiffness in x-θ plane
E	elastic modulus
E_b	elastic modulus of bottom plate in radial direction
E_t, E_s	tangent and secant moduli of elasticity
E_v	viscoelastic (time-dependent) modulus (Chapters 2 and 3)
E_{tv}, E_{sv}	viscoelastic (time-dependent) tangent and secant moduli
$E_{\theta v}$	long term viscoelastic modulus in circumferential direction
E_x, E_θ, E_ϕ	elastic modulus in x, θ (circumferential), and ϕ(meridional) directions
F	line load per unit length in parallel plate test of pipe
F_b, F_c	reaction forces at b and c
G	shear modulus
G_c	modulus of shearing rigidity of core of sandwich section
h	height of fluid
$H_{\phi k}$	horizontal edge load on spherical cap
i	section moment of inertia per unit width
i_θ, i_ϕ, i_x	section moment of inertia per unit width in circumferential, meridional, and x directions
i_f	section moment of inertia per unit width of sandwich shell having symmetrical transformed section based on facings modulus of elasticity, E_f
I, I_θ	moment of inertia of section, moment of inertia in circumferential direction
k_o, k_n, k_s	reduction (knockdown) factors for buckling coefficient
k_p	correction factor for effect of internal pressure on buckling coefficients
K_{ic}	correction factor for curvature

L	length of cylindrical shell
L_e	edge length that "lifts up" at bottom plate
L_s	length of uniform thickness shell between circumferential stiffeners
$\overline{LF}$	load factor
ℓ_b	wavelength of buckle
M	bending moment per unit width (stress resultant)
M_θ, M_ϕ	bending moment per unit width in circumferential and meridional directions
M_{ϕ_k}	bending moment at edge of spherical cap
M_b	bending moment at point b
M_o	bending moment at circumferential edge of cylindrical shell
M_x, M_y	bending moment in x and y directions
$M_{\phi\theta}$, $M_{\theta\phi}$	twisting moments per unit width on $\phi\theta$ and $\theta\phi$ sections
n_t, n_b	coefficients
N	axial force per unit width (stress resultant)
N_{sc}	critical buckling axial force in slant direction of cone
$N'_{s\theta c}$, $N'_{\theta c}$	pseudo-critical buckling shear force and circumferential force in a cone
N_x, N_y	axial force per unit width in x and y directions
N_{xy}	shear force per unit width in xy plane
N_θ, N_ϕ, N_r	axial forces per unit width in θ, ϕ, and r directions
$N_{\phi\theta}$, $N_{\theta\phi}$	shear forces per unit width in $\phi\theta$ plane
N_{xc}, $N_{\theta c}$, $N_{\phi c}$	critical buckling axial force in x, θ (circumferential), and ϕ(meridional) directions
N'_x, N'_{xc}	axial and critical buckling axial forces per unit width in x direction caused by overall bending of cylindrical shell (as a tubular beam)
$N_{\theta xc}$	critical buckling shear force in θx plane

N_1, N_2	axial stress resultants in principal directions 1 and 2
N_{1c}, N_{2c}	buckling axial stress resultants in directions with principal radii of curvatures, R_1 and R_2
p	pressure
p_e	uniform weight load on unit area
p_s	uniform load on unit area of horizontal projection
p_b, p_t	pressure in the bottom and in the top regions
p_x, p_y, p_z	pressure in directions x, y, and z
p_o, p_1	pressure at a designated point, o or 1.
p_w	pressure due to wind load
p_{cr}	critical buckling pressure
p_L	line load per unit length on edge perimeter
P	total load
P_c	concentrated load that locally buckles spherical shell
P_{cr}	overall total concentric load applied on upper and lower edges that buckles a cone
P_ϕ	total symmetrical load on shell of revolution above opening angle ϕ
$\overline{PS}_o$	short-term pipe stiffness
q	uniformly distributed lateral or internal pressure
q_b, q_o	pressure at tank bottom, top
q_f, q_r, q_t	fluid pressure, radial and tangential pressures
Q	transverse shear force per unit width (stress resultant), concentrated load
Q_b	transverse shear force at point b
Q_o	radial shear force per unit width on edge of shell
Q_x, Q_y	radial shear force per unit width on section perpendicular to x and y axis
Q_θ, Q_ϕ	radial shear force per unit width on sections perpendicular to circumferential and meridional directions
$\bar{Q}_{s1}, \bar{Q}_{sn}$	first moment of the area above (or below) centroidal plane 1-1 about axis in 1-1; above plane n-n about axis in 1-1.

R	mean radius
R_c	radius of cylinder
R_1, R_2	radius of top and bottom edges of cone; also principal radii of doubly curved shell in directions 1 and 2
$R_e, R_{e\theta}, R_{es}$	equivalent cylinder radius for buckling of cone under various types of load
R_k	knuckle radius
R_o	radius of bottom plate, radius at edge of spherical portion of torispherical head
R_o'	required radius of annular base ring
R_s	radius of sphere
s	slant distance from apex of cone
s_o	slant distance from apex to opening of cone
s, s_θ, s_x	section modulus per unit width in circumferential and longitudinal directions
S	section modulus
t	thickness of shell or pipe wall
t_b	thickness of bottom plate
t_c	thickness of sandwich core
t_e	effective thickness of ribbed or sandwich shell
t_f	thickness of sandwich facing
t_1, t_2	thickness of layers 1 and 2; time 1 and 2
T_1, T_2	temperatures on inside and outside of shell; temperature at time 1 or 2
T_{cr}	overall total torque applied at upper edge that buckles a cone
V_θ	transverse shear force per unit width (stress resultant) in a ring or curved beam
w	radial deflection
w_o	radial deflection at edge
w_b	radial deflection at b, bottom plate
w_{bm}	radial deflection at b due to membrane action

W	total load per unit width
α	angle; coefficient of thermal expansion
α_1, α_2	helix angle at layers 1 and 2
β	cylindrical shell constant; bedding angle
Δ	deviation from spherical radius
Δ_r	radial deviation from theoretical radius of shell
η	plasticity reduction factor for non-linear stress strain behavior
γ	density
λ	spherical shell constant; constant
λ_s	shell stiffening factor
ν	Poisson's ratio
ν_x, ν_θ	Poisson's ratio for stress in x and θ directions
ϕ	meridional angle
ϕ_o	meridional opening angle
ϕ_k	meridional angle from apex to edge
ψ	angle between direction of pressure and z axis; angle from edge of spherical shell
σ	normal stress
σ_b	bending stress, elastic beam theory
σ_{ic}	maximum bending stress on inside of curved ring
$\sigma_\phi, \sigma_\theta, \sigma_r$	normal stress in meridional (ϕ), circumferential, (θ), and radial (r), directions
σ_f	stress in filament
σ_x, σ_y	stress in x and y directions
σ_u	ultimate strength of material
σ_{fu}	ultimate strength in direction of filament
$\sigma_{xc}, \sigma_{\theta c}, \sigma_{\phi c}$	critical buckling stress in x, θ and ϕ directions

τ	shear stress
$\tau_{s\theta c}$	critical buckling shear stress in cone
τ_{xy}	shear stress in xy plane
τ_{xyc}	critical buckling shear stress in xy plane
τ_{θ}	shear stress on cross section normal to θ direction
θ	circumferential angle from origin to location of stress resultants
θ_b	rotation at point b, bottom edge
θ_{bb}	rotation at b due to a unit moment at b
θ_{bm}	rotation at b due to membrane effects
ω	angle between hypar x and y axes with skew coordinates
ρ	radius from axis of concentrated load or moment to point of stress resultant
ρ_m	radius of zone of significant bending moment caused by concentrated load or moment
ρ_T	radius of zone of significant thrust caused by concentrated load or moment
$\phi(\beta x)$, $\theta(\beta x)$, $\tau(\beta x)$, $\psi(\beta x)$	shell functions for long cylindrical shells
χ_1, χ_2, χ_3	shell functions for short cylindrical shells

CHAPTER 9 - THIN RINGS AND SHELLS

F.J. Heger

9.1 INTRODUCTION

Plastics and reinforced plastics may be molded to form curved ring and shell elements with ease. For applications such as pipe, liquid containers, pressure vessels, roof structures, and other structural components, shell configurations often provide an effective means of minimizing the quantity of material required for both enclosure and load transfer. In such applications, plastics may provide economical solutions to the problem of structural enclosure.

In addition to their easy adaptability to molding, plastics have many desirable properties, both structural and non-structural, which contribute to their effective use in curved components. See Chapters 1 to 4 for descriptions of those structural and non-structural characteristics that should be considered when choosing materials for ring and shell structures. The high unit materials cost of most plastics and reinforced plastics requires efficient design and demands economical fabrication techniques. Their use can often be justified by design for minimum weight of material in a form susceptible to economical fabrication. Ring and shell structures offer a means for attaining this efficiency. This is particularly the case in applications such as fluid storage vessels, pressure pipe, air ducts and buried pipe where the excellent corrosion resistance of plastics further enhances their cost effective performance as shell structures.

Methods and design aids are provided in this Chapter for analysis and design of pipes and other rings, shells of many configurations, curved panels and curved membranes that behave structurally as thin rings or shells, as defined later in this chapter. Design methods and design concepts which lead most directly to optimum structural design for plastics shell structures are emphasized.

Structural properties of plastics, along with their fabrication techniques, differ markedly from traditional structural materials; thus, as in the previous Chapters on plates, beams and axially stressed members, and sandwich structures, some new methods and new concepts that may be unfamiliar to engineers used to working with wood, metals, or reinforced concrete are required for effective design with the plastics and reinforced plastics family of structural materials. As discussed in Chapters 2, 3 and 4, plastics are frequently not ductile; hence, much greater accuracy of stress analysis is essential with these materials compared to most steel or reinforced concrete shell structures. Discontinuity stresses near edge supports are usually very important considerations in plastic shells. Also, the generally lower ratio of stiffness to strength with plastics, compared to metals, requires accurate consideration of stability in plastics shells subject to compression. Large size plastic shells often require stiffening by the use of ribs or sandwich construction in order to attain needed buckling resistance with reasonable quantities of plastics.

Plastics based composites are often used when plastics shell structures are of substantial size, or are subject to high loads. For many plastic composite shell components having conventional shapes, the stress and buckling analyses presented in this Chapter will provide sufficient accuracy for final design. In such analyses, materials properties are approximated by their average isotropic or orthotropic materials constants. These are usually based on test results for the entire laminate. as described in Section 3.5.

Advanced composites, comprised of layers of oriented fibers in a resin matrix are often used in aerospace and other transportation vehicle applications to reduce weight. Such laminates may be designed to optimize stiffness or strength as explained briefly in Section 4.9. Components fabricated from such layered materials are non-homogeneous anisotropic shells and require special refined theories for accurate analysis (9.1). These are not treated in this Chapter. Results in the form of simplified equations are not available, and lack of space precludes presentation in sufficient detail to meet the objectives of this Design Manual. However, the analyses described in this Chapter may be useful for developing the preliminary design of the these types of components. More accurate computer aided analyses can then be performed using approaches and programs such as those described in Section 4.9.

9.2 ANALYSIS AND DESIGN OF THIN RINGS

Rings may be circular or other continuous curved shapes. They may be narrow or wide, but their essential characteristic that distinguishes them from cylindrical shells is their two-dimensional behavior under load. A ring is essentially a plane frame. When transverse diaphragms or ribs are provided at one or more points along the longitudinal axis of a wide ring, applied loads are transferred in three-dimensions and the structure is termed a cylindrical shell. A ring differs from a shell in the same way that a beam differs from a plate.

Pipe are often analyzed as very wide rings, although restraints at joints and connection points may cause three-dimensional transfer of applied load in the vicinity of these points. This behavior produces "discontinuity" longitudinal bending stresses near the connections. These are determined by the cylindrical shell edge bending analyses described in Section 9.7.

Curved two-dimensional members that do not form a closed ring are often termed arches or curved beams, depending on the edge support conditions. Arches are treated extensively in reference texts on indeterminate stress analysis (9.2). They are not included in the scope of this Chapter.

Rings Under Direct Stress

Rings provide great structural efficiency in resisting those distributed loads whose funicular line (Section 4.4 and Fig. 4-1) coincides with the ring centroid. An example is uniform internal or external pressure on a circular pipe (Fig. 9-1a). Without longtitudinal discontinuities, the applied uniform pressure causes only circumferential thrust (hoop) forces in the pipe ring as follows:

$$N_{\theta} = p R \qquad \text{Eq. 9.1}$$

$$\sigma_{\theta} = \frac{p R}{a_{\theta}} \qquad \text{Eq. 9.2}$$

For a ring of uniform thickness:

$$\sigma_{\theta} = \frac{p R}{t} \qquad \text{Eq. 9.3}$$

Radial deflection is:

$$w = \frac{N_\theta R}{E_\theta a_\theta} \qquad \text{Eq. 9.4}$$

For a wide ring of uniform thickness:

$$w = \frac{N_\theta R}{E_\theta t} = \frac{\sigma_\theta R}{E_\theta} \qquad \text{Eq. 9.5}$$

Rings Under Bending

Any other load distribution on a circular ring produces bending, axial and shear stress resultants. Conventional relationships between these stress resultants for straight members are modified by the curvature or rings. Equations relating bending, axial and shear stress resultants in curved members are given below. Sign convention is shown in Fig. 9-1. For rings subject to common load distributions, these stress resultants may be determined using the moment, thrust and shear coefficients for particular points in a loaded ring structure given with the following equations:

$$M_\theta = M_{\theta o} - \int_o^\theta V_\theta R \, d\theta = c_M W R \qquad \text{Eq. 9.6a}$$

$$N_\theta = N_{\theta o} - \int_o^\theta (V_\theta + q_t r) \, d\theta = c_N W \qquad \text{Eq. 9.6b}$$

$$V_\theta = V_{\theta o} + \int_o^\theta (N_\theta - q_r R) \, d\theta = c_V W \qquad \text{Eq. 9.6c}$$

The coefficients c_M, c_N, and c_V are determined for any particular load and support arrangements by an indeterminate structural analysis of the ring as a plane frame. For many common loading and support arrangements, they may be found in handbooks such as (9.3). These are applicable only for thin rings as defined later in this Section.

Six common loading and support arrangements for circular rings are shown in Fig. 9-1. The constant circumferential thrust for the uniform pressure case (a) is given by Eq. 9.1. Plots of the moment, shear and thrust coefficients in Eqs. 9.6 are given in Fig. 9-2 for loading cases (b), (c), (d) and (e) of Fig. 9-1, and in Fig. 9-3 for case (f) of Fig. 9-1, using several different values of the bedding angle, β (9.4). The sign convention used is shown in both Figures.

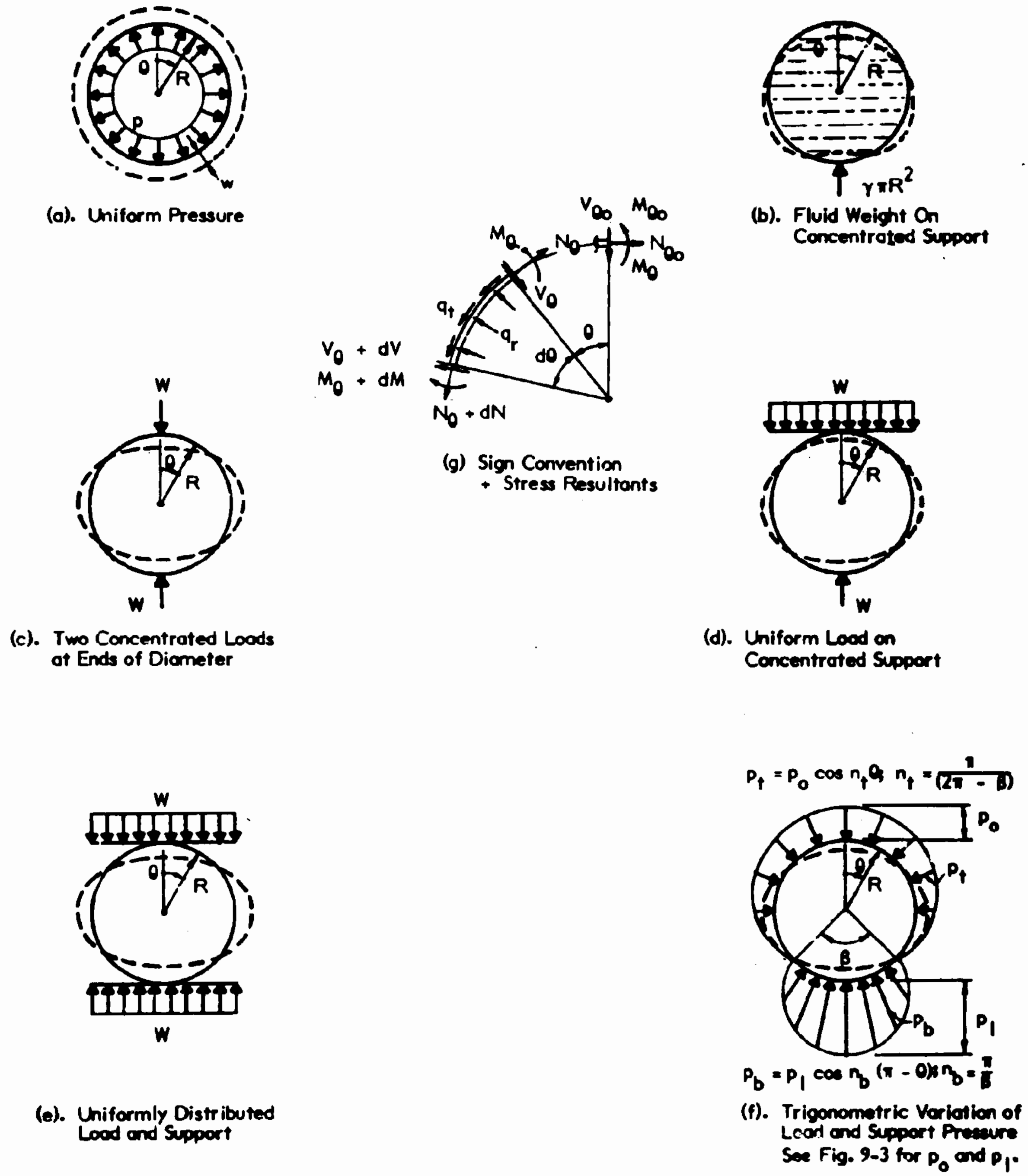

(a). Uniform Pressure

(b). Fluid Weight On Concentrated Support

(g) Sign Convention + Stress Resultants

(c). Two Concentrated Loads at Ends of Diameter

(d). Uniform Load on Concentrated Support

(e). Uniformly Distributed Load and Support

(f). Trigonometric Variation of Load and Support Pressure See Fig. 9-3 for p_o and p_1.

Fig. 9-1 SIX COMMON LOADING AND SUPPORT ARRANGEMENTS FOR CIRCULAR RINGS

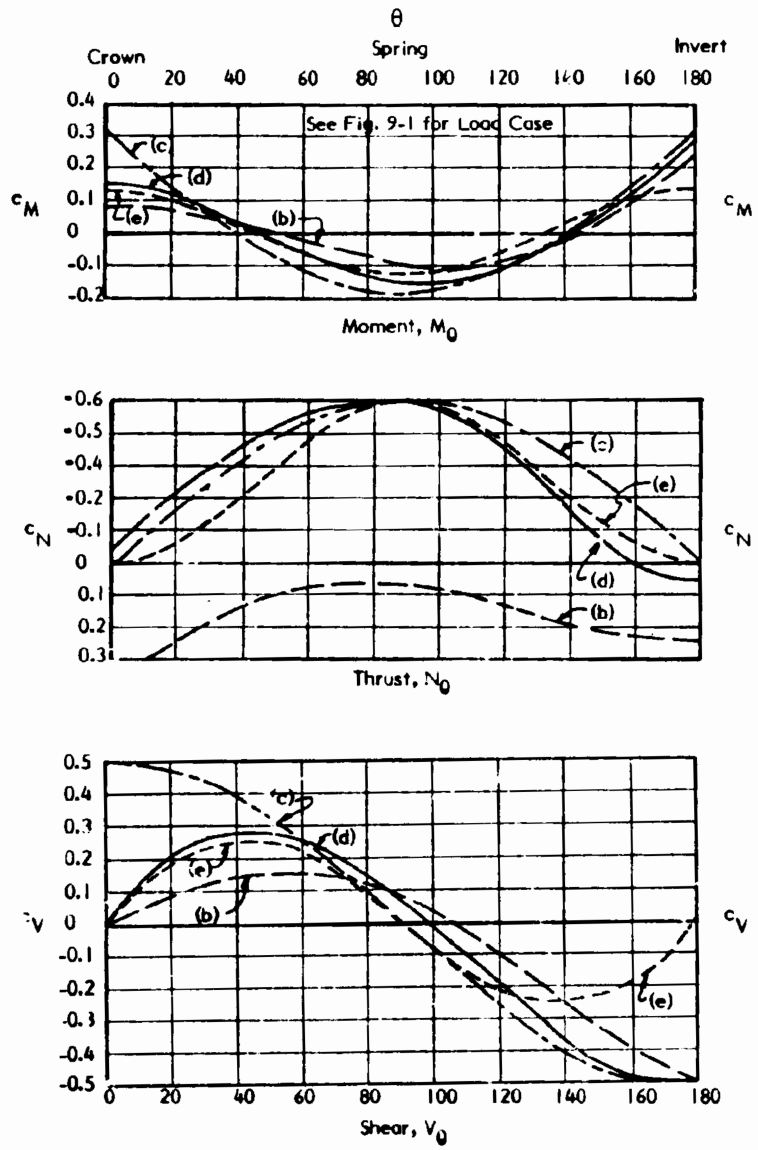

Note: See Fig. 9-1 for Load Cases (b), (c), (d) & (e)

Fig. 9-2 COEFFICIENTS FOR MOMENTS, THRUSTS AND SHEARS FOR A THIN RING SUBJECT TO VARIOUS LOAD DISTRIBUTIONS

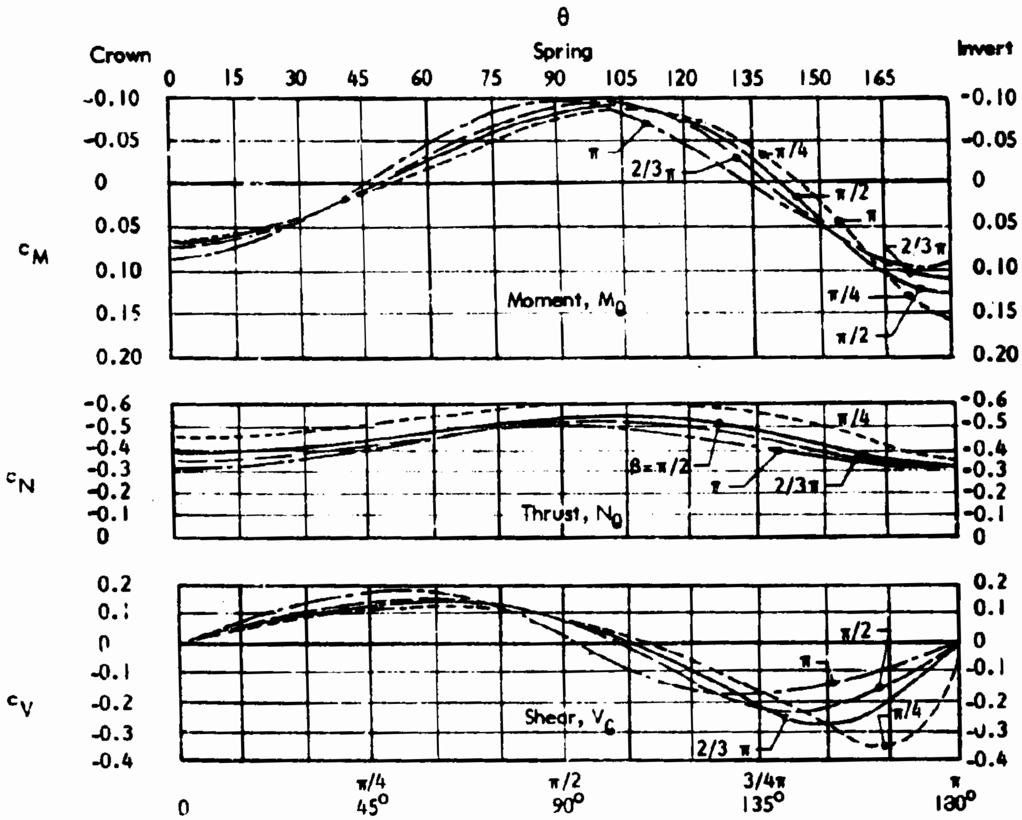

$p_o = W/C_oR$

$p_I = W/C_IR$

β	C_o	C_I
π/4	1.57	0.49
π/2	1.70	0.94
2/3π	1.71	1.20
π	1.57	1.57

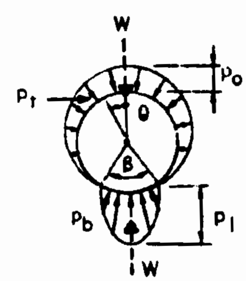

Loading Case f,
Fig. 9-1

$p_t = p_o \cos n_t\, \theta$

$n_t = \pi/(2\pi - \beta)$

$p_b = p_I \cos n_b\, (\pi - \theta)$

$n_b = \pi/\beta$

Fig. 9-3 COEFFICIENTS FOR MOMENTS, THRUSTS, AND SHEARS, FOR THIN RING SUBJECT TO TRIGONOMETRIC DISTRIBUTION OF LOADING AND SUPPORT PRESSURES (9.4)

The moment, shear and circumferential thrust stress resultants produce normal (bending and axial), transverse and interlaminar shear and radial stresses on the ring cross section as shown in Fig. 9-4. In a curved bar subject to bending, stresses will be higher on the inside edge and lower on the outside edge than stresses determined using conventional elastic bending theory, as derived from an assumption of linear strain variation across the section. This increase in maximum stress because of curvature may be neglected for rings of moderate to low curvature, say with $R \geq 5t$ to $10t$, depending on the accuracy desired. The moment, thrust, and shear values obtained with the coefficients given in Figs. 9-2 and 9-3 are all obtained from "thin ring" analyses that neglect the non-linear variation of stress on a curved cross-section.

An estimate of the maximum bending stress on the inside of a curved member may be obtained by multiplying stresses on the inside surface determined using conventional elastic beam theory, σ_b, by a correction factor for curvature, K_{ic}, as follows:

$$\sigma_{ic} = K_{ic}\,\sigma_b \qquad \text{Eq. 9.7}$$

See Fig. 9-4 (c) for a graphic presentation of these notations and stresses. For rectangular sections, the correction factor, K_{ic}, is calculated using Eq. 9.8 (9.5):

$$K_{ic} = 1.0 + \frac{t}{6}\left[\frac{1}{(R - .5t)} + \frac{1}{R}\right] \qquad \text{Eq. 9.8}$$

For other shape cross sections, such as **I**, hollow rectangular, circular or elliptical, reasonably accurate correction factors are given by (9.5):

$$K_{ic} = 1.0 + B\left(\frac{I}{bc^2}\right)\left[\frac{1}{(R - c)} + \frac{1}{R}\right] \qquad \text{Eq. 9.9}$$

B is 0.5 for **I** or hollow rectangular sections and 1.05 for circular or elliptical cross sections. See Fig. 9-4 (c) for the other symbols.

A pipe bend is an example of a curved member with a hollow circular cross section. These are actually toroidal (donut shaped) shells. Such shells are treated in Section 9.5.

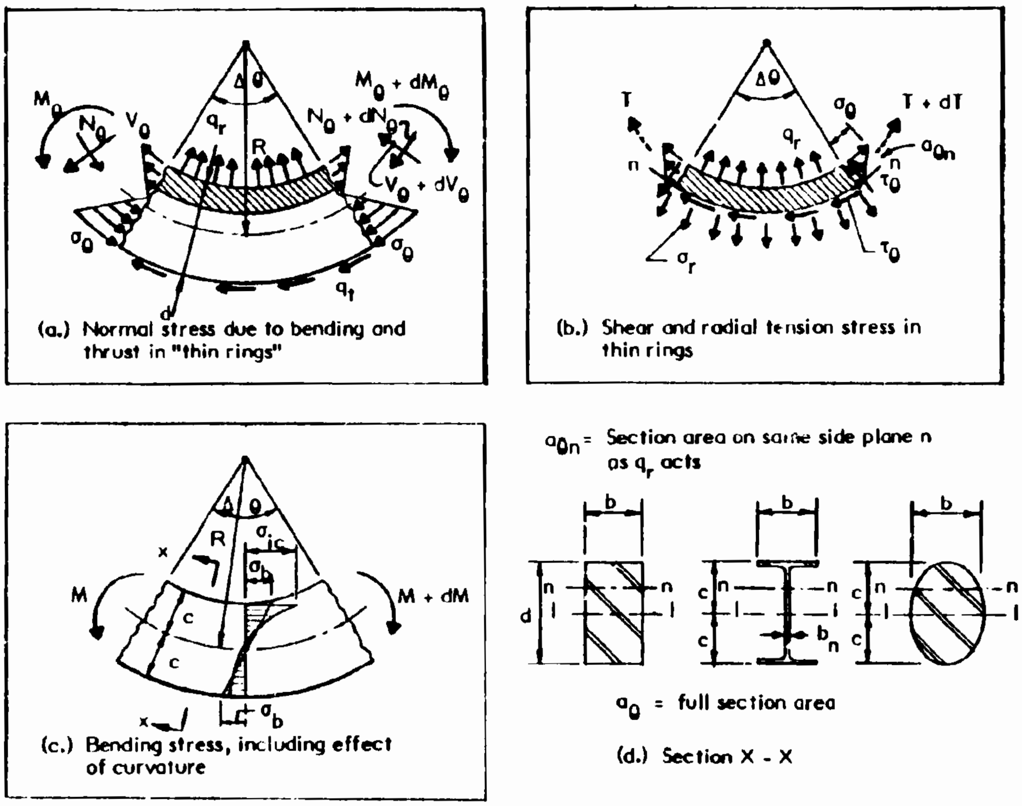

Fig. 9-4 NORMAL, SHEAR AND RADIAL STRESSES ON RING CROSS SECTION

Eq. 9.8 shows that for rectangular sections, maximum bending stresses determined using conventional beam theory are about 7.0% too low at R/t = 5, and 3.4% too low at R/t = 10. In the following discussion, rings are termed "thin rings" when the increased maximum stresses resulting from the geometry of the curvature are considered negligible for design.

For thin rings, the maximum stresses at a given cross section are:

maximum circumferential normal stress: $$\sigma_\theta = \frac{N_\theta}{a_\theta} \pm \frac{M_\theta}{s_\theta} \qquad \text{Eq. 9.10}$$

maximum shear stress (with $q_t = 0$): $$\tau_\theta = c_s \frac{V_\theta}{a_\theta} \qquad \text{Eq. 9.11}$$

maximum radial normal stress (with $q_r = 0$): $$\sigma_r = c_r \frac{M_\theta}{a_w R} \qquad \text{Eq. 9.12}$$

The coefficients, c_s and c_r, depend on the shape of cross section. For maximum shear stress, c_s is obtain by applying Eq. 5.30 at the neutral plane, giving c_s = $(\bar{Q}_{sl}\, a_\theta)/(b_n\, I_\theta)$. It may be shown that when q_r = 0, σ_r has the same variation as τ_θ, giving $c_r = c_s$. In this case:

For a rectangular section: $c_s = c_r = 1.5$.

For an I section with a thin web and a_θ = area of web: $c_s = c_r = 1.0$

When $q_r \neq 0$, the radial stress produced by q_r, $\sigma_{rq} = q_r b/b_n\,(1 - a_{\theta n}/a_\theta)$ must be added to the radial stress produced by the bending moment, as given by Eq. 9.12 (except determine c_r using $\bar{Q}_{sn}$ for the plane n of maximum combined radial stress, rather than for the neutral plane). See Fig. 9-4(d) for b_n, a_n and a_θ for several section shapes. The same reasoning applies to shear stress when $q_t \neq 0$. The part of the N_θ thrusts that are not associated with q_r do ot produce radial normal stresses, since they result from a change in shear stress resultant with angular position (see Eq. 9.6b), and their radial components equilibrate shear stress variations with angular position.

Radial stresses produce distortion of the cross section of thin tubular curved beams. This reduces both the strength and the stiffness of the tubular section. See (9.3) for correction factors that account for this distortion in curved members whose curvature is not excessively sharp (thin rings).

When rings are subject to significant bending moments, bending deflections are usually much greater than deflections resulting from axial or shear stress resultants. These latter deflections are generally neglected in practical calculations and maximum bending deflections are determined from:

$$w = \frac{c_w\, P\, R^3}{E_\theta\, I_\theta} \qquad \text{Eq. 9.13}$$

For a ring of unit width, subject to a load, W, per unit width:

$$w = \frac{c_w\, W R^3}{E_\theta\, i_\theta} \qquad \text{Eq. 9.13a}$$

For long tubes (wide rings), restraint of deformation transverse to the ring stiffens the ring somewhat, as explained in Chapter 6. Thus, $E_\theta\, i_\theta$ should be replaced with D_θ, where D_θ is given in Table 6-1, and:

$$w = c_w \frac{WR^3}{D_\theta} \qquad \text{Eq. 9.13b}$$

Values for the coefficient c_w for various common loading cases are given in handbooks such as (9.3). Values of c_w for vertical and horizontal diametral changes are given below for the load cases shown in Fig. 9-1:

Coefficients for Deflection of Rings for Loading Cases in Fig. 9-1

Load Case Fig. 9-1		Change in Diameter Vertical c_w	Change in Diameter Horizontal c_w
b		-0.074	0.068
c		-0.149	0.137
d		-0.116	0.110
e		-0.083	0.083
f	$\beta = \pi/4, \pi/2, 2\pi/3, \pi$	-0.060	0.030

Buckling

When rings are subject to significant axial compression under uniform or non-uniform loads, their structural capacity may be limited by their resistance to buckling. The maximum circumferential compressive force (ring thrust), as limited by buckling, is usually taken as the buckling resistance of a circular ring subject to uniform external pressure. This is:

$$N_{\theta c} = \frac{3 E_\theta i_\theta}{R^2} \qquad \text{Eq. 9.14}$$

The critical external pressure that buckles the ring is:

$$p_{cr} = \frac{3 E_\theta i_\theta}{R^3} \qquad \text{Eq. 9.15}$$

For a long tube of uniform wall thickness:

$$p_{cr} = \frac{E_\theta \; t^3}{4(1 - \nu_\theta \nu_x) R^3} \qquad \text{Eq. 9.16}$$

The critical circumferential stress that buckles the ring or tube is:

$$\sigma_{\theta c} = \frac{E_\theta \; t^2}{4(1 - \nu_\theta \nu_x) R^2} \qquad \text{Eq. 9.17}$$

The buckled configuration of the ring is shown in Fig. 9-5.

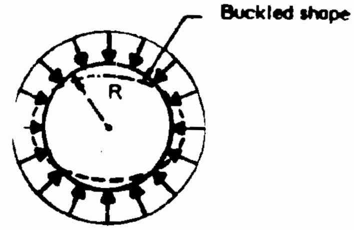

Fig. 9-5 BUCKLED CONFIGURATION OF RING SUBJECT TO UNIFORM EXTERNAL PRESSURE

Example 9-1 illustrates the use of the equations for rings subject to uniform pressure to determine the required wall thickness of a plastic pressure pipe. The maximum external pressure that causes buckling is also calculated. **Example 9-2** illustrates the use of the equations and coefficients for non-uniform load to obtain an approximate evaluation of the stresses and deflections expected in a parallel plate test of a plastic pipe.

Buried plastic pipe behaves as thin flexible rings that are both loaded and restrained by their embedment soil. These require special design approaches that rely on soil-structure interaction for control of pipe deflection. A brief explanation of the principal considerations for analysis and design of buried plastic pipe systems is presented in Section 9.14 at the end of this Chapter.

Curved components that support loads by three dimensional systems of internal stress resultants are termed shells. These are treated in the sections that follows.

9.3 SHELL GEOMETRY

Typical configurations for plastics shells were discussed in Chapter 4, Section 4.4. These generally may be classified as "cylindrical" (i.e., shells with a finite radius of curvature in only one principal direction, such as cylinders), "doubly curved with positive Gaussian curvature" (i.e., shells having radii of curvature with the same sign in each of the two principal directions, such as domes), and "doubly curved with negative Gaussian curvature" (i.e., shells having radii of curvatue with opposite signs in the two principal directions such as saddle shells). See Figs. 4-1 to 4-3 for illustrations of the above types of shells.

Shapes and equations for surface geometry of cylindrical shells and doubly curved shells of positive Gaussian curvature are given in Fig. 9-6. Doubly curved shapes include the sphere, its generalized counterpart - the ellipsoid, cones with either elliptic or circular sections, and the elliptic paraboloid. The surfaces shown in Fig. 9-6 (a), (b), (c) with $a = c$, (d) with $a = b$ and (f) with $a = b$ are surfaces of revolution, formed by revolving a straight or curved line about an axis. The surfaces shown in these figues are also translational surfaces, formed by translating a straight or curved line along another straight or curved line. The surface shown in (e) is another translational surface, formed by translating one parabola over another parabola. This surface is useful for covering areas with rectangular plans, using arches supporting each edge, as explained in more detail in Section 9.6. It is also useful for approximating portions of other surfaces covering rectangular plans such as a spherical surface.

Example 9-1: Determine the minimum wall thickness for a 12 in. diameter PVC water main (AWWA C900). Pipe is buried with shallow cover in an area where surface traffic is not anticipated. Internal pressure is 130 psi, including a 30 psi occasional surge. Also calculate adequacy against buckling with full vacuum applied briefly inside the line.*

1. Pipe Properties at Temperature of 73°F (Ref. AWWA C900)

   Outside Diameter: $2R_o = 13.2$ in; $R_o = 6.6$ in.

   Modulus of Elasticity: $E = 400{,}000$ psi (short term)

   Poissons Ratio: $\nu = 0.38$

   Hydrostatic Design Basis: HDB = 4,000 psi

2. Determine pipe wall thickness providing safety factor of 2.5. Assume that the pipe is a thin ring and that load effects due to burial are negligible.

$$t = \frac{pR}{\sigma_0} = \frac{p\left(\frac{2R_o - t}{2}\right)}{\frac{HDB}{SF}} = \frac{130\left(\frac{13.2 - t}{2}\right)}{\frac{4000}{2.5}} = 0.515 \text{ in.}$$

   Use AWWA C900 Class 100 PVC pipe with minimum $t = 0.528$ in.

3. Determine buckling resistance

$$R = \frac{13.20 - 0.528}{2} = 6.336 \text{ in.}$$

$$p_{cr} = \frac{E_0 t^3}{4(1 - \nu^2)R^3} = \frac{400{,}000 \times 0.528^3}{4(1 - 0.38^2)\,6.336^3} = 67.6 \text{ psi}$$

   Factor of safety against buckling under brief vacuum in line

$$SF = \frac{67.6}{14.7} = 4.6$$

Note: 1 psi = 0.0069 MPa, 1 in. = 25.9 mm, °C = (°F - 32) 5/9

* Design loads, design criteria (such as safety factors, load factors and capacity reduction factors, etc.), and materials properties used in design examples are for illustrative purposes only. The user of this Manual is cautioned to develop his own loads, criteria and materials properties based on the requirements and conditions of his specific design project.

Example 9-2: Determine the force per lineal inch required to achieve the 5% deflection requirement in the parallel plate loading test for stiffness of plastic pipe (ASTM D2412). (For arrangement, see Fig. 9-1c). Analyze 12 in. diameter PVC pipe (AWWA C900). Determine pipe stiffness and maximum bending stress in the pipe wall at 5% deflection.*

1. Pipe properties (See Example 9-1)

2. Deflection - 5% of mean diameter: $w = 0.05\,(2 \times 6.336) = 0.634$ in.

3. Find load to develop 5% deflection. Use short term viscoelastic modulus since test lasts a few minutes. Use Eq. 9.13b because ASTM D2412 requires a moderately wide ring (i.e., 6 in. length on 12 in. diameter and 0.515 in. wall). Neglect effects of increase in span of ring caused by increase in diameter, since such effects are small at 5% deflection.

$$W = \frac{D_0\, w}{c_w R^3} = \frac{E_0\, i_0\, w}{(1 - \nu^2)\, c_w R^3} \qquad \text{(Eq. 9.13b, rearranged)}$$

$$i_0 = \frac{t^3}{12} = \frac{0.528^3}{12} = 0.0123 \ \text{in}^3/\text{in.}$$

$c_w = 0.149$ (see table following Eq. 9.13b for case c, Fig. 9-1.)

$$W = \frac{400{,}000 \times 0.0123 \times 0.634}{(1 - 0.38^2)\, 0.149 \times 6.336^3} = 96.2 \ \text{lb/in.}$$

4. Short-term pipe stiffness, PS_o, is W/w ($W/w = F/\Delta y$, the latter being ASTM D2412 notation).

$$PS_o = \frac{W}{w} = \frac{96.2}{0.634} = 152 \ \text{psi}$$

Note that the D2412 calculation is based on the mean inside diameter or radius, rather than the mean radius of the wall as in Eq. 9.17.

5. Maximum short-term bending stress at 5% deflection

$M_0 = c_M WR$; $c_M = 0.32$ maximum at crown and invert (Fig. 9-2)

$M_0 = 0.32 \times 96.2 \times 6.336 = 195.0$ in-lb/in.; $N_0 = 0$ at crown and invert, by symmetry

$$\sigma_0 = \frac{N_0}{a_0} \pm \frac{M_0}{S_0} \quad \text{(Eq. 9.10)}$$

$$s_0 = \frac{i_0}{\frac{t}{2}} = \frac{0.0123}{\frac{0.528}{2}} = 0.0466 \ \text{in}^3/\text{in.}$$

$\sigma_0 = \pm \dfrac{195.0}{0.0466} = \pm 4185$ psi; Maximum bending stress at 5% deflection is $\pm$ 4185 psi

---

Note: 1 in. = 25.4 mm, 1 in.^{3}/in. = 645 mm^3/mm, 1 in.^{4}/in. = 16,387 mm^4/mm, 1 lb/in. = 175 N/m, 1 in.-lb/in. = 4.45 N-m/m, 1 psi = 0.0069 MPa.

* See footnote, Example 9-1, Page 9-13.

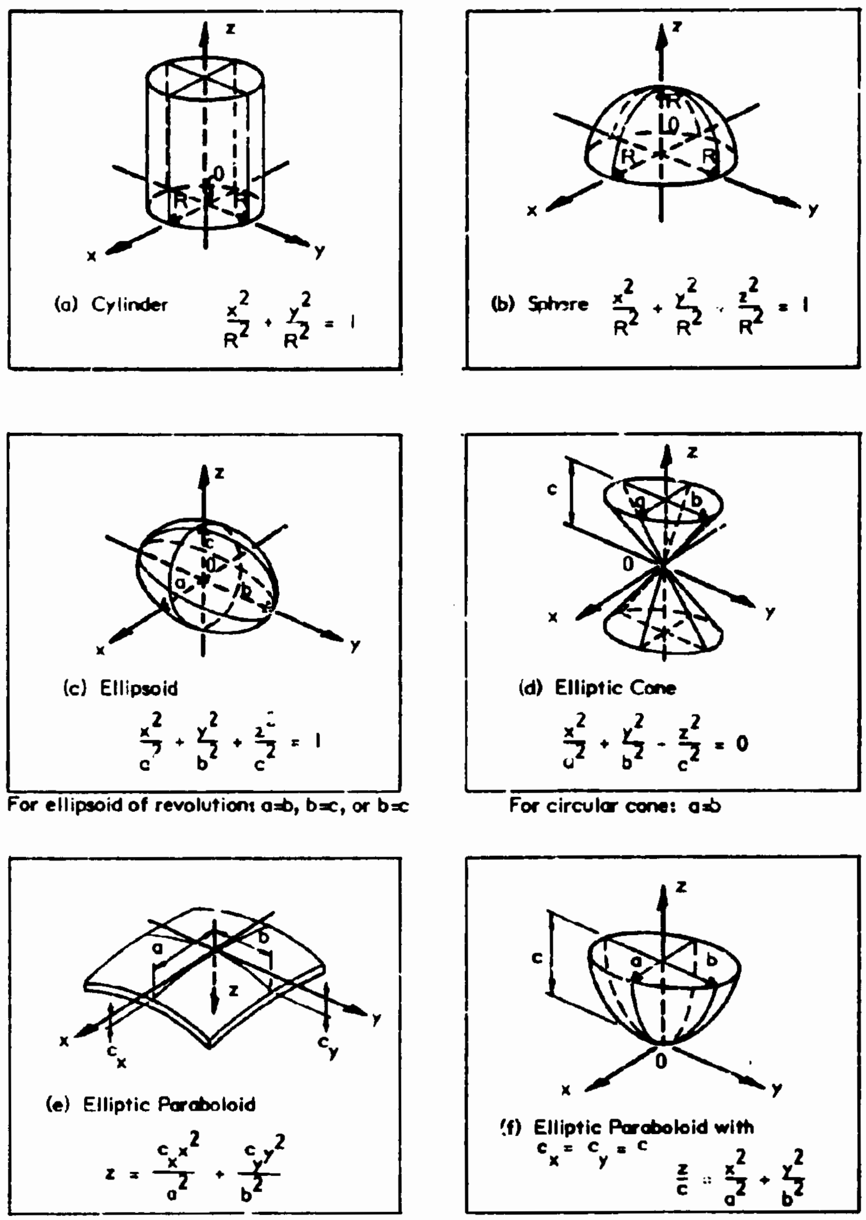

Fig. 9-6 GEOMETRY OF CYLINDRICAL SHELLS AND SHELLS OF POSITIVE GAUSSIAN CURVATURE

Shapes and equations of geometry for doubly curved shells of negative Gaussian curvature are given in Fig. 9-7. The most common such surface is the hyperbolic paraboloid shown in (a) and (b), and designated by shortened terminology as a "hypar." If reference axes x and y intersect at an angle ω less than 90°, as shown in (b), the resulting surface is termed a "skew hypar." The case of $\omega = 90^\circ$ is then termed a "right hypar." If the two edges in the x-y plane, a and b, are equal, the hypars are termed "equilateral."

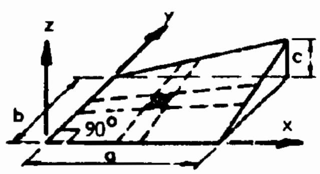

(a.) Right Hypar, Rectangular Axes, x & y:

$$z = \frac{c}{ab}xy$$

For Equalateral Right Hypar, a = b

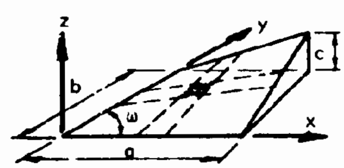

(b.) Skew Hypar, Skew Axes, x & y:

$$z = \frac{c}{ab}xy$$

For Equalateral Skew Hypar, a = b

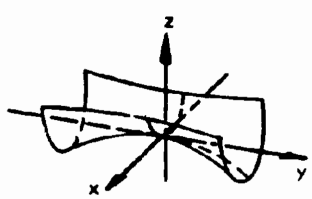

(c.) Right Hypar, Alternate Orientation of Axes Along Curved Diagonal

$$\frac{x^2}{a^2} - \frac{y^2}{b^2} = \frac{2z}{c}$$

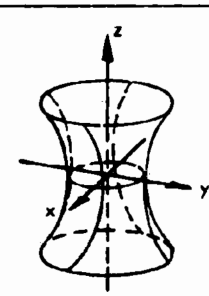

(d.) One-Sheeted Hyperboloid

$$\frac{x^2}{a^2} + \frac{y^2}{b^2} - \frac{z^2}{c^2} = 1$$

Fig. 9-7 GEOMETRY OF SHELLS OF NEGATIVE GAUSSIAN CURVATURE

Hypars are translational surfaces, formed by translating a straight line over two generator straight lines, as shown in Fig. 9-7. When the x and y axes are rotated into the directions of principal curvature, the hypar surfaces has the form of a saddle, as shown in (c). A surface of revolution having negative curvature is formed when a parabola is rotated about a central axis, as shown in (d), to form a hyperboloid of one sheet.

A torus, or donut-shaped surface, shown in Fig. 9-8a, is a doubly curved surface having positive curvature over the portion outside the radius, b, and negative curvature over the portion inside b. This shape is widely used for pipe bends, and portions of it are used for fillets at the base of cylindrical vessels with cylinder axis oriented vertically, and for junctions between cylindrical walls and spherical heads of pressure vessels. The latter type is shown in sketch b in the Figure.

As stated earlier for rings, the shells treated in this Chapter are all classed as "thin". This requires that the smallest radius be greater than about 10 times the shell thickness (9.3). Such limits are imposed so that the underlying assumptions of the stress-strain relationships in the bending and membrane theories used for the equations presented in this Chapter will be valid.

9.4 STRESS ANALYSIS OF SHELLS

Very often, simple closed form elastic formulas for stresses and deformations provide analyses of sufficient accuracy for commonly occuring shell components, such as cylindrical tanks, spherical roofs and hypar roof components subject to axisymmetric loads. Other somewhat more complex cases involving closed form solutions of differential equations have been solved in non-dimensional form and results presented in tables of shell coefficients (9.6). Still more complex shell geometries, edge restraints or loadings, which cannot be represented by mathematical functions having closed form solutions, can be analyzed using finite element computer analyses. The general approach to such problems was discussed in Chapter 4, Section 4.9. Some of the available programs were referenced in that Section.

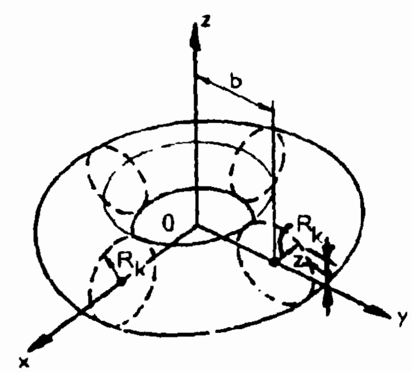

$$\frac{x^2}{\left[b \pm (R_k^2 - z^2)^{1/2}\right]^2} + \frac{y^2}{\left[b \pm (R_k^2 - z^2)^{1/2}\right]^2} = 1$$

(a) Torus

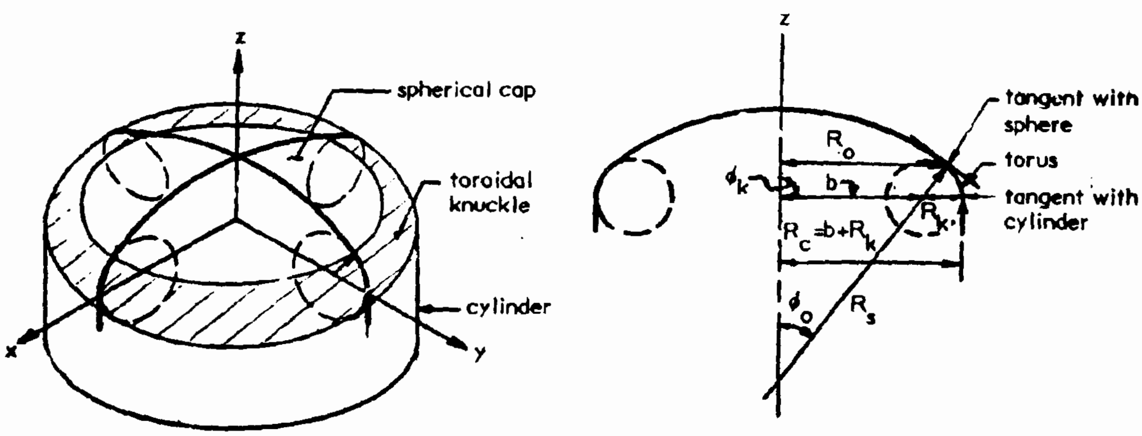

(b) Torispherical closure for end of cylinder

Fig. 9-8 GEOMETRY OF TORUS, A SHELL WITH BOTH POSITIVE AND NEGATIVE GAUSSIAN CURVATURE

Accurate Analysis for General Shells

An accurate analysis of a shell having almost any shape, subject to almost any condition of edge restraint, and comprised of almost any type of elastic or viscoelastic material is within the present state-of-the art in finite element analysis. However, the analysis may become extremely complex and expensive when non-linear analysis is required for those special types of shells whose:

- deformations result in signifiant changes in geometry,
- elastic properties change with stress level, and/or duration of load,
- restraint conditions change with stress level and duration of load, requiring non-linear analysis.

The analysis may also become complex when materials properties are "generally anisotropic" and/or layered, requiring consideration of non-symmetric elasticity.

When non-linear analyses are required for shells that are sensitive to changes in local geometry (such as analyses for buckling), curved finite elements may be required, further adding to the complexity of the solution.

General — Shell Bending Analysis

Consider first the general case where stress resultants are to be determined in a singly or doubly curved thin shell subject to an applied load. Eight unknown stress resultants exist at a point on the shell (Fig. 9-9) while only six equilibrium equations are available. Consequently, the general problem of shell analysis is indeterminate and can be solved accurately only by inclusion of deformation compatability relations in addition to equilibrium equations. While it is not difficult to set up the differential equations of equilibrium and deformation for general bending shell behavior, solutions of the equations often either are not available or are too complex for practical application.

Simplifications in Analysis

Shell analysis can be simplified greatly for many doubly curved shell structures that are subject to loads distributed over their surfaces without abrupt discontinuities, because in such shells, bending, twisting and radial shear stress resultants are relatively unimportant compared to axial and tangential shear stress resultants. If bending, twisting, and radial shear stress resultants are assumed to be zero, only three unknown stress resultants exist at any point on a shell surface. These stresses are termed the "membrane stresses" because the assumption of zero bending means that the shell is acting as a pure membrane, subjected only to tension, compression, and in-plane (tangential) shear stresses.

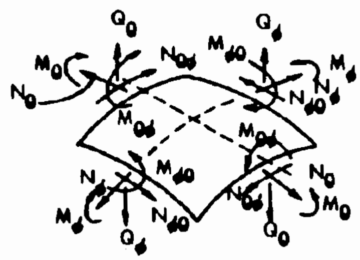

For thin shells:

$M_{\phi\theta} = M_{\theta\phi}$

$N_{\phi\theta} = N_{\theta\phi}$

Fig. 9-9 INTERNAL STRESS RESULTANTS AT A POINT IN A SHELL

The membrane stress problem is statically determinate within the shell because three equations of equilibrium are available for every point in the surface; however, for a complete membrane solution, edge support forces and deformations must be provided which exactly meet the membrane solution requirements. Practically, these support requirements may not be satisfied; in such cases, bending stresses will exist in the vicinity of supports. Fortunately, these edge bending effects usually damp out rapidly, so that approximate bending solutions for the portions of the shell near the edge supports often are sufficient for determining the significant shell bending stresses.

The approach usually taken in the simplified shell analysis is as follows:

- Assume membrane solution is valid, and calculate membrane stresses at appropriate points in the shell. Details of this analysis are presented in Section 9.6.
- Determine edge reactions and deformations required in the membrane analysis.

- If the actual shell boundary conditions cannot provide the thrust and in-plane shear reactions, nor the edge displacements and rotations required for compatibility with membrane stress conditions (the usual case), apply additional edge forces that, when added to the membrane reactions, result in support reactions, deflections and rotations compatible with the actual boundary conditions of shell. These additional edge forces produce significant bending and in-plane stress resultants in the edge regions of the shell, and the analysis to determine these stress resultants and the associated edge deformations is termed the "edge bending analysis" or "discontinuity stress analysis". Details of this analysis are presented in Section 9.7.

- The final stresses in the edge region are determined by superimposing the membrane stresses and the edge bending stresses.

The simplified shell analyses presented in the remainder of this chapter cover the following common shell types: cylindrical shells, shells of revolution, and translational shells.

Cylindrical shells have been treated more extensively in the literature than any other type. Because they have only single curvature, membrane solutions are easy to obtain for many types of loading.

Full cylindrical shells (Fig. 9-6a) under distributed load, such as pressure vessels and tanks, have edge bending disturbances only in the vicinity of circumferential edges. Generally, these circumferential edge disturbances produce longitudinal bending moments which damp out rather rapidly in a longitudinal direction into the shell. This is particularly true for long shells. Elsewhere in the shell, only the stress resultants obtained in the membrane analysis are significant; however, some stiffness is required throughout the shell for stability. This will be discussed in detail in Section 9.10

Partial cylinders, such as barrel vault roofs (Fig. 4-3), usually have significant transverse bending effects which result from longitudinal edge disturbances. For long shells, transverse bending moments extend over the entire width of the shell. Transverse bending moments are a critical design consideration in such partial cylindrical shells..

Shells of revolution of many types (Fig. 9-6), in addition to cylindrical shells, have also been treated extensively in the literature. For continuous loading on all but very flat shells, only the membrane stress resultants are significant over a major portion of the shell and bending moments usually may be ignored except in the vicinity of edges; again some bending stiffness must be provided throughout the entire shell for stability.

Translational shells, such as the hyperbolic paraboloid (hypar) (Figs. 4-2 & 9-7) also support distributed loads primarily by membrane stresses, when edge supports provide reactions and control deformations as required by the assumption of the membrane theory. Although, because of their simplicity, membrane solutions are usually employed, at least for preliminary design of hypar shells, their results have been found to be inaccurate for some commonly used shell and edge support configurations. When edge supports do not control deformation as required by the membrane theory, bending occurs in the shell and in-plane stress resultants may differ considerably from those obtained with the membrane theory. This is discussed in Section 9.6.

Equations for determining membrane stresses and edge bending effects in the above common shell types are given in Sections 9.5 and 9.6, respectively, together with references for more comprehensive solutions. Stresses resulting from thermal gradients and restraints of thermal changes at edges are treated in Section 9.9.

Normally, the thin shells treated in this Chapter have a constant thickness, t, having uniform elastic properties in all directions (isotropic). The basic solutions given later are for this case. In some structures, however, thickness may not be uniform, ribs may be present, the shell cross section may be layered or materials may be orthotropic. Since the membrane stress resultants are statically determinate, these variations do not significantly affect the membrane solutions given in the next Section. They will have a profound effect on the edge bending solutions, as is discussed further in Section 9.6, as well as on any mathematical or numerical solutions that include bending. Various approximations for including the effect of directional variations in stiffness and effects of ribs or sandwich construction are included in many of the presentations in the Sections that follow.

9.5 MEMBRANE ANALYSIS OF SHELLS

Membrane action of shell structures relies on the system of statically determinate "in-plane" or membrane" stress resultants that arise to resist a continuously distributed load on a smoothly curved shell. These in-plane stress resultants are sufficient to satisfy static requirements for support of the continuous distributed load because of the curved geometry of the shell. Membrane stress resultants are obtained by statically determinate stress analyses, involving only the geometry of the shell and the applied loads, and the equations of equilibrium. Membrane action provides an inherently efficient stress path because no bending or transverse (radial) shear is required by statics to support the applied load.

Shells of revolution.

Membrane equations of equilibrium for continuous distributed loading are given in (9.7) for two practical shell types of widespread interest:

- shells of revolution with symmetrical load distribution with respect to their axis of revolution (i.e. termed axisymmetric loading),
- shells of revolution with anti-symmetrical load distribution with respect to their axis of revolution.

Analyses of the former type do not require solution of differential equations; the latter solutions involve differential equations.

Membrane stress resultants in symmetrically loaded shells of revolution (Fig. 9-10) may be determined using the following two equations (9.7):

$$N_\phi = \frac{P_\phi}{2\pi R_2 \sin^2\phi} \qquad \text{Eq. 9.18}$$

$$\frac{N_\phi}{R_1} + \frac{N_\theta}{R_2} = -p_z \qquad \text{Eq. 9.19}$$

P_ϕ is the total symmetrical load on the shell above the opening angle ϕ, directed along the axis of revolution as shown in Figs. 9-6 and 9-10. Eq. 9.18 has a singularity at $\phi = 0$, and thus the above method cannot be used in the vicinity of the apex of shells of revolution. See (9.7) for the basic differential equations of the membrane theory.

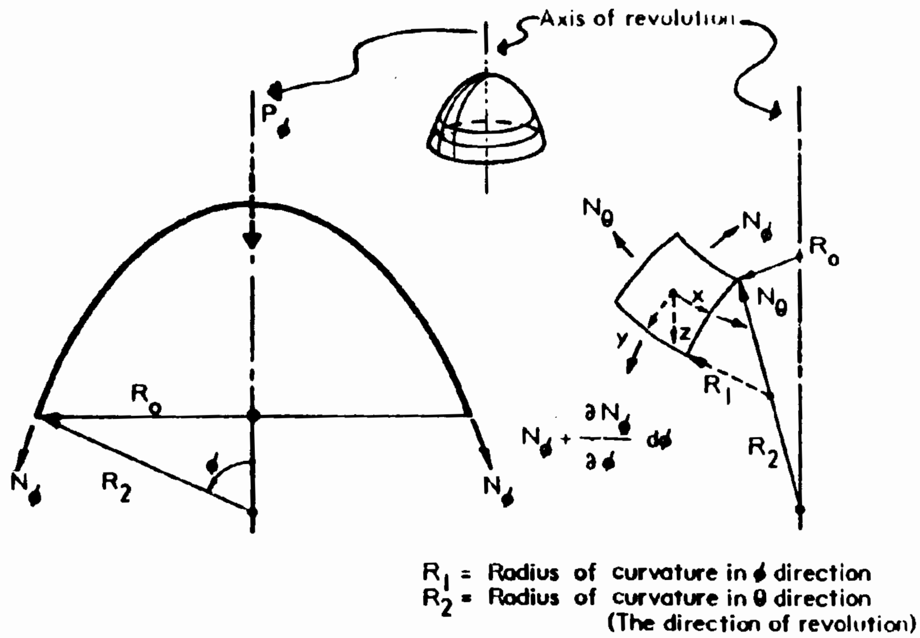

Fig. 9-10 MEMBRANE STRESS RESULTANTS IN SYMMETRICAL SHELL OF REVOLUTION WITH SYMMETRICAL LOADING

p_z is the radial unit load, normal to the surface (pressure), at a point whose coordinates are ϕ, θ.

The use of these equations to determine the membrane stress resultants in a paraboloidal shell is illustrated in Example 9-3.

Note that for a cylindrical shell, $R_1 = \infty$, $\phi = 90$ degrees, and $N_\phi = N_x$ in Table 9-1 for all locations on the shell.

Equations for the three membrane stress resultants, N_ϕ, N_θ and $N_{\phi\theta}$, are presented for several common types of distributed load of practical design interest in the following tables:

Example 9-3: Determine the membrane stress resultants at the support ring of the circular paraboloid of revolution shown in the sketch, subject to 1 psi internal pressure. Obtain geometry from Fig. 9-6, Case (f), for a = b = 50 in. and c = 30 in.*

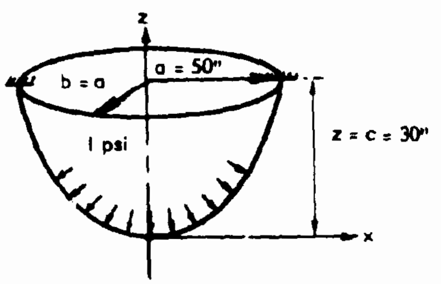

1. Fig. 9-6: Equation of surface:

$$z = \frac{cx^2}{a^2} + \frac{cy^2}{a^2}$$

2. Since any horizontal section through the surface is a circle, stress resultants are the same at all points around any horizontal circumference. Thus, consider the x-z vertical plane as representing all vertical planes.

3. Radii of curvature: At support ring where x = 50 in.

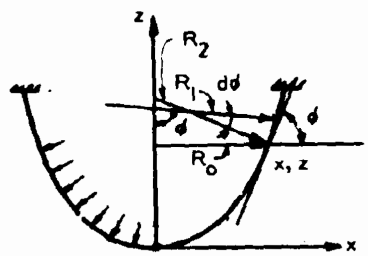

$$R_2 = \frac{R_o}{\sin\phi} = \frac{x}{\sin\phi}\,;\ \tan\phi = \frac{dz}{dx} = \frac{2cx}{a^2} = \frac{2 \times 30 \times 50}{50^2} = 1.2$$

and $\phi = 50.19$, $\sin\phi = 0.768$, $R_2 = \dfrac{50}{0.768} = 65.1$ in.

$$R_1 = \frac{ds}{d\phi} = \frac{\left[1 + \left(\frac{dz}{dx}\right)^2\right]^{3/2}}{\frac{d^2z}{dx^2}}\,;\ \frac{d^2z}{dx^2} = \frac{2c}{a^2} = \frac{2 \times 30}{50^2} = 0.0240$$

$$R_1 = \frac{\left[1 + (1.2)^2\right]^{3/2}}{0.0240} = 158.8 \text{ in.}$$

4. N_ϕ stress resultant: Eq. 9.18: $N_\phi = \dfrac{P_\phi}{2\pi R_2 \sin^2\phi}$

At the support ring: $P_\phi = p_z \pi a^2$, where P_ϕ is the component of the total pressure load below the support ring along the axis of rotation and p_z is the pressure normal (perpendicular) to the surface at any point.

$$N_\phi = \frac{p_z a^2}{2 R_2 \sin^2\phi} = \frac{1 \times 50^2}{2 \times 65.1 \times (0.768)^2} = 32.55 \text{ lbs/in.}$$

5. N_θ stress resultant: Eq. 9.19: $\dfrac{N_\phi}{R_1} + \dfrac{N_\theta}{R_2} = -p_z$; $p_z = 1.0$ psi

At the support ring: $\dfrac{32.55}{158.8} + \dfrac{N_\theta}{65.1} = 1.0$; $N_\theta = 65.1\,(1.0 - 0.206) = 51.7$ lbs/in.

Note: 1 in. = 25.4 mm, lbf/in. = 175 N/m, 1 psi = 0.0059 MPa.

* See footnote, Example 9-1, Page 9-13.

Cylindrical Shells	—	Table 9-1
Spherical Shells	—	Table 9-2
Conical Shells	—	Table 9-3
Toroidal Shells	—	Table 9-4

See (9.8) and (9.9) for extensive tables of equations for membrane stress resultants in other shells of revolution, including pointed domes (toroid shells where ring axis bisects cross section), spherical shells with unsymmetrical boundaries, paraboloids, cycloids and ellipsoids of revolution, and conical shells with support at vertex. See (9.7), (9.8), (9.9), (9.10), (9-11) and (9.12) for derivations of the equations given in Tables 9-1, 9-2, 9-3 and 9-4, for other results of membrane shell analyses, and for more detailed explanations of methods of analysis and differential equations for more complex cases of membrane stresses in shells.

Translational shells.

Another class of shells of practical design interest are translational shells. The surface geometry of these shells is formed by translating a straight or curved generator along a set of perpendicular or skewed straight or curved generatrices. Cylindrical shells belong to this class, as well as to shells of revolution. The hyperbolic paraboloid (shortened to "hypar" hereafter) is a well known translational shell, formed by translating a straight generatrix along another set of straight generatrices, as shown in Fig. 9-7(a) and (b). Another translational shell of interest is the elliptic paraboloid, formed by translating a parabolic generatrix along a set of perpendicular parabolic generatrices, as shown in Fig. 9-6(e).

Equations for membrane stress resultants in right angle hypar shells subject to dead load, snow load, fluid load and wind load are given in (9.8). For all the above loadings except snow load, both axial and shear stress resultants arise throughout the shell. Since edge members often cannot be arranged to support significant axial membrane stress resultants with adequate strength and stiffness, a system of equal and opposite edge forces must be applied to eliminate the required membrane reactions. These edge forces cause additional in-plane axial and bending stress resultants which are difficult to evaluate by simple closed form analyses, as discussed in the next Section.

Table 9-1

Membrane Stress Resultants in Closed Circular Cylindrical Shells (Source 9.8)

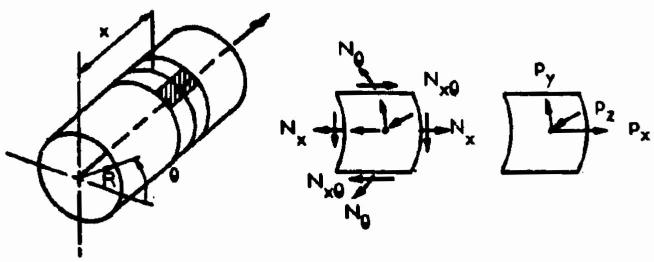

Arrangement	Equation of Load Variation	N_x	N_θ	$N_{x\theta}$
1. 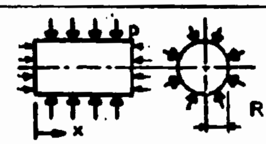	$p_z = p$ (Uniform pressure on vertical or horizontal cylinder)	$\frac{-pR}{2}$	$-pR$	0
2. 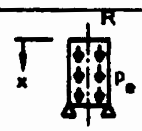	$p_x = p_e$ (Weight load on vertical cylinder)	$-p_e x$	0	0
3. 	$p_z = -\gamma x$ (Fluid load on vertical cylinder)	0	$\gamma x R$	0
4. 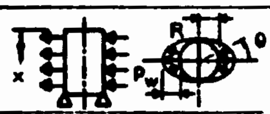	$p_z = p_w \cos\theta$ (Wind load on vertical cylinder)	$p_w \frac{x^2}{2R} \cos\theta$	$-p_w R\cos\theta$	$-p_w x \sin\theta$
5. 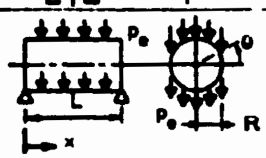	$p_y = -p_e \cos\theta$ $p_z = p_e \sin\theta$ (Weight load on horizontal cylinder)	$-p_e \frac{x}{R} (L-x) \sin\theta$	$-p_e R\sin\theta$	$-p_e (L-2x) \cos\theta$
6. 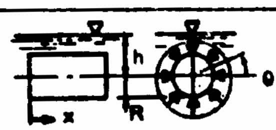	$p_z = \gamma (h - R\sin\theta)$ (Fluid load on horizontal cylinder)(external as shown, - for internal)	$\gamma \frac{x}{2} (L-x) \sin\theta$ $- \frac{\gamma R^2}{2} (\frac{h}{R} - \frac{\sin\theta}{2})$ $h \geq R$	$-\gamma R^2 (\frac{h}{R} - \sin\theta)$	$\gamma R (\frac{L}{2} - x) \cos\theta$
7. 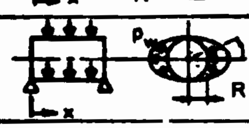	$p_z = p_w \cos\theta$ (Wind load on horizontal cylinder)	$p_w \frac{(L-x)^2}{2R} \cos\theta$	$-p_w R \cos\theta$	$-p_w (\frac{L}{2} - x) \sin\theta$

Table 9-2

Membrane Stress Resultants in Spherical Shells (Source 9.8)

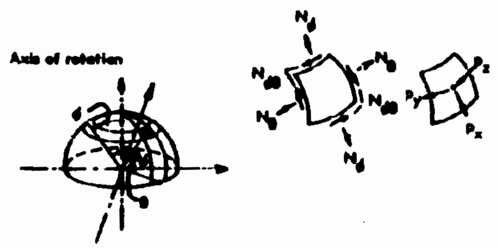

Note: Membrane reactions require support in N_ϕ direction at base as well as base support for $N_{\phi\theta}$ for the wind loading condition given in the last case below.

Arrangement	Equation of Load Variation	N_ϕ	N_θ	$N_{\phi\theta}$
1. 	$p_z = p$ (Uniform pressure)	$-\frac{pR}{2}\left(1 - \frac{\sin^2\phi_o}{\sin^2\phi}\right)$	$-\frac{pR}{2}\left(1 + \frac{\sin^2\phi_o}{\sin^2\phi}\right)$	0
		For $\phi_o = 0$ (No vertex opening)		
		$-p\frac{R}{2}$	$-p\frac{R}{2}$	0
2. 	$p_z = p_o \cos\phi$ $p_x = p_o \sin\phi$	$-p_oR\frac{(\cos\phi_o - \cos\phi)}{\sin^2\phi}$	$-N_\phi - p_oR\cos\phi$	0
	(Weight load)	For $\phi_o = 0$ (No vertex opening)		
		$-\frac{p_oR}{1+\cos\phi}$	$-N_\phi - p_oR\cos\phi$	0
3. 	$p_z = p_s \cos^2\phi$ $p_x = p_s \sin\phi\cos\phi$	$-\frac{p_sR}{2}\left(1 - \frac{\sin^2\phi_o}{\sin^2\phi}\right)$	$-N_\phi - p_sR\cos^2\phi$	0
	(Snow load)	For $\phi_o = 0$ (No vertex opening)		
		$-\frac{p_sR}{2}$	$N_\phi \cos 2\phi$	0
4. 	Upper edge load p_L	$-p_L\frac{\sin\phi_o}{\sin^2\phi}$	$-N_\phi$	0
		For $\phi_o = 0$ (No vertex opening)		
	Vertex load p_L	$-p_L\frac{1}{2\pi R^2\sin^2\phi}$	$-N_\phi$	0

Table 9-2 (cont'd)

Arrangement	Equation of Load Variation	N_ϕ	N_θ	$N_{\phi\theta}$
5. 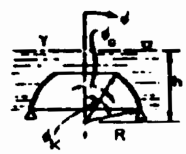	$p_z = \gamma(h - R\cos\phi)$ $(h > R\cos\phi_o)$ (Fluid load)	$-\gamma R\left[\frac{h}{2}\left(1 - \frac{\sin^2\phi_o}{\sin^2\phi}\right) - \frac{R}{3}\frac{(\cos^3\phi_o - \cos^3\phi)}{\sin^2\phi}\right]$	$-\gamma R\left[\frac{h}{2}\left(1 + \frac{\sin^2\phi_o}{\sin\phi}\right) + \frac{R}{3}\left(\frac{(\cos^3\phi_c - \cos^3\phi)}{\sin^2\phi} - 3\cos\phi\right)\right]$	0
		For $\phi_o = 0$ (No vertex opening)		
		$-\gamma R\left\{\frac{h}{2} - \frac{R}{3}\left[1 + \frac{\cos^2\phi}{(1 + \cos\phi)}\right]\right\}$	$-\gamma R\left\{\frac{h}{2} - R\cos\phi + \frac{R}{3}\left[1 + \frac{\cos^2\phi}{(1 + \cos\phi)}\right]\right\}$	0
6. 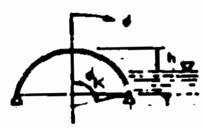	$p_z = \gamma(R - R\cos\phi - h)$ (Fluid load)	Above liquid level 0	0	0
		Below liquid level $-\frac{\gamma R}{6}\left\{h\left[\frac{1}{\sin^2\phi}\ \frac{h}{R}\ (3 - \frac{h}{R}) - 3\right] + R\left[1 + \frac{2\cos^2\phi}{(1 + \cos\phi)}\right]\right\}$	$-\gamma R^2\left[1 - \cos\phi - \frac{h}{R}\right] - N_\phi$	0
7. 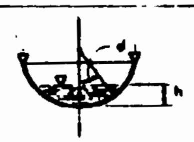	$p_z = -\gamma(R - R\cos\phi - h)$ (Fluid load)	Above liquid level $\frac{\gamma h^2}{6}\ (3 - \frac{h}{R})\ \frac{1}{\sin^2\phi}$	$-N_\phi$	0
		Below liquid level $\frac{\gamma R^2}{6}\left[3\frac{h}{R} - 1 + \frac{2\cos^2\phi}{(1 + \cos\phi)}\right]$	$R^2\left[\frac{h}{R} - 1 + \cos\phi - N_\phi\right]$	0
8. 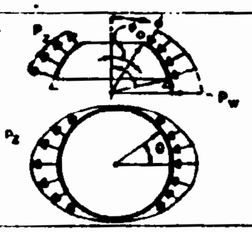	$p_z = p_w \sin\phi\cos\theta$ (Wind loading)	$-p_w\frac{R}{3}\frac{\cos\theta\cos\phi}{\sin^3\phi}\left[3(\cos\phi_o - \cos\phi) - (\cos^3\phi_o - \cos^3\phi)\right]$	$p_w\frac{R}{3}\frac{\cos\theta}{\sin^3\phi}\left[\cos\phi(3\cos\phi_o - \cos^3\phi_o) - 3\sin^2\phi - 2\cos^4\phi\right]$	$\frac{N_\phi}{\cos\phi}\tan\theta$
		For $\phi_o = 0$ (No vertex opening)		
		$-p_w\frac{R}{3}\frac{\cos\theta\cos\phi}{\sin^3\phi} \times (2 - 3\cos\phi - \cos^3\phi)$	$p_w\frac{R}{3}\frac{\cos\theta}{\sin^3\phi}(2\cos\phi - 3\sin^2\phi - 2\cos^4\phi)$	$\frac{N_\phi}{\cos\phi}\tan\theta$
8a. 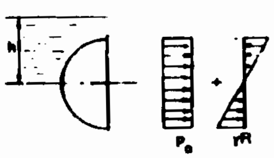	Use Case 8 also for the variable part of external (or internal) fluid pressure in Case 8a by replacing p_w with γR and adding $p_o = \gamma h$	$\left(-\frac{p_o R}{2}\ \text{for 8a}\right)$ Add to Case 8	$\left(-\frac{p_o R}{2}\ \text{for 8a}\right)$ Add to Case 8	

Table 9-3

Membrane Stress Resultants in Conical Shells (Source 9.8)

Arrangement	Loading	N_ϕ	N_θ	$N_{\phi\theta}$
1. 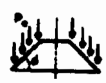	$p_x = p_e \sin\phi$ $p_z = p_e \cos\phi$ (Weight Load)	$-p_e \frac{(s^2 - s_0^2)}{2s} \frac{1}{\sin\phi}$ For $s_0 = 0$ (complete cone): $-p_e \frac{s}{2} \frac{1}{\sin\phi}$	$-p_e s \frac{\cos^2\phi}{\sin\phi}$ $-p_e s \frac{\cos^2\phi}{\sin\phi}$	0 0
2. 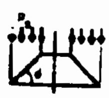	$p_x = p_s \sin\phi \cos\phi$ $p_z = p_s \cos^2\phi$ (Snow Load)	$-p_s \frac{(s^2 - s_0^2)}{2s} \operatorname{ctg}\phi$ For $s_0 = 0$ (complete cone): $-p_s \frac{s}{2} \operatorname{ctg}\phi$	$-p_s s \frac{\cos^3\phi}{\sin\phi}$ $-p_s s \frac{\cos^3\phi}{\sin\phi}$	0 0
3. 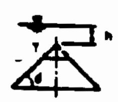	$p_z = \quad (h + s \sin\phi)$ (Fluid Load)	$-\frac{\gamma}{s}\left[h \frac{(s^2 - s_0^2)}{2} \operatorname{ctg}\phi + \frac{(s^3 - s_0^3)}{3} \cos\phi\right]$ For $s_0 = 0$ (complete cone): $-\gamma s \left(\frac{h}{2} \operatorname{ctg}\phi + \frac{s}{3} \cos\phi\right)$	$-\gamma s (h \operatorname{ctg}\phi + s \cos\phi)$ $-\gamma s (h \operatorname{ctg}\phi + s \cos\phi)$	0 0
4. 	$p_z = \gamma (s \sin\phi - h)$ (Fluid load)	Points above the liquid level: 0 Points below liquid level: $-\frac{\gamma}{6s}\left[\frac{\cos\phi}{\sin^3\phi} h^3 + s^2 (2 s \cos\phi - 3 h \operatorname{ctg}\phi)\right]$	 0 $-\gamma s (s \cos\phi - h \operatorname{ctg}\phi)$	 0 0
5. 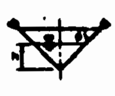	$p_z = -\gamma (h - s \sin\phi)$ (Fluid load)	Points above liquid level: $\frac{\gamma h^3}{6s} \frac{\cos\phi}{\sin^3\phi}$ Points below liquid level: $\frac{\gamma s}{2} (3 h \operatorname{ctg}\phi - 2 s \cos\phi)$	 0 $\gamma s (h \operatorname{ctg}\phi - s \cos\phi)$	 0 0
6. 	$p_z = p$ (Uniform pressure)	$-p \frac{(s^3 - s_0^2)}{2s} \operatorname{ctg}\phi$ For $s_0 = 0$ (complete cone): $-p \frac{s}{2} \operatorname{ctg}\phi$	$-p s \operatorname{ctg}\phi$ $-p s \operatorname{ctg}\phi$	0 0
7. 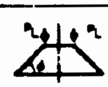	Edge load p_L Axial load P_L	$-p_L \frac{s_0}{s} \frac{1}{\sin\phi}$ For $s_0 = 0$ and axial single loads: $-P_L \frac{1}{2\pi s \sin\phi \cos\phi}$		0 0
8.  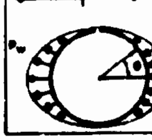	(Wind load)	$-p_w \frac{s}{2}\left[\cos\phi - \frac{1}{3\cos\phi} - \frac{s_0^2}{s^2} \times \left(\cos\phi - \frac{1}{\cos\phi}\right) - \frac{s_0^3}{s^3} \frac{2}{3\cos\phi}\right] \cos\theta$ For $s_0 = 0$ (complete cone): $-p_w \frac{s}{2}\left[\cos\phi - \frac{1}{3\cos\phi}\right] \cos\theta$	$-p_w s \cos\phi \cos\theta$ $-p_w s \cos\phi \cos\theta$	$-p_w \frac{(s^3 - s_0^3)}{3s^2} \sin\theta$ $-p_w \frac{s}{3} \sin\theta$

Table 9-4

Membrane Stress Resultants in Symmetrical Toroid Shell Whose Ring Axis Does Not Intersect the Cross Section (Source 9.9)

Arrangement	Equation of Load Variation	N_ϕ	N_θ	$N_{\phi\theta}$
1 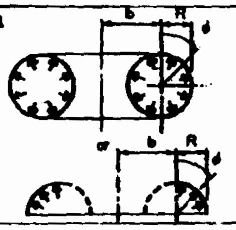	$p_z = -p$ (Uniform pressure)	$\frac{pR}{2}\frac{(2b + R\sin\phi)}{(b + R\sin\phi)}$	$\frac{pR}{2}$	0
2 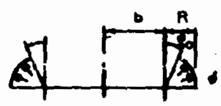	$p_z = -p$ (Uniform pressure on partial knuckle)	$\frac{p}{2(b + R\sin\phi)\sin\phi}\left[(b + R\sin\phi)^2 - (b + R\sin\phi_o)^2\right]$	$\frac{p}{2\sin^2\phi}\left[2b\sin\phi_o + R(\sin^2\phi_o + \sin^2\phi)\right]$	0
3 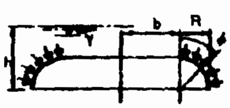	$p_z = \gamma(h - R\cos\phi)$ (Fluid pressure where γ = specific weight of fluid)	$-\frac{\gamma R}{(b + R\sin\phi)\sin\phi}\Big[b\,h\sin\phi + \frac{Rh}{2}\sin^2\phi - \frac{bR}{2}(\sin\phi\cos\phi + \phi) - \frac{R^2}{3}(1 - \cos^3\phi)\Big]$	$-\frac{\gamma R}{\sin^2\phi}\Big[\frac{h}{2}\sin^2\phi - \frac{b}{2}(\sin\phi\cos\phi - \phi) - R\left(\cos\phi\sin^2\phi - \frac{(1 - \cos^3\phi)}{3}\right)\Big]$	0

See (9.8) and (9.9) for other loading cases and configurations of toroidal shells.

For loads that are uniformly distributed over the xy plane and directed along the z axis of hypar shells, such as snow loads (Fig. 9-11), the N_x and N_y direct stress resultants are zero throughout the shell; the only stress resultants are the in-plane shear forces, N_{xy}. Along the edges, these can be resisted by edge struts having adequate axial strength and stiffness, and thus edge bending effects can be minimized. Because of the simplicity of the membrane analysis and the fairly low rise of many practical hypar shells, the solution for snow load is often used to obtain an approximate analysis for dead load and other loads which have the same approximate direction and distribution.

The following equation gives the applied load intensity on a unit surface area of the hypar (refer to Fig. 9-11):

$$p_z = -p_s \cos \psi \qquad \text{Eq. 9.20}$$

In this equation, p_z is the component of the applied load intensity in the direction of the z axis (Fig. 9-11).

For the case of loads uniformly distributed over the xy plane, $\psi = 0$ and $p_z = -p_s$. The membrane stress resultants in rectangular and skew hypar shells subject to such loads are (9.13):

$$N_x = N_y = 0 \qquad \text{Eq. 9.21}$$

$$N_{xy} = p_s \frac{ab \sin \omega}{2c} \qquad \text{Eq. 9.22}$$

When $\omega = 90^o$, the hypar is a right hypar (Fig. 9-11a).

The above system of in-plane shear stress resultants produces the following maximum direct stress resultants (principal stress resultants) in the two diagonal directions (Fig. 9-11d):

$$N_1 = N_{xy} \cot \frac{\omega}{2} \qquad \text{Eq. 9.23a}$$

$$N_2 = -N_{xy} \tan \frac{\omega}{2} \qquad \text{Eq. 9.23b}$$

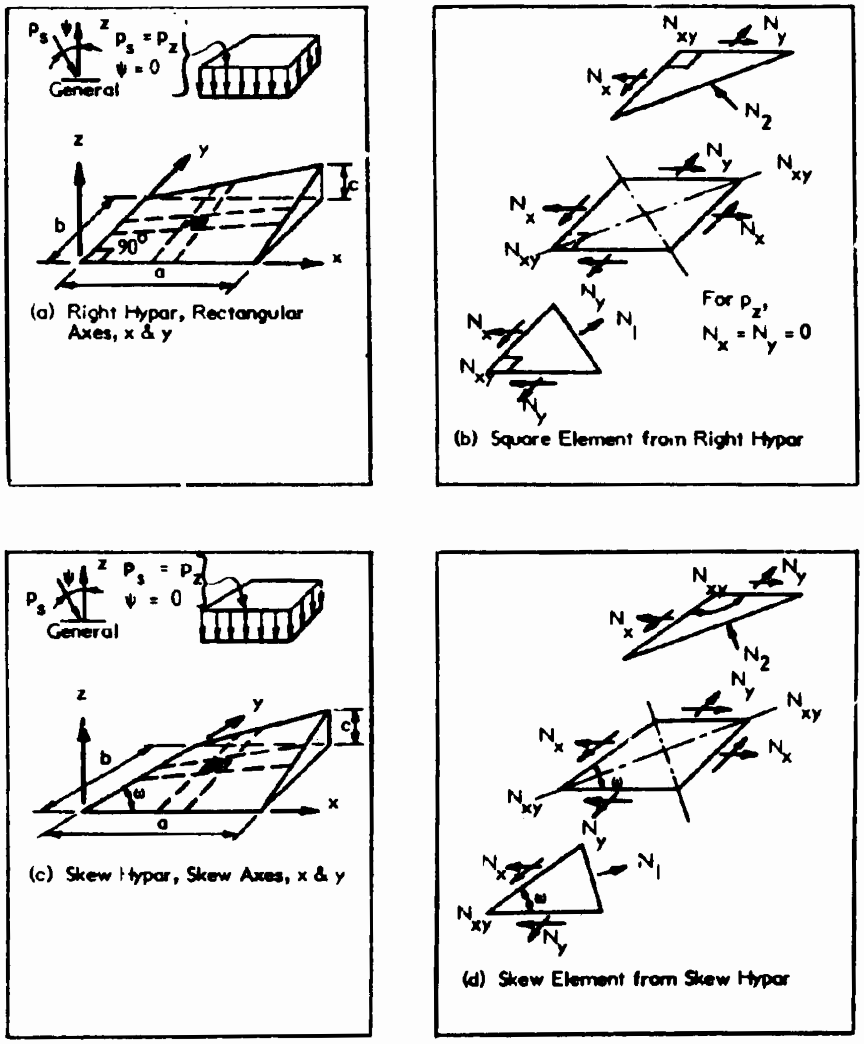

Fig. 9-11 HYPAR SHELL COORDINATE SYSTEMS AND STRESS RESULTANTS

The above principal stress results are oriented in the following directions:

N_1 at $\omega/2$ with x axis.
N_2 at $(\omega/2 + 90^o)$ with x axis.

The shear stress resultants in these directions are zero.

If N_x and N_y are set equal to 0 in Fig. 9-11 (b), or (d), these sketches illustrate how the diagonal principal stress resultants, N_1 or N_2 are equilibrated by the components in diagonal directions 1 or 2 of the two shear stress resultants, N_{xy}, acting along the x and y edges, respectively.

The error in using the above equations for dead load, where $p_z = -p_e$, or for other loads, can be estimated to some extent by noting the magnitude and variation of cos ψ (Fig. 9-11) throughout a particular shell. More complicated analyses should be used for shells wih large rise, or for shells whose z axis is not vertical.

Membrane stress resultants in elliptical paraboloid shells (Fig. 9-6(e)) are given in (9.14). These can sometimes also be used to approximate the stress resultants in similar shells formed by translation of circular arcs instead of parabolas. Generally, fabrication of components with curved surfaces having constant radii is considerably simpler than fabrication of curved surfaces with variable radii. In this case, a parabola which is passed through two sets of symmetrical points on the circular arc will provide a good approximation (Fig. 9-6(e)).

Tension Membranes

Tension membranes are used in structures such as tents and air supported enclosures and components. Air supported structures include single membranes, enclosing an entire pressurized space, and closed cell double membrane, pressurized components that can be used for covering non-pressurized spaces. Fabrics used for such membranes are often composites of flexible plastic coating and inorganic or organic fiber. Three common types are Fluroplastic (PTFE) coated glass fiber, Polyvinyl Chloride (PVC) coated Nylon or Polyester fiber, and Neoprene coated Nylon or Polyester fiber. The first type can be formulated to be non-combustible, a particularly important consideration for covering large spaces used for public assembly (see Section 10.5). See (9.15) for a "state-of-the-art" report on the application and design of air supported tension membrane structures.

As the name implies, tension membranes are capable of resisting applied load only when they are stressed in tension. When they are not given sufficient initial tension, large changes in shape may result from fluctuating loads, such as wind load, producing unsatisfactory behavior like "flapping", flutter and excessive movement. In view of this, most tension structures are pretensioned prior to application of service loads, either by tensioning against external anchorage, and internal struts, or by internal air pressure. Once the tension structure has sufficient initial tension, it can resist applied distributed loads which produce tension, compression, and/or in-plane shear, so long as the principal compression resulting from the applied loads remains below the initial tension, and the combined initial tension and applied principal tension remain below the safe tensile strength limit.

Tension membranes differ from rigid shells because they cannot resist bending and transverse shear, and they must have sufficient initial tension to counteract membrane compression due to applied loads. Usually, the initial tension forces and the applied loads produce large deformations of tension structures and the changes in structure geometry must be accounted for in accurate design analyses. This requires non-linear analysis methods that are complex and outside the scope of this Manual. However, if the final geometry of a tension structure, after application of initial tension and applied loads, can be estimated with sufficient accuracy or determined experimentally, the structure may be analyzed using the membrane analysis methods previously presented in this Section. Even when final shapes can only be roughly estimated, linear membrane analysis may be very useful for preliminary design purposes.

Tension structures require adequate anchorage to develop tension edge forces provided to develop initial tension in the membrane and edge reactions caused by applied loads. Anchorage strength frequently is developed by providing sufficient weight in foundations, or by anchoring into the ground with earth anchors having adequate pullout strength.

When initial or final stresses are larger than the safe strength of the skin fabrics, tension membranes can be reinforced with cables of nylon, aramid, fiberglass or steel. Such reinforcement may also be required if significant concentrated loads must be supported.

Netting Analysis

Netting analysis is a method that is sometimes used to design filament wound laminates for pressure vessels and pipe subject to one predominant uniform loading, such as internal pressure. This loading produces a particular set of membrane principal stress resultants in the shell. Netting analysis provides a means for determining the filament orientation that results in the same stresses in all filaments, as well as equations for determining the filament stress at this orientation for this set of membrane stress resultants. In netting analysis, it is reasoned that if all filaments are arranged to be at the same stress under the design load, their inherent strength can be fully developed (with suitable safety factors), and the design will thus be optimized with respect to strength-to-weight ratio.

In netting analysis, only the continuous filaments are assumed to have load carrying capability and in designs based upon this analysis, all fibers are arranged to be uniformly stressed in tension (or compression). One of the following four types of layered filament wound composites are usually used:

(1) An angle ply (helix wound) balanced laminate of thickness t consisting of two sets of equal strength monolayers, oriented at $\pm\,\alpha$ with the longitudinal axis (Fig. 9-12a). α is termed the winding angle of the helix.

(2) A binary angle ply (helix wound) balanced laminate consisting of two sets of equal strength monolayers oriented at $\pm\,\alpha_1$, and two sets oriented at $\pm\,\alpha_2$ with the longitudinal axis (Fig. 9-12b). The double sets of layers have total thicknesses of t_1, and t_2, respectively, for each double set. This is considered the general case of a binary oriented laminate.

(3) A three-ply laminate comprised of two equal sets of monolayers at $\pm\,\alpha$, with a total thickness t_1 (for both sets together), and one set of monolayers of thickness t_2 at 90° (circumferential) (Fig. 9-12c). This is a special condition of Case 2 with $\alpha_2 = 90^\circ$.

(4) A cross ply balanced laminate consisting of one set of monolayers (with thickness t_1) oriented in the x-direction and one set (with thickness t_2) oriented in the y-direction (Fig. 9-12d). This is a special condition of Case 3 with $\alpha_1 = 0$.

The equations of netting analysis are based on the resolution of stresses on a filament of cross section bt, oriented at an angle, α, with the x-axis and subjected to principal stresses σ_x and σ_y in the x and y directions, as shown in Figure 9-12a. When σ_x and σ_y are principal stresses, the shear stresses on planes perpendicular to the x and y axes are zero. For equilibrium of applied and resisting forces:

$\sigma_x t b_x = \sigma_f t b \cos\alpha$, where t is the equivalent thickness of the monolayer

$$b_x = \frac{b}{\cos\alpha}$$

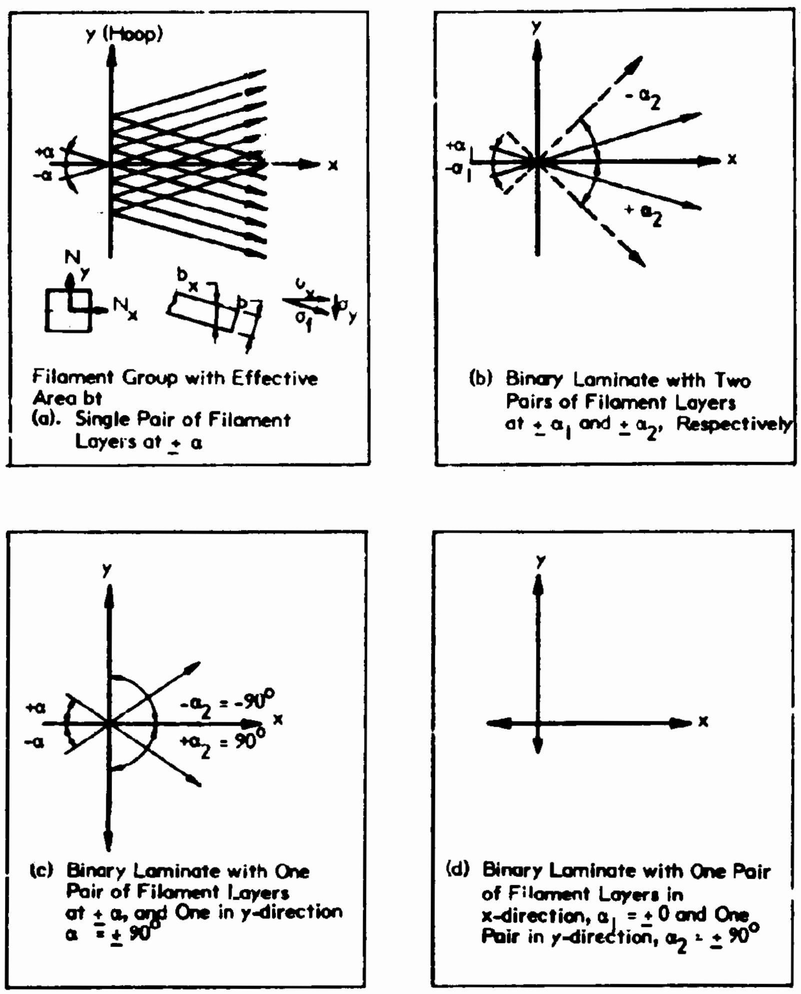

Fig. 9-12 ORIENTATION OF FILAMENTS AND MEMBRANE STRESSES FOR NETTING ANALYSIS

Thus: $\sigma_x = \sigma_f \cos^2 \alpha$ Eq. 9.24

Similiarly: $\sigma_y = \sigma_f \sin^2 \alpha$ Eq. 9.25

The above relations lead to the equations given in Table 9-5 for the laminate described in Case I above. These indicate the required angle of wind, α, as a function of the ratio of principal membrane stress resultants, N_x and N_y. Most commonly, these relations are used for designing filament wound laminates for cylindrical vessels or pipe subject to internal pressure, or to combinations of internal pressure and various axi-symmetric longtudinal stresses. The equation for filament orientation shows that the so-called optimum wind angle of $\alpha = 54.7^{\circ}$ only applies to a cylindrical component, such as a closed cylinder with internal pressure, where $N_y = 2 N_x$.

In a more general case, two winding angles or directions of filaments are used. Filament layers having an equivalent thickness of t_1, are applied at a helix angle $\pm \alpha_1$, and layers having an equivalent thickness of t_2 are applied at a helix angle $\pm \alpha_2$, as shown in Figure 9-12(b). The equations for determining the relations between layer thickness and required helix angles and the strength of layers for this more general case of a binary laminate are given in Table 9-5, Case 2.

In typical practical laminates, one "pair" of filaments is applied at approximately $\pm 90^{\circ}$ (the hoop direction), while the other pair is applied at $\pm \alpha$ (Case 3 in the Table), or in the longitudinal direction ($\alpha = 0^{\circ}$) (Case 4 in the Table).

Thus, the equations given in Table 9-5 may be used to determine the arrangements and strength of filaments in filament wound vessels and pipe subject to principal membrane stress resultants N_x and N_y. **Example 9-4** illustrates the application of these equations to design of a filament wound pressure pipe subject to both longitudinal and circumferential stresses.

In filament wound vessels with closed ends or heads, the same helix wraps used to form the cylinder are also wrapped over a doubly curved mold of proper shape to form end closures which resist internal pressure using the full strength provided by the helix wrap. Usually, polar openings are provided at the apex of the head shell as access ports and as openings needed to remove an internal collapsible or disposable mandrel used in winding the vessels.

Table 9-5

Requirements for Filament Orientation and Strength Based on Netting Analysis

Type of Laminate	Filament Orientation in Terms of Helix Angle, α, and Equivalent Thickness of Filaments t_1 and t_2 for Membrane Stress Ratio, N_y/N_x	Required Strength, σ_f, in Direction of Filament
Case 1 - laminate of thickness t with two equal sets of filaments at helix angle $\pm\alpha$ (Fig. 9-12(a)).	$\frac{N_y}{N_x} = \tan^2 \alpha$	$\sigma_f = \frac{N_x}{t \cos^2 \alpha}$ also $\sigma_f = \frac{N_y}{t \sin^2 \alpha}$
Case 2 - general binery laminate with a set of filaments at $\pm\alpha_1$ (thickness t_1) and a set of filaments at $\pm\alpha_2$ (thickness t_2). Strengths of filaments in sets 1 and 2 are all σ_f (Fig. 9-12(b)).	$\frac{N_y}{N_x} = \frac{t_1 \sin^2 \alpha_1 + t_2 \sin^2 \alpha_2}{t_1 \cos^2 \alpha_1 + t_2 \cos^2 \alpha_2}$	$\sigma_f = \frac{N_x}{t_1 \cos^2 \alpha_1 + t_2 \cos^2 \alpha_2}$ also $\sigma_f = \frac{N_y}{t_1 \sin^2 \alpha_1 + t_2 \sin^2 \alpha_2}$
Case 3 - laminate with t_1 filaments at helix angle $\pm\alpha$ and t_2 filaments at 90° i.e. in direction of y (hoop) (Fig. 9-12 (c)).	$\frac{N_y}{N_x} = \frac{t_1 + t_2}{t_1 \cos^2 \alpha} - 1$	$\sigma_f = \frac{N_x}{t_1 \cos^2 \alpha}$ also $\sigma_f = \frac{N_y}{t_1 \sin^2 \alpha + t_2}$
Case 4 - laminate with t_1 filaments in direction x (longitudinal) and t_2 filaments in direction y (hoop) (Fig. 9-12(d)).	$\frac{N_y}{N_x} = \frac{t_2}{t_1}$	$\sigma_f = \frac{N_x}{t_1}$ also $\sigma_f = \frac{N_y}{t_2}$

Example 9-4: Determine the required laminate thickness and angle of wind for helical filaments that should be used in a filament wound pressure pipe with 10-in. inside radius constructed with one half of the filaments at 90^{o} (hoop) and the other half at a helix angle $\pm\alpha$. Assume an internal pressure of 100 psi and assume that the joints and bends are supported so that maximum longitudinal tension will not be greater than 0.3 times the circumferential tension. Assume that the basic tensile strength in short-time tests of the laminate in the direction of filaments (uniaxial strength) is 60,000 psi. Use a capacity reduction factor of 0.3 for long term and cyclic stress, service exposure effects, and manufacturing variability, and use a load factor of 2.0.*

1. Uniaxial strength: $\sigma_{fu} = 0.3 \times 60{,}000 = 18{,}000$ psi

2. Table 9-5, Case 3: Let $t_1 = t_2 = 0.5\,t$, where t = total thickness of laminate

$$\frac{N_y}{N_x} = \frac{1}{0.3} = \frac{(t_1 + t_2)}{t_1 \cos^2\alpha} - 1;$$

$$\frac{1}{.3} = \frac{0.5\,(t + t)}{0.5\,t \cos^2\alpha} - 1; \cos^2\alpha = \frac{2}{4.33} = 0.461; \cos\alpha = 0.679; \alpha = 47.2^{o}$$

3. Stress Resultants:

Eq. 9.1: $N_y = N_0 = pR = 100 \times 2.0 \times 10 = 2{,}000$ lb/in.

Table 9-5, Case 3: $\sigma_f = \dfrac{N_y}{t_1 \sin^2\alpha + t_2}$; $18{,}000 = \dfrac{2{,}000}{(0.5\,t \sin^2 47.2 + 0.5\,t)}$;

$$t = \frac{2{,}000}{9{,}000\,(\sin^2 47.2 + 1)} = 0.144 \text{ in.; hoop thickness } = 0.144/2 = 0.072 \text{ in.}$$

Helix ($\alpha = \pm 47.2^{o}$ with longitudinal axis) thickness also = 0.072 in.

Use 0.036 in. at + 47.2^{o} and 0.036 in. at -47.2^{o}.

Note: 1 in. = 25.4 mm, 1 lbf/in. = 175 N/m, 1 psi = 0.0069 MPa.

* See footnote, Example 9-1, Page 9-13.

Netting analysis is also used to determine an optimized shape for the ovaloid end closure, or head shell. This requires consideration of the helix winding pattern as well as the size and type of polar opening needed at the apex. A low angle helix wind is usually used for the cylinder to provide an efficient wind angle for the ovaloid head. The shape of the ovaloid head has been developed using both analog equipment that applies pressure to a net of continuous fibers and theoretical analyses (9.16). Such analyses are beyond the scope of this Design Manual.

While netting analysis often is extrememly useful for proportioning the effective thickness or quantity of fiber to be placed at specific orientations in filament wound components, in some cases final design requires consideration of the effects of bending caused by discontinuities at supports and heads. This usually involves determination of elastic stiffness properties for laminated orthotropic plates and shells (Section 6.7), and a bending analysis of the orthotropic layered filament wound shell (Sections 4.9 and 9.6), using appropriate stiffness constants for this analysis.

9.6 EDGE BENDING ANALYSIS OF SHELLS

Efficient structural action associated with shell behavior demands adequate support at the edges of the shell. If possible, edge structure should be strong enough to provide the reactions required to support the membrane stress state. In addition, it should be stiff enough to minimize deformations in excess of those required by the membrane solution. Nevertheless, even if edge members have sufficient strength to support membrane stresses, in general, their deformation will not meet the requirements of pure membrane behavior. Consequently, bending stresses almost always must be expected in the vicinity of shell edges.

Whether or not the edge bending moments are significant for the design of the shell depends on the relative strength and stiffness of the edge supports provided. In most practical shell structures, these moments are significant near the edges, but they usually die out rapidly in a direction away from the edge. Consequently, analysis of bending effects in shells is usually limited to the edge region or other points of discontinuity, such as locations where different shells intersect, where abrupt changes in load distribution occur, or where penetrations and concentrated loads occur. This is not the case in certain hypar shells where support deformations result in large differences between the membrane stress solution and stresses obtained by numerical analyses that account for bending and support deformation (9.32) (9.33). This is also evident in model tests (9.34).

Practical, and usually approximate, methods for determining shell stress resultants in the above regions of discontinuity are presented in this Section. Solutions that are included here are limited to widely applicable approximations for commonly occurring discontinuity problems in symmetrically loaded shell edge regions. These occur in pressure vessels and many other shells of practical interest. The axisymmetric solutions are also widely used as rough approximations for many non-axisymmetric conditions. Although edge bending stresses are often considered as secondary effects and neglected in ductile metal shells, these stresses may produce cracking or other distress in the generally non-ductile plastics materials; thus, they almost always require careful consideration in design with these materials.

Long Cylinder

Under axisymmetric edge loads, structural behavior of the edge region of a shell of revolution is analogous to a beam on an elastic foundation. This is illustrated in Fig. 9-13 which shows that axisymmetric edge radial shears and moments on the end of a cylinder produce similar effects to the behavior caused by a concentrated load and moment on the end of a beam on an elastic foundation. In the edge region of a cylinder, the stiffness of the hoop direction provides continuous elastic support (i.e. "an elastic foundation") for longitudinal strips that resist the applied edge loads. These edge loads cause radial shear, Q_x, and bending moment, M_x, stress resultants in the longitudinal direction, and direct stress resultants, N_θ, in the circumferential direction. These are analogous to the longitudinal shears and moments and the foundation direct pressures which arise in a beam on an elastic foundation.

The above analogy proves useful in understanding the edge bending behavior of more complex structures such as orthotropic, ribbed or sandwich shells. The deformations and stress resultants that arise in the edge region when the axisymmetric edge forces shown in Fig. 9-13 are applied depend on the ratio of circumferential axial stiffness to longitudinal flexural stiffness, as defined by a shell constant, β.

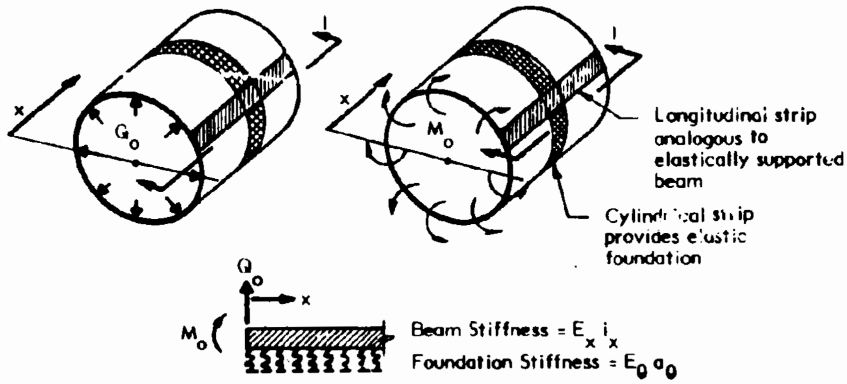

Section I-I: Analogous "Beam-On-Elastic Foundation"

Fig. 9-13 ELASTICALLY SUPPORTED BEAM ANALOGY FOR SHELL EDGE BENDING

In order to define β, it is useful to modify slightly the notation previously used in Section 6.2 to define plate stiffness, to give the circumferential axial and longitudinal flexural stiffnesses, respectively, as:

$$\bar{A}_\theta = E_\theta\, a_\theta \qquad \text{Eq. 9.26}$$

$$D_x = \frac{E_x\, i_x}{(1 - \nu_x\, \nu_\theta)} \qquad \text{Eq. 9.27}$$

For uniform thickness shells, these become:

$$\bar{A}_\theta = E_\theta\, t \qquad \text{Eq. 9.28}$$

$$D_x = \frac{E_x\, t^3}{12\,(1 - \nu_x\, \nu_\theta)} \qquad \text{Eq. 9.29}$$

The shell constant, β, defines the relationship of the above directional stiffnesses as follows:

$$\beta = \left[\frac{\bar{A}_\theta}{4\, D_x\, R^2}\right]^{1/4} \qquad \text{Eq. 9.30a}$$

For a shell of constant thickness:

$$\beta = \left[\frac{3(1-\nu_x \nu_\theta) E_\theta}{R^2 t^2 E_x}\right]^{1/4} \qquad \text{Eq. 9.30b}$$

If the material is isotropic, E_θ and E_x are equal and may be dropped from Eq. 9.30b. Also, $\nu_x = \nu_\theta = \nu$.

The following equations give the radial deflection, slope, longitudinal moment and shear, and circumferential thrust caused by the axisymmetric edge forces shown in Fig. 9-13, as a function of the distance, x, from the edge of the shell:

$$w = -\frac{1}{2\beta^3 D_x}\left[\beta M_o \psi(\beta x) + Q_o \theta(\beta x)\right] \qquad \text{Eq. 9.31}$$

$$\frac{dw}{dx} = \frac{1}{2\beta^2 D_x}\left[2\beta M_o \theta(\beta x) + Q_c \phi(\beta x)\right] \qquad \text{Eq. 9.32}$$

$$M_x = -\frac{1}{\beta}\left[\beta M_o \phi(\beta x) + Q_o \tau(\beta x)\right] \qquad \text{Eq. 9.33}$$

$$Q_x = 2\beta M_c \tau(\beta x) - Q_o \psi(\beta x) \qquad \text{Eq. 9.34}$$

$$N_\theta = -\frac{\bar{A}_\theta w}{R} \qquad \text{Eq. 9.35a}$$

$$M_\theta = \nu_\theta M_x \qquad \text{Eq. 9.35b}$$

In these equations, deflection, w, is positive when inward, the edge forces Q_o and M_o are positive when directed as shown in Fig. 9-13, and the dimension, x, is positive as shown in the same Figure. The functions of βx in the brackets are shell functions that are defined as:

$$\phi(\beta x) = e^{-\beta x}(\cos \beta x + \sin \beta x) \qquad \text{Eq. 9.36a}$$

$$\psi(\beta x) = e^{-\beta x}(\cos \beta x - \sin \beta x) \qquad \text{Eq. 9.36b}$$

$$\theta(\beta x) = e^{-\beta x} \cos \beta x \qquad \text{Eq. 9.36c}$$

$$\tau(\beta x) = e^{-\beta x} \sin \beta x \qquad \text{Eq. 9.36d}$$

These functions are plotted in Fig. 9-14 for the range of βx of practical interest. See (9.7) for more precise function values for βx, varying in 0.1 intervals from 0 to 7.0.

Eqs. 9.31 to 9.34 apply to shells that have sufficient length to make the effects of edge discontinuities at each end essentially independent. This will be the case when the shell length, $L > 3/\beta$.

For ribbed shells, the axial stiffness per unit width, $\bar{A}_0$, and the flexural stiffness per unit width, D_x, needed in Eqs. 9.30 to 9.35 may be obtained by "smearing out" (i.e. averaging over rib spacing) the respective circumferential axial and longitudinal flexural stiffnesses. The "smeared out" circumferential axial stiffness is the circumferential rib axial stiffness divided by the longitudinal spacing of these ribs. The "smeared out" longitudinal flexural stiffness is the longitudinal rib flexural stiffness divided by the circumferential spacing of these ribs.

For sandwich shells, the axial stiffness per unit width, $\bar{A}_0$, and the flexural stiffness per unit width, D_x, needed in Eqs. 9.30 to 9.35, may be obtained from the Eqs. 8.5 and 8.12 for stiffness of sandwich sections given in Table 8-1.

As is evident by inspecting Eqs. 9.31 to 9.34 for effects of a unit edge moment and shear, the variation with (βx) of deflection, w, slope, dw/dx, moment, M_x, and shear, Q_x, is the same as the variation in the appropriate functions that are plotted in Fig. 9.14. These plots illustrate how the effects of edge disturbances damp out within a distance of about $x = 3/\beta$.

The maximum moment caused by an edge shear, Q_o is:

$$\text{max. } M_x = \frac{0.323\, Q_o}{\beta} \qquad \text{Eq. 9.37}$$

$$\text{This occurs at: } x \approx \frac{0.8}{\beta} \qquad \text{Eq. 9.38}$$

The above equations are used in Example 9-5 to show that the following edge bending effects occur in a "hinged edge" cylinder subject to uniform internal pressure, q, (Fig. 9-15a):

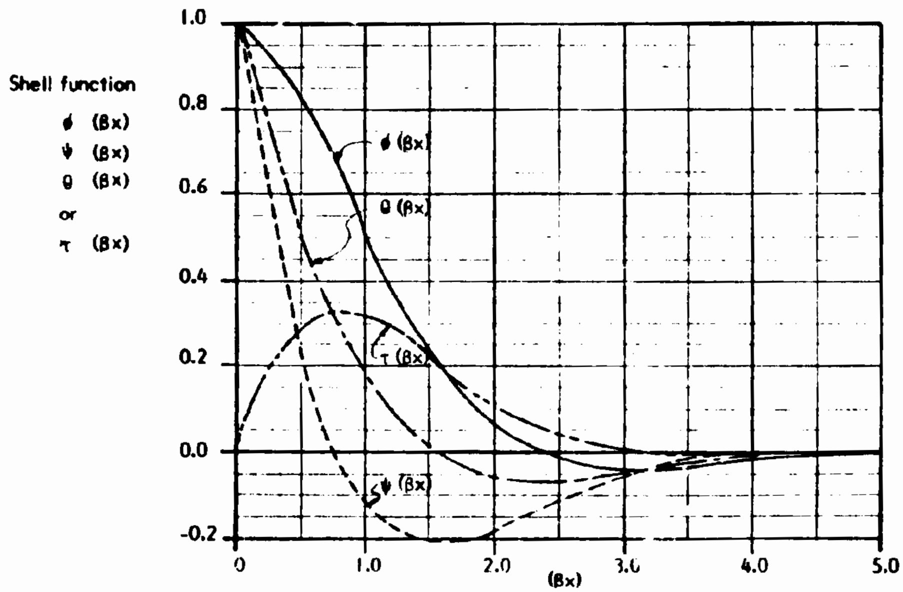

Fig. 9-14 SHELL FUNCTIONS FOR EDGE BENDING IN LONG CYLINDERS

Edge Shear: $$Q_o = \frac{-q}{2\beta} \qquad \text{Eq. 9.39}$$

Maximum Moment: $$M_x = \frac{-0.162\,q}{\beta^2} \qquad \text{Eq. 9.40}$$

The maximum shear and moment in a cylinder with rotationally fixed edges subject to internal pressure occur at the edge and are (Fig. 9-15b):

Edge Shear: $$Q_o = \frac{-q}{\beta} \qquad \text{Eq. 9.41}$$

Edge Moment: $$M_o = \frac{q}{2\beta^2} \qquad \text{Eq. 9.42}$$

The maximum shear and moment due to a radially directed concentrated line load per unit of circumference, P, around a long cylinder are (Fig. 9-15c):

Example 9-5: Determine the maximum axi-symmetric radial shear and moment stress resultants in a long cylindrical shell with a "hinged" edge (i.e., free to rotate but radial deflection prevented) subject to uniform internal pressure, q (Fig. 9-15a).

1. Radial shear at the hinged edge:

1.1 Because edge, $x = 0$, is "hinged", $M_o = 0$ and the final radial deflection, $w = 0$.

1.2 Consider that the final radial edge deflection is obtained by superimposing the radial deflection in a "free" edged tube produced by the internal pressure (membrane deflection) and the radial deflection at $x = 0$ produced by the axi-symmetric radial edge force, Q_o.

1.3 Edge deflection produced by q: Eqs. 9.5 and 9.1: $w = \dfrac{N_\theta R}{E_\theta t} = \dfrac{q R^2}{E_\theta t}$

1.4 Edge deflection produced by Q_o:

Eq. 9.31 with $M_o = 0$, $x = 0$, $(\beta x) = 0$: $w = \dfrac{-1}{2 \beta^3 D_x} \left[Q_o \, \theta(\beta x) \right]$

Fig. 9-14: $\theta(\beta x) = 1.0$ at $(\beta x) = 0$;

1.5 Equate edge deflections in 1.3 and 1.4:

$$\frac{q R^2}{E_\theta t} = -\frac{Q_o}{2 \beta^3 D_x}; \quad Q_o = -\frac{2 \beta^3 D_x q R^2}{E_\theta t}$$

Eq. 9.28: $E_\theta t = \bar{A}_\theta$; and Eq. 9.30 a: $\dfrac{2 D_x R^2}{\bar{A}_\theta} = \dfrac{1}{2 \beta^4}$; $Q_o = -\dfrac{q}{2 \beta}$

2. Maximum moment:

2.1 Only the edge load produces longitudinal moment, M_x.

2.2 M_x is obtained using Eq. 9.33 with $M_o = 0$ for a hinged edge. Thus:

$$M_x = \frac{Q_o \, \tau(\beta x)}{\beta} = -\frac{q \, \tau(\beta x)}{2 \beta^2}$$

2.2 Moment varies with the shell function $\tau(\beta x)$, as shown in Fig. 9-14. The maximum moment occurs at a point where $\beta x = 0.8$ and $\tau(\beta x) = 0.32$

Thus: $\max M_x = -\dfrac{q \times 0.32}{2 \beta^2} = -\dfrac{0.16 q}{\beta^2}$ at $x = \dfrac{0.8}{\beta}$

$$Q_a = \frac{-P}{2} \qquad \text{Eq. 9.43}$$

$$M_a = \frac{P}{4\beta} \qquad \text{Eq. 9.44}$$

where Q_a and M_a are the shear and bending stress resultants at the point of load application.

Discontinuity bending stresses that arise when a pressure pipe wall is thickened at a joint are calculated in **Example 9-6**. The pressure pipe designed in **Example 9-1** and an idealized joint configuration are used in this simplified example.

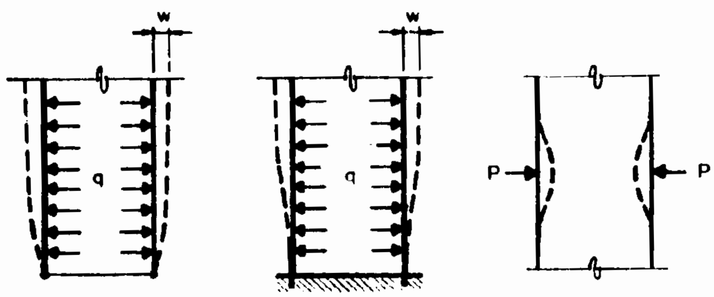

(a.) Hinged edge

(b.) Rotationally fixed edge

(c.) Radially Applied ring load

Note: Above zone of edge restraint, w is membrane deflection.

Fig. 9-15 AXI-SYMMETRIC "DISCONTINUITY" CONDITIONS IN LONG CYLINDERS

Short Cylinder

Edge-bending effects on the circumferential edges of a cylindrical shell which cannot be considered "long" are also treated in (9.7). For the special case of equal edge shears, Q_o and edge moments, M_o on each end of the "short" cylinder (Fig 9-16a), the radial deflections and slopes at the edge are given by the following equations (9.7):

$$w_o = -\frac{1}{2\beta^3 D_x}(\beta M_o \chi_2 + Q_o \chi_1) \qquad \text{Eq. 9.45}$$

$$\left(\frac{dw}{dx}\right)_o = -\frac{1}{2\beta^2 D_x}(2\beta M_o \chi_3 + Q_o \chi_2) \qquad \text{Eq. 9.46}$$

Example 9-6: Estimate the maximum longitudinal discontinuity stress that results from the use of a thickened wall at a bell joint for the pressure pipe designed in Example 9-1. Use the following idealized edge thickening and assume that a "hinged" edge condition occurs at the bell end of the pipe. See Example 9-1 for material properties.*

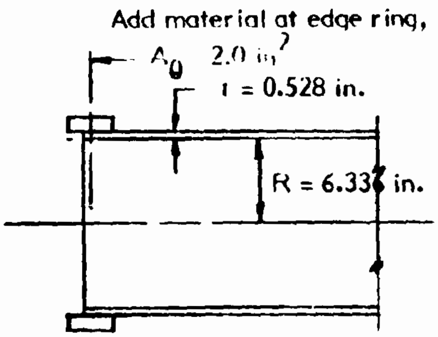

1. Shell parameter, β:

Eq. 9.30b: $\beta = \left[\dfrac{3(1-\nu_x\nu_\theta)E_\theta}{R^2 t^2 E_x}\right]^{1/4}$

$E_\theta = E_x = E = 400{,}000$ psi; $\nu_x = \nu_\theta = 0.38$

$$\beta = \left[\frac{3(1-0.38^2)}{(6.336)^2 \times (0.528)^2}\right]^{1/4} = 0.692; \; \beta^2 = 0.479$$

2. Membrane deflection: Eqs. 9.5 & 9.1: $w = \dfrac{qR^2}{Et} = \dfrac{-130 \times 6.336^2}{E \times 0.528}$; $E\,w = -9{,}884$

3. Unknown edge load, Q_o, acts on edge of pipe shell and on ring:

3.1 Deflection of shell edge due to Q_o, ($M_o = 0$ because of hinge assumption):

Eq. 9.31: $w_o = -\dfrac{Q_o}{2\beta^3 D_x}$;

Eq. 9.29: $D_x = \dfrac{E t^3}{12(1-\nu^2)} = \dfrac{0.528^3 \, E}{12(1-.38^2)} = -0.0143\,E$

$$E\,w_o = -\frac{Q_o}{2 \times (0.692)^3 \times 0.0143} = -105.5\,Q_o$$

3.2 Deflection of extra ring reinforcement:

Eqs. 9.4 & 9.1: $w_o = \dfrac{Q_o R^2}{E A_\theta}$; $E\,w_o = \dfrac{Q_o \times (6.336)^2}{2.0} = 20.1\,Q_o$

4. Equate deflection at edge of pipe (membrane, q, plus bending, Q_o) to deflection of ring reinforcement to obtain Q_o.

$-9884 - 105.2\,Q_o - 20.1\,Q_o = 0$; $Q_o = -\dfrac{9884}{(105.5 + 20.1)} = -78.7$ lbs/in.

<u>Check:</u> Q_o must be less than Q_o for "hinged" edge as given by Eq. 9.39

Hinged edge $Q_o = -\dfrac{q}{2\beta} = -\dfrac{130}{2 \times 0.692} = -93.9$ lbs/in. o.k.

---

* See footnote, Example 9-1, Page 9-13.

Example 9-6 (continued)

5. With a hinged end, maximum moment occurs at $(\beta x) = 0.8$ and is given by Eq. 9.33 with $(\beta x) = 0.32$.

$$x = \frac{0.8}{0.692} = 1.16 \text{ in. from edge; } M_x = \frac{-18.9 \times 0.32}{0.692} = 36.5 \text{ in.-lbs/in.}$$

$$s_x = \frac{1 \times t^2}{6} = \frac{1 \times .528^2}{6} = 0.0465 \text{ in.}^3\text{/in.; } \sigma_x = \frac{M_x}{s_x} = \frac{36.5}{0.0465} = 786 \text{ psi}$$

6. Comment on accuracy of assumptions.

The assumption of a hinged end and ring area concentrated at the edge probably is not very accurate, since the point of maximum discontinuity moment is only 1.16 in. from the edge. A second assumption that the edge rotation is "fixed" by the ring could be made and the resulting maximum moment calculated. These two cases would probably bracket the actual discontinuity bending condition. An upper limit of the moment for the fixed rotation assumption, applicable if the confining ring had infinite radial stiffness, is obtained with Eq. 9.42:

$$\text{max. limit of } M_{xo} = \frac{q}{2\beta^2} = \frac{130}{2 \times (0.692)^2} = 135.7 \text{ in.-lbs/in.}$$

$$\text{max. stress } \sigma_{xo} = \frac{135.7}{0.0465} = 2{,}919 \text{ psi}$$

Because the above solution does not account for the radial and rotational flexibility of the edge ring, the actual maximum longitudinal stress is probably quite a bit lower than the above value.

Note: 1 in. = 25.4 mm, 1 in.^{2} = 645 mm^2, 1 in.^{3}/in. = 645 mm^{33}/mm, 1 lbf/in. = 175 N/m, 1 psi = 0.0069 MPa, 1 in.-lbf/in. = 4.45 N-m/m.

where the terms $\chi_{1,2,3}$ are functions of (βL) as follows:

$$\chi_1 = \frac{\cosh(\beta L) + \cos(\beta L)}{\sinh(\beta L) + \sin(\beta L)}$$

$$\chi_2 = \frac{\sinh(\beta L) - \sin(\beta L)}{\sinh(\beta L) + \sin(\beta L)} \qquad \text{Eqs. 9.47}$$

$$\chi_3 = \frac{\cosh(\beta L) - \cos(\beta L)}{\sinh(\beta L) + \sin(\beta L)}$$

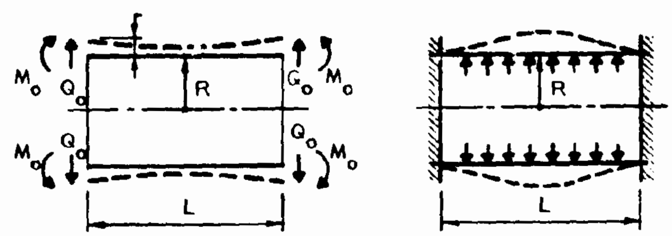

(a.) Axi-symmetric Edge shears and moments

(b.) Built in edges with internal pressure

Fig. 9-16 AXI-SYMMETRIC EDGE EFFECTS IN SHORT CYLINDERS

The functions χ_1, χ_2 and χ_3 are plotted in Fig. 9-17 for the practical range of βL. It is evident that they approach 1.0 when βL > about 3.0, indicating that in such cases, the shell behaves as a "long shell".

Eqs. 9.45 and 9.46 are similar to Eqs. 9.31 and 9.32 with x = 0, modified by the shell functions χ_1, χ_2, or χ_3.

For a short cylindrical shell with built-in edges subject to uniformly distributed load, q, (Fig. 9-16b):

$$M_o = \frac{q\,\chi_2}{2\,\beta^2} \qquad \text{Eq. 9.48}$$

The general solutions for the constants of integration for deformations of short cylindrical shells are given in (9.7), enabling more complete solutions for such problems than can be obtained with the limited equations for edge deformation given above. Also, see (9.9) for extensive tables of coefficients for a variety of edge bending solutions for both long and short cylindrical shells.

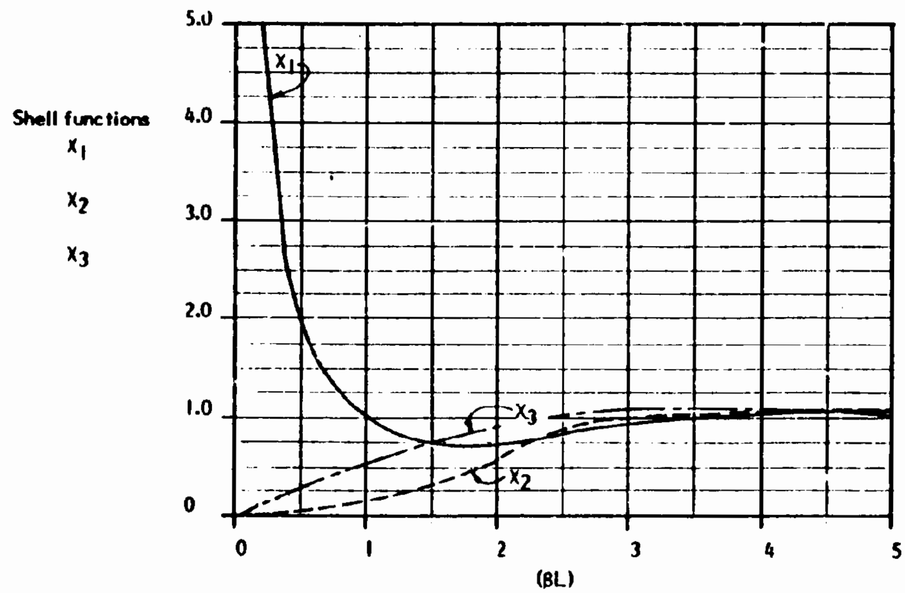

Fig. 9-17 SHELL FUNCTIONS FOR LONGITUDINAL BENDING IN SHORT CYLINDERS

Other Shells of Revolution

Edge-bending effects in many other shells of revolution such as spherical and conical shells are determined approximately by considering their edge region to behave as a tangent cylinder. This is known as the "Geckler" approximation and it has been found to give sufficient accuracy for practical design of most shells of revolution. Exceptions are excessively shallow shells, say spherical or conical shells whose rise is less than 1/12th to 1/15th their span, and shells whose R/t is less than about 50.

Equations are given in Table 9-6 for evaluating edge bending in spherical shells. These equations are derived from Eqs. 9.31 to 9.35 by taking the sphere radius equivalent to the tangent cylinder radius and the meridional direction in the sphere equivalent to the longitudinal direction of the cylinder. Since it is convenient to consider distance from the edge of the sphere in terms of the angular displacement (See Sketch in Table 9-6), $R\psi$ is equivalent to x in the "tangent cylinder" and a new shell constant λ is defined as:

$$\lambda = R\beta = \left[\frac{\bar{A}_0 R^2}{4 D_\phi}\right]^{1/4} \qquad \text{Eq. 9.49}$$

$$\bar{A}_0 = E_0 a_0 \qquad \text{(circumferential direction)} \qquad \text{Eq. 9.50}$$

$$D_\phi = E_\phi i_\phi \qquad \text{(meridional direction)} \qquad \text{Eq. 9.51}$$

Equations are given in the Table for determining the significant edge bending effects in a spherical shell subject to horizontal edge loads, $H_{\phi K}$ and edge moments, $M_{\phi K}$. Usually, $H_{\phi K}$ and $M_{\phi K}$ are determined from the edge forces required in the membrane condition and the equations of deformational compatibility at the edge. This is illustrated in **Example 9-7** for a simple dome with an edge ring having negligible rotational restraint at the edge. Once $H_{\phi K}$ and $M_{\phi K}$ are determined, the remaining equations in the Table may be used to determine the moments and thrusts in the edge region due to the edge loads. These are added to the thrusts determined in a membrane analysis as illustrated in **Example 9-7.**

Similar relations have been developed for other shells of revolution by considering the edge region as a tangent cylinder. In (9.9) extensive tables of formulas and coefficients are presented for determining edge bending effects in cylindrical, spherical and conical shells with a variety of edge conditions.

Torispherical and Ellipsoidal Pressure Vessel Heads

Torispherical shells of revolution are widely used as heads for cylindrical pressure vessels because they provide a smooth transition between the cylinder and the head, while providing a relatively low rise closure. The torispherical shape is comprised of a spherical surface from the crown or apex jointed with a torroidal knuckle shell that is tangent with the spherical surface near the edge with the cylinder at the edge. This geometry is shown in Fig. 9-8(b) in Section 9.3. Ellipsoidal surfaces also can provide a similar smooth transition with the cylinder and have been widely used as pressure vessel heads. General ellipsoid geometry is shown in Fig. 9-6(c) in Section 9.3.

Table 9-6

Edge Deformations, Moments and Thrusts Due to Edge Forces on Spherical Shells

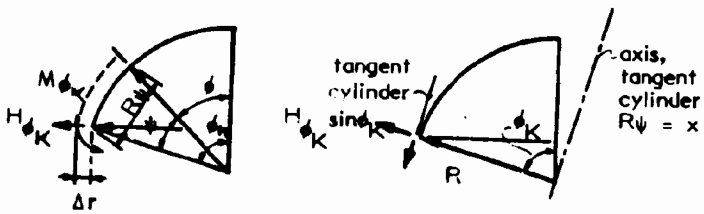

shell constant $\lambda = \left(\frac{\bar{A}_\theta}{4D_\phi} R^2\right)^{1/4} = \left(\frac{E_\theta a_\theta R^2}{4E_\phi i_\phi}\right)^{1/4} = R\beta$

isotropic, uniform t: $\lambda = \left(\frac{3(1-\nu^2)R^2}{t^2}\right)^{1/4}$

	Edge Load, H_{ϕ_K}	Edge Moment, M_{ϕ_K}
Edge radial deformation in base plane, Δr	$\frac{2\lambda R \sin^2\phi_K}{E_\theta a_\theta} H_{\phi_K}$	$\frac{2\lambda^2 \sin\phi_K}{E_\theta a_\theta} M_{\phi_K}$
Edge rotation	$-\frac{2\lambda^2 \sin\phi_K}{E_\theta a_\theta} H_{\phi_K}$	$-\frac{4\lambda^3}{E_\theta a_\theta R} M_{\phi_K}$
Meridional moment, M_ϕ	$\frac{R \sin\phi_K H_{\phi_K}}{\lambda} \frac{\sin(\lambda\psi)}{e^{\lambda\psi}}$	$\sqrt{2} M_{\phi_K} \frac{\sin(\lambda\psi + \frac{\pi}{4})}{e^{\lambda\psi}}$
Maximum meridonal moment, max M_ϕ	$\frac{0.322 R \sin\phi_K H_{\phi_K}}{\lambda}$, at $\lambda\psi = 0.8$	M_{ϕ_K}, at $\lambda\psi = 0$
Meridional thrust, N_ϕ	$\sqrt{2} \sin\phi_K H_{\phi_K} \frac{\cot\phi_K \sin(\lambda\psi - \frac{\pi}{4})}{e^{\lambda\psi}}$	$\frac{-2\lambda \cot\phi_K M_{\phi_K} \sin\lambda\psi}{R \; e^{\lambda\psi}}$
Circumferential thrust, N_θ	$-2\lambda \sin\phi_K H_{\phi_K} \frac{\sin(\lambda\psi - \frac{\pi}{2})}{e^{\lambda\psi}}$	$\frac{-2\sqrt{2}\lambda^2 M_{\phi_K} \sin(\lambda\psi - \frac{\pi}{4})}{R \; e^{\lambda\psi}}$
Circumferential moment, M_θ	$\nu_\theta M_\phi$	$\nu_\theta M_\phi$

Example 9-7: Determine the stress resultants at the edge and at the apex of the spherical shell shown in the sketch *:

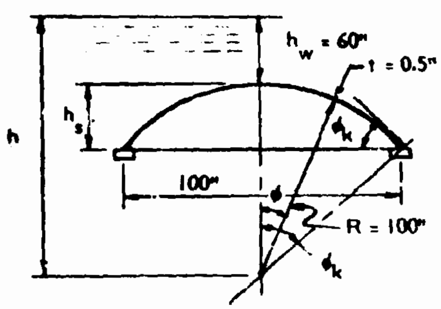

h_w = 60 in.; γ = 64 lbs/ft.^{3} = 0.0370 lbs/in.^{3}

t = 0.5 in.; transparent glass reinforced polycarbonate shell

Ring: Aluminum shape with A = 1.5 in^2 and E = 10 x 10^6 psi; $\bar{A}_0$ = EA = 15 x 10^6 lbs.

Shell: E = 800,000 psi; for long term load, use 0.8E; thus, long term E = 640,000 psi; ν = 0.3

1. Geometry:

$$\sin\phi_k = \frac{50}{100} = 0.5;\ \phi_k = 30^\circ;\ h_s = 100(1-\cos\phi_k) = 13.4 \text{ in.};\ h = R + 60 = 160 \text{ in.}$$

2. Membrane Stress resultants at edge:

2.1 Membrane stress resultants - Table 9-2

First Fluid Load Case: $N_\phi = -\gamma R \left\{\frac{h}{2} - \frac{R}{3}\left[1 + \frac{\cos^2\phi}{(1+\cos\phi)}\right]\right\}$

$$N_\phi = -0.037 \times 100 \left\{\frac{160}{2} - \frac{100}{3}\left[1 + \frac{\cos^2 30}{(1+\cos 30)}\right]\right\} = -123 \text{ lbs/in};\ \sigma_\phi = -\frac{123}{.5} = -246 \text{ psi}$$

$$N_\theta = -\gamma R\left\{\frac{h}{2} - R\cos\phi + \frac{R}{3}\left[1 + \frac{\cos^2\phi}{(1+\cos\phi)}\right]\right\}$$

$$N_\theta = -0.037 \times 100 \left\{\frac{160}{2} - 100\cos 30 + \frac{100}{3}\left[1 + \frac{\cos^2 30}{(1+\cos 30)}\right]\right\} = -148.5 \text{ lbs/in};$$

$$\sigma_\theta = -\frac{148.5}{0.5} = -297 \text{ psi}$$

2.2 Membrane edge displacement of shell.

Edge radial displacement: From Eq. 9.35a

$$\Delta r_m = \frac{N_\theta r_o}{Et};\ E\Delta r_m = \frac{-148.5 \times 50}{0.5} = -14{,}850 \text{ lbs/in; inward}$$

2.3 Radial displacement of ring due to membrane reactions:

$H_m = N_{\phi k}\cos\phi_k$; $\bar{A}_0$ = 15 x 10^6 lbs

Eqs. 9.4 and 9.1: $\Delta r = \dfrac{H_m r_o^2}{\bar{A}_0}$

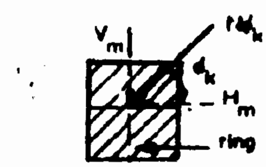

---

* See footnote, Example 9-1, Page 9-13.

Example 9-7 (continued)

$$E_{shell}\,\Delta r = \frac{.64 \times 10^6 \times 123(\cos 30) \times 50^2}{15 \times 10^6} = 11{,}362 \text{ lbs/in.}$$

3. Apply horizontal edge reaction, $H_{\phi k}$, to impose equal deflections on shell and ring.

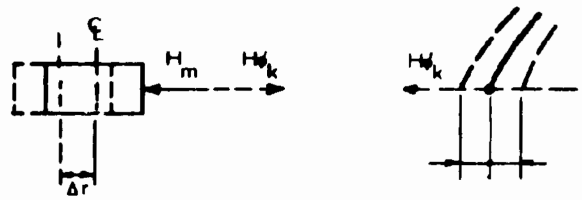

Edge bending analysis, using equations in Table 9-6.

3.1 Shell constants: $\lambda = \left[\dfrac{3(1-\nu^2)R^2}{t^2}\right]^{1/4} = \left[\dfrac{3(1-0.3^2)\,100^2}{0.5^2}\right]^{1/4} = 18.2;\ \phi_k = 30^\circ$

3.2 Edge radial displacement of shell for $H_{\phi k}$: Table 9-6:

$$E\,\Delta r = \frac{2\,\lambda\, R \sin^2\phi_k\, H_{\phi k}}{t} = \frac{2 \times 18.2 \times 100 \times H_{\phi k} \sin^2 30}{0.5} = 1820\, H_{\phi k}$$

3.3 Edge radial displacement of base ring for $H_{\phi k}$:

Eqs. 9.4 and 9.1: $\Delta r = \dfrac{H_{\phi k} r_o^{\,2}}{\bar{A}_0} = \dfrac{H_{\phi k} \times 50^2}{15 \times 10^6}$

$$E_{shell}\,\Delta r = \frac{.64 \times 10^6 \times 2500\, H_{\phi k}}{15 \times 10^6} = 107\, H_{\phi k}$$

3.4 Determine $H_{\phi k}$ by equating shell (membrane + bending) radial edge deflection to ring radial deflection:

$$-14{,}850 + 1820\, H_{\phi k} = 11{,}362 - 107\, H_{\phi k}$$

$$H_{\phi k} = \frac{11{,}362 + 14{,}850}{1820 + 107} = 13.6 \text{ lbs/in}$$

4. Determine maximum bending moment and flexural stress caused by $H_{\phi k}$: Table 9-6:

$$\max M_\phi = \frac{0.322\, R \sin\phi_k\, H_{\phi k}}{\lambda} = \frac{0.322 \times 100(\sin 30) \times 13.6}{18.2} = 12.0 \text{ in.-lbs/in.}$$

$s_\phi = \dfrac{1 \times 0.5^2}{6} = 0.0417 \text{ in}^3;\ \max \sigma_\phi = \dfrac{12.0}{0.0417} = 288$ psi

$\lambda\psi = 0.8;\ \psi = \dfrac{0.8}{18.2} = 0.044$ radians $\times \dfrac{180}{\pi} = 2.52$ deg.; $R\psi = .044 \times 100 = 4.4$ inches from edge

Max $M_\theta = \nu M_\phi = 0.3 \times 12.0 = 3.6$ in-lbs/in. at the same location as for max. M_ϕ

Example 9-7 (continued)

5. Maximum combined stress @ ϕ = 30 – 2.5 = 27.5°; ϕ_K = 30°

N_ϕ: membrane stress: @ ϕ = 30° is close enough = - 123 lbs/in.

edge bending - Table 9-6: @ ϕ = 27.5°, ψ = 2.5°

$$N_\phi = \sqrt{2}\ (\sin 30) \times 13.6\ \frac{\cot 27.5 \sin(.8 - \frac{\pi}{4})}{e^{0.8}} = 0.1 \text{ lbs/in. negligible}$$

$$\max \sigma_\phi = \frac{-123}{0.5} \pm 288 = -534 \text{ psi, or } +43 \text{ psi}$$

N_θ: membrane stress @ ϕ = 30° is close enough = -148.5 lbs/in.

edge bending - Table 9-6:

$$N_\theta = -2 \times 18.2 \sin 30^\circ \times 13.6\ \frac{\sin(0.8 - \frac{\pi}{2})}{e^{0.8}} = 77.5 \text{ lbs/in.}$$

$$\sigma_\theta = \frac{-148.5 + 17.5}{.5} \pm \frac{3.6}{0.0417} = -56 \text{ psi or } -228 \text{ psi}$$

6. Compute N_θ at support, ϕ = 30°, and check radial displacement of shell against radial displacement of ring.

Table 9-6, for $\lambda\psi$ = 0, for edge bending:

$$N_\theta = -2 \times 18.2 \sin 30 \times 13.6\ \frac{\sin(-\pi/2)}{e^{0}} = +247.5 \text{ lbs/in}$$

$$\text{Net } N_\theta = -148.5 + 247.5 = 99. \text{ lbs/in}$$

shell: $$\Delta r = \frac{99 \times 50}{640{,}000 \times 0.5} = 0.0155 \text{ in.}$$

ring: $$H = H_m - H_{\phi k} = (123 \cos 30 - 13.6) = 92.9 \text{ lbs/in}$$

$$\Delta r = \frac{92.9 \times 50^2}{10{,}000{,}000 \times 1.5} = 0.0155 \text{ in. o.k.}$$

ring thrust, $T_\theta = Hr_o$ = 92.9 x 50 = 4,645 lbs, tension; σ_θ = 4645/1.5 = 3,097 psi

7. Membrane stress resultants at apex; Table 9-2:

$$N_\phi = -0.037 \times 100 \left\{\frac{160}{2} - \frac{100}{3}\left[1 + \frac{\cos^2 0}{(1 + \cos 0)}\right]\right\} = -111 \text{ lbs/in} < N_\phi \text{ at edge}$$

$$N_\theta = -0.037 \times 100 \left\{\frac{160}{2} - 100 \cos 0 + \frac{100}{3}\left[1 + \frac{\cos 0}{(1 + \cos 0)}\right]\right\} = -111 \text{ lbs/in.}$$

Check: Because of symmetry, apex stress resultants must be the same as for the uniform pressure case:

$$N_\phi = N_\theta = -p R/2 = -0.037 \times 60 \times 100/2 = -111 \text{ lbs/in.} \quad \text{o.k.}$$

Note: 1 in. = 25.4 mm, 1 in.^{2} = 645 mm^2, 1 in.^{3} = 16387 mm^3, 1 lbf = 4.45 N, 1 lbf/in. = 175 N/m, 1 lb/in.^{3} = 271000 N/m^3, 1 lbf/ft^3 = 157 N/m^3, 1 psi = 0.0069 MPa, 1 in-lb/in. = 4.45 N-m/m.

Practical elastic shell analysis solutions for bending and membrane stress resultants in torispherical and ellipsoidal heads did not become available until they could be obtained with finite difference or finite element computer analysis in the late 1960's. The results of extensive parametric studies that provide elastic and membrane stress resultants for torispherical and ellipsoidal heads with various angles ϕ_o, ratios of cylinder diameter to thickness R_c/t, and ratios of sphere radius to thickness, R_s/t are presented in a paper, "Elastic Stresses in Pressure Vessel Heads" by Kraus (reprinted from Welding Research Council Bulletin 129, 1968 in Vol 2. of (9.17)). The plots are too extensive to repeat here, but are very useful for the analysis of torispherical and ellipsoidal heads that can be designed based on isotropic elastic shell analysis. When such approximations are not appropriate, computer analyses for specific cases may be performed using a finite difference or finite element program such as one of those discussed in Section 4.9. See also (9.35) for design formulas for maximum stress in the toroispherical head shell in a pressure vessel.

Tanks and Silos

In (9.36) extensive tables of coefficients for determining edge bending effects in cylindrical tanks and silos with either uniform or tapered walls are presented. A method of determining edge effects in flat bottom tanks and pressure vessels having a toroidal knuckle shell at the base is presented in Section 9.7 which follows. "Lift-up" of the bottom edge is also considered.

Barrel Shells

When cylindrical shells, such as barrel vaults (Fig. 4-3), have longitudinal edges, edge bending effects often extend throughout the entire shell, particularly if the opening angle of a transverse cross section is less than about 120 degrees. These transverse bending effects from disturbances on longitudinal edges have been extensively treated in the literature, but their exact determination involves solutions of differential equations. Because these solutions cannot be formulated in concise explicit equations, they are not presented here. Practically, stress resultants in cylindrical barrel shells are determined using tables of shell coefficients, based on solution of the differential equations for edge loadings, and presented in (9.6), or they are determined with computer analyses. Also, an approximation known as the "beam-arch" analogy (9.18) is sometimes useful.

See (9.12) for a concise explanation of the differential equations for edge disturbances in cylindrical barrel shells, as well as an excellent discussion of several different approximations used in solving the differential equations, and a detailed consideration of the approximations involved in using the "beam-arch" analogy.

Hypars

Edge-bending stress resultants arise in hypar shells whenever edge support deformations differ from those required by the membrane theory. Behavior is much more complex to define mathematically than in the case of axi-symmetric deformations of shells of revolution. Solutions for edge bending stress resultants are given in Table 9-7 for several cases of idealized edge support conditions which are discussed in (9.11). In most actual hypar structures, the edge members will not provide the idealized restraints used in the solutions given in the Table. Very often this will result in larger bending effects, particularly in hypars with low values of λ, but simplified solutions are not available for quantitative estimates of the amplified bending stress resultants. Cases where stress resultants differ markedly throughout the shell from the stress resultants obtained with the membrane theory are discussed in (9.32)(9.33)(9.34).

Hypar shells comprised of one or more layers of corrugated sheet have also been developed and analyzed (9.37). When a single corrugated sheet is used, substantial bending moments arise in the direction of the corrugations, but some of the benefits of in-plane shear resistance, typical of smooth hypar shells are also derived in the corrugated hypar (9.37).

If, in the designer's judgement, bending stresses may be significant in particular hypar shell structures, these stresses may be determined using finite element computer analyses. These are available in several general structural analysis programs as described in Section 4.9. See also (9.32). Program improvements and simplifications undoubtedly will continue to occur, making such approaches even more practical and cost effective in the future.

Table 9-7

Maximum Moments and Forces at Edges of Hypar Shells (9.11)

Condition	Maximum Negative M At Center of Edge	Maximum Positive M Opposite Center of Edge		Maximum Reaction Perpendicular to Edge Beam
	M_y	M_y	Location y, out from edge	R_y
Edges at y = 0 supported to fully restrain translation and rotation in all directions	$-\frac{0.511\, p_s a^2}{\lambda^{4/3}}$	$\frac{0.1[illegible]\, p_s a^2}{\lambda^{4/3}}$	$\frac{0.85a}{\lambda^{1/3}}$	$\frac{3\, p_s a}{\lambda}$
Edges at y = 0 supported to fully restrain translation in all directions, hinged perpendicular to edge	0	$\frac{0.149\, p_s a^2}{[illegible]}$	$\frac{0.55a}{\lambda^{1/3}}$	$\frac{3\, p_s a}{\lambda^3}$

Notes:

1. $\lambda = \frac{c}{t}$, edge bending parameter. See Fig. 9-11a for c.
2. Equations were developed for isotropic, equilateral 90° hypar, of uniform thickness, as shown in Fig. 9-11a for a = b.
3. If hypar is rectangular, with plan dimension a and b, use dimensions a for effects along edge a and dimensions b for effects along edge b. In this case, calculate λ using a modified value of c determined for an equilateral hypar with sides a, or with sides b, respectively.

Edge and Discontinuity Reinforcement

It should already be evident from the above discussions of edge-bending stress resultants in several of the common types of shells that structural members of adequate strength and stiffness should be provided along edges and around openings in singly and doubly curved shells to develop the inherent strength and structural efficiency of these shells.

In cases where edge members cannot be provided, the shells must be designed to resist substantial bending and transverse shear stress resultants. Edge regions may have to be designed as curved beams or arches, with greatly increased requirements for strength and stiffness compared to membrane shells. Bending effects may penetrate significant distances into the shell from the edges which will increase with increasing radii of curvature (i.e., with increasing flatness).

Also to be avoided in efficient application of thin shell structures are sharp discontinuities in load or shell stiffness. For example, concentrated loads cause localized bending. These effects are covered later in Section 9.8. Increases in thickness at joints in pressure pipe often cause significant bending stress as illustrated in Example 9-6. Restraints at flanges and connections between pipe and pressure vessels cause similar effects.

Summary

Many failures of plastic shell structures have occurred because so called secondary bending stresses at edges or other discontinuities were not taken into account in the design. Because most reinforced plastic materials behave elastically up to failure instead of yielding in a ductile manner like metals, it is essential that designs, for plastic shells be based on accurate, or conservatively approximate, determinations of both membrane and "discontinuity bending" stress resultants. The methods given in this Section and the previous Section will enable the designer to determine these stress resultants with sufficient accuracy for many common shell types. In more complex cases, computer analyses or prototype test programs may be required to achieve the necessary accurate determination of maximum stresses.

Examples given in Sections 9.12 and 9.13 illustrate the application of the above-described analyses to some shell problems representative of actual structural design practice.

9.7 SPECIAL EDGE CONDITIONS – CYLINDRICAL VESSELS WITH FLAT BOTTOMS AND KNUCKLES

Two problems that are of frequent concern to tank and pressure vessel designers are determination of edge bending effects at the base of vessels with flat, uniformly supported bottom plates, and determination of bending and hoop stresses in toroidal knuckle fillets located at the junction of walls with bottoms or covers. These conditions are shown in Fig. 9-18 for a cylindrical fluid storage vessel having a vertical axis and a flat, unyielding base support such as a concrete slab.

Sketch "a" in the Figure shows the first case, a 90 degree junction between the wall and a flat base. Sketch "b" shows a typical condition where the base limits membrane radial deflection at the bottom of the wall and also partially restrains wall rotation at this point. This rotational restraint produces an edge moment that, in turn, causes a short length, L_e, at the edge of the base to "lift off" its foundation, as shown in Sketch "b".

Sketch "c" in the Figure shows the second case, a knuckle junction between wall and base in a cylindrical tank with fluid contents, but no overpressure to cause uplift tension on the cylinder wall. In this case, the knuckle partially restrains the membrane radial deflection and rotation at the bottom of the wall. This produces radial bending, and both radial and circumferential axial stress resultants in the knuckle. Again, the flat base limits radial deflection of the inside of the knuckle and also partially restrains rotation at this point, resulting in the type of base edge deformation and "lift off" shown in Sketch "b".

Sketch "d" shows another bottom knuckle and base "lift off" condition that occurs in closed tanks with internal gas pressure and without external "hold-down" connections to the base slab. In this case, the overpressure causes uplift forces on the wall, and the edge of the base lifts off until the total downward force due to pressure on the knuckle and base edge equals the total upward force on the upper end of the knuckle due to pressure on the closed cover. This type of behavior usually produces large radial bending stresses and circumferential direct compression stresses which rapidly increase with increases in internal pressure, a very undesirable type of structural behavior. The rapid non-linear increase in edge bending occurs because of the increase in "lift off" length as internal pressure increases. In view of this, cylindrical vessels with closed tops, flat bottoms, and internal pressure should normally be designed with "hold-down" connections directly to a substantial base structure. The thin flat bottom plate should not be used to develop the "hold-down" resistance of the bottom pressure.

Vertical Cylinder Base with Flat Bottom:

This base joint condition is shown in Fig. 9-18, "a" and "b", for an open top cylindrical tank with internal fluid pressure. A portion of bottom plate, L_e, lifts off the base due to edge rotation. This length is determined from the laws of static equilibrium and the inside boundary requirement that in regions beyond the "lift off" length, the bottom plate must be flat (i.e.: without curvature). A state of zero moment and zero shear must exist whenever the curvature and the change in the curvature of a structural member are zero (9.20).

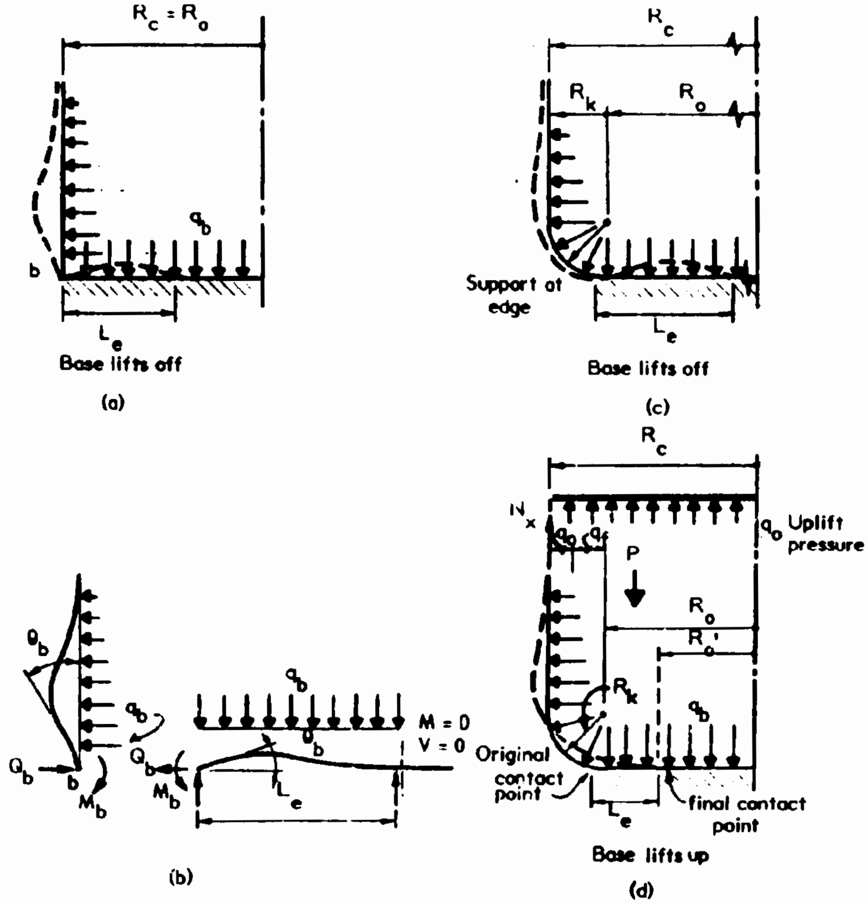

Fig. 9-18 BASE JOINT BEHAVIOR IN VERTICAL CYLINDER

If the lifted off length in the edge region is small compared to the radius of the bottom plate (the usual case), the bottom plate may be assumed to behave as a series of rectangular strips whose lengths extend in a radial direction. In this case, referring again to Fig. 9-18(b), the following relationships between the lifted off length, L_e, the base rotation, θ_b, and the edge moment are derived in **Example 9-8:**

$$M_b = \frac{q_b L_e^2}{4} ; \quad L_e = 2 \left(\frac{M_b}{q_b}\right)^{0.5} \qquad \text{Eq. 9.52}$$

$$\theta_b = \frac{M_b^{1.5}}{3 D_r (q_b)^{0.5}} \qquad \text{Eq. 9.53}$$

The radial deflection of the flat bottom plate due to a radial base reaction per unit of circumferential length, Q_b, is:

$$w_b = \frac{Q_b R_o (1 - \nu)}{E_b t_b} \qquad \text{Eq. 9.54}$$

The deflection and rotation of the cylindrical shell wall were discusssed in the previous Section. The membrane deflection and rotation at the bottom edge of the cylinder are obtained as follows:

$$N_\theta = q_b R_c \qquad \text{Eq. 9.55}$$

$$w_{bm} = \frac{N_\theta R_c}{\bar{A}_\theta} = \frac{q_b R_c^2}{\bar{A}_\theta} \qquad \text{Eq. 9.56}$$

For hydrostatic pressure varying from 0 at the top of the tank to $q_b = \gamma h$ at the bottom, on a tank of uniform wall thickness:

$$\theta_{bm} = \frac{w_{bm}}{h} = \frac{\gamma R_c^2}{\bar{A}_\theta} \qquad \text{Eq. 9.57}$$

The deflection and rotation of the bottom edge of the cylinder due to radial shear Q_b and moment M_b are given by Eqs. 9.31 and 9.32, with $\beta x = 0$.

The moment, M_b, and shear, Q_b, at the wall bottom are determined by equating the membrane and Q_b and M_b edge loading deflections and rotations of the cylindrical wall bottom to the Q_b edge deflection and the M_b edge rotation of the bottom plate. This requires solution of two simultaneous equations for compatible deflections and rotations at the junction of base and wall:

w_b wall cylinder $=$ w_b bottom plate

Q_b wall cylinder $=$ Q_b bottom plate edge region

In most practical vessels, the radial deflection at the junction of shell with bottom plate is very small and may be taken as zero. This occurs because the deflection, w_b, given by Eq. 9.54 is usually too small to have a significant effect on edge bending in the adjacent cylinder. Also friction between the loaded bottom plate and the base support provides a further reduction of radial deflection at the edge. If w_b is assumed equal to zero, the effect of restraint at the base of a vessel of uniform wall thickness containing a fluid with a unit weight of γ may be determined using the following approximate equation:

$$\frac{\gamma R_c^{\,2}\,(\beta h - 1)}{A_\theta} - \frac{M_b}{2\beta D_x} = \frac{M_b^{\,1.5}}{3\,D_r\,(\gamma h)^{\,0.5}} \qquad \text{Eq. 9.58}$$

This equation is derived in the third and fourth Sections in **Example 9-8.** It is most readily solved by a trial solution procedure. It can also be used as a reasonable approximation for vessels with non-uniform wall thickness if the cylinder wall in the base region is approximately uniform over a height of at least $3/\beta$ above the base, and if the bottom plate thickness is reasonably uniform over a distance, L_e, (Eq. 9.52) in from the base junction.

In order to determine stress resultants in the cylinder caused by base restraint, the edge shear, Q_b, must also be calculated as follows:

$$Q_b = -\frac{(\gamma h)}{2\,\beta} - \beta M_b \qquad \text{Eq. 9.59}$$

This equation is also derived in **Example 9-8.**

The longitudinal bending moment at any point in the cylindrical shell may readily be determined using Eq. 9.33 with $Q_o = -Q_b$ and $M_o = M_b$, together with the shell functions plotted in Fig. 9-14. The maximum moment will either be at the base (M_b) or at the point above the base where Q_x (Eq. 9.34) is zero.

The maximum circumferential bending moment is:

$$M_\theta = \nu_\theta M_x \qquad \text{Eq. 9.60}$$

Example 9-8: Determine the base moment that results from restraint of membrane displacements in a cylindrical pressure vessel with a vertical axis and flat bottom. Account for lifting of the bottom away from a flat foundation that supports downward load only (i.e., give the derivations of Eqs. 9.52, 9.53, 9.58 and 9.59).

1. End slope (rotation) of bottom plate:

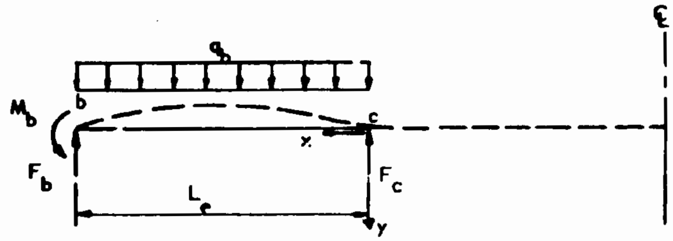

1.1 Assume that the edge of the flat bottom behaves as a series of flat strips of unit width (circumferentially) subject to an end moment, M_b, as shown in the sketch.

1.2 Boundary Conditions: at b: $y = 0$, $M = M_b$

at c: $y = 0$; slope, $\frac{dy}{dx} = 0$; $M = 0$

1.3 Equations of Statics:

$$\Sigma M_b = 0;\ M_b = \frac{q_b L_e^2}{2} - F_c L_e;\ F_c = \frac{q_b L_e}{2} - \frac{M_b}{L_e}$$

$$\Sigma F_y = 0;\ F_b = q_b L_e - F_c = \frac{q_b L_e}{2} + \frac{M_b}{L_e}$$

1.4 Equations of Beam Theory:

$$M_x = D_r \frac{d^2 y}{d x^2} = F_c x - \frac{q_b x^2}{2} = \left(\frac{q_b L_e}{2} - \frac{M_b}{L_e}\right) x - \frac{q_b x^2}{2}$$

$$D_r \frac{dy}{dx} = \left(\frac{q_b L_e}{2} - \frac{M_b}{L_e}\right) \frac{x^2}{2} - \frac{q_b x^3}{6} + C_1$$

at $x = 0$, $\frac{dy}{dx} = 0$; thus: $C_1 = 0$

$$D_r y = \left(\frac{q_b L_e}{2} - \frac{M_b}{L_e}\right) \frac{x^3}{6} - \frac{q_b x^4}{24} + C_2$$

at $x = 0$, $y = 0$; thus: $C_2 = 0$

at $x = L_e$, $y = 0$; thus: $0 = \left(\frac{q_b L_e}{2} - \frac{M_b}{L_e}\right) \frac{L_e^3}{6} - \frac{q_b L_e^4}{24}$; $\frac{M_b}{6} = \frac{q_b L_e^2}{24}$

Example 9-8 (continued)

1.5 Solution for Edge Moment and Rotation:

$$M_b = \frac{q_b L_e^2}{4} \text{ ; This is Eq. 9.52; solving for } L_e = 2\sqrt{\frac{M_b}{q_b}}$$

$$\text{at } x = L_e,\ D_r \frac{dy}{dx} = D_r \theta_b$$

$$D_r \theta_b = \left(\frac{q_b L_e}{2} - \frac{M_b}{L_e}\right)\frac{L_e^2}{2} - \frac{q_b L_e^3}{6} = \frac{q_b L_e^3}{12} - \frac{M_b L_e}{2};$$

$$\text{Substitute } M_b = \frac{q_b L_e^2}{4} \text{ ; } D_r \theta_b = \frac{M_b L_e}{3} - \frac{M_b L_e}{2} = -\frac{M_b L_e}{6}$$

$$\text{Substitute } L_e = 2\sqrt{\frac{M_b}{q_b}};\ D_r \theta_b = -\frac{M_b^{1.5}}{3\,(q_b)^{0.5}} \text{ ; This is Eq. 9.53}$$

2. Edge Deflection of bottom plate:

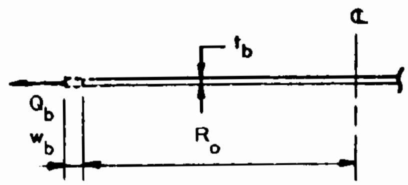

For a disk under radial load:

$$w_b = \frac{Q_b R_o (1 - \nu)}{E_b t_b} =$$ negligible compared to edge deflection of cylinder for most practical cases

w_b will be assumed = 0 to simplify the following derivation.

3. Bottom slope (rotation) of cylinderical shell due to fluid pressure and base moment for zero radial deflection:

3.1

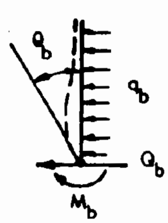

If, as in step 2, the radial deflection of the bottom plate is assumed = 0, the edge forces on the cylinder, Q_b and M_b, are related to each other by equating their radial deflection at b (Eq. 9.31) to the radial deflection produced by the applied pressure, q_b, on the free shell (Eq. 9.35 with N_θ = membrane hoop stress resultant at b).

Using Eq. 9.31 at $\beta x = 0$, $\psi(\beta x) = \theta(\beta x) = 1.0$ and Eq. 9.35:

$$w = -\frac{M_b}{2\beta^2 D_x} - \frac{Q_b}{2\beta^3 D_x} - \frac{N_\theta R_c}{\bar{A}_\theta} = 0;\ Q_b = -\frac{2 N_\theta R_c \beta^3 D_x}{\bar{A}_\theta} - \beta M_b$$

For the case of fluid pressure: $N_\theta = (\gamma h) R_c$

$$Q_b = -\frac{2\beta^3 D_x R_c^2 (\gamma h)}{\bar{A}_\theta} - \beta M_b; \text{ and from Eq. 9.30a: } \frac{4 D_x R_c^2}{\bar{A}_\theta} = \frac{1}{\beta^4}$$

Example 9-8 (continued)

$$Q_b = -\frac{(\gamma h)}{2\beta} - \beta M_b; \text{ This is Eq. 9.59}$$

3.2 Slope at base due to M_b and Q_b:

Eq. 9.32 at x = 0, $M_o = M_b$; $Q_o = Q_b$; $\theta(\beta x) = \phi(\beta x) = 1.0$

$$\theta_b = \frac{M_b}{\beta D_x} + \frac{Q_b}{2\beta^2 D_x} = \frac{M_b}{\beta D_x} - \frac{2 N_\theta R_c \beta^3 D_x}{2 \bar{A}_\theta \beta^2 D_x} - \frac{M_b}{2\beta D_x}$$

$$\theta_b = \frac{M_b}{2\beta D_x} - \frac{N_\theta R_c \beta}{\bar{A}_\theta}$$

3.3 Slope at base due to membrane stresses.

If N_θ results from fluid pressure on a tank of uniform wall thickness in the vicinity of the base, membrane stresses cause a base rotation of

$$\theta_{bm} = \frac{w_{bm}}{h} = -\frac{N_\theta R_c}{\bar{A}_\theta h} = -\frac{\gamma R_c^2}{\bar{A}_\theta}$$

If the vessel wall thickness is tapered to maintain a constant stress due to fluid pressure that varies with depth, $\theta_{bm} = 0$. As shown below, θ_{bm} is usually small compared to the slope caused by Q_b and M_b, and is often not included, particularly in vessels having tapering wall thickness in the region above the base.

3.4 Slope at base of cylinder with zero radial deflection:

For fluid pressure: $N_\theta = \gamma R_c h$ at base

Thus, summing 3.2 and 3.3 for fluid pressure on a cylinder with zero radial deflection at the base:

$$\theta_b = \frac{M_b}{2\beta D_x} - \frac{\beta(\gamma h R_c) R_c}{\bar{A}_\theta} + \frac{\gamma R_c^2}{\bar{A}_\theta}$$

$$\theta_b = \frac{M_b}{2\beta D_x} - \frac{\gamma R_c^2 (\beta h - 1)}{\bar{A}_\theta}$$

4. Equate θ_b due to M_b at edge of bottom plate, to θ_b due to M_b, Q_b and membrane stresses at edge of cylinder

$-\theta_b$ cylinder = $-\theta_b$ bottom plate; and $q_b = h$

$$\frac{\gamma R_c^2 (\beta h - 1)}{\bar{A}_\theta} - \frac{M_b}{2\beta D_x} = \frac{M_b^{1.5}}{3(\gamma h)^{0.5}} \text{ : This is Eq. 9.58}$$

If the wall thickness of the cylinder tapers over the length βh above the base, 1 may be dropped from the term $(\beta h - 1)$.

Example 9-9 illustrates the design of a cylindrical fluid storage vessel with vertical axis and a flat bottom. The edge bending effects in this vessel are determined using the equations presented above.

Base Joint with Knuckle

This base condition is shown in Fig. 9-18(c) for an open top cylindrical tank with internal fluid pressure. The knuckle geometry and the internal pressure and edge forces applied on the knuckle shell are shown in Fig. 9-19. A 90 degree knuckle is a quarter segment of a toroidal (donut) shell. Geometry of such shells is described in Section 9.3.

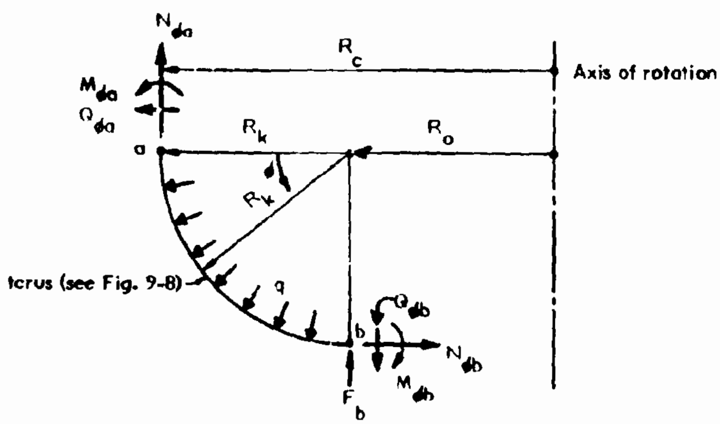

Fig. 9-19 GEOMETRY OF KNUCKLE AND PRESSURES AND EDGE FORCES APPLIED ON KNUCKLE

Membrane stress resultants for toroidal shells are given in Table 9-4. For a complete solution, however, bending effects must also be determined. These generally are significant throughout the entire knuckle.

Relatively simple approximations of the type described in Section 9.6 for determining edge effects in long cylinders, and spherical or conical domes are not applicable to a toroidal knuckle. The sharp curvature of meridional strips and the highly variable stiffness of circumferential strips produce complexities that make the "beam-on-elastic-foundation" analogy too complex for practical application to the toroidal shell segments normally used for tank and pressure vessel knuckles.

Example 9-9: Determine the required shell and bottom thickness of a cylindrical chemical storage tank with a vertical axis and a flat bottom as shown in the Figure.*

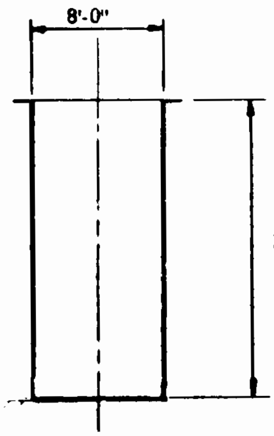

The vessel will be an open top tank and may be filled to the top by a fluid having a maximum specific gravity of 1.4 and a maximum temperature of 120°F. The tank and its contents are supported by uniformly distributed bearing over the flat bottom shell. The tank is to be used in an interior location, and fixed in position by guides at the top stiffening ring that prevents overturning due to any accidental lateral effects.

Use a shell laminate comprised of 0.10 in. chopped strand polyester resin spray-up on the inside (liquid seal) and for the balance of the required thickness a circumferential filament winding tape with polyester resin. In addition, assume that 0.02 in. thick mat reinforced surfacing layers are used on the inside and outside surfaces of the shell. Use a chopped strand polyester resin laminate with 0.02 in. thick interior mat reinforced surfacing layer for the bottom. Assume that the minimum practical thicknesses of the shell and bottom laminates both are 0.20 in. Assume the following strength and stiffness characteristics for the above materials.

Stiffness is characterized with the standard test (short-time) elastic moduli of the filament winding, spray-up liquid seal, and surfacing mat layers in tension for the circumferential direction and in flexure for the determination of longitudinal (vertical) and bottom shell discontinuity effects.

Assume the following values for these moduli:

1. Cylinder Shell (Orthotropic)

Circumferential elastic modulus in tension	$E_\theta = \dfrac{(6.0\, t_{fw} + 0.8\, t_{cs})\, 10^6}{(t_{fw} + t_{cs})}$ where t_{fw} is the thickness of the filament winding and t_{cs} is the thickness of the chopped strand spray-up and mat layers.
Longitudinal elastic modulus in flexure	$E_x = 0.8 \times 10^6$ psi
Poisson's Ratio	$\nu_\theta = 0.38$

---

* See footnote, Example 9-1, Page 9-13.

Example 9-9 (continued)

2. Flat Bottom Shell (Isotropic)

Elastic modulus in flexure for any direction $E_r = E_\theta = 1.0 \times 10^6$ psi

Poisson's Ratio $\nu = 0.3$

Strength under long-term load or repeated load is characterized by limiting the maximum circumferential tension strain to 0.001 and the maximum longitudinal and bottom shell flexural strain to 0.0015, based on the above short time moduli.

1. Membrane stress resultant at bottom

Eq. 9.1: $N_\theta = p\,R = \gamma\, h\, R = 1.4 \times 62.4 \times 26.75 \times \frac{4}{12} = 779$ lbs/in.

2. Trial design of laminate at bottom:

$t_{cs} = 0.10 + 0.02 \times 2 = 0.14$ in. and try $t_{fw} = 0.10$;

$$E_\theta = \frac{(6.0 \times 0.10 + 0.8 \times 0.14) \times 10^6}{0.14 + 0.10} = 3.0 \times 10^6$$

allow $\sigma_\theta = e_{allow}\, E_\theta = 0.001 \times 3.0 \times 10^6 = 3{,}000$ psi

req'd $t = \frac{779}{3000} = 0.26$ in.

Increase t_{fw} to 0.12 in.; $E_\theta = 3.2 \times 10^6$; allow $_\theta = 3{,}200$ psi, allow $N_\theta = 832$ lbs/in.;

$t = 0.26$ in. o.k.

3. Reduce wall thickness higher up the wall to min $t_{fw} = 0.06$ in., with $E_\theta = 2.3 \times 10^6$

allow $N_\theta = 0.20 \times .001 \times 2.3 \times 10^6 = 460$ lbs/in.

reduced $h = \frac{460}{779} \times 26.75 = 15.8$ ft from top

reduce thickness to 0.20 in. by reducing filament winding to 0.06 in. at 15 ft below the top.

4. Investigate vertical bending at base and design bottom thickness. Trial bottom thickness is 0.20 in.

4.1 Shell constant, β:

Eq. 9.30b: $$\beta = \left[\frac{3\,(1 - \nu_x\, \nu_\theta)\, E_\theta}{R^2\, t^2\, E_x}\right]^{1/4}$$

Example 9-9 (continued)

$E_\theta = 3.2 \times 10^6$ psi; $E_x = 0.8 \times 10^6$ psi; $\nu_\theta = 0.38$;

Eq. 6.4d: $\nu_x = \nu_\theta \dfrac{E_x}{E_\theta} = 0.38 \times \dfrac{0.8}{3.2} = 0.10$

$$\beta = \left[\frac{3\,(1 - 0.38 \times 0.10) \times 3.2}{48^2 \times 0.26^2 \times 0.8}\right]^{1/4} = 0.522$$

4.2 Obtain base moment by solving Eq. 9.58

$$\frac{\gamma R_c^{\,2}\,(\beta h - 1)}{\bar{A}_\theta} - \frac{M_b}{2\,\beta\,D_x} = \frac{M_b^{\,1.5}}{3\,D_r\,(\gamma h)^{0.5}}$$

$\bar{A}_\theta = 3.2 \times 10^6 \times 0.26 = 0.83 \times 10^6$; $D_x = \dfrac{0.8 \times 10^6 \times 0.26^3}{12\,(1 - 0.38 \times 0.10)} = 1{,}218$;

$$D_r = \frac{1.0 \times 10^6 \times 0.20^3}{12\,(1 - 0.3^2)} = 733$$

$\gamma = 1.4 \times 62.4/1728 = 0.051$ lbs/in^3; $h = 26.75 \times 12 = 321$ in.; $\gamma h = 16.2$ psi

$$\frac{0.051 \times 48^{\,2}(0.522 \times 321 - 1)}{830{,}000} - \frac{M_b}{2 \times 0.522 \times 1{,}218} = \frac{M_b^{\,1.5}}{3 \times 733 \times (16.2)^{0.5}}$$

$0.0233 - 0.00079\,M_b = .000113\,M_b^{\,1.5}$; $23.3 - 0.79\,M_b = 0.113\,M_b^{\,1.5}$

Cut and Try Solution

Trial M_b	$23.3 - 0.79\,M_b$	$0.113\,M_b^{\,1.5}$
15	11.45	6.56
20	7.50	10.11
18	9.08	8.63
18.3	8.84	8.85

$M_b = 18.3$ **in.-lbs/in. at junction of wall base.**

4.3 Obtain base shear in cylinder from Eq. 9.59.

$$Q_b = -\frac{(\gamma h)}{2} - \beta M_b = -\frac{16.2}{2 \times 0.522} - 0.522 \times 18.3$$

$Q_b = -15.52 - 9.55 = -25.07$ lbs/in.

Example 9-9 (continued)

4.4 Calculate maximum cylinder wall moment above the base:

Eq. 9.34: $Q_x = 2 \times 0.522 \times 18.3\ \tau(\beta x) - (-25.1)\ \psi(\beta x) = 0$ at location of max. wall moment

$19.1\ \tau(\beta x) = -25.1\ \psi(\beta x);\ \tau(\beta x) = -1.31\ \psi(\beta x)$

Fig. 9-14: $(\beta x) = 1.3$

Eq. 9.33: $M_x = \frac{1}{0.522}\left[0.522 \times 18.3\ \phi(1.3) - 25.1\ \tau(1.3)\right]$

Fig. 9-14: $M_x = 18.3 \times 0.34 - 48.1 \times 0.26 = 6.22 - 12.50 = -6.28$ in-lbs/in.

4.5 Calculate stresses:

Wall: $s = \frac{0.26^2}{6} = 0.0113$ in^3/in; Floor: $s = \frac{0.20^2}{6} = 0.00667$ in^3/in.

Wall at base: $\sigma_x = \frac{18.3}{0.0113} = 1{,}619$ psi

Wall at $\beta x = 1.3$; $x = \frac{1.3}{.522} = 2.5$ in.: $\sigma_x = \frac{6.28}{0.0113} = 556$ psi

Wall allowable σ_x $0.8 \times 10^6 \times 0.0015 = 1{,}200$ psi $<$ 1619 psi

Floor at base: $\sigma_r = \frac{25.1}{0.20} \pm \frac{18.3}{0.00667} = 126 \pm 2{,}744 = 2870$ psi max. at joint b.

Floor allowable $\sigma_r = 1.0 \times 10^6 \times 0.0015 = 1{,}500$ psi $<$ 2870 psi

4.6 Calculate lift off length, L_e

Eq. 9.52: $18.3 = \frac{16.2\ L_e^2}{4}$; $L_e = \sqrt{4.52} = 2.13$ in.

5. Conclusion: Increase wall and floor thicknesses very locally at corner intersection.

6. Recommendation: Investigate the use of a knuckle joint to facilitate a more practical detail at this location. See Example 9-10.

Note: 1 in. = 25.4 mm, 1 in.^{3}/in. = 645 mm^3/mm, 1 ft = 0.3048 m, 1 lbf/in. = 175 N/m, 1 psi = 0.0069 MPa, 1 lbf/in.^{3} = 0.27 MN/m^3, 1 in.-lbf/in. = 4.45 N-m/m, ^{o}C = 0.55 (^{o}F-32).

Fortunately, the direct determination of stress resultants in axisymmetric shells using computer analysis based on finite element or finite difference, has become practical and relatively inexpensive. Programs such as BOSOR, and portions of NASTRAN, have been specifically developed to provide efficient analysis and simple input for axisymmetric shells of arbitrary shape. These solutions are easier to implement than an approximate analysis using curved meridional strips restrained by circumferential strips of varying stiffness. The computer programs ANSYS and MARC both have additional capabilities for modeling contact surfaces with interface elements that can transmit compression only. An iterative solution is used to determine which elements finally have a gap status and which elements are in contact.

When the simpler computer programs are used to analyze bottom supported vertical tanks, "lift off" of the bottom plate under applied forces (Fig. 9-18) is not directly considered. However, "lift-off" behavior in vessels subject to rotation at the junction may be analyzed using a two step procedure similiar to the approach suggested earlier in this Section for analyzing the junction of a cylindrical wall with a flat base (Fig. 9-18a). As was done in developing Eq. 9.58, in the first step, the vessel is assumed to have a hinged connection at the junction of knuckle and flat base (Fig. 9-20a). Computer analyses of this structure for the applied loads (Fig. 9-20a) and for a "unit" moment applied along edge b (Fig. 9-20b) provide the edge rotation and stress resultants in the knuckle and cylinder for these loading conditions. The net rotation at b is that due to the applied load on a hinged joint less M_b times the rotation due to a unit restraining moment. In the second step, the net rotation (Fig. 9-20c), of the shell is equated to the edge rotation of the flat bottom plate, as given by Eq. 9.53, as follows:

$$\theta_{bm} - M_b\theta_{bb} = \frac{{M_b}^{1.5}}{3\,D_r\,(q_b)^{0.5}} \qquad \text{Eq. 9.61}$$

This equation is easily solved for M_b. A trial procedure usually provides the most practical solution. The final stress resultants in the shell are those obtained from the computer analysis for the applied loads on the "hinged base" shell plus M_b times those obtained from the computer analysis for the unit base moment at the "hinged base" shell.

Example 9-10 illustrates the investigation of edge bending effects in a base joint with a knuckle for the same vertical cylindrical fluid storage vessel that was designed in **Example 9-9.** It is worth noting that the introduction of the knuckle has not diminished the stresses at the most highly stressed point at the intersection of knuckle and bottom. This is because of the additional bending introduced by the weight of fluid over the knuckle. The knuckle does provide a more practical detail for connecting the base to the wall and does tend to reduce the discontinuity stresses in the lower part of the cylinder wall, compared to the sharply intersecting case.

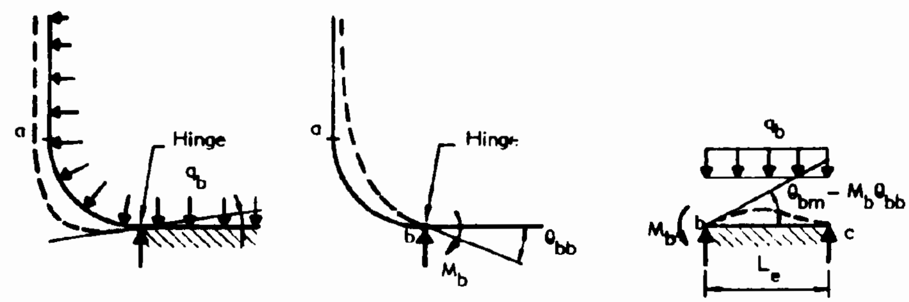

Fig. 9-20 STRUCTURE INDEALIZATION AND LOAD CASES FOR BASE JOINT WITH KNUCKLE

Although the knuckle base arrangement shown in Fig. 9-18(d) involving uplift of the entire knuckle and edge region of the bottom plate without external "hold-down" connections should not be used in practical design, it may be necessary to analyze such a condition for various reasons. This case may be solved by a direct computer analysis of the assembly of axisymmetric cylinder, knuckle and that portion of the bottom plate that lifts off the base. The idealized shell structure is shown in Fig. 9-21. The extent of annular bottom plate to be included in the structure is only the area below the weight of structure, contents and internal pressure that just balances the upward force on the top of the cylinder (See Fig. 9-21). As shown in the Figure, the boundary conditions at the point where the lifted off edge region contacts the base are zero deflection, rotation, moment and shear. These must exist because the bottom plate remains flat and in contact with the rigid base beyond this point.

Example 9-10: Modify the base detail of the tank designed in **Example 9-9,** by introducing a knuckle as shown in the sketch. Assume that the knuckle laminate has the same properties as the bottom laminate of the tank in **Example 9-9.***

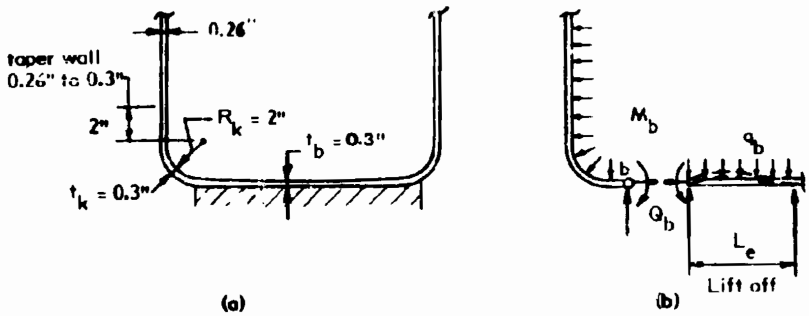

1. Analyze the shell structure with the hinged support shown in sketch (b) for two loading conditions: (1) internal fluid pressure, and (2) unit moment applied at the hinge. This is accomplished using a computerized "finite difference" analysis for axi-symmetric loadings on axi-symmetric shell of revolution. Program name is BOSOR.

2. BOSOR results provide φ_{bm} and φ_{bb} as follows:

   Fluid Pressure loading; $\varphi_{bm} = 4.64 \times 10^{-2}$ rad

   Unit moment at b: $\varphi_{bb} = 8.98 \times 10^{-4}$ rad

3. Solve for M_b using Eq. 9.61. Modify D_R from Example 9-9 for t_b = 0.3". $D_R = (.3^3/.2^3)733 = 2474$

$$4.64 \times 10^{-2} - 8.98 \times 10^{-4}\ M_b = \frac{M_b^{1.5}}{3 \times 2474\sqrt{16.2}}\ ;\ M_b = 41.64 \text{ in/lbs}$$

4. The final stresses in the shell are calculated from the superposition of the results of the fluid pressure loading case plus M_b times the results of the unit moment loading case.

5. Investigate maximum stresses from plots of stress resultants:

5.1 At knuckle region, point b:

   max M_x = 41.64 in-lb/in.; max N_x = 42.88 lb/in. tension

   $s_x = t^2/6 = 0.3^2/6 = 0.015$ in^3/in; $a = t = 0.3$ in^2/in.

---

* See footnote, Example 9-1, Page 9-13.

Example 9-10 (continued)

Allowable bending stress = .0015 x (1 x 10^6) = 1500 psi

Allowable tensile stress = .001 x (1 x 10^6) = 1000 psi

Interaction relation for combined bending and tension stress in x direction:

$$\frac{\frac{41.64}{0.015}}{1500} + \frac{\frac{42.88}{0.3}}{1000} = 1.99 > 1.0 \qquad \text{N.G.}$$

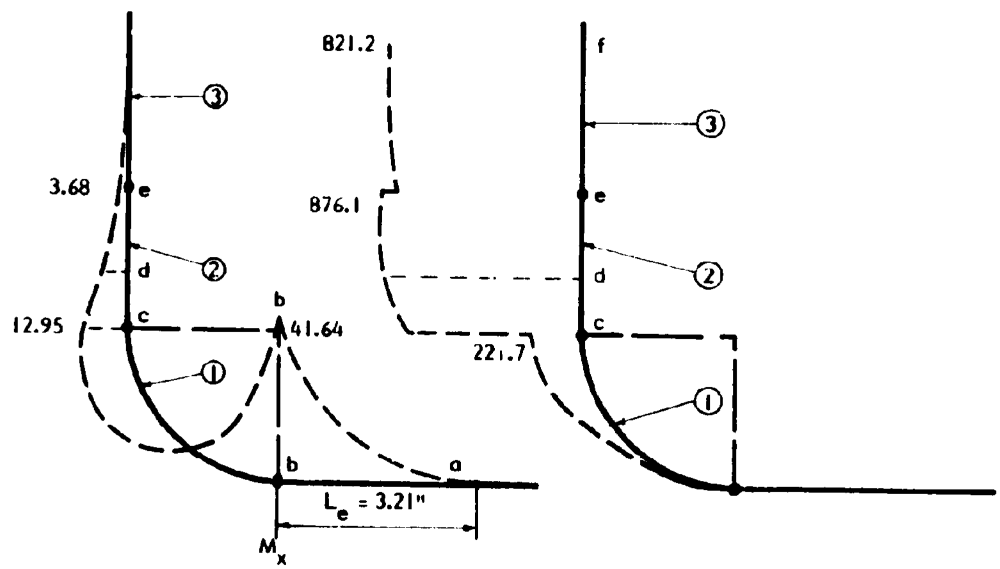

Tension Side

Tensile + N_θ

5.2 At knuckle region, point c: $N_{\theta\, max}$ = 221.7 lb/in.; M_θ = 4.65 in-lb/in.

Interaction relation for combined bending and tension in θ direction:

$$\frac{\frac{4.65}{0.015}}{1500} + \frac{\frac{221.7}{0.3}}{1000} = 0.95 < 1.0 \qquad \text{o.k.}$$

5.3 At tapered wall region, point c: max M_x = 12.95 in.-lb/in.; max N_x = 0.38 lb/in. (neglect); $s_x = 0.3^2/6 = 0.015$ in.^{3}/in.; Allowable bending stress = 0.0015 x (0.8 x 10^6) = 1200 psi

σ_x = 12.95/0.015 = 863 psi < 1200 psi o.k.

5.4 At tapered wall region, point d:

max N_θ = 876.1 lb/in. tension; M_θ = 2.18 in.-lb/in.

Use average thickness, t = 0.28; a = t = 0.28 in.^{2}

Allowable bending stress: 0.0015 (3.4 x 10^6) = 5100 psi

Allowable tensile stress = 0.0010 (3.4 x 10^6) = 3400 psi

Example 9-10 (continued)

Interaction relation for combined bending and tension in θ direction:

$$\frac{\frac{2.18}{0.13}}{5100} + \frac{\frac{876.1}{.28}}{3400} = 0.92 < 1.0 \quad \text{o.k.}$$

5.5 At uniform wall region, point e: max $M_x = 3.68$ in-lb/in; $N_x = 0$

$s_x = .26^2/6 = 0.011 \text{ in}^3/\text{in.}$

Allowable bending stress $= 0.0015\ (0.8 \times 10^6) = 1200$ psi

$$\sigma_x = \frac{3.68}{0.011} = 335 < 1200 \qquad \text{o.k.}$$

5.6 At uniform wall region, point f: max $N_\theta = 821.2$ lbs/in; $M_\theta = 1.04$ in-lbs/in.

$s_x = .26^2/6 = 0.011 \text{ in}^3/\text{in.}$; $a = t = 0.26 \text{ in}^2/\text{in.}$

Allowable bending stress $= 0.0015\ (3.2 \times 10^6) = 4800$ psi

Allowable tensile stress $= 0.0010\ (3.2 \times 10^6) = 3200$ psi

Interaction relation for combined bending and tension in θ direction:

$$\frac{\frac{1.04}{0.011}}{4800} + \frac{\frac{821.2}{0.26}}{3200} = 1.01 \approx 1.0 \qquad \text{o.k.}$$

6. Calculate lift-off length, L_e:

Eq. 9.52: $41.64 = \frac{16.4}{4} L_e^2$; $L_e = \sqrt{10.28} = 3.21$ in.

7. Comments:

7.1 Knuckle substantially increases the theoretical peak bending stress at the junction with base as compared with the flat base in **Example 9-9.** However, knuckle material is overstressed in only a very small region at the junction with the base.

7.2 Peak overstress could be decreased by using a material with a higher stiffness and allowable strength in both directions for the knuckle and the edge of the bottom (such as mat - woven roving), by increasing thickness at junction with bottom, and/or by reducing knuckle radius to the smallest practical size for good quality construction.

7.3 Some theoretical overstress maybe tolerable at the local region at the juction with the base.

7.4 The use of a knuckle, compared to a 90° corner, is desirable from a fabrication viewpoint.

Note: 1 in. = 25.4 mm, 1 in.^{2}/in. = 25.4 mm^2/mm, 1 in.^{3}/in. = 645 mm^3/mm, 1 lbf/in. = 175 N/m, 1 psi = 0.0069 MPa, 1 in.-lbf = 0.113 N-m, 1 in.-lbf/in. = 4.45 N-m/m.

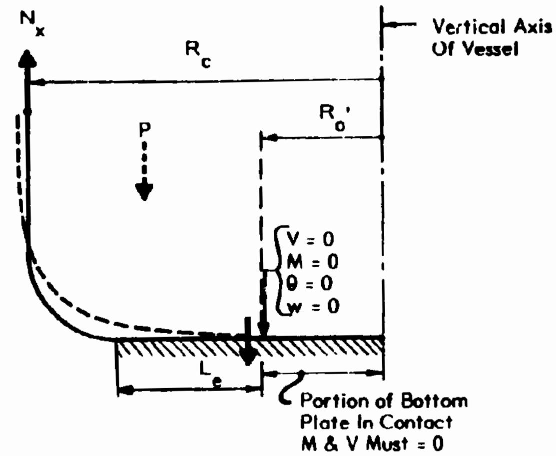

P = weight of structure contents, and internal pressure force on area of edge region that lifts off rigid base to balance total upward force on structure

R_o' = required radius of annular base ring to satisfy: $P = 2\pi R_c N_x$

Fig. 9-21 BASE UPLIFT IN CLOSED PRESSURIZED VESSEL WITHOUT WALL HOLD-DOWN TO RIGID BASE

9.8 CONCENTRATED LOAD EFFECTS

As stated previously, when concentrated loads, or moments, are applied to thin shells, significant bending and axial thrust stress resultants arise in local regions surrounding the points of force application. The paper, "Local Stresses in Spherical and Cylindrical Shells due to External Loadings" by K. Wichman, A. Hopper and J. Mershon (reprinted from Welding Research Council Bulletin 107, 1968 in Vol. 2 of (9.17)), provides an exhaustive summary of the available hand calculation methods for analyzing concentrated load effects, including extensive charts and design aids. The material is too extensive to be included here. Instead, equations for approximating moment and thrust stress resultants due to a concentrated radial load and a concentrated moment load on a spherical shell are presented in this Section. These may be used to determine if a more complete analysis is warranted.

Two common types of concentrated applied forces, radial load and bending moment, are shown in Fig. 9.22, a and b, respectively. Significant effects from the concentrated forces extend over a radius, :

For moment: $\rho_m = 2\left(\frac{i}{\bar{a}}\right)^{1/4} R^{1/2}$ Eq. 9.62

For thrust: $\rho_T = 4\left(\frac{i}{\bar{a}}\right)^{1/4} R^{1/2}$ Eq. 9.63

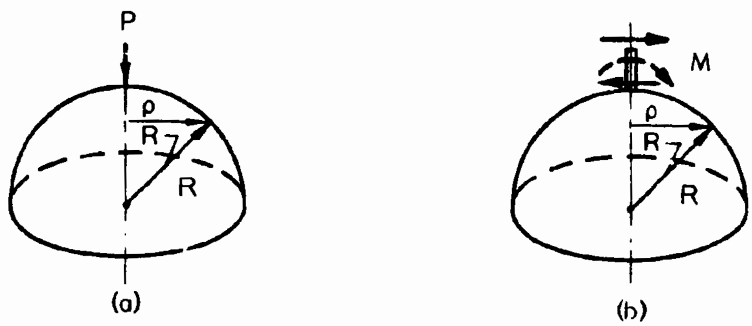

Fig. 9-22 CONCENTRATED RADIAL LOAD AND MOMENT ON SPHERICAL SHELL

Equations for approximate maximum stress resultants produced by these concentrated radial forces or moments on a spherical shell with approximately equal moment of inertia per unit width, i, and area per unit width, $\bar{a}$, in each direction are given in Table 9-8, Part I. These simplified equations are based on more comprehensive relations given in (9.19).

The above relations are considerably simplified for an isotropic uniform thickness shell. Significant effects extend over a radius, :

For moment: $\rho_m = 1.1\sqrt{Rt}$ Eq. 9.64

For thrust: $\rho_T = 2.2\sqrt{Rt}$ Eq. 9.65

Table 9-8

Approximate Stress Resultants in Spherical Shells Subject to Concentrated Radial Loads and Moments *

Stress Resultant	Applied Concentrated Radial Force, P	Applied Concentrated Moment, M
1. General non-prismatic shell with approximately equal i and $\bar{a}$ in all directions		
M_ϕ	$\dfrac{0.06\,P\left(\frac{i}{\bar{a}}\right)^{1/4}\sqrt{R}}{\rho}$	$\dfrac{0.16\,M\cos\theta}{\rho}$
M_θ	$\dfrac{0.04\,P\left(\frac{i}{\bar{a}}\right)^{1/4}\sqrt{R}}{\rho}$	$\dfrac{0.08\,M\cos\theta}{\rho}$
N_ϕ	$-\dfrac{0.04\,P\left(\frac{\bar{a}}{i}\right)^{3/8}R^{1/4}}{\sqrt{\rho}}$	$-\dfrac{0.02\left(\frac{\bar{a}}{i}\right)^{5/8}M\cos\theta}{R^{1/4}\sqrt{\rho}}$ **
N_θ	$\dfrac{-.06\,P\,R^{1/2}\left(\frac{\bar{a}}{i}\right)^{1/4}}{\rho}+.03\,P\left(\frac{\bar{a}}{i}\right)^{1/2}$ **	$-\dfrac{0.035\left(\frac{\bar{a}}{i}\right)^{1/2}M\cos\theta}{\rho}$ **
	(only up to min $\rho = 0.18\,\rho_T$)	(only up to min $\rho = 0.10\,\rho_T$)
w	max $w = \dfrac{0.12\,P\,R}{E\sqrt{i\bar{a}}}$	See 9.19
2. Uniform shell thickness, t		
M_ϕ	$\dfrac{0.03\,P\sqrt{Rt}}{\rho}$	$\dfrac{0.16\,M\cos\theta}{\rho}$
M_θ	$\dfrac{0.02\,P\sqrt{Rt}}{\rho}$	$\dfrac{0.08\,M\cos\theta}{\rho}$
N_ϕ	$-\dfrac{0.10\,P\,R^{1/4}}{t^{3/4}\sqrt{\rho}}$	$-\dfrac{0.10\,M\cos\theta}{t^{5/4}R^{1/4}\sqrt{\rho}}$ **
N_θ	$-\dfrac{.12\sqrt{R}\,P}{\rho\sqrt{t}}+0.10\,\dfrac{P}{t}$ **	$-\dfrac{.12\,M\cos\theta}{t\,\rho}$ **
	(only up to min $\rho = 0.18\,\rho_T$)	(only yp to min $\rho = 0.10\,\rho_T$)
w	max $w = \dfrac{0.40\,P\,R}{E\,t^2}$	See 9.19

* Adapted from (9.19). See charts in 9.19 for greater accuracy.

** These approximations are of varying accuracy. See (9.19) for charts that give more accurate approximations.

Equations for approximate maximum stress resultant produced by these forces or moments on an isotropic uniform wall spherical shell are given in Table 9-8, Part 2.

9.9 THERMAL STRESSES

Uniform temperature change does not produce stresses in shells with free edges. However, if edges are connected to elements which do not undergo the same thermal change as the shell, edge restaints arise and generally cause edge bending, thrust and shear stress resultants. These may be determined by establishing equations of deformational compatibility as explained in Section 9.6.

Temperature change in the form of a thermal gradient across the thickness of a shell often produces significant stresses which should be taken into account in the design of shell components. Points at sufficient distance from the edge of a shell are completely restained from curling to conform with the free relative deformations caused by thermal gradients. Bending moments arise that produce the strains needed to accommodate the effects of thermal gradients. The bending moment due to a uniform thermal gradient with temperature T_1 on the outside and T_2 on the inside of an isotropic shell is (9.7):

$$M_\theta = M_x \text{ (or } M_\phi) = \frac{E\,\alpha\,(T_1 - T_2)\,t^2}{12\,(1-\nu)} \qquad \text{Eq. 9.66}$$

The stress in the shell is:

$$\sigma_\theta = \sigma_x \text{ (or } \sigma_\phi) = \frac{E\ \ (T_1 - T_2)}{2\,(1-\nu)} \qquad \text{Eq. 9.67}$$

If the edges of the shell are free, the maximum circumferential stress in the vicinity of the edge is increased (9.7):

$$\sigma_\theta = \frac{E\,\alpha\,(T_1 - T_2)}{2\,(1-\nu)}\left[(1 - \nu + \sqrt{\frac{(1-\nu^2)}{3}}\right] \qquad \text{Eq. 9.68}$$

The coefficient of expansion, α, of many plastics materials is relatively high and this increases the magnitude of the possible stress state in a plastic shell resulting from thermal gradients or overall thermal change. However, the effects of a high coefficient of expansion are offset, to some extent, by the low modulus of elasticity, E, of many plastics.

If the shell is a symmetrical sandwich shell subject to a uniform temperature gradient across its overall thickness, $(t_c + 2t_f)$, the fully restrained bending moment caused by the thermal gradient is:

$$M_\theta = M_x \text{ (or } M_\phi) = \frac{E\alpha_f (T_1 - T_2)\, i}{(t_c + 2t_f)} \qquad \text{Eq. 9.69}$$

if $t_f << t_c$:

$$M_\theta = M_x \text{ (or } M_\phi) \quad \frac{E\alpha_f (T_i - T_2)\, t_f (t_f + t_c)}{2} \qquad \text{Eq. 9.70}$$

$$\sigma_\theta = \sigma_x \text{ (or } \sigma_\phi) \quad \frac{E\sigma_f (T_1 - T_2)}{2} \qquad \text{Eq. 9.71}$$

Eq. 9.71 is essentially the same as Eq. 9.67 for uniform thickness shells. However, because of the good thermal insulation provided by plastic core sandwich constructions, $(T_1 - T_2)$ may be much larger than in thin shells of uniform thickness. Because of this, stresses caused by thermal gradients may be much more significant in sandwich shells than in thin shells of single thickness. Thermal stresses are calculated in sandwich cylinders having a variety of facing materials in **Example 9-11**.

If thermal gradients are not uniform, or if walls are non-uniform or ribbed, evaluation of the effects of thermal change usually is much more complex, requiring the application of finite element computer analysis techniques for both heat transfer and stress analyses.

Example 9-11: Estimate the thermal stress in regions away from the ends for a $100^{o}F$ temperature gradient across the walls of sandwich cylinders having the thin facing materials and properties shown below.*

Eq. 9.71: $\sigma_{\theta} = \sigma_x = \dfrac{E\,\alpha\,(T_1 - T_2)}{2}$

Material	E psi	α in./in./^{o}F	$\sigma_{\theta} = \sigma_x$ for $(T_1 - T_2) = 100^{o}F$ psi
Steel	30×10^{6}	6×10^{-6}	$\pm$ 9,000
Aluminum	10×10^{6}	12×10^{-6}	$\pm$ 6,000
FRP - 50% glass	2×10^{6}	12×10^{-6}	$\pm$ 1,200
FRP - 30% glass	1×10^{6}	18×10^{-6}	$\pm$ 900
PVC	0.5×10^{6}	35×10^{-6}	$\pm$ 875
Polycarbonate	0.4×10^{6}	35×10^{-6}	$\pm$ 700
HDPE	0.15×10^{6}	70×10^{-6}	$\pm$ 525

Note: $1^{o}F = 0.55^{o}C$, 1 psi = 0.0069 MPa, 1 in./in./^{o}F = 1.82 mm/mm^{o}C

* See footnote, Example 9-1, Page 9-13.

9.10 STABILITY ANALYSIS

Stability analysis is particularly important for the design of plastic shell structures. The high strength-to-stiffness ratio of most plastics and the economic need to minimize thickness of these materials both result in designs often governed by stability rather than strength considerations. Methods of stability analysis for shell structures, particularly with ribbed or sandwich construction, are not widely treated in the literature. However, approximate methods based on buckling analyses for certain basic structure and load arrangements, have been proposed (9.9, 9.21, 9.22) as sufficiently accurate for practical design of the shell configurations described in Section 9.3. These approximate methods for stability analysis of uniform thickness, sandwich, or ribbed shells are summarized in this Section.

Material Stiffness

This stiffness or modulus of elasticity of the shell material must be known or estimated to evaluate the stability of a shell structure. For many plastics materials, this property is dependent on the duration of load and/or the service temperature. The concept of the time-temperature dependent viscoelastic modulus, E_v, was introduced in Chapter 2 as a practical way to account for the reduction in stiffness (often termed creep) that occurs under long time stress and with increasing temperature. The viscoelastic modulus is defined in Chapter 2 as the initial slope (or practically, the slope at a low stress) of the isochronous stress-strain curve at a particular time duration of stress, t_1 and temperature T_1. The isochronous stress-strain curve is a plot of stress vs. time-dependent strain for several test samples at different-stress magnitudes, with each stress level held constant for a time, t_1, and temperature T_1. The initial elastic modulus for short term load, E, and the viscoelastic modulus, E_v, for several stress durations, t_1, t_2, are illustrated in the stress-strain plots shown in Fig. 9-23.

Modulus of elasticity may also depend on the magnitude of the short or long term stress. In this case, the short term and/or long term stress-strain curves are not linear at the stress level of interest. When an isochronous stress-strain curve is not linear, its slope at any particular stress level is termed the viscoelastic tangent modulus, E_{tv}, for this stress, and the slope of a line joining the origin with the curve at that stress level is termed the viscoelastic secant modulus, E_{sv}. These moduli are also illustrated in Fig. 9-23.

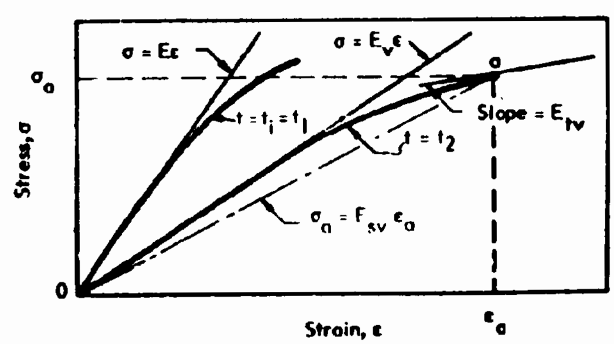

Fig. 9-23 ELASTIC MODULI FOR USE IN BUCKLING EQUATIONS

The buckling equations given in this section are written in terms of the initial elastic modulus, E, for short term loading, and for stresses within the range where stress is E times strain. For a particular maximum duration of long term load, and maximum service temperature, E_v for that duration of stress and temperature should be used in place of E in the equations given in this Section. When stress is outside the linear elastic or linear viscoelastic range, the tangent modulus, E_{tv}, and the secant modulus, E_{sv}, may be used to estimate a plasticity correction factor, η. This correction factor may be applied to reduce the critical buckling stress obtained using E, (E_v in the case of long term stress).

Methods for estimating η, based largely on experiments and theory for thin metal shells, are given in this Section for various types of shell buckling behavior. These require verification for application to plastic materials, particularly if buckling stresses exceed the "viscoelastic limit" as defined in Chapters 2 and 3.

Idealized Shell Buckling Behavior

Approximate stability analyses for many shells may be based on consideration of three basic types of structural action of a cylinder:

- **Longitudinally loaded cylinder** — longitudinal stress is compressive. (Figs. 9-24, 9-28).
- **Radially loaded cylinder** — circumferential stress is compressive. (Fig. 9-29).
- **Torsionally loaded cylinder** — diagonal stress is compressive. (Fig. 9-30).

Cylindrical Shells

Longitudinally loaded long cylinder. In Fig. 9-24(a), a long cylinder under longitudinal load is divided into longitudinal strips of unit width around the entire circumference, and circumferential hoops of unit width along the entire length. Each longitudinal strip behaves as a slender end-loaded bar with continuous elastic support from the circumferential hoops (Fig. 9-24(b)). Cylinder buckling resistance is a function of both the longitudinal bending rigidity, D_x, and the circumferential hoop rigidity, $\bar{A}_0/R$.

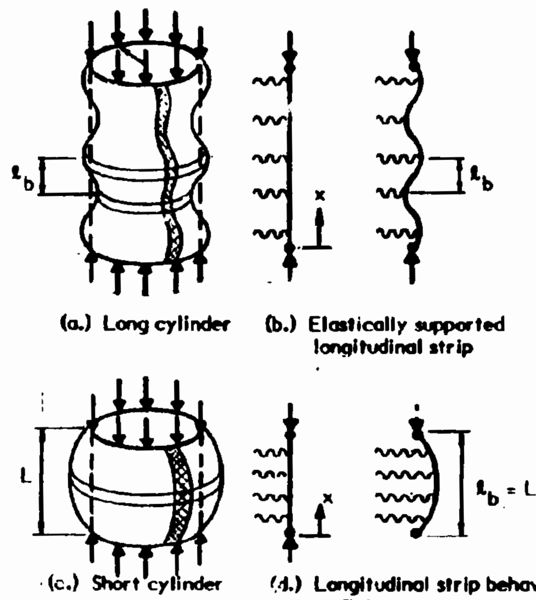

Fig. 9-24 BUCKLING OF LONGITUDINALLY COMPRESSED CYLINDER

The longitudinal axial force per unit of circumferential length which buckles the cylinder is (9.23):

$$N_{xc} = \frac{2\sqrt{3}\ C\ \sqrt{D_x \bar{A}_0}}{R} \qquad \text{Eq. 9.72}$$

This equation is valid only for a "long" cylinder which buckles into one and a half, or more, longitudinal waves. For buckle patterns with fewer waves, it represents a lower limit of buckling resistance. Other limitations are discussed below. Buckling of short cylinders is discussed later in this Section.

The half-wave length of each longitudinal buckle is (9.23):

$$\ell_b = \pi \left[\frac{D_x R^2}{\bar{A}_0}\right]^{1/4} \qquad \text{Eq. 9.73}$$

For isotropic, uniform thickness shells, Eq. 9.72 reduces to the more familiar cylindrical shell buckling equation:

$$\sigma_{xc} = \frac{N_{xc}}{t} = \frac{C\,E\,t}{R} \qquad \text{Eq. 9.74}$$

The half-wave length of each longitudinal buckle is:

$$\ell_b = 1.72\sqrt{R\,t} \qquad \text{Eq. 9.75}$$

In order for Eq. 9.72 to be applicable to orthotropic, or ribbed cylindrical shells, the following criteria for relative longitudinal, circumferential and shearing stiffnesses must be met (9.9):

$$\frac{\bar{A}_x D_\theta}{\bar{A}_\theta D_y} \geq 1.0 \qquad \text{Eq. 9.76}$$

$$\frac{\dfrac{D_{x\theta}'}{D_x} + \nu_\theta}{\dfrac{\bar{A}_\theta (1 - \nu_x \nu_\theta)}{2\bar{A}_{x\theta}'} - \nu_\theta} \geq 1.0 \qquad \text{Eq. 9.77}$$

The above stiffness parameters are defined in Table 6-1 of Chapter 6, with x and θ replacing directions 1 and 2.

In most practical designs for orthotropic or ribbed shells, the above criteria are, or should be, met. See (9.9) for solutions when these criteria are not satisfied.

For orthotropic, ribbed or sandwich shells that meet the above criteria, Eq. 9.74, may be used in lieu of Eq. 9.72, if "t" is replaced by t_e, an effective thickness given by Eqs. 9.82 or 9.83 below. Thus:

$$\sigma_{xc} = \frac{C\,E_x\,t_e}{R} \qquad \text{Eq. 9.78}$$

The term C in the above equations is a shell buckling coefficient that is determined as follows:

$$C = k_o k_n k_s \qquad \text{Eq. 9.79}$$

where: k_o = buckling coefficient from classical linear mathematical derivations for cylindrical shell buckling, given by:

$$k_o = \frac{1}{3(1-\nu^2)} \approx 0.6 \text{ , when } \nu = 0.3 \qquad \text{Eq. 9.80}$$

k_n = "knockdown factor" (less than 1.0) for reduction of buckling stress in thin cylinders due to imperfections (see later discussion). k_n may be estimated for cylindrical shells of uniform thickness from the following semi-empirical relation, based on many tests on thin isotropic metal and plastic cylinders (9.24):

$$k_n = 1.0 - 0.91\left(1 - \frac{1}{e^{0.06\sqrt{R/t}}}\right) + 1.5\left(\frac{R}{L}\right)^2\left(\frac{t}{R}\right) \qquad \text{Eq. 9.81}$$

e, the Naperian Base, equals 2.7183

The experimental data that provide the basis for Eq. 9.81 cover a range of R/t from 100 to 4,000 and R/L from 0.2 to 33 for unstiffened, uniform wall thickness cylinders. The terms containing R/L are not significant for smaller values than R/L = 0.2. See also (9.26) for discussion of k_n.

Eq. 9.81 is plotted in Fig. 9-25 for cases where the term involving R/L is not significant.

The following alternate equation for k_n is recommended in (9.39), based on a study of available test data on fabricated steel and aluminum cylinders subject to axial load.

$$k_n = 1.53 - 0.477 \log\frac{R}{t} \leq 0.21 \qquad \text{Eq. 9.81a}$$

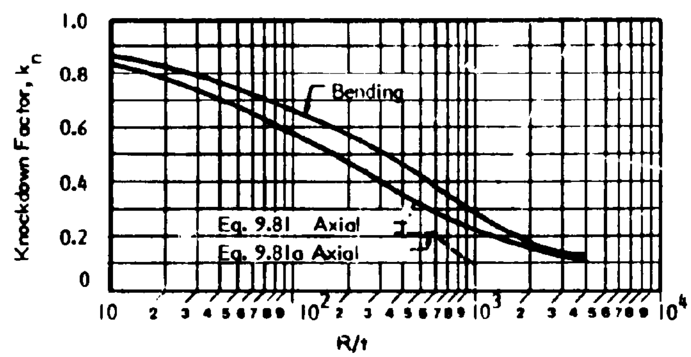

Fig. 9-25 KNOCKDOWN FACTOR FOR LONGITUDINALLY COMPRESSED OR BENT CYLINDERS (Source 9.9)

This equation is also plotted in Fig. 9-25 for R/t between 600 and 1000. Obviously, it gives more conservative results than Eq. 9.81 because it is based on tests of components with larger imperfections, presumably more representative of actual metal shells. The cut off at $k_n = 0.21$, representing R/t = 600, is suggested in (9.39) because of the absence of test data for lower R/t values. However, note that test data from small scale tests reviewed in (9.39) suggests a cut off of max. $k_n = 0.57$, as well as an increase in the constant 1.53 to 1.60 in Eq. 9.81a. If the latter coefficient is used in Eq. 9.81a in place of 1.53, the k_n values obtained with Eq. 9.81a agree quite well with Eq. 9.81 up to the cut off point.

The accuracy of either Eq. 9.81 or 9.81a for use with plastics shell components will depend primarily on the accuracy of fabrication. Tests of full scale components should be undertaken as a basis for confirming or modifying these relations.

A further modification of Eqs. 9.81 and 9.81a for k_n to include the increased buckling strength that can be provided by circumferential stiffening ribs is presented later in this Section.

Applicability of the above knockdown factor to ribbed or sandwich cylinders by substitution of t_e for t requires verification by tests.

k_s = reduction factor (less than 1.0) for shear deflection. This is usually only significant for sandwich shells, and is given in Fig. 9-26.

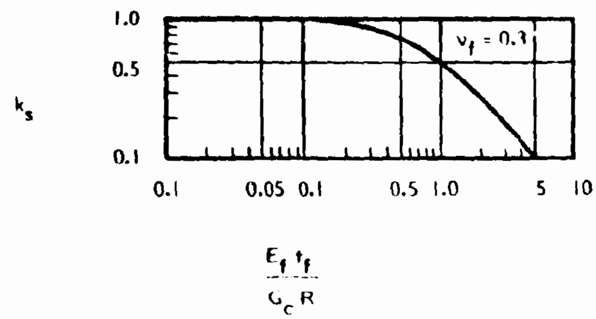

Fig. 9-26 REDUCTION FACTOR FOR SHEAR DEFORMATION IN BUCKLING OF LONGITUDINALLY COMPRESSED LONG SANDWICH CYLINDER WITH ISOTROPIC FACINGS AND SHEAR FLEXIBLE CORE (Source 9.9)

Discussion of knockdown factor k_n: The buckling analysis used for bars and plates is based on an assumption of elastic behavior and a deformed position of differential elements in the compressed component only slightly different than the initial theoretical geometry. When this type of analysis is applied to shells, the equations for critical buckling stress or stress resultant given above are obtained with $C = k_o$. In real shells, however, prebuckling rotations usually are not negligibly small, and they have to be taken into account in determining buckling resistance. This requires a non-linear analysis, as well as consideration of initial deviations of the shell geometry from the assumed perfect cylindrical shape. Initial deviations result from imperfections such as waviness and "flat spots" in the actual shell geometry. Further deviations occur when the shell deforms under load. These prebuckling changes in the shells geometry usually reduce its buckling resistance to only about 1/4 to 1/8 of the resistance obtained in a linear elastic small deflection analysis. However, because a direct non-linear analysis is usually too complex and unwieldly for practical design, a "knockdown factor", k_n, given by Eq. 9.81 or 9.81a, is usually applied to the results of linear theory, producing the buckling coefficient given by Eq. 9.79.

For a long cylinder under longitudinal compression, the buckling resistance developed in the classical linear analysis depends on the axial stiffness of the circumferential or ring strips. In a thin shell, these ring strips have a very low bending stiffness relative to their axial stiffness. Deviations from a perfect ring and from perfectly straight longitudinal strips cause small unsymmetrical lateral forces which produce circumferential bending deformations. When a typical "imperfect" longitudinally loaded cylinder buckles, a diamond-shaped buckle pattern arises rather than the axi-symmetric wave pattern shown in Fig. 9-24(a). The size and shape of the diamond-shaped pattern is a function of both the circumferential axial and bending stiffness, as well as the longitudinal bending stiffness.

When circumferential stiffeners are provided at a spacing, L_s, that is greater than the half wave length of longitudinal buckling, ℓ_b, (see Fig. 9.24), the preceeding buckling theory indicates that the critical buckling load is the buckling capacity of the shell between stiffeners. Theoretically, this strength is not affected by the length of the shell between stiffeners when $L_s > \ell_b$. However, tests reported in (9.39) show that the longitudinal buckling strength of such circumferentially ribbed shells is increased significantly over the strength of a similar shell without the stiffeners. The increased strength may be taken into account by modifying the knockdown coefficient, k_n, given previously by Eq. 9.81 or 9.81a. If a shell stiffening factor,

$$\lambda_s = \frac{L_s}{\sqrt{Rt}} \qquad \text{Eq. 9.82}$$

is defined, then the following knockdown factor for buckling of the shell between ribs, suggested in (9.39) for use with fabricated steel cylinders, is probably also applicable to plastic shells fabricated to the same level of accuracy:

$$k_n = (3.13 - 0.82 \log \frac{R}{t}) \lambda_s^{-0.6} \leq 0.87 \lambda_s^{-0.6} \qquad \text{Eq. 9.81b}$$

Obviously, k_n, need not be less than the value given by Eq. 9.81a.

The bending stiffness of the circumferential stiffeners do not appear in the above equation. This stiffness must be at least equivalent to the bending stiffness of an unstiffened shell of uniform thickness that has the increased buckling strength given by Eq. 9.81b together with Eqs. 9.74 and 9.79. For the usual case of ribs that act compositely with the shell, a length of shell equal to $.76\sqrt{Rt}$ on each side of the rib, but not greater than 0.5 L_s, may be considered as a part of the rib.

The above qualitative discussion indicates that the knockdown factor, k_n, should be a function of the ratio of circumferential bending stiffness to circumferential axial stiffness. For an isotropic shell of uniform thickness, this ratio is $t^2/12$. For a planar isotropic sandwich shell with thin equal faces, this ratio is $(t_c + t_f)^2/4$. Also, the effective thickness of the above sandwich shell which produces the same critical buckling stress with Eqs. 9.72 and 9.76 is:

$$t_e = \sqrt{3}\,(t_c + t_f) \qquad \text{Eq. 9.83}$$

With the above value of t_e, $t_e^2/12 = (t_c + t_f)^2/4$. Thus, R/t_e may be used in place of R/t in Eqs. 9.81 and 9.81a for determining k_n for sandwich shells, although as stated above, this should be verified by tests.

The equations for longitudinal buckling stress resultant and knockdown factors presented above cover the cases of unstiffened isotropic or orthotropic shells (Eqs. 9.74 or 9.72 with 9.79 and 9.81 or 9.81a), circumferentially stiffened shells that buckle in the uniform thickness region between stiffeners (Eqs. 9.74 or 9.72 with 9.79 and 9.81, 9.81a or 9.81b), and sandwich shells (Eqs. 9.78 and 9.82, or 9.72, with Eq. 9.81 as lower bound for k_n.) Consideration of the longitudinal buckling stress resultant for cylindrical shells that have both longitudinal and circumferential stiffeners also is of interest This case also covers the sub-case of the longitudinal buckling strength of cylindrical shells that have only circumferential ribs, but whose buckled shape includes bending of the ribs (termed "general instability" as compared to "local buckling" of the shell between ribs.) This stiffened shell case may also be evaluated using the buckling theory presented above by defining an effective thickness:

$$t_e = \frac{2\sqrt{3}}{\bar{A}_x}\sqrt{D_x\,\bar{A}_\theta} \qquad \text{Eq. 9.84}$$

Eq. 9.84 may be applied to ribbed shells that meet the criteria given by Eqs. 9.76 and 9.77 (9.21) by using the knockdown factors given by Eqs. 9.81 or 9.81a based on R/t_e. When circumferential ribs provide greater bending strength, D_θ, than the minimum required in Eq. 9.76, the knockdown coefficient given by Eq. 9.81 becomes increasingly more conservative. Eq. 9.84, together with Eq. 9.78 may be used to determine the resistance to general instability of a longitudinally compressed cylinder with circumferential ribs only, but if the ribs are closely spaced, the k_n coefficients given by Eq. 9.81 will be very conservative. Tests of cylinders that failed with buckles that include the ribs have shown that the high circumferential bending stiffness of the rib compared to the longitudinal bending stiffness of the shell increases the buckling coefficient, k_n (9.39).

Creep and non-linear behavior. For shells subject to long term stress and/or elevated temperatures, the viscoelastic modulus should be used in the stiffness terms of the above equations. If isochronous stress-strain relations are not linear, k_n should be multiplied by the following plasticity correction factor (isotropic materials) (9.9):

$$\eta = \frac{\sqrt{E_t E_s}}{E}, \text{ or } \frac{\sqrt{E_{tv} E_{sv}}}{E_v} \qquad \text{Eq. 9.85}$$

E_t is the tangent modulus of the plastic at an ultimate stress equal to the design stress times a suitable load factor. E_s is the secant modulus at that ultimate stress and E is the initial modulus. These moduli are obtained from a stress-strain curve for the material, taken at least up to the required ultimate stress. (Fig. 9-23).

When stress is long term, an isochronous stress-strain curve for the material loaded under the design time duration (or extrapolated to that duration) should be used to obtain the viscoelastic moduli, E_{tv}, E_{sv}, and E_v. (Fig. 9-23)

Pressurized longitudinally loaded cylinder. If a cylindrical shell is pressurized internally, resulting in circumferential tension, the knockdown factor is increased. The effect of the circumferential tension is to stabilize the longitudinal strips which are subject to compression, thereby increasing the longitudinal buckling stress. An estimate of the increased buckling strength of a pressurized shell may be obtained using a correction factor to the buckling coefficient given by Eq. 9.79 as follows (9.9):

$$C = (k_o \; k_n \; + \; k_p) \, k_s \qquad \text{Eq. 9.79a}$$

The correction coefficient for effects of internal pressure, k_p, is given in Fig. 9-27.

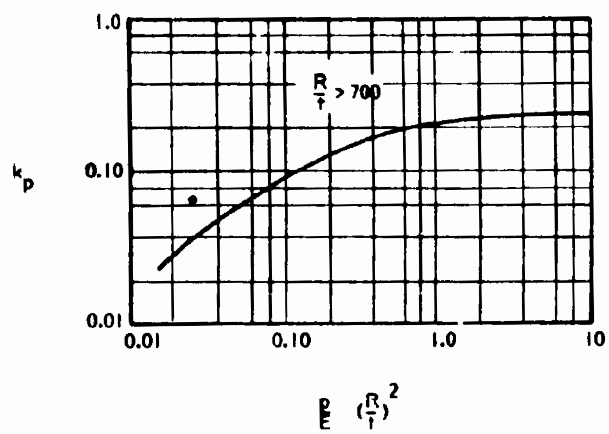

Fig. 9-27 CORRECTION FACTOR FOR PRESSURIZED LONGITUDINALLY COMPRESSED CYLINDER (Source 9.9)

If, conversely a cylindrical shell is subject to circumferential compression, the knockdown factor is decreased, and thus, the longitudinal buckling stress is decreased. The effect of combined radial and longitudinal compressive stresses may be evaluated using the interaction equation given later in this Section.

See (9.24) and (9.9) for summaries of many studies of longitudinal buckling stress. Included are various suggested provisions for reductions due to imperfections, plasticity, creep and shear deformation effects.

Longitudinally loaded short cylinder Length of shell does not appear in Eqs. 9.72 or 9.74. For long shells, length does not affect the longitudinal buckling stress. However, very short longitudinally loaded cylindrical shells may have a larger buckling capacity than given by Eqs. 9.72 or 9.74. Such shells buckle into only one half-wave length, as shown in Fig. 9.24(c). See Eq. 9.73 or 9.75 for the theoretical half-wave length of buckle. For short shells, the critical longitudinal stress resultant that produces buckling may be determined using Eq. 6.72 in Chapter 6 for buckling of wide plates. This equation is essentially Euler's formula for a long slender column.

In short shells, the axial strips derive their principal resistance to buckling from their longitudinal bending stiffness. This is in contrast to long shells whose buckling resistance is enhanced by elastic support from the circumferential stiffness of the shell. Obviously, in a short shell, the rotational stiffness of the ends of the cylinder, as well as its length, greatly affects the buckling strength.

The effect of shell length for intermediate length shells where the length of the shell, or the spacing of circumferential stiffeners, L_s, is more than the half wave length of buckle, ℓ_b, is included in Eq. 9.81b for knockdown coefficient. This provides a transition range where the combined resistance to buckling as an Euler strip with elastic support from the hoop stiffeners of the shell is taken into account.

Whenever Eq. 6.72, with the appropriate end restraint coefficient, gives a higher buckling stress than Eqs. 9.72 or 9.74, together with Eqs. 9.79 and 9.81 or 9.81b, the shell is a "short shell" and the higher critical stress represents the buckling strength.

Example 9-12 illustrates application of the above buckling equations and the procedure described for estimating knockdown coefficients to the calculation of the longitudinal buckling stress resultant for an orthotropic cylindrical shell. The shell stiffness is orthotropic because the circumferential elastic modulus differs from the longitudinal elastic modulus, and also because circumferential ribs are provided, without longitudinal ribs.

Cylinder Under Longitudinal Bending. The preceding equations may also be used to determine the longitudinal buckling stress resultant in a cylindrical shell which is subject to overall bending, as shown in Fig. 9-28. In this case, longitudinal stress resultants vary within the shell, and the buckling stress at the most highly compressed point can be determined using Eqs. 9.72 or 9.74 with a slightly modified value of the buckling coefficient. Instead of the knockdown coefficient given by Eq. 9.81, a higher k_n, given by the upper curve in Fig. 9-25, may be used.

Example 9-12: Determine the longitudinal stress resultant, N_{xc}, that will buckle a filament wound, circumferentially ribbed, FRP tube with materials properties and dimensions shown in the sketch.*

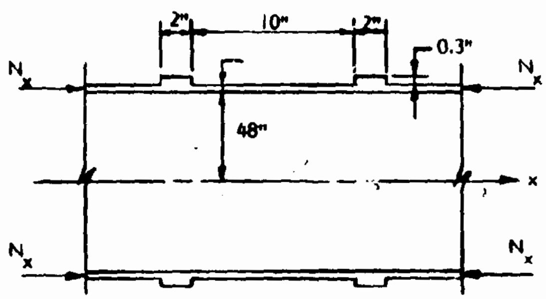

$E_\theta = 3 \times 10^6$
$E_x = 0.8 \times 10^6$ psi
$\nu_x = 0.11$
$\nu_\theta = 0.41$
$t = 0.3$ in.
Ribs: $A_\theta = 0.3$ in^2/rib

1. Longitudinal and circumferential stiffnesses per unit width

1.1 For buckling between ribs

Eq. 6.5a: $\bar{A}_\theta = \frac{E_\theta t}{(1 - \nu_\theta \nu_x)} = \frac{3 \times 10^6 \times 0.3}{(1 - 0.41 \times 0.11)} = 0.94 \times 10^6$ lbs/in.

Eq. 6.6a: $D_x = \frac{E_x i_x}{(1 - \nu_\theta \nu_x)} = \frac{0.8 \times 10^6 \times 0.3^3}{12(1 - .41 \times .11)} = 1.89 \times 10^3$ lbs-in.

Eq. 6.5b: $\bar{A}_x = \frac{0.8 \times 10^6 \times 0.3}{(1 - 0.11 \times 0.41)} = 0.25 \times 10^6$ lbs/in.

Eq. 9.82 $\lambda_s = \frac{L_s}{\sqrt{Rt}} = \frac{10}{\sqrt{48 \times 0.3}} = 2.64$

1.2 For buckling including ribs - smear out to get average stiffness per unit width

$$\bar{A}_\theta = \frac{E_\theta a_\theta}{(1 - \nu_\theta \nu_x)} = 3 \times 10^6 \times \frac{(0.3 \times 12 + 0.3 \times 2)}{12(1 - 0.41 \times 0.11)} = 1.10 \times 10^6 \text{ lbs/in}$$

$D_x = 1.89 \times 10^3$ lbs-in

1.3 Check stiffness ratios:

Eq. 9.76: $\frac{\bar{A}_x D_\theta}{\bar{A}_\theta D_x} \geq 1.0$

Between ribs: $\bar{A}_x = \frac{0.8}{3.0} \bar{A}_\theta$; $D_\theta = \frac{3.0}{0.8} D_x$, and thus $\frac{\bar{A}_x D_\theta}{\bar{A}_\theta D_x} = 1.0$

Including ribs: D_θ increases more than $\bar{A}_\theta$ increases while D_x and A_x do not change, and thus inequality is satisfied.

---

* See footnote, Example 9-1, Page 9-13.

Example 9-12 (continued)

2. Check half wave length of buckle between ribs to determine whether shell can buckle between ribs.

Eq. 9.73: $$\ell_b = \pi \left[\frac{D_x R^2}{\bar{A}_0}\right]^{1/4} = \pi \left[\frac{1.89 \times 10^3 \times 48^2}{0.94 \times 10^6}\right]^{1/4} = 4.6 \text{ in.}$$

Conclusion: Shell can buckle between ribs.

3. Check buckling strength between ribs:

Eq. 9.72: $$N_{xc} = \frac{2\sqrt{3}\ \ C\sqrt{D_x \bar{A}_0}}{R}$$

Eq. 9.79: $C = k_o k_n k_s$; $k_o = 0.6$, $k_s = 1.0$

Eq. 9.84: $$t_e = \frac{2\sqrt{3}}{\bar{A}_x}\sqrt{D_x \bar{A}_0} = \frac{2\sqrt{3 \times 1.89 \times 10^3 \times 0.94 \times 10^6}}{0.25 \times 10^6} = 0.584 \text{ in.}$$

$$\frac{R}{t_e} = \frac{48}{0.584} = 82; \text{ Fig. 9 - 25:} k_n = 0.6$$

$$N_{xc} = \frac{2\sqrt{3}\ \times 0.6 \times 0.6\sqrt{1.89 \times 10^3 \times 0.94 \times 10^6}}{48} = 1095 \text{ lbs/in.}$$

4. Check for potential increased longitudinal buckling strength due to effect of rib spacing:

Eq. 9.81b: $k_n = (3.13 - 0.82 \log \frac{R}{t})\ \ \lambda_s^{-0.6} \leq\ 0.8\ \ \lambda_s^{-0.6}$

$k_n = (3.13 - 0.82 \log 80)\ 2.64^{-0.6} = 0.88,$

or max. $k_n = 0.8 \times 2.64^{-0.6} = 0.45 < 0.60$ from step 3

No increase expected from circumferential ribs; however, they probably make this shell considerably less "imperfection sensitive" than a comparable shell without the ribs. Tolerances for deviations from the design geometry can probably be somewhat greater because of the stiffening effect of the ribs.

5. Check whether Eq. 6.72 with k = 1.0 (Euler's formula) gives a higher N_{xc}:

$$N_{xc} = \frac{k\ \ \pi^2 D_x}{c^2} = \frac{1.0\ \ \pi^2 \times 1.89 \times 10^3}{(10)^2} = 18\text{[illegible] lbs/in} \quad 1095 \text{ lbs/in.}$$

This result was expected since ℓ_b (in step 2) << a, the clear rib spacing.

6. Conclusion: longitudinal buckling strength is governed by sections between circumferential ribs, maximum N_{xc} = 1095 lbs/in., and longitudinal buckling stress is;

$$\sigma_{xc} = \frac{1095}{0.3} = 3650 \text{ psi.}$$

Note: 1 in. = 25.4 mm, 1 in.^{2} = 645 mm^2, 1 lbf-in. = 0.113 N-m, 1 lbf/in. = 175 N/m, 1 psi = 0.0069 MPa

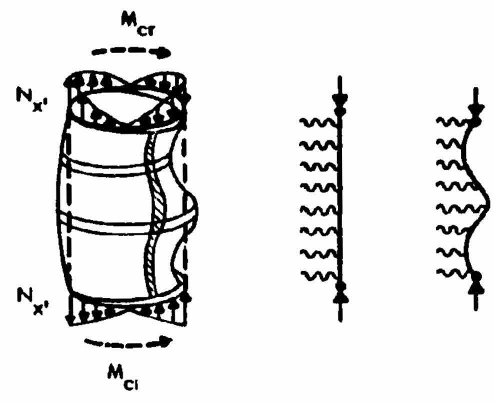

(a.) Bent long cylinder (b.) Elastically supported longitudinal strip

Fig. 9-28 BUCKLING OF LONGITUDINALLY BENT LONG CYLINDER

Radially loaded cylinder. In Fig. 9-29, a cylinder loaded by radial pressure is shown divided into circumferential hoops along its entire length. For very long cylinders in the regions away from the ends of the cylinder, these hoops behave like slender radially loaded rings. These rings derive little support from the end diaphragms which are too far away. The shell buckling resistance is the same as the buckling resistance of the strips acting as rings, given in Section 9.2. For cylinders of moderate length, shell buckling resistance is increased over the ring buckling capacity because of the resistance to ovalling developed from tangential (membrane) shear stiffness. Very short cylindrical shells under radial pressure or circumferential stress behave the same as long, narrow plates with supported edges parallel to the direction of stress, developing still greater buckling resistance than "moderate length" cylinders.

The circumferential buckling stress and external pressure for a <u>long</u> cylindrical shell (Fig. 9-29c) is given by Eqs. 9.14 to 9.17 in Section 9.2.

The circumferential buckling stess resultant for a <u>moderate</u> length cylinder (Figs. 9-29a, d) is (9.21):

$$N_{\theta c} = \sigma_{\theta c}\, a_\theta = \frac{5.5\, k_n\, (\bar{A}_x)^{1/4}\, (D_\theta)^{3/4}}{L\sqrt{R}} \qquad \text{Eq. 9.86}$$

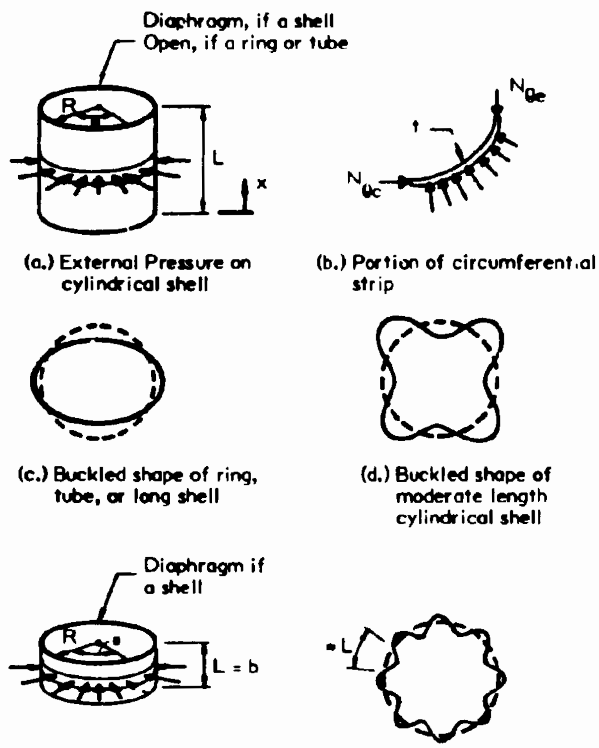

(a.) External Pressure on cylindrical shell

(b.) Portion of circumferential strip

(c.) Buckled shape of ring, tube, or long shell

(d.) Buckled shape of moderate length cylindrical shell

(e.) Short shell

(f.) Buckled shape of short cylindrical shell

Fig. 9-29 BUCKLING OF RADIALLY COMPRESSED CYLINDER

In terms of the external pressure that buckles the shell, this becomes:

$$p_{cr} = \frac{5.5\, k_n\, (\bar{A}_x)^{1/4}\, (D_\theta)^{3/4}}{L\, R \sqrt{R}} \qquad \text{Eq. 9.86a}$$

The circumferential buckling stress for an isotropic, uniform thickness, <u>moderate</u> length cylinder is (9.21):

$$\sigma_{\theta c} = \frac{0.855 \quad k_n\ E\ t}{(1 - \nu^2)^{3/4}\, L \sqrt{R/t}} \qquad \text{Eq. 9.87}$$

In terms of the external pressure that buckles the shell, this becomes:

$$p_{cr} = \frac{0.855 \quad k_n\ E\ t^2}{(1 - \nu^2)^{3/4}\, L\, R \sqrt{R/t}} \qquad \text{Eq. 9.87a}$$

The coefficient, k_n, is a knockdown coefficient for effect of imperfections on buckling of moderate length cylindrical shells under radial pressure. These shells derive their buckling resistance from the combined action of circumferential bending stiffness and in-plane shear and axial cylindrical membrane stiffnesses that restrain "ovalling" of the ring during buckling. This behavior is not "imperfection sensitive", consequently the knockdown coefficient required to obtain agreement with test results is much larger than in the case of a longitudinally loaded cylinder. A constant knockdown coefficient, $k_n = 0.9$, is suggested (9.9) for use in Eqs. 9.86 and 9.87.

For shells subject to long term stress and/or elevated temperatures, the viscoelastic modulus should be used in place of E in the above equations. If stress-strain relations are not linear, k_n should be multiplied by the following approximate plasticity correction factor (isotropic materials) (9.9):

$$\eta = \frac{E_s}{E}\left[\frac{1}{4} + \frac{3}{4}\frac{E_t}{E_s}\right] \qquad \text{Eq. 9.88}$$

For sandwich shells with "shear soft" cores, a suitable reduction factor for shear deformation should be applied to the flexural stiffness, D_θ, in Eq. 9.82. See Fig. 9-26.

The buckling stress resultant for an isotropic uniform thickness cylinder of <u>short</u> length (Fig. 9-29e, f) is given by Eq. 6.71 (Chapter 6) for a longitudinally loaded "long" plate, with coefficients obtained from Table 6-3 for various conditions of restraint along the edges. In this case, the long direction of the plate is the circumference of the "short" cylinder. The width, b, of the plate is the length, L, of the "short" cylinder. No general "knockdown factor" for imperfections is required in the case of short shells.

For an orthotropic "short" cylinder, use Eqs. 6.92, or 6.94, depending on rotational restraint of edges.

For a sandwich short cylinder, use Eq. 6.71 in Chapter 6 and the buckling coefficients given in Fig. 8-18 in Chapter 8.

In order to determine whether a particular radially loaded cylindrical shell behaves as a long, moderate length, or short cylinder, the buckling stress resultant, $N_{\theta c}$, stress $\sigma_{\theta c}$, or pressure, p_{cr}, may be calculated for each type.

The **highest** calculated buckling stress resultant determines the buckling strength and the mode of buckling (i.e: length, classification).

Example 9-13 illustrates application of the above equations to determine the external pressure that will produce buckling of the cylindrical tube sketched in Example 9-12 when heavy rib supports or end diaphragms are spaced at 20 ft longitudinally.

Torsionally loaded cylinder. In Fig. 9-30, a cylinder is shown loaded in torsion, producing a state of pure shear in the x and θ directions, and diagonal compression and tension at a 45-degree helix angle. Here, the shell buckles into inclined circumferential waves that spiral along the cylinder. Again, cases involving a long cylinder, a moderate length cylinder and a short cylinder are considered.

The shear buckling stress for an isotropic, uniform thickness, long cylinder or tube loaded in torsion is (9.26):

$$\tau_{x\theta c} = \frac{0.27k_n E}{(1-\nu^2)^{3/4}} \left[\frac{t}{R}\right]^{3/2} \qquad \text{Eq. 9.89}$$

The shear buckling stress resultant for a ribbed or sandwich long cylinder or tube loaded in torsion is (9.27):

$$N_{x\theta c} = \frac{1.75\,(\bar{A}_x)^{1/4}\,(D_\theta)^{3/4}}{R^{3/2}} \qquad \text{Eq. 9.90}$$

The shear buckling stress for an isotropic uniform thickness moderate length cylinder loaded in torsion is (9.26):

$$\tau_{x\theta c} = \frac{0.70k_n E}{(1-\nu^2)^{5/8}} \left[\frac{t}{R}\right]^{5/4} \left[\frac{R}{L}\right]^{1/2} \qquad \text{Eq. 9.91}$$

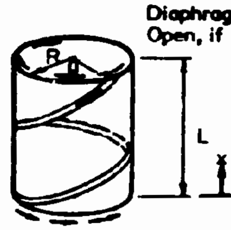

Fig. 9-30 BUCKLING OF TORSIONALLY LOADED CYLINDER

Example 9-13: Determine the external pressure that will produce radial buckling of the cylindrical ribbed tubular section shown in **Example 9-12** if diaphragms or very stiff ribs are provided at a longitudinal spacing of 20 ft.*

1. Longitudinal and circumferential stiffness properties per unit length for use in Eq. 9.86a: See **Example 9-12** for material properties.

$$\bar{A}_x = \frac{E_x t}{1 - \nu_x \nu_\theta} = \frac{0.8 \times 10^6 \times 0.3}{(1 - 0.11 \times 0.41)} = 0.25 \times 10^6 \text{ lbs/in}$$

D_θ is obtained by determining the averaged (smeared out) properties of a 12 inch length. A portion of shell having a length of $0.76 \sqrt{Rt}$ on each side acts with the rib. Thus, rib width = $2 + 2 \times .76 \sqrt{48 \times 0.3} = 7.77$ in. < 12 in.

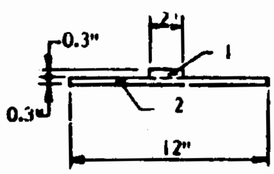

	A	y	Ay	$\bar{y}$	$A\bar{y}^2$		Io
1. 2×0.3 =	0.6	0	0	0.238	0.034	$2 \times .3^3/12$ =	0.0045
2. 7.77×0.3 =	2.3	0.3	0.69	0.062	0.009	$7.77 \times .3^3/12$ =	0.0175
	2.9		0.69		0.043		0.0220
							0.0430
						I_θ =	0.0650

$$\bar{y} = \frac{0.69}{2.9} = 0.238 \text{ in.}$$

$$i_\theta = I/12 = 0.00542 \text{ in.}^4\text{/in.}$$

$$D_\theta = \frac{E_\theta i_\theta}{1 - \nu_x \nu_\theta} = \frac{3 \times 10^6 \times 0.00542}{(1 - 0.41 \times 0.11)} = 1.70 \times 10^4 \text{ lbs-in}$$

2. Buckling pressure, based on general buckling of the 20 ft. long ribbed shell:

Eq. 9.86a: $$p_{cr} = \frac{5.5\, k_n\, (A_x)^{1/4}\, (D_\theta)^{3/4}}{LR\sqrt{R}}; \text{ Take } k_n = 0.9.$$

$$p_{cr} = \frac{5.5 \times 0.9 \times (25 \times 10^4)^{1/4}\, (1.70 \times 10^4)^{3/4}}{240 \times 48\sqrt{48}} = 2.06 \text{ psi}$$

Also check Eq. 9.15 for long tube buckling:

$$p_{cr} = \frac{3\,D_\theta}{R^3} = \frac{3 \times 1.70 \times 10^4}{48^3} = 0.46 \text{ psi} < 2.06 \text{ psi; use } p_{cr} = 2.06 \text{ psi}$$

3. Check local buckling of shell between ribs; consider as intermediate length shell, L = 10 in.:

$$D_\theta = \frac{E_\theta t^3/12}{1 - \nu_\theta \nu_x} = \frac{3.0 \times 10^6 \times 0.3^3/12}{(1 - 0.41 \times 0.11)} = 0.71 \times 10^4 \text{ psi; } \bar{A}_x \text{ same as above.}$$

$$p_{cr} = \frac{5.5 \times 0.9 \times (25 \times 10^4)^{1/4}\, (0.71 \times 10^4)^{3/4}}{10 \times 48\sqrt{48}} = 25.7 \text{ psi} > 2.06 \text{ psi}$$

Thus, radial buckling between local ribs does not govern. No need to check using short shell equations since general buckling of 20 ft long shell governs.

Note: 1 in. = 25.4 mm, 1 in.^{4}/in. = 16387 mm^4/mm, 1 ft = 0.305 m, 1 lbf-in. = 0.113 Nm, 1 lbf/in. = 175 N/m, 1 psi = 0.0069 MPa.

* See footnote, Example 9-1, page 9-13.

The shear buckling stress resultant for a ribbed or sandwich moderate length cylinder loaded in torsion is (9.27):

$$N_{x\theta c} = \frac{3.46\,(\bar{A}_x)^{3/8}\,(D_0)^{5/8}}{L^{1/2}\,R^{3/4}} \qquad \text{Eq. 9.92}$$

Long and moderate length cylinders stressed in shear are not as sensitive to reductions in buckling strength from geometrical imperfections as longitudinally compressed cylinders. Also, they do not experience as much of a drop in post buckling strength as a longitudinally compressed cylinder. This is because shear induced by torsion represents compression in one diagonal direction accompanied by tension in the orthogonal diagonal direction. Nevertheless, experiments show some reduction from the buckling strength determined using linear elastic analysis (9.9). In the absence of specific experimental data for a particular design, a knockdown coefficient, $k_n = 0.8$, is suggested, based on test data given in the literature (9.9).

The effect of creep may be taken into account by using the viscoelastic modulus, E_v, for a particular duration of load and maximum temperature design criteria in place of E in Eqs. 9.89 and 9.91 above, and in the stiffness terms, $\bar{A}_x$ and D_0, in the other equations. Also for sandwich shells, the effect of core shear deformation may be significant. An appropriate reduction coefficient, k_s, may be applied to the flexural stiffness, D_0 in Eqs. 9.90 and 9.92.

The shear buckling stress, or stress resultant, for a short cylinder loaded in torsion is obtained using plate shear buckling equations given in Chapter 6. Use Eqs. 6.84 for isotropic short shells and 6.102 for orthotropic (including ribbed) short shells. For a complete cylinder of length L and radius R, b = L and a = $2\pi R$ in the plate buckling equations.

The highest value of the shear buckling stress, as determined by the appropriate equations given above for long, moderate and short length shells is the proper calculated buckling strength. The length associated with this stress establishes the proper length classification.

The above equations for shear buckling of cylinders loaded in uniform shear resulting from torsion provide a lower bound for the shear buckling strength of cylindrical shells subject to conditions of varying shear. One common case occurs when a cylindrical shell behaves as a tubular beam, resulting in conditions of a maximum membrane shear stress resultant at locations at the end of the beam span and at the neutral axis of the beam on the sides of the cylinder. Elsewhere in the cylinder, shear is lower, and thus, the torsional loading case provides a conservative "lower bound" shear buckling estimate. See **Example 9-15** in Section 9.12 for an illustration of the use of the above equations to estimate the shear buckling strength of a horizontal cylindrical vessel on saddle supports.

Combination of Longitudinal and Circumferential Compression and Shear Stress. The following interaction equation provides a conservative means to account for the effect of combinations of longitudinal and circumferential compression and shear stresses on the buckling of a cylindrical shell:

$$\frac{N_x}{N_{xc}} + \frac{N'_x}{N_{xc'}} + \frac{N_\theta}{N_{\theta c}} + \left(\frac{N_{x\theta}}{N_{x\theta c}}\right)^2 \leq 1.0 \qquad \text{Eq. 9.93}$$

The terms with c subscripts in the denominators are the critical buckling stress resultants without the presence of other types of stress. The terms in the numerator are the calculated simultaneously applied ultimate stress resultants of each type. The unprimed N_x term is the uniform longitudinal stress resultant, and the primed N_x' term is the non-uniform (bending) longitudinal stress resultant at a critical point of a cylindrical shell.

The preceding equation is similar to Eqs. 6.87 and 6.82 for plate buckling under combined stresses. See (9.24) for a summary of more extensive analyses of combined stress cases.

Other Solutions for Buckling of Cylindrical Shells. See (9.24) for equations applicable to isotropic uniform wall, ribbed or sandwich cylindrical shells under axial and radial compression and shear that differ somewhat from some of the preceding equations. Plasticity reduction factors are also suggested for each type of buckling.

Conical Shells.

Like the cylinder, the surface of a circular cone is formed by revolving a straight line about a longitudinal axis. In the case of the cone, the generating line is inclined to the axis of revolution, while in a cylinder it is parallel to it. Thus, like the cylinder, a cone has an infinite radius of curvature in one principal direction, but in the other direction, its radius of curvature varies with distance from the apex. Because of its similarity to a cylinder, buckling relations for conical shells may be determined using an equivalent cylinder. The equivalent cylinder radii are shown in Fig. 9-31 for the three basic types of buckling behavior. The following transformation relations are suggested (9.9):

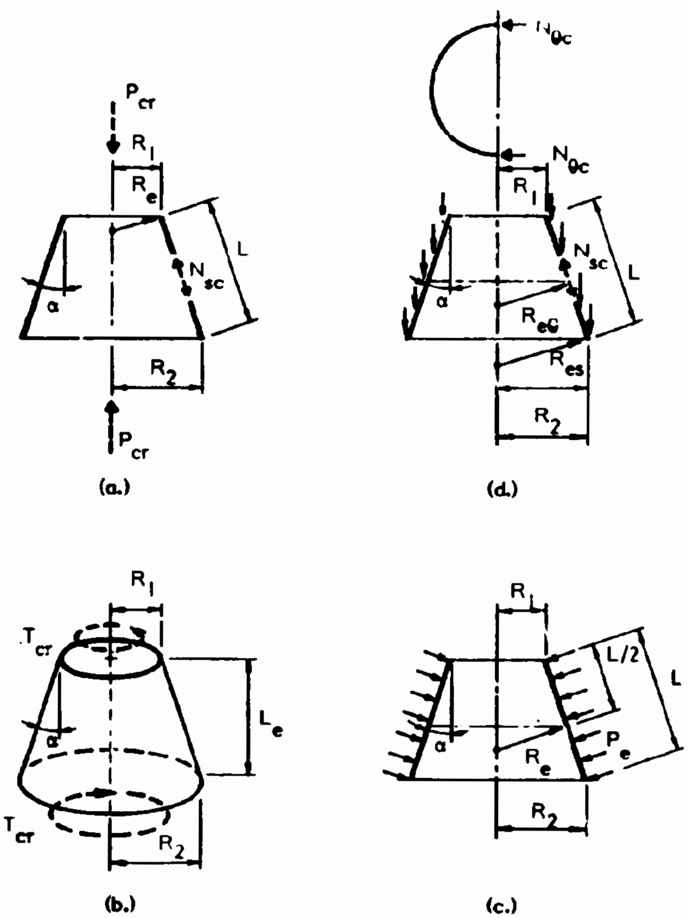

Fig. 9-31 EQUIVALENT CYLINDER RADII FOR BUCKLING OF CONICAL SHELLS

Longitudinally compressed cone (Fig 9-31a): Determine N_{sc} (or σ_{sc}) at the small end of the cone using Eqs. 9.72 or 9.73 for a longitudinally compressed cylinder, and the following equivalent cylinder radius, R_e (9.9):

$$R_e = \frac{R_1}{\cos\alpha} \qquad \text{Eq. 9.94}$$

$$P_{cr} = 2\pi R_2 N_{sc} \cos^2\alpha \qquad \text{Eq. 9.95}$$

The same equivalent cylinder approach may be used to analyze the buckling of cylinders under non-uniform longitudinal compression caused by an applied bending moment (9.9).

Cone under torsion (Fig. 9-31b): Determine a pseudo-shear buckling stress resultant, $N'_{s\theta c}$ (or $\tau'_{s\theta c}$), at the small end of the cone using Eqs. 9.92, or 9.91, for a cylinder loaded in torsion, and the following equivalent cylinder radius, R_e, (9.9):

$$R_e = R_1 \cos\alpha \left[1 + \left(\frac{1 + R_2/R_1}{2}\right)^{1/2} - \left(\frac{1 + R_2/R_1}{2}\right)^{-1/2}\right] \qquad \text{Eq. 9.96}$$

Determine the actual critical shear stress resultants at the small end as:

$$N_{s\theta c} = \left(\frac{R_1}{R_e}^2\right) N'_{s\theta c} \qquad \text{Eq. 9.97}$$

For a constant thickness cone:

$$\tau_{s\theta c} = \frac{N_{s\theta c}}{t} \qquad \text{Eq. 9.98}$$

Also: $$T_{cr} = 2\pi R_1^2 N_{s\theta c} \qquad \text{Eq. 9.99}$$

Cone under external pressure (Fig. 9-31c): For a cone subject to external pressure on the sides only (no loads on top and bottom ends), determine a pseudo buckling stress resultant, $N_{\theta c}'$, (or $\sigma_{\theta}'_c$), at the large end of the cone using Eqs. 9.86, or 9.87, for circumferential buckling of a cylinder, and the following equivalent cylinder radius, R_e, at mid-length of the cone, (9.9):

$$R_e = \frac{(R_1 + R_2)}{2 \cos \alpha} \qquad \text{Eq. 9.100}$$

Determine the actual critical circumferential stress resultant at the large end:

$$N_{\theta c} = N'_{\theta c} \frac{R_2}{R_e \cos\alpha} \qquad \text{Eq. 9.101}$$

$$\text{Also: } p_{cr} = \frac{N_{\theta c} \cos \alpha}{R_2} = \frac{N_{\theta}'{}_c}{R_e} \qquad \text{Eq. 9.102}$$

For a constant thickness cone:

$$\sigma_{\theta c} = \frac{N_{\theta c}}{t} \qquad \text{Eq. 9.103}$$

Cone under distributed dead loading (Fig. 9-31d): First investigate buckling, due to circumferential stress resultants. Determine $N'_{\theta c}$ (or $\sigma_{\theta}'{}_c$) at the large end of the cone using Eqs. 9.86, or 9.87 for circumferential buckling of a cylinder, and the following equivalent cylinder radius, $R_{e\theta}$, at mid-length of the cone:

$$R_{e\theta} = \frac{(R_1 + R_2)}{2 \cos \alpha} \qquad \text{Eq. 9.104}$$

Determine the actual critical circumferential stress resultant at the large end:

$$N_{\theta c} = N_{\theta}'{}_c \frac{R_2}{R_{e\theta} \cos \alpha} \qquad \text{Eq. 9.105}$$

For a constant thickness cone:

$$\sigma_{\theta c} = \frac{N_{\theta c}}{t} \qquad \text{Eq. 9.103}$$

Also investigate buckling due to longitudinal stress resultants. Determine N_{sc} (or σ_{sc}) at the large end of the cone using Eqs. 9.72 and 9.74 for a longitudinally compressed cylinder, and the following equivalent radius, R_{es}:

$$R_{es} = \frac{R_2}{\cos \alpha} \qquad \text{Eq. 9.106}$$

Compare the above critical stress resultants for circumferential and longitudinal buckling with the appropriate circumferential and longitudinal membrane stress resultants at the large end of the cone.

The same approach, using the equivalent radii given in Eqs. 9.104 and 9.106, may be used for conical shells subject to other types of distributed load such as snow load or fluid load.

See Table 9-3 for membrane stress resultants in conical shells under various distributed loadings.

Spherical Shells.

The theoretical buckling stress resultant in a sphere under uniform external pressure is exactly the same as the longitudinal buckling stress resultant in a longitudinally compressed cylinder. The meridional direction of the sphere is analogous to the longitudinal direction of the cylinder, while the circumferential direction is analogous to the cylinder hoops. Thus, for a spherical shell (9.21):

$$N_{\phi c} = \frac{2\sqrt{3}\ C\sqrt{D_{\phi}\bar{A}_{\theta}}}{R} \qquad \text{Eq. 9.107}$$

$$P_{cr} = \frac{4\sqrt{3}\ C\sqrt{D_{\phi}\bar{A}_{\theta}}}{R^2} \qquad \text{Eq. 9.107a}$$

For an isotropic, uniform thickness, shell:

$$\sigma_{\phi c} = \frac{C\,E\,t}{R} \qquad \text{Eq. 9.108}$$

$$P_{cr} = \frac{2\,C\,E\,t^2}{R^2} \qquad \text{Eq. 9.108a}$$

The term, C, is a shell buckling coefficient that is determined as follows:

$$C = k_o\,k_n\,k_s \qquad \text{Eq. 9.79}$$

The coefficients k_o, k_n, and k_s were described previously under cylindrical shells. The buckling coefficient from the classical linear buckling analysis, k_o, is the same as the coefficient given for longitudinally compressed cylindrical shells given by Eq. 9.74. The knockdown coefficient, k_n, is estimated from one of the methods given below. The reduction factor for shear deformation is not significant, except in certain sandwich shells with "shear soft" cores, and is taken as 1.0 for other spherical shells.

In one approach (9.9), the knockdown coefficient is:

$$k_n = 0.14 + \frac{3.2}{\lambda^2} \quad \text{for } \lambda > 2.0 \qquad \text{Eq. 9.109}$$

$$\text{where } \lambda = 2\left[12(1-\nu^2)\right]^{1/4}\left(\frac{R}{t}\right)^{1/2} \sin\frac{\phi_k}{2} \qquad \text{Eq. 9.110}$$

ϕ_k = half the included angle of the shell (see Table 9-3)

The above value of k_n gives a conservative lower bound for buckling pressure, based on data for shallow spherical caps and may also be used for deeper shells (9.9).

Another semi-empirical equation for k_n is (9.28):

$$k_n = 0.25\,(1 - 0.175\,\frac{(\phi_k - 20^\circ)}{20^\circ})\,(1 - \frac{0.07\,R/t}{400}) \qquad \text{Eq. 9.111}$$

for $20^\circ \leq \phi_k \leq 60^\circ$ and $400 \leq \frac{R}{t} < 2000$

As a rough approximation, k_n may be taken as 0.16 to 0.20 when $R/t > 400$.

In **Example 9-14**, the shell that was analyzed for membrane and edge bending stress resultants in **Example 9-7** is checked for stability using the above equations for buckling and knockdown coefficient. See also **Example 9-17** in Section 9.13 for an illustration of the use of the above equations for determining the required thickness of a transparent plastic dome shell.

Example 9-14: Determine the factor of safety against buckling for the spherical shell that was analyzed in Example 9-7. $t = 0.5$ in., $R = 100$ in., $E = 640{,}000$ psi, $\phi_k = 30^o$.*

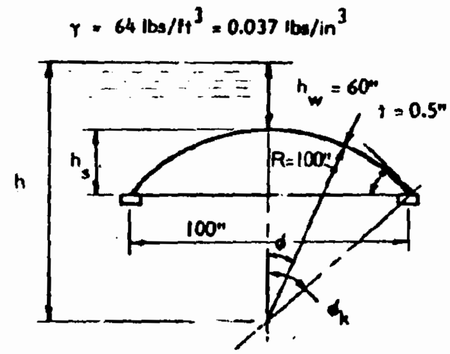

Eq. 9.108 $\quad \sigma_{\phi c} = \frac{C E t}{R}$; $C = k_o\, k_n\, k_s$; $k_o = 0.6$ and $k_s = 1.0$; try several methods for k_n:

Eq. 9.109: $\quad k_n = 0.14 + \frac{3.2}{\lambda^2}$

Eq. 9.110. $\quad \sigma = 2 \left[12 (1 - 0.3^2)\right]^{1/4} \left(\frac{100}{.5}\right)^{1/2} \sin \frac{30}{2} = 13.3$

$$k_n = 0.14 + \frac{3.2}{(13.3)^2} = 0.158$$

Alternate:

Eq. 9.111: $\quad k_n = 0.25 \left[1 - 0.175 \frac{(30 - 20)}{20}\right] \left[1 - \frac{0.07 \times 100/0.5}{400}\right] = 0.22$

Use average $k_n = (0.16 + 0.22) \times 0.5 = 0.19$

$$\sigma_{\phi c} = \frac{0.6 \times 0.19 \times 640{,}000 \times 0.5}{100} = 365 \text{ psi}$$

$$SF = \frac{365}{246} = 1.48 \text{ near edge, and } \frac{365}{222} = 1.64 \text{ near apex}$$

Note: 1 in. = 25.4 mm, 1 psi = 0.0069 MPa, 1 lbf/ft^3 = 157 N/m^3, 1 lbf/in.^{3} = 271000 N/m^3.

* See footnote, Example 9-1, Page 9-13.

In another approach, Eq. 9.108 is used with the following value of $k_o k_n$ covering the effects of using uniformly distributed ribs or sandwich construction, as well as imperfections and plasticity (9.19):

$$k_o k_n = -0.54 \frac{\Delta}{\bar{a}} - 0.145 \left[9.9 \left(\frac{\Delta}{\bar{a}} \right)^2 + 37 \frac{i}{\bar{a}^3} \right]^{1/2} + \left\{ 1.09 \left(\frac{\Delta}{\bar{a}} \right)^2 - 0.03 \frac{\Delta}{\bar{a}} \left[9.9 \left(\frac{\Delta}{\bar{a}} \right)^2 + 37 \frac{i}{\bar{a}^3} \right]^{1/2} + 4.31 \frac{i}{\bar{a}^3} \right\}^{1/2} \qquad \text{Eq. 9.112}$$

Δ is the · ιum deviation from the theoretical curvature, including deflection.

If $\Delta = 0$ (no imperfections):

$$k_o k_n = 1.21 \frac{(i\,\bar{a})^{1/2}}{\bar{a}^2} \qquad \text{Eq. 9.113}$$

but $k_o k_n$ should not be taken greater than one half the value given by Eq. 9.113 for any practical shell.

In shells subject to long term stress, E should be replaced by E_v for the particular duration of stress and maximum surface temperature for that duration. If isochronous stress-strain relations are not linear, a plasticity reduction factor, η, should be applied to E or E_v, as described previously for cylindrical shells.

In the case of a sandwich shell with a "shear soft" core, the reduction factor, k_s, given in Fig. 9.26 for cylindrical shells may be used for spherical shells together with one of the above estimates for knockdown coefficient, k_n.

Buckle wave length is:

$$\ell_b = 3.72 \sqrt{R} \left(\frac{i}{\bar{a}} \right)^{1/4} \qquad \text{Eq. 9.114}$$

For a shell of uniform thickness:

$$\ell_b = 2\sqrt{Rt} \qquad \text{Eq. 9.115}$$

Eq. 9.108 may be used for investigating the buckling of a spherical segment of shell between ribs or supports with restricted wave length, where distance between ribs each way, $d \leq 2\sqrt{Rt}$, using the following buckling coefficient (9.29):

$$C = 0.00226\,\frac{d^2 t}{R^3} + \frac{3.7\,t^3}{d^2 R} \qquad \text{Eq. 9.116}$$

An equation for the buckling coefficient for spherical shells with various patterns of radial and circumferential ribs is given in (9.30).

When a spherical shell is subject to significant concentrated loads, the following buckling case may provide a useful indication of whether the shell has adequate safety against local buckling from the concentrated loads. The approximate concentrated load, P_c, at the apex of a isotropic uniform thickness spherical cap that buckles the shell is (9.9):

$$P_c = \frac{\lambda^2 E t^3}{24 R} \qquad \text{Eq. 9. 117.}$$

where λ is given by Eq. 9.110, and may extend over a range from 4 to 18. This equation is a lower bound relationship for shells with unrestrained edges. When λ is less than about 4, "snap through" buckling generally will not occur (9.9). This conclusion should be checked experimentally for any particular shell, material, and loading combination.

Other Shells of Positive Double Curvature

For a shell having radii of principal curvature, R_1 and R_2, the theoretical buckling stress resultant in the direction with principal curvature R_1 is the same as the longitudinal buckling stress resultant in a cylinder with a radius of R_2. Thus:

$$N_{1c} = \frac{2\sqrt{3}\,C\sqrt{D_1 \bar{A}_2}}{R_2} \qquad \text{Eq. 9.118a}$$

$$N_{2c} = \frac{2\sqrt{3}\, C\sqrt{D_2 \bar{A}_1}}{R_1} \qquad \text{Eq. 9.118b}$$

D_1 is the flexural stiffness and $\bar{A}_1$ is the axial stiffness in the direction having radius R_1, while D_2 and $\bar{A}_2$ are the respective flexural and axial stiffnesses in the direction having radius R_2. The buckling coefficient, C, may be estimated using the R/t ratio for the principal direction orthogonal to the direction of critical compression stress, as described previously.

See (9.9) for specific buckling relations for various doubly curved shapes such as complete ellipsoidal shells, ellipsoidal and torispherical heads, complete circular toroidal (donut shape) shells, and bowed out toroidal segments. Note that with some of these shapes, internal pressure produces compression in certain parts of the shell, thereby requiring consideration for buckling resistance even though the major stress resultants in the shell are tensile. See Vol. 2 of (9.17) for several discussions of conditions that produce buckling of torispherical and ellipsoidal heads under internal pressure.

Hypars

A hypar has negative Gaussian curvature. It has radii of principal curvature which are of opposite sign. For the "skew hypar" shown in Fig. 9-11c, d, approximate equations for the radii of principal curvature are (9.31):

Long diagonal: $$R_1 = \frac{2ab}{c} \cos^2 \frac{\omega}{2} \qquad \text{Eq. 9.119a}$$

Short diagonal: $$R_2 = \frac{2ab}{c} \sin^2 \frac{\omega}{2} \qquad \text{Eq. 9.119b}$$

Membrane stresses in hypar shells subject to uniform lateral pressure are given in Section 9.5. In either a right hypar or the more general skew hypar, the diagonal direction which is "arched up" toward the load is in compression, while the diagonal direction which is "sagged down" is in tension. The diagonal which is in compression is analagous to the longitudinal direction in a longitudinally compressed cylinder. The radius of the opposite tension diagonal is analagous to the radius of a longitudinally compressed cylinder. Thus, the buckling stress resultant of a skew hypar (Fig. 9-11c, d) is (9.31), for compressive principal stress in the, Long diagonal: $$N_{1c} = \frac{c}{a\, b \sin^2 \frac{\omega}{2}} \sqrt{D_1 \bar{A}_2}$$ Eq. 9.120a

Short diagonal: $$N_{2c} = \frac{c}{a\, b \cos^2 \frac{\omega}{2}} \sqrt{D_2 \bar{A}_1}$$ Eq. 9.120b

For an isotropic uniform thickness hypar, the buckling stress is (9.31):

For compressive principal stress in the

Long diagonal: $$\sigma_{1c} = \frac{c\ E\ t}{a\, b \sin^2 \frac{\omega}{2} \sqrt{3\,(1 - \nu^2)}}$$ Eq. 9.121a

Short diagonal: $$\sigma_{2c} = \frac{c\ E\ t}{a\, b \cos^2 \frac{\omega}{2} \sqrt{3\,(1 - \nu^2)}}$$ Eq. 9.121b

The uniformly distributed pressure which buckles a skew hypar is (9.31):

$$p_{cr} = \frac{2\, c^2\, E\, t^2}{a^2\, b^2 \sin^2 \omega \sqrt{3\,(1 - \nu^2)}}$$ Eq. 9.121c

Note that in the above equations, $\omega \leq 90^{\circ}$, and a, b and c are the dimensional parameters of the hypar (Fig. 9-11c).

Eq. 9.121c for buckling of a skew hypar was derived by approximating the hypar as a longitudinally loaded cylinder (direction of principal compression is taken as longitudinal) with radius equal to the "averaged" radius of the tension parabola (Eqs. 9.119, a or b) and longitudinal axis in direction of compression parabola. The "averaged" radius of the tension parabola is obtained by approximating the radius of curvature of this parabola by the second derivative of its geometrical equation (9.31). Reisner (9.38) derived exactly the same equation for an equilateral right hypar ($\omega = 90^{\circ}$, $a = b$) using classical linear buckling theory.

Unlike the buckling relations for longitudinally loaded cylinders and doubly curved shells of positive Gaussian curvature, the above equations for buckling of hypars do not include a knockdown factor. This is because in a hypar under uniform lateral pressure, whenever compression exists in the one principal direction, tension exists in the orthogonal direction, and this greatly reduces the imperfection sensitivity of the thin hypar shell. However, the designer should be cautious in choice of safety factors since research is needed to determine the actual effects of imperfections, edge deformations, and other deviations from theoretical conditions in hypar shells. The more flat the shell, the greater the expected reductions from theoretical buckling strength. Corrections should also be introduced for creep and shear deformation in cases where such behavior may be significant.

Use of the above equations for determining the required thickness of a skew hypar shell for adequate buckling strength is illustrated in **Example 9-18** in Section 9.13. A high load factor is used in this example because of uncertainties about the accuracy of the knockdown factor and the validity of the membrane theory for predicting diagonal compressive stress resultants in certain hypar shells. It was noted previously in Section 9.4 that significant differences have been found between membrane compression stress resultants and compression stress resultants determined by more accurate analyses that take into account bending introduced by support deformations in certain types of hypar shells (9.32)(9.33). These findings indicate that the actual buckling strength of these types of hypars will be significantly less than indicated by the above equations that are based on membrane stress resultants in the main part of the shell. Thus, without tests on models that accurately represent shell geometry and edge support conditions, the above equations provide only an upper bound (unconservative) approximation of the true buckling strength of many hypar shells.

9.11 SANDWICH SHELLS

Sandwich construction provides an efficient structural cross section for utilizing plastics in large lightly loaded shells, typical of roof structures. The membrane and edge bending stress resultants in such shells may be determined using the concepts and equations given previously in this Chapter. However, the design of sandwich shells is often governed by buckling. Buckling resistance of sandwich shells may be determined using the equations given in the preceding Section. Flexural rigidity, D_m, and extensional rigidity, $\bar{A}$, are given in Table 8-1 of Section 8.4. The shell buckling coefficient, C, in Eqs. 9.72, 9.78, 9.79, 9.107, 9.118 should include a reduction factor, k_s, for core shear deformation whenever "shear flexible" cores are used. This term is defined in Section 8.3. For buckling equations that do not include a buckling coefficient, C, a reduction factor for core shear deformation, k_s, should be applied to the flexural rigidity, D_m. k_s is given in Fig. 9-26.

Because of their relatively greater overall thickness, buckling resistance of sandwich shells is usually less sensitive to imperfections. The knockdown factor, k_n, to be used in determining the buckling coefficient, C, should be based on the effective thickness, t_e, of the sandwich. For an isotropic sandwich with thin stiff faces of equal thickness and relatively thick "soft" core; t_e is given by Eqs. 9.82. For a more complex sandwich section, t_e, may be determined using Eq. 9.83 and the methods given in Section 8.4 for calculating D_m and $\bar{A}$.

See (9.24) (9.9) for summaries of more extensive special solutions for buckling of sandwich shells. Summaries of test results are also presented.

Determining Optimum Proportions When Buckling Governs Design.

The usual design problem with a sandwich shell is to determine the proportions required for adequate strength and stability. In regions away from edges where membrane stresses predominate, sandwich section proportions are largely governed by requirements for buckling resistance.

In the majority of shells where behavior is similar to buckling of a longitudinally loaded cylinder, it is often desirable to optimize the proportions of the composite sandwich section to obtain the required quantity: $D_m \bar{A} = E_f\sqrt{i_f \bar{a}_f}$ for the least cost of the core and face materials. This type of optimization is an extension of the concepts for optimizing sandwich proportions to obtain a required section modulus or moment of inertia as explained previously in Section 8.9.

For a sandwich with two symmetrical facings that are both thin and stiff relative to the core structure (see Section 8.9 in Chapter 8 for limitations), the face thickness, t_f, and core thickness, t_c, that provide the least cost of the composite panel (for given face and core material) for a required $i_f \bar{a}_f$ are (9.21):

$$t_f = \sqrt{\frac{C_c \sqrt{i_f \bar{a}_f}}{(2\,C_f - C_c)}} \qquad \text{Eq. 9.122}$$

$$t_c = \left(\frac{2\,C_f}{C_c} - 2\right) t_f \qquad \text{Eq. 9.123}$$

The minimum combined materials cost for these proportions are:

$$\text{min. materials cost/unit area} = \sqrt{C_c\,(2\,C_f - C_c)\sqrt{i_f\,\bar{a}_f}} \qquad \text{Eq. 9.124}$$

In some practical cases, the optimum face thickness, t_f, is thinner than can be fabricated with proper quality assurance, or is thinner than a minimum required for adequate resistance to local effects of handling and usage. Also, sometimes strength requirements, instead of stability, may determine minimum facing thickness. When the preceding conditions apply, a minimum value for face thickness, t_f, is chosen and required proportions are selected as follows:

$$\bar{a}_f = 2\,t_f \qquad \text{Eq. 9.125}$$

$$t_c = \sqrt{\frac{i_f\,\bar{a}_f}{t_f}} - t_f \qquad \text{Eq. 9.126}$$

The minimum combined materials cost for these proportions is:

$$\text{min. materials cost/unit area} = 2\,C_f\,t_f + C_c\,t_c \qquad \text{Eq. 9.127}$$

In those cases where shell buckling is governed by $E_f\,i_f$, rather than by $E_f\sqrt{i_f\,\bar{A}_f}$, (i.e., long cylinder under radial load), Eqs. 8.114 and 8.115 (Chapter 8) for optimum proportions for the case when cross sectional stiffness, $E_f\,i_f$, governs should be used.

Edge bending effects in sandwich shells may be determined using the procedures given in Section 9.6 and stiffness properties determined using procedures given in Chapter 8. Stress may be evaluated using sectional properties and analysis methods given in Chapter 8.

See **Example 9-19** in Section 9.13 for an illustration of how the equations given in this section may be used to proportion sandwich shell cross sections. Also, see Chapter 8 for other considerations in the design of sandwich sections used in shells, such as local buckling of facings away from the core.

9.12 DESIGN EXAMPLES – VESSELS

Fluid storage vessels are important applications for structural plastics because of the widespread need for corrosion resistant containers for storage of corrosive chemicals that often aggressively attack conventional metals. Designs for several types of cylindrical vessels are presented in this Section and in Section 9.7 to illustrate the application of some of the concepts and simplified analysis methods developed earlier in this Chapter.

Examples 9-9 and **9-10** presented in Section 9.7 illustrate the design of an open top, vertically oriented, cylindrical tank with a flat bottom supported on a flat concrete slab. In **Example 9-9**, the vessel has a sharp intersection of wall base and flat bottom and in **Example 9-10** the same cylindrical vessel is provided with a toroidal knuckle transition at the base. Each of the vessels in these examples are fabricated by filament winding continuous glass fibers in a polyester resin matrix to form the cylinder shell, while the bottom and knuckle regions are fabricated by spray-up of chopped glass fiber and polyester resin over a mold.

Example 9-15 in this Section illustrates the design of a cylindrical vessel with axis oriented horizontally, supported on two saddles with stiff ribs at the saddles and with hemispherical head shells. The cylinder is fabricated by spray-up of chopped glass fiber and polyester resin over a mandrel (endless helix) while the head shell is sprayed-up over a mold off mandrel. The ribs at the saddles are formed with alternating layers of woven roving and mat layed up over a cardboard form.

In **Example 9-16**, the design of another horizontally oriented tank, a buried petroleum storage tank, is illustrated. Ribs are provided to resist buckling under external pressure. The overall design considerations that led to the selection of the materials and configuration of this buried petroleum storage tank are discussed in Section 4.15.

See (9.22) and (9.43) for discussions of design approaches and safety factors and for examples of material properties and design results for glass fiber reinforced tanks and vessels, and vessels reinforced with advanced fibers in aerospace applications.

Example 9-15: Develop a preliminary design for the saddle supported horizontal cylindrical 10,000 gal capacity chemical storage tank shown in the sketch. Use a chopped strand fiberglass reinforced plastic laminate applied by spray-up over a mandrel for the cylinder and heads and a mat-woven roving laminate for the ribs that are located at saddles. Laminate properties in any direction are:

		Chopped Strand	Mat-Woven Roving for Rib at Saddle
Tension strength		10,000 psi	18,000 psi
Flexure strength		12,000 psi	24,000 psi
Compression Strength		15,000 psi	18,000 psi
Elastic moduli,	E	800,000 psi	1,600,000 psi
	G	300,000 psi	—
	ν	0.3	0.25

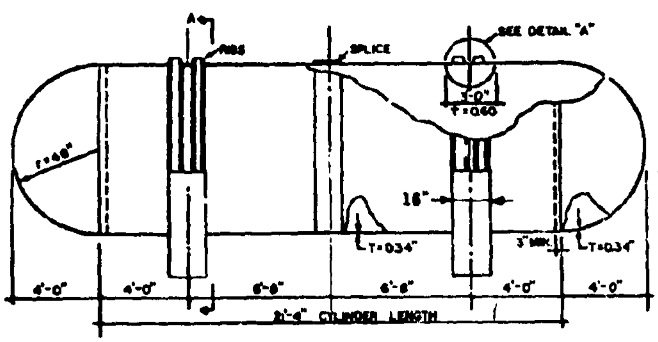

The design fluid specific gravity is taken as 1.1, including an allowance of 0.06 for the weight of the tank, and the tank should be designed for a potential maximum overpressure of 5 psi. The tank should also be capable of resisting a negative internal pressure (or an external pressure) of 0.21 psi (30 psf) when empty.*

1. Location of saddles and load on saddles: The saddles are located to equalize the total shear force on each side of the saddle. This minimizes the shear stress resultant, a design goal since buckling of the tank shell due to in-plane shear is likely to be a design parameter that governs the required shell thickness. Shear forces on each saddle support are equalized when the volume of fluid in the region between the centerline of saddles equals the volume in both the regions beyond the saddles. The 10,000 gallon capacity requires a total volume of 1,337 cu ft. Each hemispherical head has a volume of $2/3\ \pi r^3 = (2\pi \times 4^3)/3 = 134$ cu ft. Thus, the required cylinder volume = 1,337 - 2 x 134 = 1,069 cu ft, requiring a length of $1{,}069/\pi \times 4^2 = 21.3$ ft. To provide one half the volume, the cylinder length between centerlines of saddles should be $1{,}337/2\pi \times 4^2 = 13.3$ ft, or 13 ft-4 in. The cylinder should extend (21.3 - 13.3)/2 or 4.0 ft beyond the centerline of support on each end.

   The total load on each support saddle will be:

   $Q = W/2 = (1337 \times 1.1 \times 62.4)/2 = 45{,}900$ lbs

   The maximum unit weight of fluid and allowance for tank weight is 1.1 x 62.4 = 68.6 lbs/cu ft = 0.040 lbs/cu in.

---

* See footnote, Example 9-1, Page 9-13.

Example 9-15 (continued)

2. Membrane stresses in wall — See Table 9-1.

(a) Circumferential: h = R for fluid load case in Table 9-1

$N_\theta = \gamma R^2 (\frac{R}{R} - \sin \theta)$ with $\theta = 0$ at horizontal diameter

crown: $\theta = 90^\circ$; $N_\theta = 0.040 \times 48^2 \times (1 - 1) = 0$

side: $\theta = 0$; $N_\theta = 92.2\ (1 - 0) = 92.2$ lbs/in.

bottom: $\theta = -90$; $N_\theta = 92.2\ (1 + 1) = 184.4$ lbs/in.

Add for possible 5 psi overpressure (uniform pressure case in Table 9-1):

$$N_\theta = p\,R = 5 \times 48 = 240 \text{ lbs/in.}$$

(b) Shear — fluid load case in Table 9-1

$N_{x\theta} = \gamma R\, (\frac{L}{2} - x) \cos \theta$; max $N_{x\theta} = \gamma R\, \frac{L}{2}$ at sides adjacent to support

If shell is thickened for a width of 1 ft-6 in. on each side of the saddle centerline to resist local stresses at supports, the critical section for shear will be at L'/2 = 80 - 18 = 62 in.

max $N_{x\theta} = 0.04 \times 48 \times 62 = 119$ lbs/in.

(c) Longitudinal Stress

Adjust the N_x stresses given in Table 9-1, fluid load case, for a cylindrical beam with simply supported span, L, to reflect the effect of the overhangs, as follows:

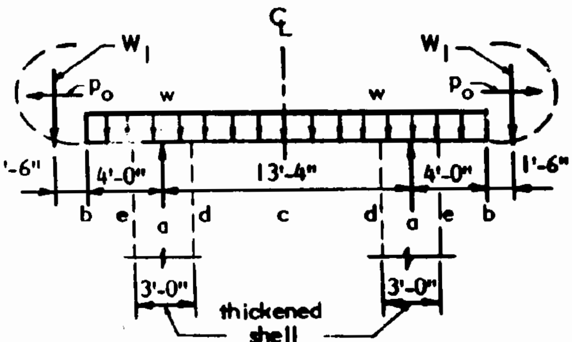

<u>Effect of Vertical Loads:</u>

w = 1069 × 68.6/(21.3 × 12)
= 287 lbs/in.

W_1 = 134 × 68.6
= 9,192 lbs

centroid of half sphere = $\frac{3}{8}$ r
= $\frac{3}{8}$ × 48 = 18 in.

$M_a = -9192 \times (18 + 48) + 287 \times \frac{48^2}{2} = -937{,}300$ in.-lbs

$M_c = \frac{287 \times 160^2}{8} - 937{,}300 = -18{,}900$ in.-lbs

$M_d = -937{,}300 - \frac{287 \times 18^2}{2} + \frac{45{,}900 \times 18}{2} = -570{,}694$ in.-lbs

$M_e = -9192 \times 48 - 287 \times \frac{30^2}{2} = -570{,}366$ in.-lbs

Example 9-15 (continued)

Modifying Case 6 in Table 9-1 for moment distribution with overhang instead of simple beam:

at support a: $N_x = -\gamma \sin \theta \frac{L^2}{8} \quad \frac{M_a}{M_s}$

where M_s = simple beam moment = $\frac{287 \times 160^2}{8}$ = 918,400 in.-lbs

From vertical loads:
at top and bottom: $N_x = -0.04 \times (\pm 1.) \times \frac{160^2}{8} \times (\frac{-937,300}{918,400}) = \mp 131$ lbs/in.

From fluid pressure on ends: $N_x = \frac{\gamma R^2}{2} (\frac{h}{R} - \frac{\sin \theta}{2})$; h = R
(Case 6, Table 9-1)

at top: $\theta = 90^\circ$; $N_x = \frac{0.04 \times 48^2}{2} \quad (1 - \frac{1}{2}) = 23$ lbs/in.

at sides: $\theta = 0$ $N_x = 46 (1 - 0) = 46$ lbs/in.

at bottom: $\theta = -90^\circ$ $N_x = 46 (1 + \frac{1}{2}) = 69$ lbs/in.

From 5 psi overpressure: $N_x = \frac{pR}{2} = \frac{5 \times 48}{2}$ = 120 lbs/in.

Combined N_x at a and d (or e) (Point c is not critical):

	at a		at d	
top:	131 + 23 + 120	= + 274 lbs/in.	$131 \times \frac{570.7}{937.3}$ + 23 + 120	= + 223 lbs/in.
sides:	0 + 46 + 120	= + 166 lbs/in.		= + 166 lbs/in.
bottom:	-131 + 69	= - 62 lbs/in.	-80 + 69	= - 11 lbs/in.

3. Trial wall thickness for strength:

3.1 Capacity reduction factors: Use ϕ = 0.25 for long-term and environmental effects:

tension σ_{xu} = 10,000 x 0.25 = 2,500 psi

compression σ_{xu} = 15,000 x 0.25 = 3,750 psi

3.2 Load factor: Use 2.0 to cover uncertainties in load and analysis.

3.3 Bottom section: N_θ = 184 + 240 = 424 lbs/in.

req'd $t = \frac{424 \times 2}{2,500}$ = 0.34 in.

3.4 Side section at d: N_θ = 92 + 240 = + 332 or + 92 lbs/in.

$N_{x\theta}$ = + 119 or + 119 lbs/in.

N_x = + 166 or + 46 lbs/in.

Example 9-15 (continued)

Eq. 6.69a for principal stress:

$$N_p = \frac{N_\theta + N_x}{2} \pm \sqrt{\left(\frac{N_\theta - N_x}{2}\right)^2 + N_{x\theta}^2}$$

For maximum tension:

$$N_p = \frac{332 + 166}{2} + \sqrt{\left(\frac{332 - 166}{2}\right)^2 + 119^2} = 394 \text{ lbs/in.} < 424 \text{ lbs/in.}$$

For minimum tension, or maximum compression:

$$N_p = \frac{92 + 46}{2} - \sqrt{\left(\frac{92 - 46}{2}\right)^2 + 119^2} = -53 \text{ lbs/in.}$$

Angle of principal compression:

Eq. 6.69b: $\tan 2\phi = -\frac{2 N_{x\theta}}{(N_\theta - N_x)} = -\frac{2 \times 119}{(92 - 46)} = 5.17;\ 2\phi = 79.1^\circ;\ \phi = 39.5^\circ$

3.5 Top section: minimum $N_\theta = 0$

4. Check cylinder shell wall for buckling:

4.1 Shear, or diagonal compression, is governing compressive condition in shell. Torsion buckling of cylindrical shell is the closest case and will probably give conservative results.

Eq. 9.91 for intermediate length cylinder: $\tau_{x\theta c} = \frac{0.70\, k_n E}{(1 - \nu^2)^{5/8}} \left(\frac{t}{R}\right)^{5/4} \left(\frac{R}{L}\right)^{1/2}$

k_n = 0.8 – see discussion in Section 9.10

L = 144 in., the clear distance between inside edge of saddles.

4.2 Use ϕ = 0.7 for elastic moduli because of long term load, aggressive environment and manufacturing variations

$$E = 0.7 \times 800{,}000 = 560{,}000$$

4.3 Try the 0.34 in. thick wall needed for strength:

$$\tau_{x\theta c} = \frac{0.70 \times 0.8 \times 560{,}000}{(1 - .3^2)^{5/8}} \left(\frac{0.34}{48}\right)^{5/4} \left(\frac{48}{144}\right)^{1/2} = 395 \text{ psi}$$

$N_{x\theta c}$ = 395 x .34 = 134 lbs/in.

Furnished load factor = $\frac{134}{53}$ = 2.5 o.k.

A check using Eq. 9.89 for "long cylinder" buckling gives a much lower buckling stress, showing that this cylinder behaves as an intermediate length cylinder.

4.4 The highest longitudinal compressive stress resultant in the thin area between saddles (or in overhang) is 11 lbs/in. and it can be shown using Eq. 9.74 that the buckling resistance is much higher.

Example 9-15 (continued)

4.5 Check circumferential buckling of empty tank to determine sensitivity.

$$\text{Eq. 9.87a: } p_{cr} = \frac{0.855\, k_n\, E\, t^2}{(1-\nu^2)^{3/4}\, L\, R\, \sqrt{R/t}} = \frac{0.855 \times 0.8 \times 560{,}000 \times 0.34^2}{(1-.3^2)^{3/4} \times 144 \times 48\, \sqrt{48/0.34}} = 0.58 \text{ psi}$$

For L.F. = 2.5 for buckling: limit max. external pressure, or internal vacuum, to 0.58/2.5 = 0.23 psi (or 33 psf). Thus, the tank should be adequately vented against a vacuum and should not be unloaded too rapidly.

5. Determine maximum membrane stress resultants in hemispherical head shells:

5.1 Equation of pressure variation:

$$p_z = p_o - \gamma\, r \sin\phi \cos\theta$$

5.2 Stress resultants for p_o: $N_\phi = N_\theta = \frac{p_o\, r}{2} = \frac{\gamma\, r^2}{2} = \frac{.04 \times 48^2}{2} = 46$ lbs/in.

$$N_{\theta\phi} = 0$$

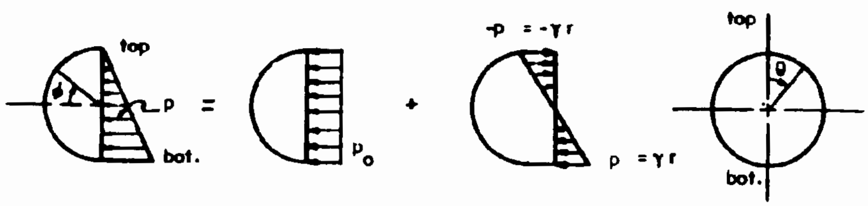

End Section

5.3 Stress resultants for $\gamma\, r \sin\phi \cos\theta$ — same as Table 9-2, wind loading, Case 8, with $\gamma r = p_w$ (Case 8a) and $\phi_o = 0$

$$N_\phi = -\frac{\gamma\, r^2}{3}\, \frac{\cos\theta \cos\phi}{\sin^3\phi}\, (2 - 3\cos\phi + \cos^3\phi)$$

$$N_\theta = +\frac{\gamma\, r^2}{3}\, \frac{\cos\theta}{\sin^3\phi}\, (2\cos\phi - 3\sin^2\phi - 2\cos^4\phi)$$

$$N_{\theta\phi} = \frac{N_\phi \tan\theta}{\cos\phi} = -\frac{\gamma r^2}{3}\, \frac{\sin\theta}{\sin^3\phi}\, (2 - 3\cos\phi + \cos^3\phi)$$

Some trial calculations show that maximum N_ϕ is at $\theta = 0$, $\cos\theta = 1.0$, and $\phi = -55^o$.

$$N_\phi = -\frac{0.04 \times 48^2}{3}\, \frac{1.0\cos(-55)}{\sin^3(-55)}\, (2 - 3\cos(-55) + \cos^3(-55)) = +15 \text{ lbs/in.}$$

Maximum compressive N_θ is at $\theta = 0$ and $\phi = 90^o$ (top)

$$N_\theta = +\frac{.04 \times 48^2}{3}\, \frac{1.0}{1.0}\, (0 - 3 \times 1 - 0) = -92.2 \text{ lbs/in.}$$

Example 9-15 (continued)

Maximum $N_{\theta\phi}$ where $\theta = 90^o$, $\sin\theta = 1.0$, $\phi = \pm 90^o$, $\sin\phi = 1$, $\cos\phi = 0$

$$N_{\theta\phi} = \frac{.04 \times 48^2}{3} \quad \frac{1.0}{1.0} \quad (2 - 0 + 0) = \pm 61.5 \text{ lbs/in.}$$

5.4 Stress resultants for 5 psi overpressure:

$$N_\phi = N_\theta = \frac{p\,r}{2} = \frac{5 \times 48}{2} = 120 \text{ lbs/in.}$$

5.5 Maximum combined membrane stress resultants in head

Tension: N_θ at bottom: $46 + 92 + 120 = 258$ lbs/in.

N_ϕ @ $55^o = 46 + 15 + 120 = 181$ lbs/in.

Compression: (without overpressure):

N_θ at top: $46 - 92 = -46$ lbs/in.

Shear: Determine principal compression at point of maximum shear, without overpressure

$N_\phi = N_\theta = 46$ lbs/in., $N_{\phi\theta} = 62$ lbs/in.

$$\text{neg. } N_p = \frac{46 + 46}{2} - \sqrt{\left(\frac{46 - 46}{2}\right)^2 + 62^2} = -16 \text{ lbs/in.}$$

6. Design thickness of heads – same material as cylinder

6.1 Strength: $\text{req'd } t = \frac{258 \times 2}{2500} = 0.21$ in.

6.2 Buckling: Maximum compression is circumferential at joint with cylinder. Since no rib is provided at this location, the structure behaves like a cylindrical shell of intermediate length, with equivalent length equal to the distance between edge of rib at saddle and effective support point somewhere in the surface of the head where slope is low enough to provide diaphragm action. Estimate effective length,

$$L = 48'' - \text{half rib width} + \frac{2}{3}\,r = 48 - 8 + \frac{2}{3} \times 48 = 72 \text{ in.}$$

Eq. 9.87: $$N_{\theta c} = \frac{0.855\, k_n\, E\, t^2}{(1 - \nu^2)^{3/4}\, L \sqrt{r/t}} = \frac{0.855 \times 0.8 \times 560{,}000 \times 0.21^2}{(1 - .3^2)^{3/4}\; 72 \sqrt{48/.21}}$$

$= 16.6$ lbs/in. $< 46 \times$ L.F. N.G.

Example 9-15 (continued)

Try increasing t to 0.34 in., thickness required for cylinder

$$N_{\theta c} = 16.66 \times \left(\frac{.34}{.21}\right)^{2.5} = 55.6 \text{ lbs/in.}$$

L.F. = 55.6/46 = 1.20. However, N_{θ} = - 46 lbs/in. occurs in only one small location at the top. It very likely will be reduced by continuity with the cylinder where N_{θ} = 0 under fluid load without overpressure (Step 3.5). Thus, a thickness of 0.34 in. will be tentatively adopted for the head shells.

7. Support Ring Rib and Saddles

7.1 General: Stiff rings must be provided at each saddle support to carry the membrane shear stress resultants that deliver the shell loads to the saddle supports. Without such rings, the shell will be subject to very high circumferential and longitudinal bending stress resultants in the saddle region. Longitudinal direct stress resultants will increase as the shell over the saddles deflects, softening the effective beam action of the cylinder. See (9.40) for a detailed discussion of the behavior of saddle supported horizontal vessels without ring ribs.

If a ring is used, an analysis for the moments, thrusts and shears that result from loading by the shell membrane in-plane shear stress resultants and support on a saddle may be obtained by superimposing the appropriate ring analysis cases given in (9.3). The following superposition of cases provides an approximate analysis for the required ring in this problem.

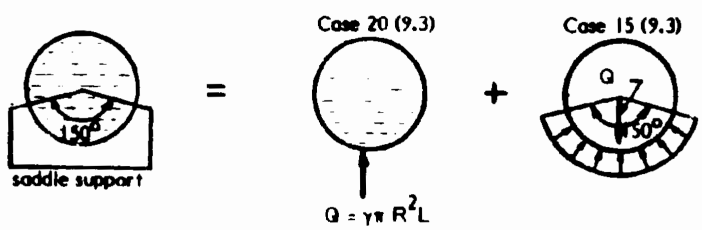

7.2 Investigation of the equations for moment thrust and shear in the above cases in (9.3) gives the following maximum values:

max M = -0.034 Q R, max N = -0.25 Q — at sides, tension on outside

max M = +0.033 Q R, max N = +0.135 Q — at crown, compression on outside

max V = 0.10 Q — at 75° above the base

Q ≈ 46,000 lbs from step 1

at sides:	M = -0.034 x 46,000 x 48	= -75,000 in.-lbs
	N = -0.25 x 46,000	= -11,500 lbs
at crown:	M = 0.033 x 46,000 x 48	= 73,000 in.-lbs
	N = +0.135 x 46,000	= 6,200 lbs
at 75° above bottom:	V = 0.10 x 46,000	= 4,600 lbs

Example 9-15 (continued)

7.3 Check to determine if the following trial rib design provides the necessary resistance to the above stress resultants:

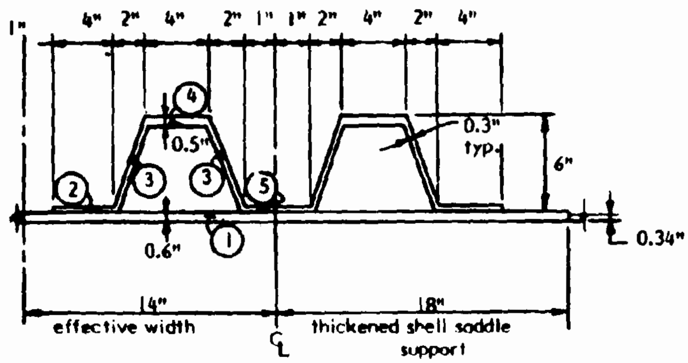

Effective projection of shell wall beyond rib = $0.76\sqrt{Rt} = 0.76\sqrt{48 \times 0.9} = 5$ in.

Section Properties of Half of Rib — Transformed Section to E = 1,600,000 (0.6 to .3)

	Area	A	y	Ay	y_o	Ay_o^2	I_o
1	0.6 x 14 x 0.8/1.6 =	4.2	0	0	2.09	18.3	-
2	0.3 x 4 =	1.2	0.45	0.5	1.64	3.2	-
3	0.3 x 5.9 x 2 =	3.5	3.05	10.7	0.96	3.2	$\frac{3.5 \times 5.5^2}{12} = 8.8$
4	0.5 x 4 =	2.0	6.05	12.1	3.96	31.4	-
5	0.3 x 1 =	0.3	0.45	0.1	1.64	8	
		11.2		23.4		56.9	8.8

$\bar{y} = \frac{23.4}{11.2} = 2.09$ $\qquad I = (8.8 + 56.9) \times 2 = 131.4 \text{ in.}^4$

$S_{top} = \frac{131.4}{4.21} = 31.2 \text{ in.}^3$; $\qquad S_{bot} = \frac{131.4}{2.39} = 55.0 \text{in.}^3$

$A = 2 \times 11.2 = 22.4 \text{ in.}^2$

At sides: outside: $\sigma_t = \frac{M}{S} - \frac{N}{A} = \frac{75{,}000}{31.2} - \frac{11{,}500}{22.4} = 1{,}890$ psi

inside transformed: $\sigma_c = -\frac{75{,}000}{55.0} - \frac{11{,}500}{22.4} = 1{,}877$ psi

transform σ_c back to stress in actual material with E = 800,000 psi:

inside actual: $\sigma_c = \frac{1877}{2} = 939$ psi

Example 9-15 (continued)

At top: outside: $\sigma_c = -\frac{73{,}000}{31.2} + \frac{6{,}200}{22.4} = -2{,}063$ psi

inside transformed: $\sigma_t = +\frac{73{,}000}{55} + \frac{6{,}200}{22.4} = 1{,}604$ psi

transform σ_t back to actual material:

inside: $\sigma_t = \frac{1604}{2} = 802$ psi

7.4 Check transverse stresses in flanges due to radial forces from curvature

Radial pressure, $p_r = \frac{N_0}{R} = \frac{\sigma t}{R}$

Outer flange: $p_{ro} = \frac{2063 \times 0.5}{48 \times 6} = 19.1$ psi

Inner flange: $p_{ri} = \frac{939 \times 0.6}{48} = 11.7$ psi

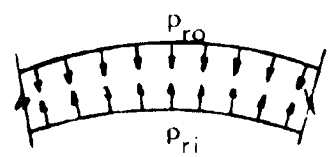

Outer flange, transverse bending: $M = \frac{19.1 \times (4 - 0.6)^2}{10} = 22.1$ in./lbs/in.

$\sigma_f = \frac{22.1}{1 \times 0.5^2/6} = 530$ psi o.k.

Inner flange, transverse bending: $M = \frac{11.7 \times (8 - 0.6)^2}{10} = 64$ in.-lbs/in.

$\sigma_f = \frac{64}{1 \times 0.6^2/6} = 1{,}068$ psi o.k.

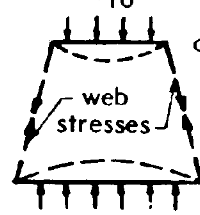

Radial load on web = 19.1 x 2 = 38.2 lbs/in.; low

Note: The maximum web radial force should include the inclined value of 38.2 plus the radial effect of circumferential stress in the web beyond the point of zero stress. This will be of the same order as the 38 lbs/in. and thus the web stresses due to radial loads will be about 200 to 300 psi, well below the allowable strength.

7.5 Check compressive buckling of rib flanges. Use plate buckling equations because under circumferential stress flanges are very "short" shells and behave like plates whose length corresponds to the circumferential length of the rib flange and whose width corresponds to the clear width of the flange.

Eq. 6.71a: $\sigma_{xc} = \frac{k \pi^2 \phi E}{12(1 - \nu^2)} \left(\frac{t}{b}\right)^2$ and k = 4.0

Outer flange: $\sigma_{xc} = \frac{4. \times \pi^2 \times 0.7 \times 1{,}600{,}000}{12(1 - .25^2)} \left(\frac{0.5}{3.4}\right)^2 = 85{,}000$ psi

Inner flange: $\sigma_{xc} = \frac{4. \times \pi^2 \times .7 \times 800{,}000}{12(1 - .3^2)} \left(\frac{0.6}{7.4}\right)^2 = 13{,}300$ psi

Both flanges have adequate safety against buckling. By inspection, the same is true of the webs.

Example 9-15 (continued)

7.6 Approximate check of shear in web: max V = 4,600 lbs

$$\text{approx } \tau = \frac{V}{A_w} = \frac{4{,}600}{3.5 \times 2} = 657 \text{ psi, low}$$

8. Summary: The required cylinder shell thickness is governed by tensile strength under the circumferential stress resultant at the bottom and buckling resistance under the principal diagonal compressive stress near the supports. The hemispherical head shells are made the same thickness as the cylinder shell to obtain adequate resistance to buckling under circumferential compressive stress at the top junction with the cylinder. A stiff rib with substantial bending strength is provided at the saddle locations to reduce local bending effects in the adjacent shells, thereby permitting the use of a shell that is only 0.34 inch thick. A tubular section is used to obtain large bending strength in the rib without excessive material.

Because of the curvature of the rib, the flanges are subject to transverse bending across their width from radial components of the flange forces, and the web is subject to in-plane tensile and compressive stresses in the radial direction. The thin flanges and web of the ring ribs must also be checked for adequate local buckling resistance.

9. Final Comment: Lack of space precludes further examination of secondary bending effects from differences in radial deflection of the rib and membrane shell, local rib stresses due to bearing in the saddle, discontinuity bending stresses at the junction of the head and cylinder, etc.

The preliminary design obtained in this example should be checked by a finite element analysis of the vessel and its support system and/or by the test of a prototype vessel using a fluid with a specific gravity that is greater than 1.1. Drilling mud is a possible candidate material.

If a design without a full ring rib at the support channel is desired, the shell will have to be thickened substantially in the vicinity of the saddles and a check of the stresses in the shell using a finite element computer analysis is absolutely essential. See (9.40) for a guide to estimating design requirements near the saddles in such vessels. However, often assumptions are made for design of steel vessels based on static requirements and the premise that the structure will yield at points of high local bending stress. This is not a valid assumption for plastics vessels.

Note: 1 in. = 25.4 mm, 1 ft = 0.305 m, 1 in.^{2} = 645 mm^2, 1 in.^{3} = 15376 mm^3, 1 ft^3 = 0.028 in.^{3}, 1 in.^{4} = 416231 mm^4, 1 lbf = 4.45 N, 1 lbf/in. = 175 N/m, 1 in.-lbf/in. = 4.45 N-m/m, 1 psi = 0.0069 MPa, 1 psf = 47.9 Pa, 1 lbf/in.^{3} = 0.27 MN/m^3, 1 lbf/ft.^{3} = 157 N/m^3, 1 in.-lbf = 0.113 N-m.

Example 9-16: Develop a preliminary design for a 10,000 gal. buried petroleum storage tank of the type described in Section 4.15. Use the same FRP materials as used in **Example 9-15.***

1. Shape, orientation, general configuration and general approach to design of tank: This is described in Section 4.15. See Fig. 4-25 for arrangement of tank with horizontal axis.

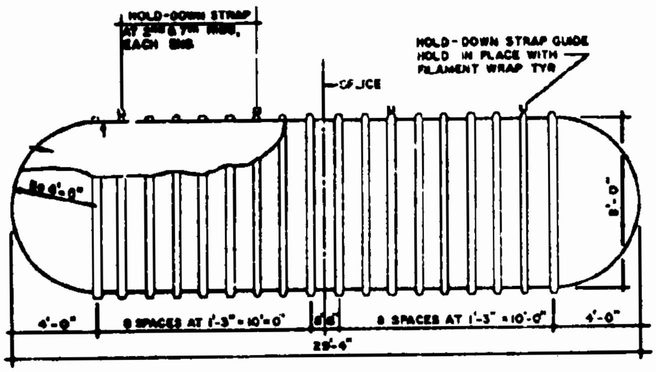

2. Design criteria: These are described in Section 4.15 and are briefly summarized below:
   - Earth cover over top of tank: 3 ft.
   - Depth of ground water over top of tank: 3 ft.
   - Hold-down straps to resist buoyant uplift on empty tank: 4 (See above sketch).
   - Stored product: Petroleum with maximum specific gravity of 0.7.
   - Bedding: well compacted granular material
   - Air pressure test: 5 psi.

3. Design approach: This is described in Section 4.15. The tank design is first developed to have adequate buckling resistance under external earth and water pressure. Prototype tanks are built to meet the design required for this criterion, and are tested for adequacy to meet other design criteria that are less susceptible to theoretical evaluation by rational methods of shell analysis. This avoids the necessity of defining the specific earth and bedding pressure distributions that result when the tank is loaded with 10,000 gals. of fluid, and/or by concentrated wheel pressures at ground surface over the tank.

4. Effect of restraint by earth on buckling resistance: Preliminary tests are performed on a prototype tank shell without ribs to determine whether the earth envelope around the tank increases its resistance to buckling under external pressure. These tests show no significant increase in buckling resistance resulting from earth restraint. This is because the tank is approximately in a state of "neutral buoyancy", with the upward buoyant force of external ground water approximately equal to the submerged weight of the tank and earth cover. Thus, the external earth pressure is nearly zero in the bottom region of the tank, while the water pressure is maximum at this location. Further, the circumferential buckle wave length of a cylindrical shell of intermediate length (the tank) is short compared to the tank circumference so that to be effective, earth restraint must act over the bottom region of the tank. Since earth pressure is zero in this region, no earth restraint is provided. Thus, the tank is designed to resist the external water pressure without restraint of buckling by the earth.

5. Design for buckling resistance:

5.1 Ribs are provided to attain required buckling resistance without an excessively thick shell (without ribs, required shell thickness is over 1 in.). Ribs are formed over cardboard or

---

*See footnote, Example 9-1, Page 9-13.

Example 9-16 (continued)

foam plastic cores to obtain the thin-wall trapezoidal tubular section shown in the sketch. This shape can be fabricated by wet lay-up when the tank shell is being manufactured on a mandrel. See sketch of rib section in Step 5.4.

5.2 Shell thickness is determined based on required resistance to local buckling between ribs. The trial number and arrangement of ribs shown in the sketch results in a center to center spacing of ribs of 15 in. and an assumed effective length of shell between ribs of 10.5 in.

(a) First the thickness is determined for resistance to maximum circumferential compression. This occurs at the bottom of the tank and is produced by an 11 ft. head of ground water with the tank empty.

$$N_\theta = pr = \frac{11 \times 62.4 \times 48}{144} = 228 \text{ lbs/in.}$$

(1) Thickness required for strength: Use material properties given in Example 9-15, with $\phi = 0.4$ and load factor (L.F.) = 2.5. In compression, $\sigma_{\theta u} = 0.4 \times 15000 = 6000$ psi.

$$t = \frac{N_\phi}{\sigma_{\theta u}} = \frac{228 \times 2.5}{6000} = 0.10 \text{ in.}$$

(2) Thickness required for buckling resistance: Use $\phi = 0.8$, giving $E = 800{,}000 \times 0.8 = 640{,}000$ psi, and use L.F. = 2.5

First try "short shell" equation, based on plate buckling:

$$\text{Eq. 6.71:}\quad N_{\theta c} = \frac{k\pi^2 E\, t^3}{12(1-\nu^2)\, b^2}$$

$N_{\theta c} = 228 \times 2.5 = 570$ lbs/in.; estimate k = 5. (Increased above 4. because of edge restraint)

$$t = \left[\frac{570 \times 12(1-.3^2) \times 10.5^2}{5.0\, \pi^2\; 640{,}000}\right]^{1/3} = 0.28 \text{ in.}$$

Also try intermediate length shell equation, with $k_n = 0.8$

$$\text{Eq. 9.87:}\quad N_{\theta c} = \sigma_{\theta c} t = \frac{0.855\, k_n\, E\, t^{2.5}}{(1-\nu^2)^{3/4}\, L\, \sqrt{R}}$$

$$t = \left[\frac{570 \times (1-0.3^2)^{3/4} \times 10.5\sqrt{48}}{0.855 \times 0.8 \times 640{,}000}\right]^{1/2.5} = 0.38 \text{ in.}$$

Use t = 0.28 in. as adequate for buckling resistance. Note that the length assumption giving the **highest** buckling resistance, or the **lowest** thickness requirement is the correct assumption.

(b) Next, the thickness obtained for circumferential compression is checked for adequacy to resist the maximum longitudinal compression stress resultant. This also occurs at the bottom under an external water pressure head of 11 ft. with the tank empty. If hold down straps are positioned at equal spaces, as shown in the sketch, the tank behaves as a tubular beam subject to a net upward load equal to the bouyant force of the water reduced by the buoyant weight of the tank and earth

Example 9-16 (continued)

over the tank. If the earth weight is 110 lbs/cu. ft. and only the weight directly over the tank is considered, the following net upward load is obtained:

Upward bouyant water pressure: $W_w = \pi\, 4^2 \times 62.4 = 3137$ lbs/ft.

Downward earth: $W_e = (7 \times 8 - \frac{\pi\, 4^2}{2})(110\text{-}62.4) = -\underline{1469 \text{ lbs/ft.}}$

Net upward load: 1668 lbs/ft.

Span between straps: L = 5 spaces x 1.25 = 6.25 ft.

approx. $M = \frac{1668 \times 6.25^2 \times 12}{16} = 48{,}860$ in.-lbs.

From Table 5-3, Case 10, for a thin ring: $S = \pi r^2 t = \pi\, 48^2 t = 7{,}238t$ in.^{3}

$$\sigma_x = \frac{M}{S} = -\frac{48{,}860}{7{,}238t} = -\frac{6.75}{t}\,;\; N_x = -6.75 \text{ lbs/in.;}$$

Add axial compression from fluid and earth pressure on ends. Use an equivalent fluid weight of 100 lbs/cu.ft. for water plus submerged lateral earth pressure. Since the pressure on the hemisphere end caps is assumed to act normal to its surface, the resultant passes through the axis of the tank at the junction of cylinder and hemisphere. Thus there is no net moment at the junction of the hemisphere and cylinder due to its pressure variation on the hemisphere and the axial force in the cylinder from pressure on the end shell is produced by the average pressure at the cylinder and hemisphere axis of rotation. Thus:

$$N_x = -\frac{\gamma h_o R^2}{2R} = -\frac{\gamma h_o R}{2} = -\frac{100 \times 7 \times 12 \times 48}{1728 \times 2} = -117 \text{ lbs/in.}$$

(1) Check adequacy of strength with t = 0.28 in.

$$\sigma_x = \frac{(117 + 7)}{0.28} = 443 \text{ psi} < 6000 \text{ psi}$$

(2) Check adequacy of resistance to longitudinal buckling.

First, check short shell equation based on wide plate (Euler) buckling relations:

Eq. 6.72a: $\sigma_{xc} = \frac{k\pi^2 E}{12(1-\nu^2)} \left(\frac{t}{a}\right)^2$; k = say 2.0 - partial end fixity

$$\sigma_{xc} = \frac{2.0\,\pi^2 \times 640{,}000}{12(1-.3^2)} \left(\frac{0.28}{10.5}\right)^2 = 823 \text{ psi}$$

Second, check axially loaded shell buckling with R/t = 48/0.28 = 171.

Eq. 9.74: $\sigma_{xc} = \frac{CE\,t}{R}$; $C = k_o k_n k_s$; $k_o = 0.6$ & $k_s = 1.0$

Fig. 9-25 for R/t = 171: k_n = 0.5 and C = 0.6 x 0.5 = 0.3

Check for intermediate length case, Eq. 9.81b:

Eq. 9.81(b): $k_n = (3.13 - 0.83 \log \frac{R}{t})\, \lambda_s^{-0.6} < 0.87\, \lambda_s^{-0.6}$

Eq. 9.82: $\lambda_s = \frac{L_s}{\sqrt{Rt}} = \frac{10.5}{\sqrt{48 \times 0.28}} = 2.86$

Example 9-16 (continued)

$$k_n = (3.13 - 0.83 \log 171)\, 2.86^{-0.6} = 0.68$$

$$\text{or max } k_n = 0.8 \times (2.86)^{-0.6} = 0.43 < 0.5$$

Continue to use $k_n = 0.5$ and $C = 0.3$

$$\sigma_{xc} = \frac{0.3 \times 640{,}000}{171} = 1120 \text{ psi} > 823 \text{ psi}$$

Use shell buckling case: $\text{Furn. } \overline{L.F.} = \frac{1120}{443} = 2.53 > 2.5$ o.k.

Conclusion: Adopt a 0.23 inch minimum shell thickness with an effective clear distance between ribs of 10.5 in. (Ribs are spaced 15 in. center-to center.)

5.3 Determine minimum rib stiffness for adequate resistance to general instability of the entire tank shell. This is governed by buckling resistance to circumferential compression. (The previous calculations have already shown that the shell has adequate resistance to longitudinal compression, with or without ribs.)

Eq. 9.86a: $$p_{cr} = \frac{5.5 k_n (\bar{A}_x)^{1/4} (D_\theta)^{3/4}}{L R \sqrt{R}} \quad \text{and } k_n = 0.8$$

at bottom: $$\text{req'd } p_{cr} = \gamma h_{bottom} \times \overline{L.F.} = \frac{62.4 \times 11 \times 2.5}{144} = 11.9 \text{ psi}$$

effective $L = (21.25 + 2/3 \times 4 \times 2) \times 12 = 319$ in.; $R = 48$ in.

$$\bar{A}_x = \frac{Et}{1 - \nu^2} = \frac{0.28E}{1 - .3^2}\ ; \ D_\theta = \frac{E i_\theta}{1 - \nu^2} = 1.1\, E i_\theta$$

$$11.9 = \frac{5.5 \times 0.8 \times 1.1 \times 640{,}000\ (0.28)^{1/4} (i_\theta)^{3/4}}{319 \times 48^{1.5}}$$

req'd $i_\theta = 0.462$ in.^{4}/in.

For each rib, req'd $I = 0.462 \times 15 = 6.9$ in.^{4}*

*Note: this is based on rib properties transformed to $\phi E = 640{,}000$ psi

5.4 A rib having a thin wall trapezoidal section comprised largely of an 0.25 in. thick mat woven roving laminate with 0.05 in. layers of filament winding applied to the inner and outer flanges to hold the rib in position during fabrication is provided, as shown in the sketch below.

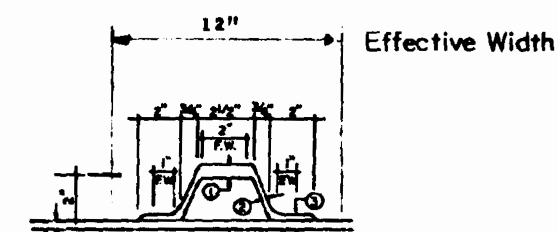

DETAIL "A" - RIB CONSTRUCTION

Example 9-16 (continued)

The "transformed" section properties based on ϕE = 640,000 psi are determined below. The modular ratio is assumed to be 2.0 for woven roving and 8.0 for filament winding (i.e. E's of 1,600,000 and 6,400,000 psi, respectively). The effective width of the inner flange (tank shell) is assumed to extend $0.76\sqrt{Rt}$ beyond the rib, but the maximum width is 15 inches, the center to center spacing of ribs.

$0.76\sqrt{Rt} = 0.76\sqrt{48 \times 0.28} = 2.8$ in., or $0.76\sqrt{48 \times (0.28 + 0.31)} = 4.0$ in.

Use an effective flange width of 12 in. as shown in the sketch.

	Transformed Area ϕE = 640,000 psi	A	y	Ay	y_o	Ay_o^2	I_o
1.	0.06 x 2 x 8 0.25 x 2.13 x 2 x 2	= 2.21	2.32	5.13	1.51	5.04	
2.	0.25 x 2.13 x 2 x 2	= 2.13	1.14	2.52	0.33	0.23	$2.13 \times 2^2/12$ = 0.71
3.	$0.06 \times 1 \times 8 \times 2^2$ 0.25 x 1.7 x 2 x 2	= 2.66	.29	0.77	0.52	0.72	
4.	0.28 x 12	= 3.36	0	0	0.81	2.20	
Σ		10.36		8.42		8.19	0.71

$\bar{y} = \frac{8.42}{10.36} = 0.81$ in. $\qquad I = \frac{8.19}{8.90}$ in.^{4}

Furn. I = 8.90 6.9 in.^{4} req'd; Furn $S_{out} = \frac{8.9}{1.66} = 5.36$ in.^{3}; $S_{in} = \frac{8.9}{9.5} = 9.36$ in.^{3}

6. Check design for adequate strength to support the full load of petroleum stored in tank plus the weight of earth and wheel loads above the tank.

This can be done by field tests, assisted by theoretical and experimental determinations of rib bending strength. The required calculations for estimating rib bending strength should include consideration of buckling of both the outer flange and the inner flange (shell at rib) in circumferential compression, as well as transverse bending of these flanges caused by radial components of the curved flange forces. This is illustrated for the ring rib design in **Example** 9-15, and will not be repeated here. Bending at hold down straps should also be investigated. Case 24 in (9.3) is useful for this analysis.

7. Determine thickness of head shell, based on buckling resistance to external pressure.

7.1 As shown in **Example** 9-15, the maximum stress resultant due to internal or external pressure in head shells subject to varying pressure is N_θ at the bottom. Since a rib is located adjacent to this location and will restrain the shell from buckling, determine the maximum N_θ some distance away from the bottom, say at $\phi = 75^\circ$. Thus, using a uniform pressure p_o, at the axis of rotation plus Case 8 in Table 9-2 for the effect of pressure variation from p_o, we get for $\phi = 75^\circ$, $\theta = 0$:

$$\text{Max. } N_\theta = -\frac{p_o R}{2} + \frac{\gamma R^2}{3} \frac{\cos 0}{\sin^3 75} (2 \cos 75 - 3\sin^2 75 - 2\cos^4 75)$$

$$= -0.5\ \gamma hR - 0.85\ \gamma R^2$$

Example 9-16 (continued)

Using γ = 62.4 lbs/cu.ft. (= 0.036 lbs/cu. in.) and neglecting any restraint of buckling by the soil:

Max. $N_\theta = -\dfrac{0.036 \times 7 \times 12 \times 48}{2} - 0.85 \times 0.036 \times 48 \times 48 = -143$ lbs/in. (compression)

It is conservative to design thickness for buckling of a spherical shell with $N_\phi = N_\theta$ everywhere in the shell (uniform pressure case)

Eq. 9.108: $\sigma_{\phi c} = \sigma_{\theta c} = \dfrac{CEt}{R}$; $N_{\theta c} = \sigma_{\theta c} t$; $t = \left(\dfrac{RN_{\theta c}}{CE}\right)^{1/2}$

Eq. 9.79 $C = k_o k_n k_s = 0.6\, k_n$

Eqs. 9.109 & 9.110: $k_n = 0.14 + \dfrac{3.2}{\lambda^2}$; $\lambda = 2\left[12(1-\nu^2)\right]^{1/4} \left(\dfrac{R}{t}\right)^{1/2} \sin\dfrac{\phi_k}{2}$

Try $t = 0.28$; $\lambda = 2(12 \times .91)^{1/4} \left(\dfrac{48}{0.28}\right)^{1/2} \sin\dfrac{90}{2} = 33.6$

$k_n = 0.14 + \dfrac{3.2}{(33.6)^2} = 0.143$; $C = 0.6 \times 0.143 = 0.086$

$N_{\theta c} = 143 \times$ L.F. $= 143 \times 2.5 = 357$ lbs/in.

req'd $t = \left(\dfrac{48 \times 357}{0.086 \times 640{,}000}\right)^{1/2} = 0.56$ in.

Conclusion: Provide a 0.56 in. thick hemispherical head for buckling resistance.

Max $\sigma = \dfrac{143}{0.56} = 255$ psi

Check required thickness at mid-height:

$N_\phi = N_\theta = -\dfrac{.036 \times 7 \times 12 \times 48}{2} = -72.6$ lbs/in $\times 2.5 = 181$ lb/in

req'd $t = -\left[\dfrac{48 \times 181}{0.086 \times 640{,}000}\right]^{1/2} = 0.40$ in.

The shell thickness could be tapered from 0.40 in. constant over the top half linearly to 0.56 in. 75° below the horizontal diameter and constant to the bottom.

8. Note that the tank design developed in this example is intended as a preliminary design, for use in further reinfinement in materials selection, materials properties, prototype testing etc. It is not the final design used for any particular commercially produced tank known to the author.

Note: 1 in. = 25.4 mm, 1 ft = 0.305 m, 1 in.^{2} = 645 mm^2, 1 in.^{3} = 16,387 mm^3, 1 in.^{4}/in. = 16,387 mm^4/mm, 1 in.^{4} = 4.16 x 10^5 mm^4, 1 lbf/in. = 175 N/m, 1 lbf/ft = 14.6 N/m, 1 psi = 0.0069 MPa, 1 lbf/cu. in. = 2.71 x 10^5 N/m^3, 1 lbf/ft^3 = 157 N/m^3, 1 in.lbf = 0.113 N-m, 1 gallon = 3.785 liters.

9.13 DESIGN EXAMPLES – ROOFS AND SKYLIGHTS

Plastic shells have been widely used in building construction for skylight components. Occasionally, they are used as the entire roof structure to obtain special shapes or particular aesthetics. Curved components that provide both roof and wall enclosure have been marketed for housing and small buildings with some success. Sandwich construction has been used for large shell roof or building enclosure components.

Example 9-17 illustrates the design of the transparent acrylic plastic skin panels whose overall design and configuration were discussed in Section 4.15. The required panel thickness is goverened by the buckling resistance required for snow and ice load.

In **Example 9-18,** a skew hypar component is designed as a skylight over a cental assembly area in a church or meeting room. Fiberglass reinforcement is used to enhance the toughness and stiffness of the transparent thermoplastic polycarbonate resin in this fairly large component. Although each unit is about 30 ft long, a width of about 8 ft is achieved by the use of the skew hypar geometry permitting shipment by truck. Also, the hypar configuration provides a doubly curved surface that resists wind and snow loads by both membrane tension and compression, thereby improving buckling resistance under both inward and outward load. However, a high load factor is used in the analysis for buckling because of the reasons given in Section 9.10.

The development of proportions and a preliminary investigation of thermal gradient stresses and edge bending stresses in a large spherical dome of sandwich construction is illustrated in **Example 9-19.** This dome forms the roof over a sewage digester tank and provides desired thermal insulation in addition to its primary function as a structural enclosure. Prefabricated panels with mat reinforced FRP facings and a polyurethane foam plastic core, arranged in an "orange peel" layout, form the dome. Details for connecting panels developed here are not included due to space limitations.

Lack of space precludes the inclusion of more extensive shell design examples. However, detailed design examples for a large sandwich dome, and a space frame dome with skew hypar roof panels, are presented in (9.21). See also (9.41) and (9.42) for other shell roof design examples.

Example 9-17: Determine the sheet thickness required for the acrylic domed transparent skin panel, or skylight panel, described in Section 4.15. See Figs. 4-28 and 4-29 for photos of the actual unit. Assume that the acrylic material has an elastic modulus of 400,000 psi and tensile, compressive and flexural strengths in excess of 10,000 psi.*

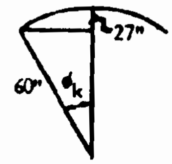

1. Design criteria - see Section 4.15 for complete description:

   Inward pressure (snow): 43 psf; Outward pressure (wind): 65 psf

2. Geometry -- see Section 4.15 for more complete description.

   Rise: 27 in.; Radius of curvature in major region away from base: 60 in.; Hexagonal base inscribed within 12 ft by 10 ft rectangle.

3. Thickness determination based on buckling under inward load. Apply ϕ = 0.8 to E in determining buckling with snow load, and use a load factor of 2.0.

   Eq. 9.108a: $p_{cr} = \dfrac{2\,C\,E\,t^2}{R^2}$; req'd $p_{cr} = \dfrac{43}{144} \times 2.0 = 0.60$ psi

   Eq. 9.79 $C = k_o\,k_n\,k_s$; $k_o = 0.6$; $k_s = 1.0$; Eqs. 9.109 and 9.110: $k_n = 0.14 \times \dfrac{3.2}{\lambda^2}$

   $$\lambda = 2\left[12\,(1-\nu^2)\right]^{1/4}\left(\frac{R}{t}\right)^{1/2}\sin\frac{\phi_k}{2} \quad \text{and trial } t = 0.25 \text{ in.}$$

   $$\cos\phi_k = \frac{60-27}{60} = 0.550;\ \phi_k = 56.6^{\circ};\ \sin\frac{\phi_k}{2} = 0.474$$

   $$\lambda = 2\ (12 \times .91)^{1/4}\left(\frac{60}{0.25}\right)^{1/2} \times .474 = 26.7$$

   $$k_n = 0.14 + \frac{3.2}{(26.7)^2} = 0.144;\ C = 0.6 \times 0.144 = 0.087$$

   $$t = \left[\frac{0.60 \times 60^2}{2 \times 0.087 \times 0.8 \times 400{,}000}\right]^{1/2} = 0.20 \text{ in.}$$

4. Check shell stress under wind load

   $$p_w = \frac{65}{144} \times 2.0 = 0.90 \text{ psi};\ \sigma_u = \frac{p\,R}{2\,t} = \frac{0.90 \times 60}{2 \times 0.20} = 135 \text{ psi} \qquad \text{o.k.}$$

   $$p_s = \frac{43}{144} \times 2.0 = 0.60 \text{ psi};\ \sigma_u = \frac{0.60 \times 60}{2 \times 0.23} = 78 \text{ psi}$$

5. Investigate base connection (see Fig. 4-30)

   Wind uplift and snow load produce local bending at the lip around the perimeter of the shell, resulting in the highest level of stress in the structure. The resistance of the shell to edge bending under at least 2.0 times the inward and outward design loads is determined by testing a full-scale phototrype structure mounted on an airtight box to simulate the restraints provided by the connection shown in Fig. 4-30. The prototype is subject to at least 2.5 times the design pressures applied as vacuum (snow) and pressure (wind) loadings.

Note: 1 in. = 25.4 mm, 1 ft = 0.305 m, 1 psi = 0.0069 MPa, 1 psf = 47.9 Pa.

* See footnote, Example 9-1, Page 9-13.

Example 9-18: Determine the required thickness of a glass reinforced polycarbonate thermoplastic transparent skew hypar skylight having the geometry shown in the sketch.*

Equation of surface: $z = \frac{c}{ab} xy$

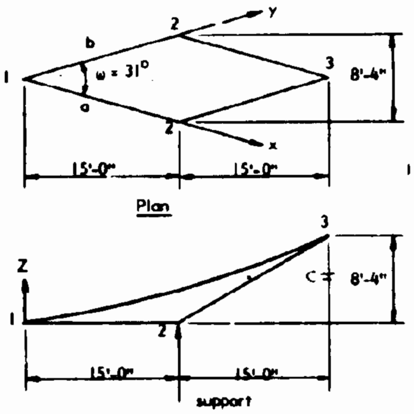

Elevation 1-3

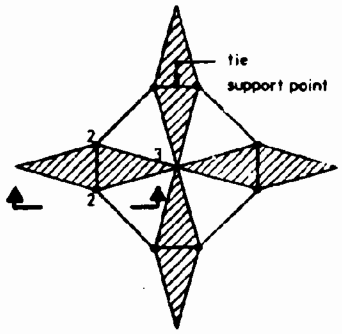

Plan of Four Unit "Star Skylight" over Central Area

The design loads are: snow and dead load = 42 lbs/sq ft downward; wind load = 20 lbs/sq ft upward.

Assume an elastic modulus, based on short time tests of 800,000 psi and short time test strengths in tension, compression and flexure above 9,000 psi.

1. Factors for limit analysis

(a) Use capacity reduction factors ϕ as follows:

	Strength	Elastic Moduli (Buckling)
Snow load	0.4	0.5
Wind load	0.5	0.6

The low capacity reduction factors for buckling are used becuase local deviations in surface geometry from assumed shape may reduce buckling strength of a thin shell.

(b) Use a load factor of 3.0 for uncertainties about analysis and variations in design loads.

2. Geometry: see Figs. 9-7 and 9-11; $a = b = 12\sqrt{15^2 + 4.17^2} = 186.8$ in; $c = 8.33 \times 12 = 100$ in.; $\tan \omega/2 = 4.17/15 = 0.278$; $\omega/2 = 15.54^{o}$; $\omega = 31.1^{o}$

---

* See footnote, Example 9-1, Page 9-13.

Example 9-18 (continued)

3. Membrane stress resultants:

(a) Snow load: $p_s = 42/144 = 0.29$ psi

Eq. 9.22: $N_{xy} = p_s \dfrac{ab \sin}{2c} = \dfrac{0.29 \times 186.8^2 \sin 31.1}{2 \times 100} = 26.3$ lbs/in

Eq. 9.23, a & b: $N_1 = N_{xy} \cot \omega/2 = 26.3 \cot 15.54 = 94.6$ lbs/in.

$N_2 = -N_{xy} \tan \omega/2 = -26.3 \tan 15.54 = -7.3$ lbs/in.

(b) Wind load: $p_s \approx -20/144 = -0.14$ psi

Note: p_w is assumed equivalent to a uniformly distributed load, p_s normal to the plane 1-2, (horizontal plane). This gives a suitable approximate analysis.

$N_{xy} = \dfrac{-0.14}{0.29} \times 26.3 = -12.7$ lbs.in.

$N_1 = \dfrac{-0.14}{0.29} \times 94.4 = -45.6$ lbs/in.; $N_2 = \dfrac{-0.14}{0.29} \times (-7.3) = +3.5$ lbs/in.

4. Buckling governs required thickness:

Eq. 9.121c: $p_{cr} = \dfrac{2c^2\, Et^2}{a^2\, b^2 \sin^2 \omega \sqrt{3(1-\nu^2)}}$

For a load factor of 3.0; req'd $p_{cr} = 0.29 \times 3.0 = 0.87$ psi

$$t = \frac{ab \sin\omega}{c\sqrt{2E}} \left[3\,(1-\nu^{22})\right]^{1/4} = \frac{186.8^2 \sin 31.08 \sqrt{0.87}\left[3(1-.3^2)\right]^{1/4}}{100\sqrt{2} \times 0.5 \times 800{,}000} = 0.242 \text{ in.}$$

Use t = 0.25 in.

Factored Stresses: $\tau_{xy} = \dfrac{26.3 \times 3.0}{0.25} = 316$ psi; $\sigma_1 = \dfrac{94.6 \times 3.0}{0.25} = 1135$ psi, (tension)

$\sigma_2 = \dfrac{-7.4 \times 3.0}{0.25} = -89$ psi, (compression)

5. Approximate edge bending stress for "hinged" edge with translation prevented by edge member:

Table 9-7: $M = \dfrac{0.149\, p_s\, a^2}{\lambda\ 4/3}$; $\lambda = \dfrac{c}{t} = \dfrac{100}{0.25} = 400$

$M = \dfrac{0.15 \times 0.29 \times 186.8^2}{(400)^{1.33}} = 0.53$ in-lbs/in; $\sigma_b = \dfrac{0.53 \times 6}{0.25^2} = 51$ psi, low

Example 9-18 (continued)

6. Edge load and Support Reaction: The edge load is the summation of shears along the edges.

Horizontal edges: Length = a = 186.8 in.

Snow load: max P = $-N_{xy}a$ = -26.3 x 186.8 = -4,913 lbs, (compression)

Wind load: max P = 12.7 x 186.8 = 2372 lbs, (tension)

Inclined edges: Length = $\sqrt{a^2 + c^2} = \sqrt{186.8^2 + 100^2}$ = 211.9 in.

Snow load: max P = -26.3 x 211.9 = -5573 lbs, (compression)

Wind load: max P = 12.7 x 211.9 = 2691 lbs, (tension)

Support Reaction at Points 2:

Snow load: Vertical, $P_V = -5573 \times \frac{100}{211.9}$ = -2630 lbs at each point 2.

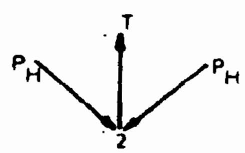

Horizontal (direction 2-3), $R_H = -5573 \times \frac{186.8}{211.9}$ = -4913 lbs

also P for horizontal edges = P_H

Thus, tie force, $T_{22} = 2 \times 4913 \times \frac{50}{186.8}$ = 2630 lbs

Check total load on horizontal projected area = 0.29 x 15 x 12 x 100 x 2/2 = 5,220 ≈ 2 x R_V o.k.

Wind load: The above reactions are all multiplied by -0.14/0.29 = -0.48

Note: In this case wind load is assumed to be uniformly distributed normal to the horizontal projection of surface, instead of normal to the surface.

Note: 1 in. = 25.4 mm, 1 ft = 305 m, 1 lbf = 4.45 m, 1 lbf/in. = 175 N/m, 1 psi = 0.0069 MPa, 1 psf = 47.9 Pa.

Example 9-19: Develop sandwich section proportions and estimate stresses caused by a 100°F thermal gradient across the sandwich section, and by edge bending effects for preliminary design of a sandwich dome for a sewage digester tank. The base diameter and rise of the dome are 80 ft and 10 ft, respectively, as shown below. Assume that the sandwich section is comprised of mat reinforced FRP faces and a polyurethane foam plastic core. Also, assume that the base of the dome will be supported on a continuous wall, and that a stainless steel ring that can freely move radially relative to the wall below (i.e., ring is supported on a rubber pad having low shear rigidity) will be provided to resist the radial thrust at the base. The ring will be given sufficient section area so that the maximum tensile stress in the ring will be 10,000 psi under full design snow load. The centroid of the ring is concentric with the line of action of dome thrust and wall support.

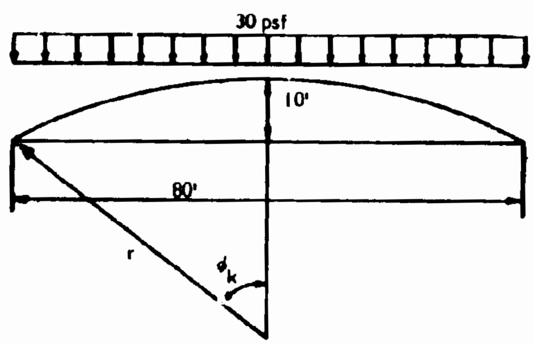

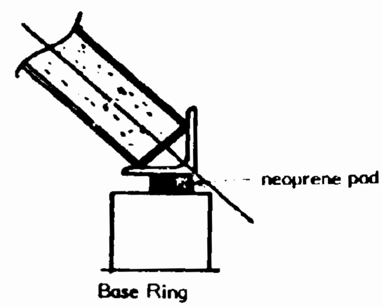

Use a load factor of 3.0 for strength and buckling, and 1.5 for thermal gradient. Use the following materials properties and capacity reduction factors.*

Property	Face (mat FRP)	Core (foam plastic)
Unit volume cost, C_f or C_c, \$/in^3	0.08	0.005
Ultimate tensile strength and capacity reduction factor for snow load, $\phi\sigma_u$, psi	0.6 x 10,000	
Ultimate compression strength and capacity reduction factor for snow load, $\phi\sigma_u$, psi	0.6 x 15,000	
Ultimate shear strength and capacity reduction factor for snow load, $\phi\tau_u$, psi		0.5 x 35
Modulus of elasticity and capacity reduction factor, ϕE_f, psi or ϕE_c, psi	$0.8 \times 0.9 \times 10^6$	0.7 x 2,000
Poisson's Ratio, ν_f	0.3	
Modulus of rigidity and capacity reduction factor, ϕG, psi		0.7 x 1,000
Coefficient of thermal expansion of faces, α_f, in./in./°F.	20×10^{-6}	

* See footnote, Example 9-1, Page 13.

Example 9-19 (continued)

1. Geometry of dome:

   $r^2 = (40 \times 12)^2 + (r - 10 \times 12)^2$; $r = 1020$ in.; $\sin \phi_k = \frac{480}{1020} = 0.4706$; $\phi_k = 28.07^\circ$

2. Required $\sqrt{i_f a_f}$ for buckling resistance. Assume dead load = 2 lbs/sq ft.

2.1 req'd $p_{cr} = (30 + 2)/144 \times 3.0 = 0.67$ psi

2.2 $N_\phi = N_\theta = \frac{p_s r}{2} = \frac{0.67 \times 1020}{2} = 342$ lbs/in.

2.3 Buckling resistance given by Eq. 9.107: $N_{\phi c} = \frac{2\sqrt{3}\, C\sqrt{D_\phi \bar{A}_\theta}}{R}$

Eq. 9.79: $C = k_o k_n k_s$; $k_o = 0.6$

Need R/t_e to determine k_n, and $E_f t_f/G_c R$ to determine k_s from Fig. 9-26.

For first trial assume $C = 0.12$

From Table 6-1: $\sqrt{D_\phi \bar{A}_\theta} = \frac{E_f \sqrt{i_f a_f}}{(1 - \nu^2)}$, when properties in ϕ and θ directions are the same.

req'd $\sqrt{i_f a_f} = \frac{1020 \times 342 \times (1 - 0.3^2)}{720{,}000 \times 2\sqrt{3} \times 0.12} = 1.061$

3. Optimum proportions to obtain req'd $\sqrt{i_f a_f}$ using sandwich section with two symmetrical faces that are both thin and stiff relative to the core:

3.1 Eq. 9.122: $t_f = \sqrt{\frac{C_c \sqrt{i_f a_f}}{(2C_f - C_c)}} = \sqrt{\frac{0.005 \times 1.061}{(2 \times 0.08 - 0.005)}} = 0.185$ in., facing thickness

Eq. 9.123: $t_c = (\frac{2C_f}{C_c} - 2)\, t_f = (\frac{2 \times 0.08}{0.005} - 2)\, 0.185 = 5.55$ in., core thickness

3.2 Eq. 9.83: $t_e = \sqrt{3}\,(t_c + t_f) = \sqrt{3}\,(0.185 + 5.55) = 9.93$ in., equivalent thickness

3.3 Check C:

k_n: $R/t_e = \frac{1020}{9.93} = 103$; First try Eqs. 9.109 and 9.110, as the most conservative:

$\lambda = 2\left[12\,(1 - 0.3^2)\right]^{1/4} (103)^{1/2} \sin \frac{28.07}{2} = 8.95$; $k_n = 0.14 + \frac{3.2}{(8.95)^2} = 0.18$

Also, try Eq. 9.111 with $R/t_e = 400$, the lowest R/t in the range of applicability:

$k_n = 0.25\,(1 - 0.175\,\frac{(28.07 - 20)}{20})\,(1 - \frac{0.07 \times 400}{400}) = 0.216$

Use $k_n = 0.21$

k_s: $\frac{E_f t_f}{G_c r} = \frac{720{,}000 \times 0.185}{700 \times 1020} = 0.187$; from Fig. 9-26, $k_s \approx 0.95$

$C = 0.6 \times 0.21 \times 0.95 = 0.12$; checks initial assumption.

Example 9-19 (continued)

3.4 Use trial proportions of facings = 0.18 in. and core = 6.0 in.

4. Local buckling resistance:

Eq. 8.107: $\sigma_{wr} = 0.5\,(E_f\,E_c\,G_c)^{1/3} = 0.5(720{,}000 \times 1400 \times 700)^{1/3} = 4{,}450$ psi

5. Membrane stress - snow load:

max. $\sigma_\phi = \sigma_\theta = \dfrac{0.67 \times 1020}{2 \times 0.18 \times 2} = 949$ psi $< 4{,}450$ psi local buck. str. $< 9{,}000$ psi ult. str.

6. Thermal gradient stress:

6.1 Eq. 9.71: $\sigma_\phi = \sigma_\theta = \pm \dfrac{E\,\alpha_f\,(T_1 - T_2)}{2} = \pm \dfrac{900{,}000^{*} \times 20 \times 10^{-6} \times 100}{2} = \pm\, 900$ psi

* Note: Maximum E without ϕ is used for upper bounds.

6.2 Multiply by load factor of 1.5 for ultimate strength checks: $\sigma_\phi = \sigma_\theta = \pm\, 900 \times 1.5 = \pm\, 1350$ psi

7. Combined thermal and load stresses for ultimate strength check in regions away from the edge.

max $\sigma_\phi = \sigma_\theta = -949 - 1350 = -2300$ psi $< 4{,}450$ psi o.k.

8. Estimate edge bending stress:

8.1 If stainless steel (E = 28,000,000 psi) base ring is sized to have a final circumferential stress of 10,000 psi, the final radial deflection of the base will be:

ultimate $\Delta r = \dfrac{\sigma_r\, r \times LF}{E_r} = \dfrac{10{,}000 \times 40 \times 12 \times 3}{28{,}000{,}000} = 0.514$ in.

8.2 Approximate membrane deformation of shell at edge due to maximum design load times load factor of 3.0 = 0.67 psi:

$\Delta r_m = \dfrac{\sigma_{\theta m}\, r}{E_\theta}$ (Note: this equation neglects Poisson effects).

Table 9-2, Case 3: $N_\theta = -\dfrac{p_s R}{2}\cos 2\phi_k = -\dfrac{.67 \times 1020}{2}\cos(2 \times 28.07) = -190$ lbs/in.

$\sigma_{\theta m} = \dfrac{-190}{2 \times 0.18} = -529$ psi; $\Delta r_m = -\dfrac{529 \times 480}{720{,}000} = -0.353$ in.

8.3 Total radial deflection that must be applied by edge bending reaction, $H\phi_k$, is 0.514 + 0.353 = 0.867 in.

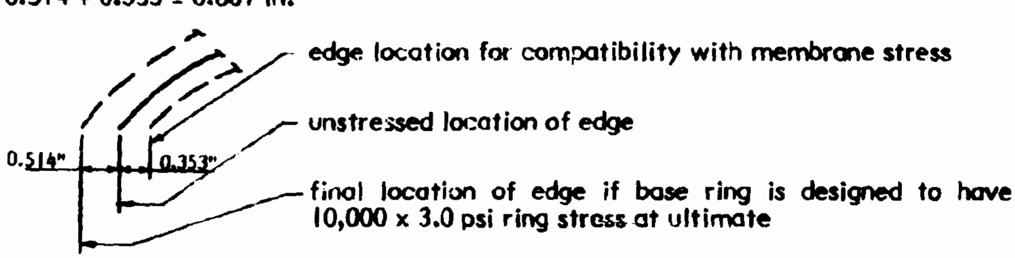

Example 9-19 (continued)

8.4 Determine H_{ϕ_k} to produce ultimate Δr = 0.867 in. Use equations in Table 9-6.

$$\Delta r = \frac{2\lambda R \sin^2\phi_k\, H_{\phi_k}}{E_\theta a_\theta};\; H_{\phi_k} = \frac{E_\theta a_\theta \Delta r}{2\lambda R \sin^2\phi_k};\; \lambda = \left[\frac{E_\theta a_\theta R^2}{4E_\phi i_\phi}\right]^{1/4} = \left(\frac{a_f R^2}{4 i_f}\right)^{1/4}$$

Table 8-1: $a_f = 2 \times 0.18 = 0.36$ in.^{2}/in.; $i_f = \frac{1 \times 0.18 \times (6.0 + 0.18)^2}{2} = 3.44$ in^4/in.

$$\lambda = \left(\frac{0.36 \times 1020^2}{4 \times 3.44}\right)^{1/4} = 12.84$$

$$\text{Ultimate } H_{\phi_k} = \frac{720{,}000 \times 0.36 \times 0.867}{2 \times 12.84 \times 1020 \times \sin^2 28.07} = 38.8 \text{ lbs/in.}$$

8.5 Maximum meridional moment and associated meridional thrust:

$$\text{Table 9-6: max. } M_\phi = \frac{0.322\, R \sin\phi_k\, H_{\phi_k}}{\lambda} = \frac{0.322 \times 1020 (\sin 28.07)\, 36.8}{12.84} = 467 \text{ in.-lbs/in.}$$

$$\text{Location is } \psi = \frac{0.8}{\lambda} = \frac{0.8}{12.84} = 0.0623 \text{ radians} = 0.0623 \times \frac{180}{\pi} = 3.57^\circ$$

Distance in from edge = $R\psi$ = $1020 \times 0.0623 = 63.5$ in.

Meridional thrust due to H_{ϕ_k} at $\psi = 3.57^\circ$:

$$N_\phi = -\sqrt{2} \sin\phi_k\, H_{\phi_k} \frac{\cot\phi_k \sin(\lambda\psi - \frac{\pi}{4})}{e^{\lambda\psi}} = \frac{-\sqrt{2} (\sin 28.07)\, 38.8 \cot 28.07 \sin(0.8 - \frac{\pi}{4})}{e^{0.8}} = \text{negl.}$$

Meridional thrust due to membrane conditions at $\psi = 3.57^\circ$, $\phi = 28.07 - 3.57 = 24.5^\circ$:

$$N_\phi = \frac{p_s R}{2} = -\frac{0.67 \times 1020}{2} = -342 \text{ lbs/in.}$$

8.6 Maximum meridional facing stress:

Table 8-1: section modulus/unit length. $s = 2i/d = 2 \times 3.44/6.18 = 1.11$ in^3/in.

check: $s = 1 \times td = 1 \times 0.18 \times 6.18 = 1.11$ in^3/in.

$$\sigma = \frac{N_\phi}{a} \pm \frac{M_\phi}{s} = \frac{-342}{0.36} \pm \frac{467}{1.11} = -950 \pm 421 = -1371 \text{ psi}$$

add stress due to thermal gradient = -1350

Total stress (ultimate) -2721 psi

Upper bound maximum ultimate meridional stress in dome < 4,450 psi, local wrinkling stress.

Example 9-19 (continued)

8.7 Maximum circumferential facing stress.

Stress at edge is compatible with 10,000 x 3 = 30,000 psi edge ring stress: Thus,

$\sigma_\theta = 30{,}000 \times \frac{720{,}000}{28{,}000{,}000} = 771$ psi

Check membrane and bending stress: $N_\theta = \frac{-p_s R \cos^2 \phi_k}{2} + (-2)\lambda \sin\phi_k H_{\phi_k} \frac{\sin(\lambda\psi - \frac{\pi}{2})}{e^{\lambda\psi}}$

(From 8.2):

$N_\theta = -190 - 2 \times 12.84 \sin 28.07 \times 38.8 \frac{\sin(-\frac{\pi}{2})}{e^0} = +279$ lbs/in.

$\sigma_\theta = \frac{279}{0.36} = +775$ psi $\approx +771$ psi

To get approximate maximum stress, add maximum thermal gradient stress:

Eq. 9.68: $\sigma_\theta = \frac{E\alpha(T_1 - T_2)}{2(1-\nu)} \left(1 - \nu + \sqrt{\frac{1-\nu^2}{3}}\right) \times CF = 900\left[1 - 0.3 + \sqrt{\frac{(1 - 0.3^2)}{3}}\right] \times 1.5$

$= \pm 1{,}689$ psi

Combined ultimate circumferential tension stress at edge: + 2460 psi < 6,000 psi, tensile strength

Maximum circumferential bending stress occurs at $\lambda\psi = 0.8$ and is equal to $\pm \nu M_\phi$ $= \pm 0.3 \times 467 = \pm 140$ psi

This should be added to circumferential direct stresses due to load and thermal gradient that are slightly lower at $\psi = 0.8/\lambda$ than calculated above for the edge, $\psi = 0$. Thus, maximum ultimate circumferential stress will be less than -2600 psi.

Note: 1 in. = 25.4 mm, 1 ft = 0.305 m, 1 in.^{2}/in. = 25.4 mm^2/mm, 1 in.^{3}/in. = 645 mm^3/mm, 1 in.^{4}/in. = 16387 mm^4/mm, 1 lbf/in. = 175 N/m, 1 psf = 47.9 Pa, 1 psi = 0.0069 MPa, 1 in.-lbf/in. = 4.45 N-m/m, °C = (°F - 32) (0.55), 1 in./in./°F = 1.8 mm/mm/°C, 1 \$/in.^{3} = 0.006 ¢/mm^3.

9.14 ANALYSIS AND DESIGN OF BURIED PIPE - (See Table 9-9 for Notations used in this Section).

Most plastic pipe used in buried pipe systems behave as flexible rings that obtain support for vertical load transfer from the surrounding soil. Rational structural analysis of such pipe requires an evaluation of soil-structure interaction. Finite element methods have been used to obtain accurate soil-structure interaction analyses but they are not yet economical for routine design of practical buried pipe systems. Thus, buried plastic pipe are normally designed based on semi-empirical relationships for soil-structure interaction response.

The practical approach for design of flexible buried pipe systems is based on simplified theory, tests, field observations and experience (9.44, 9.45). It is basically a method for determining the quality of installation required to permit the use of a given pipe for given soil and surface wheel loading criteria.

Soil load criteria include unit weight of soil and height of cover over the pipe. Surface wheel load criteria include wheel footprint, type of pavement (if any), magnitude and frequency of load, and required impact allowance.

Typically, for non-pressure applications, buried plastic pipe systems of a particular material are supplied in only one or two structural configurations. Nevertheless, these may be suitable for a wide range of cover heights and wheel loading conditions, if they are properly installed to meet the design requirements. For conditions of deep fill or shallow fill with typical truck wheel loads, stiff embedments are required. These are achieved with angular crushed stone, or well-graded gravel and/or coarse sand materials compacted to near or above the top of the pipe.

A well compacted side fill with support material carefully placed under the haunches of the pipe promotes a uniform reactive pressure around the pipe, limiting bending stresses and deflections to acceptable levels (Fig.9-32). Trench width is usually held to the minimum which will still permit proper installation of embedment material. In wide trenches or where trench walls are especially soft, compacted material should extend at least 2.5 diameters each side of the pipe for small pipe; special study is required for minimum compacted width for larger pipe.

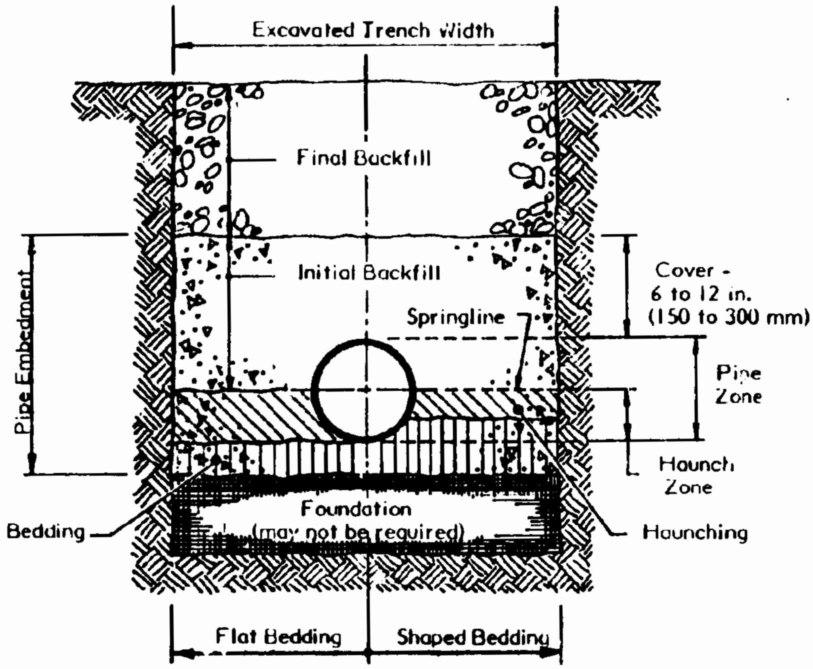

Fig. 9-32 INSTALLATION DETAILS

The design process is to select a trial pipe-soil system, and then to evaluate the adequacy of the pipe for supporting the design fill height, surface wheel load configuration, and internal pressure, if present. The installation is adequate, if, under design loads:

- Deflection is within a maximum limit based on service requirements
- Strains or stresses are less than limits set for long term load and environmental exposure, or for fatigue due to multiple applications of wheel loading
- Buckling resistance is adequate

Since maximum strain can be related approximately to maximum deflection, the pipe will be structurally adequate if its installed deflection is less than a specified limiting deflection and provided that it possesses sufficient buckling resistance.

A semi-empirical procedure for evaluating the behavior of a buried pipe system having a uniform wall thickness is given in Table 9-9 as adapted from (9.45). The method, as presented, applies only to smooth-wall pipe without ribs or corrugations. The pipe material is assumed to be homogeneous; thus, for fiberglass reinforced plastics, distribution of circumferential reinforcement throughout the thickness must be reasonably uniform, balanced, and symmetrical (Section 2.5).

The approach may be adapted to evaluate corrugated-wall pipe, ribbed-wall pipe, or double-wall "truss" pipe, providing the structural properties of the shaped wall system are known. In these kinds of pipe, ring bending produces direct tension or compression on the thin wall elements; thus, limiting stresses and strains should be based on tension or compression properties, rather than on bending properties of the wall material. Local buckling of such thin elements may also prove critical.

Table 9-9, together with subsequent tables and graphs, provides relationships for pipe deflection and pipe strain resulting from soil loads, internal and external pressure, surface wheel loads, and initial installation effects. These values are then compared to limiting performance criteria for deflection based on ultimate strain. Also, maximum external pressure is compared to an estimated critical buckling pressure. If any criterion is not met, soil properties can be upgraded by a change in materials or density requirements, or a different pipe system can be tried. Procedures given in Table 9-9 are explained in more detail below.

Design Criteria

The first step in the design procedure is to set design criteria. These include characteristics of the installation, dimensional, strength, and stiffness properties of the pipe, and properties of the embedment material surrounding the pipe. Key considerations are as follows:

Stiffness Properties: Stiffness properties of the pipe and surrounding soil are required for both deflection and stability calculations. ASTM standards for plastic pipe systems intended for burial frequently contain requirements for short-term pipe stiffness, $\overline{PS}_o$, measured in accordance with ASTM 2412 (see Example 9-2). Short-term pipe stiffness can also be calculated if the circumferential short-term elastic modulus and pipe dimension are known or specified, as follows:

$$\overline{PS}_o = \frac{F}{\Delta y} = 6.7 \frac{E_o i}{R^3} \qquad \text{Eq. 9.154}$$

where the following notations are taken directly from ASTM D2412

F = test load per unit length of pipe at 5% deflection.

Δy = deflection, or change in vertical diameter at the test load (i.e. 5% of vertical diameter)

See Notations for definition of other terms.

Long-term pipe stiffness, usually established at 10 years of load duration (50 years in Europe) in the case of buried pipe, can be obtained by substituting extrapolated estimates of the viscoelastic modulus (Eq. 3.1) into Eq. 9.154. Or, if the creep factor $\overline{CF} = E_o/E_{10}$ (same as R in Table 2-2) is known, the long-term pipe stiffness becomes:

$$\overline{PS}_{10} = \frac{\overline{PS}_o}{\overline{CF}} \qquad \text{Eq. 9.155}$$

Embedment soil stiffness, E', is the modulus of soil reaction, or stiffness of the soil. Average values for common embedment soils are given in Table 9-10. These values are empirical, and are back-calculated from measurements on actual pipe installations.

Material Strength: There are few codes or industry concensus standards available to provide guidance on strength design of plastic pipe for the loading conditions encountered when buried. For example, methods are not available to determine strength under constant strain (relaxation), combined strains from sustained internal pressure and bending due to ovalling, and various other combinations including cyclic loads, except in some cases for fiberglass reinforced plastic water pipe (9.46). Until such guidance is available the strength equations (Eq. 9.156 a & b) in Table 9-11 together with interaction relations given in Table 9-9 provide a basis for strength design which is consistent for both fiberglass-reinforced-plastic and thermoplastic pipe (9.45). Note that strength is expressed in terms of strain rather than stress in Table 9-11.

Table 9-9

Design Procedure for Buried Plastic Pipe with Uniform Wall Thickness (See End of Table for Notation)

1. Design Criteria

   a. Pipe Properties

   Tabulate pipe dimensions, modulus, and ultimate strength and pipe stiffness. Determine ultimate strength (in terms of strain) from Table 9-11 or other source. Calculate pipe stiffness if not available in specifications.

   Establish capacity reduction factor for pipe stiffness (ϕ'') and pipe strength (ϕ). Calculate reduced ultimate strengths: $\epsilon_{Ru} = \phi\epsilon_R$; $\epsilon_{Cu} = \phi\epsilon_C$ — Eq. 9.128a, b

   b. Soil Properties

   Select modulus of soil reaction, Table 9-10, and deflection lag factor. Establish capacity reduction factor, (ϕ'), for modulus of soil reaction.

   c. Load Factors

   Select load factors for each loading condition.

2. Pressures due to applied loads:

a.	Earth load (γ_s = soil density)	$p_s = \gamma_s h$	Eq. 9.129
b.	Earth load reduced for buoyancy	$p_b = p_s C_w$	Eq. 9.130
		$C_w = 1 - \frac{h_w}{3h}$	Eq. 9.130a
c.	H20 wheel load (p_{wh} from Fig. 9-33)	$p_w = p_{wh}(1 + \overline{IF})$	Eq. 9.131
	Impact factor	$\overline{IF} = p_{wh}/(p_{wh} + p_s)$	Eq. 9.132
d.	Ground water (γ_w = water density)	$p_g = \gamma_w h_w$	Eq. 9.133
e.	Vacuum in line	p_v	
f.	Internal pressure	p_f	
	Determine factored or ultimate pressures	$p_{nu} = p_n \times \overline{LF}$	Eq. 9.134a
		$p'_{nu} = p_n \times \overline{LF}'$	Eq. 9.134b

3. Maximum deflection due to earth and surface wheel service loads, and installation:

a.	Average earth load deflection $\overline{PS}_o$ from Eq. 9.154 or pipe specification, K_b from Table 9-12	$\frac{\Delta s}{2R} = \left[\frac{K_b p_s}{0.149\,\overline{PS}_o + 0.061\,E'}\right] \times \overline{DF}$	Eq. 9.135
b.	Average surface wheel load deflection	$\frac{\Delta w}{2R} = \frac{K_b p_w}{0.149\,\overline{PS}_o + 0.061\,n\,E'}$	Eq. 9.136
c.	Installation deflection	$\frac{\Delta i}{2R}$ = from Table 9-13	
d.	Maximum estimated deflection	$\frac{\Delta}{2R} = \frac{\Delta s}{2R} + \frac{\Delta w}{2R} + \frac{\Delta i}{2R}$	Eq. 9.137

4. Strain components:

   a. Ring bending strain from external loads ($\overline{MF}$ from Table 9-12)

Earth	ϵ_{bsu}	$= 2.14\left(\frac{t}{R}\right)\overline{MF} \times \frac{\Delta s}{2R} \times \overline{LF}$	Eq. 9.138a
Vehicle	ϵ_{bwu}	$= 2.14\left(\frac{t}{R}\right)\overline{MF} \times \frac{\Delta w}{2R} \times \overline{LF}$	Eq. 9.138b
Installation	ϵ_{biu}	$= 2.14\left(\frac{t}{R}\right)\overline{MF} \times \frac{\Delta i}{2R} \times \overline{LF}$	Eq. 9.138c
Total	ϵ_{bu}	$= \Sigma$ Eq. 9.138a to c	Eq. 9.138d

   b. Ring tension strain from internal pressure $\epsilon_{tu} = \frac{p_{fu} R_i}{t\,F_o}$ — Eq. 9.139

Table 9-9 continued

c. Ring compression strain from external loads

Earth:	Maximum	ϵ_{csu}				p_{su}	Eq. 9.140a
	Minimum	ϵ'_{csu}				p_{su}'	Eq. 9.140b
Vehicle:	Maximum	ϵ_{cwu}	=	$\frac{R_o}{t E_o}$	x	p_{wu}	Eq. 9.140c
	Minimum	ϵ'_{cwu}				p'_{wu}	Eq. 9.140d
Vacuum		ϵ_{cvu}				p_{vu}	Eq. 9.140e

5. Strength Adequacy

a. Maximum compression strain for all pipes

$$R_a = \frac{\epsilon_{bu}}{\epsilon_{Ru}} \left[\frac{1}{1 - \frac{\epsilon_{csu} + \epsilon_{cwu}}{\epsilon_{Cu}}} \right] \qquad \text{Eq. 9.141}$$

b. Tension at perforations in non-pressure pipe

$$R_b = \frac{\epsilon_{bu}}{\epsilon_{Ru}} \left[\frac{PF}{1 - \frac{\epsilon_{csu} + \epsilon_{cwu}}{\epsilon_{Cu}} \times PF} \right] \qquad \text{Eq. 9.142}$$

c. Tension in pressure pipe. Minimum factored compression strain is used for conservative result (RF = 1 for non-pressure pipe). Investigate cases with and without wheel load acting.

$$R_c = \frac{\epsilon_{bu}}{\epsilon_{Ru}} \left[\frac{RF}{1 - \frac{\epsilon_{tu} - \epsilon'_{csu} - \epsilon'_{cwu}}{\epsilon_{Cu}}} \right] \qquad \text{Eq. 9.143}$$

RF for pressurized pipe

$$RF = \left[1 + \frac{2p_f R_i}{(p_s + p_w) R_o} \left(\frac{\Delta}{2R}\right) \right]^{-1} \qquad \text{Eq. 9.144}$$

Redesign if $R_{a,b,c} > 1$.

6. Allowable total deflection of pipe as installed

a. Governed by maximum compression for all pipe

$$\frac{\Delta}{2R}\max = \frac{1}{R_a}\left(\frac{\Delta}{2R}\right) \qquad \text{Eq. 9.145}$$

b. Governed by tension at perforations of non-pressure perforated pipe

$$\frac{\Delta}{2R}\max = \frac{1}{R_b}\left(\frac{\Delta}{2R}\right) \qquad \text{Eq. 9.146}$$

c. Deflection before pressurization governed by tension in pressure pipe after rerounding

$$\frac{\Delta}{2R}\max = \frac{1}{R_c}\left(\frac{\Delta}{2R}\right) \qquad \text{Eq. 9.147}$$

7. Buckling capacity:

a. Modified AWWA formula

$$p_{cr} = 0.77 \left[\left(\frac{\left(1 - \frac{\Delta}{2R}\right)}{\left(1 + \frac{\Delta}{2R}\right)^2} \right)^3 (C_w\, B'(E'\phi)(PS_{10}\,\phi^m) \right]^{1/2} \qquad \text{Eq. 9.148}$$

For $0 < \frac{h}{2R_o} < 5$ $\qquad B' = (0.015 + 0.041 \frac{h}{2R_o})$ $\qquad$ Eq. 9.149

For $5 < \frac{h}{2R_o} < 80$ $\qquad B' = (0.15 + 0.014 \frac{h}{2R_o})$ $\qquad$ Eq. 9.150

See Eq. 9.130a for C_w

Use $\Delta/2R$ max in Eq. 9.148 if Eq. 9.145 to 9.147 are used in determining maximum deflections.

Buckling resistance is adequate if $\qquad R_d = (p_{bu} + p_{gu} + p_{vu} + p_{wu}) \div (p_{cr}) \leq 1$ $\qquad$ Eq. 9.151

b. Buckling under hydrostatic component of load: $\qquad p_{cr}' = 0.5\, C_a\, PS_{10}\phi' \phi^m$ $\qquad$ Eq. 9.152

C_a = 2 to 3 for softer soils, ranging up to 6 for rigid mortar encasement

Buckling resistance under hydrostatic loads is adequate if $\qquad R_e = (p_{gu} + p_{vu}) \div (p'_{cr}) \leq 1$ $\qquad$ Eq. 9.153

Table 9-10

Average Values of E' for Equations 9.135, 9.136 & 9.148 (9.44)

Embedment Material per Unified Soil Classification System ASTM D 2487	Average E' for Degree of Compaction of Bedding (lb/in.^{2}) [1, 3]			
	Dumped	Less than 85% of Maximum Density	85 to 95% of Maximum Density	Greater than 95% of Maximum Density
Crushed Rock	1,000	3,000	3,000	3,000
Coarse-grained Soil with Little or No Fines GW, GP, SW, SP contains less than 5 percent fines	200	1,000	2,000	3,000
Coarse-grained Soils with Fines GW, GC, SM, SC contains more than 12 percent fines	100	400	1,000	2,000
Fine-grained Soils (LL < 50) [2] Soils with medium to no plasticity CL, ML, ML-CL, with more than 25 percent coarse-grained particles	50	200	400	1,000
Fine-grained Soils (LL < 50) [2] Soils with medium to no plasticity CL, ML, ML-CL, with less than 25 percent coarse-grained particles	50	200	400	1,000
Fine-grained Soils (LL > 50) [2] Soils with medium to high plasticity CH, MH, CH-MH	No data available			

Notes:
1. Source ASTM D3839-79
2. LL = Liquid limit.
3. Maximum Density determined in accordance with AASHTO T-99.
4. 1 lb/in^2 = 1 psi = 6.9 kPa

Notations for Table 9-9.

B'	empirical coefficient of elastic support
C_a	buckling coefficient for hydrostatic pressure loading on pipe
C_w	correction factor to account for loss of buckling restraint by soil weight, due to ground water
$\overline{CF}$	creep factor; same as R in Section 3.3.
$\overline{DF}$	deflection lag factor
E_o	short term elastic modulus
E_{10}	apparent elastic modulus after 10 years under constant stress or strain in linear viscoelastic range
E'	modulus of soil reaction of embedment material (See Table 9-10)
h	height of soil above top of pipe
h_w	height of ground water above top of pipe
HDB	hydrostatic design basis or 10-year strength of plastic pipe under sustained hydrostatic internal pressure
$\overline{IF}$	impact factor
K_b	bedding constant for deflection (See Table 9-12)
$\overline{LF}$	load factor
$\overline{LF}'$	minimum load factor; may be less than 1.0
$\overline{MF}$	moment factor (bedding factor for ring bending) (Table 9-12)
n	reduction factor for soil modulus
p_b	pressure on bottom region; earth load reduced for buoyancy
p_{cr}	critical buckling pressure on pipe; critical buckling external pressure on lateral sides of cone, without pressure on top and bottom ends
p'_{cr}	critical buckling pressure on pipe under hydrostatic loading
p_f	hydrostatic pressure in pipe due to internal fluid
p_g	hydrostatic pressure on pipe due to ground water
p_n	pressures applied to pipe, under loading "n"
p_{nu}	factored ultimate pressures applied to pipe, under loading "n"
p_s	pressure at top of buried pipe due to earth weight
p_v	negative pressure due to vacuum in pipe
p_w	pressure due to wind load; pressure at top of buried pipe due to surface wheel loads, including impact
p_{wh}	pressure at top of buried pipe due to surface wheel loads (see Fig. 9-33)
$\overline{PF}$	strain concentration factor (See Table 9-14)
$\overline{PS}_v$	time-dependent pipe stiffness
$\overline{PS}_o$	short-term pipe stiffness
$\overline{PS}_{10}$	long-term (10 year) pipe stiffness
R	mean radius
$\bar{R}_a$	index of strength adequacy for compression strain
$\bar{R}_b$	index of strength adequacy for tension strain
$\bar{R}_c$	index of strength adequacy for tension in pressure pipe
$\bar{R}_d$	index of buckling strength adequacy based on modified AWWA formula
$\bar{R}_e$	index of buckling strength adequacy based on hydrostatic buckling loads
R_i	inside radius of pipe
R_o	outside radius of pipe
$\overline{RF}$	rerounding factor for pressurized pipe
t	thickness of pipe wall
Δ	buried pipe deflection
Δ_s	average pipe deflection due to earth weight
Δ_w	average deflection due to wheel load
ϵ_b	ring bending strain in pipe
ϵ_{bsu}	factored strain due to earth weight
ϵ_{bu}	sum of factored bending strains
ϵ_{biu}	factored strain due to installation deflections
ϵ_{bwu}	factored strain due to surface wheel loads
ϵ_c	ring compression strain in pipe
ϵ_{csu}	factored strain due to earth weight
ϵ'_{csu}	ring strain due to earth weight with minimum load factor applied
ϵ_{cwu}	factored strain due to surface wheel load
ϵ'_{cwu}	ring strain due to surface wheel load with minimum load factor applied
ϵ_{cvu}	factored strain due to vacuum in pipe
ϵ_C	initial ultimate strain in creep or constant stress
ϵ_{Cu}	initial reduced ultimate strain in creep
ϵ_R	initial ultimate strain in relaxation or constant strain
ϵ_{Ru}	initial reduced ultimate strain in relaxation
ϵ_{tu}	maximum ring tensile strain due to internal pressure in pipe
γ_s	density of earth cover
γ_w	density of water
ϕ	capacity reduction factor on material strength
ϕ'	capacity reduction factor for soil modulus of soil reaction
ϕ''	capacity reduction factor for long-term pipe stiffness

Table 9-11 also shows examples of ultimate strengths in terms of strain, calculated using the strength equations, for several specific types of thermoplastic and fiberglass-reinforced plastic materials that have a demonstrated long term strength capacity (HDB) (See Sections 3.4 and 3.5). These limits should be valid for water exposures and non-aggressive environments for the specific materials given in the table. The ultimate strains are to be reduced by capacity reduction factors, and then compared to short-term strains calculated for service loads, and increased by load factors. It is recognized that the short-term values are expected to change during creep and relaxation of the material.

Table 9-11

Ultimate Long-Term Strengths (Strains) of Pressure-Rated Plastic Pipe Materials

Material	Polyvinyl-chloride (PVC)	Polyethylene (PE)	Fiberglass Reinforced (RTR)	Fiberglass Reinforced (RPM)
Type or Class	1120(2)	(3)	200(4)	50(4)
HDB, psi	4,000	1,450	14,100	6,700
E_o, psi	0.4×10^6	0.1×10^6	3.0×10^6	2.0×10^6
$\overline{CF} = E_o/E_{10}$	2	2	1.25	1.25
Strength in Creep (Constant Stress) $\epsilon_C = \frac{HDB}{E_o}$, % (Eq. 9.156a)	1.0	1.5	0.48	0.34
Strength in Relaxation (Constant Strain) $\epsilon_R = \frac{HDB \times \overline{CF}}{E_o}$, % (Eq. 9.156b)	2.0	2.9	0.59	0.42

(1) See R in Table 2-2 for creep factor ($\overline{CF}$) estimates
(2) ASTM D1785
(3) ASTM F714
(4) Appendix of (9.46)
(5) Consult manufacturer for actual values of HDB, E_o & E_{10}
(6) 1 psi = 6.9 kPa

Other strength criteria are needed to evaluate the effects of cyclic fatigue, in such cases as a shallowly buried installation subjected to heavy traffic, or a pipe subjected to cyclic internal pressures. For example, limited data on pressure-rated PVC pipe materials indicate that fatigue effects become important when cyclic strain amplitude exceeds 25% of the total strain amplitude (3.15). In some reinforced-plastics-based pipe, the long-term HDB is obtained by cyclic pressurization (ASTM D2992, D2143) and hence fatigue strength is already reflected in the HDB.

Capacity Reduction Factors: Capacity reduction factors are applied to stiffness and strength properties to reflect variations in materials properties from those established in test or by specification.

Capacity reduction factors used in specific designs should account for such factors as aggressive environments, scratches, gouges and other unavoidable damage, cyclic internal pressures, exposure to ultraviolet radiation during storage, difficulties anticipated in installation, and the consequences of failure.

Load Factors: Load factors ($\overline{LF}$) are applied to increase loads or stresses to account for the potential for overloads, and other unknowns related to the loads and the analysis, as is done in structural design with conventional structural materials. See Section 3.2, 4.2, 4.10 and 8.11. As will be illustrated in **Example 9-20,** different load factors may be applied to different components of load. For example, the load factor applied to vacuum might be lower than that for internal pressure. That is, the maximum pressure due to vacuum is well defined, being that of the atmosphere, while internal pressure in the line may be difficult to predict, particularly with regard to surges.

In some cases such as in the evaluation of the effects of combined loadings (Eq. 9.143), the use of the design load or a load factor greater than one may produce an unconservative result. Therefore load factors less than one should be considered for use in such situations.

Loads: Soil pressure on the pipe due to earth weight is determined simply as the weight of the column of earth directly above the pipe, as given by Eq. 9.129 in

Table 9-9. This load is reduced by the buoyancy resulting from groundwater as indicated in Eq. 9.130. Soil pressure produced by surface wheel loads depends on the depth of burial, and also the impact (rapid load) factor which also varies with depth of cover (Eq. 9.131 and 9.132). The soil pressure caused by earth load, H-20 live load, and combined earth and live load are plotted versus depth of earth cover in Fig. 9-33. The reduction factor, C_w, given by Eq. 9.143a, is applied when a pipe is submerged below ground water level.

Loads due to internal pressure should include the effects of surges. If frequent surges are anticipated, and these surges are large compared to the normal operating pressure, special study may be required for fatigue effects. (See above discussion on **Material Strength.**) Negative pressures accompanying surges in pressure pipe may be significant. Some producers of plastic pipe design their pipe for full vacuum, although refined dynamic analysis might result in lower values.

Deflection

Usually a design objective is to maintain changes in vertical and horizontal diameter, resulting from installation and loading, within a specified percentage of pipe diameter. Average deflection due to earth load is estimated using the semi-empirical relationship for soil-structure interaction given by Eq. 9.135 in Table 9-9. As is usual practice with other structural materials, deflections are calculated on service, not factored, loads. This should be a primary consideration in setting maximum deflection limits, and establishing acceptance criteria for the project.

Historically, maximum deflection has been frequently limited by specifications, somewhat arbitrarily, to 3 to 7.5 percent of the diameter, depending upon characteristics of a given plastic pipe system. Such deflection limits are needed to retain fluid tightness at joints, and to permit cleaning by plug pulling. A specific limiting deflection based on maximum acceptable strengths should also be established for each plastic pipe system. Furthermore, to meet a maximum strength criterion, a lower deflection limit is required at joints that have thicker walls than at the thinner pipe barrel away from the joints.

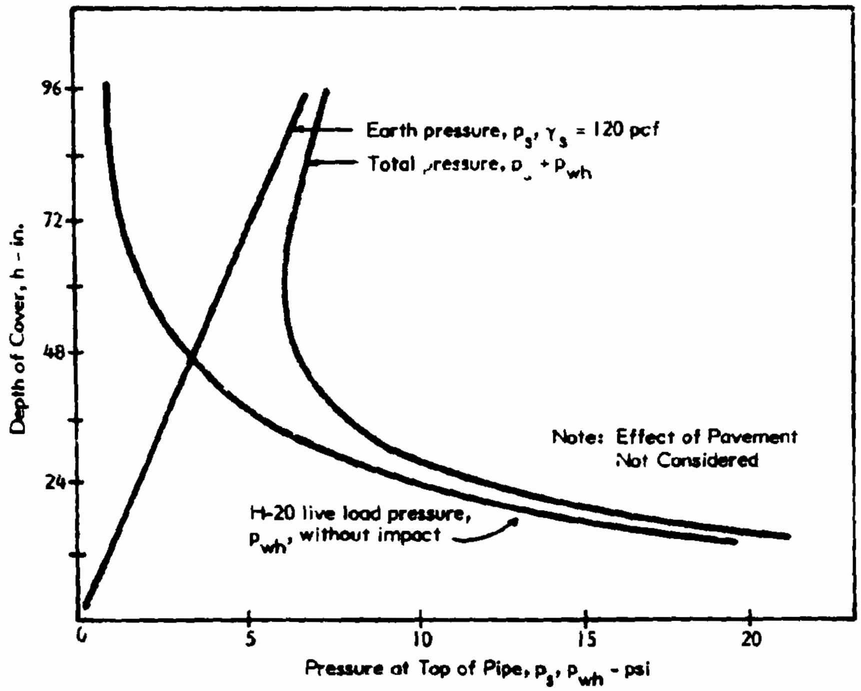

Note: 1 psi = 6.9 kPa; 1 in. = 25.4 mm

Fig. 9-33 VARIATION IN SOIL PRESSURES WITH INCREASING DEPTH OF COVER

Initial Deflection: The expression inside the brackets of Eq. 9.135 is used to determine the initial pipe deflection due to earth load, based on the short-term pipe stiffness, $\overline{PS}_o$, the modulus of subgrade reaction, E', and a bedding factor, K_b, which depends on the uniformity of embedment support near the pipe invert (Table 9-12).

Table 9-12

Constants for Deflection and Ring Bending Equations (9.45)

Coefficient	Symbol	Haunched & Field Monitored	Haunched & Not Monitored	Not * Haunched
Bedding Constant for Deflection (Eqs. 9.135 & 9.136)	K_b	0.09	0.11	0.13
Ring Bending Moment Factors for (Eq. 9.138)	$\overline{MF}$ (Crown)	0.75	0.75	0.75
	$\overline{MF}$ (Springline)	0.75	0.75	1.0
	$\overline{MF}$ (Invert)	0.75	1.0	1.5

* Omission of haunching not recommended.

The initial short-term pipe deflection, as calculated above, is increased by the deflection lag factor, $\overline{DF}$, which reflects a "lag" in the development of maximum or final deflection that is frequently observed in field installations of flexible pipe. This delayed deflection is attributable to the additional consolidation or densification of the embedment soil around the pipe, which occurs after installation. This deflection lag phenomenon is observed with flexible metal pipe as well as plastic pipe, and is usually related more to soils and trench characteristics than to the creep, or time-dependent reduction in the modulus of the plastic pipe material. The magnitude of the deflection increase is a function of soil type and degree of compaction; $\overline{DF}$ is frequently taken as 1.5 although much higher values have been recorded.

Field tests demonstrate that deflection lag effects in the soil may develop very soon after installation as a result of construction traffic, or heavy rains, and that the pipe deflection remains stable thereafter. While there is some further small deflection due to creep in the pipe material, it is usually sufficiently accurate to assume that the pipe shape is "frozen" in an oval configuration after the deflection lag has developed, and that the pipe is in a state of constant bending strain (relaxation) thereafter.

Deflections due to surface applied wheel loads are calculated using Eq. 9.136, which is similar to the equation discussed above for earth loads. The coefficient "n" is used to reduce the soil modulus E' to account for the effects of a reduction in soil support which occurs under the localized wheel load. A tentative value of n = 0.5 is recommended, provided $p_w > 0.25\, p_s$.

Installation Deflection: Measurements made during the installation of flexible plastic pipe systems shows that an allowance should be made for deflections resulting from conditions that might occur during installation and compaction of soil around the pipe. These are in addition to the initial deflections calculated by conventional pipe-soil interaction formulas discussed above. The more flexible the pipe and the less stiff the embedment soil, the greater the expected installation deflection, $\Delta_i/2R$. Suggested tentative values for $\Delta_i/2R$ for three embedment conditions are given in Table 9-13. Obviously, if installation is not properly performed, such deflections become unpredictable and large.

Table 9-13

Tentative Installation Deflections for Haunched Pipe (9.45)

	Installation Deflection ($\Delta_i/2R$) (%) (1)		
Pipe Stiffness PS_o (lb/in./in.) (4)	Embedment Less Than 85% of Max. Dry Density (2) or Dumped (3)	Embedment 85% to 95% of Max. Dry Density (2)	Embedment Greater Than 95% of Max. Dry Density(2)
Less Than 40	6+	4	3
40 to 100	4+	3	2
Greater Than 100	2+	2	1

Notes:
1. Deflections of unhaunched pipe are significantly larger.
2. Maximum dry density determined in accordance with AASHTO T 99.
3. Dumped materials and materials with less than 85% of maximum dry density are not recommended for embedment. Deflection values are provided for information only.
4. 1 lb/in./in. = 1 psi = 6.9 kPa

Strains in Pipe Wall

Strains in the pipe wall result from bending or ovalization under non-uniform radial loads and from direct circumferential stress resulting from radial pressure distributions.

Ring Bending Strain: Maximum ring bending strains resulting from earth and surface wheel loads, as well as from installation deflections normally occur at the invert. However, under some conditions, strains at other locations may be important depending on strength limits established for environmental exposures inside and outside the pipe. For example, tensile strains at the crown may govern the design of FRP or RPM pipe, since exposure of the crown interior surface to sewer acids may reduce ultimate strength below that experienced in a water environment, as is the case for values given in Table 9-11.

The moment factor, $\overline{MF}$, required for Eq. 9.138 a to c, accounts for the effects of bedding on bending moments and strains. Tentative values for the moment factor are given in Table 9-12. Strains occurring under service loads are increased by the load factor appropriate for each loading condition.

Ring Tension and Compression Strains: Factored ring or hoop tension strains resulting from the applied internal pressure, if any, are calculated using Eq. 9.139. And Eqs. 9.140 a to d are used to calculate the initial ring compression strains in the pipe. These strains are assumed to be constant around the full pipe circumference, although in the real structure, particularly in large pipe, these strains may be less at the crown than at the invert.

Both maximum and minimum ring compression strains under earth and vehicle loads are required in this ultimate strength approach. The maximum strain is used in later determination of the maximum compression strain in the wall (Eq. 9.141), and the minimum strain is needed for determination of the maximum tension strains in the ring (Eqs. 9.142 & 9.143).

Strength Adequacy

Adequacy to resist the combinations of strain components calculated above is evaluated in a manner similar to that given in Eq. 8.130. In this case, an interaction index is proposed that reflects different strengths in creep (fixed stress or load) and relaxation (fixed strain). The interaction equations from which Eqs. 9.141 to 9.143 are derived are expressed in terms of strain, below:

$$\frac{\epsilon_{bu}}{\epsilon_{Ru}} + \frac{\epsilon_{cu}}{\epsilon_{Cu}} \leq 1 \quad \text{and} \quad \frac{\epsilon_{bu}}{\epsilon_{Ru}} + \frac{\epsilon_{tu}}{\epsilon_{Cu}} \leq 1 \qquad \text{Eq. 9.156a, b}$$

Non-Pressure Pipe: Adequacy of buried non-pressure pipe is usually governed by maximum compression at extreme fibers resulting from combined ring bending and ring compression. This may not be the case for reinforced plastic pipe where the compression strength may be significantly greater than the tension strength, depending on the materials and construction. If this is the case, adequacy under both maximum combined tension and compression should be evaluated.

Perforated Pipe: When a buried pipe is perforated, stress or strain concentrations in a tensile stress field can be significant. Thus, a check of the effects of perforations should be made in accordance with Eq. 9.139. This is in addition to that for maximum combined compression, discussed above. Table 9-14 provides "stress (strain) concentration factors" to be applied to the maximum tensile stress or strain calculated at the perforation location. If perforations are located at or near inflection points, the effects of strain concentrations can be neglected.

Pressure pipe: Maximum strains in pressure pipe are the combined result of hoop stress due to internal or external pressures, bending due to earth and vehicle loads, and any reduction in bending due to "rerounding" of the ovalled buried pipe upon pressurization as discussed below. When a buried pipe is subjected to internal pressure, circumferential (hoop) stresses develop, and deflection due to installation and earth pressure is reduced. The pipe returns to a more circular shape or "rerounds." This rerounding reduces bending strains caused by external loads. The rerounding factor ($\overline{RF}$, Eq. 9.144) proposed in (9.45) accounts for the effects of internal pressure on bending strains in a very flexible buried pipe subjected to external loads and installation deflections. Note that the above check for maximum compression in non-pressure pipe should be made for pressure pipe as well since compression strength may govern design for periods when no pressure is applied.

Table 9-14

Perforation Factors for Strain Concentrations (9.44)

Perforation Type	Perforation Factor ($\overline{PF}$)
Circular hole, smooth-wall pipe in bending	2.3
Circular hole, uniform tension (e.g. in one shell of ABS Composite or in flanges of corrugated tubing)	3.0
Circumferential slot, rounded ends, assume aspect ratio = 8:1 (e.g. 1 in. (25 mm) circumferential slot, 1/8 in. (3 mm) wide; factor varies with actual aspect ratio	1.3

Allowable Deflections Based on Ultimate Strain

For purposes of writing specifications, or when establishing deflection limit criteria for existing or new products, it is useful to calculate the maximum allowable deflection. Eqs. 9.145 and 9.147, based on strength limits (in terms of strain) given above, provide a means for calculating the maximum installed deflections of the pipe barrel.

Buckling

The resistance of the pipe ring to buckling under external pressure becomes very important in large-diameter thin-walled plastic pipe, or in pipe with low modulus materials, such as PE. Resistance to buckling is significantly enhanced by the restraint of the embedment soil. The stiffer the embedment, the greater is the buckling resistance, as is shown by Eq. 9.148 in Table 9-9. The calculated factored compression stress should be less than the buckling resistance times the capacity reduction factor. Methods for predicting buckling strength are currently under review by industry, and the following approaches may be revised based on new research.

The buckling resistance of pipe under long term earth load reduces with time because of creep. Little is known about the effect of creep on buckling of buried pipe. For the present, it appears conservative to use the long term time-dependent pipe stiffness, $\overline{PS}_{10}$ in buckling calculations, Eq. 9.148. $\overline{PS}_{10}$ is determined directly from special, non-standard long term parallel plate tests, or from Eq. 9.155.

When the pipe is submerged in ground water, it is assumed that the pipe remains empty. The factor, C_w, accounts for the reduction in buckling resistance that occurs when the confining soil pressure is reduced by the buoyancy of the ground water. In this case, the external pressure in Eq. 9.151 is the combined pressure caused by ground water, the weight of saturated earth above the water table, and the buoyant weight of submerged earth below the water table.

Some experiments with polyethylene pipe indicate that buckling is caused solely by the uniform hydrostatic component of pressure from ground water and internal vacuum, if any, rather than the pressure of earth combined with water and vacuum. Buckling resistance on this basis may be less than given by Eq. 9.148. Various investigators suggest that the maximum buckling strength under this approach is in the range of 3 to 6 times the buckling resistance of a simple tube subject to hydrostatic pressure without constraint from the soil; the critical buckling load for this case is given by Eq. 9.152.

A reduction in buckling resistance may also occur for shallow buried pipe when the upward force of buoyancy equals, or exceeds, the submerged weight of soil over the pipe. Obviously, in this case, the pipe requires anchor straps to restrain it from "floating" out of the embedment. More research is needed to determine the effects of such "neutral buoyancy" conditions on the buckling resistance of the pipe. A lower limit of such resistance is given by Eq. 9.15 for buckling of rings under external pressure with no restraint from surrounding soil.

Eq. 9.152 may govern over Eq. 9.148 in the case of large hydrostatic pressures. The actual range of material modulus, pipe stiffness, cover depths and embedment stiffness over which each of the two buckling equations is valid remains to be determined.

Other Considerations: The above procedure covers only the structural adequacy of the pipe barrel in the circumferential direction. Joints, connections, and fittings display stiffness, strength, and stiffness-to-strength relationships, which are significantly different from those provided in the barrel. A comprehensive structural evaluation of a plastic pipe system should include behavior evaluation of these parts of the system.

Dynamic surge pressures, impact loadings, longitudinal membrane and bending stress resultants due to internal pressure, unbalanced thrust forces resulting from changes in flow direction at bends, changes in flow cross-section area or line termination, and restraint of Poisson's contraction by soil friction may result in significant stress or strains and must be considered in any detailed evaluation of a specific installation. Also, as experience has shown, bending of the whole tubular cross section as a beam can add significantly to ring deflections, as well as to stresses and strains as calculated herein. See (9.44), (9.45) and (9.46) for more complete presentations of design considerations for buried plastic pipe.

Design Example

The application of the above procedure for evaluating the adequacy of a 32-inch diameter uniform wall polyethylene (PE) gravity flow industrial waste line is illustrated in **Example 9-20.**

Example 9-20 Buried Polyethylene Industrial Waste Line: Determine the adequacy of a polyethylene pipe, 32 in. in diameter, IPS (ANSI B36-10) sizing system, with minimum wall thickness of 1.882 in. Operating pressure is 45 psi. Burial depth varies from 4 ft to 15 ft, proposed embedment is well-graded gravel with less than 5% fines, compacted to 90% of maximum dry density. Groundwater varies from below pipe to 5 ft below grade. Site will be trafficked. (See Table 9-9 for procedure and notations.)*

1. **Design Criteria:**

a. **Pipe Properties**

Outside diameter: $2R_o = 32.0$ in.; $R_o = 16.0$ in.

Wall thickness: $t = 1.882$ in.

Mean diameter: $2R = 30.1$ in.; $R = 15.1$ in.

Inside diameter: $2R_i = 28.2$ in.; $R_i = 14.1$ in.

Short term elastic modulus: $E_o = 100{,}000$ psi

Creep factor: assume $\overline{CF} = 2.0$

Calculate pipe stiffness since governing specification does not contain a pipe stiffness requirement.

Moment of inertia: $i = 1/12\ t^3 = 1/12 \times 1.882^3 = 0.555$ in.^{4}/in.

Pipe Stiffness: $$\overline{PS}_o = \frac{6.7\,E_o\,i}{R^3} = \frac{6.7 \times 100{,}000 \times 0.555}{15.1^3} = 108 \text{ psi}$$

$$\overline{PS}_{10} = \frac{\overline{PS}_{10}}{\overline{CF}} = \frac{108}{2.0} = 54 \text{ psi}$$

Capacity Reduction Factors: Pipe strength $\phi = 0.80$
Pipe stiffness for buckling $\phi'' = 0.75$

Ultimate strength (strain basis, Table 9-11): $\epsilon_{Cu} = \phi\epsilon_C = 0.80 \times 1.5 = 1.2\%$

$\epsilon_{Ru} = \phi\epsilon_R = 0.80 \times 2.9 = 2.3\%$

b. **Soil Properties**

Modulus of Soil Reaction (Table 9-10): $E' = 2{,}000$ psi; for well-graded gravel @ 90% density

Capacity reduction factor for soil modulus in buckling equation: $\phi' = 0.50$

Deflection Lag Factor: $\overline{DF} = 1.5$

---

* See footnote, Example 9-1, Page 9-13.

Example 9-20 (continued)

c. **Load Factors ($\overline{LF}$)**

Earth, ground water and installation: 1.5

Minimum when earth load increases strength: 0.8

Internal Pressure: 2.0

Vehicle: 1.8 (max. vehicle wheel pressure unlikely to occur with factored internal pressure)

Vacuum: 1.8 (vacuum cannot exceed atmospheric pressure)

2. **Loads:**

			15 ft. cover	4 ft. cover
a.	Burial Depth		15 ft. cover	4 ft. cover
b.	Earth:	$p_s = \gamma_s h$	$\frac{120 \times 15}{144} = 12.5$ psi	$\frac{120 \times 4}{144} = 3.3$ psi
		$p_{su} = p_s \times \overline{LF}$	12.5 x 1.5 = 18.8 psi	3.3 x 1.5 = 5.0 psi
		$p'_{su} = p_s \times \overline{LF}'$	12.5 x 0.8 = 10.0 psi	3.3 x 0.8 = 2.6 psi
c.	Buoyant Earth:	$C_w = 1 - \frac{h_w}{3h}$	$1 - \frac{10}{3 \times 15} = 0.778$	1 - 0 = 1
		$p_b = p_s C_w$	12.5 x 0.778 = 9.7 psi	3.3 psi
		$p_{bu} = p_b \times \overline{LF}$	9.7 x 1.5 = 14.6	3.3 x 1.5 = 5.0
d.	Vehicle:	p_{wh} (Fig. 9-33)	0.8 psi	3.3 psi
		$\overline{IF} = \frac{p_{wh}}{p_{wh} + p_s}$	$\frac{0.8}{0.8 + 12.5} = 0.06$	$\frac{3.3}{3.3 + 3.3} = 0.5$
		$p_w = p_{wh}(1 + \overline{IF})$	0.8 x 1.06 = 0.8 psi	3.3 (1.5) = 5.0 psi
		$p_{wu} = p_w \times \overline{LF}$	0.8 x 1.8 = 1.4 psi	5.0 x 1.8 = 9.0 psi
		$p'_{wu} = p_w \times \overline{LF}'$	0.8 x 0.8 = 0.6 psi	5.0 x 0.8 = 4.0 psi
e.	Groundwater:	$p_g = 0.43\, h_w$	0.43 x 10 = 4.3 psi	0.43 x 0 = 0 psi
		$p_{gu} = p_g \times \overline{LF}$	4.3 x 1.5 = 6.5 psi	0
f.	Vacuum:	$p_v =$	14.7 psi	14.7 psi
		$p_{vu} = p_v \times \overline{LF}$	14.7 x 1.8 = 26.5 psi	14.7 x 1.8 = 26.5 psi
g.	Internal Pressure:	$p_f =$	45 psi	45 psi
		$p_{fu} = p_f \times \overline{LF}$	45 x 2.0 = 90 psi	45 x 2.0 = 90 psi

Example 9-20 (continued)

3. Maximum Deflection

a). Earth load ($\overline{DF}$ = 1.5, K_b = 0.11 from Table 9-12)

$$\frac{\Delta s}{2R} = \frac{K_b\, P_s}{0.149\,\overline{PS}_o + 0.061\,E'} \times \overline{DF} = \left(\frac{0.11 \times 12.5}{0.149 \times 108 + 0.061 \times 2000}\right) \times 1.5 = 0.0149 \text{ in./in.} = 1.49\%$$

b). Live load at 15 ft depth is small (neglect)

$$\frac{\Delta w}{2R} = 0$$

c). Installation deflection (for $\overline{PS}_o$ = 108 psi)

$$\frac{\Delta i}{2R} = 2.0\% \text{ (from Table 9-13)}$$

d). Total deflection

$$\frac{\Delta}{2R} = \frac{\Delta s}{2R} + \frac{\Delta w}{2R} + \frac{\Delta i}{2R} = 1.49\% + 0 + 2.0\% \simeq 3.5\%$$

4. Strain Components

a. Ring Bending — Haunching is specified, inspection is expected to be nominal. Select $\overline{MF}$ = 1.0 from Table 9-12.

$$\begin{vmatrix} \epsilon_{bsu} \\ \epsilon_{bwu} \\ \epsilon_{biu} \end{vmatrix} = 2.14\left(\frac{t}{R}\right)\overline{MF} \times \begin{vmatrix} \frac{\Delta s}{2R} \times \overline{LF} \\ \frac{\Delta w}{2R} \times \overline{LF} \\ \frac{\Delta i}{2R} \times \overline{LF} \end{vmatrix} = 2.14\left(\frac{1.882}{15.1}\right) \times 1.0 \times \begin{vmatrix} 1.49 \times 1.5 \\ 0 \times 1.8 \\ 2.0 \times 1.5 \end{vmatrix} = \begin{vmatrix} 0.60\% \\ 0 \\ \underline{0.80\%} \end{vmatrix}$$

$$\epsilon_{bu} = \epsilon_{bsu} + \epsilon_{bwu} + \epsilon_{biu} = 1.40\%$$

b. Ring tension

$$\epsilon_{tu} = \frac{P_{fu} R_i}{t\,E_o} = \frac{90 \times 14.1}{1.882 \times 100{,}000} = 0.0067 \text{ in./in.} = 0.67\%$$

c. Ring compression

$$\begin{vmatrix} \epsilon_{csu} \\ \epsilon'_{csu} \\ \epsilon_{cwu} \\ \epsilon_{cvu} \end{vmatrix} = \frac{R_o}{t\,E_o} \begin{vmatrix} P_{su} \\ P'_{su} \\ P_{wu} \\ P_{vu} \end{vmatrix} = \frac{16.0 \times 100}{1.882 \times 100{,}000} \times \begin{vmatrix} 18.0 \\ 10.0 \\ 0 \\ 26.5 \end{vmatrix} = \begin{vmatrix} 0.16\% \\ 0.085\% \\ 0\% \\ 0.23\% \end{vmatrix}$$

Example 9-20 (continued)

5. **Strength Adequacy**

a. Maximum compression before pressurization

$$\bar{R}_a = \frac{\varepsilon_{bu}}{\varepsilon_{Ru}} \left[\frac{1}{1 - \frac{\varepsilon_{csu} + \varepsilon_{cwu} + \varepsilon_{cvu}}{\varepsilon_{Cu}}} \right] = \frac{1.4}{2.3} \left[\frac{1}{1 - \frac{0.16+0+0.23}{1.2}} \right] = 0.90 \leq 1 \qquad \text{o.k.}$$

b. Maximum tension

$$\overline{RF} = \left[1 + \frac{2\, p_f\, R_i}{(p_s + p_w)\, R_o} \left(\frac{\Delta}{2R}\right) \right]^{-1} = \left[1 + \frac{2 \times 45 \times 14.1}{(12.5 + 0)\, 16.0} \; (0.035) \right]^{-1} = 0.818$$

$$\bar{R}_c = \frac{\varepsilon_{bu}}{\varepsilon_{Ru}} \left[\frac{\overline{RF}}{1 - \frac{\varepsilon_{tu} - \varepsilon'_{csu}}{\varepsilon_{Cu}}} \right] = \frac{1.4}{2.3} \left[\frac{0.818}{1 - \frac{0.67 - 0.085}{1.2}} \right] = 0.97 \leq 1 \qquad \text{o.k.}$$

Note that rerounding reduces flexural strains by (1 - 0.818) = 0.18 or 18%.

6. **Buckling**

a. Modified AWWA formula

$$p_{cr} = 0.77 \left[\left(\frac{(1 - \frac{\Delta}{2R}\max)}{(1 + \frac{\Delta}{2R}\max)^2} \right)^3 C_w\, B'\, (E'\, \phi')\, (\overline{PS}_{10}\, \phi'') \right]^{1/2}$$

C_w = 0.778 (From Step 2c)

$$\frac{h}{2R_o} = \frac{15}{2 \times 16.0 \times \frac{1}{12}} = 5.63$$

$$B' = 0.150 + 0.014 \frac{h}{2R_o} = 0.150 + (0.014 \times 5.63) = 0.229$$

$$p_{cr} = 0.77 \left[\left(\frac{(1 - 0.035)}{(1 + 0.035)^2} \right)^3 \times 0.778 \times 0.229 \times 2000 \times 0.5 \times 54 \times 0.75 \right]^{1/2} = 55.9 \text{ psi}$$

$\bar{R}_d = (p_{bu} + p_{gu} + p_{vu})/(p_{cr}) = (14.6 + 6.5 + 26.5)/(55.9) = 0.85 \leq 1$ o.k.

b. Buckling under hydrostatic component of load.

$p'_{cr} = 0.5\, C_a\, \phi'\, \overline{PS}_{10} \times \phi''$

Say C_a = 3 for well compacted gravel

p'_{cr} = 0.5 x 3 x 0.5 x 54.0 x 0.75 = 30.5 psi

$\bar{R}_e = (p_{gu} + p_{vu})/(p_{cr}') = (6.5 + 26.5)/(30.5) = 1.09$ Overstress is 9%

Example 9-20 (continued)

7. Check pipe design at 4 ft minimum cover

a. Loads - See Step 2

b. Maximum deflection

$$\frac{\Delta s}{2R} = \frac{K_b\,P_s}{0.149\,\overline{PS}_o + 0.061\,E'} \times \overline{DF} = \frac{0.11 \times 3.3}{0.149 \times 108 + 0.061 \times 2000} \times 1.5 = 0.0039 \text{ in./in.} = 0.39\%$$

$$\frac{p_w}{p_s} = \frac{5.0}{3.3} = 1.5 \geq 0.25 \text{ (Therefore use n = 0.5)}$$

$$\frac{\Delta w}{2R} = \frac{K_b\,P_w}{0.149\,\overline{PS}_o + 0.061\,n\,E'} = \frac{0.11 \times 5.0}{0.149 \times 108 + 0.061 \times 0.5 \times 2000} = 0.0071 \text{ in./in.} = 0.71\%$$

$$\frac{\Delta i}{2R} = 2.0\%$$

$$\frac{\Delta}{2R} = \frac{\Delta s}{2R} + \frac{\Delta w}{2R} + \frac{\Delta i}{2R} = 0.39 + 0.71 + 2.0 = 3.1\% = 0.031 \text{ in./in.}$$

c. Strain components

$$\begin{vmatrix} \varepsilon_{bsu} \\ \varepsilon_{bwu} \\ \varepsilon_{biu} \end{vmatrix} = 2.14\left(\frac{t}{R}\right)\overline{MF} \times \begin{vmatrix} \frac{\Delta s}{2R} \times \overline{LF} \\ \frac{\Delta w}{2R} \times \overline{LF} \\ \frac{\Delta i}{2R} \times \overline{LF} \end{vmatrix} = 2.14\left(\frac{1.882}{15.1}\right) \times 1.0 \times \begin{vmatrix} 0.39 \times 1.5 \\ 0.71 \times 1.8 \\ 2.0 \times 1.5 \end{vmatrix} = \begin{vmatrix} 0.16\% \\ 0.34\% \\ \underline{0.80\%} \end{vmatrix}$$

$$\varepsilon_{bu} = \varepsilon_{bsu} + \varepsilon_{bwu} + \varepsilon_{biu} = 1.30\%$$

$$\begin{vmatrix} \varepsilon_{csu} \\ \varepsilon'_{csu} \\ \varepsilon_{cwu} \\ \varepsilon'_{cwu} \end{vmatrix} = \frac{R_o}{t\,E_o} \begin{vmatrix} p_{su} \\ p'_{su} \\ p_{wu} \\ p'_{wu} \end{vmatrix} = \frac{16.0 \times 100}{1.882 \times 100{,}000} \times \begin{vmatrix} 5.0 \\ 2.6 \\ 9.0 \\ 4.0 \end{vmatrix} = \begin{vmatrix} 0.04\% \\ 0.02\% \\ 0.08\% \\ 0.03\% \end{vmatrix}$$

$\varepsilon_{tu} \doteq 0.0067$ in./in. = 0.67% (Step 4b)

d. Strength adequacy

$$\overline{R}_a = \frac{\varepsilon_{bu}}{\varepsilon_{Ru}}\left[\frac{1}{1 - \dfrac{\varepsilon_{csu} + \varepsilon_{cwu} + \varepsilon_{cvu}}{\varepsilon_{Cu}}}\right] = \frac{1.30}{2.3}\left[\frac{1}{1 - \dfrac{0.04 + 0.08 + 0.23}{1.2}}\right] = 0.80 < 1 \quad \text{o.k.}$$

$$\overline{RF} = \left[1 + \frac{2p_f\,R_i}{(p_s + p_w)\,R_o}\left(\frac{\Delta}{2R}\right)\right]^{-1} = \left[1 + \frac{2 \times 45 \times 14.1}{(3.3 + 5.0)\,16.0}\,(0.031)\right]^{-1} = 0.77$$

Example 9-20 (continued)

$$\bar{R}_c = \frac{\varepsilon_{bu}}{\varepsilon_{Ru}}\left[\frac{\overline{RF}}{1 - \frac{\varepsilon_{tu} - \varepsilon'_{csu} - \varepsilon'_{cwu}}{\varepsilon_{Cu}}}\right] = \frac{1.30}{2.3}\left[\frac{0.77}{1 - \frac{0.67 - 0.02 - 0.03}{1.2}}\right] = 0.89$$

A separate check without wheel load, with $p_w = 0$, $\Delta/2R = 0.024$, $\varepsilon_{bu} = 0.96$, and $\varepsilon'_{cwu} = 0$, indicates $\overline{RF} = 0.63$ and $R_c = 0.78$. Therefore, above condition governs.

e. Buckling

Modified AWWA formula

$$p_{cr} = 0.77\left[\left(\frac{(1 - \frac{\Delta}{2R}\max)}{(1 + \frac{\Delta}{2R}\max)^2}\right)^3 C_w B' (E'\phi') (\overline{PS}_{10}\,\phi'')\right]^{1/2}$$

$$C_w = 1;\ \frac{h}{2R_o} = \frac{4 \times 12}{2 \times 16.0} = 1.50;\ B' = 0.015 + 0.041\frac{h}{2R_o} = 0.077$$

$$p_{cr} = 0.77\left[\left(\frac{(1 - 0.031)}{(1 + 0.031)^2}\right)^3 \times 1 \times 0.077 \times 2000 \times 0.5 \times 54 \times 0.75\right]^{1/2} = 37.4 \text{ psi}$$

$$\bar{R}_d = (p_{bu} + p_{wu} + p_{vu})/(p_{cr}) = (5.0 + 9.0 + 26.5)/(37.4) = 1.08$$

Buckling becomes critical at shallow burial mainly because B', an indicator of stiffness of soil confinement, reduces drastically with decreasing depth according to the AWWA formula. (Compare with Step 6a.)

Hydrostatic Buckling (vacuum only, no ground water)

p'_{cr} = 30.5 psi (from Step 6b)

$\bar{R}_e = p_{vu}/p'_{cr} = 26.5/30.5 = 0.87$

8. **Summary**

Following is a summary of results:		15 ft Burial	4 ft Burial
Deflection		3.5%	3.1%
Maximum Compression	$\bar{R}_a$	0.90	0.80
Maximum Tension	$\bar{R}_c$	0.97	0.89
AWWA Buckling	$\bar{R}_d$	0.85	1.08
Hydrostatic Buckling	$\bar{R}_e$	1.09	0.87

The design meets all criteria except for AWWA buckling at shallow burial and hydrostatic buckling at deep burial.

Example 9-20 (continued)

The following options are available.

a. Accept 8% and 9% overstress in buckling since accuracy of analysis is not high. Note that 8% overstress exists at shallow burial only when maximum vehicle wheel load and short-term occasional vacuum due to surge occur simultaneously. The likelihood of both of these loads acting simultaneously is small, as indicated in the AWWA Standard.

b. Increase compaction requirements of gravel to greater than 95%. This will increase E' by 50%. The increase in E' will result in an increase in buckling resistance such that R_d and $\bar{R}_e$ < 1 for shallow depths.

c. Change from gravel to crushed stone at 90% density. This will produce results similar to (b.).

d. Increase wall thickness of pipe.

Note: 1 in. = 25.4 mm, 1 ft = 0.3048 m, 1 in./in. = 1 mm/mm, 1 $in.^4$/in. = 16,387 mm^4/mm, 1 psi = 0.0069 MPa.

REFERENCES – CHAPTER 9

9.1 Widera, G.E.O. and Logan, D.L., "Refined Theories for Nonhomogeneous Anistropic Cylindrical Shells: Part I – Deviation and Part II –Application", Journal of the Engineering Mechanics Division, Papers 15933 and 15934, Vol. 106, No. EM6, American Society of Civil Engineers, New York, December 1980.

9.2 Lentovich, V., Frames & Arches, New York, McGraw-Hill, 1959

9.3 Roark & Young, Formulas for Stress and Strain, 5th Edition, New York, McGraw-Hill, 1975. (See also 4th edition, 1965, for certain additional formulas.)

9.4 Olander, H.C., Stress Analysis of Concrete Pipe, U.S. Bureau of Reclamation, Eng. Monograph No. 6.

9.5 Peterson, R.E., Stress Concentration Factors, Wiley, New York, 1974.

9.6 ASCE, Manual of Engineering Practice - No. 31, Design of Cylindrical Concrete Shell Roofs, ASCE, 1951.

9.7 Timoshenko, S., and Woinowsky-Krieger, S., Theory of Plates and Shells, 2nd Ed., New York, McGraw-Hill, 1959.

9.8 Pfluger, A., Elementary Statics of Shells, New York, F.W. Dodge, 1961.

9.9 Baker, E.H., Kovalevsky, L., and Rish, F.L.; Structural Analysis of Shells, New York, McGraw-Hill, 1972.

9.10 Flugge, W., Stresses in Shells, Berlin, Springer-Verlag, 1960.

9.11 Haas, A.M., Design of Thin Concrete Shells, Vols I & II, New York, Wiley, 1962.

9.12 Billington, D.P., Thin Shell Concrete Structures, New York, McGraw-Hill, 1965.

9.13 Candela, F., General Formulae for Membrane Stresses in Hyperbolic Paraboloidical Shells, ACI Journal, 353 (October 1960).

9.14 Parme, A.L., Hyperbolic Paraboloids and Other Shells of Double Curvature, ASCE Trans., 989 (1958).

9.15 "State-of-the-Art Report on Air Supported Structures", American Society of Civil Engineers, New York, 1979.

9.16 Rosato, D.V. & Grove, C.S., Jr., Filament Winding, Interscience, 1964.

9.17 Pressure Vessels and Piping: Design and Analysis, Vol. I – Analysis, Vol. II – Components and Structural Dynamics, (A compilation of technical papers), American Society of Mechanical Engineers, New York, 1972.

9.18 Lundgren, H., Cylindrical Concrete Shell Roofs, Copenhagen, The Danish Technical Press, 1951.

9.19 Buchert, K.P., Buckling of Shell & Shell-Like Structures, Columbia, Missouri, K.P. Buchert & Assoc., 1973.

9.20 Crandall, S.H., & Dahl, N.C.; An Introduction to the Mechanics of Materials, New York, McGraw-Hill, 1959, p. 370.

9.21 Heger, F.J., "Design of Reinforced Plastic Shell Structures", Chapter 6 in Plastics in Building, edited by Skeist, I., New York, Reinhold, 1966.

9.22 Heger, F.J., "Design of FRP Fluid Storage Vessels", Journal of Structural Division, ASCE, Nov. 1970.

9.23 Timoshenko, S.P. and Gere, J.M., Theory of Elastic Stability, 2nd Ed., New York, McGraw-Hill, 1961.

9.24 Column Research Committee of Japan, Handbook of Structural Stability, Tokyo, Corona, 1971.

9.25 Buckling of Thin-Walled Circular Cylinders, NASA SP 8007, 1968.

9.26 Gerard, G. and Becker, H.: Handbook of Structural Stability: III, Buckling of Curved Plates and Shells, NACA TN 3783, 1957.

9.27 Becker, H., General Instability of Stiffened Cylinders, NACA TN 4237 Washington, 1958.

9.28 Kloppel, K. and Jungbluth, O., "Beitrag Zum Durchschlagproblem dunnwandiger Kugelschalen" Der Stahlbau, vol. 22, p. 121, 1953 (in German).

9.29 Structural Stability Research Council, B.G. Johnston, Ed., Guide to Stability Design Criteria for Metal Structures, 3rd Ed., 1976.

9.30 Kloppel, K. and Roos, E. "Beitrag zum Durchschlagproblem dunnwandiger versteifter und unversteifter Kugelschalen fur Voll-und halbseitage Belastung, Der Stahlbau, vol. 25, p. 49, 1956.

9.31 Heger, F.J., Chambers, R.E., Dietz, A.G.; "On the Use of Plastics and Other Composite Materials for Shell Roof Structures", World Conference on Shell Structures, San Francisco, 1967.

9.32 Schnobrich, W. C., "Analysis of Hipped Roof Hyperbolic Paraboloid Structures", Journal of Structural Division, Vol. 93, ST7, American Society of Civil Engineers, New York, July 1972.

9.33 Shaaban, A. and Ketchum, M., "Design of Hipped Hypar Shells", Journal of Structural Division, Vol. 102, ST11, American Society of Civil Engineers, New York, November 1976.

9.34 White, R., "Reinforced Concrete Hyperbolic Paraboloid Shells", Journal of Structural Division, Vol. 101, ST9, American Society of Civil Engineers, New York, September 1975.

9.35 Ranjan, G. V. and Steel, C. R., "Analysis of Torispherical Pressure Vessels", Journal of Engineering Mechanics Division, Vol. 102, EM4, American Society of Civil Engineers, New York, August 1976.

9.36 Ghali, A., Circular Storage Tanks and Silos, London, Spon, 1979.

9.37 McDermott, J. F., "Single-Layer Corrugated-Steel-Sheet Hypars", Journal of the Structural Division, Vol. 94, ST6, American Society of Civil Engineers, New York, June 1968.

9.38 Reisner, E., "On Some Aspects of the Theory of Thin Elastic Shells", Journal of the Boston Society of Civil Engineers, Vol. 42, No. 2, Boston Society of Civil Engineers, April 1955.

9.39 Miller, C. D., "Buckling of Axially Compressed Cylinders", Journal of the Structural Division, Vol. 103, No. ST3, American Society of Civil Engineers, New York, March 1977.

9.40 Zick, L. P., "Stresses in Large Horizontal Cylindrical Pressure Vessels on Two Saddle Supports", The Welding Journal Research Supplement, September 1951, Reprinted in Vol. 2, Ref. (9.17)

9.41 Heger, F. J., Chambers, R. E., "Design, Analysis and Economics of Fiberglass Reinforced Plastics World's Fair Structures", Proceedings, 21st Annual Technical and Management Conference, Reinforced Plastics Division, Society of the Plastics Industry, Inc., New York, 1966.

9.42 Heger, F. J., "Engineering Concepts in the Design of Two FRP Shell Roof Structures", Proceedings, 19th Annual Technical and Management Conference, Reinforced Plastics Division, The Society of the Plastics Industry, Inc., New York, 1964.

9.43 Kulkarni, S. and Zweben, C. (ed.), Composites in Pressure Vessels and Piping, PVP - PB - 021, American Society of Mechanical Engineers, New York, 1977.

9.44 Chambers, R.E., McGrath, T.J. and Heger, F.J., Plastic Pipe for Subsurface Drainage of Transportation Facilities, National Cooperative Highway Research Program Report 225, Transportation Research Board, National Research Council, Washington, DC, October 1980.

9.45 Chambers, R.E., McGrath, T.J., "Structural Design of Buried Plastic Pipe", Proceedings, ASCE International Conference on Underground Plastic Pipe, New Orleans, LA, March 1981.

9.46 The American Water Works Association, "Standard for Glass Fiber Reinforced Thermosetting Resin Pressure Pipe," (AWWA C950-80), 1980.

ASCE Structural Plastics Design Manual

CHAPTER 10 — FIRE SAFETY CONSIDERATIONS

By Albert G. H. Dietz

T A B L E   O F   C O N T E N T S

CHAPTER 10 - FIRE SAFETY CONSIDERATIONS

A. G. H. Dietz

10.1 INTRODUCTION

When plastics are employed structurally, their behavior in fire must be considered, as is true of other structural materials. Ease of ignition, rate of flame spread, rate of heat release, smoke release, toxicity of products of combustion, and other factors must be taken into account. Plastics are organic materials and, like other organic construction materials, can be destroyed by fire. Some burn readily, others with difficulty, and still others do not support their own combustion. Behavior in fire depends upon the nature and scale of the fire and the surrounding conditions. Fire is a highly complex, variable phenomenon, and the behavior of organic materials, including plastics, in a fire is equally complex and variable.

No attempt at an exhaustive treatment is made here. Differences between behavior of plastics in controlled laboratory-scale fires and in large actual fires are set forth. There is some discussion of the products of combustion including smoke and gases. Steps taken to modify the susceptibility of plastics to fire are briefly outlined.

Fire tests of plastics, like fire tests generally, are frequently highly specific and the results are specific to the tests. The results of one type of test may not correlate directly with another. Some tests are intended mainly for screening purposes during research and development; others, such as the large-scale tests, more nearly approximate actual fires. Consequently, such often-used terms as "self-extinguishing" and "flame spread" must be understood in the context of the specific tests with which they are employed. Commonly-used tests are summarized in this chapter and their limitations indicated.

The principles of good design for fire safety are as applicable to plastics as to other materials. The specific design must be carefully considered, the properties of the materials taken into account, and engineering judgment applied.

Experience and tests have indicated approaches that may be utilized and applications that have been found satisfactory.

Building codes have incorporated provisions for plastics since about 1955. The model codes contain such provisions. These are summarized as examples, but in any specific instance the local code that has jurisdiction must be followed.

10.2 STEPS LEADING TO COMBUSTION

Small-Scale Burning (10.1) *

In small-scale fire tests, as in many laboratory screening tests, several stages are involved. At relatively low temperatures, such as 175-212°F (80-100°C), slow oxidation occurs, a feature also characteristic of aging, which is often enhanced as temperatures increase. As the temperature is raised, the process is accelerated. When the temperature becomes high enough, in the range 390-570°F (200-300°C), the process in the presence of air (oxygen) becomes exothermic, that is, heat is evolved, giving off decomposition products which are often flammable. Thermoplastics soften or melt, whereas thermosets characteristically maintain their shapes. If more heat is added, auto-ignition occurs at approximately 750°F (400°C), resulting in combustion. (See Appendix A for more detailed description.)

Large-Scale Burning (10.2) (10.8) (10.10)

The foregoing description of the successive stages of decomposition and ignition of plastics is for small-scale fires, as in laboratory tests. In real fires, as in a room, the same reactions probably take place, but the scale and temperatures involved are much larger and more complex, leading to phenomena not found in small-scale controlled laboratory burning. The following stages are generally encountered:

---

* Numbers in parentheses refer to the list of references at the end of this chapter.

Ignition: A fire can start in many ways, not necessarily involving a plastic material. The location, temperature, energy output, and duration of an ignition source are important. A burning match, a lighted cigarette, an electrical short, or any one of many sources may start a fire slowly or rapidly. At this stage, the decomposition temperature and behavior, ease of ignition, extent of exposure, and extent of involvement of plastics are important.

Build-up and Spread. This and following stages are strongly influenced by ventilation, fuel load, composition, availability, configuration and moisture content of materials. Temperatures of materials rise as the fire continues and contributes heat. Easily-ignited materials catch fire. Fire may begin to spread on flammable surfaces such as finishes. Combustible and toxic gases begin to evolve and smoke is produced; these constitute a hazard to occupants. Early warning, as by smoke and fire detectors, may be crucial.

Flashover. This phenomenon is familiar to firefighters and is the critical point in a fire. At this stage, most or all of the combustible materials reach the ignition temperatures because of radiation, convection, and conduction from the original fire. An entire room and its contents, for example, seem suddenly to burst into flame simultaneously. Ease of ignition, surface flammability, extent of exposure, evolution of combustible gases and extent of involvement of all combustibles, including plastics, are important.

Fully-Developed Fire. All of the combustibles are essentially involved. The total heat contributed by the materials is now important. This is a function of the unit heat of combustion and the quantity of material. Fire gases and smoke production are critical. Occupants may find it impossible to escape.

Propagation. Whether the fully-developed fire will spread to adjacent areas depends upon the dimensions of the compartment, the fire resistance of the boundaries, and such deterrents as sprinklers. If walls, floors, and ceilings are resistant to fire, and if openings can be closed to stop the spread, the fire may be contained. If not, it may spread to other parts of the structure.

Fig. 10-1 illustrates fire-intensity phases in an energy-time relationship during fires that undergo flashover and those that do not. The latter involve little energy and may be confined to their points of origin. Flashover fires, on the other hand, involve large amounts of energy and may propagate across incombustible zones if not effectively blocked. Intensity may be high and of short duration, as in fires involving readily-available combustibles and plenty of ventilation, or intensity may be low and of long duration, as in damped fires involving less-readily burned materials, which may smolder for a considerable period.

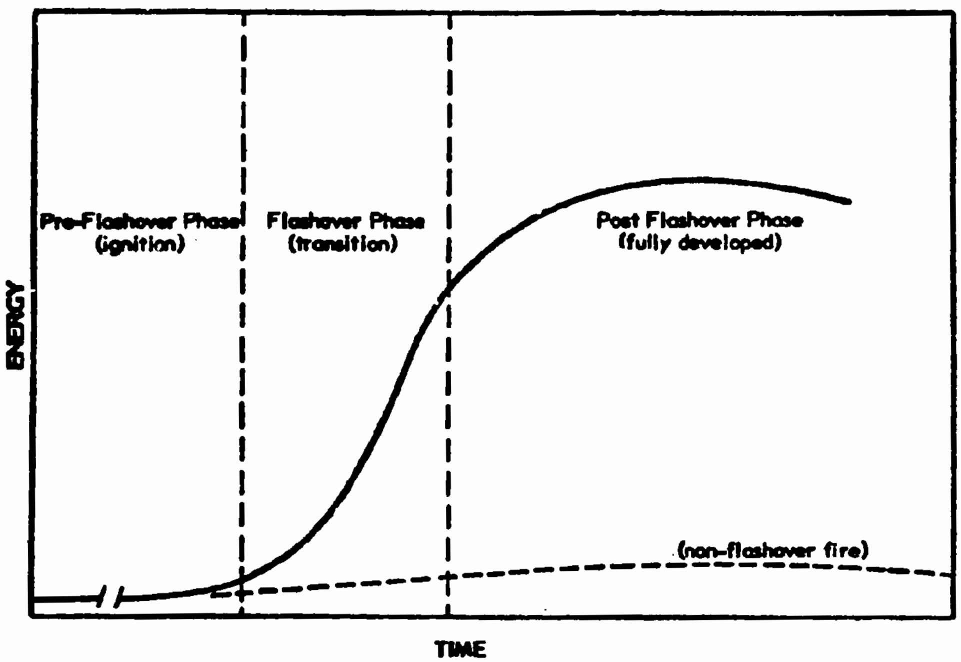

Fig. 10-1 FIRE INTENSITY PHASES (10.8)

Smoke (10.2) (10.3) (10.4) (10.7) (10.10) (10.11) (10.12) (10.13) (10.14) (10.15) (10.16) (10.17)

Smoke is recognized by firefighters as in many ways more dangerous than actual flame because it (1) obscures vision, making it impossible to find safe means of egress and leading to panic, (2) makes help or rescue difficult or impossible, and (3) leads to physiological reactions such as choking and lachrymation. Smoke usually contains toxic gases such as carbon monoxide, often accompanied by noxious gases that may lead to nausea and other debilitating effects, as well as panic. Smoke particles may carry aerosols such as HCl on their surfaces.

Whether plastics give off light or heavy smoke and toxic or noxious gases depends upon composition and the conditions under which burning occurs. Some burn with a fairly clean flame in the presence of plentiful air, but may give off dense smoke under smoldering conditions. Others are inherently smoke producing. The composition of the smoke depends upon the composition of the plastic and the burning conditions, as is true of other organic materials of construction. In a particular application, therefore, careful consideration should be given to the relative importance of flame and smoke, including design favoring the rapid elimination of smoke by venting, for example, or fending off smoke as in pressurized corridors and stair towers.

Table 10-1 presents flame spread and smoke evolved from a number of tests on plastics materials performed in the fire tunnel, ASTM E84 (see comments in Section 10.4). These are to be taken as examples that show the range of results brought about by differences in composition, thickness, and configurations of plastic materials, including high-pressure laminates, molded plastics, reinforced plastics, polymer concrete, and miscellaneous materials when tested by this particular method. Variations and anomalies in smoke and flame-spread values are not unusual for several test runs of the same material in this tunnel test and in other tests.

Toxic and Noxious Gases (10.7) (10.10) (10.11) (10.12) (10.13) (10.14) (10.15)

The subject of toxic and noxious gases generated by the decomposition and combustion of plastics is so large, complex, and incompletely understood that no attempt is made here to treat it exhaustively.

Table 10-1

Burning Characteristics of Selected Plastics
Flamespread Test ASTM E84

		Flame Spread	Smoke Developed
High-Pressure Laminates (a)			
(1)	Unbonded General Purpose	60	135-170
	Unbonded Fire Resistant	5	25
	Bonded to CA Board		
	General Purpose	25-40	0-25
	Fire Resistant	5	5
(2)	Unbonded General Purpose	115	400
	Unbonded Fire Resistant	45-70	65
	Bonded to CA Board		
	General Purpose	70	110-160
	Fire Resistant	25	5
(3)	Unbonded General Purpose	320-350	200-250
	Unbonded Fire Resistant	55	85-140
	Bonded to CA Board		
	General Purpose	55-70	35-55
	Fire Resistant	15	10-30
Molded Plastics (a)			
	Open-Grid Panels	25	450-over 500
	Open-Grid Panels	130-160	over 800
	Translucent Panels	10	125
	Translucent Panels	25	400-450
Glass Fiber Reinforced Plastics (a)			
	1	15	over 500
	2	20	140-200
	3	25	300-400
	4	30	200
	5	50	250
	6	70	over 500
	7	75	over 500
Polyester Concrete (b)		3	55
Miscellaneous Materials (c)			
	Solid Vinyl Tile	90	
	Vinyl Flooring	80	
	Vinyl Asbestos Tile	235	
	Asphalt Tile	82	
	Lauan Mahogany	242	
	White Pine Panelling	130	
	Hollow-Core Wood Doors	325-420	
	White Vinyl Ceiling Panels	20	

(a) Reference (5.10)
(b) Manufacturer's Data
(c) Reference (5.17)

Like organic materials generally, plastics and other polymers may generate both toxic and noxious gases, as well as smoke, when exposed to high heat and during burning. The gases that will be generated depend upon the composition of the plastic and the burning conditions. If the plastic contains only carbon, hydrogen and oxygen, and if it burns under favorable conditions in the presence of plentiful oxygen, the products may be mainly water vapor and carbon dioxide. Under unfavorable conditions, such as deficient oxygen, great quantities of carbon monoxide may be generated. Some carbon monoxide is generated in any fire. Carbon monoxide is by far the most dangerous gas because it may be present in large quantities, but has no odor or other identifying features.

Again depending upon composition and burning conditions, plastics containing such elements as chlorine, nitrogen, phosphorous, and others may generate hydrogen chloride, corrosive to many materials and to living tissue, hydrogen cyanide, phosgene, acrolein, aldehydes, and others, as well as release the basic monomers of which the molecular chains were composed. Frequently, small amounts of these gases are so noxious as to be intolerable before lethal levels are attained.

It is difficult to ascertain actual levels of gases in real fires; hence, the uncertainty respecting the hazards presented by burning plastics. Considerable research into and measurements of gases as well as smoke is consequently being undertaken, in light of the increasing uses of plastics in construction. Similar research is underway to diminish the levels of noxious and toxic gases as well as smoke. (see, also, Section 10.4.) Generally-accepted tests to evaluate toxicity are lacking.

10.3 MODIFICATION FOR IMPROVED BEHAVIOR IN FIRE (10.1) (10.2) (10.3) (10.5) (10.17)

Susceptibility of unfilled, unmodified plastics to fire can be diminished in manufacture by (1) development of plastics whose structures are inherently resistant to ignition when exposed to heat and oxygen, (2) modification, and (3) incorporation of additives. Whatever the material, including plastics, the design of a structure to minimize fire danger may be more important than any of these.

The first approach is problematical in many building fires. Polymers resistant to high temperatures are possible and are produced, but it is doubtful that any foreseeable structurally-useful ones can withstand the temperatures and heat found, in fully-developed building fires, although some will propogate flame much less rapidly than others.

The second and third approaches are actively pursued in the attempt to provide plastics of varying resistance to fire.

Modification of the polymeric structure by incorporating reactive flame retardants and by incorporating additives usually involves one or more of the following approaches to achieve:

1. Decomposition and combustion products which are non-combustible, or heavy enough to blanket the plastic and prevent or retard interaction with air.

2. Decomposition and combustion reactions that involve reduced heats of combustion.

3. Reduced ease of ignition, involving increased ignition or decomposition temperature, or increased energy needed for decomposition.

4. Increased amount of solid residue so as to maintain structural integrity and impede access of heat and oxygen. Char formation, similar to the char formed on structural timber, is one of the best ways to achieve this objective. Carbon monoxide and carbon dioxide formation releases large quantities of energy and the products go off as gases, whereas carbon as char releases no energy, protects the substrate, and helps to retain the integrity of the part. Other favorable aspects are impeded access of heat and oxygen, lessened oxygen depletion and reduced toxic gas (carbon monoxide). Decomposition of silicone plastics leaves a residue of silica.

5. Increased specific heat or thermal conductivity to prevent or retard local hot spots.

6. Decreased amount of resin and other combustibles by use of incombustible fillers or reinforcements such as mineral particles and glass fibers.

The chemistry involved in accomplishing these ends is more fully set forth in Appendix A.

Zones of time vs. temperature in which various plastics retain 50 percent of their mechanical and physical properties are shown in Appendix B.

Weathering (10.18)

Fire retardants frequently lead to decreased resistance to weathering. For example, the translucent glass fiber-reinforced polyester sheets commonly employed in flat or corrugated form for wall and roof covering and in sandwich panels may turn yellow and darken upon exposure to sunlight if the polyester is one of the chlorinated types. This phenomenon may be accompanied by more rapid erosion of the surface, leading to exposure of fibers, than is true of the more highly weather-resistant types.

Because this type of deterioration is caused by ultraviolet radiation, it can be combated by employing overlays of ultraviolet-screening films. It has been found, for example, that applying a thin film (several mils) of polyvinyl fluoride to the surface of glass fiber-reinforced chlorinated polyester sheet greatly reduces surface breakdown, and such protected sheets are employed in regions of intense sunlight.

Surface erosion can frequently be repaired and surfaces restored by the application of liquid acrylic films which harden in place, protecting the fibers from exposure to the elements and retaining translucence. Opaque paints and other finishes can also be used to protect plastics from weathering. Although surface-protecting films may inherently exhibit higher or lower flame-spread characteristics than the substrate, depending upon the nature of the film, they frequently are so thin as to have little or no effect. Upon burning or decomposing, some may evolve noxious or toxic gases.

10.4 TESTS FOR EVALUATING MATERIALS

The structural engineer considering fire-related aspects of materials in his design has access to quantities of fire data, drawn from a variety of tests. In assessing such data, he must have some understanding of the tests and their limitations in order to avoid relying upon data where they are not applicable. In this section, an attempt is made to assess the tests most commonly employed for plastics.

Fire testing in general, not only for plastics, is undergoing intensive review. Test methods have evolved with inadequate understanding of the growth of fires, with the consequence that such tests and standards have often necessarily been piecemeal, applicable essentially to limited test conditions, and difficult, if not impossible, to correlate.

Knowledge of fire behavior has recently advanced considerably, and the devising of new test methods based on fire dynamics is proceeding, albeit many such tests are still largely in the development stage.

Laboratory-scale flammability test methods have evolved over many years. Their sponsorship by consensus organizations such as the American Society for Testing and Materials (ASTM) is formalized after an intensive screening process performed by committees of experts.

Many of the approximately 118 ASTM flammability test methods were adopted to cope with specific situations. It is therefore necessary for authorities concerned with the writing of codes and regulations to select those standards which most closely meet their requirements. In order to do this, the authorities must have a thorough knowledge of the standards and be aware of the techniques used and the limitations inherent in each. The long and successful application of these standards by code and regulatory bodies demonstrates their usefulness.

New testing procedures involving the calorimetric determination of ignition conditions, rate of heat and smoke release and other parameters at several heat flux levels have been developed and are being examined by the standards organizations. When these procedures have been developed as standards, they will probably replace many of the current laboratory tests in providing quantifiable fire parameters that will more closely relate these tests to the behavior of materials in actual fires.

Large-scale and full-scale tests have been proposed with the objective of providing better understanding of the behavior of materials and components in actual fires. Although the performance of these tests can be useful, no standard methods for their performance have been developed. One of the reasons for this is the very large number of variables that are associated with real fires. Another problem is that they can be very expensive to run.

With these observations in mind, the present status of fire testing as it relates to plastics may be reviewed, realizing that the situation is subject to considerable change.

The most-commonly used tests are those of the American Society for Testing and Materials (ASTM), although model codes (Section 10.6) often designate their own standards based upon accepted ASTM tests. There are others such as those of the Underwriters' Laboratories (UL), the National Fire Protection Association (NFPA), and the Factory Mutual System (FM). Many are similar. Many of these standards are adopted by the American National Standards Institute and become ANSI standards as well.

As any engineer knows, the results of tests must be interpreted and employed with caution and judgment. They cannot simulate all conditions of use. Tests are run under specified conditions, which are an approximate average of use conditions. Nowhere is this more the case than with fire tests. Different tests are used for different purposes, and the results may appear to be widely different, depending upon test conditions. Some materials that behave well in a small-scale laboratory bench test, and may appear to be nonburning or self-extinguishing, may burn vigorously in a larger-scale test or in actual use. It is therefore necessary to understand the test procedures and know their limitations.

In the past, some proponents of new materials have used favorable results of small-scale tests to designate their materials "non-flammable" or "fireproof" or, more moderately, "slow-burning", with some disastrous results in actual use. As a consequence, the Federal Trade Commission found it necessary, in the case of cellular plastics, to issue a complaint respecting such claims. The Society of the Plastics Industry incorporates this caution:

"This numerical flamespread rating is not intended to reflect hazards presented by this or any other material under actual fire conditions." (See ASTM E84 below.)

ASTM adds this caution to its fire tests:

"This standard should be used solely to measure and describe the properties of the materials, products, or systems in response to heat and flame under controlled laboratory conditions and should not be considered or used for the description, appraisal, or regulation of the fire hazards of materials, products, or systems under actual fire conditions."

This puts it squarely up to the designer and the building official to interpret the results of fire tests according to their appraisal of the conditions surrounding any particular building design. Nevertheless, ASTM and other tests are the available and accepted tests, and are commonly used as indicators of the comparative behavior of materials such as plastics among themselves and with other materials employed by the designer. Codes (Section 10.6) customarily refer to them as requirements for the guidance of building officials and designers.

With these general observations in mind, some of the commonly-used ASTM and other tests are reviewed. Some are specifically for plastics, but others are for materials generally. The larger-scale tests reviewed first relate to materials generally, not only to plastics. The smaller-scale bench or laboratory tests, many for polymer testing, are mainly useful as screening tests during research and development.

ASTM E119, NFPA 251, UL 253
Fire Tests of Building Construction and Materials

These methods are frequently called the "Standard Fire Tests" and the performance is usually expressed as "2-h", "1/2-h", etc., h meaning hours of resistance as defined by this test.

The methods are applicable to bearing and non-bearing walls and partitions, columns, girders, beams, slabs, composite beams and slabs, and other assemblies such as surface protection for combustible framing and combustible facings. They apply to all materials and combinations, including plastics.

The standard is intended to determine the period of time that a test assemblage (Fig. 10-2) will contain fire or retain its structural integrity, or both, when subjected to a standard fire exposure which may or may not be followed by a stream of water from a standard fire hose. It provides a relative measure of fire performance of comparable assemblies of materials under these fire conditions.

The standard does not provide information as to performance of assemblies of sizes other than specified, nor does it evaluate products of combustion. It does not measure flame spread (see ASTM E84), nor effects of joints or such elements as pipe and electrical receptacles unless specifically provided for (see below).

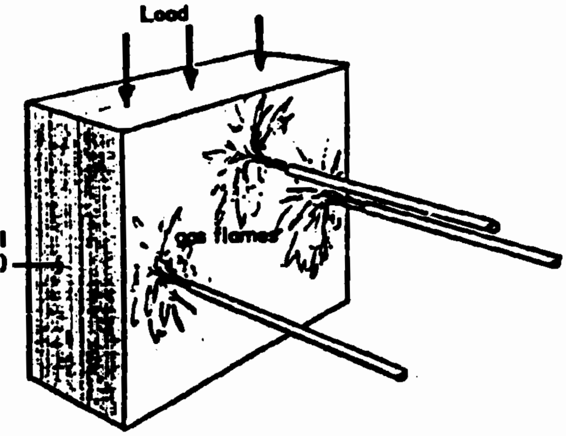

(Note: Test wall may be horizontal, e.g., floor, roof.)

Fig. 10-2 ASTM E119, FIRE ENDURANCE TEST (10.19)

Gas burners in the furnace are arranged to raise the temperature in accordance with the time-temperature relation shown in Fig. 10-3. Flames may or may not impinge directly upon the face of the specimen, which is often horizontal, rather than vertical as shown. The specimen is left exposed for the prescribed period of time, or until failure occurs as defined for that type of specimen, including penetration by flame or gases, unacceptable rise in temperature on the unexposed side, and unacceptable rise in temperature of protected framing members.

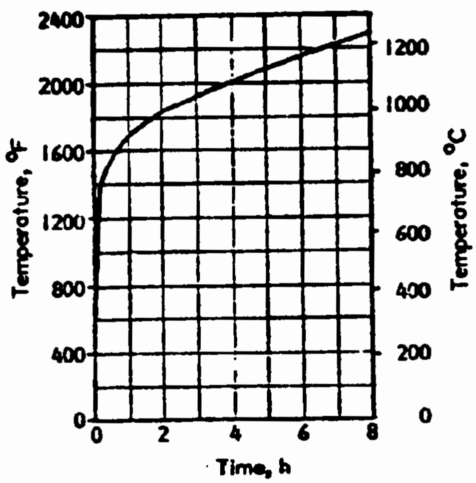

Fig. 10-3 ASTM E119, TIME-TEMPERATURE CURVE (10.19)

One point not covered by the test is the effect of pipes, conduits, ducts, and other members that pass through a wall or ceiling and may therefore allow fire to penetrate through or around the member. The insulation on electrical cable, for example, may burn and carry fire through an otherwise acceptable wall. Steps are being taken to establish tests and standards for such features.

This is one of the most widely-specified tests in building codes. Hourly ratings established by the test are the basis for permitting the use of materials and combinations or excluding them from various occupancies as defined in codes. It is probably the one standard fire test that most nearly approximates actual fire conditions.

ASTM E84, UL 723, NFPA 255
Surface Burning Characteristics of Building Materials

This test is also extensively referred to in codes. It is often called the "flame-spread" or Steiner "tunnel" test. Its purpose is to determine comparative surface burning characteristics of materials by measuring the rate of flame spread over their surfaces when exposed to the test fire. Fuel contributed and smoke density are also recorded, although there is no necessary relationship among the three measurements, and fuel contributed is often omitted.

The test chamber or "tunnel" is a horizontal duct approximately 25 ft (7.62 m) long, lined with insulating fire-resistive material such as refractory fire brick (Fig. 10-4). Test panels are placed in the ceiling of the duct. Windows provided along one side permit observation of the fire as it spreads along the lower surface of the test material. Two gas burners deliver flames upward against the test material at the "fire" end of the tunnel. At the other, or "vent," end is placed a photo-electric cell to measure smoke-caused loss in light transmission.

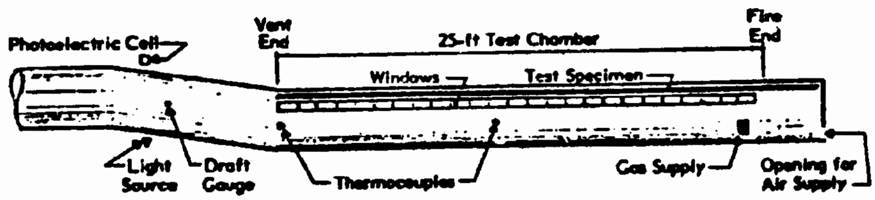

Fig. 10-4 ASTM E84, FLAME-SPREAD TUNNEL TEST (10.19)

The tunnel is first calibrated by lining the top with 23/32-inch (18.3 mm) thick select red oak flooring at 6 to 8 percent moisture content. The flame is applied and the time required to reach the end of the test specimen is determined. Temperatures and smoke density, as measured by photo-electric cell readings, are recorded. Following the red oak trials, the test calibration is repeated with cement-asbestos board. Time to travel the length of the tunnel, and the smoke density in the red oak trials are arbitrarily rated 100, whereas the cement-asbestos is rated zero.

Materials to be evaluated are tested in the same manner. Depending upon the time required for the flame to travel along the tunnel and the relative amount of smoke involved, the material may have flame-spread ratings of less or more than 100, and, similarly, smoke-density ratings of less or more than 100.

This is the test most widely specified in building codes for flame-spread on materials, including interior finish. Materials are, or are not, permitted in various building occupancies, depending upon flame-spread and smoke-density ratings. For example, a flame-spread rating of less than 25 may allow a material to be used in occupancies closed to intermediate ratings such as 25 - 50 and 51 - 200. A high flame-spread rating may rule out a material completely.

Although the test is commonly specified, its validity is challenged on the basis of larger tests such as the corner, corridor, and room tests (see below) and actual experience in fires. Materials with favorable ratings in the tunnel test may burn readily and rapidly in these other tests and in actual use. Results are strongly dependent upon the geometry of the test. The test does not show flashover. It appears to be sensitive to small variations in test conditions, and results may differ from test to test and from laboratory to laboratory. Its results have been used for other purposes than their intended use, which is flame spread and not fire endurance. It measures flame spread on the bottom of a horizontal surface, not on vertical surfaces. Thermoplastic materials may melt and fall and require special support not representative of actual use. The rate of fuel supply has been criticized as too low to reflect actual fire conditions. Smoke is measured on a linear scale (photo-electric) but light obscuration is a log function. A 75X reading, therefore, does not indicate optical density 3 times as much as 25X, but more nearly 8 to 10 times.

Nevertheless, it is widely used; many test data (e.g., Table 10-1) are available, and are relied upon in design. They must be employed judiciously, recognizing the limitations of the test.

Corner Tests and Room Tests (10.12) (10.24) (10.25) (10.26)

Because many of the standard tests do not correlate well with the observed behavior of plastics and other organic materials in actual fires, efforts are underway to develop tests that more nearly approximate such fires.

One such test is the corner test (Fig. 10-5). It consists of a corner where two vertical walls meet and are surmounted by a ceiling, forming a three-way corner. Generally, the surfaces of the walls and ceiling are made of the material to be tested, although, in some instances, either the ceiling or the walls may be a fire-resistant material such as concrete or cement-asbestos board.

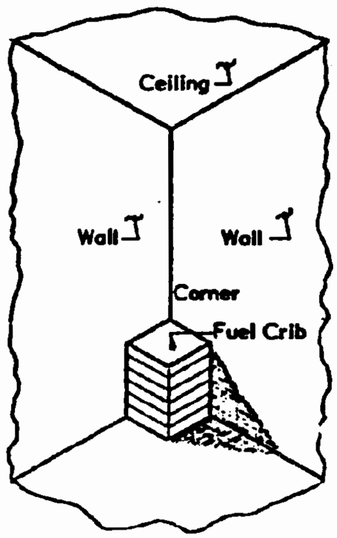

Fig. 10-5 CORNER TEST (10.12) (10.25)

A given fire source is placed on the floor near the corner and ignited. The behavior of the material in walls and ceilings is observed visually and timed. Thermocouples measure temperatures at selected spots. Critical points, such as the time that sudden rapid propagation of flame occurs (if at all), are carefully noted.

Dimensions of corner test installations vary. The largest are up to 25 ft (8 m) high with side walls up to 50 ft (16 m) long. Smaller ones are of the order of 6 to 10 ft (1.8 to 3 m) high, with correspondingly shorter walls. In larger installations, wood cribs or stacks of wood pallets, of weighed quantities and specified moisture content, are employed for fuel. Gas burners are also being used by leading laboratories for consistency and cleaner fires. Other types of fuel may also be used. For example, fuel in smaller installations may consist of weighed polyethylene wastebaskets filled with milk cartons of coated paper.

These tests are considered to be closer approximations of actual fire conditions than the smaller laboratory tests or the tunnel test. However, the larger ones, in particular, are obviously expensive and require large amounts of material, not always easy to obtain with new materials under development. Investigations of smaller corner tests and methods of scaling them to correspond to the larger tests are therefore underway.

Room tests are one step beyond the corner tests. Rooms of various dimensions, usually with standard door and window openings, are built with walls and ceilings made of the materials to be tested. Some are essentially corner tests with additional walls to form an enclosure, and openings such as doors for ventilation and observation. Specified quantities of fuel, such as wood cribs, or specified furniture such as chairs, beds, mattresses, draperies, and others, are placed in the room and ignited. As in the corner tests, progress of fire, flashover, and temperatures are carefully noted and timed.

Somewhat similar to room tests are corridor tests. Dimensions approximating those of corridors, and openings commonly found in corridors, are used. Measurements are similar to those made in corner and room tests.

Determinations of quantitative performance levels from these tests are not so easily made as from some of the small-scale laboratory tests, but are much more likely to provide better judgment of behavior in actual fire conditions.

ASTM D635- Rate of Burning and/or Extent and Time of Burning of Self-Supporting Plastics in a Horizontal Position

This small-scale laboratory test is designed to compare the relative rate of burning, extent, and time of burning of self-supporting plastics bars molded to size or cut from sheets, plates, or panels, when tested in a horizontal position.

Specimens are 125 ± 5 mm (4.92 ± .20 in.) long, 12.5 ± 0.2 mm (.492 ± .01 in.) wide, and thickness of the material normally supplied.

At least ten specimens are employed. Each specimen is clamped at one end with its long axis horizontal and transverse axis at 40 degrees to the horizontal. The tip of a specified bunsen burner flame is placed in contact with the free end of the specimen for 30 seconds. The progress of the flame along the specimen is timed until it goes out or has burned 100 mm (3.94 in.) along the specimen. This is called the burning mark.

If two or more specimens burn to the burning mark, the average burning rate, in cm/min, for all specimens that burn to the mark, is reported as the average burning rate (ABR).

If none of ten specimens, or no more than one of twenty specimens burns to the mark, the average time of burning (ATB) and the average extent of burning are reported.

Although widely used as an exploratory laboratory test, it is only that. The results are limited to the test conditions. It is only a horizontal test and does not measure the vertical component of burning. On a vertical specimen ignited at the bottom, flame spread may be many times as rapid and extensive.

ASTM D1929 - Ignition Properties of Plastics

Self-ignition and flash-ignition temperatures of plastics are determined by this laboratory test.

A 102-mm (4-in.) diameter tubular furnace 216 to 254 mm (8-1/2 to 10 in.) high surrounds a 76-mm (3-in.) diameter inner tube of the same length. Granular or stacked 19-mm (3/4-in.) square specimens are placed in the furnace, and heated air flows past them. A pilot flame is provided at the top of the furnace.

In the Flash-Ignition Test, the pilot flame is ignited and air at various velocities is passed through the furnace. The temperature of the air is set to rise at various rates until a lowest temperature is found at which combustible gases evolved from the specimen are ignited by the pilot light.

In the Self-Ignition Test, essentially the same process is employed, but without the pilot flame. Self-ignition occurs when the specimen flames, explodes, or glows.

Both tests are repeated with air at constant temperatures.

The minimum temperatures at which flash occurs are reported as Flash Ignition Temperature and Self-Ignition Temperature.

ASTM E662, NFPA 258 - Smoke Generated by Solid Materials

The method uses a chamber in which smoke is generated, and measures the smoke by photometric system. It employs either a radiant energy source for non-flaming pyrolitic decomposition of the test specimen or a six-tube propane-air burner for flaming conditions.

The specimen is 76.2 mm (3 in.) square. For non-flaming tests, a central 65.1-mm (2-9/16-in.) square area is exposed to the radiant source. For flaming conditions, flamelets are applied to the lower edge of the vertically-placed specimen. A vertical light beam passes upward through the chamber to a photomultiplier tube above the top. Smoke density is measured by loss in transmission of light, from which the specific optical density is computed. Other parameters such as maximum rate of smoke accumulation, and time to a specific optical density level, may be obtained.

ASTM E162 - Surface Flammability of Materials Using a Radiant Energy Source

Surface flammability is measured with an inclined specimen placed in front of a vertical radiant heat source composed of a ceramic plate heated by a gas flame.

The carefully preconditioned specimen is 152 x 457 mm (6 x 18 in.) and the radiant source is 305 x 457 mm (12 x 18 in.). Opaque specimens are backed as they would be in practice. Transparent specimens are backed with highly-reflective aluminum foil. The radiant panel is of porous refractory material capable of operating at temperature up to 816°C (1500°F). A pilot flame at the top of the specimen is present principally to initiate ignition and to ignite combustible evolving gases.

Rate and extent of burning and liberation of heat are determined. A flame-spread index is derived from the rate of progress of the flame front and the rate of heat liberation. Special note is made if flash occurs during the test.

This is a laboratory test and is intended for research and development only. It is considered by many practitioners to be superior to the widely-used ASTM E84 test.

ASTM D3675.

A comparison test, ASTM D3675-78, has been approved for testing of foamed plastics, specifically. It is almost identical to ASTM E162.

ASTM D3014 - Flame, Time of Burning, and Loss of Weight of Rigid Cellular Plastics in a Vertical Position

This is a small-scale screening test for comparing relative extent of burning and loss of weight of rigid cellular plastics when burning from the bottom in an upright position.

A specimen 254 x 19 x 19 mm (10 x 3/4 x 3/4 in.) is supported in an upright position in a vertical test chimney. A propane or natural gas burner applies a flame to the bottom of the specimen. A small aluminum pan under the specimen catches any drippings.

The flame is applied for 10 seconds. The height of flame produced and the time to extinction are recorded. After flaming has stopped, the specimen, holder, and drip pan are weighed, and the weight loss of material determined. At least six specimens are tested and the average results determined.

ASTM 2863 - Oxygen Index

Because many of the standard tests only roughly distinguish the relative flammability of plastics and other materials, a test known as the Oxygen Index Flammability Test, also called the Limiting Oxygen Index Test has been devised. In it, a test sample is held upright inside a tube and a precisely-controlled mixture of oxygen and nitrogen is passed upward around the specimen. A pilot flame is touched to the top of the specimen to ignite it. The percentage of oxygen in the oxygen-nitrogen mixture is adjusted until it will just maintain the flame. The index is 100 times the ratio of the amount of oxygen to the total oxygen-nitrogen mixture.

Since the percentage of oxygen in normal air is approximately 21, a lower oxygen index generally indicates a material that will burn readily, the lower the more flammable, whereas a higher index indicates that the material will not burn readily, the higher the index, the less flammable. The test has been found to be considerably more sensitive and reproducible than ASTM D635, for example.

Like all tests, this must be interpreted within its context. It measures relative flammability under controlled conditions. It does not model energy feedback, or measure flame spread, dripping, ignition temperature, and heat and smoke production, although it can probably be modified to include some of these. It is an indicator of relative oxygen requirements. The test is of interest primarily as a laboratory technique for the evalution and guidance of the development of new materials.

FM Construction Materials Calorimeter (10.16)

In this test, the heat contributed by a test specimen when exposed to flame is measured. The specimen is a panel (such as a wall or roof) of the whole construction to be tested. It forms the horizontal cover of the liquid fuel-fired furnace with the top of the sample exposed to the open atmosphere. The fuel is ignited and fed at a predetermined rate. Flue temperature is recorded versus time until no further significant combustion occurs.

The test is repeated with an incombustible panel. Auxiliary burners in the test chamber are adjusted to produce the same flue temperature-time curve as the test panel. The fuel required to match the performance of the test sample is a measure of the fuel contributed by the test sample in the original test.

NBS Differential Bomb Calorimeter (10.34)

The National Bureau of Standards has developed a bomb calorimeter used to measure potential heat of materials. Representative values obtained on a number of materials are given in Appendix C.

Toxicity Tests (10.7)

Tests for, and determination of, incapacitation and death commonly involve animals such as mice and rats exposed to gases and smoke evolved by burning materials. Incapacitation is deemed to have occurred when the animal loses control of his movements, as by falling from a revolving support. Death is determined by cessation of breathing. Whereas incapacitation by these tests may be determined within quite narrow time limits, death is more difficult to ascertain. Furthermore, anir removed from the test before death may die hours or days later. The same delayed deaths have been observed in human victims of fires.

The problem of toxicity is highly complex. Currently, there are no widely accepted toxicity tests.

10.5 DESIGN APPROACHES FOR FIRE SAFETY (10.5) (10.6) (10.7) (10.8) (10.9) (10.13) (10.14) (10.15) (10.17)

In structural or load-bearing applications, plastics and combinations employing plastics should be judged on the same basis as any other structural materials under the same loading and fire conditions. Much can be done to minimize fire hazard by employing the same basic principles of design for fire safety as are applied to any structure. The objective is to minimize hazard, irrespective of materials utilized.

In structural design the foremost considerations respecting fire are prevention of (1) loss of life, (2) loss of property, and (3) loss of services such as files, office equipment, and others. Good design involves (1) prevention of ignition, (2) controlling or managing a fire once started, and (3) extinguishing the fire.

Reduction of hazard involves early warning of a fire as by smoke and heat detectors. This is of paramount importance in saving life and bringing in fire-control equipment. Occupants, once alerted, must be able to leave a structure rapidly by protected paths and exits. Other design features include, for example, containment by thermal barriers and fire-spread breaks, knockout panels, venting as by roof vents, minimization of fuel content, avoidance of build-up and concentration of heat and smoke, and prompt fire suppression. Automatic supression systems such as sprinklers can go far toward stopping a fire in its crucial early stages. "Active" devices such as sensors and sprinklers must be maintained in working condition; otherwise, false reliance will be placed upon them. These are general considerations not confined to any particular materials.

In considering fire hazards of plastics, it should be kept in mind that thermoplastics may soften, distort, melt, drip, and flow, whereas thermosetting plastics generally keep their shapes, although they may soften to some degree and distort. Different plastics, depending upon composition, behave differently at different temperatures (see Appendix B).

The softening qualities of thermoplastics are sometimes put to use in fires. Thermoplastic translucent sheets in ceiling illumination, for example, may soften and fall at temperatures well below ignition. This may remove them from a ceiling fire, and may expose sprinklers situated above the translucent ceiling, but may fall into and augment a fire below. Frequently, codes permit such sprinkler installations, as with egg-crate diffusers or thin thermoplastics; in other cases, sprinklers must be below the translucent ceiling, and sometimes sprinklers are required both above and below.

Skylights, such as domed transparent or translucent plastic skylights, are frequently designed to be self-venting by springing open at specified temperatures by means of fusible links. If not, they may burn through to open vents, or may be broken. Windows, similarly, may burn or be broken. Some tough transparent plastics are not easily shattered; in such cases, it is often recommended that they be installed in openable sash.

Foams

Because of their excellent thermal insulation properties (Chapter 1), plastics foams are widely used as thermal insulation and in composites such as structural sandwiches (Chapter 8). Their very large surface areas coupled with resistance to inward heat flow leads to rapid flame spread. Because of their low densities they may contribute relatively little fuel to a fire, if quantities involved are small, but foams are frequently used in large quantities. Fuel contribution is significant because the rate of heat release is high, which can cause temperatures to rise rapidly. Combustion is usually complete. Smoke and toxic gas (HCN) emission are very significant in overall fire hazard evaluation (See Section

10.2 — Smoke). Some thermoplastic foams melt and retract from a heat source such as a flame, but falling molten droplets may contribute to a fire. Thermo-setting foams tend to retain their shapes instead of retracting, but some, such as the phenolics, form a surface char resistant to fire.

Plastic foams have been subjected to considerable examination and test under all conditions from small-scale laboratory tests to large corner and room tests. As a consequence, thermal barriers to shield the plastic from fire are strongly recommended for use with both thermosetting and thermoplastic foams and are required in some States. A common specification requires at least a 15-minute rating for such barriers, e.g., 26-gauge (0.45 mm) steel, 0.5-in. (13 mm) gypsum board or 0.75-in. (19 mm) fire-retardant plywood, fastened through the foam to a firm substrate to make sure the barrier stays in place for the specified time even if the foam underneath should soften. The same holds true of metal lath and plaster. Some States require sprinklers. Local codes should be consulted.

When thermal barriers are employed with some foams, especially thermoplastics such as polystyrene, the foam may, upon being heated through the barrier, contract and retract away from the barrier, leaving an insulating air space. If hot enough, however, the foam may melt, and if it can run out at the bottom of a wall panel, for example, it may ignite and help to spread the fire. If fire can penetrate an air space between foam and cover, it may ignite the foam. Barriers should be designed to prevent melting, running, and ingress of flame. Foam-cored sandwich panels may be sealed along the edges for this reason. However, some foams will decompose under such conditions, releasing combustible gases.

A retracting foam laid horizontally, as over a ceiling, may be protected from flame or heat above by a layer of loose fill such as vermiculite. If the foam does retract, the fill settles and follows, avoiding an air gap.

All foamed plastics may be employed in cavity masonry walls and under concrete floors where the cover is at least 0.5 in. (13 mm) thick. When used in roofs, depending upon the rating of the roofing, foams over sheet metal roof supports may need a barrier of incombustible material. (Codes, Section 10.6). Thermo-setting foams are not prone to melt and drip through seams in the roof, as thermoplastics may.

With sandwich panels, depending upon the composition of facing and foamed plastic core, sprinklers may or may not be required. If facings are metal, steel must be at least 26 gauge (0.45 mm), and aluminum at least 0.032 in. (0.8 mm) thick, and sprinklers are usually required.

Care must be exercised to avoid undue hazard with foamed plastics during construction. Board stock should be stored at least 50 ft (15 m) from a building or important structure. In sprinklered buildings, it may be stored in piles up to 6 ft (1.8 m) high. Only limited quantities should be placed in unsprinklered areas. As installation proceeds, the thermal barriers should follow closely, so as to avoid having large areas exposed.

Thermosetting Plastics

Because thermosetting plastics, as described in Chapter 1, consist of crosslinked or interlinked molecular aggregations, they tend to retain their configurations as temperatures rise to the combustion point, unlike thermoplastics which characteristically soften and may melt and drip. This attribute of thermosetting materials may be favorable or unfavorable in a given situation.

Depending upon molecular structure, thermosetting materials have varying degrees of resistance to temperature and flame. Phenolics, for example, are difficult to burn under ordinary conditions of flame exposure, and properties do not begin to degrade until temperatures of 500°F (260°C) are reached. They produce surface chars difficult to burn that protect the material underneath. Because phenolics are commonly modified with fillers, their fire behavior depends to some degree upon the nature and amount of filler present, e.g., wood flour, cotton flock, mica, asbestos or glass. Silicones, because of their stable silicon-oxygen linkage, are highly resistant to flame and elevated temperatures. The amines, urea formaldehyde and melamine formaldehyde, and the polyesters are less so. The burning characteristics of the unsaturated polyesters widely used in reinforced plastics (see below) can be modified by chemical modification of the monomer constituents, by the addition of organic fire retardants, the addition of inorganic fillers, and the chemical introduction of organometallic compounds. Epoxy resins, similar, can have their flammability reduced by introducing phosphorous and halogen-containing monomers or additives.

Reinforced Plastics

The relative resistance of glass-reinforced phenolics, silicone, melamine, and polyester when exposed to different temperatures is shown in Fig. 10-6. At still higher temperatures, the rate of weight loss increases, as shown in Fig. 10-7 for asbestos-filled silicones. Even at the highest temperatures shown, some silicones do not burn, and have been known to resist short-time temperatures as high as 2000°F (1100°C) without actually burning through (Appendix B).

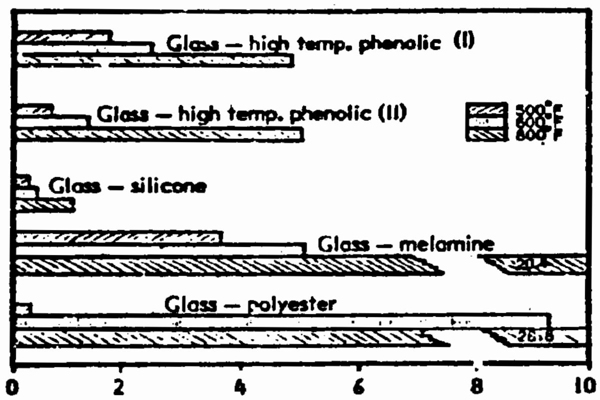

Fig. 10-6 PERCENT WEIGHT LOSS OF LAMINATES AFTER VARIOUS BAKING TEMPERATURES (10.17)

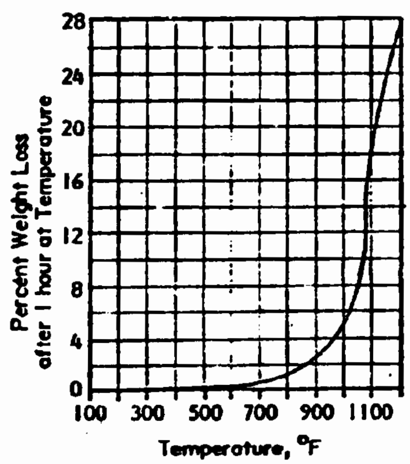

Fig. 10-7 WEIGHT LOSS OF SILICONE-ASBESTOS LAMINATES (10.17)

Reinforced plastics panels, whether fire-retardant treated or not, may be expected to burn in building fires, but the thin panels ordinarily employed frequently burn through quickly, creating openings or vents through which heat can escape. Under these conditions, temperatures may drop quickly, and flames stop propagating. It is therefore recommended that space for venting be provided behind such panels to allow the ready escape of heat. This is particularly true of hung ceiling panels; the space above should be sufficient to prevent the build-up of heat and to allow for the escape of hot gases.

Several examples may illustrate suggested applications:

1. In sprinklered areas, walls and roof bands, up to 30 ft (9 m) high and of unlimited horizontal length may be constructed of commonly-found fire-retardant panels such as those 1/16 in. (1.5 mm) thick, weighing 8 oz/sq ft (24 kg/m2) and having a flame spread of 25 or less in the ASTM E84 test.

2. In unsprinklered areas, such bands may be up to 8 ft (2.4 m) high. Successive tiers should be separated far enough to avoid jumping of fire from one to another.

3. Similar considerations hold for interior partitions and space dividers.

Epoxies are similar to the polyesters in their general flammability behavior. As indicated in Chapter 1, because of their higher cost they are normally employed only where polyesters are inadequate. In addition to glass fiber, reinforcements are commonly synthetic high-strength high-modulus fibers. Flammability characteristics of such composites have not been extensively investigated.

Furans, like phenolics, have inherently good resistance to fire, and glass fiber-reinforced furans are reported to have superior resistance to flame. They are difficult to process.

Composites

Composites are frequently relied upon to provide performance not otherwise attainable. Glass fiber reinforced polyesters may be faced with a thin acrylic cover, and backed with foam in turn covered with still another material to obtain a combination of surface color and texture, strength, insulating value, and protection against damage. Fire resistance of combinations may or may not be superior to that of the constituents alone, and should, therefore, be subjected to flammability tests.

A composite consisting of layers of materials often exhibits better fire endurance (resistance to penetration) than the sum of the endurances of the layers exposed to fire separately. A foam-cored sandwich panel, for example, is likely to resist fire better than the facings and core separately. Closely related to this generalization is the observation that the farther an air gap or cavity is from the surface exposed to fire, the more beneficial it is. Foamed plastics in a cavity wall, for example, are more useful in retarding heat flow through the wall if protected by a thick effective thermal barrier than if exposed to high heat through a thin thermal barrier which may permit the foam to be destroyed. Plastics foams have low thermal conductivities. Thus when they are used in a layered structure, such as a wall, floor, ceiling or roof, they can be highly effective in retarding heat flow from the exposed to the unexposed side. This slows the rise in temperature on the unexposed side, and may increase the hourly fire resistance rating of the entire assembly. However, previous comments respecting flammability of foams should be noted.

Particular composites, such as polymer-impregnated concrete and polymer concrete, in which the great mass of the material is heavy mineral particles, can be expected to retard penetration of flame because of the small percentage of polymer compared with the mass and heat capacity of the minerals. However, polymer concrete cannot be expected to have the fire resistance of all-mineral concrete.

Area Interruptions

Building Codes (Section 10.6) limit or prohibit the use of materials that exhibit rapid surface flame spread or evolve large quantities of smoke. In general, combustible materials should not be applied continuously over large areas or for long distances. Breaks wide enough to stop flame spread should be provided at frequent intervals. This is particularly true of ceilings.

Protective Coatings

Fire-retardant coatings attempt to delay the time to reach ignition temperature and to reduce the spread of flame. They are of three types: heat-resistant, flame retardant, and insulative.

Heat-resistant coatings usually can withstand elevated temperatures. Silicones, for example, are effective to 650°F (340°C); zinc or aluminum pigments may raise this to 1000°F (540°C) and ceramic frits to 1400°F (760°C), but may not withstand direct flame. Flame-retardant coatings, such as fluorocarbons and polyimides, retard the spread of flame but do not necessarily protect the substrate.

Insulative coatings, commonly called intumescents, when heated by flame, bubble and swell to form an insulating mass of char. One ingredient in the coating forms a carbonaceous foam, another makes the foam resistant to flame, and a third forms a non-ignitable gas trapped in the foam. Other ingredients decompose and absorb heat, lowering the temperature below the ignition temperature. Such coatings are used not only on plastics but on wood and other combustible materials.

Considerations with Air Supported Structures (10.35)

Membranes used in air supported structures are either plastic films or flexible composites comprised of plastic coatings on organic or inorganic fiber fabrics. The most commonly used fabrics are organics: nylon and polyester, both readily combustible. Most commonly, these fabrics are coated with vinyl formulated to limit flame spread so that the coated fabrics conform with NFPA Standard 701-71, a vertical flame test that requires extinction of combustion within 2 seconds. As a protection against leaching out of the retardants, the Standard requires that the test material be artificially aged in a weatherometer.

The vinyl coated fabric is generally considered to have a service life of 7 to 10 years, when it must be recoated. Obviously, if limitation of flame spread is a design consideration, the material used in the recoating must continue to provide this protection.

A relatively new and more expensive composite fabric of fluoroplastic (PTFE, Chapter 1) coated fiberglass can achieve a flame spread rating of "incombustible," on the basis of tests that check for flame spread, smoke generation, no fuel contribution and structural integrity. The fiberglass fabric has a high temperature resistance; the PTFE coating melts at temperatures in the range 600 - 700°F. Under elevated temperature, the fabric strength is limited by the strength of the PTFE seams which may soften if the temperature rise is sufficient.

Flexible membrane materials do not provide fire barriers or barriers to prevent temperature build-up on the far side. They would melt or burn in tests for fire resistance. Although many building codes do not require a fire-resistive rating for arches and roof decks located more than 20 ft (6.1 m) above floor level if the materials of the roof structures are incombustible, such structures have been vulnerable in fires. However, such code stipulations may permit the use of PTFE-coated fiberglass fabric in certain applications if fire load and height separation preclude loss of structural integrity of the fabrics from elevated temperature.

Fire Barriers Against Penetration Around Pipe, etc.

Fire may penetrate an otherwise fire-resistant wall or other barrier by moving along a cable, pipe, conduit or other fixture that passes through a barrier, or in a pipe chase not adequately blocked, for example, at floor levels. Various materials have been developed to close such openings. Some are designed to form a char upon exposure to fire, thus retarding penetration. Others, such as those based upon silicones, are resistant to high temperatures. Such barriers may be annular rings, foamed in place (dense foam), or designed to be sprayed, poured, trowelled, or forced as mastics into the openings to be blocked.

10.6 BUILDING CODES (10.9) (10.27) (10.28) (10.29) (10.30) (10.31)

There are no Federal building codes. However, the Department of Housing and Urban Development (HUD) and the General Services Administration (GSA) have their own regulations, as mentioned below. Many States have building codes, but these may not be completely binding unpon municipalities. Consequently, for any given building design, it is necessary to consult the local code and officials to be certain what regulations apply.

On the other hand, several organizations write model building codes that may be and frequently are adopted by municipalities with or without modification. Three of the most widely-employed are those written by Building Officials and Code Administrators, International (BOCA); International Conference of Building Officials (ICBO); and Southern Building Code Conference, International (SBCC). Their provisions for plastics are similar, and undergo periodic changes as the uses of plastics in construction grow and change. In this discussion, these codes are used to illustrate the types of provisions to be found in building codes, but it must be emphasized again that in any specific instance the local code having jurisdiction must be consulted and followed. Furthermore, codes are subject to change, sometimes rapid in an evolving area such as plastics.

Coverage (10.9)

The model codes have general provisions respecting fire that must be met by all materials. They also have specific provisions for plastics.

General

Fire safety measures generally cover:

1. Regulations respecting egress. These are based upon type and physical condition of occupants, and time required to reach a place of safety or to leave the building. Regulations also cover type of building construction, detection systems, self-closing doors, number and location of exits, etc.

2. Protection of structural members. This is generally in the form of an incombustible insulating barrier such as concrete, masonry, plaster or gypsum. The required resistance ratings measured in hours are based upon occupancy, fire loading, and height and areas of a building.

3. Prevention of the spread of fire and smoke. This is accomplished by subdividing the building into limited areas by means of fire-resistant walls, floor-ceiling assemblages, and fire doors.

4. Restrictions on combustibility. Combustible building materials are not permitted in some occupancies and are limited in area and exposure in others. Flame spread of interior surfaces of ceilings, walls, and floors is

limited according to results of tests such as ASTM E84 (Section 10.4). Smoke generation is limited according to the results of either ASTM E84 or ASTM D2843. Some Federal agencies utilize NFPA 258 or ASTM E162. Some codes have specified that products of combustion of interior finishes must be no more toxic than burning wood, but these are being discontinued as too uncertain and difficult to measure.

5. Fire detection and alarm systems. These are being increasingly required, e.g., smoke detectors in residential living units, hotel rooms, nursing homes, etc., are required in some jurisdictions. Voice alarm and communication systems and smoke detectors are sometimes required in retail stores, apartment buildings, and office buildings that have floors more than 75 ft (23 m) above the level of access by fire equipment. Manual fire alarm systems are generally required in schools, hospitals and similar occupancies in buildings more than three stories high.

6. Fire-suppression systems. Various requirements for fire extinguishing systems and automatic sprinklers depend upon floor area, occupancy, and access by fire departments Several States now require sprinklers in all buildings over five stories high.

7. Size of building unit. Permitted heights and areas vary with types of occupancy, type of construction, and requirements for fire extinguishing systems.

Plastics

All three codes named above have specific sections covering Light-Transmitting Plastics and Plastic Foams. Other applications are implied in these and other sections of the codes. Structural applications of plastics, for example, must meet the same general safety requirements as other structural materials.

Light-Transmitting Plastic Construction

The BOCA provisions in effect in 1978 are used as a basis in this discussion, with variations, if any, among the other two codes noted. ICBO and SBCC have adopted essentially the same provisions. It should be emphasized that local codes must be consulted in each individual case.

Approved materials are those that meet the strength, durability, sanitary and fire-resistive requirements of the code. Among the tests cited are ASTM D635 Standard Method of Test for Flammability of Self-Supporting Plastics, ASTM D374 Method of Testing for Thickness, ASTM D1929 Method of Testing for Ignition Properties of Plastics, ASTM E662, NFPA 258 Smoke Generated by Solid

Materials, and ASTM E84 Method of Test for Surface Burning Characteristics of Building Materials. Approved plastics, thermoplastic, thermosetting, or reinforced, must have self-ignition temperature 650°F (350°C) or above when tested according to ASTM D1929, a smoke density rating no greater than 450 when tested according to the way intended for use by ASTM E84, or a smoke density rating no greater than 75 according to ASTM D2843.

Two combustibility classes are:

- C-1, burning extent 1 in. (2.54 cm) or less, 0.060 in. (1.5 mm) thick material, or the thickness intended for use, tested in accordance with ASTM D635.
- C-2, burning rate 2.5 in. (6.35 cm) per min. or less, 0.060 in. (1.5 mm) thick material, or the thickness intended for use, tested in accordance with ASTM D635.

Types of application are:

- Glazing
- Plastic wall panels
- Roof panels
- Skylights
- Light-diffusing systems

Three classes of plastics are:

- Glass fiber reinforced (20 percent or more glass fiber by weight)
- Thermosetting
- Thermoplastic.

Approval of a plastic material requires suitable technical information and identification by trade formula number, name, or other acceptable identification.

In addition to fire-safety requirements, design and installation must meet strength and durability requirements of the code, as well as recognize the properties peculiar to plastics, such as large coefficients of expansion.

Glazing of Unprotected Openings

In unprotected frame construction and in factory and industrial buildings, such doors, sash, and framed openings as are not required to be fire-resistance rated, may be glazed with approved plastics. In other classes of construction, such openings as are not required to be fire-resistance rated may be glazed with approved plastics if:

- the area is not more than 25 percent of the wall face of the story in which it is installed; area of each pane above five stories not more than 16 sq ft (1.49 m2), not more than 4 ft (1.22 m) high, a minimum 3-ft-high (91 cm) vertical spandrel between stories, and installed not more than 75 ft (23 m) above ground. (Note: ICBO requires 4 ft (1.22 m) vertical panels, or flame barriers extending 30 in. (76 cm) beyond exterior wall in plane of floor, and limited to installations not more than 65 ft (19.8 m) above ground.
- **Exception:** If each floor above the first has a 3-ft-wide (91 cm) horizontal architectural projection (fire canopy), thermoplastic materials may be installed up to 50 percent of the wall area of each story in buildings less than 150 ft (46 m) high. Sizes and dimensions of glazed units are unlimited except to meet structural loading requirements.

If a complete approved automatic fire suppressant system is supplied, the 25 percent area restriction above may be increased 100 percent. ICBO permits a maximum 50 percent increase if sprinklered, and SBCC permits a 50 percent increase of the area permitted under the exception with the use of canopies, and waives the basic area provisions.

Exterior Panel Walls

Approved plastics may be used as wall panels in exterior walls of all buildings not required to have a fire resistance rating, except theaters, dance halls and similar high-hazard and institutional buildings, provided that:

- They do not alter the type-of-construction classification.
- They are not installed more than 75 ft (23 m) above ground, except as noted above under Glazing of Unprotected Openings. (The ICBO limit is 40 ft (12.2 m).
- Vertical spandel wall separations between stories are:

Class C-1, at least 3 ft (91 cm)

Class C-2, at least 4 ft (1.22 m)

If there is a fire canopy (see above, Glazing of Unprotected Openings), no vertical separation is needed except thickness of canopy.

If a complete approved automatic fire suppressant system is provided, maximum area of exterior wall and maximum square feet of single area may be increased 100 percent, but not more than 50 percent of total wall area, and is exempt from height limitations.

Combinations of plastic glazing and plastic wall panels are subject to the same limitations as are applicable to the class of plastic for plastic wall panels alone.

Roof Panels

Approved plastics may be used in roof panels of all buildings except theaters, dance halls and similar occupancies, amusement and recreation buildings without stage, and high-hazard and institutional buildings, provided that:

- Roofs are not required to meet the fire resistance requirements.
- Roof panels meet the requirements for roof coverings of the particular occupancy.
- The roof is protected by a complete approved automatic fire suppressant system.
- Roof panels must be separated at least 4 ft (1.22 m) horizontally.
- If exterior wall openings must be fire-resistance rated, roof panels must be at least 6 ft (1.83 m) away from such walls.

Individual Class C-1 plastic panels are limited to 300 sq ft (27.9 m^2), and to a total of 30 percent of the floor area directly below the roof. For individual Class C-2 panels the corresponding limits are 100 sq ft (9.3 m^2) and 25 percent.

Area limitations are waived for one-story buildings not more than 16 ft (4.87 m) high, not exceeding 1200 sq ft (111.3 m^2) in area, and at least 11 ft (3.35 m) from another building. They are also waived for low-hazard buildings such as swimming pool shelters and greenhouses, provided that the building is not more than 5,000 sq ft (465 m^2) in area and at least 11 ft (3.35 m) from a property line or another building. Approved plastics may be used as roof coverings over terraces and patios of one and two-family dwellings.

Skylight Assemblies

Except in high-hazard buildings, skylight assemblies of approved plastics may be used, provided that:

- They are mounted on curbs at least 4 in. (10.2 cm) above the plane of the roof and of material consistent with requirements for the type of construction.
- Edges of plastic are protected by noncombustible material.
- Dome-shaped skylights rise at least 10 percent of maximum span, or not less than 5 in. (12.7 cm).
- Maximum area per skylight within curb is not more than 100 sq ft (9.3 m2).
- Aggregate area of skylights is not more than 33 percent for C-1 plastics and 25 percent for C-2 plastics of floor area directly below.
- Skylights are separated at least 4 ft (1.22 m) horizontally. If exterior wall openings must be fire resistance rated, skylights must be at least 6 ft (1.83 m) from that wall.

Except in high-hazard and institutional buildings, the aggregate area of skylights may be increased 100 percent if skylights are used as fire venting systems, or the building has a complete automatic fire-suppression system. The provisions are waived for one-story buildings at least 30 ft (9.15 m) from adjacent buildings and the space below the roof is not classed as high hazard or institutional or means of egress, or if the plastic meets the fire-resistance requirements of the roof.

Combinations of roof panels and skylights must meet the same requirements as roof panels.

Light-Diffusing Systems

Plastic light-diffusing systems are prohibited in high-hazard and institutional buildings, and in exit ways unless protected by a fire-suppressant system. They must comply with interior finish requirements unless they will fall from their mountings at temperatures at least 200°F (93°C) below their ignition temperatures, but remain in place at ambient temperatures of 175°F (79°C) for at least 15 minutes. Diffusers must be supported directly or indirectly by incombustible hangers.

Individual panels may not exceed 30 sq ft (2.79 m^2) in area, nor 10 ft (3.05 m) in length.

If the building has a complete fire-suppressant system, sprinklers must be both above and below the diffuser panels, unless specifically approved for only above. Diffuser areas are not limited, if protected by an approved fire-suppressant system.

Plastic light-transmitting and light-diffusing panels installed in electrical lighting fixtures must conform with interior finish requirements unless they meet the retention and falling requirements described above. In fire exits and corridors, the area of approved plastics materials must not be greater than 30 percent of the total area of the ceiling unless the occupancy is protected by an approved fire-suppressant system.

Partitions

Partitions incorporating plastics must meet code requirements for partitions in the occupancy class involved.

Bathroom Accessories

Approved plastics are permitted in shower doors, bathtub enclosures, and similar accessory units.

Awnings and Similar Structures

Approved plastics may be used in conformity with provisions of the code.

Greenhouses

Approved light-transmitting plastics may be used in place of plain glass.

Foam Plastics

The model codes have similar language for foam plastics. A general requirement, except where specifically exempted, is that foam plastics shall have a flame-spread rating of not more than 75 and a smoke developed rating of not more than 450 when tested according to ASTM E84 (the tunnel test) or the equivalent Underwriters' Laboratories (UL 723) or model code tests, (e.g., ICBO 42-1). However, insurance companies consider E84 an unsuitable and frequently misleading test for foams. A further general requirement, now being eliminated in most cities, is that the products of combustion shall be no more toxic than those of untreated wood burned under similar conditions. The requirement is hard to enforce because of the difficulty of measuring toxicity under the conditions specified. Codes typically require thermal barriers, sprinklers, or both in conjunction with foam plastics (see below). Some localities do not permit foam plastics.

Specific Requirements: These requirements, unless otherwise specified, apply to all uses of foam plastics in or on walls, ceilings, attics, roofs, floors, crawl spaces or similar areas.

Foam plastics may be used:

a. Within the cavities of masonry or concrete walls regardless of type of construction.

b. On room side surfaces, such as walls or ceilings, if the foam plastic is protected on the interior side by a thermal barrier having a finish rating of at least 15 minutes, e.g., 1/2-inch (12.7 mm) gypsum wallboard, installed to stay in place at least 15 minutes.

c. Within wall cavities, or as elements of walls classified as combustible non-fire resistive, if installed according to (b) above.

d. Within wall cavities, or as elements of walls classified as combustible fire-resistive, provided fire tests are conducted according to ASTM E119, or equivalent Underwriters' Laboratories or model code tests, and the protection from the interior is at least equivalent to (b) above.

In cold-storage rooms and similar installations requiring thick insulation, foam plastics insulation having a flame spread of 75 or less when tested according to ASTM E84 in a thickness of 4 in. (10.2 cm) may be used in thicknesses of up to 10 in. (25.4 cm) when the room is protected inside by a thermal barrier having a 15-minute finish rating (e.g., portland cement plaster) as determined by ASTM E119 or equivalent Underwriters' Laboratories or model code tests. Thermal barriers must stay in place at least 15 minutes.

Except where codes require noncombustible or fire-resistive construction, foam plastics having a flame-spread rating of 25 or less may be used in thicknesses not greater than 4 in. (10.2 cm) in or on walls if the foam is covered by not less than 0.032-in. (0.81-mm) thick aluminum, or 26-gauge (0.45 mm) galvanized steel, and the insulated space is protected by automatic sprinklers.

Codes specify barriers and types of foams used with Class A, B, C and ordinary roofing materials, similarly for foam cores of doors that do not require a fire-resistive rating, and foam plastic backerboard for siding.

Foams for applications not meeting the above requirements may be approved on the basis of tests such as ASTM E84, ASTM E119, corner tests, and tests related to actual end-use items, or upon considerations of quantity, location, and similar pertinent items where tests are not applicable or practical. These must be taken up with the building official. An example might be sandwich roof panels for cold-storage warehouses in which the foam core not only acts as insulation but as an essential part of the load-bearing element. In that case, structural and fire requirements for the class of building involved must be met in addition to the fire requirements set forth above.

Department of Housing and Urban Development

HUD Minimum Property Standards. The Department of Housing and Urban Development issues standards governing construction of One and Two-Family Dwellings (No. 4900.1) Multi-Family Housing (No. 4910.1), and Care-Type Housing (No. 4920.1). These apply to HUD's numerous housing programs, and should be consulted for any specific design.

The standards, especially as they apply to fire safety, are general and are as applicable to plastics as to any other materials. Fire-resistance ratings are determined by ASTM E119, or by judgment based on tests of similar assemblages. HUD has issued Materials Use Bulletins for plastics materials.

Mobile Homes. The Department issues similar standards covering mobile homes. The standards cover all materials including plastics. Like the Minimum Property Standards, the Mobile Home Standards should be consulted in cases involving the design of such structures.

Other Federal Agencies

Other Federal agencies issue specifications and standards covering materials, including plastics, utilized in structures under their jurisdiction. These are exempt from local codes and should be consulted for designs of such structures.

Life Safety Code, NFPA No. 101, National Fire Protection Association (10.31)

This Code for Safety to Life from Fire in Buildings and Structures, issued by the National Fire Protection Association, is widely quoted. It contains provisions for classifications of occupancy and hazards of contents, means of egress, features of fire protection, building service equipment, and nine classes of occupancies. Of particular interest in applications of plastics as interior finish are the following:

Interior Finish (NFPA 255, ASTM E84, UL 723)

Class A.	Flame spread 0-25, smoke developed 0-450.
Class B.	Flame spread 26-75, smoke developed 0-450.
Class C.	Flame spread 76-200, smoke developed 0-450.

The Life Safety Code does not have provisions for the use of light-transmitting plastics materials for glazing, skylights and similar uses.

Cellular or foamed plastics may be permitted on the basis of fire tests which reasonably substantiate their intended combustibility characteristics, under actual fire conditions. They may be used as trim, if density is not less than 20 pcf (321 kg/m^3), and the aggregate wall surface covered is not greater than 10 percent. With these restrictions, Class C interior finish materials may be used in occupancies where Class A or B is required. Model building codes have similar restrictions.

10.7 SUMMARY

Plastics are organic materials and should be handled in much the same manner as other organic materials, keeping in mind their own distinctive properties.

Behavior in a fire depends upon the chemical structure and composition of plastics, as well as the nature of the fire itself. All plastics burn. Behavior in fire is variable, including rate of burning and emission of smoke and noxious or toxic gases. Various chemical and physical means are employed to modify the fire behavior of plastics.

Results of fire tests, by and large, are specific to the conditions of the test, and cannot readily be correlated with other tests. Small-scale tests can provide a great deal of information, provided the data user understands how the test is conducted, and its limitations. Larger-scale tests that more nearly approximate actual fire conditions come closer to depicting behavior, but even these do not necessarily predict how materials will behave under actual fire conditions. The field is undergoing active development.

Design and manner of use of plastics in structures are frequently more significant than their inherent fire properties. Fire hazards can be reduced by good design for rapid evacuation of inhabited structures and by confining fire by suitable enclosures, fire breaks, thermal barriers, and venting, as well as by judicious selection of materials for a particular application.

Building codes, in addition to general requirements respecting fire, incorporate specific sections respecting plastics. In the model codes, these are related particularly to foams and to light-transmitting plastics materials and installations. In any specific design, the local code having jurisdiction must be followed.

As is true of any material, plastics must be utilized in such a way as to take advantage of their favorable properties and to minimize their limitations, including their behavior in fire.

APPENDIX 10-A - DESCRIPTION OF COMBUSTION (10.1)

All polymers, natural and synthetic, undergo progressive degradation and, ultimately, destruction including combustion, as temperatures are raised progressively to the critical points in a favorable environment, usually normal air. Some burn reacily, others slowly, and still others do not support combustion in ordinary atmospheres.

Steps Leading to Combustion

Several stages are involved. Most polymers and objects made of them are reasonably stable at ordinary temperatures, and exposure for several hours even at 175-212°F (80-100°C) has no appreciable effect, even though slow oxidation resulting in hydroperoxyl groups occurs. The rate of oxidation depends upon composition. Some groups, such as cyanide (CN), and halogens (Cl, for example), retard the reaction, while others, such as methyl (CH_3), promote it.

The formation of hydroperoxyl groups is a feature of the slow progressive degradation known as aging, which is often accelerated by elevated temperatures. It can be counteracted by chain transfer agents (antioxidants) such as amines and phenols. A relatively small amount suffices to protect an object against deterioration for months or years.

As the temperature is raised, e.g., to 212°F (100°C), the process is accelerated to form more hydroperoxyl groups by scission of polymer chains, the rate depending upon composition. Degradation also occurs because of accelerated scission or separation of -C-C-bonds in the polymeric chains. Here again the stabilizers mentioned above serve to reduce this reaction to prevent degradation, and are effective at processing temperatures such as 355-390°F (180-200°C).

At still higher temperatures, in the range of 390-570°F (200-300°C), the rate of reaction increases rapidly enough to overcome stabilizers, the chain reaction in the presence of oxygen becomes exothermic and raises the temperature, chemical decomposition of the polymer produces volatile flammable products, and many polymers, especially thermoplastics, soften or may even melt, leading to deformation and possibly to increased surface area accessible to oxygen.

If more heat is added and oxygen is available, open flame or autoignition may develop at approximately 750°F (400°C). The steps leading to combustion are complete.

Among the steps that can be taken to lessen flammability are the incorporation of flame-retardant ingredients that decompose to give off non-combustible gases such as water vapor, carbon dioxide, and ammonia, and form inhibitors, such as HBr, against radical chain reactions. Finely-powdered inorganic fillers such as carbon black, alumina, silica, and limestone increase the thermal conductivity and thus reduce local hot spots and at the same time raise the softening temperature. Still other additives such as borates, phosphates, and silicates can form glassy coatings around the polymeric mass, thereby reducing the access of oxygen and the escape of volatile flammable gases, increasing the thermal conductivity, and preventing flaming and dripping.

Phosphoric acid salts, preferably, or heavy metals such as zinc and molybdenum in addition to mineral fillers, assist in char formation. Others include chromated zinc chloride and antimony oxides, sometimes combined with tricresyl phosphate.

Among the most effective flame retardants are the halogens, especially chlorine and bromine. These are employed in a variety of ways, e.g., halogenated plasticizers, additions to the polymer chain, halogenated hardeners as in epoxies, and halogenated blowing agents as in polyurethane foam.

Phosphorous is another effective flame retardant, as in the promotion of char mentioned above. It is used in various ways, e.g., in plasticizers.

Alumina trihydrate, by giving off water as it decomposes, absorbs a great deal of energy and holds down temperatures as the water is released and vaporizes.

Inorganic fillers, especially those having high thermal conductivities, densities, and specific heats, assist in retarding ignition by absorbing energy and preventing high local temperatures.

Synergism

Some halogen (Cl, Br) compounds useful in fire retardation are listed in Table 10-2. Because some are ordinarily volatile and may be lost at temperatures below the critical ones, e.g., below 570°F (300°C), other ingredients are added that combine with the halogens and keep them in place. Among them is antimony trioxide (Sb_2O_3) which displays outstandingly this "synergistic" effect. The amount of halogen needed to be effective as a flame retardant can frequently be markedly reduced by the Sb_2O_3, thus alleviating property losses that might be caused by high halogen content. Zinc salts and bromine compounds act well together. The effectiveness of phosphorous compounds is often increased by adding bromine compounds. Phosphites, metaphosphites and silicates of zinc, titanium and other heavy metals display similar synergism.

Table 10-2
Representative Halogenated Flame Retardants

Chlorendic acid
Chlorinated bisphenyl
Chlorinated paraffin
Hexachloro-cyclo-pentadiene
Tetrabromo-bis-phenol
Tetra-bromo-phthalic anhydride
Tribromo-phenol

Summary

To summarize, the important components of a system modified by a flame-retardant chemical are:

1. Chain transfer agents to retard free radical chain reactions.
2. Reduction of flammable gases, and keeping flash-points of decomposition gases high.
3. Formation of glossy coatings.
4. Char formation.
5. Reduction of volatility and synergistic retention of important components of flame-proofing systems.
6. Fixing of flame-retardants.

Additional factors affecting flammability include the following:

1. Glass transition temperature, Tg, below which amorphous and partially crystalline polymers become glassy. Pipes sag and plates warp above this temperature (Table 10-3). Structural components cannot be permitted to reach this temperature.

2. Melting point, Tm, at which crystalline polymers abruptly change into mobile liquids, losing all mechanical properties (Table 10-4).

3. Decomposition temperature range, Td, in the presence of oxygen, with generation of volatile products, many flammable. The rate and extent of decomposition are increased with increasing temperature. This depends strongly upon not only the chemical composition, but the configuration, e.g., chunk, rod, plate, film, fiber, sponge or foam, web, or other shape (Table 10-5).

Specific heats and heat conductivities are additional important aspects (Tables 10-6, 1-2).

Finally, the flash ignition and autoignition temperatures at which polymers react with oxygen to start burning are important (Table 10-7). The flash-ignition temperature is the temperature at which a material flashes into enveloping flame in the presence of an igniting flame. The self-ignition temperature is the temperature at which the same effect occurs without an igniting flame (see ASTM D1929, Section 10.4).

Table 10-3
Glass Transition (T_g) Values for Various Polymers

	°F	°C
Polyethylene	-184	-120
Polypropylene	-8	-22
Polybutylene	-13	-25
Polybutadiene	-112	-80
Polyvinyl fluoride	-4	-20
Polyvinyl chloride	185	85
Polyvinylidene chloride	-4	-20
Polystyrene	203	95
Poly acetal	-112	-80
6-Nylon	158	70
66-Nylon	122	50
Polyester	230	110
Polycarbonate	302	150
Polytetrafluoroethylene	-175	-115
Silicone	-193	-125

Table 10-4
Melting Temperatures (T_m) for Various Crystalline Polymers *

	°F	°C
Low density polyethylene	230	110
High density polyethylene	266	130
Polypropylene (isotactic)	347	175
6-Nylon	419	215
66-Nylon	500	260
Polyester	500	260
Polytetrafluoroethylene	626	330
Polyarylamides	716	380

* Amorphous polymers exhibit a softening range of temperatures.

Table 10-5
Decomposition Ranges (T_d) Ranges for Various Polymers

	°F	°C
Polyethylene	645-825	340-440
Polypropylene	610-750	320-400
Polyvinyl acetate	420-600	215-315
Polyvinyl chloride	390-570	200-300
Polyvinyl fluoride	700-880	370-470
Polytetrafluoroethylene	930-1020	500-550
Polystyrene	570-750	300-400
Polymethyl methacrylate	355-535	180-280
Polyacrylonitrile	480-570	250-300
Cellulose acetate	480-590	250-310
Cellulose	535-715	280-380
6-Nylon	570-660	300-350
66-Nylon	610-750	320-400
Polyester	535-610	280-320

Table 10-6
Specific Heats for Various Materials

	cal/g. °C
Polyethylene	0.55
Polypropylene	0.46
Polytetrafluoroethylene	0.25
Polyvinyl chloride	0.25
Polyvinyl fluoride	0.30
Polystyrene	0.32
SBR (Styrene Butadiene Rubber)	0.45
ABS (Acrylonitrile Butadiene Styrene)	0.35
Cellulose acetate	0.40
6-Nylon	0.38
66-Nylon	0.40
Polyester	0.30
Phenol formaldehyde	0.40
Epoxy resins	0.25
Polyimide	0.27

Table 10-7
Ignition Temperatures of Various Polymers

	Self Ignition		Flash Ignition	
	°F	°C	°F	°C
Polyethylene	662	350	644	340
Polypropylene	1022	550	968	520
Polytetrafluoroethylene	1076	580	1040	560
Polyvinyl chloride	842	450	734	390
Polyvinyl fluoride	896	480	788	420
Polystyrene	914	490	662	350
SBR (Styrene Butadiene Rubber)	842	450	680	360
ABS (Acrylonitrile Butadiene Styrene)	896	480	734	390
Polymethyl methacrylate	806	430	572	300
PAN (Polyacrylonitrile)	1040	560	896	480
Cellulose (paper)	446	230	410	210
Cellulose acetate	878	470	644	340
66 Nylon cast	842	450	788	420
66 Nylon spun and drawn	986	530	914	490
Polyester	896	480	824	440

APPENDIX 10-B - EFFECT OF TEMPERATURE ON MECHANICAL PROPERTIES (10.17) (10.32)

Figure 10-8 and Table 10-8 present information respecting the ability of eight classes of plastics to retain 50 percent of their mechanical properties in various temperature ranges for various periods of time. Figure 10-8 shows temperature-time zones, and Table 10-8 lists the plastics that fall in the various zones.

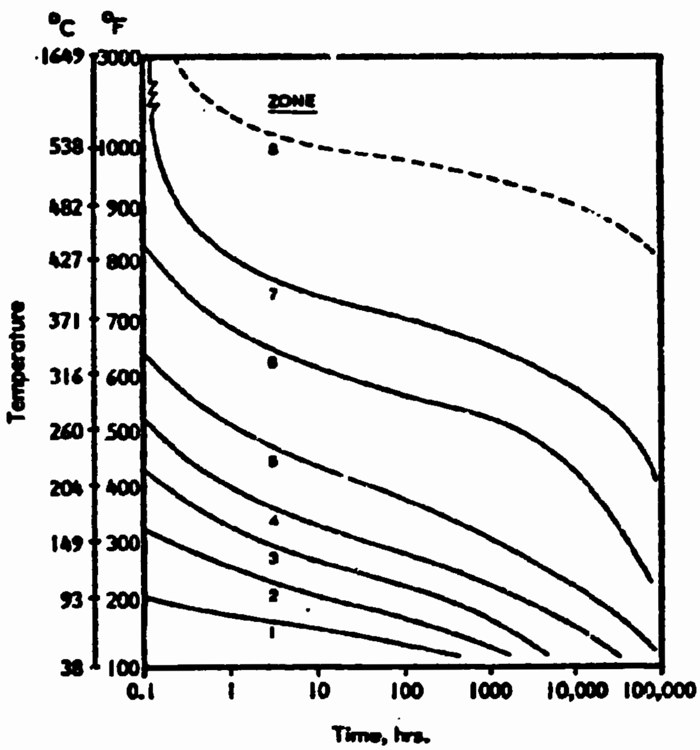

Fig. 10-8. HOW PLASTICS PERFORM ON THE BASIS OF TEMPERATURE AND TIME (10.17) (10.32)

Table 10-8

Plastics Retaining 50% Mechanical or Physical Properties Tested at Temperatures in Air

Zone 1 - Fig. 10-8

Acrylic
Cellulose acetate (CA)
Cellulose acetute-butyrate (CAB)
Cellulose acetate propionate (CAP)
Cellulose nitrate (CN)
Cellulose propionate
Polyallomer
Polyethylene, low-density (LDPE)
Polystyrene (PS)
Polyvinyl acetate (PVAC)
Polyvinyl alcohol (PVAL)
Polyvinyl butyral (PVC)
Polyvinyl chloride (PVC)
Styrene-acrylonitrile (SAN)
Styrene-butadiene (SBR)
Urea-formaldehyde

Zone 2

Acetal
Acrylonitrile-butadiene-styrene (ABS)
Chlorinated polyether
Ethyl cellulose (EC)
Ethylene vinyl acetate copolymer (EVA)
Furan
Ionomer
Phenoxy
Polyamides
Polycarbonate (PC)
Polyethylene, high-density (HDPE)
Polyethylene, cross-linked
Polyethylene terephthalate (PETP)
Polypropylene (PP)
Polyvinylidene chloride
Urethane

Zone 3

Polymonochlorotrifluoroethylene (CTFE)
Vinylidene fluoride

Zone 4

Alkyd
Fluorinated ethylene propylene (FEP)
Melamine-formaldehyde
Phenol-furfural
Polyphenylene oxide (PPO)
Polysulfone

Zone 5

Acrylic thermoset
Diallyl phthalate (DAP)
Epoxy
Phenol-formaldehyde
Polyester
Polytetrafluoroethylene (TFE)

Zone 6

Parylene
Polysulfone
Polybenzimidazole (PBI)
Polyphenylene
Silicone

Zone 7

Polyamide-imide
Polyimide

Zone 8

Plastics now being developed using intrinsically rigid linear macromolecules rather than the usual crystallization and cross-linking.

References (10.17) (10.32)

APPENDIX 10-C - POTENTIAL HEAT OF PLASTICS (10.34)

Table 10-9 lists potential heat values obtained with the National Bureau of Standards Differential Bomb Calorimeter (Section 10.4).

Table 10-9
Potential Heat of Selected Building Materials

Material	Thickness (in.)	Density (lb/ft^3)	Potential Heat: Weight basis (Btu/lb)	Potential Heat: Volume basis (Btu/ft^3)
1. Woods				
a. Douglas fir, untreated	0.75	38.0	8,400	319×10^3
b. Douglas fir (retardant treatment "[illegible]")	0.75	37.2	8,290	308.0
c. Douglas fir (retardant treatment "B")	0.75	47.2	7,860	371.0
d. Douglas fir (retardant treatment "C")	0.75	38.8	7,050	274.0
e. Maple, soft, untreated	1.0	39.5	[illegible],940	314.0
f. Hardboard, untreated	0.25	59.8	8,530	510.0
2. Plastics				
a. Polystyrene, wall tile	0.075	65.4	17,420	1,140.0
b. Rigid, polyvinyl chloride, retardant treated	0.147	86.0	9,290	799.0
c. Phenolic laminate	0.063	76.4	7,740	592.0
d. Polycarbonate resin	0.25	78.7	13,330	1,050.0
3. Insulation				
a. Glass fiber, semirigid, no vapor barrier	1.0	3.0	3,040	9.1
b. Rock wool batting, paper enclosure	3.0	2.4	1,050	2.5
c. Roof insulation board	1.0	10.4	3,380	35.1
d. Cork (reconstituted cork sheet)	0.25	14.8	[illegible],110	164.0
e. Cellulose mineral board	2.0	47.8	2,250	108.0
4. Concrete				
a. Cinder aggregate		93.0	3,090	286.0
b. Slag aggregate		110.1	80	8.9
c. Shale aggregate		80.5	10	0.5
d. Calcareous gravel aggregate		133.1	-250	-33.[illegible]
e. Siliceous gravel aggregate		166.8	-40	-6.7
5. Cement Board				
a. Asbestos cement board	3/16	117.0	80	[illegible].2
b. Asbestos cement board + 20 mil paint	3/16	159.2	390	62.4
6. Gypsum				
a. $CaSO_4 \cdot 2H_2O$, hydrated neat gypsum	0.41	137.9	-290	-31.3
b. Perlite aggregate plaster, 21 percent aggregate	1.0	53.2	70	4.0
c. Sand aggregate plaster, 68 percent aggregate	1.0	101.8	-50	-5.4
d. Vermiculite aggregate plaster, 15 percent aggregate	1.0	51.2	-90	-4.6
e. Gypsum board "A"	3/8	50.5	760	38.4
f. Gypsum board "A" with paper removed	3/8	46.6	-270	-12.5
g. Gypsum board "A" + alkyd gloss paint	3/8	46.[illegible]	860	41.2
h. Gypsum board "B"	0.50	51.2	650	33.0
7. Miscellaneous				
a. Paint "E" (dried paint film)	0.05		3,[illegible]40	
b. Asphalt shingles (fire retardant)	0.25	70.7	8,320	588.0
c. Building paper (asphalt impregnated)	0.042	42.8	13,620	583.0
d. Building paper (rosin sized)	0.018	23.6	7,650	181.0
e. Linoleum tile	1/8	86.0	7,760	667.0
f. Brick, red, face	2.25	139.1	20	2.2
g. Charcoal, coconut			13,870	

Note: All weights and percentages refer to original air-dry weight. Ref. 10.34

REFERENCES - CHAPTER 10

10.1 Mark, Herman F. "Combustion of Polymers and Its Retardation." Proceedings, National Symposium on Fire Safety Aspects of Polymeric Materials. Carnegie Institution, Washington, D.C., 6-8 June 1977.

10.2 Hilado, Carlos J. Flammability Handbook for Plastics. 2d ed. Fire and Flammability Series, Technomic Publishing Co., Inc., Westport, Conn., 1974.

10.3 Hilado, Carlos J., ed. Flammability of Solid Plastics. Vol. 7. Fire and Flammability Series, Technomic Publishing Co., Inc., Westport, Conn., 1974.

10.4 Hilado, Carlos J., ed. Flammability of Cellular Plastics. Vol. 8. Fire and Flammability Series, Technomic Publishing Co., Inc., Westport, Conn., 1974.

10.5 Fire Safety Aspects of Polymeric Materials, Vol. 1: Materials: State of the Art. Report by National Materials Advisory Board, Pub. NMAB 318-1, National Academy of Sciences, Washington, D.C., 1977.

10.6 Fire Safety Aspects of Polymeric Materials, Vol. 2: Test Methods, Specifications, Standards, Glossary. Report by National Materials Advisory Board, Pub. NMAB 318-1, National Academy of Sciences, Washington, D.C., 1977.

10.7 Fire Safety Aspects of Polymeric Materials, Vol. 3: Smoke and Toxicity. Report by National Materials Advisory Board, Pub. NMAB 318-1, National Academy of Sciences, Washington, D.C., 1977.

10.8 Fire Safety Aspects of Polymeric Materials, Vol. 4: Fire Dynamics and Scenarios. Report by National Materials Advisory Board, Pub. NMAB 318-1, National Academy of Sciences, Washington, D.C., 1977.

10.9 Fire Safety Aspects of Polymeric Materials, Vol. 7: Buildings. Report by National Materials Advisory Board, Pub. NMAB 318-1, National Academy of Sciences, Washington, D.C., 1977.

10.10 Building Materials List, 1978. Underwriters' Laboratories, Northbrook, Illinois.

10.11 Factory Mutual Guide, 1978. Factory Mutual Engineering Corporation, Norwood, Mass.

10.12 Factory Mutual Building Corner Fire Test Procedure. Fire Test Procedure Publication A880. Factory Mutual Engineering Corporation, Norwood, Mass. June 1972.

10.13 Loss Prevention Data, 1-57; Rigid Foamed Polyurethane and Polyisocyanurate for Construction. Factory Mutual Engineering Corporation, Norwood, Mass., Dec. 1978.

10.14 Loss Prevention Data, 1-58; Foamed Polystyrene for Construction. Factory Mutual Engineering Corporation, Norwood, Mass. June, 1978.

10.15 Loss Prevention Data, 1-59; Reinforced Plastic Panels in Construction. Factory Mutual Engineering Corporation, Norwood, Mass. June, 1978.

10.16 Thompson, N. J. and Cousins, E. W. "The FM Construction Materials Calorimeter." Quarterly of the National Fire Protection Association. Vol. 52, No. 3, Jan. 1959.

10.17 Wilson, E. L. "Flammability and High-Temperature Characteristics of Composites." Vol. 3, Flame Retardance of Polymer Materials. Marcus Dekker, Inc., New York, N. Y. 1975.

10.18 Blaga, A. and Yamasaki, R. S. "Outdoor Durability of a Common Type (Tetrachlorophthalic Acid-Based) Fire Retardant Glass Fiber Reinforced Polyester (GRP) Sheet." DBR Paper 757, National Research Council of Canada, Division of Building Research, Ottawa, Canada. 1977.

10.19 ASTM 1978 Annual Book of Standards, Parts 18, 35. American Society for Testing and Materials, Philadelphia, Pa.

10.20 Standard Methods of Fire Tests of Building Construction. NFPA 251, National Fire Protection Association, Boston, Mass. 1972.

10.21 Method of Test of Surface Burning Characteristics of Building Materials. NFPA 255, National Fire Protection Association, Boston, Mass. 1972.

10.22 Standard Test Method for Measuring the Smoke Generated by Solid Materials. NFPA 258. National Fire Protection Association, Boston, Mass. 1976.

10.23 Underwriters' Laboratories Tests. Underwriters' Laboratories, Inc., Chicago, Ill.

10.24 "A Fire Study of Rigid Cellular Plastic Materials for Insulated Wall and Roof/Ceiling Construction, Parts 1, 2, 3." Summaries from Society of Plastics Industry, N. Y. Urethane Safety Group Bulletins U-100R, U-102R. Factory Mutual Research Corporation, Westport, Conn.

10.25 Williamson, R. B. and Baron, F. M. "A Corner Fire Test to Simulate Residential Fires." Flammability of Cellular Plastics. Vol. 8, Fire and Flammability Series. ed. Hilado, Carlos J. Technomic Publishing Company, Inc., Westport, Conn. 1974.

10.26 Benjamin, I. A. "Development of a Room Fire Test." Special Technical Publication 614, American Society for Testing and Materials, Philadelphia, Pa. 1977.

10.27 Basic Building Code, 1975. Building Officials and Code Administrators International, Inc., Chicago, Ill.

10.28 Uniform Building Code 1976, and 1978 Supplements. International Conference of Building Officials, Whittier, Cal.

10.29 Standard Building Code 1976, and 1977 Revision. Southern Building Code Congress International, Inc., Birmingham, Ala.

10.30 HUD Minimum Property Standards. 4900.1, One and Two-Family Dwellings; 4910.1, Multi-Family Housing; 4920.1, Care-Type Housing. U. S. Department of Housing and Urban Development, Washington, D. C. 1973.

10.31 Life Safety Code. National Fire Protection Association, Boston, Mass. 1976.

10.32 Rosato, D. V.; Fallon, W. K.; Rosato, D. V. Markets for Plastics. Van Nostrand Reinhold Co., New York, N. Y. 1969.

10.33 Nelson, Gordon L. "Plastics Flammability." National Symposium on Fire Safety Aspects of Polymeric Materials. Carnegie Institution, Washington, D. C. 6-8 June 1977.

10.34 "Potential Heat of Materials in Building Fires." NBS Technical News Bulletin, Nov. 1960. National Bureau of Standards, Washington, D. C.

10.35 "State-of-the-Art Report Air Supported Structures." American Society of Civil Engineers, New York, N. Y. 1979.

*U.S. GOVERNMENT PRINTING OFFICE: 1982 522-046/8565 1-3